frontiers | Research Topics

Microbes from marine distinctive environments

Edited by
Shan He, Ming Ma and Slava Epstein

Coordinated by
Yongchao Yin

Published in
Frontiers in Microbiology
Frontiers in Marine Science

ISSN 1664-8714
ISBN 978-2-8325-4170-8
DOI 10.3389/978-2-8325-4170-8

About Frontiers

Frontiers is more than just an open access publisher of scholarly articles: it is a pioneering approach to the world of academia, radically improving the way scholarly research is managed. The grand vision of Frontiers is a world where all people have an equal opportunity to seek, share and generate knowledge. Frontiers provides immediate and permanent online open access to all its publications, but this alone is not enough to realize our grand goals.

Frontiers journal series

The Frontiers journal series is a multi-tier and interdisciplinary set of open-access, online journals, promising a paradigm shift from the current review, selection and dissemination processes in academic publishing. All Frontiers journals are driven by researchers for researchers; therefore, they constitute a service to the scholarly community. At the same time, the *Frontiers journal series* operates on a revolutionary invention, the tiered publishing system, initially addressing specific communities of scholars, and gradually climbing up to broader public understanding, thus serving the interests of the lay society, too.

Dedication to quality

Each Frontiers article is a landmark of the highest quality, thanks to genuinely collaborative interactions between authors and review editors, who include some of the world's best academicians. Research must be certified by peers before entering a stream of knowledge that may eventually reach the public - and shape society; therefore, Frontiers only applies the most rigorous and unbiased reviews. Frontiers revolutionizes research publishing by freely delivering the most outstanding research, evaluated with no bias from both the academic and social point of view. By applying the most advanced information technologies, Frontiers is catapulting scholarly publishing into a new generation.

What are Frontiers Research Topics?

Frontiers Research Topics are very popular trademarks of the *Frontiers journals series*: they are collections of at least ten articles, all centered on a particular subject. With their unique mix of varied contributions from Original Research to Review Articles, Frontiers Research Topics unify the most influential researchers, the latest key findings and historical advances in a hot research area.

Find out more on how to host your own Frontiers Research Topic or contribute to one as an author by contacting the Frontiers editorial office: frontiersin.org/about/contact

Microbes from marine distinctive environments

Topic editors
Shan He — Ningbo University, China
Ming Ma — Peking University, China
Slava Epstein — Northeastern University, United States

Topic coordinator
Yongchao Yin — Northeastern University, United States

Citation
He, S., Ma, M., Epstein, S., Yin, Y., eds. (2023). *Microbes from marine distinctive environments*. Lausanne: Frontiers Media SA. doi: 10.3389/978-2-8325-4170-8

Table of contents

frontiers | Frontiers in Microbiology

TYPE Editorial
PUBLISHED 06 December 2023
DOI 10.3389/fmicb.2023.1300210

OPEN ACCESS

EDITED AND REVIEWED BY
Michael Rappe,
University of Hawaii at Manoa, United States

*CORRESPONDENCE
Shan He
✉ heshan@nbu.edu.cn

RECEIVED 23 September 2023
ACCEPTED 24 November 2023
PUBLISHED 06 December 2023

CITATION
He S, Ma M, Epstein S and Yin Y (2023) Editorial: Microbes from marine distinctive environments. *Front. Microbiol.* 14:1300210. doi: 10.3389/fmicb.2023.1300210

Editorial: Microbes from marine distinctive environments

Shan He[1]*, Ming Ma[2], Slava Epstein[3] and Yongchao Yin[3]

[1]Li Dak Sum Yip Yio Chin Kenneth Li Marine Biopharmaceutical Research Center, Health Science Center, Ningbo University, Ningbo, Zhejiang, China, [2]School of Pharmaceutical Sciences, Health Science Centre, Peking University, Beijing, China, [3]Department of Biology, Northeastern University, Boston, MA, United States

KEYWORDS

microbes, marine, diversity, natural product, deep sea, enzyme, symbiosis

Editorial on the Research Topic
Microbes from marine distinctive environments

Marine distinctive environments, such as the deep sea, polar seas, hydrothermal vents, the mesophotic zone, holobionts, and mangroves, are unique habitats for microorganisms, with distinctive environmental properties in terms of temperature, pressure, light, and salinity. Innumerous and distinctive microbial biodiversity in these environments awaits exploration. Major advances in manned submersibles, underwater robots (e.g., ROVs and AUVs), and SCUBA deep diving have enabled extensive observation and sample collection in these environments in recent decades. These environments are important resources for bioprospecting, including drug discovery and novel enzymes. The advent of new microbial cultivation approaches, as well as metagenomics and bioinformatics tools, provide unprecedented opportunities to study microbes from these special habitats. Thus, there are continuous research and development efforts to analyze, understand, and utilize these microbial resources. This Research Topic falls between microbiology and marine sciences. The aim was to gather recent insights into microbes from marine distinctive environments.

Symbiosis is very common in marine life. In a holobiont, the host can leverage its symbiotic microbes as producers of bioactive compounds for chemical defense and other ecological purposes. Zhao et al. investigated natural products from a marine-algal-derived endophytic fungus *Aspergillus* sp. Tennessenoid A, a novel polyketide-terpene hybrid metabolite, was discovered. The compound featured an unprecedented structure, with antifungal activities against eight plant pathogenetic fungi. Hmani et al. have cultivated epibiotic bacteria of *Ulva* from the Tunisian coast. The enzymatic and antimicrobial activities of *Ulva*-associated bacteria were evaluated. The report highlighted the enzymatic activities of seaweed epibiotic bacteria, with potential uses in the industrial sector.

The deep sea is a unique environment characterized by no sunlight penetration, high hydrostatic pressure, and low temperature. Microbes inhabiting the deep sea have evolved unique biodiversity, chemical diversity, and functional diversity. Lv et al. analyzed secondary metabolites from a deep-sea-derived fungus. Two new indole diketopiperazines, along with several known analogs with anti-microbial and anti-cancer activities, were characterized. These reports revealed the potential of discovering novel microbial natural products from marine distinctive environments for future drug development.

Marine sediments are rich in organic matter. Taurine, a naturally occurring organic sulfonate, acts as an important component of organic sulfur in marine sediments, while polyvinyl alcohol is the world's highest output water-soluble synthetic polymer, exerting

an adverse effect on marine ecological environments. Tan et al. cultured a *Marmoricola* sp. actinobacterium from a deep-sea cold seep, which exhibited the prominent capability of degrading and utilizing taurine and polyvinyl alcohol for energy production.

Historic shipwrecks are anthropogenic landmarks in the marine environment, some of which have become sites of seeing, visited by SCUBA divers and submersibles. However, their influence on the local geochemistry and microbiology remains largely unexplored. Van Landuyt et al. targeted a World War II shipwreck that was hit by two aerial bombs before sinking. Chemical and microbial analyses of the samples indicated that, even after 80 years, the historic shipwreck can still significantly steer the surrounding sediment chemistry and microbial ecology.

Hydrothermal vents are unique marine environments where geothermally heated water is expelled through fissures in the Earth's crust. Their environmental conditions are extreme and significantly different from those in other marine habitats, for example, high temperature and the enrichment of organic volatiles and heavy metals. Wang L. et al. investigated the functions of microbial communities from Kueishan Island hydrothermal vents using metagenomics. This study provided insights into the microbial community in this distinctive habitant and helped understand how they survive and interact in such extreme conditions. In another case, Fonseca et al. addressed the structure, diversity, and spatial distribution patterns of the bacterial community of one of the world's largest subsurface sulfidic benthic systems. The community was dominated by sulfur-associated bacteria. A spatial pattern was unveiled along the study area, to which the family Desulfobulbaceae contributed the most to the spatial variance.

New microbial cultivation approaches enable the cultivation of previously uncultured marine microbes. Ding et al. modified iChip, an *in situ* cultivation technique, and applied the new device to access the hidden microbial diversity in marine sediments. Two novel species from the family Flavobacteriaceae were successfully cultured and systematically described. In another article, two previously uncultured novel species belonging to the genus *Kordiimonas* were cultured and reported by Ye et al.. Comparative genomic analysis indicated that the genus is a rich source of homoserine lactones, some of the most important signaling molecules in the quorum-sensing system of Gram-negative bacteria.

Marine blue holes are underwater sinkholes considered to be time capsules providing evidence of Earth's history regarding past climate change, karst processes, and life evolution. The Sansha Yongle blue hole (301.19 m depth) in the South China Sea is the world's deepest blue hole. Chen et al. unveiled a distinct separation of communities in different oxic and anoxic layers in deep gradients, and significant day-night differences were detected in the upper-layer microbial community, indicating potential vertical migration.

Coral reef ecosystems are one of the most diverse and productive habitats on Earth. Microbes in reef-overlying waters are key players in maintaining this ecosystem by regulating biogeochemical and ecological processes. Liu et al. shed light on the bacterial biodiversity of coral reefs and the importance of stochastic process in structuring bacterial communities.

Seagrass forms highly productive ecosystems in coastal environments. Pan et al. demonstrated that seagrass imposed significant ecological effects on the diversity and community organization of underground microbial eukaryotes.

Marine pathogens impose challenges to aquaculture, fishery productivity, and marine conservation. Several marine habitats, such as mangroves and wetlands, can serve as aquatic filtration systems to reduce marine pathogens. The perspective by Klohmann and Padilla-Gamiño reviewed how mangroves, shellfish beds, seagrasses, and constructed wetlands can reduce pathogen pressure in coastal ecosystems.

Dissolved oxygen is one of the key factors impacting microbial community composition in marine environments. Wang J. et al. investigated variations in the bacteria community in oxygen-depleted water, providing new insights into the potential role of denitrifying bacteria under oxygen depletion in Bohai Sea for the first time. In oceanic oxygen minimum zones (OMZs), the abundance of aerobic organisms significantly decreases, and energy shifts from higher trophic levels to microorganisms while the microbial communities become critical drivers of marine biogeochemical cycling activities. Guo et al. investigated microbial community distribution patterns across oxygen gradients, including oxygenic zones (OZs), oxygen limited zones (OLZs), and OMZs.

Planktonic microbes play vital roles in marine environments. *In situ* measurement of different size-fractionated chlorophyll *a* concentrations (Chl *a*) of phytoplankton assemblages are essential for understanding the microbial phytoplankton size structure, primary production in the ocean, and the marine biogeochemical cycle. Wei et al. showed significant differences in microbial phytoplankton size structure in different sea areas through a comparative analysis of total and size-fractionated Chl *a*.

Xie et al. focused on a ubiquitous marine fungus-like protistan group, the Labyrinthulomycetes, with a huge biomass that can exceed that of bacterioplankton in coastal oceans. The report revealed their partitioning of spatial patterns and multifaceted roles in coastal marine microbial food webs. Kim et al. investigated the physicochemical properties and bacterioplankton community of rearing water in a Biofloc technology (BFT)–based *Litopenaeus vannamei* aquaculture system. The metataxonomic results indicated a highly dynamic bacterioplankton community.

The publications in this Research Topic exhibit a broad scope, covering microbial diversity, ecology, evolution, resource mining, natural products, and enzyme discovery. To summarize, the Research Topic showcases not only the diversity of themes and contributors but also the wide scales in Marine distinctive environments, from deep sea extremes to near shore ecosystems and from hydrothermal vents to the world's deepest blue hole. Research teams from eight countries (China, United States, South Korea, Denmark, Chile, Belgium, Myanmar, and Tunisia) published 18 articles in this exciting collection of research papers and perspectives. The editorial team would like to thank all the authors and reviewers for their great contributions, helping achieve the goal of the Research Topic. The oceans link us all. We believe that this Research Topic will certainly draw more attention to the intersection of microbiology and marine sciences. With these joint

efforts, we can better understand and utilize microbes from marine distinctive environments.

Author contributions

SH: Writing – original draft, Writing – review & editing. MM: Writing – review & editing. SE: Writing – review & editing. YY: Writing – review & editing.

Funding

The author(s) declare that no financial support was received for the research, authorship, and/or publication of this article.

Conflict of interest

The authors declare that the research was conducted in the absence of any commercial or financial relationships that could be construed as a potential conflict of interest.

Publisher's note

frontiers | Frontiers in Microbiology

ORIGINAL RESEARCH
published: 06 May 2022
doi: 10.3389/fmicb.2022.903159

Comparative Analysis of Total and Size-Fractionated Chlorophyll *a* in the Yellow Sea and Western Pacific

Yuqiu Wei[1,2], *Zhengguo Cui*[1,2*], *Xingzhou Wang*[3], *Guangliang Teng*[1], *Keming Qu*[1,2] *and Jun Sun*[3,4*]

[1] *Key Laboratory of Sustainable Development of Marine Fisheries, Ministry of Agriculture and Rural Affairs, Yellow Sea Fisheries Research Institute, Chinese Academy of Fishery Sciences, Qingdao, China,* [2] *Laboratory for Marine Fisheries Science and Food Production Processes, Pilot National Laboratory for Marine Science and Technology (Qingdao), Qingdao, China,* [3] *Research Centre for Indian Ocean Ecosystem, Tianjin University of Science and Technology, Tianjin, China,* [4] *State Key Laboratory of Biogeology and Environmental Geology, China University of Geosciences, Wuhan, China*

Measurements of different size-fractionated chlorophyll *a* concentrations (Chl *a*) of phytoplankton assemblages *in situ* are vital for advancing our understanding of the phytoplankton size structure and thus the marine biogeochemical cycle. In the present study, we thus made a comparative analysis of total and size-fractionated Chl *a* in the Yellow Sea (YS) and Western Pacific (WP). Our results suggest that the total Chl *a* was highly variable in the YS (averaging ∼1.02 μg L^{-1}) and was generally 3–4-fold more than that in the WP (averaging ∼0.30 μg L^{-1}). The pico-sized Chl *a* had a significant contribution to total Chl *a* in the WP (range 75–88%), while the average contributions of the nano-sized and pico-sized Chl *a* to total Chl *a* in the YS were 47 and 38%, respectively, suggesting that a majority of the total Chl *a* in the YS was associated with nano- and picophytoplankton. Moreover, we applied the generalized additive models (GAMs) to explore the relationships between the total Chl *a* and that contained in each of the three size classes. These GAMs relationships suggested a continuum from picophytoplankton dominated waters to large phytoplankton (cells> 2 μm) domination with increasing Chl *a*. Finally, we made a comparison of the total Chl *a* obtained with GF/F filters and that measured from size-fractionated filtration and revealed that their corresponding concentrations are in good agreement, indicating the size-fractionated filtration had no effect on total Chl *a* determination.

Keywords: phytoplankton, chlorophyll a, size-fractionated filtration, Yellow Sea, Western Pacific

OPEN ACCESS

Edited by:
Shan He,
Ningbo University, China

Reviewed by:
Yuchuan Fan,
University of Florida, United States
Xuerong Sun,
University of Exeter, United Kingdom
Franco Decembrini,
Institute of Polar Sciences (CNR), Italy

***Correspondence:**
Jun Sun
phytoplankton@163.com
Zhengguo Cui
cuizg@ysfri.ac.cn

Specialty section:
This article was submitted to Aquatic Microbiology, a section of the journal Frontiers in Microbiology

Received: *24 March 2022*
Accepted: *11 April 2022*
Published: *06 May 2022*

Citation:
Wei Y, Cui Z, Wang X, Teng G, Qu K and Sun J (2022) Comparative Analysis of Total and Size-Fractionated Chlorophyll a in the Yellow Sea and Western Pacific. Front. Microbiol. 13:903159. doi: 10.3389/fmicb.2022.903159

INTRODUCTION

As a ubiquitous photosynthetic pigment in phytoplanktonic species and also a readily available ocean color product, the chlorophyll *a* (Chl *a*) is generally thought to be the most widely used proxy of biological indicators, such as total phytoplankton biomass and primary productivity (Falkowski and Kiefer, 1985; Behrenfeld and Boss, 2006). At present, the Chl *a* concentration can be estimated using satellite remote sensing, *in situ* with fluorometers, or measured on filtered discrete samples though pigment or fluorometric analyses and so forth (Welschmeyer, 1994; O'Reilly et al., 1998). Whatman CF/F glass fiber filters (which have a nominal pore size of 0.7 μm and a median retention size of 0.2 μm) or 0.2-μm Nuclepore membrane filters have traditionally been used for

the filtration of those discrete samples to concentrate planktonic organisms (Prepas et al., 1988; Chavez et al., 1995). However, after the discovery of photoautotrophs smaller than 2–3 μm (called picophytoplankton), such as picocyanobacteria and picoeukaryotes, the essential role of the size structure of phytoplankton in the food webs and marine ecosystems has been realized (Marañón et al., 2001; Sun et al., 2018, 2019; Richardson, 2019). Also, a suite of phytoplankton biochemical functions is controlled by cell size, including nutrient uptake, metabolic rate, growth, and sinking rate (Moloney and Field, 1991; Finkel et al., 2010; Marañón, 2015). As such, accurate measurements of the size structure of natural phytoplankton assemblages *in situ* are vital for advancing our understanding of the marine biogeochemical cycling (Marañón et al., 2001; Sun et al., 2018, 2019; Brewin et al., 2019). Conventionally, phytoplankton size structure can be quantified by partitioning total Chl *a* into three typical size classes, that is, pico- (<2 μm), nano- (2–20 μm), and micro-phytoplankton (>20 μm) (Sieburth et al., 1978). However, in biological oceanography, Whatman GF/F and 0.2-μm Nuclepore membrane filters are not adequate for the determination of size-based Chl *a* concentrations, much less identifying the different size types of phytoplankton. Consequently, size-fractionated filtration associated with membrane filters of varied composition has been developed in order to retain different size-structure Chl *a* contents.

Over the last decades, measurements of size-fractionated Chl *a* are of particular significance to the biogeochemical community and are therefore used extensively in biological oceanographic research. For instance, size-fractionated Chl *a* approach has complemented the flaw of remote-sensing algorithms with respect to the estimates of size-fractionated biomass and primary production (Varela et al., 2002; Kameda and Ishizaka, 2005). Meanwhile, measurements of size-fractionated Chl *a* have also been used to estimate the export production (Guidi et al., 2009) or used for the validation of size-based food web models and marine biogeochemical models (Marañón et al., 2001). Size fractionations have the advantage of making a explicit partition of the size structure of phytoplankton assemblages. However, this approach involving filters of different sizes (e.g., 0.2, 2 and 20 μm) poses a problem in that planktonic organisms may break apart during the continual filtration process, ultimately resulting in a certain portion of cellular Chl *a* passing through the filters into seawater (Brewin et al., 2014). On the contrary, the size-fractionated filtration is also time-consuming and thus probably alters the Chl *a* concentration, as Chl *a* fluorescence is particularly vulnerable to continuous light exposure. Such a filtration step is often taken for granted as being a relatively conservative step in an extraction procedure (Knefelkamp et al., 2007); however, its impact on the results may be underestimated. Considering the potential influence of size-fractionated filtration on the Chl *a* determination, the main question we wish to address in this paper is that: Is total Chl *a* concentration measured from size-fractionated filtration approximately equal to that obtained with Whatman GF/F filters?

Many comparisons between different filters in terms of Chl *a* retention have been carried out in previous studies. For example, both Chavez et al. (1995) and Moran et al. (1999) have compared Chl *a* measurements obtained from field samples using Whatman GF/F and Nuclepore 0.2-μm filters and verified no significant difference between the total Chl *a* concentrations estimated from these two filters. Analogously, size-fractionated Chl *a* for three size classes (i.e., < 2 μm, 2–20 μm, and > 20 μm) estimated from measurements of size-fractionated filtration and HPLC analysis have also been compared quantitatively, but there are significant biases between these two methods, with HPLC analysis underestimating picoplankton Chl *a* obviously (Brewin et al., 2014). In addition, the relationship between total Chl *a* and that contained in each of the three size classes has been studied relying on a three-component model (Brewin et al., 2010, 2019). To date, however, little is known about the degree to which size-fractionated filtration impact Chl *a* determination. In the present work, we thus make use of an expanded dataset collected from coastal waters of the Yellow Sea and from oligotrophic waters of the Western Pacific, consisting of measurements of total Chl *a* and size-fractionated Chl *a*, to quantify the relationship between total Chl *a* obtained with GF/F filters and that measured from size-fractionated filtration. More importantly, the total and size-fractionated Chl *a* data in these two distinct regions of the ocean have rarely been compared.

MATERIALS AND METHODS

Study Area and Water Sampling

Results presented here encompass data from two oceanographic cruises located in the Yellow Sea, China (YS; 32–37°N, 122–124°E), and the Western Pacific (WP; 13–21°N, 130°E), covering 10 multiple spatial stations that employ very similar sampling strategies (**Figure 1**). The cruise for YS took place from September to October 2021 aboard R/V *Hailan* 101, while the cruise for WP was undertaken from October to November 2018 aboard R/V *Kexue* 3. Thus, a variety of oceanographic conditions and habitats, for example, the high-biomass coastal YS (Huo et al., 2020) and the nutrient-depleted WP affected by the Kuroshio (Yasuda, 2003), were sampled during these two cruises. Water sampling and parallel measurements of temperature and salinity were performed using 12-L Niskin bottles equipped with a Sea-Bird CTD (conductivity, temperature, and depth) rosette sampler (SBE 19 Plus). Seawater samples for the Chl *a* analysis were taken at up to 3 depths in the YS and 6 depths within the upper 200 m in the WP, respectively (**Table 1**). In total, 180 Chl *a* samples (comprising total and size-fractionated Chl *a*) were available, 60 from the YS and 120 from the WP, respectively. Both total and size-fractionated Chl *a* were measured on water collected from the same bottles, and all samples were collected during daylight hours (9:00–16:00 local time).

Total and Size-Fractionated Chl *a* Analyses

The size-fractionated filtration method for measuring Chl *a* concentration in each size class involves filtering water through different filters with decreasing pore sizes. Polycarbonate (PC) membrane filters typically used for the size-fractionated filtration have a higher precision in pore size, as they are manufactured with a laser (Brewin et al., 2014). In this study, for each water

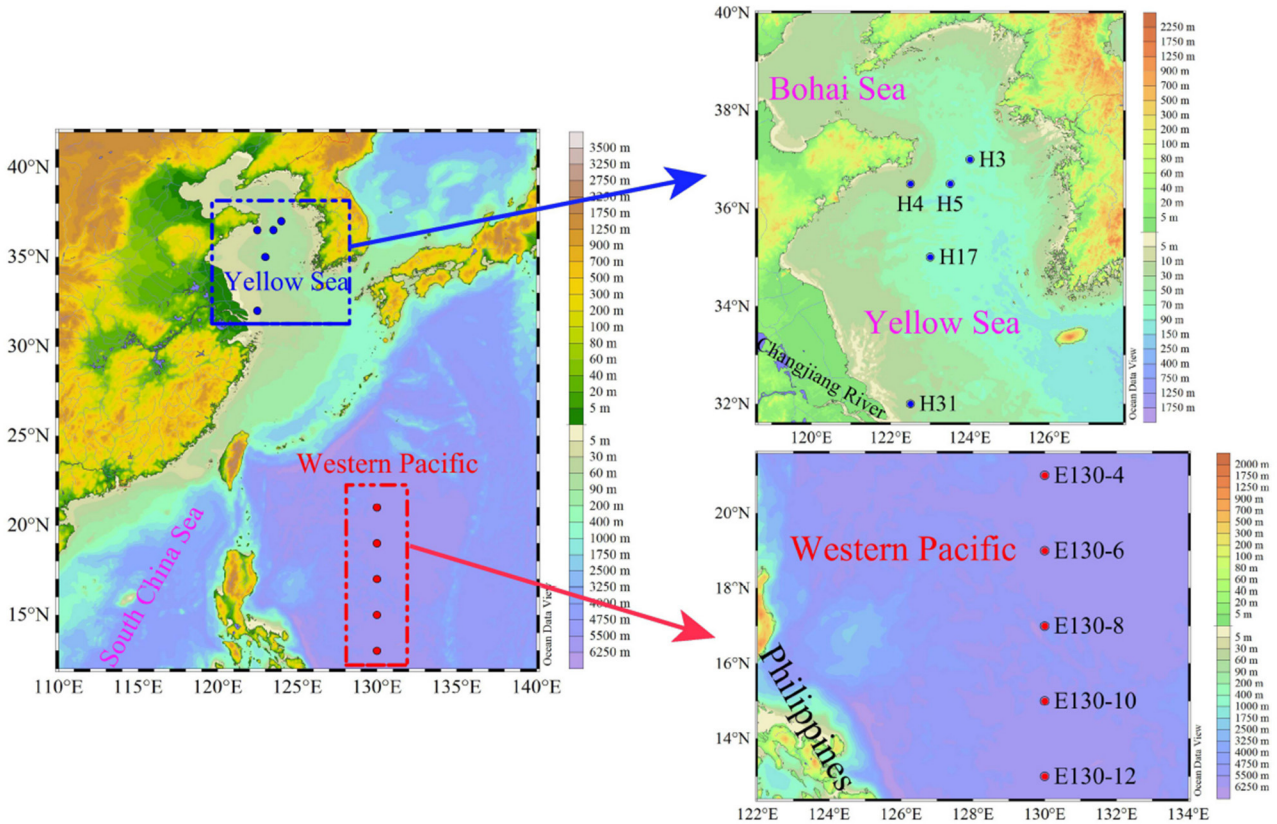

FIGURE 1 | Study area and sampling stations in the Yellow Sea (blue dots) and the Western Pacific (red dots).

TABLE 1 | Information of sampling stations and depths for the Chl *a* analysis during the two cruises.

Yellow Sea				Western Pacific			
Station	**Latitude (°E)**	**Longitude (°N)**	**Sampling depth (m)**	**Station**	**Latitude (°E)**	**Longitude (°N)**	**Sampling depth (m)**
H3	124	37	2, 29, 71	E130–4	130	21	5, 25, 50, 82, 150, 200
H4	122.5	36.5	2, 8, 17	E130–6	130	19	5, 25, 50, 93, 150, 200
H5	123.5	36.5	2, 32, 71	E130–8	130	17	5, 25, 50, 100, 150, 200
H17	123	35	2, 33, 67	E130–10	130	15	5, 25, 50, 120, 150, 200
H31	122.5	32	2, 12, 24	E130–12	130	13	5, 25, 50, 115, 150, 200

sample collected from the YS and WP, ∼1,000 mL of seawater was filtered sequentially through 20-μm nylon membrane, and 2- and 0.2-μm PC membrane filters (47 mm; Merck Millipore Ltd.) under low-vacuum pressure (<0.04 MPa). In addition, we particularly defined the Chl *a* concentration in each size class that we used throughout the article so that our intended meaning was more clear. Unless otherwise noted, in this study, we used the terms pico-sized Chl *a*, nano-sized Chl *a*, and micro-sized Chl *a* for the size ranges of 0.2 to 2 μm, 2 to 20 μm, and > 20 μm, respectively (Sieburth et al., 1978). Thereafter, the total Chl *a* content (called "total size-fractionated Chl *a* concentration") was estimated from the sum of the three size classes for each sample.

Although the minimum pore size of PC filters (i.e., 0.2 μm) used above is lower than that of the GF/F filters (nominal size ∼0.7 μm), no significant difference has been found for the Chl *a* retention capability between these two filters, because the GF/F filter has a median retention size (i.e., effective pore size) of ∼0.2 μm. In particular, the GF/F filters have long been considered as a standard for phytoplankton Chl *a* determination (Chavez et al., 1995; Moran et al., 1999). During the two cruises, we thus applied the GF/F filters for the measurements of total phytoplankton Chl *a* content (referred to as "total Chl *a* concentration"). For this purpose, ∼1,000 mL of seawater samples was directly filtered through the Whatman GF/F

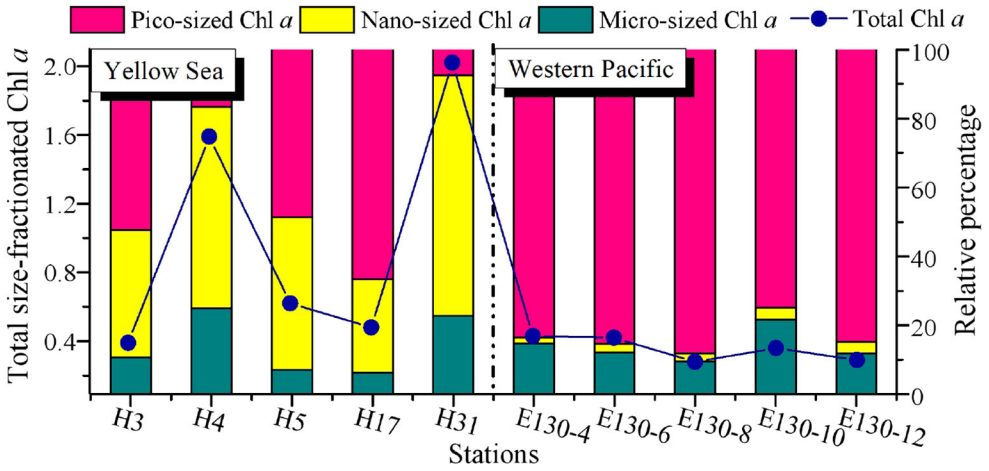

FIGURE 2 | Spatial variations of total size-fractionated Chl *a* concentrations (μg L^{-1}) and the relative proportion (%) for each size class among sampling stations in the Yellow Sea and the Western Pacific. Blue dots and lines denote the total size-fractionated Chl *a* concentrations, which were the sum of the three size classes. Note that all the size-fractionated Chl *a* data were expressed as depth-weighted averages, corresponding to the *y*-axis on the left.

filters (47 mm; Whatman Corp.) under the same low-vacuum pressure (<0.04 MPa).

Following filtration, these Chl *a* filters were folded in quarters and stored in liquid nitrogen at −80°C until processing. Subsequently, pigment extraction was made by submerging the filters in 90% acetone for 24 h at 4°C. After removal of the filters, extracted pigments were then determined using a CE Turner Designs Fluorometer following the standard method of Welschmeyer (1994).

Statistical Tests

Average data were given as values ± standard deviation (i.e., SD). The non-linear regression models (i.e., Gauss and Lorentz models; Origin v8.5) and *t*-test (Prism v8.3) were used to plot the fitting curves and thus to explore the vertical trends of the size-fractionated Chl *a*. Spearman's correlation analysis (*r* and *p*-values; SPSS, v25) and linear regression (R^2; Origin v8.5) were used to evaluate the relationship between total Chl *a* obtained with GF/F filters and that measured from size-fractionated filtration (Wei et al., 2020). Furthermore, to establish the relationship between total Chl *a* and that in three size classes (Brewin et al., 2014, 2019), we applied the generalized additive models (GAMs) that were performed using R software in version 4.0.2. The GAMs were fitted with the mgcv package (GAMs with GCV smoothness estimation). All statistical significance levels were set to $p < 0.05$. Unless otherwise stated, the total and size-fractionated Chl *a* concentrations used for presenting spatial variation or for comparison among stations were expressed as depth-weighted averages (See **Figure 2** below), which were calculated by dividing the trapezoidal integration of measured values for each variable by the maximum sampling depth (Crosbie and Furnas, 2001). The depth-weighted equation was calculated as follows:

$$\mathrm{Chl}_a = \left[\sum_{1}^{n} \frac{(\mathrm{Chl}_{ai} + \mathrm{Chl}_{ai+1})}{2} \times (D_{i+1} - D_i)\right] / (D_{MSL} - D_S)$$

where "Chl *a*" is the depth-weighted average (μg L^{-1}) over the sampling water column; "Chl a_i" is the Chl *a* concentration (μg L^{-1}) at sampling layer *i*; "*n*" is the number of sampling layers in the YS ($n = 3$) and WP ($n = 6$), and "D_i" is the depth at sampling layer *i* (m); "D_{MSL}" and "D_S" are the depths of maximum sampling layer and the surface sampling depth, respectively (**Table 1**).

RESULTS AND DISCUSSION

Total and Size-Fractionated Chl *a* Concentrations

Horizontal Distribution

There was a wide range of variability in the magnitude of total size-fractionated Chl *a* concentrations (referred to as "Chl $a_{>0.2\mu m}$") among sampling stations across the YS and WP, but significant contribution of pico-sized Chl *a* (i.e., 0.2–2-μm size class) to Chl $a_{>0.2\mu m}$ was observed in the WP (**Figure 2**). The Chl $a_{>0.2\mu m}$ was highly variable in the YS, ranging from 0.39 to 2.02 μg L^{-1}, with an average value (±SD) of 1.02 ± 0.73 μg L^{-1} (**Table 2**). In particular, the station H31 had the highest Chl $a_{>0.2\mu m}$ than other stations in the YS, while the Chl $a_{>0.2\mu m}$ was relatively low at station H3. The station H31 was observed near the Changjiang River estuary (**Figure 1**), which receives strong influences from nutrient-rich fresh water of the Changjiang River (Liu et al., 2016), thereby resulting in seasonally and spatially high phytoplankton Chl *a*, biomass, and primary production

TABLE 2 | Depth-weighted averages of total and size-fractionated Chl *a* concentrations (μg L^{-1}) among sampling stations in the Yellow Sea and the Western Pacific.

Cruise	Station	Micro-sized Chl *a*	Nano-sized Chl *a*	Pico-sized Chl *a*	Chl $a_{>0.2\mu m}$
Yellow Sea	H3	0.04	0.14	0.21	0.39
	H4	0.40	0.93	0.26	1.59
	H5	0.04	0.27	0.30	0.62
	H17	0.03	0.13	0.32	0.48
	H31	0.46	1.41	0.15	2.02
Western Pacific	E130–4	0.06	0.01	0.36	0.43
	E130–6	0.05	0.01	0.36	0.42
	E130–8	0.03	0.01	0.24	0.28
	E130–10	0.08	0.01	0.27	0.36
	E130–12	0.03	0.01	0.25	0.29

(Gong et al., 2003; Guo et al., 2014). Differently, the station H3 was dramatically influenced by the Yellow Sea Cold Water Mass (YSCWM, T < 10°C; Fu et al., 2018), which forms large temperature difference between the surface and bottom, reaching up to ∼1°C (Lee et al., 2016). Conceivably, the relatively low Chl $a_{>0.2\mu m}$ at station H3 may be controlled by the cold water in the YSCWM. On the contrary, this result may be due to the YSCWM nutrient-depleted surface water, with N and P concentrations near the analytical detection limit (Fu et al., 2018), although the YSCWM represents a large nutrient reservoir in the bottom layer of the YS. Indeed, the Chl $a_{>0.2\mu m}$ in the YS was strongly related to temperature ($p < 0.05$) and dissolved inorganic N, P, and Si ($p < 0.05$) in our correlation analysis (**Supplementary Figure 1A**), suggesting that temperature and nutrients were the two key factors regulating the variation of Chl $a_{>0.2\mu m}$ in the YS. On the contrary, the Chl $a_{>0.2\mu m}$ in the WP was lower and less variable, averaging 0.30 ± 0.06 μg L^{-1} (range 0.24–0.36 μg L^{-1}; **Figure 2** and **Table 2**). The mean Chl $a_{>0.2\mu m}$ in the WP was generally 3–4-fold lower than that in the YS. Similarly, the Chl $a_{>0.2\mu m}$ was positively correlated with nutrients ($p < 0.05$) in the WP (**Supplementary Figure 1B**), indicating that the observed low Chl $a_{>0.2\mu m}$ in the WP was largely caused by nutrient limitation. We thus suggested that the dynamic of Chl $a_{>0.2\mu m}$ in the WP could be reasonably driven by the Kuroshio current (Wei et al., 2020), since it is characterized by substantially higher temperature and salinity, and yet very low nutrient concentrations (Yasuda, 2003).

The Chl *a* concentration in particles > 20 μm (i.e., micro-sized Chl *a*) was relatively low in the YS (average 0.19 ± 0.21 μg L^{-1}) and WP (average 0.05 ± 0.02 μg L^{-1}) (**Table 2**), and thus, the contribution of micro-sized Chl *a* to the Chl $a_{>0.2\mu m}$ across both regions was only between 6 and 25% and averaged 14 ± 7% (**Figure 2**). Likewise, the contribution of 2–20 μm Chl *a* concentration (i.e., nano-sized Chl *a*) to the Chl $a_{>0.2\mu m}$ was comparatively low in the WP, averaging at 3 ± 1% and ranging from 2 to 4%. Our understanding of why the Chl *a* concentration is high or low in the ocean could be guided by analyzing the phytoplankton community data. Hence, these low contributions were not surprising given that the dominants of phytoplankton in the oligotrophic WP are not micro/nano-sized species, where large diatoms only represent on average ∼15% of total C biomass compared to small picophytoplankton (∼47%) (Wei et al., 2020). In comparison, the nano-sized Chl *a* at the coastal YS was between 27 and 70% of the Chl $a_{>0.2\mu m}$ and averaged 47 ± 17%, which was consistent with previously reported contribution of the nano-sized Chl *a* in the Garolim and Asan bays of the YS (range 17–71% and average 40 ± 14%; Lee et al., 2020). Furthermore, Soria-Píriz et al. (2017) have also shown that nanoplankton was the dominant fraction of Chl *a* in the coastal estuary (e.g., the Gulf of Nicoya) representing 51–78% of total Chl *a*. In our previous study, we indeed found that the phytoplankton community in the YS basin was mainly dominated by the nano-sized *Paralia sulcata*, *Thalassiosira angulata*, *Thalassiosira excentricus*, and *Skeletonema* cf. *costatum* (Wei et al., 2017). It is noteworthy that the station H31 situated near the Changjiang River estuary also had a greater nano-sized Chl *a* concentration (1.41 μg L^{-1}, ∼70% of the Chl $a_{>0.2\mu m}$), which may be associated with the dominant species *Skeletonema* cf. *costatum* therein (Guo et al., 2014).

Across the WP, the Chl *a* concentration in < 2-μm size class (i.e., pico-sized Chl *a*) was higher but less variable than that in other size classes among sampling stations (range 0.24–0.36 μg L^{-1}, average ∼0.29 μg L^{-1}; **Figure 2** and **Table 2**). The average contribution of pico-sized Chl *a* to the Chl $a_{>0.2\mu m}$ in the WP was close to 83 ± 9% (range 75–88%), indicating that a majority of the Chl $a_{>0.2\mu m}$ was in picoplankton size fraction, and the Chl $a_{>0.2\mu m}$ variability was largely driven by the pico-sized Chl *a*. This significant fraction of pico-sized Chl *a* in the Chl $a_{>0.2\mu m}$ is broadly consistent with previous findings in open-ocean ecosystems (Fiala et al., 1998; Froneman et al., 2001; Morán et al., 2004; Richardson, 2019). In the oligotrophic NE Atlantic, for example, most of the total Chl *a* was present in small cells (< 2 μm), and picoplanktonic Chl *a* contributed approximately 75% to total values (Morán et al., 2004). Similarly, our previous studies in the oligotrophic eastern Indian Ocean and South China Sea have also revealed that the average concentration of pico-sized Chl *a* accounted for ∼50% of the total Chl *a* (Wei et al., 2020). Collectively, these high contributions could be attributable to the fact that picophytoplankton have contributed a significant proportion of the phytoplankton community in oligotrophic ecosystems, for example, the WP. In contrast to the WP, the pico-sized Chl *a* concentrations in the YS varied from 0.15 to

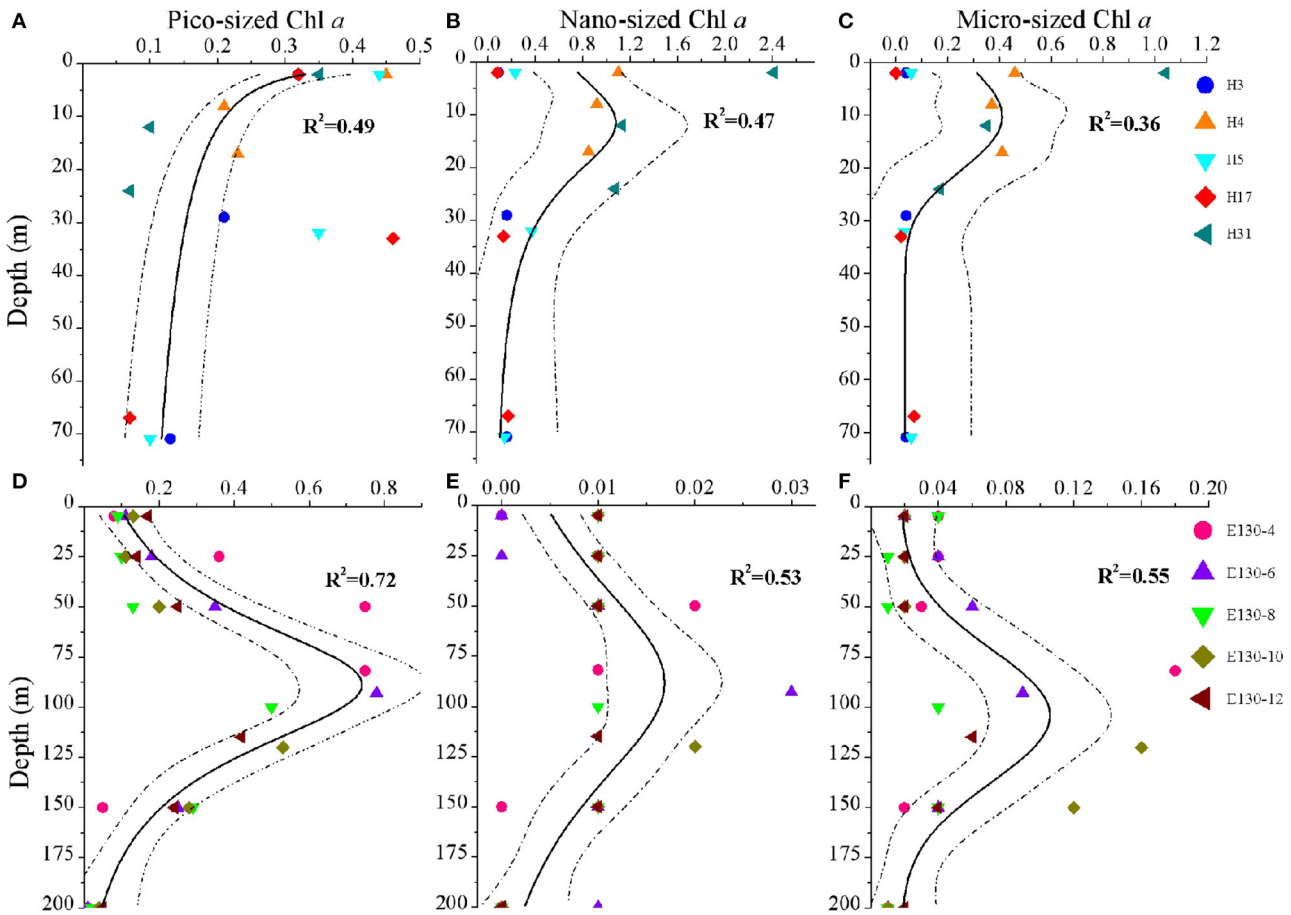

FIGURE 3 | Vertical profiles for the concentrations (μg L^{-1}) of **(A,D)** pico-sized Chl *a*, **(B,E)** nano-sized Chl *a*, and **(C,F)** micro-sized Chl *a* in the Yellow Sea (above) and the Western Pacific (below). Symbols and colors represent sampling stations. Solid lines indicate different curve-fitting trends for the size-fractionated Chl *a* data vs. depth, and dashed lines denote 95% confidence bands. R^2 is the fitting variance of the non-linear regression model. Note the different scales on the *x*-axes, reflecting variability in the magnitude of the size-fractionated Chl *a* concentrations.

0.32 μg L^{-1} with mean (±SD) of 0.26 ± 0.07 μg L^{-1}, but their contributions to the Chl $a_{>0.2\mu m}$ were lower, averaging ∼38% and ranging from 8 to 67% (**Figure 2** and **Table 2**).

Vertical Distribution

All data points of the size-fractionated Chl *a* concentrations against depth were analyzed to plot the fitting curves in **Figure 3**, and several major vertical trends were observed in the concentration of Chl *a* in each size fraction. The vertical patterns of pico-sized Chl *a*, nano-sized Chl *a*, and micro-sized Chl *a* were markedly different between the YS and the WP. Nevertheless, there were some similarities in the vertical patterns of these three size fractions collected from the same waters, especially in the WP (**Figures 3D–F**).

At the coastal YS, analysis of pico-sized Chl *a* profile showed that the pico-sized Chl *a* was generally highest in the surface waters and declined with depth (**Figure 3A**); however, for the profiles of micro-sized and nano-sized Chl *a*, they were typically low near the surface, gradually increased to a subsurface maximum at 10–15 m, and then rapidly declined to < 0.2 μg L^{-1} (**Figures 3B,C**). Information on the phytoplankton community structure is essential to understand the characteristics of size-fractionated Chl *a* distribution (Fu et al., 2018; Wei et al., 2020). Analysis of the abundance data of *Synechococcus* and picoeukaryotes also revealed that their total abundance was maximum at the surface and declined with depth (**Supplementary Figure 2A**). Therefore, the vertical variability of pico-sized Chl *a* appears to be driven largely by picophytoplankton dynamics (**Supplementary Figure 3A**). Our results are also in line with previous findings regarding the vertical structures of picophytoplankton abundance and pico-sized Chl *a* in the YS, for example, Fu et al. (2018) have reported that high picophytoplankton abundance occurs in the nutrient-depleted upper 30 m of the central YS area. A major mechanism has been proposed to explain the formation of this vertical pattern in the YS: active growth under an optimal combination of light and nutrients (Fu et al., 2018). Field data and experimental studies have suggested that nutrients are depleted in the surface waters of the central YS area (e.g., YSCWM), in particular, the phytoplankton growth is

influenced by P limitation throughout the YS (Wei et al., 2017; Yang et al., 2018). Because of their competitive advantages in low nutrient concentrations (e.g., P) and under stratification conditions, picophytoplankton could dominate in the surface mixed layer of the YS (**Supplementary Figure 2A**). Light is another long-standing hypothesis and is frequently suggested to explain the vertical decrease in the phytoplankton in the euphotic zone (Guo et al., 2014; Liu et al., 2016). In our study, the pico-sized Chl *a* was significantly associated with light irradiance (**Supplementary Figure 1A**), indicating that light is likely responsible for the vertical decrease in the pico-sized Chl *a* in the YS. Accordingly, we concluded that the active growth of picophytoplankton under an optimal combination of nutrient and light availability was the main formation mechanism for the vertical variation of pico-sized Chl *a* in the YS. The vertical trends of micro-sized and nano-sized Chl *a* also corresponded with the vertical distribution of large phytoplankton assemblages in our previous findings in the YS (Wei et al., 2017). Compared with the surface mixed layer with high irradiance, large phytoplankton assemblages could well be acclimated to the low-light but nutrient-replete subsurface layer. Therefore, nutrient availability was the most important contributing factor to the vertical trends of micro-sized and nano-sized Chl *a* in the YS (**Supplementary Figure 1A**).

The major vertical trends of the three size-fractionated Chl *a* concentrations were as expected for the WP. Within the upper 200 m, their concentrations were generally 2–4-fold higher near the subsurface 100 m than in the surface layer, with a rapid decline at depths deeper than 125 m (**Figures 3D–F**). It has been reported that nutrients are almost depleted over the surface in the oligotrophic WP due to the water stratification, whereas nutrient supply is sufficient in the deeper layer (Ma et al., 2019). Under the influence of nutrient availability, the phytoplankton assemblages characterized by a great biomass of picophytoplankton in the WP are also lower near the surface, gradually increase to a subsurface maximum at ∼100 m, and then decline rapidly from 125 to 200 m (**Supplementary Figures 2B, 3B**). Furthermore, phytoplankton growth is limited under conditions with sufficient nutrients below the euphotic layer, which may be reasonably controlled by light limitation as discussed above (Guo et al., 2014; Liu et al., 2016). In this study, similarly, we observed that the size-fractionated Chl *a* concentrations in the WP were positively correlated with nutrients (especially N and P; $p < 0.05$), but negatively correlated with light intensity ($p < 0.05$) (**Supplementary Figure 1B**), indicating nutrients and light intensity were the key factors in regulating the biogeographic variation of the size-fractionated Chl *a*. We suggested that the vertical trends for the size-fractionated Chl *a* concentrations observed in the WP were primarily attributed to the combined effects of nutrient and light availability. It is noteworthy that the vertical variation of Chl *a* in the offshore waters or the open oceans is typical of the deep chlorophyll maximum (DCM) which is formed at the thermocline layer (Gong et al., 2003; Behrenfeld and Boss, 2006; Uitz et al., 2006; Brewin et al., 2017; Sun et al., 2019). The implication is that the vertical variation of Chl *a* may be related to vertical stratification (Chen et al., 2021).

Relationships Between Total Chl *a* and That in Three Size Classes

The relationships between total Chl *a* and that contained in each of the three size classes have been studied primitively in some regions. Thereafter, these relationships have been quantified empirically, statistically, and/or mechanistically (Hirata et al., 2008), but one popular approach to modeling these relationships at present is the three-component model of Brewin et al. (2010). This model has an advantage over other empirical methods in that its variable parameters are interpretable, and the derived three-component relationship can be compared with a range of environmental factors, for instance, with temperature and light availability (Brewin et al., 2015, 2017). Moreover, the three-component model of Brewin et al. (2010) has been applied in the eastern China seas (Sun et al., 2018, 2019), such as the Bohai Sea, Yellow Sea, and East China Sea, though the Chl *a* estimations are derived from HPLC pigments. In the present study, differently, we applied the GAMs to establish the relationships between total Chl *a* and that in three size classes (**Figure 4**). The GAMs have distinct advantages over other conceptual or empirical models (Brewin et al., 2010; Hirata et al., 2011) as they allow non-linear functions of covariates to be included in regression equations and require an additive combination of functions of covariates, avoiding stringent restrictions imposed by parametric assumptions (Wood, 2006; Young et al., 2011). In the GAMs, the variable of interest is often smoothed using a locally weighted scatterplot smoothing that includes smoothing terms taking the form of non-parametric functions of predictors; thus, the GAMs using univariate or bivariate smoothers are a robust multivariate statistical method for large datasets and popular in marine studies (Young et al., 2011; Xiao et al., 2018). Altogether, the GAMs results below demonstrated that such established relationships could successfully capture the general changes in size-fractionated Chl *a* and fractions of total Chl *a* when plotted as a function of total Chl *a*, although the environmental variables were not incorporated into the models for reasons that our dataset was relatively small.

Across the coastal YS and the oligotrophic WP, the pico-sized Chl *a* increased drastically with increasing total Chl *a* when total Chl *a* was $< \sim 1\ \mu g\ L^{-1}$ (**Figure 4a**), indicating that small picophytoplankton dominate at low Chl *a* concentrations, a conclusion consistent with our observations that the pico-sized Chl *a* had a significant contribution to total Chl *a* (range 75–88%) and thus dominated in the oligotrophic WP (**Figure 2**), and previous studies that picophytoplankton dominate oligotrophic oceans, contributing > 10% of global primary productivity (Raven, 1998; Crosbie and Furnas, 2001; Flombaum et al., 2013; Visintini et al., 2021). In contrast, the pico-sized Chl *a* declined when total Chl *a* exceeded $\sim 1\ \mu g\ L^{-1}$, while the micro-sized and nano-sized Chl *a* increased gradually (**Figures 4b,c**), suggesting that large phytoplankton (cells $>2\ \mu m$) dominate at high Chl *a* concentrations. This result is also in line with previous reports that the large phytoplankton primarily including diatoms and dinoflagellates are dominant in the coastal waters with relatively high Chl *a* concentrations (Guo et al., 2014; Sun et al., 2018; Xiao et al., 2018). Indeed, there is accumulating

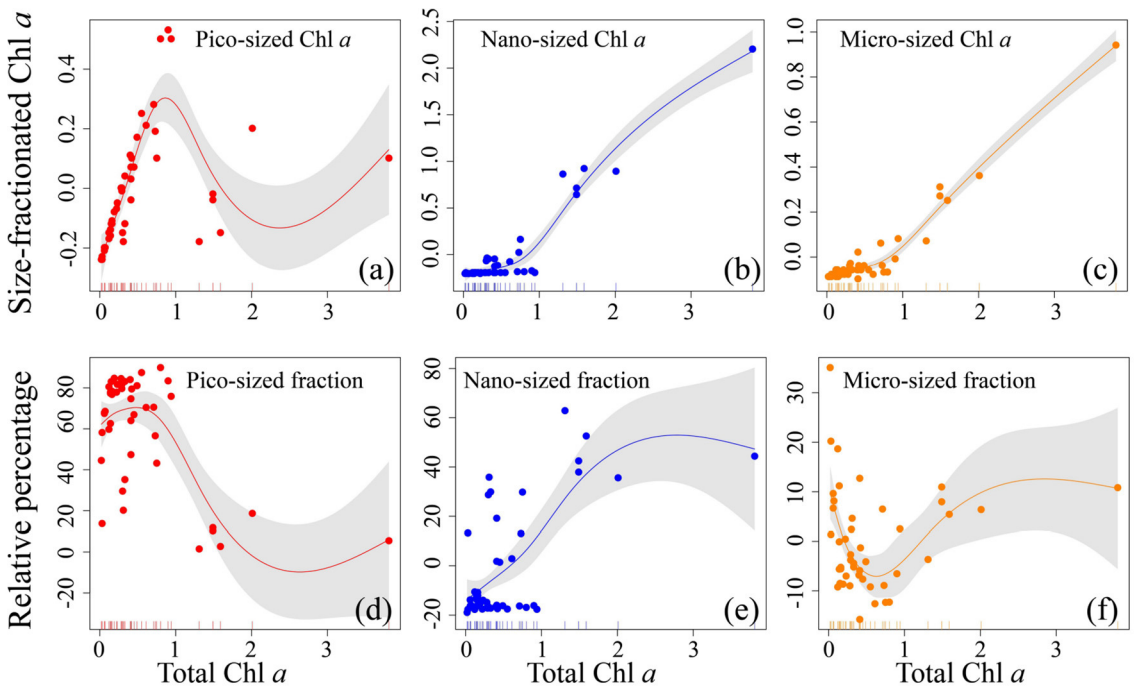

FIGURE 4 | Relationship for all size-fractionated filtration data collected in the Yellow Sea and Western Pacific. Top row **(a–c)** shows the absolute size-fractionated Chl *a* concentrations (μg L^{-1}), and bottom row **(d–f)** is the fractions (%) plotted as a function of total Chl *a* (μg L^{-1}), with the GAMs overlain. The colored dots represent residual values (that are normalized by the GAMs) of both size-fractionated Chl *a* and relative percentages, and the inward tick marks on the horizontal axes show data distributions. The solid lines represent GAMs smoothing, and shaded areas denote 95% confidence bands.

evidence that diatoms and dinoflagellates, two typical groups that form phytoplankton blooms, play key roles in marine coastal ecosystems and form the basis of many aquatic food webs (Guo et al., 2014; Spilling et al., 2018; Xiao et al., 2018; Trombetta et al., 2020). In addition, these relationships are very consistent with previous models of Brewin et al. (2010, 2019) and Sun et al. (2018, 2019) using size-fractionated Chl *a* data in the coastal Red Sea, the oligotrophic Atlantic Ocean, and the eastern China seas, with the abundance of small cells increasing to a given total Chl *a* concentration (∼1 μg L^{-1}), beyond which total Chl *a* increases through the addition of larger size classes of phytoplankton. This feature is also evident in the models of Uitz et al. (2006) who have suggested that an enhanced pico-sized Chl *a* near the surface is noted at the expense of the micro- and nano-sized Chl *a*. Meanwhile, our established relationships further confirmed the assumptions that the phytoplankton size structure (expressed here as size-fractionated Chl *a*) covaries with the total Chl *a* (Raimbault et al., 1988; GoeRicke, 2011). In other words, biomass is added only to the smallest size class until an upper limit to Chl *a* in this size class (called biomass quota) when phytoplankton communities are dominated by picophytoplankton and total biomass is low. For instance, the biomass quotas for the <1 <3, and <10 μm size classes are about 0.5, 1, and 2 μg L^{-1} Chl *a*, respectively (Raimbault et al., 1988). Once this quota has been reached, total Chl *a* is added to a system by the addition of larger size classes of phytoplankton. Therefore, the implication is that such relationships based on the GAMs could fit the size-fractionated Chl *a* data well in this study.

The relationships modeled to estimate fractional contributions of various size classes can offer the distinct advantage of providing more information than those that treat only the dominant class. For example, the column-integrated biomass and the vertical phytoplankton size class composition can be inferred by the Uitz et al. (2006) model that has related the Chl *a* concentration to the fractional contributions of three phytoplankton size classes (micro-, nano-, and picophytoplankton) to the total pigment. Here, a relationship was also developed to show the change in percentage contribution of the size-fractionated Chl *a* with increasing total Chl *a* (**Figure 4**). As anticipated, the trend of the pico-sized fraction was similar to that of the pico-sized Chl *a* observed above. The pico-sized fraction remained relatively stable increase between 0.01 and 1 μg L^{-1} total Chl *a*, whereas decreased with increasing total Chl *a* in the approximate range of ∼1–3 μg L^{-1} (**Figure 4d**). This supports the common observation that low Chl *a* environments in oligotrophic waters are essentially dominated by picophytoplankton, where they contribute as much as ∼60–90% of the total Chl *a* (Wei et al., 2020). On the contrary, the micro-sized fraction decreased with increasing total Chl *a* when total Chl *a* was low (<1 μg L^{-1}), as the total Chl *a* increased beyond ∼1 μg L^{-1} it began to increase (**Figure 4f**). This result is well-comparable to previous studies of Hirata et al. (2008), Brewin et al. (2010, 2019), and Sun et al. (2019) who have

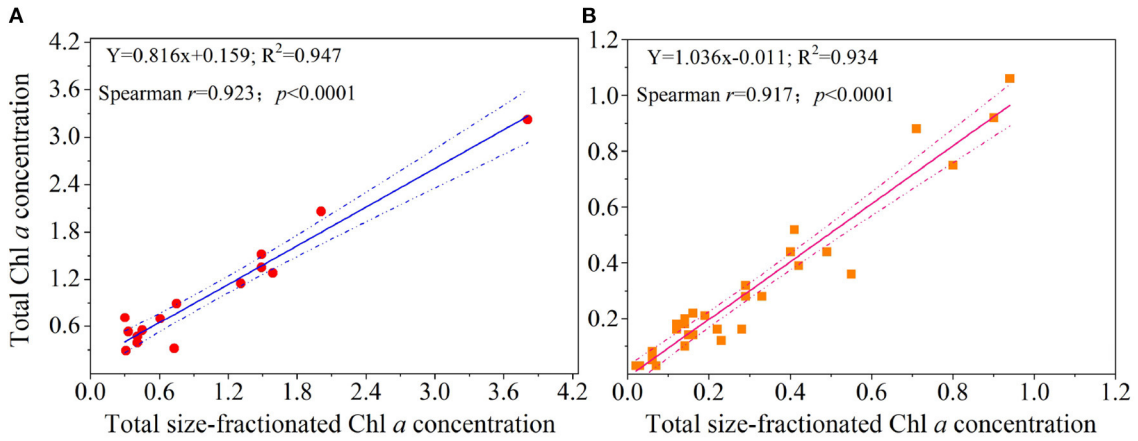

FIGURE 5 | Comparisons of the estimates of total Chl *a* concentration ($\mu g\ L^{-1}$) obtained with GF/F filters (i.e., total Chl *a* concentration) and size-fractionated PC filters (i.e., total size-fractionated Chl *a* concentration) in the **(A)** Yellow Sea and the **(B)** Western Pacific. Solid lines represent the linear regressions (Spearman's *r*, *p*-values, and regression variance R^2), and dashed lines are 95% confidence bands.

documented that microplankton begin to dominate the total population as the total Chl *a* exceeds 0.95–1.3 $\mu g\ L^{-1}$. Moreover, there was a successive increase in the nano-sized fraction with increasing total Chl *a*, indicating that nanophytoplankton are also dominant at high Chl *a* concentrations. Collectively, these relationships between total Chl *a* and that in three size classes suggested a continuum from picophytoplankton dominated waters to micro- and nanophytoplankton domination with increasing Chl *a* (Hirata et al., 2008; Brewin et al., 2010). The implication is that our GAMs relationships not only can offer direct biological interpretation but also can be applied to a continuum of Chl *a* concentrations without having to deal with discrete trophic classes. Therefore, our GAMs relationships may be used in conjunction with algorithms designed to estimate the major variations of size-fractionated Chl *a* to improve the estimates of remotely sensed primary production (Varela et al., 2002; Kameda and Ishizaka, 2005; Hirata et al., 2008). However, as this analysis was based on a relatively small dataset (180 Chl *a* samples), we recognized that additional data were required to optimize our GAMs relationships observed here. Furthermore, additional environmental knowledge could be introduced to improve the performance of our GAMs relationships. Unfortunately, these GAMs relationships are still in their infancy for the limitation of our small dataset. Though beyond the scope of the present study, future efforts are needed in this direction.

Does Size-Fractionated Filtration Affect Total Chl *a* Determination?

The size-fractionated filtration involving filters of different sizes leads to a series of problems in that (*i*) the filters may retain particles smaller than the nominal pore size (Prepas et al., 1988; Chavez et al., 1995; Moran et al., 1999), which is dependent on the morphology and cohesiveness of the particles, as well as on the filtered volume and the used filter types; (*ii*) some larger particles may also pass through the nominal pore size of the small filter (e.g., through overlapping holes) and be accounted for in smaller-size fractions (Brewin et al., 2014); (*iii*) the phytoplankton may break apart during the continual filtration process, ultimately resulting in a certain portion of cellular Chl *a* passing through the filters into seawater; finally, the size-fractionated filtration is time-consuming that may alter the Chl *a* fluorescence properties (Wei et al., 2019). Therefore, it is possible that the size-fractionated filtration could have an impact on the total Chl *a* determination. If this hypothesis is real, the influence could be substantially large in marine biogeochemistry, as the size-fractionated Chl *a* and phytoplankton size structure are two strong ecological descriptors of the marine biogeochemical cycling that co-vary with each other (Marañón et al., 2001; Brewin et al., 2019). On the contrary, if it is not real, the implications of our results may be minimal.

At present, the effect of those factors above on measurement uncertainties is difficult to quantify, and we thus conducted a simultaneous measurement of the total Chl *a* obtained with GF/F filters and PC filters to make an accurate diagnosis of uncertainty in the size-fractionated technique. Across the YS and WP, surprisingly, corresponding concentrations of the total Chl *a* measured from GF/F filters and size-fractionated PC filters are in good agreement ($R^2 > 0.93$; $r > 0.91$, $p < 0.0001$; **Figure 5**), suggesting that the hypothesis we presented above is not valid and thus the implications of our results may be minimal. Therefore, the comparison of total Chl *a* between GF/F filters and the sum of size-fractionated PC filters is promising for people who are using either method. Based on the raw data (**Figure 5**), however, our linear regressions also revealed that the overall total Chl *a* obtained with GF/F filters was slightly higher than that measured from PC filters in the YS, and an opposite trend was observed in the WP. This result reflected the fact that the size-fractionated filtration may be by no means exact, although it is encouraging to observe

significant agreement between the two approaches ($p < 0.0001$; **Figure 5**). In accord with this logic, we speculated that there would be large or small discrepancies in each size-fractionated Chl *a* by using filters with different materials as a result of inaccuracies in pore sizes, filter clogging, and/or cell breakage as discussed above. Also, another possible reason for these potential discrepancies may be the difference in two study areas. Nevertheless, we could not address this hypothesis at present due to the technological limitations. With this in mind, future efforts should be further focused toward quantifying the uncertainty in size-fractionated filtration, possibly through simultaneous measurements made by multiple types of *in situ* methods.

DATA AVAILABILITY STATEMENT

The original contributions presented in the study are included in the article/**Supplementary Material**, further inquiries can be directed to the corresponding authors.

AUTHOR CONTRIBUTIONS

JS and ZC contributed to the theoretical designs. YW, XW, and GT performed all experiments. YW and KQ analyzed all data. YW wrote the manuscript with the help of all authors. All authors contributed to the final version of the manuscript.

FUNDING

This work was financially supported by the Project funded by China Postdoctoral Science Foundation (2021M703590), the Shandong Postdoctoral Innovation Talent Support Program (SDBX2021014), the National Nature Science Foundation of China grants (41876134), the Central Public-Interest Scientific Institution Basal Research Fund, YSFRI, CAFS (20603022022010), and the Qingdao Postdoctoral Applied Research Project, and the State Key Laboratory of Biogeology and Environmental Geology, China University of Geosciences (GKZ21Y645).

ACKNOWLEDGMENTS

We would like to show our great gratitude to Prof. Xiujuan Shan and Dongliang Yuan, students Qingyuan Lu and Hongsheng Wang, as well as all captains and crews of R/V *Hailan* 101 (NORC2022-01) and *Kexue* 3 (NORC2018-09) for their assistance in our sampling process.

SUPPLEMENTARY MATERIAL

The Supplementary Material for this article can be found online at: https://www.frontiersin.org/articles/10.3389/fmicb.2022.903159/full#supplementary-material

REFERENCES

Behrenfeld, M. J., and Boss, E. (2006). Beam attenuation and chlorophyll concentration as alternative optical indices of phytoplankton biomass. *J. Mar. Res.* 64, 431–451. doi: 10.1357/002224006778189563

Brewin, R. J., Ciavatta, S., Sathyendranath, S., Jackson, T., Tilstone, G., Curran, K., et al. (2017). Uncertainty in ocean-color estimates of chlorophyll for phytoplankton groups. *Front. Mar. Sci.* 4, 104. doi: 10.3389/fmars.2017.00104

Brewin, R. J., Morán, X. A. G., Raitsos, D. E., Gittings, J. A., Calleja, M. L., Viegas, M., et al. (2019). Factors regulating the relationship between total and size-fractionated chlorophyll-a in coastal waters of the Red Sea. *Front. Microbiol.* 10, 1964. doi: 10.3389/fmicb.2019.01964

Brewin, R. J., Sathyendranath, S., Hirata, T., Lavender, S. J., Barciela, R. M., and Hardman-Mountford, N. J. (2010). A three-component model of phytoplankton size class for the Atlantic Ocean. *Ecol. Modell.* 221, 1472–1483. doi: 10.1016/j.ecolmodel.2010.02.014

Brewin, R. J., Sathyendranath, S., Jackson, T., Barlow, R., Brotas, V., Airs, R., et al. (2015). Influence of light in the mixed-layer on the parameters of a three-component model of phytoplankton size class. *Remote Sens. Environ.* 168, 437–450. doi: 10.1016/j.rse.2015.07.004

Brewin, R. J., Sathyendranath, S., Lange, P. K., and Tilstone, G. (2014). Comparison of two methods to derive the size-structure of natural populations of phytoplankton. *Deep Sea Res. Part I Oceanogr. Res.* 85, 72–79. doi: 10.1016/j.dsr.2013.11.007

Chavez, F. P., Buck, K. R., Bidigare, R. R., Karl, D. M., Hebel, D., Latasa, M., et al. (1995). On the chlorophyll a retention properties of glass-fiber GF/F filters. *Limnol. Oceanogr.* 40, 428–433. doi: 10.4319/lo.1995.40.2.0428

Chen, Z., Sun, J., Gu, T., Zhang, G., and Wei, Y. (2021). Nutrient ratios driven by vertical stratification regulate phytoplankton community structure in the oligotrophic western Pacific Ocean. *Ocean Sci.* 17, 1775–1789. doi: 10.5194/os-17-1775-2021

Crosbie, N. D., and Furnas, M. J. (2001). Abundance, distribution and flow-cytometric characterization of picophytoprokaryote populations in central (17 S) and southern (20 S) shelf waters of the Great Barrier Reef. *J. Plankton Res.* 23, 809–828. doi: 10.1093/plankt/23.8.809

Falkowski, P., and Kiefer, D. A. (1985). Chlorophyll a fluorescence in phytoplankton: relationship to photosynthesis and biomass. *J. Plankton Res.* 7, 715–731. doi: 10.1093/plankt/7.5.715

Fiala, M., Semeneh, M., and Oriol, L. (1998). Size-fractionated phytoplankton biomass and species composition in the Indian sector of the Southern Ocean during austral summer. *J. Mar. Syst.* 17, 179–194. doi: 10.1016/S0924-7963(98)00037-2

Finkel, Z. V., Beardall, J., Flynn, K. J., Quigg, A., Rees, T. A. V., and Raven, J. A. (2010). Phytoplankton in a changing world: cell size and elemental stoichiometry. *J. Plankton Res.* 32, 119–137. doi: 10.1093/plankt/fbp098

Flombaum, P., Gallegos, J. L., Gordillo, R. A., Rincón, J., Zabala, L. L., Jiao, N., et al. (2013). Present and future global distributions of the marine Cyanobacteria Prochlorococcus and Synechococcus. *Proc. Natl. Acad. Sci.* 110, 9824–9829. doi: 10.1073/pnas.1307701110

Froneman, P. W., Laubscher, R. K., and McQuaid, C. D. (2001). Size-fractionated primary production in the south Atlantic and Atlantic sectors of the Southern Ocean. *J. Plankton Res.* 23, 611–622. doi: 10.1093/plankt/23.6.611

Fu, M., Sun, P., Wang, Z., Wei, Q., Qu, P., Zhang, X., et al. (2018). Structure, characteristics and possible formation mechanisms of the subsurface chlorophyll maximum in the Yellow Sea Cold Water Mass. *Cont. Shelf Res.* 165, 93–105. doi: 10.1016/j.csr.2018.07.007

GoeRicke, R. (2011). The size structure of marine phytoplankton—What are the rules. *Calif. Coop. Ocean Fish Invest. Rep.* 52, 198–204. doi: 10.1007/s11160-011-9210-1

Gong, G. C., Wen, Y. H., Wang, B. W., and Liu, G. J. (2003). Seasonal variation of chlorophyll a concentration, primary production and environmental conditions in the subtropical East China Sea. *Deep Sea Res. Part II Top. Stud. Oceanogr.* 50, 1219–1236. doi: 10.1016/S0967-0645(03)00019-5

Guidi, L., Stemmann, L., Jackson, G. A., Ibanez, F., Claustre, H., Legendre, L., et al. (2009). Effects of phytoplankton community on production, size, and export

of large aggregates: a world-ocean analysis. *Limnol. Oceanogr.* 54, 1951–1963. doi: 10.4319/lo.2009.54.6.1951

Guo, S., Feng, Y., Wang, L., Dai, M., Liu, Z., Bai, Y., et al. (2014). Seasonal variation in the phytoplankton community of a continental-shelf sea: the East China Sea. *Mar. Ecol. Prog. Ser.* 516, 103–126. doi: 10.3354/meps10952

Hirata, T., Aiken, J., Hardman-Mountford, N., Smyth, T. J., and Barlow, R. G. (2008). An absorption model to determine phytoplankton size classes from satellite ocean colour. *Remote Sens. Environ.* 112, 3153–3159. doi: 10.1016/j.rse.2008.03.011

Hirata, T., Hardman-Mountford, N. J., Brewin, R. J. W., Aiken, J., Barlow, R., Suzuki, K., et al. (2011). Synoptic relationships between surface Chlorophyll-a and diagnostic pigments specific to phytoplankton functional types. *Biogeosciences* 8, 311–327. doi: 10.5194/bg-8-311-2011

Huo, Y., Liu, Q., Zhang, F., Li, C., Tao, Z., Bi, H., et al. (2020). Biomass and estimated production, and feeding pressure on zooplankton of chaetognaths in the Yellow Sea, China. *Terr. Atmospheric Ocean. Sci.* 31, 61–75. doi: 10.3319/TAO.2019.06.26.01

Kameda, T., and Ishizaka, J. (2005). Size-fractionated primary production estimated by a two-phytoplankton community model applicable to ocean color remote sensing. *J. Oceanogr.* 61, 663–672. doi: 10.1007/s10872-005-0074-7

Knefelkamp, B., Carstens, K., and Wiltshire, K. H. (2007). Comparison of different filter types on chlorophyll-a retention and nutrient measurements. J. *Exp. Mar. Biol. Ecol.* 345, 61–70. doi: 10.1016/j.jembe.2007.01.008

Lee, J. H., Kang, J. J., Jang, H. K., Jo, N., Lee, D., Yun, M. S., et al. (2020). Major controlling factors for spatio-temporal variations in the macromolecular composition and primary production by phytoplankton in Garolim and Asan bays in the Yellow *Sea. Reg. Stud. Mar Sci.* 36, 101269. doi: 10.1016/j.rsma.2020.101269

Lee, J. H., Pang, I. C., and Moon, J. H. (2016). Contribution of the Yellow Sea bottom cold water to the abnormal cooling of sea surface temperature in the summer of 2011. *J. Geophys. Res. Oceans* 121, 3777–3789. doi: 10.1002/2016JC011658

Liu, X., Xiao, W., Landry, M. R., Chiang, K. P., Wang, L., and Huang, B. (2016). Responses of phytoplankton communities to environmental variability in the East China Sea. *Ecosystems* 19, 832–849. doi: 10.1007/s10021-016-9970-5

Ma, J., Song, J., Li, X., Yuan, H., Li, N., Duan, L., et al. (2019). Environmental characteristics in three seamount areas of the Tropical Western Pacific Ocean: focusing on nutrients. *Mar. Pollut. Bull.* 143, 163–174. doi: 10.1016/j.marpolbul.2019.04.045

Marañón, E. (2015). Cell size as a key determinant of phytoplankton metabolism and community structure. *Ann. Rev. Mar. Sci.* 7, 241–264. doi: 10.1146/annurev-marine-010814-015955

Marañón, E., Holligan, P. M., Barciela, R., González, N., Mouriño, B., Paz,ó, M. J., et al. (2001). Patterns of phytoplankton size structure and productivity in contrasting open-ocean environments. *Mar. Ecol. Prog. Ser.* 216, 43–56. doi: 10.3354/meps216043

Moloney, C. L., and Field, J. G. (1991). The size-based dynamics of plankton food webs. I. A simulation model of carbon and nitrogen flows. *J. Plankton Res.* 13, 1003–1038. doi: 10.1093/plankt/13.5.1003

Moran, X. A., Gasol, J. M., Arin, L., and Estrada, M. (1999). A comparison between glass fiber and membrane filters for the estimation of phytoplankton POC and DOC production. *Mar. Ecol. Prog. Ser.* 187, 31–41. doi: 10.3354/meps187031

Morán, X. A. G., Fernández, E., and Pérez, V. (2004). Size-fractionated primary production, bacterial production and net community production in subtropical and tropical domains of the oligotrophic NE Atlantic in autumn. *Mar. Ecol. Prog. Ser.* 274, 17–29. doi: 10.3354/meps274017

O'Reilly, J. E., Maritorena, S., Mitchell, B. G., Siegel, D. A., Carder, K. L., Garver, S. A., et al. (1998). Ocean color chlorophyll algorithms for SeaWiFS. *J. Geophys. Res. Oceans* 103, 24937–24953. doi: 10.1029/98JC02160

Prepas, E. E., Dunnigan, M. E., and Trimbee, A. M. (1988). Comparison of in situ estimates of chlorophyll a obtained with Whatman GF/F and GF/C glass-fiber filters in mesotrophic to hypereutrophic lakes. *Can. J. Fish. Aquat. Sci.* 45, 910–914. doi: 10.1139/f88-111

Raimbault, P., Rodier, M., and Taupier-Letage, I. (1988). Size fraction of phytoplankton in the Ligurian Sea and the Algerian Basin (Mediterranean Sea): size distribution versus total concentration. *Marine Microbial. Food Webs.* 3, 1–7.

Raven, J. A. (1998). The twelfth tansley lecture. Small is beautiful: the picophytoplankton. *Funct. Ecol.* 12, 503–513. doi: 10.1046/j.1365-2435.1998.00233.x

Richardson, T. L. (2019). Mechanisms and pathways of small-phytoplankton export from the surface ocean. *Ann Rev Mar Sci.* 11, 57–74. doi: 10.1146/annurev-marine-121916-063627

Sieburth, J. M., Smetacek, V., and Lenz, J. (1978). Pelagic ecosystem structure: heterotrophic compartments of the plankton and their relationship to plankton size fractions. *Limnol. Oceanogr.* 23, 1256–1263. doi: 10.4319/lo.1978.23.6.1256

Soria-Píriz, S., García-Robledo, E., Papaspyrou, S., Aguilar, V., Seguro, I., Acuna, J., et al. (2017). Size fractionated phytoplankton biomass and net metabolism along a tropical estuarine gradient. *Limnol. Oceanogr.* 62, S309–S326. doi: 10.1002/lno.10562

Spilling, K., Olli, K., Lehtoranta, J., Kremp, A., Tedesco, L., Tamelander, T., et al. (2018). Shifting diatom—dinoflagellate dominance during spring bloom in the Baltic Sea and its potential effects on biogeochemical cycling. *Front. Mar. Sci.* 5, 327. doi: 10.3389/fmars.2018.00327

Sun, X., Shen, F., Brewin, R. J., Liu, D., and Tang, R. (2019). Twenty-year variations in satellite-derived chlorophyll-a and phytoplankton size in the Bohai Sea and Yellow Sea. *J. Geophys. Res. Oceans.* 124, 8887–8912. doi: 10.1029/2019JC015552

Sun, X., Shen, F., Liu, D., Bellerby, R. G., Liu, Y., and Tang, R. (2018). In situ and satellite observations of phytoplankton size classes in the entire continental shelf sea, China. *J. Geophys. Res. Oceans* 123, 3523–3544. doi: 10.1029/2017JC013651

Trombetta, T., Vidussi, F., Roques, C., Scotti, M., and Mostajir, B. (2020). Marine microbial food web networks during phytoplankton bloom and non-bloom periods: Warming favors smaller organism interactions and intensifies trophic cascade. *Front. Microbiol.* 11, 502336. doi: 10.3389/fmicb.2020.502336

Uitz, J., Claustre, H., Morel, A., and Hooker, S. B. (2006). Vertical distribution of phytoplankton communities in open ocean: an assessment based on surface chlorophyll. *J. Geophys. Res. Oceans* 111, C08005. doi: 10.1029/2005JC003207

Varela, M., Fernandez, E., and Serret, P. (2002). Size-fractionated phytoplankton biomass and primary production in the Gerlache and south Bransfield Straits (Antarctic Peninsula) in Austral summer 1995-1996. *Deep Sea Res. Part II Top. Stud. Oceanogr.* 49, 749–768. doi: 10.1016/S0967-0645(01)00122-9

Visintini, N., Martiny, A. C., and Flombaum, P. (2021). Prochlorococcus, Synechococcus, and picoeukaryotic phytoplankton abundances in the global ocean. *Limnol. Oceanogr. Lett.* 6, 207–215. doi: 10.1002/lol2.10188

Wei, Y., Chen, Z., Guo, C., Zhong, Q., Wu, C., and Sun, J. (2020). Physiological and ecological responses of photosynthetic processes to oceanic properties and phytoplankton communities in the oligotrophic western Pacific Ocean. *Front. Microbiol.* doi: 10.3389/fmicb.2020.01774

Wei, Y., Liu, H., Zhang, X., Xue, B., Munir, S., and Sun, J. (2017). Physicochemical conditions in affecting the distribution of spring phytoplankton community. *Chin. J. Oceanol. Limno.* 35, 1342–1361. doi: 10.1007/s00343-017-6190-6

Wei, Y., Zhao, X., Sun, J., and Liu, H. (2019). Fast repetition rate fluorometry (FRRF) derived phytoplankton primary productivity in the Bay of Bengal. *Front. Microbiol.* 10, 1164. doi: 10.3389/fmicb.2019.01164

Welschmeyer, N. A. (1994). Fluorometric analysis of chlorophyll a in the presence of chlorophyll b and pheopigments. *Limnol. Oceanogr.* 39, 1985–1992. doi: 10.4319/lo.1994.39.8.1985

Wood, S. N. (2006). *Generalized Additive Models: An Introduction With R. Chapman and Hall/CRC.*

Xiao, W., Liu, X., Irwin, A. J., Laws, E. A., Wang, L., Chen, B., et al. (2018). Warming and eutrophication combine to restructure diatoms and dinoflagellates. *Water Res.* 128, 206–216. doi: 10.1016/j.watres.2017.10.051

Yang, F., Wei, Q., Chen, H., and Yao, Q. (2018). Long-term variations and influence factors of nutrients in the western North Yellow Sea, China. *Mar. Pollut. Bull.* 135, 1026–1034. doi: 10.1016/j.marpolbul.2018.08.034

Yasuda I. (2003). Hydrographic structure and variability in the Kuroshio-Oyashio transition area. *Journal of Oceanography*, 59, 389–402. doi: 10.1023/A:1025580313836

Young, R. L., Weinberg, J., Vieira, V., Ozonoff, A., and Webster, T. F. (2011). Generalized additive models and inflated type I error rates of smoother significance tests. *Comput. Stat. Data Anal.* 55, 366–374. doi: 10.1016/j.csda.2010.05.004

Conflict of Interest: The authors declare that the research was conducted in the absence of any commercial or financial relationships that could be construed as a potential conflict of interest.

Publisher's Note: All claims expressed in this article are solely those of the authors and do not necessarily represent those of their affiliated organizations, or those of the publisher, the editors and the reviewers. Any product that may be evaluated in this article, or claim that may be made by its manufacturer, is not guaranteed or endorsed by the publisher.

frontiers | Frontiers in Microbiology

ORIGINAL RESEARCH
published: 23 May 2022
doi: 10.3389/fmicb.2022.868728

Characterization of a Deep-Sea Actinobacterium Strain Uncovers Its Prominent Capability of Utilizing Taurine and Polyvinyl Alcohol

Yingqi Tan[1,2,3,4], *Yeqi Shan*[1,2,3,4], *Rikuan Zheng*[1,2,3,4], *Rui Liu*[1,2,4] *and Chaomin Sun*[1,2,3,4]*

[1] Chinese Academy of Sciences and Shandong Province Key Laboratory of Experimental Marine Biology and Center of Deep Sea Research, Institute of Oceanology, Chinese Academy of Sciences, Qingdao, China, [2] Laboratory for Marine Biology and Biotechnology, Qingdao National Laboratory for Marine Science and Technology, Qingdao, China, [3] College of Earth Science, University of Chinese Academy of Sciences, Beijing, China, [4] Center of Ocean Mega-Science, Chinese Academy of Sciences, Qingdao, China

Actinobacteria represent a large group of important prokaryotes with great application potentials and widely distribute in diverse natural environments including the ocean. However, compared to their terrestrial cultured members, there are much less available marine *Actinobacteria*, especially deep-sea counterparts. Here, we cultured a bacterial strain of deep-sea actinobacterium, *Marmoricola* sp. TYQ2, by using a basal medium supplemented with taurine. Consistently, the growth of strain TYQ2 was significantly promoted by the supplement of taurine. Transcriptomic analysis showed that the expressions of genes encoding proteins associated with taurine metabolization and utilization as well as energy generation were evidently up-regulated when taurine was added. Moreover, strain TYQ2 was demonstrated to degrade polyvinyl alcohol (PVA) with the involvement of the redox cycle of extracellular quinol and quinone and the reduction of iron to ferrous, and strain TYQ2 could utilize the degradation products for energy production, thereby supporting bacterial growth. Overall, our experimental results demonstrate the prominent degradation capabilities of *Marmoricola* sp. TYQ2 toward the organics taurine and PVA.

Keywords: actinomyces, deep sea, cultivation, taurine, polyvinyl alcohol

OPEN ACCESS

Edited by:
Shan He,
Ningbo University, China

Reviewed by:
Xin-Peng Tian,
South China Sea Institute of Oceanology (CAS), China
Zhiyong Li,
Shanghai Jiao Tong University, China
Fatemeh Mohammadipanah,
University of Tehran, Iran

***Correspondence:**
Chaomin Sun
sunchaomin@qdio.ac.cn

Specialty section:
This article was submitted to Aquatic Microbiology, a section of the journal Frontiers in Microbiology

Received: *03 February 2022*
Accepted: *17 March 2022*
Published: *23 May 2022*

Citation:
Tan Y, Shan Y, Zheng R, Liu R and Sun C (2022) Characterization of a Deep-Sea Actinobacterium Strain Uncovers Its Prominent Capability of Utilizing Taurine and Polyvinyl Alcohol. Front. Microbiol. 13:868728. doi: 10.3389/fmicb.2022.868728

INTRODUCTION

Microorganisms play a vital role toward the decomposition of organic matter in the marine environment and the biogeological cycle (Abirami et al., 2021). Among these microbes, the microbial community in the bottom sediments of the deep sea formed an unexplored biosphere (Baker et al., 2021). Due to the difficulty of sampling and the complexity of the community structure, current researches lacked a full understanding of its unique biological and metabolic characteristics. However, it is sure that these microorganisms play crucial roles toward the global cycle of elements and nutrients in the deep biosphere (Zhang et al., 2020; Baker et al., 2021; Suzuki et al., 2021; Zheng et al., 2021).

Among the marine microorganisms, *Actinobacteria* members are considered as key members due to their wide distribution and diverse biological functions (Rathore et al., 2021). The *Actinobacteria* bacteria ubiquitously distribute in marine sediments (Solano et al., 2009), sea

water (Sheikh et al., 2019), marine organic aggregates (Lam, 2006), marine sponges (Gandhimathi et al., 2009; Sheikh et al., 2019), and deep-sea gas hydrate reservoirs (Wang et al., 2014). Notably, *Actinobacteria* have broad application potentials, such as production of large number of secondary metabolites for developing novel antibiotics (Wang et al., 2014; Kamjam et al., 2017); production of variety of enzymes including alkaline protease, xylanase, α-galactosidase (Temuujin et al., 2016; Sanjivkumar et al., 2017; Thakrar and Singh, 2019). In addition, *Actinobacteria* could degrade and metabolize foreign compounds such as heavy metals, hydrocarbons, pesticides and plastics, and they are also potential candidates for bioremediation (Rathore et al., 2021).

Nocardioidaceae members are heterotrophic aerobic bacteria belonging to the phylum *Actinobacteria*. Like other *Actinobacteria*, they are considered to be consumers of organic substances in the ecosystem. Many biological groups in this family could metabolize refractory and foreign compounds by secreting a series of extracellular enzymes (Evtushenko and Ariskina, 2015). They may also use organic matter or the input of some atmospheric gases and minerals to participate in various chemical energy and nutrient metabolic processes (Evtushenko and Ariskina, 2015).

The discovery of novel actinomycete strain with unique metabolic activity from deep-sea samples clearly illustrate that indigenous deep-sea *Actinobacteria* indeed exist in the oceans and are important sources of novel secondary metabolites, exogenous substance degradation and biosurfactant production (Rathore et al., 2021; Stubbins et al., 2021). The study of *Actinobacteria* has become one of the hot spots of current research. However, the isolation and culture of deep-sea *Actinobacteria* are still facing technological barriers associated with isolation strategies. It is crucial to cultivate novel deep-sea *Actinobacteria* with innovative approaches. In the present study, we successfully cultivated an actinomycete strain *Marmoricola* sp. TYQ2 from the deep-sea cold seep by using a medium supplemented with taurine as the only carbon source. The novel strain belonged to the *Nocardiaceae* family. Combining the physiological, genomic, and transcriptomic methods, we specifically disclosed the metabolic pathways and energy production of taurine and polyvinyl alcohol (PVA) mediated by strain TYQ2 and corresponding contributions to its growth. The utilization of taurine and PVA by strain TYQ2 was demonstrated.

MATERIALS AND METHODS

Sampling, Cultivation Conditions, and Strain Isolation

The sediment and water samples were collected by *RV KEXUE* from a deep-sea cold seep in the South China Sea in 2020. The sediment samples were diluted by the sterile seawater and spread on the solid basal medium supplemented with taurine (1.25 g/L). The components of basal medium were 60 g NaCl, 8.36 g $MgCl_2{\cdot}6H_2O$, 6.8 g $MgSO_4{\cdot}7H_2O$, 0.66 g KCl, 0.5 g NH_4Cl, 0.212 g $CaCl_2$, 15 g agar in 1 liter distilled water, pH 7.5. After autoclaving, the other components, including 4 mL/L 7.5% $NaHCO_3$, 1 mL/L phosphate solution (K_2HPO_4, 140 g/L), 1 mL/L vitamin solution (5 mg/L p-aminobenzoic acid, 2 mg/L biotin, 10 mg/L pyridoxine hydrochloride, 5 mg/L thiamine hydrochloride, 5 mg/L Ca-pantothenate, 0.1 mg/L cobalamin, 2 mg/L folic acid, 5 mg/L riboflavin, 5 mg/L niacin, 5 mg/L lipoic acid), 25 mL/L taurine solution (50 g/L), 1 mL/L trace element solution (2.1 g/L $FeSO_4{\cdot}7H_2O$, 30 mg/L H_3BO_3, 100 mg/L $MnCl_2{\cdot}4H_2O$, 190 mg/L $CoCl_2{\cdot}6H_2O$, 24 mg/L $NiCl_2{\cdot}6H_2O$, 2 mg/L $CuCl_2{\cdot}2H_2O$, 144 mg/L $ZnSO_4{\cdot}7H_2O$, 36 mg/L $Na_2MoO_4{\cdot}2H_2O$, 5.2 g/L $Na_2EDTA{\cdot}2H_2O$), were added and sterilized by filtration and stored at −20°C. In addition, to prevent fungal growth, 30 mg/L nystatin was added to the medium. Single bacterial colonies from the original medium were picked and purified. The purified strain was stored at −80°C using 1/10 2216E medium (0.5 g peptone and 0.1 g yeast extract in per liter of seawater) supplemented with 10 mM taurine and 20% (v/v) glycerol. The isolation and cultivation process and subsequent experiments were all conducted at normal atmospheric pressure and temperature.

Transmission Electron Microscopy Observation

To obtain the cellular morphological characteristics of strain TYQ2, its cell pellets were collected for observation using TEM with a JEOL JEM 12000 EX (HT7700, Hitachi, Tokyo, Japan) equipped with a field emission gun at 100 kV. Briefly, the bacteria solution of strain TYQ2 was centrifuged at 5,000 *g* for 10 min to obtain cells, then washed with 10 mM phosphate buffered saline (PBS, pH 7.4) and centrifuged at 5,000 *g* for 5 min. Washing and centrifugation operations were repeated three times as above. Then, bacterial cells were resuspended, where the copper grid coated with carbon film was immersed for 20 min. Finally, the ready-made copper grid was dried at indoor temperature for 20 min, and then observed under TEM (Buchan et al., 2014).

Studies on Physiological and Biochemical Traits of Strain TYQ2

The ranges of temperature and pH for the growth of strain TYQ2 were tested and indicated by the absorbance of OD_{600} value in the 1/10 2216E liquid medium (0.5 g tryptone and 0.1 g yeast extract in 1-liter filtered seawater). The range of NaCl concentration was tested in the modified 1/10 2216E liquid medium. Growth tests were performed at different temperatures (4, 10, 16, 28, 30, 37, and 40°C). Sodium chloride tolerance was detected in the modified medium (0.5 g tryptone and 0.1 g yeast extract dissolved in 1-liter distilled water) supplemented with 0–10% (w/v) NaCl (1.0% intervals). The pH range was tested from 2.0 to 12.0 (increments of 1 pH unit). Some of physiological characteristics were determined by using the API 20NE (Biomerieux, Lyon, France) tests. To test the utilization of various electron donors and energy sources by strain TYQ2, the 1/10 2216E liquid medium added without or with single substrates (including glucose, sucrose, fructose, lactose, maltose, xylose, rhamnose, xylan, mannose, arabinose, inositol, glycerol, sodium pyruvate, sodium acetate, sodium citrate, sodium propionate, formate, salicylic acid, succinate, mannitol, cellulose, starch, glycine,

trehalose, ethanol, polyethylene glycol, D-sorbitol) at 10 mM was used to test the growth of strain TYQ2. All the culture conditions were incubated at 28°C for 5 days. To study the effects of various sulfur sources on the growth of strain TYQ2, the growth of bacterial cells in the 1/10 2216E medium supplemented without or with 2% DMSO, 20 mM $Na_2S_2O_3$, 5 mM Na_2SO_3, or 100 mM Na_2SO_4 were measured by OD_{600} value as described above. Three biological replicates were performed for both control and experimental groups.

Genomic Sequencing and Analysis of Strain TYQ2

To determine the whole genome sequences, genomic DNA was extracted from 5 days' bacterial culture of the strain TYQ2. The DNA library was constructed by Nanopore PromethION platform and Illumina NovaSeq platform at the Beijing Novogene Bioinformatics Technology Co., Ltd. Firstly, large DNA fragments were recovered by Blue Pippin automatic nucleic acid fragment recovery system, and then repaired. Next, barcode was added by PCR-free method of EXP-NBD104 kit from Oxford Nanopore Technologies Company. The fragments' size was detected by AATI automatic capillary electrophoresis instrument to get the samples isomolarly mixed. Afterward, the SQK-LSK109 connection kit was used to connect the adapter and the library was preliminarily constructed. Then, sequencing libraries were generated by using NEBNext® Ultra™ DNA Library Prep Kit for Illumina (NEB, Ipswich, MA, United States). PE150 data and Nanopore data were combined to assemble by using Unicycler.

Phylogenetic Analysis

Phylogenetic tree based on 16S rRNA gene sequences of strain TYQ2 and some other related taxa was constructed by the maximum likelihood method. Briefly, the 16S rRNA gene (1,511 bp) of strain TYQ2 was obtained from its assembled complete genome (accession number CP076053.1). Other 16S rRNA gene sequences were obtained from the type strains in the NCBI GenBank database.[1] The multiple sequence alignment and sequences' trim were performed by the MEGA version 5.0 software. Finally, the phylogenetic tree was completed by using W-IQ-TREE web server[2] (Trifinopoulos et al., 2016) with TIM3 + F + I + G4 model. The edition was performed by the website tool: Interactive Tree of Life[3] (Letunic and Bork, 2019).

Growth Assays and Transcriptomic Analysis

To detect the effect of taurine on the growth, strain TYQ2 was cultured in the modified 1/10 2216E medium supplemented with different concentrations of taurine (0, 10, 20, 30, 40, 50 mM), and OD_{600} values were checked on the third day with a microplate reader (Infinite M1000 Pro; Tecan, Mannedorf, Switzerland). Since the experimental group had the most obvious effect of promoting growth on the third day, 3 days' cell cultures of strain TYQ2 in the above 1/10 2216E medium supplemented with (40 mM) or without taurine were respectively collected by centrifugation at 5000 *g*, 4°C, 10 min for transcriptomic analysis. In addition, as the same as above, strain TYQ2 was cultured in the modified 1/10 2216E medium supplemented without or with 10 g/L polyvinyl alcohol, respectively. Daily growth was recorded by OD_{600} values and plotted as a growth curve. Four days' culture of the two conditions was used for transcriptomic analysis, for the same reasons as before. Three parallel replicates were set for all the growth tests above.

According to the manufacturer (Novogene, Beijing, China), the brief procedures of transcriptomic analyses were as follows. First, total RNAs of the strain TYQ2 were extracted and rRNA was removed by using probes. Purified mRNA was reversely transcribed into cDNA, and then cDNA was used to prepare the library. After accurate assessment of the library quality and cluster generation, the library preparations were sequenced on an Illumina Novaseq platform. Then, based on the high-quality clean data and genome website, Bowtie2 (Langmead and Salzberg, 2012) was used to both build index of reference genome and align clean reads to reference genome. Gene expression level was estimated by FPKM (Trapnell et al., 2009). Differential expression analysis of two conditions/groups was performed using the DESeq R package (Anders and Huber, 2010). GO and KEGG enrichment analyses of differentially expressed genes were tested by the GOseq R package (Young et al., 2010) and KOBAS software respectively.

RESULTS AND DISCUSSION

Cultivation and Phylogeny of a Deep-Sea Actinobacterium

Given that taurine is an important nutrient source for marine prokaryotes (Clifford et al., 2019), we developed an approach for enrichment of taurine-utilization microorganisms by using a basal medium supplemented with taurine (**Figure 1A**). With that, deep-sea cold seep samples diluted with sterile seawater were spread on plates containing a basal medium supplemented with appropriate amount of taurine and incubated at 28°C. After 2 weeks, we only observed a few white colonies on the plate. Through successive generations of purification and 16S rRNA gene sequencing confirmation, a pure bacterial strain named TYQ2 was obtained (**Figure 1A**). It is observed under TEM as shown in **Figure 1B**. According to the 16S rRNA sequence analysis, strain TYQ2 was identified as a member of the phylum *Actinobacteria*.

To gain a deeper insight into strain TYQ2, its entire genome was sequenced and analyzed (**Supplementary Figure 1**). The whole genome size of strain TYQ2 was 3,600,424 bp, and the DNA G + C content was 71.99%. The annotation of the genome of strain TYQ2 revealed that it consisted of 3,440 predicted genes, including 52 RNA genes (6 rRNA genes, 46 tRNA genes) (**Supplementary Table 1**).

To further clarify the taxonomic status of the strain TYQ2, we performed the phylogenetic analysis with 16S rRNA genes of the cultured type strains of *Nocardiaceae* and other actinomycete

[1] https://www.ncbi.nlm.nih.gov/

[2] http://iqtree.cibiv.univie.ac.at/

[3] https://itol.embl.de/

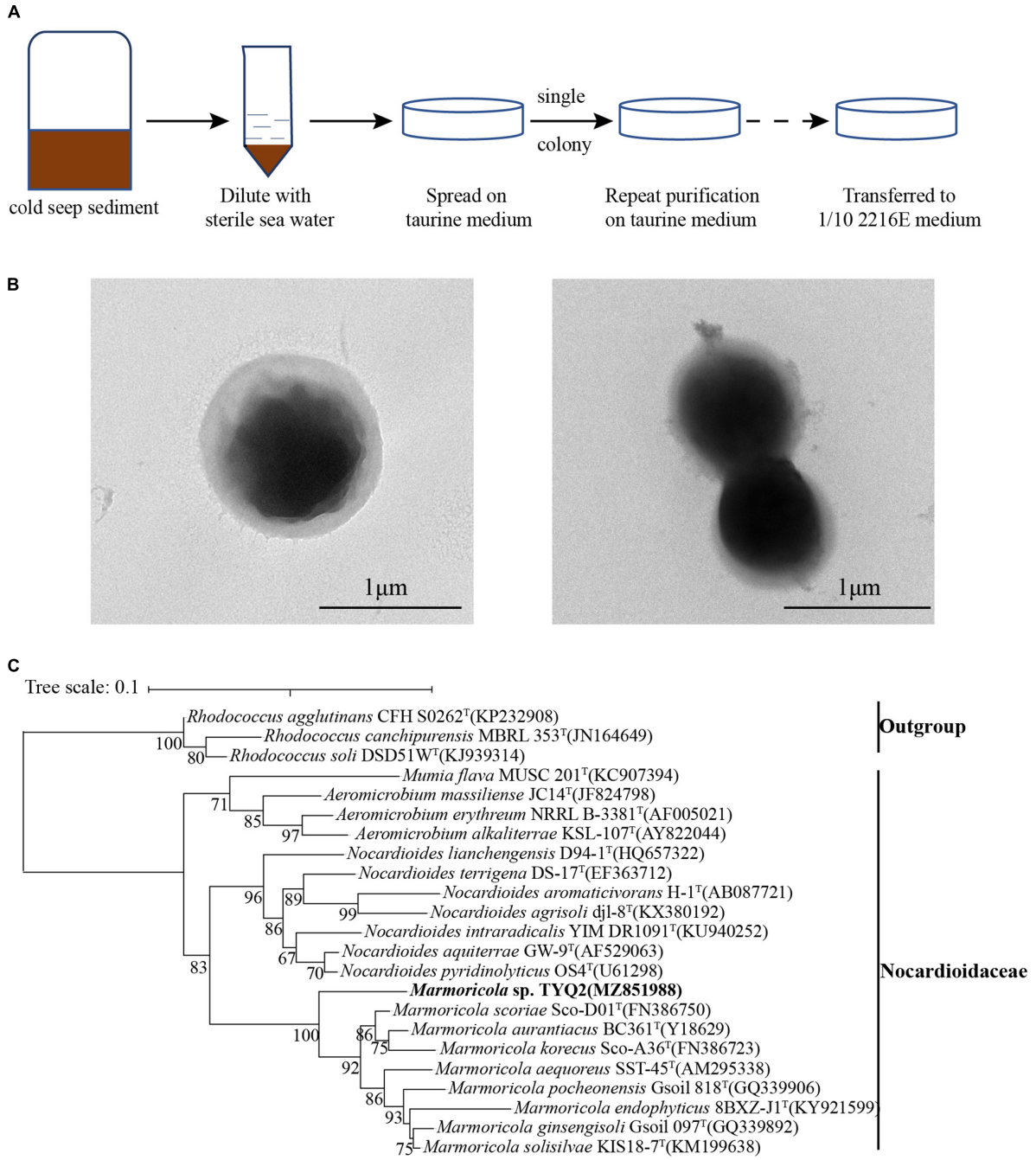

FIGURE 1 | Cultivation, morphology, and phylogeny of *Marmoricola* sp. TYQ2 isolated from the deep-sea cold seep. **(A)** Diagram of enrichment and cultivation of strain TYQ2 by using a taurine supplemented medium. **(B)** Observation of the cell morphology of strain TYQ2 through the transmission electron microscopy. Bar is 1 μm. **(C)** Maximum likelihood 16S rRNA gene phylogenetic tree showing the position of strain TYQ2 as well as the family *Nocardioidaceae* within the *Actinobacteria* phylum. The accession number of each 16S rRNA gene is shown in the parentheses after corresponding strain name. The numbers by the side of branch node indicated statistical support for bootstrap values, respectively. Scale bar, 0.1 substitutions per nucleotide position.

groups as outgroup by using the maximum likelihood method (**Figure 1C**). Based on the 16S rRNA sequence of strain TYQ2, the sequence similarity calculation using the NCBI server showed that strain TYQ2 was closely related to the *Marmoricola aurantiacus* strain BC 361^T (95.94% similarity), which was a type strain of the genus *Marmoricola* isolated from a marble statue (Urzl et al., 2000).

It is noting that we also obtained some species belonging to the phylum *Actinobacteria* from the deep-sea cold seep sediments through the same enrichment and cultivation method,

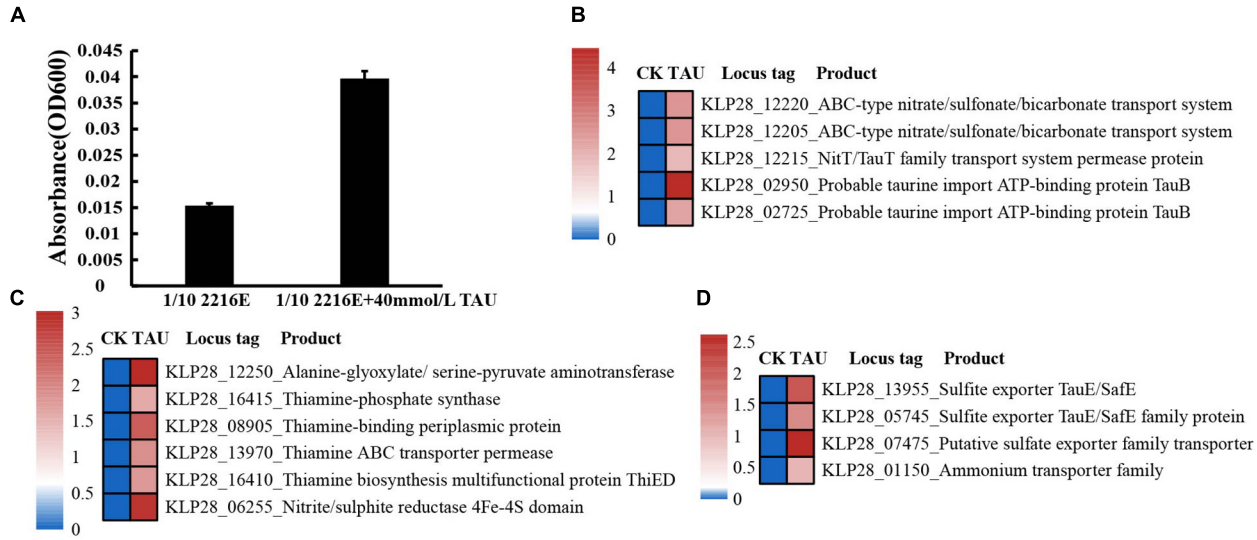

FIGURE 2 | Strain TYQ2 effectively utilizes taurine. **(A)** Growth assays of strain TYQ2 in the 1/10 2216E medium supplemented either without or with 40 mM taurine. **(B)** A heat map based on transcriptomics analysis showing the up-regulated genes associated with taurine and sulfonate transport. **(C)** A heat map based on transcriptomics analysis showing the up-regulated genes associated with the metabolism of taurine. **(D)** A heat map based on transcriptomics showing the up-regulated genes involved in metabolites export.

suggesting the actinomycete group has a universal trait of metabolizing taurine. Since taurine was an organic sulfonate widely distributing in diverse marine environments (Clifford et al., 2017, 2019), it would be an available way to cultivate other uncultured microorganisms in the future.

Physiological and Biochemical Characteristics

The basic physiological and chemical characteristics of strain TYQ2 were summarized in the **Supplementary Table 2**. In detail, the colony of strain TYQ2 was round, smooth, convex, and light yellow in color. Transmission electron microscopic (TEM) observation showed that strain TYQ2 possessed a regular-shaped spherical cell (about 0.4–1.0 μm in size) without flagellum (**Figure 1B**). Gram-reaction-positive, aerobic, non-motile. Growth was detected at temperatures between 10°C and 37°C, but no growth was detected at temperatures below 10°C or above 37°C, and the optimal growth temperature was 28°C. Strain TYQ2 could grow at a pH value of 5.0–10.0, and the optimum pH was 7.0. Growth was detected between 0 and 8.0% NaCl concentration, and the optimum salinity was 4%. Oxidase was negative. In API 20NE tests, positive for aesculin hydrolysis, acid production from glucose and arginine dihydrolase, urease and gelatinase activities, but negative for nitrate and nitrite reduction and indole production. P-Nitro-β-D galactose, glucose, arabinose, mannose, N-acetyl-glucosamine, maltose, gluconate, malic acid, citric acid, and phenylacetic acid were utilized, but mannitol, capric acid, and adipic acid were not. In supplemental growth assays, growth of strain TYQ2 was stimulated by adding glucose, sucrose, fructose, maltose, xylose, rhamnose, xylan, mannose, arabinose, glycerol, sodium pyruvate, sodium acetate, sodium citrate, sodium propionate, cellulose, starch, trehalose or D-sorbitol as a carbon source or electron donor. But adding lactose, inositol, formate, salicylic acid, succinate, mannitol, glycine, ethanol, or polyethylene glycol could not promote growth. In addition, the effects of different sulfur sources on the growth of strain TYQ2 were observed, including 2% DMSO, 20 mM $Na_2S_2O_3$, 5 mM Na_2SO_3, and 100 mM Na_2SO_4 (**Supplementary Figure 2A**). It was found that 2% DMSO, 20 mM $Na_2S_2O_3$, and 5 mM Na_2SO_3 inhibited the growth of strain TYQ2. 100 mM Na_2SO_4 could promote the growth of strain TYQ2. The strain *Marmoricola* sp. TYQ2 was isolated from the deep-sea cold seep sediments in the South China Sea.

Strain TYQ2 Possessed a Prominent Capability of Utilizing Taurine

Based on our strategy of using taurine as the sole carbon source for isolation and cultivation of strain TYQ2, we speculate that this strain should be able to utilize taurine. We thus checked the growth of strain TYQ2 in a basal 1/10 2216E medium supplemented with taurine at a final concentration of 0, 10, 20, 30, 40, or 50 mM (**Supplementary Figure 2B**). The results showed that the growth of strain TYQ2 was promoted along with the increase of the concentration of taurine. Especially at the concentration of 40 mM, the growth rate was increased by nearly 3 times compared with the control group (**Figure 2A**). To further disclose the details of taurine utilization by strain TYQ2, we performed a transcriptome analysis of strain TYQ2 grown in 1/10 2216E medium supplemented without or with taurine (at a final concentration of 40 mM). Indeed, when 40 mM taurine was added to the medium, the expressions of many genes encoding key factors associated with taurine transport (**Figure 2B**), taurine degradation (**Figure 2C**), and

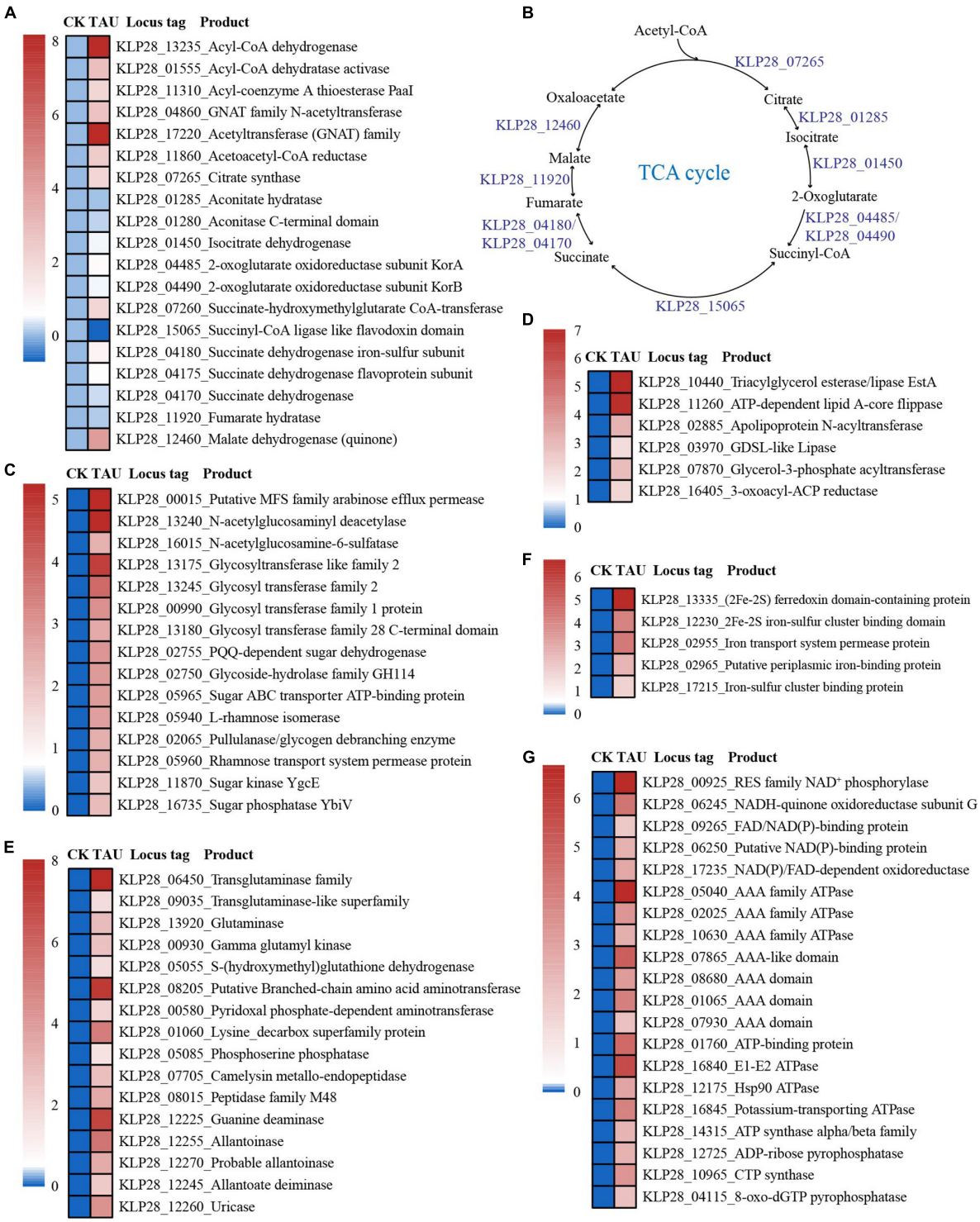

FIGURE 3 | Transcriptomic analysis of essential metabolic pathways for energy production in strain TYQ2 that cultured in the medium supplemented with taurine. **(A)** A heat map based on transcriptomics showing the up-regulated genes involved in acetyl-CoA synthesis and metabolism and the tricarboxylic acid cycle. **(B)** The diagram of the tricarboxylic acid cycle of strain TYQ2. The gene numbers are the same to those shown in panel **(A)**. **(C)** A heat map based on transcriptomics showing all the up-regulated genes involved in sugar transport and metabolism. **(D)** A heat map based on transcriptomics showing all up-regulated genes related to lipid metabolism. **(E)** Transcriptomics-based heat map showing all up-regulated genes related to amino acid and nucleotide metabolism. **(F)** A heat map based on transcriptomics showing all up-regulated genes encoding iron-sulfur proteins. **(G)** A heat map based on transcriptomics showing the up-regulation of all genes related to NAD(P)/FAD/NADH oxidoreductase and ATPase.

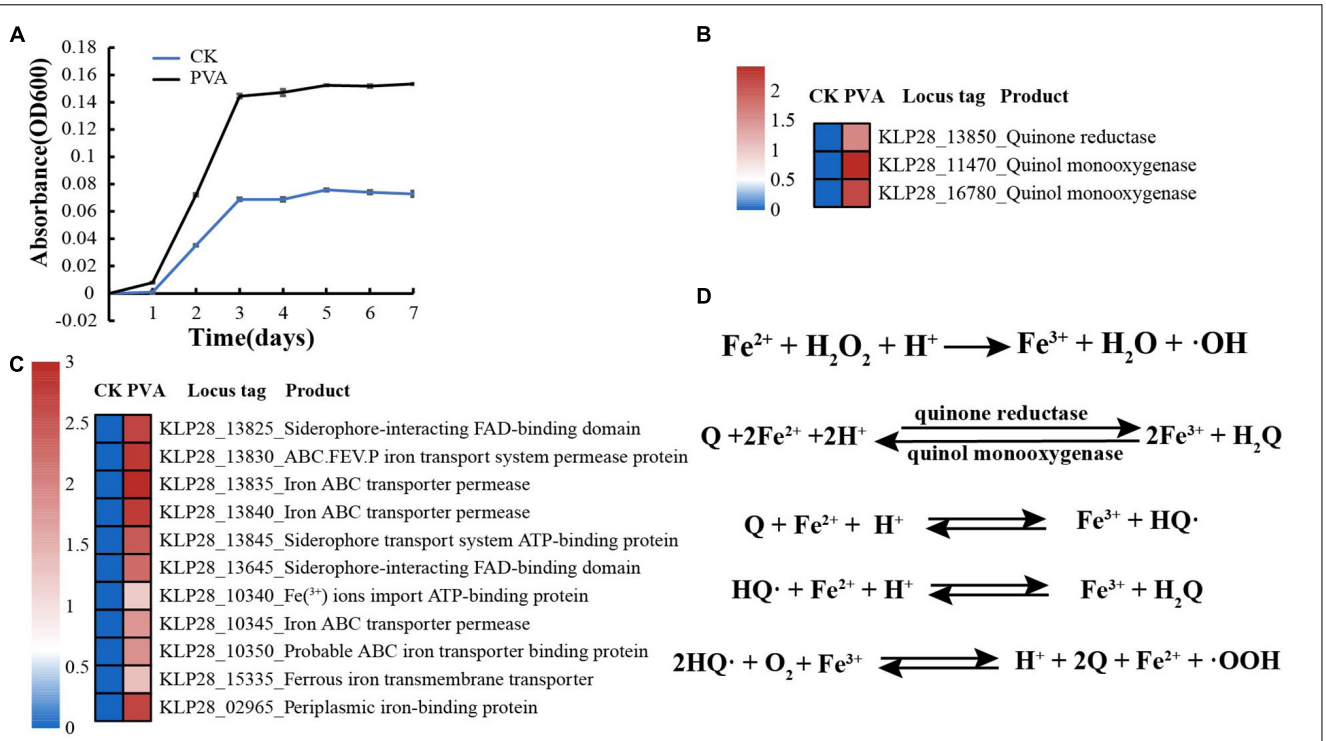

FIGURE 4 | Strain TYQ2 effectively utilizes PVA. **(A)** Growth assays of strain TYQ2 in the 1/10 2216E medium supplemented either without or with 10 g/L PVA. **(B)** A heat map based on transcriptomics analysis showing the up-regulation of genes encoding the quinone reductase and quinol monooxygenase. **(C)** A heat map based on transcriptomics analysis showing the up-regulated genes related to iron/ferrous iron transmembrane transporters and relevant FAD/ATP-binding proteins. **(D)** The proposed Fenton reaction driven by the redox process of quinone and quinol. Q, quinone; H_2Q, quinol; HQ, semiquinone; OOH, perhydroxyl radical.

metabolites export (**Figure 2D**) were evidently up-regulated. Similar to the reported metabolic process of taurine (Cook and Denger, 2006; Nishikawa et al., 2018), taurine or sulfonate transporter could transport taurine into the cell (**Figure 2B**); transamination enzyme and thiamine-phosphate synthase then promoted the destruction of taurine structure (**Figure 2C**); finally, the metabolites were exported by sulfite exporters and ammonium export genes (**Figure 2D**). The destruction of taurine's structure was accompanied by the production of acetyl-CoA, thereby entering the tricarboxylic acid cycle (Cook and Denger, 2006; Nishikawa et al., 2018).

Consistently, the expressions of genes encoding key proteins associated with the acetyl-CoA utilization and tricarboxylic acid cycle (including citrate synthase, aconitate hydratase, isocitrate dehydrogenase, 2-oxoglutarate oxidoreductase, succinyl-CoA ligase, succinate dehydrogenase, fumarate hydratase, and malate dehydrogenase) were mostly up-regulated (**Figures 3A,B**). In addition, the expression levels of genes encoding essential proteins closely related to saccharide metabolism (**Figure 3C**), lipid metabolism (**Figure 3D**), amino acid and nucleotide metabolism (**Figure 3E**), iron-sulfur proteins (**Figure 3F**) were also significantly up-regulated. Consequently, the expression levels of many proteins related to ATP production [including ATP synthase, ATPase, FAD/NAD(P)-binding protein] were also significantly up-regulated (**Figure 3G**). The above results strongly suggested that the metabolization and utilization of taurine could effectively promote the energy production, thereby facilitating the growth of strain TYQ2.

Taurine was an amino acid-like compound containing +5 oxidation state sulfur atom, belonging to the naturally occurring organic sulfonates (Cook and Denger, 2002). Taurine was found in a variety of organisms in the marine environment, including algae, oysters, copepods, diatoms, and various marine metazoans. It acts as an osmotic protective agent or performs other important physiological functions like amino acid metabolism in the organisms, and can be released into the ocean through different pathways (Jackson et al., 1992; Pierce et al., 1992; Clifford et al., 2017, 2019). Previous research reported that organic sulfonates accounted for 20–40% of the total organic sulfur in marine sediments (Vairavamurthy et al., 1994), and taurine acted as one of important components. Diverse bacteria have the ability to degrade taurine, and the degradation products (sulfate, sulfite, sulfide, thiosulfate, low-molecular-weight organic sulfonates, ammonium, alanine, etc.) may also be vital elements and energy sources for other metabolic processes (Lie et al., 1999; Visscher et al., 1999; Cook and Denger, 2006; Krejcik et al., 2008). Due to zooplankton and other metazoans releasing taurine in some nutrient-limited environments, taurine was particularly important for meso- and bathypelagic prokaryotes (Clifford et al., 2019). *Actinobacteria* members widely distributed in the ocean, and they were believed to be essential players driving the biogeographic cycle process of marine environments

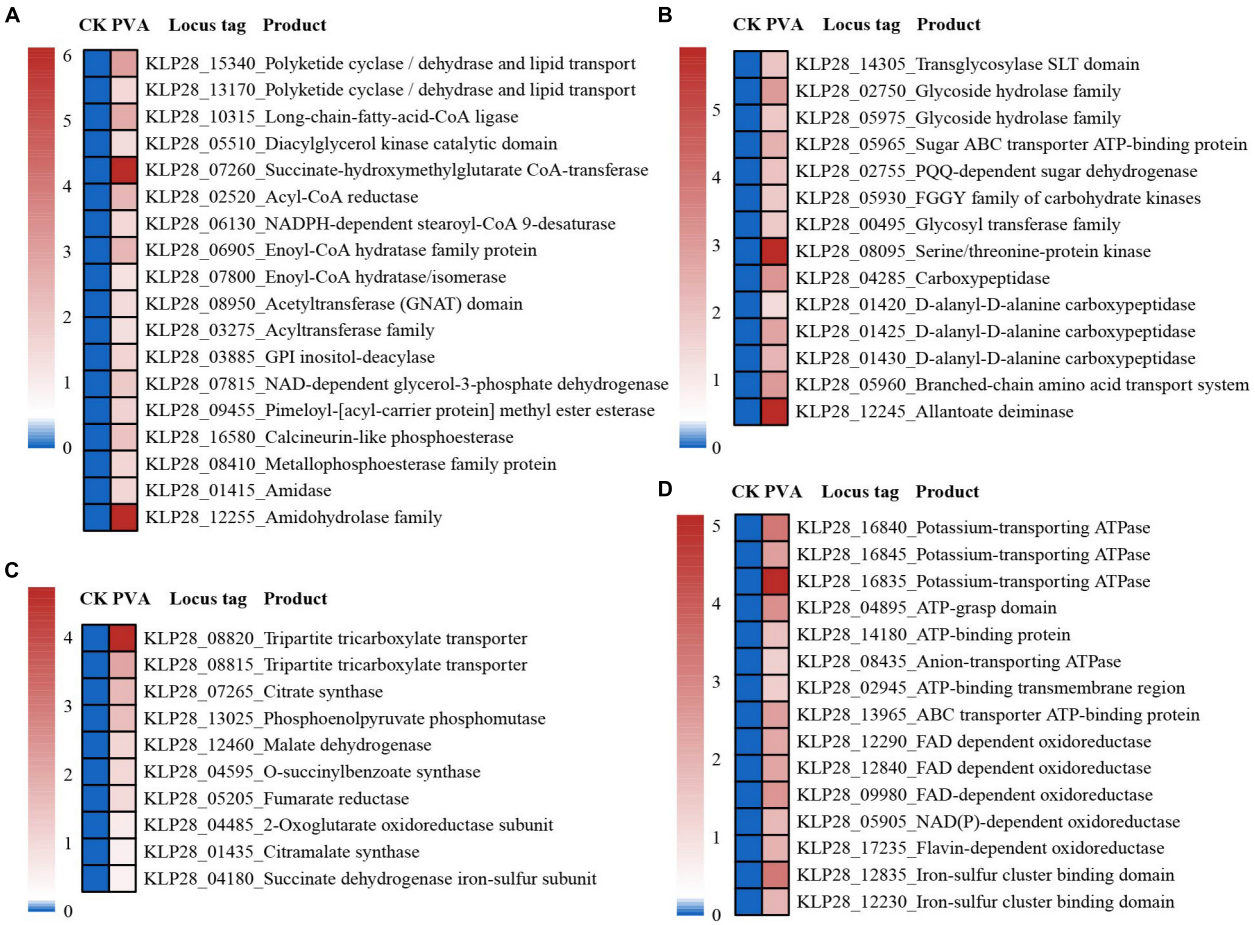

FIGURE 5 | Transcriptomic analysis of essential metabolic pathways for energy production in strain TYQ2 that cultured in the medium supplemented with PVA. **(A)** A heat map based on transcriptomics analysis showing the up-regulated genes related to lipid metabolism. **(B)** A heat map based on transcriptomics showing all the up-regulated genes associated with sugar/amino acid/nucleotide metabolism. **(C)** A heat map based on transcriptomics analysis showing all up-regulated genes related to tricarboxylic acid cycle. **(D)** A heat map based on transcriptomics analysis showing all up-regulated genes encoding proteins associated with ATP generation.

(Mincer et al., 2002; Miralles et al., 2021; Rathore et al., 2021). Metabolism of taurine by *Actinobacteria* may promote deep-sea elements and nutrient cycling processes. However, until now, there is rarely information on the metabolism of taurine by marine *Actinobacteria*, especially the deep ocean.

In the present study, we enrich and culture a deep-sea actinomycete strain TYQ2 with taurine as the sole carbon source, demonstrate its prominent capability toward the degradation and utilization of taurine, and discover the preference for taurine of *Actinobacteria*. Based on the current research, the process of bacterial degradation of taurine has been reported mostly through the same metabolic pathway. The biotransformation of taurine in bacteria usually requires specialized sulfonate transporters to be transported into the cell, and the intracellular taurine is transformed to alanine, HSO_3^-, and acetyl phosphate under the combined action of transamination enzyme and thiamine-phosphate synthase. Bisulfite or sulfate ions participates in intracellular sulfur metabolism or be excreted through transporters. Alanine participates in intracellular amino acid metabolism, and acetyl phosphate can generate acetyl-CoA to participate in intracellular tricarboxylic acid cycle and energy metabolism (Cook and Denger, 2006; Nishikawa et al., 2018). In conclusion, the entire process of strain TYQ2's taurine metabolism involves energy production and the flow of carbon, nitrogen, and sulfur elements.

Strain TYQ2 Possessed a Prominent Capability of Utilizing Polyvinyl Alcohol

When we investigated the proper metabolized substrates of strain TYQ2, we found that PVA could significantly accelerate its growth (2∼3 times) (**Figure 4A**). To explore the degradation and utilization mechanisms of PVA by strain TYQ2, we performed the transcriptomic analysis of strain TYQ2 cultured in the medium supplemented with PVA. According to previous reports (Kerem et al., 1999; Larking et al., 1999; Jensen et al., 2001; Baldrian and Valaskova, 2008; Kawai and Hu, 2009), some microorganisms could use the redox cycle of extracellular quinol

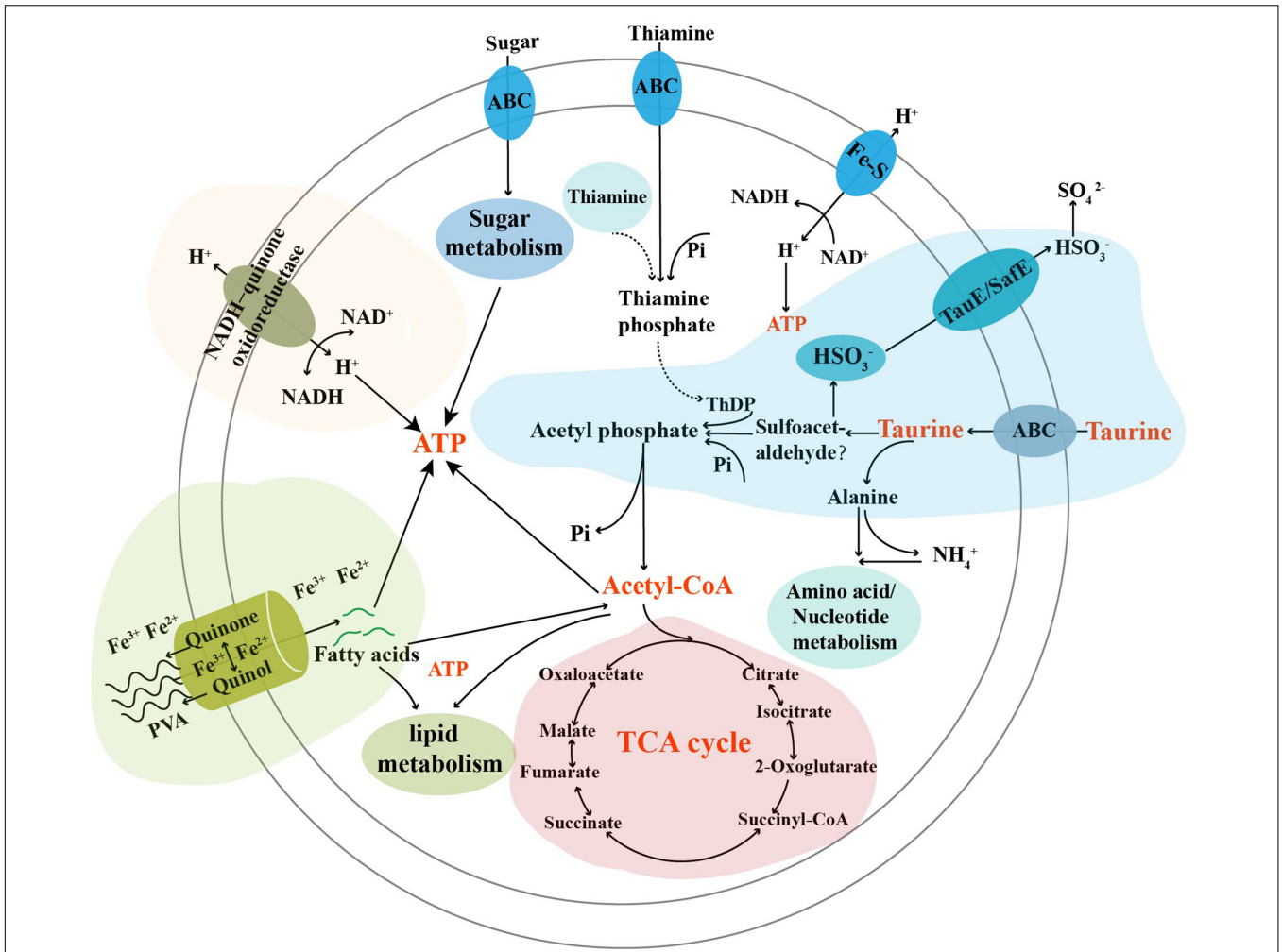

FIGURE 6 | Diagram of a proposed model describing degradation and utilization of taurine and PVA by *Marmoricola* sp. TYQ2. In this model, the metabolization of taurine and PVA as well as the contribution to energy production was highlighted. ThDP, thiamine diphosphate; Pi, phosphate group.

and quinone to reduce iron ions to ferrous ions and produce H_2O_2, which enabled microorganisms to degrade various organic compounds. Based on our transcriptomic results, the expressions of genes encoding quinone reductase and quinol monooxygenase were significantly up-regulated (**Figure 4B**). Additionally, the expressions of many genes encoding Fe^{2+}/Fe^{3+} transmembrane transporters and relevant FAD/ATP-binding proteins were also markedly up-regulated (**Figure 4C**). Therefore, we speculate that strain TYQ2 could degrade PVA through the same pathway shown in **Figure 4D**. In fact, when the conversion process above happened, quinol (H_2Q) was oxidated by Fe^{3+} to semiquinone radicals (HQ·), the semiquinone could reduce O_2 to produce ·OOH and quinone. Strongly oxidizing peroxides like H_2O_2 originated from perhydroxyl radicals (·OOH). Meanwhile, Fe^{3+} was reduced by semiquinone to Fe^{2+} and quinone could be reduced back to quinol again by ferrous ions. In this way, the whole reaction process was carried out cyclically, a complete Fenton system and lots of perhydroxyl radicals were continuously generated (Kerem et al., 1999; Larking et al., 1999; Jensen et al., 2001; Baldrian and Valaskova, 2008; Kawai and Hu, 2009). The whole process was shown the same as **Figure 4D** and these strongly oxidizing perhydroxyl radicals could destroy the structure of polyvinyl alcohol effectively. These indicated that the strain TYQ2 could also reduce iron ions to ferrous ions through the extracellular quinone reduction and quinol oxidation process and generate perhydroxyl radicals. Then, the cyclic Fenton reaction got achieved and the structure of polyvinyl alcohol was destroyed to be utilized. On the other hand, according to previous reports, esterase and lipid metabolism-related genes could promote the metabolism of low-molecular-weight PVA components (Sakai et al., 1998; Chiellini et al., 2003). Consistent with growth promotion of strain TYQ2 by the supplement of PVA in the medium, the expressions of many genes related to lipid metabolism (**Figure 5A**), sugar/amino acid/nucleotide metabolism (**Figure 5B**), tricarboxylic acid cycle (**Figure 5C**), and ATP generation (**Figure 5D**) were significantly up-regulated, suggesting strain TYQ2 not only degraded PVA but also utilized corresponding degradation products as an energy source.

Polyvinyl alcohol was currently the world's highest output water-soluble synthetic polymer, and its earlier annual output could reach 650,000 tons (Tokiwa et al., 2001). As the global production and consumption of PVA were expected to continuously increase, the content of PVA flowing into the environment accordingly showed an increasing trend (Kawai and Hu, 2009). As a potential plastics contaminant, PVA has an adverse effect on the ecological environment, especially the marine environment (Chiellini et al., 2003). Some microorganisms like strain TYQ2 could utilize PVA, which may alleviate the contamination (Suzuki et al., 2021). On the other hand, it is noting that plastics are predominantly carbon at the elemental level (Stubbins et al., 2021). Accumulated studies reveal the quantities of plastics and corresponding degraded intermediates present in some ecosystems rival the quantity of natural organic carbon and impact the carbon cycling of the world (Stubbins et al., 2021), suggesting that geochemists and ecologists should now consider plastics in their analyses. In the same way, combined with the metabolic utilization of PVA by strain TYQ2, this metabolic process involves the utilization and flow of carbon elements.

Combining the data on the metabolization of taurine and PVA, as well as the growth promotion of strain TYQ2, we proposed a model representing the central metabolism of strain TYQ2 (**Figure 6**). In this model, taurine was transported into the cells by special transporters, and then was degraded thereby entering into the sulfur cycle; the degraded products might be utilized by strain TYQ2 and transformed to ATP through different metabolic pathways, thereby promoting bacterial growth. On the other hand, PVA might be degraded with the involvement of the redox cycle of extracellular quinol and quinone and the reduction of iron to ferrous; the degradation products could also be utilized by strain TYQ2, thereby promoting the energy production and supporting bacterial growth. In addition, amplicon sequencing analysis of our deep-sea sediment samples revealed the distribution and abundance of *Actinobacteria* here (**Supplementary Figure 3**). Combined with a lot of previous reports, *Actinobacteria* are widely distributed in marine and deep-sea environments, whether nearshore or pelagic, deep-sea troughs or trenches, ordinary seas or extreme deep-sea environments such as cold seeps and hydrothermal vents (Colquhoun et al., 1998a,b; Bull et al., 2005; Prieto-Davó et al., 2013; Li and Wang, 2014; Mamaeva et al., 2016; Han et al., 2018). Therefore, the members of *Actinobacteria* may play a key role in the degradation and utilization of endogenous or exogenous organic matter, thereby contributing to the nutrient and elements cycling of the deep biosphere. In conclusion, this study explored, revealed and discussed the outstanding metabolic capacity and complete metabolic process of taurine and PVA by the actinomycete strain TYQ2, which involved energy production and flow of several types of elements, and the potential value of deep-sea *Actinobacteria* was prospected.

DATA AVAILABILITY STATEMENT

The 16S rRNA gene sequence and complete genome sequence of *Marmoricola* sp. TYQ2 have been, respectively, deposited in the GenBank database under the accession numbers MZ851988.1 and CP076053.1. The original sequencing reads for transcriptomic analysis have been deposited to the NCBI Short Read Archive. The accessions were, respectively, SAMN21031663, SAMN21031664, SAMN21031665, and SAMN21031666. The raw amplicon sequencing data have been deposited to the NCBI Short Read Archive under the accession number PRJNA675395. Strain TYQ2 has been preserved in the China General Microbiological Culture Collection Center, Beijing, China (accession number: CGMCC1.19148).

AUTHOR CONTRIBUTIONS

YT and CS conceived and designed the study and led the writing of the manuscript. YT conducted most of the experiments. YS collected the samples from the deep-sea cold seep. RZ helped to isolate the bacterium. RL helped to perform the OTU analysis. All authors reviewed the manuscript and approved the submitted version.

FUNDING

This work was funded by the Strategic Priority Research Program of the Chinese Academy of Sciences (Grant No. XDA22050301), China Ocean Mineral Resources R&D Association Grant (Grant No. DY135-B2-14), Key Deployment Projects of Center of Ocean Mega-Science of the Chinese Academy of Sciences (Grant No. COMS2020Q04), Shandong Provincial Natural Science Foundation (Grant No. ZR2021ZD28), Major Research Plan of the National Natural Science Foundation (Grant No. 92051107), and Taishan Young Scholar Program of Shandong Province (Grant No. tsqn20161051) for CS.

SUPPLEMENTARY MATERIAL

The Supplementary Material for this article can be found online at: https://www.frontiersin.org/articles/10.3389/fmicb.2022.868728/full#supplementary-material

REFERENCES

Abirami, B., Radhakrishnan, M., Kumaran, S., and Wilson, A. (2021). Impacts of global warming on marine microbial communities. *Sci. Total Environ.* 791:147905. doi: 10.1016/j.scitotenv.2021.147905

Anders, S., and Huber, W. (2010). Differential expression analysis for sequence count data. *Genome Biol.* 11:R106. doi: 10.1186/gb-2010-11-10-r106

Baker, B. J., Appler, K. E., and Gong, X. Z. (2021). New microbial biodiversity in marine sediments. *Annu. Rev. Mar. Sci.* 13, 161–175. doi: 10.1146/annurev-marine-032020-014552

Baldrian, P., and Valaskova, V. (2008). Degradation of cellulose by basidiomycetous fungi. *Fems Microbiol. Rev.* 32, 501–521. doi: 10.1111/j.1574-6976.2008.00106.x

Buchan, A., LeCleir, G. R., Gulvik, C. A., and Gonzalez, J. M. (2014). Master recyclers: features and functions of bacteria associated with phytoplankton blooms. *Nat. Rev. Microbiol.* 12, 686–698. doi: 10.1038/nrmicro3326

Bull, A. T., Stach, J. E., Ward, A. C., and Goodfellow, M. (2005). Marine actinobacteria: perspectives, challenges, future directions. *Antonie Van Leeuwenhoek* 87, 65–79. doi: 10.1007/s10482-004-6562-8

Chiellini, E., Corti, A., D'Antone, S., and Solaro, R. (2003). Biodegradation of poly (vinyl alcohol) based materials. *Prog. Polym. Sci.* 28, 963–1014. doi: 10.1016/S0079-6700(02)00149-1

Clifford, E. L., Hansell, D. A., Varela, M. M., Nieto-Cid, M., Herndl, G. J., and Sintes, E. (2017). Crustacean zooplankton release copious amounts of dissolved organic matter as taurine in the ocean. *Limnol. Oceanogr.* 62, 2745–2758. doi: 10.1002/lno.10603

Clifford, E. L., Varela, M. M., De Corte, D., Bode, A., Ortiz, V., Herndl, G. J., et al. (2019). Taurine is a major carbon and energy source for marine prokaryotes in the North Atlantic Ocean off the Iberian Peninsula. *Microb. Ecol.* 78, 299–312. doi: 10.1007/s00248-019-01320-y

Colquhoun, J. A., Heald, S. C., Li, L., Tamaoka, J., Kato, C., Horikoshi, K., et al. (1998a). Taxonomy and biotransformation activities of some deep-sea actinomycetes. *Extremophiles* 2, 269–277. doi: 10.1007/s007920050069

Colquhoun, J. A., Mexson, J., Goodfellow, M., Ward, A. C., Horikoshi, K., and Bull, A. T. (1998b). Novel rhodococci and other mycolate actinomycetes from the deep sea. *Antonie Van Leeuwenhoek* 74, 27–40. doi: 10.1023/a:1001743625912

Cook, A. M., and Denger, K. (2002). Dissimilation of the C2 sulfonates. *Arch. Microbiol.* 179, 1–6. doi: 10.1007/s00203-002-0497-0

Cook, A. M., and Denger, K. (2006). "Metabolism of taurine in microorganisms," in *Taurine 6*, eds S. S. Oja and P. Saransaari (Boston, MA: Springer US), 3–13. doi: 10.1007/978-0-387-33504-9_1

Evtushenko, L., and Ariskina, E. (2015). "Nocardioidaceae," in *Bergey's Manual of Systematics of Archaea and Bacteria*, ed. W. B. Whitman (Hoboken, NJ: wiley-blackwell), 1–18.

Gandhimathi, R., Kiran, G. S., Hema, T. A., Selvin, J., Raviji, T. R., and Shanmughapriya, S. (2009). Production and characterization of lipopeptide biosurfactant by a sponge-associated marine actinomycetes *Nocardiopsis alba* MSA10. *Bioproc. Biosyst. Eng.* 32, 825–835. doi: 10.1007/s00449-009-0309-x

Han, Y., Gonnella, G., Adam, N., Schippers, A., Burkhardt, L., Kurtz, S., et al. (2018). Hydrothermal chimneys host habitat-specific microbial communities: analogues for studying the possible impact of mining seafloor massive sulfide deposits. *Sci. Rep.* 8:10386. doi: 10.1038/s41598-018-28613-5

Jackson, A. E., Ayer, S. W., and Laycock, M. V. (1992). The effect of salinity on growth and amino acid composition in the marine diatom *Nitzschia pungens*. *Can. J. Bot.* 70, 2198–2201. doi: 10.1139/b92-272

Jensen, K. A., Houtman, C. J., Ryan, Z. C., and Hammel, K. E. (2001). Pathways for extracellular fenton chemistry in the brown rot basidiomycete *Gloeophyllum trabeum*. *Appl. Environ. Microb.* 67, 2705–2711. doi: 10.1128/Aem.67.6.2705-2711.2001

Kamjam, M., Sivalingam, P., Deng, Z. X., and Hong, K. (2017). Deep sea actinomycetes and their secondary metabolites. *Front. Microbiol.* 8:760. doi: 10.3389/fmicb.2017.00760

Kawai, F., and Hu, X. P. (2009). Biochemistry of microbial polyvinyl alcohol degradation. *Appl. Microbiol. Biot.* 84, 227–237. doi: 10.1007/s00253-009-2113-6

Kerem, Z., Jensen, K. A., and Hammel, K. E. (1999). Biodegradative mechanism of the brown rot basidiomycete *Gloeophyllum trabeum*: evidence for an extracellular hydroquinone-driven fenton reaction. *Febs Lett.* 446, 49–54. doi: 10.1016/S0014-5793(99)00180-5

Krejcik, Z., Denger, K., Weinitschke, S., Hollemeyer, K., Paces, V., Cook, A. M., et al. (2008). Sulfoacetate released during the assimilation of taurine-nitrogen by *Neptuniibacter caesariensis*: purification of sulfoacetaldehyde dehydrogenase. *Arch. Microbiol.* 190, 159–168. doi: 10.1007/s00203-008-0386-2

Lam, K. S. (2006). Discovery of novel metabolites from marine actinomycetes. *Curr. Opin. Microbiol.* 9, 245–251. doi: 10.1016/j.mib.2006.03.004

Langmead, B., and Salzberg, S. L. (2012). Fast gapped-read alignment with Bowtie 2. *Nat. Methods* 9, 357–U354. doi: 10.1038/Nmeth.1923

Larking, D. M., Crawford, R. J., Christie, G. B. Y., and Lonergan, G. T. (1999). Enhanced degradation of polyvinyl alcohol by *Pycnoporus cinnabarinus* after pretreatment with Fenton's reagent. *Appl. Environ. Microb.* 65, 1798–1800. doi: 10.1128/AEM.65.4.1798-1800.1999

Letunic, I., and Bork, P. (2019). Interactive tree of life (iTOL) v4: recent updates and new developments. *Nucleic Acids Res.* 47, W256–W259. doi: 10.1093/nar/gkz239

Li, T., and Wang, P. (2014). Bacterial diversity in sediments of core MD05-2902 from the Xisha Trough, the South China Sea. *Acta Oceanol. Sin.* 33, 85–93. doi: 10.1007/s13131-014-0543-1

Lie, T. J., Clawson, M. L., Godchaux, W., and Leadbetter, E. R. (1999). Sulfidogenesis from 2-aminoethanesulfonate (taurine) fermentation by a morphologically unusual sulfate-reducing bacterium, *Desulforhopalus singaporensis* sp nov. *Appl. Environ. Microb.* 65, 3328–3334. doi: 10.1128/AEM.65.8.3328-3334.1999

Mamaeva, E. V., Galach'yants, Y. P., Khabudaev, K. V., Petrova, D. P., Pogodaeva, T. V., Khodzher, T. B., et al. (2016). Metagenomic analysis of microbial communities of the sediments of the Kara Sea Shelf and the Yenisei Bay. *Mikrobiologiia* 85, 187–198. doi: 10.1134/S0026261716020132

Mincer, T. J., Jensen, P. R., Kauffman, C. A., and Fenical, W. (2002). Widespread and persistent populations of a major new marine actinomycete taxon in ocean sediments. *Appl. Environ. Microb.* 68, 5005–5011. doi: 10.1128/Aem.68.10.5005-5011.2002

Miralles, I., Ortega, R., and Montero-Calasanz, M. D. C. (2021). Studying the microbiome of cyanobacterial biocrusts from drylands and its functional influence on biogeochemical cycles. *Research Square* 2021:252045.

Nishikawa, M., Shen, L. H., and Ogawa, K. (2018). Taurine dioxygenase (tauD)-independent taurine assimilation in *Escherichia coli*. *Microbiol-Sgm.* 164, 1446–1456. doi: 10.1099/mic.0.000723

Pierce, S. K., Rowlandfaux, L. M., and Obrien, S. M. (1992). Different salinity tolerance mechanisms in Atlantic and Chesapeake Bay conspecific oysters - glycine betaine and amino-acid pool variations. *Mar. Biol.* 113, 107–115. doi: 10.1007/Bf00367644

Prieto-Davó, A., Villarreal-Gómez, L. J., Forschner-Dancause, S., Bull, A. T., Stach, J. E., Smith, D. C., et al. (2013). Targeted search for actinomycetes from nearshore and deep-sea marine sediments. *FEMS Microbiol. Ecol.* 84, 510–518. doi: 10.1111/1574-6941.12082

Rathore, D. S., Sheikh, M., and Singh, S. P. (2021). "Marine *Actinobacteria*: New horizons in bioremediation," in Recent Developments in Microbial Technologies, ed. R, Prasad, V, Kumar, J, Singh and C.P, Upadhyaya (Singapore: Springer) 425–449.

Sakai, K., Fukuba, M., Hasui, Y., Moriyoshi, K., Ohmoto, T., Fujita, T., et al. (1998). Purification and characterization of an esterase involved in poly(vinyl alcohol) degradation by *Pseudomonas* vesicularis PD. *Biosci. Biotechnol. Biochem.* 62, 2000–2007. doi: 10.1271/bbb.62.2000

Sanjivkumar, M., Silambarasan, T., Palavesam, A., and Immanuel, G. (2017). Biosynthesis, purification and characterization of β-1,4-xylanase from a novel mangrove associated actinobacterium *Streptomyces olivaceus* (MSU3) and its applications. *Protein Expr. Purif.* 130, 1–12. doi: 10.1016/j.pep.2016.09.017

Sheikh, M., Rathore, D. S., Gohel, S., and Singh, S. P. (2019). Cultivation and characteristics of the marine *Actinobacteria* from the sea water of Alang, Bhavnagar. *Indian J. Geo-Mar. Sci.* 48, 1896–1901.

Solano, G., Rojas-Jimenez, K., Jaspars, M., and Tamayo-Castillo, G. (2009). Study of the diversity of culturable actinomycetes in the North Pacific and Caribbean coasts of Costa Rica. *Anton. Leeuw. Int. J. G.* 96, 71–78. doi: 10.1007/s10482-009-9337-4

Stubbins, A., Law, K. L., Munoz, S. E., Bianchi, T. S., and Zhu, L. X. (2021). Plastics in the Earth system. *Science* 373, 51–55. doi: 10.1126/science.abb0354

Suzuki, M., Tachibana, Y., and Kasuya, K.-I. (2021). Biodegradability of poly(3-hydroxyalkanoate) and poly(ε-caprolactone) *via* biological carbon cycles in marine environments. *Polymer J.* 53, 47–66. doi: 10.1038/s41428-020-00396-5

Temuujin, U., Park, J. S., and Hong, S. K. (2016). Molecular characterization of the α-galactosidase SCO0284 from *Streptomyces coelicolor* A3(2), a family 27 glycosyl hydrolase. *J. Microbiol. Biotechnol.* 26, 1650–1656. doi: 10.4014/jmb.1606.06010

Thakrar, F. J., and Singh, S. P. (2019). Catalytic, thermodynamic and structural properties of an immobilized and highly thermostable alkaline protease from a haloalkaliphilic *Actinobacteria*, *Nocardiopsis alba* TATA-5. *Bioresource Technol.* 278, 150–158. doi: 10.1016/j.biortech.2019.01.058

Tokiwa, Y., Kawabata, G., and Jarerat, A. (2001). A modified method for isolating poly(vinyl alcohol)-degrading bacteria and study of their degradation patterns. *Biotechnol. Lett.* 23, 1937–1941. doi: 10.1023/A:1013785817554

Trapnell, C., Pachter, L., and Salzberg, S. L. (2009). TopHat: discovering splice junctions with RNA-Seq. *Bioinformatics* 25, 1105–1111. doi: 10.1093/bioinformatics/btp120

Trifinopoulos, J., Nguyen, L. T., von Haeseler, A., and Minh, B. Q. (2016). W-IQ-TREE: a fast online phylogenetic tool for maximum likelihood analysis. *Nucleic Acids Res.* 44, W232–W235. doi: 10.1093/nar/gkw256

Urzl, C., Salamone, P., Schumann, P., and Stackebrandt, E. (2000). *Marmoricola aurantiacus* gen. nov., sp nov., a coccoid member of the family *Nocardioidaceae* isolated from a marble statue. *Int. J. Syst. Evol. Micr.* 50, 529–536.

Vairavamurthy, A., Zhou, W. Q., Eglinton, T., and Manowitz, B. (1994). Sulfonates - a novel class of organic sulfur-compounds in marine-sediments. *Geochim. Cosmochim. Ac.* 58, 4681–4687. doi: 10.1016/0016-7037(94)90200-3

Visscher, P. T., Gritzer, R. F., and Leadbetter, E. R. (1999). Low-molecular-weight sulfonates, a major substrate for sulfate reducers in marine microbial mats. *Appl. Environ. Microb.* 65, 3272–3278. doi: 10.1128/AEM.65.8.3272-3278.1999

Wang, W. P., Cai, B. B., and Shao, Z. Z. (2014). Oil degradation and biosurfactant production by the deep sea bacterium *Dietzia maris* As-13-3. *Front. Microbiol.* 5:711. doi: 10.3389/fmicb.2014.00711

Young, M. D., Wakefield, M. J., Smyth, G. K., and Oshlack, A. (2010). Gene ontology analysis for RNA-seq: accounting for selection bias. *Genome Biol.* 11:R14. doi: 10.1186/gb-2010-11-2-r14

Zhang, J., Liu, R., Xi, S. C., Cai, R. N., Zhang, X., and Sun, C. M. (2020). A novel bacterial thiosulfate oxidation pathway provides a new clue about the formation of zero-valent sulfur in deep sea. *Isme J.* 14, 2261–2274.

Zheng, R. K., Liu, R., Shan, Y. Q., Cai, R. N., Liu, G., and Sun, C. M. (2021). Characterization of the first cultured free-living representative of *Candidatus Izemoplasma* uncovers its unique biology. *Isme J.* 15, 2676–2691. doi: 10.1101/2020.11.18.388454

Conflict of Interest: The authors declare that the research was conducted in the absence of any commercial or financial relationships that could be construed as a potential conflict of interest.

Publisher's Note: All claims expressed in this article are solely those of the authors and do not necessarily represent those of their affiliated organizations, or those of the publisher, the editors and the reviewers. Any product that may be evaluated in this article, or claim that may be made by its manufacturer, is not guaranteed or endorsed by the publisher.

frontiers | Frontiers in Microbiology

ORIGINAL RESEARCH
published: 24 May 2022
doi: 10.3389/fmicb.2022.906864

Niche Partitioning of Labyrinthulomycete Protists Across Sharp Coastal Gradients and Their Putative Relationships With Bacteria and Fungi

*Ningdong Xie[1,2], Zhao Wang[2], Dana E. Hunt[2,3], Zackary I. Johnson[2,3], Yaodong He[1] and Guangyi Wang[1,4]**

[1]Center for Marine Environmental Ecology, School of Environmental Science and Engineering, Tianjin University, Tianjin, China, [2]Marine Laboratory, Duke University, Beaufort, NC, United States, [3]Biology Department, Duke University, Durham, NC, United States, [4]Key Laboratory of Systems Bioengineering (Ministry of Education), Tianjin University, Tianjin, China

OPEN ACCESS

Edited by:
Shan He,
Ningbo University, China

Reviewed by:
Jun Gong,
Sun Yat-sen University, China
Lu Yang,
Mayo Clinic, United States

***Correspondence:**
Guangyi Wang
gywang@tju.edu.cn

Specialty section:
This article was submitted to Aquatic Microbiology, a section of the journal Frontiers in Microbiology

Received: 29 March 2022
Accepted: 05 May 2022
Published: 24 May 2022

Citation:
Xie N, Wang Z, Hunt DE, Johnson ZI, He Y and Wang G (2022) Niche Partitioning of Labyrinthulomycete Protists Across Sharp Coastal Gradients and Their Putative Relationships With Bacteria and Fungi.
Front. Microbiol. 13:906864.
doi: 10.3389/fmicb.2022.906864

While planktonic microbes play key roles in the coastal oceans, our understanding of heterotrophic microeukaryotes' ecology, particularly their spatiotemporal patterns, drivers, and functions, remains incomplete. In this study, we focus on a ubiquitous marine fungus-like protistan group, the Labyrinthulomycetes, whose biomass can exceed that of bacterioplankton in coastal oceans but whose ecology is largely unknown. Using quantitative PCR and amplicon sequencing of their 18S rRNA genes, we examine their community variation in repeated five-station transects across the nearshore-to-offshore surface waters of North Carolina, United States. Their total 18S rRNA gene abundance and phylotype richness decrease significantly from the resource-rich nearshore to the oligotrophic offshore waters, but their Pielou's community evenness appears to increase offshore. Similar to the bacteria and fungi, the Labyrinthulomycete communities are significantly structured by distance from shore, water temperature, and other environmental factors, suggesting potential niche partitioning. Nevertheless, only several Labyrinthulomycete phylotypes, which belong to aplanochytrids, thraustochytrids, or unclassified Labyrinthulomycetes, are prevalent and correlated with cohesive bacterial communities, while more phylotypes are patchy and often co-occur with fungi. Overall, these results complement previous time-series observations that resolve the Labyrinthulomycetes as persistent and short-blooming ecotypes with distinct seasonal preferences, further revealing their partitioning spatial patterns and multifaceted roles in coastal marine microbial food webs.

Keywords: heterotrophic protist, coastal ocean, environmental gradient, spatial distribution, community structure, microbial interaction

INTRODUCTION

With the growth and cohesion of human population and industries in coastal regions worldwide, the coastal oceans are increasingly modified by strong terrestrial inputs of organic and nutrient pollution, making these ecosystems highly productive and more crucial in global carbon cycling and climate change regulation (Bauer et al., 2013; Zhang et al., 2017). Due to the terrestrial influences by both anthropogenic and natural causes, the coastal oceans normally feature sharp environmental gradients from the resource-rich, temporally variable nearshore to the oligotrophic, less-variable offshore habitats, which may result in heterogeneous microbial communities and functions (Fortunato et al., 2012; Connell et al., 2017; Satinsky et al., 2017). As found in other aquatic ecosystems, planktonic microbes have long been considered as major contributors to primary and secondary production and fundamental drivers of biogeochemical processes in the coastal oceans (Sherr and Sherr, 1991; Azam and Malfatti, 2007; Jiao et al., 2014). Therefore, how these microbes interact with each other and respond to the spatiotemporally varied environmental factors has become a central question to marine ecologists and biogeochemists (Chafee et al., 2017; Wang et al., 2019).

Nevertheless, the dynamics, patterns, and drivers for different microbial taxa across the sharp coastal gradients remain elusive, partially due to a limited number of observations at the appropriate scales (e.g., repeated nearshore-to-offshore transects) and a poor characterization of many potentially important groups (e.g., heterotrophic microeukaryotes; Wang et al., 2012, 2019; Massana et al., 2014). These gaps may hinder our understanding to marine biogeochemical processes and further distort predictions of global environmental changes (Worden et al., 2015). Prior research on spatiotemporal patterns and drivers across the coastal gradients largely focuses on phytoplankton and bacterioplankton, with both groups exhibiting partitioning across coastal gradients, likely in response to environmental conditions including temperature and distance from shore (a proxy for a number of environmental factors such as productivity, terrestrial input, and nutrients), suggesting the differential niches within either group (Bouman et al., 2006; Tréguer et al., 2018; Wang et al., 2019). While recent evidence has revealed a significant biomass of diverse heterotrophic microeukaryotes in the coastal oceans (Gao et al., 2009; Heywood et al., 2010; Bong and Lee, 2011; Choi et al., 2012), efforts to investigate their community-level patterns remain rare and constrained to few taxa such as fungi (Taylor and Cunliffe, 2016; Duan et al., 2018b). In contrast to bacterioplankton populations, which display clear patterns associated with distance from shore and/or temperature (Wang et al., 2019), fungal work across the nearshore-to-offshore transects identified extremely-patchy phylotype distributions, suggesting narrow niches, stochasticity, or strong density-dependent selection, but similar to the bacterial communities, the fungal communities are also shaped by temperature and distance from shore (Duan et al., 2021). These findings shed light on the complexity regarding the spatiotemporal patterns, environmental associations, and ecological and biogeochemical functions of different microbial groups in the coastal oceans, but also expose the need to further investigate otherwise overlooked heterotrophic taxa, which may complement our understanding to the structuring and functioning of marine microbial food webs.

In this study, we focus on a ubiquitous marine fungus-like protistan group, namely Labyrinthulomycetes, whose biomass often exceed that of bacterioplankton in coastal environments but whose niches and functions are yet to be elucidated (Raghukumar and Damare, 2011; Ueda et al., 2015; Liu et al., 2017; Pan et al., 2017; Xie et al., 2018; Duan et al., 2018a). Culture-based studies show this heterotrophic group can live on both terrestrial and oceanic resources *via* multiple strategies, including degrading particulate detritus by secreted enzymes, assimilating dissolved organic matter from surrounding seawater, and consuming invertebrates, seagrasses, algae, and bacteria as parasites, symbiotes, or predators (Raghukumar, 1992, 2002; Wong et al., 2005; Rubin et al., 2017; Hamamoto and Honda, 2019). However, culture-independent studies reveal high molecular diversity within this class and find most phylotypes belonging to uncultured, novel clades with largely unknown physiology and ecology, suggesting their putative roles in the ecosystem and food webs still await evidence from solid field observations (Collado-Mercado et al., 2010; Liu et al., 2017; Bai et al., 2019; Xie et al., 2021). Up to now, only a few studies have explored their spatiotemporal patterns in the context of broad ecological factors and complex microbial interactions (Xie et al., 2018, 2021; Bai et al., 2019). Obvious seasonal dynamics in the composition of cultured and uncultured Labyrinthulomycetes have been detected in the coastal waters of Japan and China, respectively (Ueda et al., 2015; Xie et al., 2018). Our weekly observations at a nearshore site (Piver's Island Coastal Observatory, PICO) in North Carolina further identified two patterns in the Labyrinthulomycetes: a few persistent, seasonally fluctuating phylotypes and those with brief (weeks to a month) annually repeating blooms (Xie et al., 2021). These studies highlight the temperature as a key factor for the community structure of Labyrinthulomycetes (Xie et al., 2018, 2021). Although our understanding of temporal patterns is improving, the spatial patterns of the Labyrinthulomycete communities remain to be investigated. In the coastal waters of the Bohai Sea, a set of nearshore and offshore samples across different seasons have been sequenced, but no apparent spatial patterns are identified, perhaps due to limited sampling and inconsistent environmental gradients in the semi-closed bay (e.g., offshore stations sometimes are more eutrophic than nearshore stations; Xie et al., 2018). Although habitat segregation between estuarian and coastal waters has been reported for some culturable strains (Ueda et al., 2015), we still lack clarity on how the Labyrinthulomycetes respond to the trophic and other environmental conditions across nearshore to open ocean transitions without large salinity changes.

Here we examine the community dynamics of Labyrinthulomycetes in 17 repeated five-station transects from the nearshore PICO time-series site at Beaufort, North Carolina, United States, to the offshore oligotrophic waters at the

continental shelf break, as part of the Piver's Island Coastal Observatory-Longitudinal Oceanographic Variability Experiment (PICO-LOVE); the concurrent metadata, including the bacterial, fungal, algal, and environmental data sets, were incorporated for comparing spatiotemporal patterns and inferring potential microbial interactions (Wang et al., 2019; Duan et al., 2021). Referring to the annual patterns in the previous nearshore time-series, the expanded spatial scale in the present study to the oligotrophic waters adjacent to the Sargasso Sea offers unique insights into spatial partitioning of Labyrinthulomycetes across heterogeneous coastal habitats and their relationships with other marine microbes. The goal is to integrate the Labyrinthulomycete protists into the marine microbial food webs and fill the knowledge gap regarding the microbial spatiotemporal patterns, drivers, and functions in the coastal oceans.

MATERIALS AND METHODS

Environmental Samples and Metadata

Monthly or quarterly cruises were performed from July 2014 to August 2016, as part of the Piver's Island Coastal Observatory-Longitudinal Oceanographic Variability Experiment (PICO-LOVE; Wang et al., 2019; Duan et al., 2021). The repeated sampling transects began at the mouth of the Newport River estuary near the Beaufort Inlet, outreaching 87 km to the continental shelf break in Sargasso Sea (**Figure 1**). Seawater samples were collected at 1 m depth from the nearshore station A (34.7181°N 76.6707°W), shelf stations B (34.6084°N 76.6708°W) and C (34.3584°N 76.4725°W), and offshore stations D (34.1944°N 76.3328°W) and E (34.0345°N 76.1972°W), despite several samples not collected due to field conditions (**Supplementary Table S1**). Genomic DNA was collected by filtering ~1 L seawater through 0.22-μm Sterivex filter units (Millipore, United States), extracted by using the Gentra Puregene Yeast/Bacteria kit (QIAGEN, United States) supplemented with bead beating, and purified by using the Zymo OneStep PCR inhibitor removal kit. Corresponding environmental parameters, including daily blue-sky insolation, water temperature, pH, salinity, turbidity, nutrients, chlorophyll *a*, dissolved inorganic carbon, dissolved oxygen, dissolved oxygen saturation, and abundances of phytoplankton, bacterioplankton, and mycoplankton, were determined as described previously (Johnson et al., 2013; Ward et al., 2017; Duan et al., 2018b; Wang et al., 2019; Xie et al., 2021). The complete sample information and environmental metadata can be found in the **Supplementary Material**.

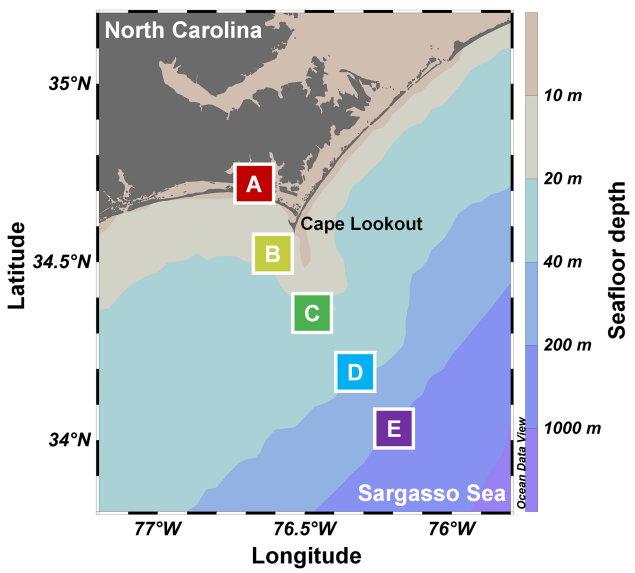

FIGURE 1 | Stations of the repeated sampling transects from July 2014 to August 2016. The transects begin at the estuarine Piver's Island Coastal Observatory time-series site (station A), continuing 87 km offshore until the continental shelf break (station E). The color gradient for the background of the map indicates ocean bathymetry.

Quantitative PCR of Labyrinthulomycete 18S rRNA Genes

Total abundance of Labyrinthulomycete 18S rRNA genes per liter seawater was determined by quantitative PCR following the described protocol (Xie et al., 2021). The 10-μl reaction mixture included 1× SYBR premix Ex Taq (Takara, Japan), 0.25 μM forward primer LABY-A (5′-GGGATCGAAGATGATTAG-3′), 0.25 μM reverse primer LABY-Y (5′-CWCRAACTTCCTTCCGGT-3′), and ~10 ng DNA template. The standard curve was built by known amounts of a modified pGEM-T vector (Promega, United States) containing the target gene from a cultured thraustochytrid (PKU#SW8, GenBank: JX847378.1) genome. The reaction program was performed on a Mastercycler ep realplex (Eppendorf, Germany) as follows: initial denaturation at 95°C for 2 min, followed by 40 cycles of 95°C for 5 s, annealing at 50°C for 30 s, elongation at 72°C for 1 min, and acquisition of fluorescence data at the end of each cycle.

Sequencing of Labyrinthulomycete 18S rRNA Genes

Partial Labyrinthulomycete 18S rRNA genes were amplified using primers LABY-A and LABY-Y with added Illumina adapters and indexes (Stokes et al., 2002; Liu et al., 2017; Xie et al., 2018, 2021; Bai et al., 2019). The 25 μl PCR reaction mixture contained 1× QIAGEN Multiplex Mastermix, 0.2 μM each primer, and ~10 ng of DNA template. The PCR program was run with an initial denaturation at 95°C for 15 min, followed by 31 cycles of 30 s at 94°C, 1.5 min at 50°C, and 1.5 min at 72°C, and a final extension at 72°C for 10 min. Duplicate PCR products for each sample were pooled and purified using QIAquick Gel Extraction Kit (QIAGEN, Germany). The resulting 69 amplicon libraries were quantified using Qubit 3 (Invitrogen, United States) and pooled at 5 ng per library. Illumina paired-end (2 × 250 bp) MiSeq sequencing was performed at Duke Center for Genomic and Computational Biology. Raw sequences were deposited under the NCBI BioProject PRJNA437132.

Processing of Labyrinthulomycete 18S rRNA Gene Sequences

In order to integrate this study with a previous study examining 3 years of nearshore (station A) weekly samples, the amplicon sequences generated in this study were processed after pooling with those described previously (Xie et al., 2021). Raw sequences were demultiplexed using CASAVA software (Illumina) and trimmed when the average Q < 25 in a 10-bp running window. The trimmed paired-end sequences were joined when they had a ≥10 bp overlap with ≤3 mismatches. Then, the Deblur workflow (Amir et al., 2017) was performed in QIIME 2 (Bolyen et al., 2019) to denoise the joined sequences and resolve amplicon sequence variants (ASVs), using "silva_132_99_18S.fna"[1] as the positive filtering database, with "sequence trim length" set as 380 bp and other parameters set to default values (e.g., retaining only ASVs appearing ≥10 times across all libraries). The resulting ASVs were annotated by the BLAST+ consensus taxonomy classifier (Camacho et al., 2009) against the SILVA database, and those not belonging to the class Labyrinthulomycetes were removed from downstream analyses. Libraries were rarified to 10,857 sequences.

Characterization of Labyrinthulomycete Communities

Amplicon sequence variant richness, Pielou's evenness, and Shannon's diversity of each rarified library were calculated in USEARCH 10 (Edgar, 2010). The dynamics of these α-diversity indexes as well as the total Labyrinthulomycete 18S rRNA gene abundance across stations was compared using one-way ANOVA and *post hoc* Tukey's HSD test, and their relationships with environmental gradients were explored using principal component analysis (PCA) and pairwise correlation test. Before performing PCA, variables were filtered to exclude collinearity at the threshold of $R = 0.9$ and then normalized; a few samples with >3 missing values were excluded; and the remaining few missing values were replaced with the mean. Non-metric multidimensional scaling (NMDS) ordination based on Bray–Curtis dissimilarity was applied to evaluate the variation in ASV composition of the Labyrinthulomycetes, and differences between stations were tested by PERMANOVA after equal dispersion was identified. Environmental parameters without missing values were input for a stepwise selection based on Akaike information criterion, using canonical correlation analysis (CCA), to find constrained parameters that were potentially associated with the Labyrinthulomycete composition. The Canoco 5 software was used to evaluate the explanatory power of each parameter to the overall community variability in terms of conditional effects and check the statistical significance by partial Monte Carlo permutation tests (999 permutations) and Benjamini–Hochberg false discovery rate correction (Benjamini and Hochberg, 1995; Verhoeven et al., 2005; Šmilauer and Lepš, 2014). And these selected key environmental parameters were finally fitted onto the NMDS plot to demonstrate their relationships with the Labyrinthulomycete composition.

[1]https://www.arb-silva.de/download/archive/qiime/

To obtain detail insights into the distribution patterns of different Labyrinthulomycete taxa, the most abundant 100 ASVs were extracted based on relative abundances, and their absolute 18S rRNA gene abundances were estimated by multiplying the total Labyrinthulomycete 18S rRNA gene abundance in the seawater. Potential biomarkers for nearshore, shelf, and offshore habitats among these ASVs were identified by LEfSe analyses, in which all-against-all (more-strict) and one-against-all (less-strict) strategies were performed for multiclass analysis, and alpha values for the factorial Kruskal–Wallis test among classes <0.05 and logarithmic LDA scores >2 were considered as significant (Segata et al., 2011; Afgan et al., 2018). A maximum likelihood tree for the 100 most abundant ASVs was constructed in MEGA 7, using the automatically selected best-fit substitution model, after the sequences were aligned with MUSCLE and curated manually (Kumar et al., 2016). Both the relative abundance and the estimated absolute abundance of these ASVs were illustrated in heatmaps, with the environmental samples clustered by Ward's hierarchical agglomerative method (Ward, 1963; Murtagh and Legendre, 2014) and the ASVs ordered following the phylogenetic tree. Environmental affiliations (location and temperature) and LEfSe associations were labeled on samples and ASVs, respectively. Pairwise Spearman correlation coefficients (ρ) between the estimated absolute abundances of the 100 most abundant ASVs and environmental parameters were calculated, and the significant correlations with adjusted p (Benjamini–Hochberg false discovery rate) < 0.05 were visualized by heatmap, with ASVs and environmental parameters both clustered by Ward's hierarchical method and the ASVs labeled with taxonomic affiliations. Typical distribution patterns of specific ASVs across the stations and the temperature gradient were demonstrated using the ggplot2 R package.

Construction of Microbial Correlation Networks

To discover potential relationships between Labyrinthulomycetes and other microbes in the coastal ocean, we obtained the relative abundances of prokaryotic/chloroplast 16S rRNA gene and fungal internal transcribed spacer (ITS) amplicon library data sets for the corresponding samples, and picked the most abundant (relative abundance >0.1%) and prevalent (present in >10% libraries) phylotypes of the Labyrinthulomycetes, fungi, eukaryotic algae, cyanobacteria, and heterotrophic bacteria for the correlation analysis. With environmental data integrated with the relative abundances, the pairwise Spearman's rank correlation coefficients (ρ) were calculated, and the strong correlations with $|\rho| > 0.6$ and adjusted p (Benjamini–Hochberg false discovery rate) < 0.05 were visualized in a network using Gephi (Bastian et al., 2009).

RESULTS AND DISCUSSION

Spatial Variations in Total Abundance and Diversity Metrics

We investigated the Labyrinthulomycete abundance and diversity across the PICO-LOVE coastal ocean transects (**Figure 1**;

Supplementary Table S1) and maintained consistency with previous studies (Wang et al., 2019; Duan et al., 2021) in grouping of stations: nearshore (station A), shelf (stations B and C), and offshore (stations D and E). The total abundance of the Labyrinthulomycete 18S rRNA genes varied from 2.02×10^3 to 3.68×10^5 copies per liter seawater (**Figure 2A**), representing a typical range in coastal waters where their biomass comprises a significant fraction of heterotrophic communities (Liu et al., 2017, 2019; Bai et al., 2019). Their abundance exhibited a sharp decrease from the nearshore station A to the shelf and offshore stations B–E (ANOVA, $p < 10^{-4}$; Turkey, $p < 0.005$), but no significant differences were identified between stations B–E (Turkey, $p > 0.05$; **Figure 2A**). Similar trends were observed in bacterial and fungal abundances, suggesting a consistent control by sharp coastal gradients (e.g., primary production and resource availability) from nearshore to offshore waters (Wang et al., 2019; Duan et al., 2021). Several cruises in the coastal waters off Japan and northern China also found the Labyrinthulomycetes more abundant at stations closer to the shore or estuaries (Kimura et al., 1999; Ueda et al., 2015; Xie et al., 2018; Duan et al., 2018a). Here we confirm this pattern by sufficient repeated transects and compare and contrast spatial distributions with those of the bacteria and fungi over a larger longitudinal scale from the coast to the open ocean.

Similar to their total 18S rRNA gene abundance, the Labyrinthulomycete ASV richness was significantly higher at the nearshore station A than the other four stations (ANOVA, $p < 10^{-7}$; Turkey, $p < 10^{-4}$; **Figure 2B**). It resembles the richness pattern of bacteria (Wang et al., 2019) but differs from that of fungi, which did not show an obvious spatial variation (Duan et al., 2021). While not significantly different (ANOVA/Turkey, $p > 0.05$), the Labyrinthulomycete Shannon's diversity

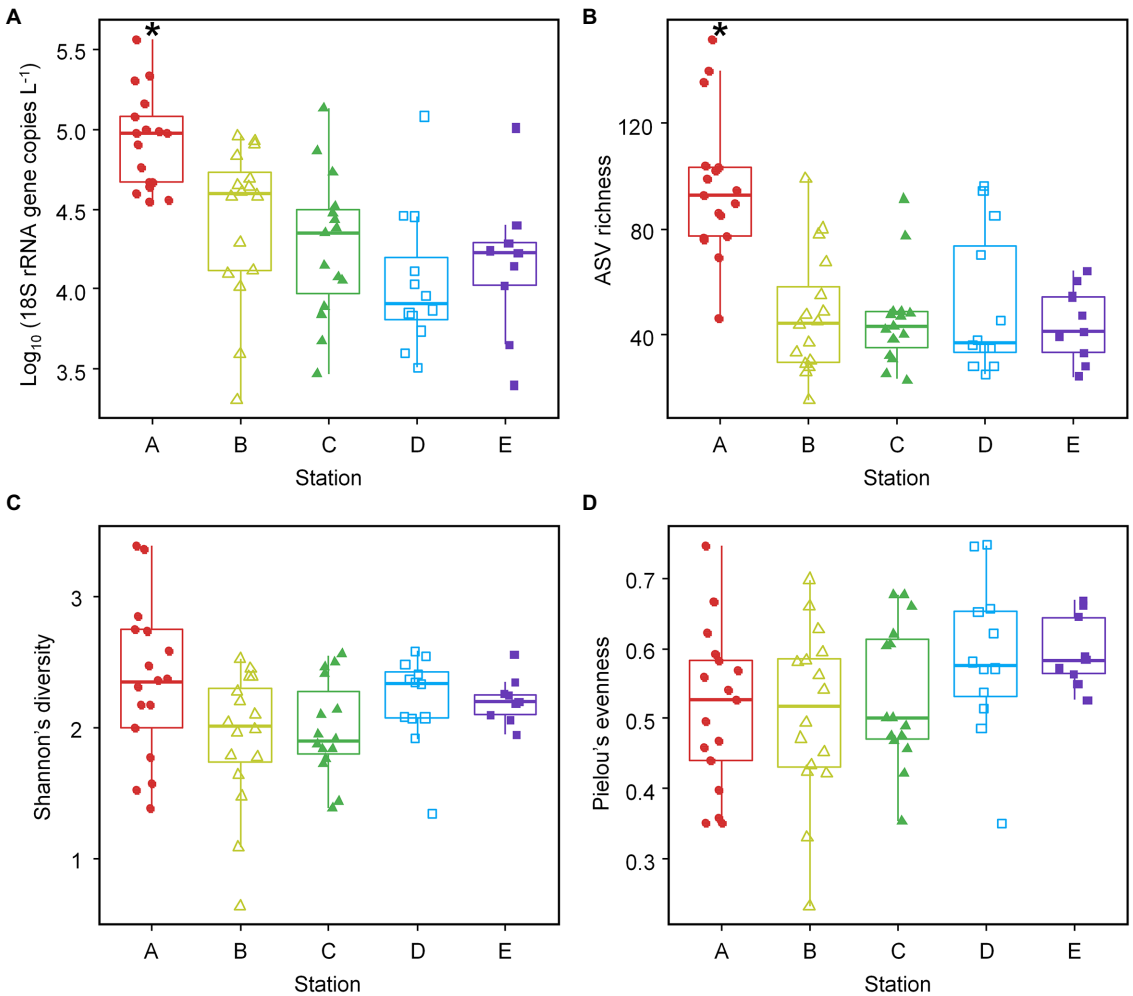

FIGURE 2 | Total abundance of the Labyrinthulomycete 18S rRNA genes **(A)** and their ASV richness **(B)**, Shannon's diversity **(C)**, and Pielou's evenness **(D)** across the nearshore-to-offshore stations (stations A–E). The box for each sampling site represents the 25th and 75th percentiles of its temporal variation; the horizontal line within the box represents the median value; the whiskers represent the lowest and highest values (excluding the outliers); the jittered shapes represent individual sample values. The asterisks above the boxes for the abundance and richness at the nearshore station A indicate statistically higher values than those at the other four stations (ANOVA, $p < 0.05$).

appeared higher at the nearshore station A and offshore stations D and E but lower for the shelf stations B and C (**Figure 2C**). This U-shaped pattern was more evident in bacteria and fungi, although bacterial Shannon's diversity was low at station D (Wang et al., 2019; Duan et al., 2021). Moreover, compared to the nearshore and shelf stations A–C, the Pielou's evenness of Labyrinthulomycete communities at the offshore stations D and E appeared higher (**Figure 2D**), which contributed to higher offshore Shannon's diversity. It contrasts the nearshore Labyrinthulomycetes whose richness and Shannon's diversity were both high, while evenness was low, which could be due to temporally variable environmental conditions and diverse, plentiful resources derived from both terrestrial and autochthonous origins (Waide et al., 1999; Gibbons et al., 2016). In contrast, higher evenness and Shannon's diversity for the offshore Labyrinthulomycetes could be attributed to the more constant environmental conditions and variable influence of the Gulf Stream (Martin-Platero et al., 2018). However, differential patterns in richness and evenness leave open questions regarding their ecological drivers and mechanisms.

To further examine these spatial patterns of abundance and diversity in the context of complex environmental gradients, we performed PCA and correlation tests with environmental metadata. Although environmental variables have been filtered to exclude strong collinearity at the threshold of $R = 0.9$, the PCA ordination provides an overview for the nonlinear and intercorrelated environmental gradients across the nearshore to the open ocean, which are represented by the first principal component (PC1; **Figure 3**). The nearshore station A exhibited high chlorophyll *a* concentration and abundances of picophotoeukaryotes, bacteria, and fungi, as well as high Labyrinthulomycete abundance and richness; this station clearly separates from the other four stations in environmental conditions (**Figure 3**). Pearson coefficients also indicate extensive correlations between these variables and the abundance and richness of Labyrinthulomycetes; the strongest associations of the total Labyrinthulomycete 18S rRNA gene abundance and their ASV richness are with fungal abundance ($R = 0.654$, $p < 10^{-7}$, $N = 59$) and picoeukaryotic phytoplankton abundance ($R = 0.704$, $p < 10^{-8}$, $N = 57$), respectively (**Supplementary Table S2**). The Labyrinthulomycete Shannon's diversity also shows significant correlations with fungal abundance ($R = 0.486$, $p < 10^{-4}$, $N = 59$) and other parameters (**Supplementary Table S2**). But these microbial indexes' correlations mainly reflect co-peaks at the coast, as most (except between Labyrinthulomycete richness and picoeukaryotic phytoplankton abundance) became insignificant when excluding the data of the nearshore station A (**Supplementary Table S3**). Their Pielou's evenness, however, was most associated with temperature ($R = 0.366$, $p < 0.005$, $N = 69$), which was generally higher in the offshore waters as well (**Supplementary Table S2**; **Figure 3**). While we are not able to disentangle direct or indirect drivers for the Labyrinthulomycete abundance and diversity metrics, their distribution across the two groups of environmental gradients (PC1 and PC2 in **Figure 3**) can provide guidance for future laboratory examinations through mesocosm manipulations to resolve the true environmental drivers (**Figure 3**).

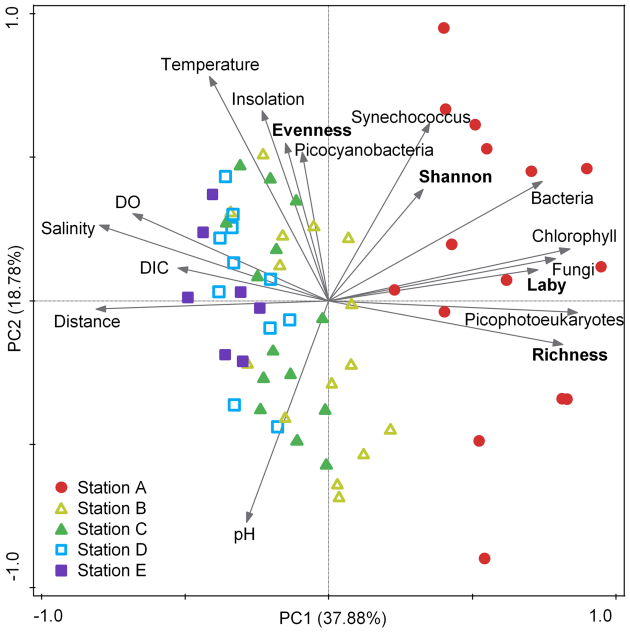

FIGURE 3 | Principal component analysis (PCA) ordination for the environmental gradients with the Labyrinthulomycete abundance (Laby) and diversity metrics (richness, evenness, and Shannon's). Taxonomic labels indicate abundances of corresponding groups as measured using flow cytometry (bacteria, picocyanobacteria, *Synechococcus*, and picophotoeukaryotes) or qPCR (Labyrinthulomycetes and fungi). Temperature: seawater temperature; DO: dissolved oxygen saturation; DIC: dissolved inorganic carbon; chlorophyll: chlorophyll *a*; Distance: distance from the shore; insolation: daily blue-sky insolation, which indicates the sampling date of the year.

Community Structure and Key Environmental Factors

NMDS ordination resolved Labyrinthulomycete communities into three significantly different groups (PERMANOVA, $p < 0.05$): the nearshore communities at the station A, the shelf communities at the stations B and C, and the offshore communities at the stations D and E (**Figure 4**; **Supplementary Table S4**). It is consistent with the pattern in the bacteria across the same transects (Wang et al., 2019), but different from that in the fungi, which did not show significant difference beyond separation of the nearshore communities, e.g., station A (Duan et al., 2021). Similar to both the bacteria and fungi, however, the Labyrinthulomycete communities at all stations exhibited statistically equal dispersion (betadisper, $p > 0.05$; **Supplementary Figure S1**), despite decreasing environmental variabilities from nearshore to offshore stations (**Figure 3**). Environmental changes have long been regarded as a major driver for microbial community variability (Zhou and Ning, 2017). Given the measured environmental parameters are less variable offshore, the obvious community variability can be attributed to the temporally variable influence of the Gulf Stream, which introduces waters with distinct environmental histories (Martin-Platero et al., 2018). Alternatively, offshore microbiomes might possess high sensitivity to minor environmental variability (Wang et al., 2019, 2021).

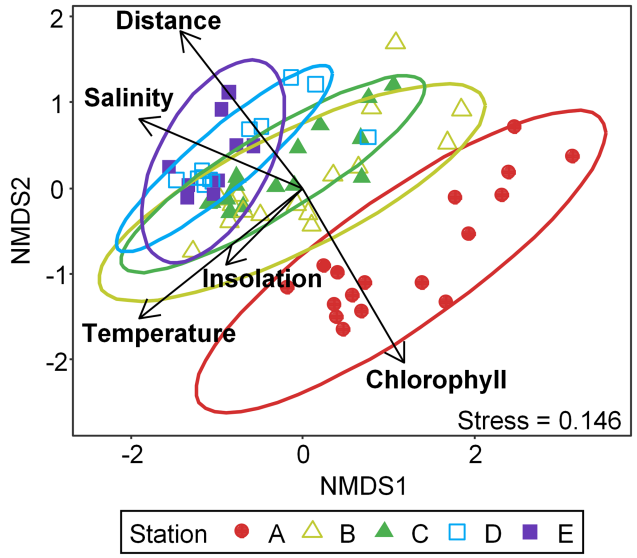

FIGURE 4 | Non-metric multidimensional scaling (NMDS) ordination based on Bray–Curtis dissimilarity of Labyrinthulomycete composition, fitted with the significant environmental factors (assessed by permutation tests in constrained ordination; $p < 0.01$). Temperature: seawater temperature; Chlorophyll: chlorophyll *a*; Distance: distance from the shore; insolation: daily blue-sky insolation, which indicates the sampling date of the year. PERMANOVA tests identified significant dissimilarities ($p < 0.05$) between the nearshore (station A), shelf (stations B and C), and offshore (stations D and E) communities.

Meanwhile, CCA identified temperature, salinity, distance from shore, daily blue-sky insolation, chlorophyll *a* as significant environmental factors for the Labyrinthulomycete composition in terms of conditional effects (999 permutations, $p < 0.01$; **Figure 4**; **Supplementary Table S5**). These parameters may serve as direct ecological drivers or proxies for unmeasured factors. For example, temperature has been reported as an important factor for the Labyrinthulomycete composition in previous studies, potentially through regulating metabolic activities and interactions between taxa (Ueda et al., 2015; Bai et al., 2019). The significant relationship of their composition with salinity (a good indicator for inputs of terrestrial materials) and chlorophyll *a* supports the hypothesis that some phylotypes mainly use terrestrial-derived organic matter, while others mainly use phytoplankton-derived resources, aligning with multiple trophic modes found in cultured Labyrinthulomycete strains (Raghukumar, 1992, 2002; Wong et al., 2005; Rubin et al., 2017; Duan et al., 2018b; Hamamoto and Honda, 2019). Distance from shore and insolation can function as indicators of the spatial and temporal (seasonal) patterns, respectively, but the light can also mediate heterotrophic communities by regulating quantity and quality of primary production. Using the same statistical examination at the same significance threshold as used for the bacteria and fungi, the community composition of the Labyrinthulomycetes is found to be associated with a broader range of environmental factors than that of bacteria and fungi, suggesting differential ecology (e.g., more niche partitioning) of this heterotrophic protistan group.

Differential Distribution Patterns Across Phylotypes

To investigate distribution patterns for phylotypes within the Labyrinthulomycetes, we use heatmaps to visualize the spatiotemporal variations of the 100 most abundant ASVs, which account for 95.87% of the total Labyrinthulomycete sequences. Both heatmaps for the relative (**Supplementary Figure S2**) and estimated absolute (**Figure 5**) abundances show similar patterns. Clearly, there are several universal or highly prevalent ASVs in the Labyrinthulomycetes (**Figure 5**); this pattern is more common in the bacteria but rarer in the fungi (Wang et al., 2019; Duan et al., 2021). Importantly, as the dominant phylotype, the aplanochytrid ASV1 appears in every library and represents 36.01% of the Labyrinthulomycete sequences (**Supplementary Figure S3**). This ASV also dominates the nearshore weekly time-series (PICO) communities, persisting all year round a peak in summer (**Supplementary Figure S3**). Other universal phylotypes include the unclassified Labyrinthulomycetes ASV2 and ASV4, which appear in >90% libraries and account for 9.45% and 4.86% of total sequences, respectively (**Supplementary Figure S3**). Unlike the bacterial OTUs in the same transects, whose abundances vary with habitats and seasons but can generally be detected in more than half of the libraries (Wang et al., 2019), only 18 of the 100 most abundant Labyrinthulomycete ASVs are detected in >50% libraries. Nevertheless, the Labyrinthulomycete ASVs are not as patchy as fungal OTUs; only one of the fungal OTUs are detected in >50% libraries from the same transects (Duan et al., 2021). Previous nearshore time-series observations have identified the Labyrinthulomycetes consisting of a few persistent ASVs and many short-blooming ASVs, whose annual patterns resemble that of bacteria and fungi, respectively. Here we reveal their distribution patterns in a larger spatial scale as either the more-prevalent (but with environmental preferences), bacterial-like patterns or the more-patchy, fungal-like patterns.

Similar to the bacterial and fungal communities, the Labyrinthulomycete communities are significantly structured by nearshore-to-offshore environmental gradients and water temperature; these patterns are evident in the NMDS ordination (**Figure 4**) as well as by the heatmap clustering (**Supplementary Figure S2**; **Figure 5**). Based on the relative abundance of the 100 most abundant Labyrinthulomycete ASVs, LEfSe identifies a number of biomarkers for specific locations (**Supplementary Figure S2**). Due to the overall higher total Labyrinthulomycete 18S rRNA gene abundance in the nearshore waters, when focusing on the estimated absolute abundances of the 100 most abundant ASVs, more nearshore but fewer offshore biomarkers can be identified (i.e., 13 nearshore and five offshore biomarkers using the more-strict, all-against-all strategy for multiclass analysis; 36 nearshore, seven shelf, and 18 offshore biomarkers using the less-strict, one-against-all strategy; **Figure 5**). As expected, the nearshore biomarkers are also abundant, while the offshore biomarkers are rare in the PICO time series (**Supplementary Figure S4**), supporting strong habitat segregation for these taxa. The differential nearshore or offshore preference within the Labyrinthulomycetes has also been reported for the culturable strains in the estuarine and coastal waters of Japan (Ueda et al., 2015). Over recent decades,

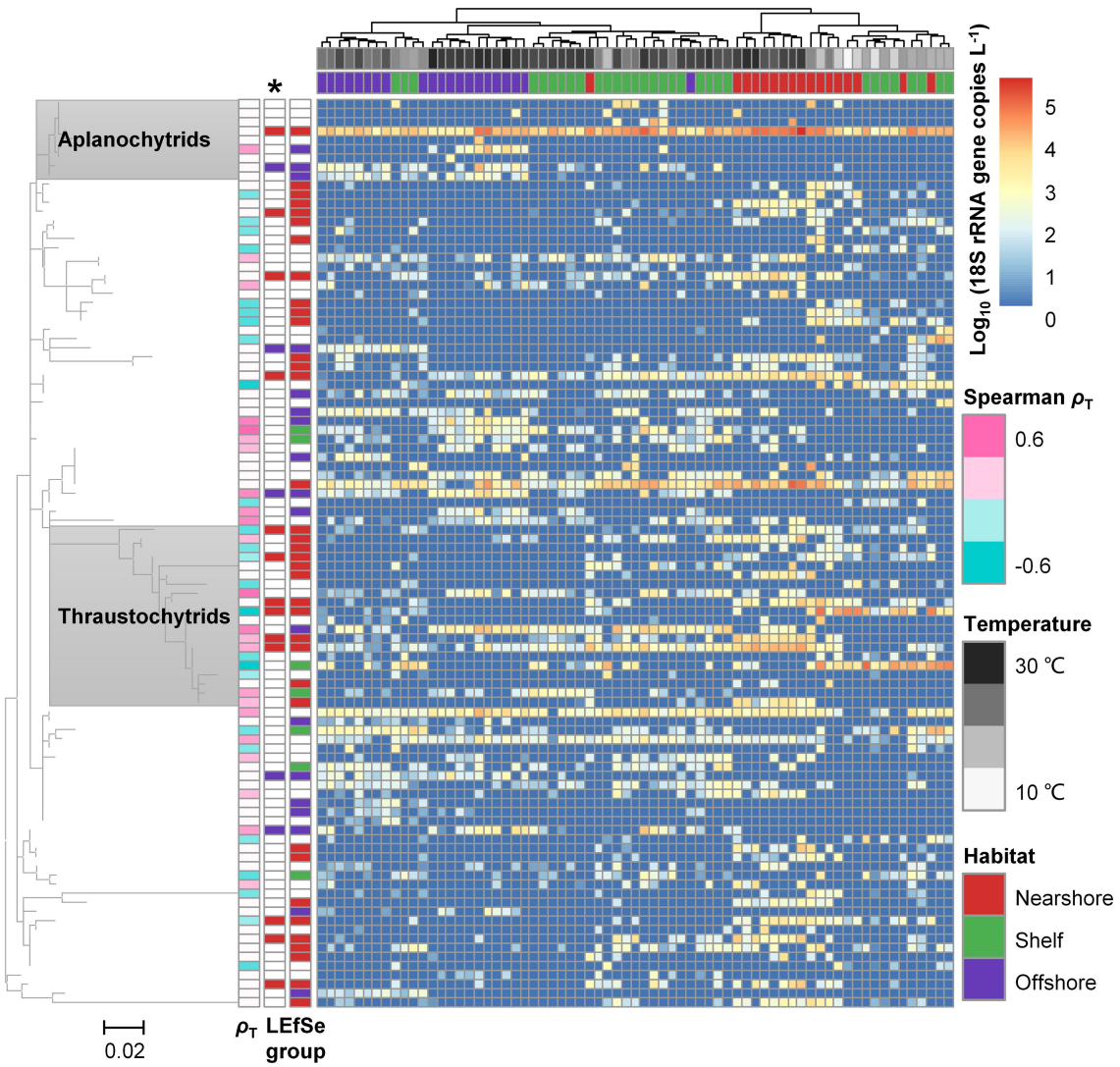

FIGURE 5 | Heatmap showing the estimated absolute 18S rRNA gene abundance variations and putative habitat preferences (assessed by LEfSe) of the 100 most abundant Labyrinthulomycete ASVs. The ASVs (rows) are organized by a maximum likelihood phylogenetic tree with the dominant and well-classified clades (aplanochytrids and thraustochytrids) labeled. Samples (columns) are clustered by similarity using Ward's hierarchical agglomerative method and labeled with water temperature and sampling locations (nearshore station A, shelf stations B and C, and offshore stations D and E). The LEfSe affiliation columns with and without the asterisk above indicate all-against-all (more-strict) and one-against-all (less-strict) strategies performed for multiclass analysis, respectively. The ASVs are also annotated by Spearman correlation coefficients (ρ_T) with water temperature when the correlations are significant (adjusted $p < 0.05$); the blank squares indicate the correlations are not significant (adjusted $p > 0.05$).

a series of field and laboratory studies have revealed the Labyrinthulomycetes as important decomposers in the nearshore eutrophic ecosystems (e.g., estuaries, mangroves, sediments, and polluted seawater; Coleman and Vestal, 1987; Raghukumar et al., 1994; Bremer and Talbot, 1995; Bongiorni et al., 2005; Wong et al., 2005; Damare and Raghukumar, 2006; Taoka et al., 2009; Nagano et al., 2011; Raghukumar and Damare, 2011; Liu et al., 2017; Xie et al., 2018; Bai et al., 2019), but few efforts have investigated the prevalence and spatial partitioning of this group in the oligotrophic open ocean (Damare and Raghukumar, 2008; Bai et al., 2021). Our repeated transects from the nearshore to the open ocean, however, identify diverse offshore-associated phylotypes with high absolute abundances (**Figure 5**), suggesting their potential importance in the oligotrophic marine ecosystems. Beyond the distinct habitat partitioning, as with the bacteria and fungi, the Labyrinthulomycete ASVs also show differential sensitivities and responses to temperature and other seasonal environmental factors (**Figure 5**; **Supplementary Figure S5**). For example, there are 23 and 25 ASVs showing positive and negative correlations with temperature (Spearman, adjusted $p < 0.05$), respectively, suggesting their potential preferences to either warm or cold environments; however, the other 52 of the 100 most abundant ASVs are statistically either insensitive or

non-monotonically correlated to the temperature (Spearman, adjusted $p > 0.05$; **Figure 5**). In our data set, the temperature mainly serves as a proxy of seasonality but also somewhat relies on locations (e.g., it never gets below 22°C offshore). Correlations between a broader range of environmental parameters and the 100 most abundant Labyrinthulomycete ASVs can provide insights to take home in potential associations (**Supplementary Figure S5**), but future work is still in need to resolve the true environmental drivers.

With the heatmap phylotypes arranged by a tree, we can see the distribution patterns of the 100 most abundant ASVs are somewhat associated with their phylogeny, but partitioning still exists between closely related taxa (**Figure 5**; **Supplementary Figure S2**). For example, most thraustochytrid ASVs are more abundant nearshore, with several ASVs completely absent from the offshore stations (**Figure 5**; **Supplementary Figure S2**). It aligns with the fact that existing culturable thraustochytrid strains are mostly isolated from coastal, especially nearshore habitats (Liu et al., 2014). Nevertheless, the thraustochytrid ASV6 are more abundant offshore and ASV3 and ASV16 appear more abundant at the shelf stations, suggesting their distinct habitat preference from the nearshore-associated thraustochytrids (**Supplementary Figure S3**). Unlike the thraustochytrids, most of the aplanochytrid ASVs, except the universal but nearshore-associated ASV1, are either patchily distributed or exclusively prevalent in offshore waters (**Figure 5, Supplementary Figure S2**). These ASVs are absent or only present as transient blooms in the PICO time series (**Supplementary Figure S4**). Our findings in the PICO-LOVE transects suggest differential causes for the nearshore "blooming" populations, i.e., they could be spatially patchy and detected as "blooms" in the time series, or they could be prevalent in offshore waters and captured occasionally at the nearshore. Additionally, most of the thraustochytrid ASVs show strong but partitioning associations to either warm or cold environment (**Figure 5**), as observed in the PICO time series (**Supplementary Figure S4**). In contrast, the aplanochytrid ASVs are generally less correlated with temperature and other seasonal factors (**Figure 5, Supplementary Figure S5**). But notably, a couple of aplanochytrid ASVs, which are abundant across different locations, only appear within narrow temperature ranges (e.g., 26.8–28.5°C for ASV25 and 27.0–30.1°C for ASV18; **Supplementary Figure S3**), suggesting their high-temperature specialization.

Correlations With Other Marine Microbes

Previous culture-based studies have observed Labyrinthulomycete's interactions with bacteria, algae, and other marine organisms in multifarious ways such as competition, decomposition, predation, parasitism, and symbiosis (Raghukumar, 1992, 2002; Sharma et al., 1994; Ralph and Short, 2002; Stokes et al., 2002; Raghukumar and Damare, 2011; Rubin et al., 2017; Hamamoto and Honda, 2019), but their overall roles and how extensively they participate in the marine microbial food webs remain to be inferred from integrative microbial communities. In this study, the concurrently sequenced amplicons of the Labyrinthulomycete 18S rRNA genes, the prokaryotic/chloroplast 16S rRNA genes, and the fungal internal transcribed spacer (ITS) provide ideal data sets for investigating their putative associations with other major components in the coastal microbiomes. To avoid false relationships between rare or sporadic taxa, we focus on the strongest pairwise correlations (Spearman, $|\rho| > 0.6$, adjusted $p < 0.05$) between the most abundant (relative abundance >0.1%) and meanwhile prevalent (present in >10% of libraries) phylotypes from these three amplicon library data sets. The results show the bacterial OTUs are largely intercorrelated as cohesive communities, but the fungal OTUs mostly co-occur with just a couple of other phylotypes (**Figure 6**). In the correlation network, several Labyrinthulomycete ASVs show extensive correlations with, and similar patterns to, the cohesive bacterial OTUs, while the other ASVs show few connections (**Figure 6A**). Within the phototrophs, a few cyanobacteria and eukaryotic algae (chloroplasts) dominate the correlations with the heterotrophic bacteria and Labyrinthulomycetes (**Figure 6A**), indicating their potential role as foundational primary producers with strong spatial patterns. These correlations may represent either direct interactions between taxa or their common responses to environmental gradients. Nevertheless, strong correlations also exist between some Labyrinthulomycetes and specific bacteria, fungi, and algae, whose abundances are not related to the measured environmental variables (**Figure 6A**), suggesting their potential interactions.

Most fungal OTUs, as nodes outlying the core of the network, display few linkages with environmental factors but strongly correlated with certain Labyrinthulomycete ASVs, with the average numbers of qualified connections (Spearman, $|\rho| > 0.6$, adjusted $p < 0.05$) from a fungal OTU to Labyrinthulomycetes and environmental factors being 1.3 and 0.2, respectively (**Figure 6A**). Therefore, we expect an additional, simplified network for fungi and Labyrinthulomycetes can provide a clearer picture to compare the two heterotrophic eukaryotic groups and infer their co-occurrence patterns. In this subset of network (**Figure 6B**), temperature, chlorophyll, and distance from shore show partitioning (positive or negative) correlations with different phylotypes of either group, but extensive concurrences are also identified between phylotypes that are not related to the measured, continuous environmental variables. Amongst the 63 Labyrinthulomycete ASVs for the network analysis (relative abundance >0.1%, present in >10% of libraries), one-third (six thraustochytrid ASVs and 15 unclassified Labyrinthulomycete ASVs) are present in less than a quarter of libraries and barely correlated with environmental gradients (Spearman, $|\rho| < 0.6$), suggesting their patchiness in distribution; of them, more than a half (two thraustochytrid ASVs and 10 unclassified Labyrinthulomycete ASVs) show strong correlations (Spearman, $|\rho| > 0.6$, adjusted $p < 0.05$) with specific fungal OTUs. Their concurrences are consistent with the reports that Labyrinthulomycetes and fungi are both enriched in some patchily distributed microhabitats including marine snow and terrestrial detritus (Kimura et al., 2001; Naganuma et al., 2006; Li et al., 2013; Bochdansky et al., 2017). Additionally, we find a number of negative correlations among the Labyrinthulomycete ASVs, but those are absent among fungal OTUs (**Figure 6B**), perhaps due to the higher patchiness of fungi. Unlike

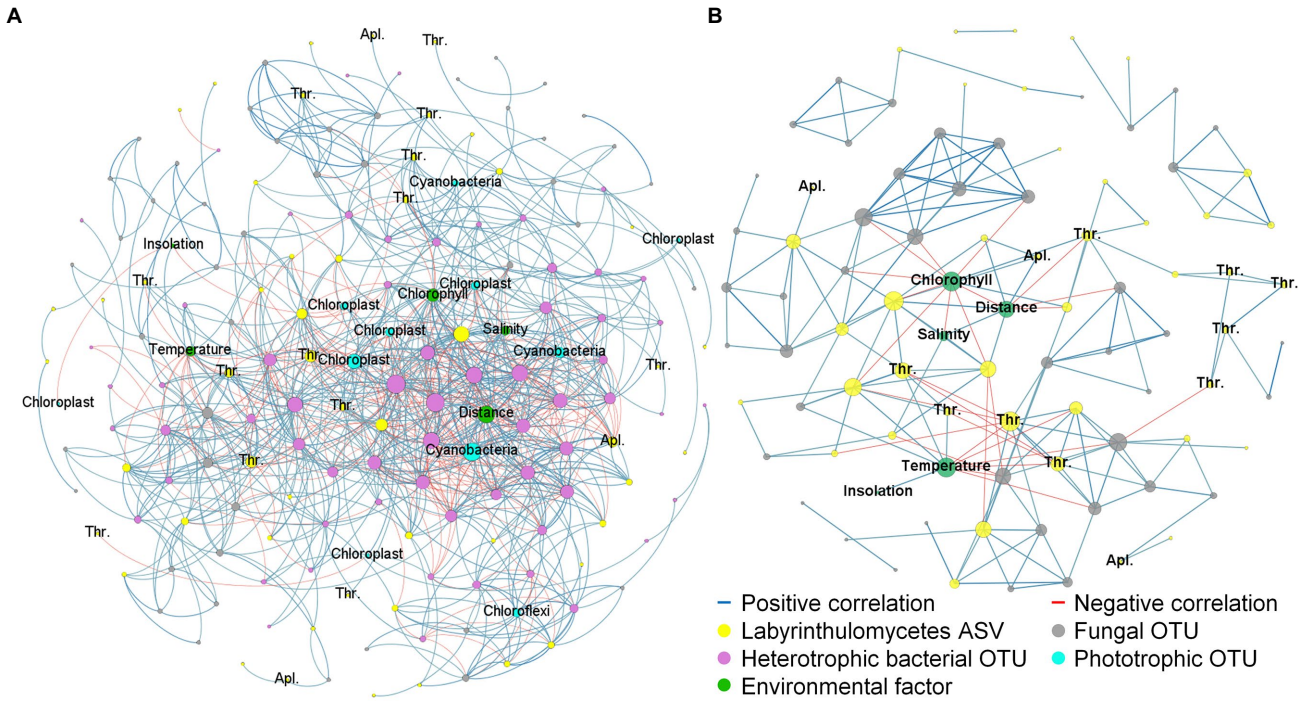

FIGURE 6 | Network **(A)** showing strong Spearman correlations ($|\rho| > 0.6$, adjusted $p < 0.05$) between key environmental factors and the most abundant (relative abundance >0.1%) and meanwhile prevalent (present in >10% libraries) phylotypes from Labyrinthulomycete 18S rRNA gene libraries, fungal ITS libraries, and prokaryotic/chloroplast 16S rRNA gene libraries, attached with a subset of the network **(B)** focusing on concurrences between Labyrinthulomycetes and fungi.

thraustochytrids and many unclassified Labyrinthulomycetes, aplanochytrids seem not related to fungi (**Figure 6B**), suggesting differential ecological roles of this abundant but less-understood genus within the Labyrinthulomycetes. Recent studies show some aplanochytrid strains can prey on living diatoms and facilitate the formation of fast-sinking aggregates (Hamamoto and Honda, 2019), but are also associated with zooplankton (Damare and Raghukumar, 2010), potentially playing a key role in carbon sequestration. Their capability to glide *via* ectoplasmic nets (Leander et al., 2004) and potential to sink as aggregates may strengthen their mobilities and distribution patchiness, potentially resulting in a rapid turnover and difficulties in capturing their dynamics and drivers.

CONCLUSION

Labyrinthulomycetes, as a typical group of marine fungus-like protists, are known to possess high biomass and diversity in the coastal oceans, but have long been neglected, like many of other heterotrophic microeukaryotes, in the marine microbial food webs and biogeochemical models. Despite a limited number of cultured Labyrinthulomycete strains showing diverse trophic modes and associations with other organisms, our understanding of their community structure, environmental associations, and ecological roles remains elusive. Using quantitative PCR and amplicon sequencing, our repeated transect observations reveal their spatiotemporal patterns across the sharp coastal gradients from the nearshore to the open ocean. Their total 18S rRNA gene abundance decreases nearshore to offshore, which is consistent with the spatial patterns of the bacterial and fungal abundances and a range of environmental gradients. Dynamics in their diversity metrics, however, are somewhat different from that of bacteria and fungi, indicating differential drivers for the three important microbial groups in the coastal ocean. Like the bacterial and fungal communities, the Labyrinthulomycete communities are structured by the nearshore-to-offshore habitats, temperature, and other environmental factors, suggesting potential niche partitioning within this closely related protistan class. Nevertheless, only several Labyrinthulomycete ASVs are as prevalent as bacterial OTUs and have extensive correlations with the cohesive bacterial communities, while more ASVs are as patchy as fungal OTUs and often co-occur with the specific fungi. Overall, this study complements previous time-series observations that resolve the Labyrinthulomycetes as persistent (bacteria-like) and short-blooming (fungi-like) ecotypes, highlighting their partitioning distribution patterns and multifaceted roles in the coastal marine microbial food webs. However, the correlation-based inferences on the biotic/abiotic environmental drivers are largely exploratory and need further verification through manipulating mesocosm studies. To test the universality of ecological patterns identified here, more observations on Labyrinthulomycetes and other heterotrophic microeukaryotes across different coastal regions are also in need. Besides, the significant uncultured diversity

of Labyrinthulomycetes identified in this study suggests that there are significant gaps in our understanding of their physiology and metabolic potential. Future meta-transcriptomic and single-cell techniques may facilitate our understanding to the ecophysiology, biochemistry, and functions of different uncultured Labyrinthulomycete taxa.

DATA AVAILABILITY STATEMENT

Raw sequences were deposited under the NCBI BioProject PRJNA437132.

AUTHOR CONTRIBUTIONS

NX performed conceptualization, formal analysis, funding acquisition, investigation, methodology, visualization, writing—original draft, and writing—review and editing. ZW did methodology, visualization, and writing—review and editing. DH and ZJ were involved in data curation, funding acquisition, methodology, and writing—review and editing. YH done project administration and writing—review and editing. GW did conceptualization, funding acquisition, methodology, and writing—review and editing. All authors contributed to the article and approved the submitted version.

FUNDING

This work was financially supported by NSFC (32170063) and National Key R&D Program of China (2016YF0601401) to GW, a US-NSF grant (OCE: 14-16665) to DH and ZJ, and a CSC scholarship (201806250109) to NX.

ACKNOWLEDGMENTS

We acknowledge Doris L. Juarez and Sara K. Blinebry for help with measuring environmental parameters. We also appreciate Thomas Schultz's assistance in sharing the qPCR instrument.

SUPPLEMENTARY MATERIAL

The Supplementary Material for this article can be found online at: https://www.frontiersin.org/articles/10.3389/fmicb.2022.906864/full#supplementary-material

REFERENCES

Afgan, E., Baker, D., Batut, B., van den Beek, M., Bouvier, D., Čech, M., et al. (2018). The galaxy platform for accessible, reproducible and collaborative biomedical analyses: 2018 update. *Nucleic Acids Res.* 46, W537–W544. doi: 10.1093/nar/gky379

Amir, A., McDonald, D., Navas-Molina, J. A., Kopylova, E., Morton, J. T., Zech Xu, Z., et al. (2017). Deblur rapidly resolves single-nucleotide community sequence patterns. *mSystems* 2:e00191. doi: 10.1128/mSystems.00191-16

Azam, F., and Malfatti, F. (2007). Microbial structuring of marine ecosystems. *Nat. Rev. Microbiol.* 5, 782–791. doi: 10.1038/nrmicro1747

Bai, M., Sen, B., Wang, Q., Xie, Y., He, Y., and Wang, G. (2019). Molecular detection and spatiotemporal characterization of Labyrinthulomycete protist diversity in the coastal waters along the Pearl River Delta. *Microb. Ecol.* 77, 394–405. doi: 10.1007/s00248-018-1235-8

Bai, M., Xie, N., He, Y., Li, J., Collier, J. L., Hunt, D. E., et al. (2021). Vertical community patterns of Labyrinthulomycetes protists reveal their potential importance in the oceanic biological pump. *Environ. Microbiol.* 24, 1703–1713. doi: 10.1111/1462-2920.15709

Bastian, M., Heymann, S., and Jacomy, M. (2009). Gephi: an open source software for exploring and manipulating networks. *Proceedings of the International AAAI Conference on Web and Social Media* 3, 361–362. doi: 10.13140/2.1.1341.1520

Bauer, J. E., Cai, W.-J., Raymond, P. A., Bianchi, T. S., Hopkinson, C. S., and Regnier, P. A. G. (2013). The changing carbon cycle of the coastal ocean. *Nature* 504, 61–70. doi: 10.1038/nature12857

Benjamini, Y., and Hochberg, Y. (1995). Controlling the false discovery rate: a practical and powerful approach to multiple testing. *J. R. Stat. Soc. Ser. B Methodol.* 57, 289–300. doi: 10.1111/j.2517-6161.1995.tb02031.x

Bochdansky, A. B., Clouse, M. A., and Herndl, G. J. (2017). Eukaryotic microbes, principally fungi and Labyrinthulomycetes, dominate biomass on bathypelagic marine snow. *ISME J.* 11, 362–373. doi: 10.1038/ismej.2016.113

Bolyen, E., Rideout, J. R., Dillon, M. R., Bokulich, N. A., Abnet, C. C., Al-Ghalith, G. A., et al. (2019). Reproducible, interactive, scalable and extensible microbiome data science using QIIME 2. *Nat. Biotechnol.* 37, 852–857. doi: 10.1038/s41587-019-0209-9

Bong, C. W., and Lee, C. W. (2011). The contribution of heterotrophic nanoflagellate grazing towards bacterial mortality in tropical waters: comparing estuaries and coastal ecosystems. *Mar. Freshw. Res.* 62, 414–420. doi: 10.1071/MF10213

Bongiorni, L., Pusceddu, A., and Danovaro, R. (2005). Enzymatic activities of epiphytic and benthic thraustochytrids involved in organic matter degradation. *Aquat. Microb. Ecol.* 41, 299–305. doi: 10.3354/ame041299

Bouman, H. A., Ulloa, O., Scanlan, D. J., Zwirglmaier, K., Li, W. K. W., Platt, T., et al. (2006). Oceanographic basis of the global surface distribution of *Prochlorococcus* ecotypes. *Science* 312, 918–921. doi: 10.1126/science.1122692

Bremer, G. B., and Talbot, G. (1995). Cellulolytic enzyme activity in the marine protist *Schizochytrium aggregatum*. *Bot. Mar.* 38, 37–42. doi: 10.1515/botm.1995.38.1-6.37

Camacho, C., Coulouris, G., Avagyan, V., Ma, N., Papadopoulos, J., Bealer, K., et al. (2009). BLAST+: architecture and applications. *BMC Bioinformatics* 10:421. doi: 10.1186/1471-2105-10-421

Chafee, M., Fernàndez-Guerra, A., Buttigieg, P. L., Gerdts, G., Eren, A. M., Teeling, H., et al. (2017). Recurrent patterns of microdiversity in a temperate coastal marine environment. *ISME J.* 12, 237–252. doi: 10.1038/ismej.2017.165

Choi, K.-H., Yang, E. J., Kim, D., Kang, H.-K., Noh, J. H., and Kim, C.-H. (2012). The influence of coastal waters on distributions of heterotrophic protists in the northern East China Sea, and the impact of protist grazing on phytoplankton. *J. Plankton Res.* 34, 886–904. doi: 10.1093/plankt/fbs046

Coleman, N. K., and Vestal, J. R. (1987). An epifluorescent microscopy study of enzymatic hydrolysis of fluorescein diacetate associated with the ectoplasmic net elements of the protist *Thraustochytrium striatum*. *Can. J. Microbiol.* 33, 841–843. doi: 10.1139/m87-147

Collado-Mercado, E., Radway, J. C., and Collier, J. L. (2010). Novel uncultivated Labyrinthulomycetes revealed by 18S rDNA sequences from seawater and sediment samples. *Aquat. Microb. Ecol.* 58, 215–228. doi: 10.3354/ame01361

Connell, P. E., Campbell, V., Gellene, A. G., Hu, S. K., and Caron, D. A. (2017). Planktonic food web structure at a coastal time-series site: II. Spatiotemporal variability of microbial trophic activities. *Deep-Sea Res. I Oceanogr. Res. Pap.* 121, 210–223. doi: 10.1016/j.dsr.2017.01.007

Damare, V., and Raghukumar, S. (2006). Morphology and physiology of the marine straminipilan fungi, the aplanochytrids isolated from the equatorial Indian Ocean. *Indian J. Mar. Sci.* 35, 326–340.

Damare, V., and Raghukumar, S. (2008). Abundance of thraustochytrids and bacteria in the equatorial Indian Ocean, in relation to transparent exopolymeric particles (TEPs). *FEMS Microbiol. Ecol.* 65, 40–49. doi: 10.1111/j.1574-6941.2008.00500.x

Damare, V., and Raghukumar, S. (2010). Association of the stramenopilan protists, the aplanochytrids, with zooplankton of the equatorial Indian Ocean. *Mar. Ecol. Prog. Ser.* 399, 53–68. doi: 10.3354/meps08277

Duan, Y., Sen, B., Xie, N., Paterson, J. S., Chen, Z., and Wang, G. (2018a). Flow cytometry for rapid enumeration and biomass quantification of thraustochytrids in coastal seawaters. *Microbes Environ.* 33, 195–204. doi: 10.1264/jsme2.ME17162

Duan, Y., Xie, N., Song, Z., Ward, C. S., Yung, C.-M., Hunt, D. E., et al. (2018b). High-resolution time-series reveals seasonal patterns of planktonic fungi at a temperate coastal ocean site (Beaufort, North Carolina, USA). *Appl. Environ. Microbiol.* 84: e00967-18 doi: 10.1128/aem.00967-18

Duan, Y., Xie, N., Wang, Z., Johnson, Z. I., Hunt, D. E., Wang, G., et al. (2021). Patchy distributions and distinct niche partitioning of mycoplankton populations across a nearshore to open ocean gradient. *Microbiol. Spectr.* 9:e01470-21. doi: 10.1128/Spectrum.01470-21

Edgar, R. C. (2010). Search and clustering orders of magnitude faster than BLAST. *Bioinformatics* 26, 2460–2461. doi: 10.1093/bioinformatics/btq461

Fortunato, C. S., Herfort, L., Zuber, P., Baptista, A. M., and Crump, B. C. (2012). Spatial variability overwhelms seasonal patterns in bacterioplankton communities across a river to ocean gradient. *ISME J.* 6, 554–563. doi: 10.1038/ismej.2011.135

Gao, Z., Johnson, Z. I., and Wang, G. (2009). Molecular characterization of the spatial diversity and novel lineages of mycoplankton in Hawaiian coastal waters. *ISME J.* 4, 111–120. doi: 10.1038/ismej.2009.87

Gibbons, S. M., Scholz, M., Hutchison, A. L., Dinner, A. R., Gilbert, J. A., and Coleman, M. L. (2016). Disturbance regimes predictably alter diversity in an ecologically complex bacterial system. *MBio* 7:e01372-16. doi: 10.1128/mBio.01372-16

Hamamoto, Y., and Honda, D. (2019). Nutritional intake of *Aplanochytrium* (Labyrinthulea, Stramenopiles) from living diatoms revealed by culture experiments suggesting the new prey–predator interactions in the grazing food web of the marine ecosystem. *PLoS One* 14:e0208941. doi: 10.1371/journal.pone.0208941

Heywood, J. L., Sieracki, M. E., Bellows, W., Poulton, N. J., and Stepanauskas, R. (2010). Capturing diversity of marine heterotrophic protists: one cell at a time. *ISME J.* 5, 674–684. doi: 10.1038/ismej.2010.155

Jiao, N., Robinson, C., Azam, F., Thomas, H., Baltar, F., Dang, H., et al. (2014). Mechanisms of microbial carbon sequestration in the ocean – future research directions. *Biogeosciences* 11, 5285–5306. doi: 10.5194/bg-11-5285-2014

Johnson, Z. I., Wheeler, B. J., Blinebry, S. K., Carlson, C. M., Ward, C. S., and Hunt, D. E. (2013). Dramatic variability of the carbonate system at a temperate coastal ocean site (Beaufort, North Carolina, USA) is regulated by physical and biogeochemical processes on multiple timescales. *PLoS One* 8:e85117. doi: 10.1371/journal.pone.0085117

Kimura, H., Fukuba, T., and Naganuma, T. (1999). Biomass of thraustochytrid protoctists in coastal water. *Mar. Ecol. Prog.* 189, 27–33. doi: 10.3354/meps189027

Kimura, H., Sato, M., Sugiyama, C., and Naganuma, T. (2001). Coupling of thraustochytrids and POM, and of bacterio- and phytoplankton in a semi-enclosed coastal area: implication for different substrate preference by the planktonic decomposers. *Aquat. Microb. Ecol.* 25, 293–300. doi: 10.3354/ame025293

Kumar, S., Stecher, G., and Tamura, K. (2016). MEGA7: molecular evolutionary genetics analysis version 7.0 for bigger datasets. *Mol. Biol. Evol.* 33, 1870–1874. doi: 10.1093/molbev/msw054

Leander, C. A., Porter, D., and Leander, B. S. (2004). Comparative morphology and molecular phylogeny of aplanochytrids (Labyrinthulomycota). *Eur. J. Protistol.* 40, 317–328. doi: 10.1016/j.ejop.2004.07.003

Li, Q., Wang, X., Liu, X., Jiao, N., and Wang, G. (2013). Abundance and novel lineages of thraustochytrids in Hawaiian waters. *Microb. Ecol.* 66, 823–830. doi: 10.1007/s00248-013-0275-3

Liu, X., Sen, B., Zhao, Y., Bai, M., He, Y., Xie, Y., et al. (2019). Gradients of three coastal environments off the South China Sea and their impacts on the dynamics of heterotrophic microbial communities. *Sci. Total Environ.* 659, 499–506. doi: 10.1016/j.scitotenv.2018.12.405

Liu, Y., Singh, P., Liang, Y., Li, J., Xie, N., Song, Z., et al. (2017). Abundance and molecular diversity of thraustochytrids in coastal waters of southern China. *FEMS Microbiol. Ecol.* 93:fix070. doi: 10.1093/femsec/fix070

Liu, Y., Singh, P., Sun, Y., Luan, S., and Wang, G. (2014). Culturable diversity and biochemical features of thraustochytrids from coastal waters of southern China. *Appl. Microbiol. Biotechnol.* 98, 3241–3255. doi: 10.1007/s00253-013-5391-y

Martin-Platero, A. M., Cleary, B., Kauffman, K., Preheim, S. P., McGillicuddy, D. J., Alm, E. J., et al. (2018). High resolution time series reveals cohesive but short-lived communities in coastal plankton. *Nat. Commun.* 9:266. doi: 10.1038/s41467-017-02571-4

Massana, R., del Campo, J., Sieracki, M. E., Audic, S., and Logares, R. (2014). Exploring the uncultured microeukaryote majority in the oceans: reevaluation of ribogroups within stramenopiles. *ISME J.* 8, 854–866. doi: 10.1038/ismej.2013.204

Murtagh, F., and Legendre, P. (2014). Ward's hierarchical agglomerative clustering method: which algorithms implement Ward's criterion? *J. Classif.* 31, 274–295. doi: 10.1007/s00357-014-9161-z

Nagano, N., Matsui, S., Kuramura, T., Taoka, Y., Honda, D., and Hayashi, M. (2011). The distribution of extracellular cellulase activity in marine eukaryotes, thraustochytrids. *Mar. Biotechnol.* 13, 133–136. doi: 10.1007/s10126-010-9297-8

Naganuma, T., Kimura, H., Karimoto, R., and Pimenov, N. V. (2006). Abundance of planktonic thraustochytrids and bacteria and the concentration of particulate ATP in the Greenland and Norwegian seas. *Polar Biosci.* 20, 37–45.

Pan, J., Campo, J., and Keeling, P. J. (2017). Reference tree and environmental sequence diversity of Labyrinthulomycetes. *J. Eukaryot. Microbiol.* 64, 88–96. doi: 10.1111/jeu.12342

Raghukumar, S. (1992). Bacterivory - a novel dual role for thraustochytrids in the sea. *Mar. Biol.* 113, 165–169. doi: 10.1007/BF00367650

Raghukumar, S. (2002). Ecology of the marine protists, the Labyrinthulomycetes (thraustochytrids and labyrinthulids). *Eur. J. Protistol.* 38, 127–145. doi: 10.1078/0932-4739-00832

Raghukumar, S., and Damare, V. S. (2011). Increasing evidence for the important role of Labyrinthulomycetes in marine ecosystems. *Bot. Mar.* 54, 3–11. doi: 10.1515/Bot.2011.008

Raghukumar, S., Sharma, S., Raghukumar, C., Sathe-Pathak, V., and Chandramohan, D. (1994). Thraustochytrid and fungal component of marine detritus IV. Laboratory studies on decomposition of leaves of the mangrove *Rhizophora apiculata* Blume. *J. Exp. Mar. Biol. Ecol.* 183, 113–131. doi: 10.1016/0022-0981(94)90160-0

Ralph, P. J., and Short, F. T. (2002). Impact of the wasting disease pathogen, *Labyrinthula zosterae*, on the photobiology of eelgrass *Zostera marina*. *Mar. Ecol. Prog. Ser.* 226, 265–271. doi: 10.3354/meps226265

Rubin, E., Tanguy, A., Pales Espinosa, E., and Allam, B. (2017). Differential gene expression in five isolates of the clam pathogen, quahog parasite unknown (QPX). *J. Eukaryot. Microbiol.* 64, 647–654. doi: 10.1111/jeu.12400

Satinsky, B. M., Smith, C. B., Sharma, S., Landa, M., Medeiros, P. M., Coles, V. J., et al. (2017). Expression patterns of elemental cycling genes in the Amazon River plume. *ISME J.* 11, 1852–1864. doi: 10.1038/ismej.2017.46

Segata, N., Izard, J., Waldron, L., Gevers, D., Miropolsky, L., Garrett, W. S., et al. (2011). Metagenomic biomarker discovery and explanation. *Genome Biol.* 12:R60. doi: 10.1186/gb-2011-12-6-r60

Sharma, S., Raghukumar, C., Raghukumar, S., Sathe-Pathak, V., and Chandramohan, D. (1994). Thraustochytrid and fungal component of marine detritus II. Laboratory studies on decomposition of the brown alga *Sargassum cinereum*. *J. Exp. Mar. Biol. Ecol.* 175, 227–242. doi: 10.1016/0022-0981(94)90028-0

Sherr, E. B., and Sherr, B. F. (1991). Planktonic microbes: tiny cells at the base of the ocean's food webs. *Trends Ecol. Evol.* 6, 50–54. doi: 10.1016/0169-5347(91)90122-E

Šmilauer, P., and Lepš, J. (2014). *Multivariate Analysis of Ecological Data Using CANOCO 5*. Cambridge: Cambridge University Press.

Stokes, N. A., Calvo, L. M. R., Reece, K. S., and Burreson, E. M. (2002). Molecular diagnostics, field validation, and phylogenetic analysis of quahog parasite unknown (QPX), a pathogen of the hard clam *Mercenaria mercenaria*. *Dis. Aquat. Org.* 52, 233–247. doi: 10.3354/dao052233

Taoka, Y., Nagano, N., Okita, Y., Izumida, H., Sugimoto, S., and Hayashi, M. (2009). Extracellular enzymes produced by marine eukaryotes, thraustochytrids. *Biosci. Biotechnol. Biochem.* 73, 180–182. doi: 10.1271/bbb.80416

Taylor, J. D., and Cunliffe, M. (2016). Multi-year assessment of coastal planktonic fungi reveals environmental drivers of diversity and abundance. *ISME J.* 10, 2118–2128. doi: 10.1038/ismej.2016.24

Tréguer, P., Bowler, C., Moriceau, B., Dutkiewicz, S., Gehlen, M., Aumont, O., et al. (2018). Influence of diatom diversity on the ocean biological carbon pump. *Nat. Geosci.* 11, 27–37. doi: 10.1038/s41561-017-0028-x

Ueda, M., Nomura, Y., Doi, K., Nakajima, M., and Honda, D. (2015). Seasonal dynamics of culturable thraustochytrids (Labyrinthulomycetes, Stramenopiles) in estuarine and coastal waters. *Aquat. Microb. Ecol.* 74, 187–204. doi: 10.3354/ame01736

Verhoeven, K. J. F., Simonsen, K. L., and McIntyre, L. M. (2005). Implementing false discovery rate control: increasing your power. *Oikos* 108, 643–647. doi: 10.1111/j.0030-1299.2005.13727.x

Waide, R. B., Willig, M. R., Steiner, C. F., Mittelbach, G., Gough, L., Dodson, S. I., et al. (1999). The relationship between productivity and species richness. *Annu. Rev. Ecol. Syst.* 30, 257–300. doi: 10.1146/annurev.ecolsys.30.1.257

Wang, Z., Juarez, D. L., Pan, J.-F., Blinebry, S. K., Gronniger, J., Clark, J. S., et al. (2019). Microbial communities across nearshore to offshore coastal transects are primarily shaped by distance and temperature. *Environ. Microbiol.* 21, 3862–3872. doi: 10.1111/1462-2920.14734

Wang, Z., Tsementzi, D., Williams, T. C., Juarez, D. L., Blinebry, S. K., Garcia, N. S., et al. (2021). Environmental stability impacts the differential sensitivity of marine microbiomes to increases in temperature and acidity. *ISME J.* 15, 19–28. doi: 10.1038/s41396-020-00748-2

Wang, G., Wang, X., Liu, X., and Li, Q. (2012). "Diversity and biogeochemical function of planktonic fungi in the ocean," in *Biology of Marine Fungi*. ed. C. Raghukumar (Berlin, Heidelberg: Springer Berlin Heidelberg), 71–88.

Ward, J. H. (1963). Hierarchical grouping to optimize an objective function. *J. Am. Stat. Assoc.* 58, 236–244. doi: 10.1080/01621459.1963.10500845

Ward, C. S., Yung, C.-M., Davis, K. M., Blinebry, S. K., Williams, T. C., Johnson, Z. I., et al. (2017). Annual community patterns are driven by seasonal switching between closely related marine bacteria. *ISME J.* 11, 1412–1422. doi: 10.1038/ismej.2017.4

Wong, M. K., Vrijmoed, L. L., and Au, D. W. (2005). Abundance of thraustochytrids on fallen decaying leaves of *Kandelia candel* and mangrove sediments in Futian National Nature Reserve, China. *Bot. Mar.* 48, 374–378. doi: 10.1515/bot.2005.050

Worden, A. Z., Follows, M. J., Giovannoni, S. J., Wilken, S., Zimmerman, A. E., and Keeling, P. J. (2015). Rethinking the marine carbon cycle: factoring in the multifarious lifestyles of microbes. *Science* 347:1257594. doi: 10.1126/science.1257594

Xie, N., Hunt, D. E., Johnson, Z. I., He, Y., and Wang, G. (2021). Annual partitioning patterns of Labyrinthulomycetes reveal their multifaceted role in marine microbial food webs. *Appl. Environ. Microbiol.* 87:e01652-20. doi: 10.1128/aem.01652-20

Xie, N., Sen, B., Song, Z., Zhao, Y., Chen, Z., Shi, W., et al. (2018). High phylogenetic diversity and abundance pattern of Labyrinthulomycete protists in the coastal waters of the Bohai Sea. *Environ. Microbiol.* 20, 3042–3056. doi: 10.1111/1462-2920.14341

Zhang, Y., Zhao, M., Cui, Q., Fan, W., Qi, J., Chen, Y., et al. (2017). Processes of coastal ecosystem carbon sequestration and approaches for increasing carbon sink. *Sci. China Earth Sci.* 60, 809–820. doi: 10.1007/s11430-016-9010-9

Zhou, J., and Ning, D. (2017). Stochastic community assembly: does it matter in microbial ecology? *Microbiol. Mol. Biol. Rev.* 81:e00002-17. doi: 10.1128/mmbr.00002-17

Conflict of Interest: The authors declare that the research was conducted in the absence of any commercial or financial relationships that could be construed as a potential conflict of interest.

Publisher's Note: All claims expressed in this article are solely those of the authors and do not necessarily represent those of their affiliated organizations, or those of the publisher, the editors and the reviewers. Any product that may be evaluated in this article, or claim that may be made by its manufacturer, is not guaranteed or endorsed by the publisher.

frontiers | Frontiers in Marine Science

ORIGINAL RESEARCH
published: 26 May 2022
doi: 10.3389/fmars.2022.923128

Tennessenoid A, an Unprecedented Steroid–Sorbicillinoid Adduct From the Marine-Derived Endophyte of *Aspergillus* sp. Strain 1022LEF

Dong-Lin Zhao[1†], *Hai-Su Wang*[2†], *Li-Wei Gao*[1] *and Peng Zhang*[1*]

[1] Tobacco Research Institute, Chinese Academy of Agricultural Sciences, Qingdao, China, [2] College of Agronomy, Qingdao Agricultural University, Qingdao, China

Marine natural products, characterized by fascinating drug-like functionalities and promising biological activities, are important base materials for innovative drugs and agrochemicals. Chemical investigations of the marine-algal-derived endophytic fungus *Aspergillus* sp. 1022LEF residing in the inner tissue of marine red alga yielded a novel polyketide-terpene hybrid metabolite, namely tennessenoid A (**1**), as well as six known biosynthetic congeners including two steroids, ergosta-4,6,8(14),22-tetraen-3-one (**2**) and (22*E*,24*R*)-3α-ureido-ergosta-4,6,8(14),22-tetraene (**3**), and four sorbicillinoid-based compounds, saturnispol G (**4**), trichodimerol (**5**), and dihydrotrichodimer ethers A and B (**6** and **7**). Their structures were unambiguously determined based on extensive 1D/2D NMR and HRESIMS spectroscopic analyses. Tennessenoid A (**1**) was characterized as an unprecedented steroid–sorbicillinoid adduct *via* a C–C bond, which was rarely-observed in natural products. All of the isolated compounds were evaluated for their antifungal activities against eight plant pathogenetic fungi. **1**, in particular, demonstrated broad-spectrum activities against *Sclerotium rolfsii* Sacc., *Fusarium oxysporum* (Schl.) F.sp *cucumerinum* Owen, *Coniella diplodiella* Petrak et Sydow, *Physalospora piricola* Nose., *Fusarium graminearum* schw., *Alternaria mali* rob., *Colletotrichum orbiculare* Arx., and *Alternaria porri* (E11iott) Cifed., with the inhibition zone diameters ranging from 2 to 7 mm.

Keywords: steroids, sorbicillinoids, marine fungus, *Aspergillus*, antifungal activity

OPEN ACCESS

Edited by:
Shan He,
Ningbo University, China

Reviewed by:
Weiyi Wang,
State Oceanic Administration, China
Tingting Wang,
Ningbo University, China

***Correspondence:**
Peng Zhang
zhangpeng@caas.cn

[†]These authors have contributed equally to this work

Specialty section:
This article was submitted to Aquatic Microbiology, a section of the journal Frontiers in Marine Science

Received: *18 April 2022*
Accepted: *28 April 2022*
Published: *26 May 2022*

Citation:
Zhao D-L, Wang H-S, Gao L-W and Zhang P (2022) Tennessenoid A, an Unprecedented Steroid–Sorbicillinoid Adduct From the Marine-Derived Endophyte of Aspergillus sp. Strain 1022LEF. Front. Mar. Sci. 9:923128. doi: 10.3389/fmars.2022.923128

INTRODUCTION

Natural products, which possessed attractive structures and potent bioactivities, traditionally contributed significantly in the development of new innovative drugs and agrochemicals (Butler, 2005). Since the first broad-spectrum antibiotic agent penicillin has been discovered as early as 1928, the "Golden Age of Antibiotics" was sparked in the last century (Knight et al., 2003; Zhang et al., 2020). From then on, the tendency in searching for new natural-product-based drugs is uptapped. It is estimated that over half (> 60%) of approved therapeutic agents are derived from natural products or their derivatives covering the period 1981 to 2019 (Newman and Cragg, 2020). Among them, microbial natural products, also known as secondary metabolites or specialised metabolites, have played nonnegligible and irreplaceable role (Knight et al., 2003). More than 20,000 microbial natural

products, which offered incomparable chemical diversity with structural complexity and biological potency, have been described (Li et al., 2018a). Nowadays, along with the rapid development of new technologies such as functional genomics, the burgeoning microbial natural products-based drug discoveries for pharmaceutical and agrochemical applications are in a revolutionary period. Meanwhile, in spite of outstanding developments in microbial natural products over the last few years, there is still an insistent necessity for searching for more interesting microbial natural products, especially those from extreme and unexplored environments.

Marine microorganisms are one of the most notable and prolific sources of bioactive natural products (Carroll et al., 2021). Although a large amount of natural products have been discovered from marine microorganisms (Rateb and Ebel, 2011; Zhang et al., 2020), it is a matter of fact that, the trend towards finding new natural products is approaching saturation due to the redundancy of the isolation and characterization of both microorganisms and biosynthetic pathways. Consequently, the discovery of new compounds from unexplored environments has proven to be an alternative strategy for the sake of pursuing for microbial novelty (Soldatou and Baker, 2017). Marine-derived endophytic fungi residing in marine alga and mangroves are extraordinary adapted and metabolically active under extreme environmental conditions, which promote them to produce abundant novel secondary metabolites (El-Bondkly et al., 2021).

As part of our ongoing research on bioactive secondary metabolites from marine-derived endophytic fungi (Zhao et al., 2018; Yuan et al., 2020; Zhao et al., 2020), the fungal strain *Aspergillus* sp. 1022LEF isolated from the inner tissue of the marine red alga *Grateloupia turuturu* was selected for a detailed chemical investigation. A scaled-up fermentation and subsequent chromatographic purification yielded a novel polyketide-terpene hybrid metabolite tennessenoid A (**1**) and six known biosynthetic congeners including two steroids (**2** and **3**) and four sorbicillinoid-based compounds (**4**–**7**) (**Figure 1**). The newly-discovered tennessenoid A (**1**) was characterized as an unprecedented steroid–sorbicillinoid adduct *via* a C–C bond, which was rarely-observed in natural products. Furthermore, compound **1** demonstrated broad-spectrum antifungal activity against eight plant pathogenetic fungi [*Sclerotium rolfsii* Sacc., *Fusarium oxysporum* (Schl.) F.sp *cucumerinum* Owen, *Coniella diplodiella* Petrak et Sydow, *Physalospora piricola* Nose., *Fusarium graminearum* schw., *Alternaria mali* rob., *Colletotrichum orbiculare* Arx., and *Alternaria porri* (E11iott) Cifed.], which highlighted its potential as an antifungal agrochemical in agriculture. Herein we report the isolation, structural elucidation, and antifungal activities of the isolated compounds.

MATERIALS AND METHODS

General Experimental Procedures

Optical rotations data were measured by a Jasco P-1020 digital polarimeter (Jasco, Tokyo, Japan) with MeOH as solvent. UV spectra were obtained on a Shimadzu UV-2700 spectrophotometer (Shimadzu, Kyoto, Japan). NMR spectra were recorded on an Agilent DD2 NMR spectrometer (Agilent Technologies, Santa Clara, CA, United States) operating at 500 MHz for the ^{1}H channel and 125 MHz for the ^{13}C channel. HRESIMS data were acquired on a Waters ACQUITY UPLC I-Class-Vion IMS Q-TOF mass spectrometer (Waters Corp., Massachusetts, U.S.A.). Column chromatography was carried out with silica gel (200–300 mesh, Haiyang Chemical Factory, Qingdao, China), Lobar LiChroprep RP-18 (40–60 μm, Merck, Darmstadt, Germany), and Sephadex LH-20 (Merck). All solvents used for extraction and purification were of analytical grade for column chromatography, or of HPLC grade for HPLC analysis. Precoated silica gel plates were used for thin-layer chromatography (TLC) with detection at 254 nm, while preparative TLC was performed with precoated TLC plates (GF_{254}, Haiyang Chemical Factory).

Fungal Material

Following standard procedures (Li et al., 2018b), the endophytic fungal strain 1022LEF was isolated from the inner tissue of the marine red alga *Grateloupia turuturu*, which was collected from

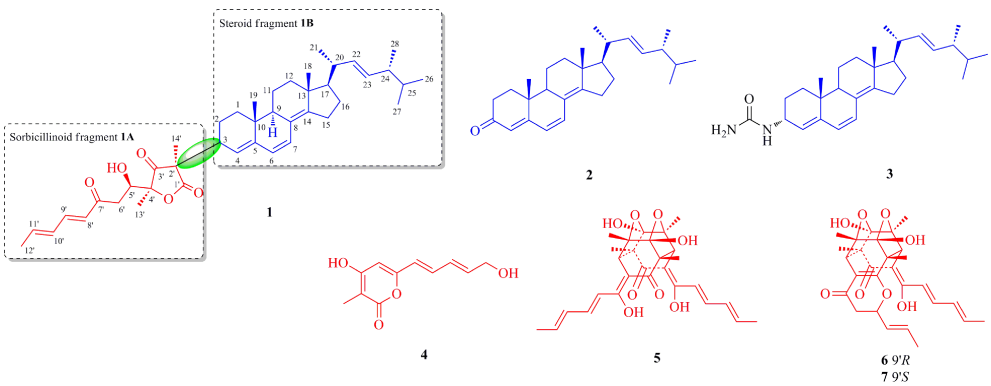

FIGURE 1 | Chemical structures of compounds **1**–**7**.

Qingdao, China. It was preliminary identified as *Aspergillus* sp. by comparing the sequence of the ITS region of the rDNA. The ITS sequence of the isolated fungus was 99% identical to that of *Aspergillus* sp. (GenBank accession: MK605984.1). The GenBank number of MH785494 was assigned to this fungal strain. This fungus was deposited in Tobacco Research Institute of Chinese Academy of Agricultural Sciences with a deposition number of 1022LEF.

Fermentation, Extraction, and Purification

The fungus *Aspergillus* sp. 1022LEF was statically cultured at 28°C in 150 × 1 L Erlenmeyer flasks, each containing 300 mL of potato dextrose broth medium (Solarbio Life Sciences CO., LTD., Beijing, China). Following fermentation for 50 days, the cultures were collected and filtered to separate the broth and mycelia. The broth and the crushed mycelia were extracted with EtOAc. Then, the separate EtOAc extracts were combined and evaporated to give 18.6 g of residue. Detailed separation process was as follows: (i) The resulting residue was subjected to silica gel vacuum liquid chromatography with a stepwise PE/EtOAc (30:1→1:1, v/v) and CH_2Cl_2/MeOH (20:1→1:1, v/v) mixture systems to afford four major fractions A–D. (ii) Fraction A eluting with PE/EtOAc 2:1 was purified by silica gel column chromatography (CC) (CH_2Cl_2/MeOH, 30:1→10:1, v/v) to yield the new compound **1** (5.8 mg). (iii) Compounds **2** (6.2 mg) and **3** (4.6 mg) were obtained from fraction B eluting with PE/EtOAc 1:1 by preparative TLC (plate: 20 × 20 cm; developing solvents: CH_2Cl_2/MeOH 30:1). (iv) Fraction C eluting with CH_2Cl_2/MeOH 20:1 was refractionated by reversed-phase C18 CC with a mixture of MeOH/H_2O system (1:9→10:0, v/v) to give five subfractions (Fraction C-1–C-5). Fraction C-1 was subjected to Sephadex LH-20 (MeOH) to yield **5** (8.9 mg). Fraction C-3 was further purified by silica gel CC (CH_2Cl_2/MeOH, 30:1→10:1, v/v), and followed by Sephadex LH-20 (MeOH) to give **6** (10.2 mg) and **7** (9.0 mg). Finally, compound **4** (11.6 mg) was separated from fraction C-4 *via* preparative TLC (plate: 20 × 20 cm; developing solvents: CH_2Cl_2/MeOH 20:1).

Tennessenoid A (**1**): amorphous powder; $[\alpha]_D^{20}$ +15.6 (*c* 0.10, MeOH); UV (MeOH) λ_{max} (log ϵ) 201 (3.29), 268 (3.05), 290 (4.19), 305 (3.10) nm; ^1H and ^{13}C NMR data (measured in $CDCl_3$), see **Table 1**; HRESIMS *m/z* 665.4183 $[M + Na]^+$ (calcd for $C_{42}H_{58}O_5Na$, 665.4182).

Antifungal Assay

Antifungal activity of compounds **1**–**8** was evaluated by modified agar diffusion test method (Ahmed et al., 2011). The test compounds were dissolved in acetone at a concentration of 1 mg/mL, and then were made up to a final concentration of 20 μg/mL. The solution was transferred to a sterile filter disk (each 50 μL), which was placed on the agar growth medium for the test pathogenetic fungi. Fungal diseases commonly found in agriculture, *Sclerotium rolfsii* Sacc., *Fusarium oxysporum* (Schl.) F.sp *cucumerinum* Owen, *Coniella diplodiella* Petrak et Sydow, *Physalospora piricola* Nose., *Fusarium graminearum* schw., *Alternaria mali* rob., *Colletotrichum orbiculare* Arx., and *Alternaria porri* (E11iott) Cifed., were chosen as the test pathogenetic fungi. The radius of the zone of inhibition was measured in millimeters starting at the middle of the filter. Prochloraz was used as the positive control.

RESULTS AND DISCUSSION

Structural Elucidation of the Isolated Compounds

Tennessenoid A (**1**) was isolated as an amorphous powder. The molecular formula of **1** was determined to be $C_{42}H_{58}O_5$ by observation of the $[M + Na]^+$ ion peak in the HRESIMS

TABLE 1 | ^1H NMR (500 MHz, δ in ppm) and ^{13}C NMR Data (125 MHz, δ in ppm) for **1** (measured in $CDCl_3$).

No.	δ_H (*J* in Hz)	δ_C, type	No.	δ_H (*J* in Hz)	δ_C, type
1	1.75, m; 1.31, m	34.4, CH_2	22	5.19, d (15.1, 7.8)	135.3, CH
2	1.77, m; 1.73, m	20.8, CH_2	23	5.24, d (15.1, 6.8)	132.2, CH
3	2.69, m	43.8, CH	24	1.87, m	42.9, CH
4	5.31, br s	119.9, CH	25	1.47, m	33.1, CH
5		146.8, C	26	0.82, d (5.9)	19.7, CH_3
6	5.84, d (9.6)	125.9, CH	27	0.84, d (5.9)	20.0, CH_3
7	6.13, d (9.6)	125.6, CH	28	0.92, d (5.8)	17.6, CH_3
8		124.7, C	1′		176.2, C
9	1.93, m	45.3, CH	2′		52.7, C
10		35.6, C	3′		214.6, C
11	1.60, m; 1.56, m	19.3, CH_2	4′		89.6, C
12	2.01, m; 1.25, m	36.4, CH_2	5′	4.35, br d (10.4)	72.5, CH
13		43.6, C	6′	3.02, dd (17.5, 10.4); 2.79, d (17.5)	40.3, CH_2
14		149.7, C	7′		199.2, C
15	2.39, m; 2.29, m	25.0, CH_2	8′	6.05, d (15.7)	127.2, CH
16	1.77, m; 1.44, m	27.9, CH_2	9′	7.18, dd (15.7, 10.1)	144.7, CH
17	1.20, m	55.9, CH	10′	6.20, dd (15.6, 10.1)	130.0, CH
18	0.92, s	19.2, CH_3	11′	6.27, dq (15.6, 6.4)	142.2, CH
19	0.81, s	18.6, CH_3	12′	1.89, d (6.4)	18.9, CH_3
20	2.11, m	39.4, CH	13′	1.48, s	18.4, CH_3
21	1.04, d (6.6)	21.2, CH_3	14′	1.41, s	16.5, CH_3

spectrum at *m/z* 665.4183 (calcd for $C_{42}H_{58}O_5Na$, 665.4182). The ^{13}C NMR spectrum of **1** (**Table 1**) revealed 42 carbon resonances, which were classified into two ketone carbonyls at δ_C 214.6 (C-3′) and 199.2 (C-7′), one ester carbonyl at δ_C 176.2 (C-1′), seven quaternary carbons including three sp^2 and one oxygenated at δ_C 89.6 (C-4′), 16 methines including nine olefinic at δ_C 127.2 (C-8′), 144.7 (C-9′), 130.0 (C-10′), 142.2 (C-11′), 119.9 (C-4), 125.9 (C-6), 125.6 (C-7), 135.3 (C-22), and 132.2 (C-23) and one oxygenated at δ_C 72.5 (C-5′), seven methylenes, and nine methyl groups with the aid of DEPT spectra. The ^1H NMR data of **1** (**Table 1**) displayed signals for nine methyl groups [including five doublets at δ_H 1.89 (d, J = 6.4 Hz), 1.04 (d, J = 6.6 Hz), 0.92 (d, J = 5.8 Hz), 0.84 (d, J = 5.9 Hz), 0.82 (d, J = 5.9 Hz), and four singlets at δ_H 1.48, 1.41, 0.92, and 0.81], nine olefinic protons (from δ_H 5.19 to 7.18), and a series of indistinguishable aliphatic multiplets. Further analysis of the 1D and 2D NMR data allowed for the establishment of fragments **1A** and **1B** for compound **1** (**Figure 2**).

Interpretation of the 2D NMR data (^1H–^1H COSY and HMBC cross-peaks) of fragment **1A**, two spin-coupling systems, H-8′/H-9′/H-10′/H-11′/H_3-12′ and H-5′/H_2-6′, were readily established. The connectivities of these spin systems, the ketone/ester carbonyls, and the methyls were achieved by analysis of the key HMBC correlations (**Figure 2**). The HMBC correlations from H_3-14′ to C-1′/C-3′ and from H_3-13′ to C-3′/C-4′generated a furan lactone moiety and it was linked to C-5′ by HMBCs from H-5′ to C-3′ and H_3-13′ to C-5′. Fragment **1A** was deduced to be a vertinolide derivative, a sorbicillinoid-type polyketide isolated from the endophytic fungus *Clonostachys rosea* B5-2 (Supratman et al., 2021).

Fragment **1B** was deduced as a steroid moiety by analysis of characteristic signals in 1D and 2D NMR spectrum. A combination of ^1H–^1H COSY and HMBC correlations (**Figure 2**) enabled us to identify the (22*E*)-ergosta-4,6,8 (14),22-tetraene nucleus, which was similar to compounds **2** and **3**. Moreover, the connection between fragments **1A** and **1B** *via* the C–C bond was established by the diagnostic HMBC correlations from H_3-14′ to C-3 and from H-3 to C-1′ (**Figure 2**). Accordingly, the planar structure of **1** was determined.

The relative stereochemistry of **1** was established by interpretation of NOESY spectrum. As for fragment **1A**, the mutual NOE correlations of H-5′/H_3-13′/H_3-14′ indicated a cofacial relationship among H-5′, H_3-13′, and H_3-14′ (**Figure 3**). In fragment **1B**, NOE correlations between H_3-19

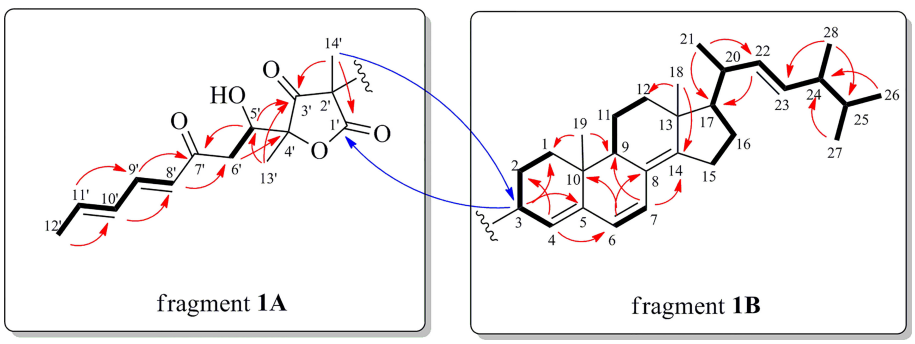

FIGURE 2 | Key ^1H-^1H COSY (bold lines) and HMBC (red and blue arrows for intra- and inter-fragments **1A** and **1B**, respectively) correlations of **1**.

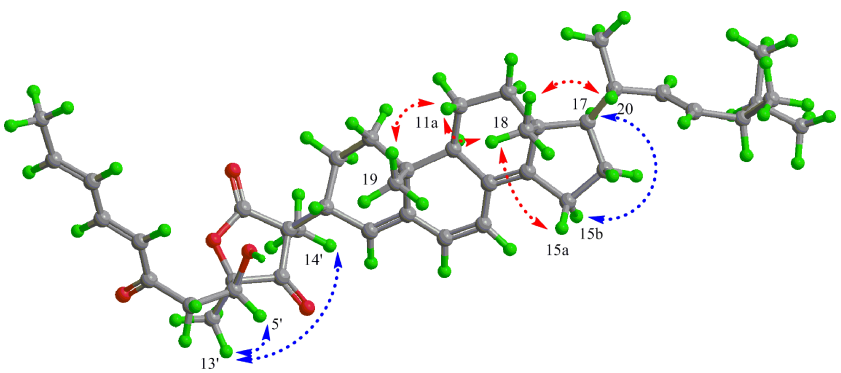

FIGURE 3 | NOESY correlations of **1**.

and H-11a, between H-11a/H_3-18, and between H_3-18 and H-15a/H-20 suggested that these groups were located at the same side of the 6/6/6/5 tetracyclic nucleus, while on the contrary, NOE correlation between H-17 and H-15b indicated they oriented towards opposite side (**Figure 3**). This deduction was also in consistance with the reported ergosteroids **2** and **3**. The β-orientations of H-20 and H-24 were deduced by biosynthesis considerations based on those in **2** and **3**. Furthermore, the coupling constants between H-8′ and H-9′ (J = 15.7 Hz) and between H-10′ and H-11′ (J = 15.7 Hz) illustrated that the double bonds at C-8' and C-10' were in the *E* configurations. However, since fragments **1A** and **1B** can be rotated freely, the high flexibility made the relative configurations of **1A** and **1B** unsolved, as well as the absolute configurations. Many attempts to cultivate single crystals which were suitable for X-ray diffraction analysis in mixed solvent systems (MeOH/H_2O, CH_2Cl_2/H_2O, acetone/H_2O, etc.) were tried. However, they all failed unfortunately.

In addition, six known biosynthetic congeners including two steroids, ergosta-4,6,8(14),22-tetraen-3-one (**2**) (Fujimoto et al., 2004) and (22*E*,24*R*)-3α-ureido-ergosta-4,6,8(14),22-tetraene (**3**) (Yoshikawa et al., 2001), and four sorbicillinoid-based compounds, saturnispol G (**4**) (Meng et al., 2018), trichodimerol (**5**) (Zhai et al., 2016), and dihydrotrichodimer ethers A and B (**6** and **7**) (Zhai et al., 2016) were isolated and identified by comparison of the spectroscopic data with those reported in the literatures. Compound **1** was characterized as an unprecedented steroid–sorbicillinoid adduct, while compounds **5**–**7** were previously reported bisorbicillinoids. The putative biosynthesis of **1** can be traced back to vertinolide and ergosteroid (**Figure 4**). The aldolization of **2** and vertinolide generated the unique C–C bond, which was rarely-observed in natural ergosteroids, while dimerization of vertinolide formed dimers **5**–**7**.

Antifungal Activity

The isolated compounds **1**–**8** were evaluated to determine their antifungal activity against eight pathogenetic fungi. As a result, the new compound **1**, in particular, exhibited modest but broad-spectrum activities against S. rolfsii, F. oxysporum, C. diplodiella, P. piricola, F. graminearum, A. mali, C. orbiculare, and A. porri, with the radius of the inhibition zone of 7, 5, 5, 5, 3, 3, 2, and 2 *mm*, respectively (**Figure 5**), while the radius of the inhibition zone of the positive control prochloraz were ranging from 7 to 12 mm. Sorbicillinoids are a family of hexaketide secondary metabolites with a characteristic sorbyl side chain residue. Previous studies reported sorbicillinoids possessed high antimicrobial activity and can be used as a biological control agent (Zhai et al., 2016). Moreover, sorbicillinoids are also found to potently inhibit fungal pathogens both in vitro and in vivo. Bisvertinolone, a bisorbicillinoid produced by Trichoderma

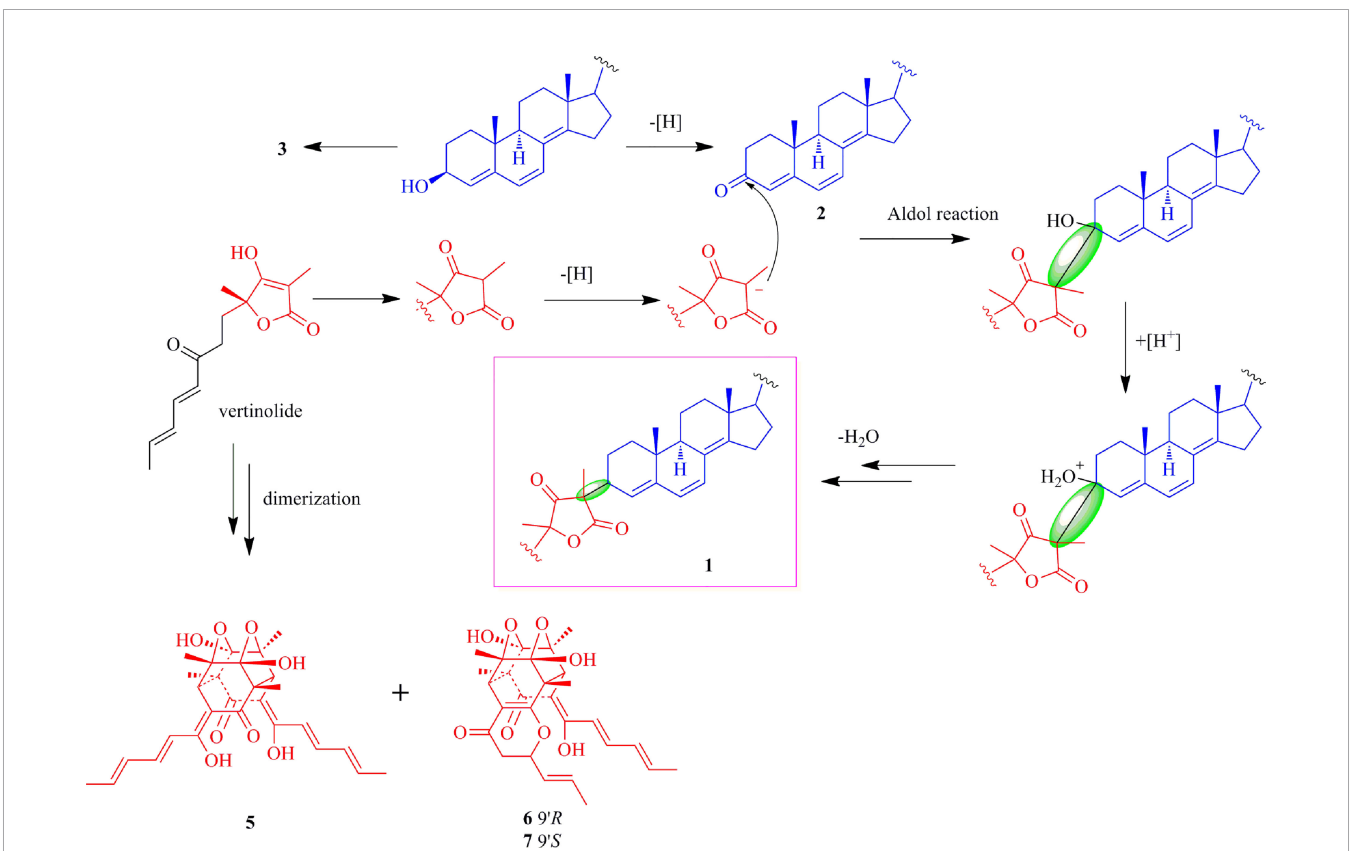

FIGURE 4 | Proposed biosynthetic pathway of **1** and related compounds.

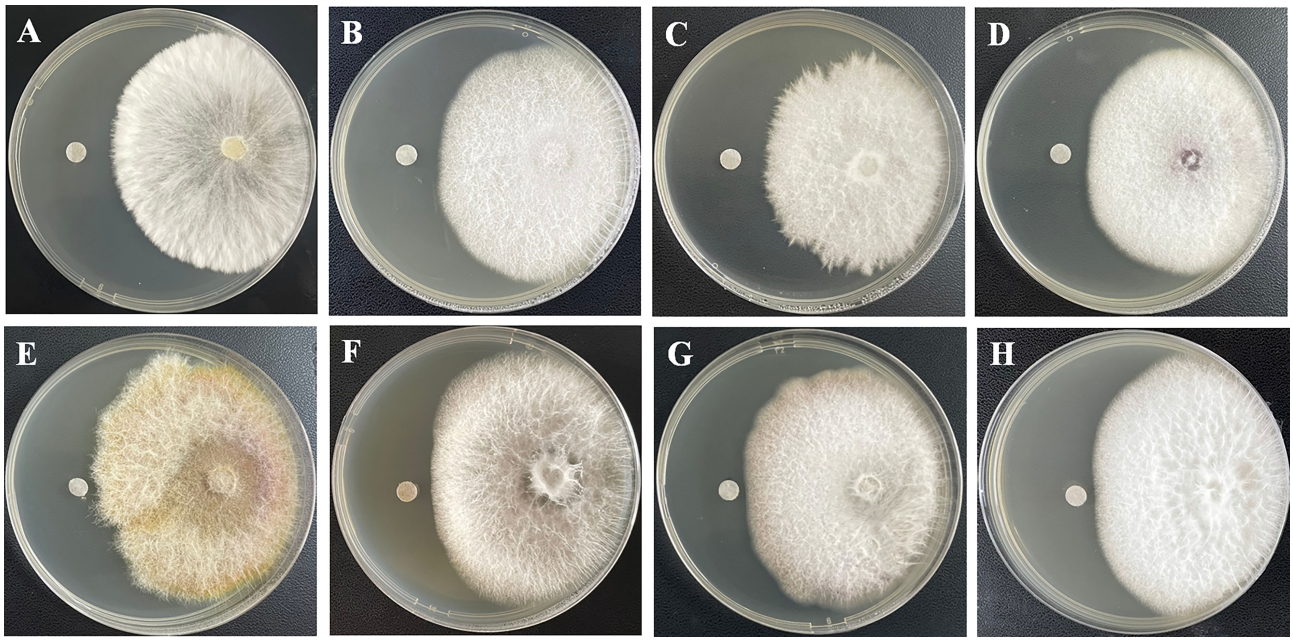

FIGURE 5 | Antifungal activities of **1** against eight plant pathogenetic fungi–*S. rolfsii* **(A)**, *F. oxysporum* **(B)**, *C. diplodiella* **(C)**, *P. piricola* **(D)**, *F. graminearum* **(E)**, *A. mali* **(F)**, *C. orbiculare* **(G)**, and *A. porri* **(H)**.

longibrachiatum SFC100166, not only showed considerable activity against phytopathogenic fungi Cladosporium coccodes, Colletotrichum coccodes, Cylindrocarpon destructans, Magnaporthe oyrzae, and Phytopathora infestans, with MIC values ranging from 6.3 to 100 μg/mL, but also reduced the development of tomato late blight disease strongly (Ngo et al., 2021). Further studies such as in vivo assay and mode of action of antifungal activities may reveal the potential of the newly-isolated steroid–sorbicillinoid adduct **1** as an antifungal agrochemical in agriculture.

CONCLUSIONS

In conclusion, a novel polyketide-terpene hybrid metabolite, tennessenoid A (**1**), as well as six known biosynthetic congeners, ergosta-4,6,8(14),22-tetraen-3-one (**2**), (22*E*,24*R*)-3α-ureido-ergosta-4,6,8(14),22-tetraene (**3**), saturnispol G (**4**), trichodimerol (**5**), and dihydrotrichodimer ethers A and B (**6** and **7**) were isolated from the marine-derived endophyte of *Aspergillus* sp. 1022LEF. Their structures were determined by detailed analysis of NMR data and HRESIMS. The steroids **2**–**3** and the sorbicillinoids **4**–**7** were common fungal secondary metabolites, whereas the new compound **1** represented the first example of steroid–sorbicillinoid adduct *via* a C–C bond. Moreover, this unprecedented compound exhibited broad-spectrum antifungal activities against several plant pathogenetic fungi. This study indicated that the marine-derived microbes were considered to be valuable resources for the development of new agrochemicals.

DATA AVAILABILITY STATEMENT

The original contributions presented in the study are included in the article/**Supplementary Material**. Further inquiries can be directed to the corresponding author.

AUTHOR CONTRIBUTIONS

Experiment implementation, D-LZ and H-SW. Writing—original draft preparation, D-LZ and L-WG. Writing—review and editing, PZ. All authors have read and approved the final manuscript.

FUNDING

This work was supported by the Central Public-interest Scientific Institution Basal Research Fund (Y2022QC32 and Y2021XK25) and the Agricultural Science and Technology Innovation Program (ASTIP-TRIC05).

SUPPLEMENTARY MATERIAL

The Supplementary Material for this article can be found online at: https://www.frontiersin.org/articles/10.3389/fmars.2022.923128/full#supplementary-material

REFERENCES

Ahmed, I., Hussain, H., Schulz, B., Draeger, S., Padula, D., Pescitelli, G., et al. (2011). Three New Antimicrobial Metabolites From the Endophytic Fungus Phomopsis Sp. *Eur. J. Org. Chem.* 2011, 2867–2873. doi: 10.1002/ejoc.201100158

Butler, M. S. (2005). Natural Products to Drugs: Natural Product Derived Compounds in Clinical Trials. *Nat. Prod. Rep.* 22, 162–195. doi: 10.1039/b402985m

Carroll, A. R., Copp, B. R., Davis, R. A., Keyzers, R. A., and Prinsep, M. R. (2021). Marine Natural Products. *Nat. Prod. Rep.* 38, 362–413. doi: 10.1039/D0NP00089B

El-Bondkly, E. A. M., El-Bondkly, A. A. M., and El-Bondkly, A. A. M. (2021). Marine Endophytic Fungal Metabolites: A Whole New World of Pharmaceutical Therapy Exploration. *Heliyon* 7, e06362. doi: 10.1016/j.heliyon.2021.e06362

Fujimoto, H., Nakamura, E., Okuyama, E., and Ishibashi, M. (2004). Six Immunosuppressive Features From an Ascomycete, *Zopfiella Longicaudata*, Found in a Screening Study Monitored by Immunomodulatory Activity. *Chem. Pharm. Bull.* 52, 1005–1008. doi: 10.1248/cpb.52.1005

Knight, V., Sanglier, J. J., DiTullio, D., Braccili, S., Bonner, P., Waters, J., et al. (2003). Diversifying Microbial Natural Products for Drug Discovery. *Appl. Microbiol. Biotechnol.* 62, 446–458. doi: 10.1007/s00253-003-1381-9

Li, Z. X., Wang, X. F., Ren, G. W., Yuan, X. L., Deng, N., Ji, G. X., et al. (2018b). Prenylated Diphenyl Ethers From the Marine Algal-Derived Endophytic Fungus *Aspergillus Tennesseensis*. *Molecules* 23, 2368. doi: 10.3390/molecules23092368

Li, Z., Zhu, D., and Shen, Y. (2018a). Discovery of Novel Bioactive Natural Products Driven by Genome Mining. *Drug Discov. Ther.* 12, 318–328. doi: 10.5582/ddt.2018.01066

Meng, J., Cheng, W., Heydari, H., Wang, B., Zhu, K., Konuklugil, B., et al. (2018). Sorbicillinoid-Based Metabolites From a Sponge-Derived Fungus *Trichoderma Saturnisporum*. *Mar. Drugs* 16, 226. doi: 10.3390/md16070226

Newman, D. J., and Cragg, G. M. (2020). Natural Products as Sources of New Drugs Over the Nearly Four Decades From 01/1981 to 09/2019. *J. Nat. Prod.* 83, 770–803. doi: 10.1021/acs.jnatprod.9b01285

Ngo, M. T., Nguyen, M. V., Han, J. W., Park, M. S., Kim, H., and Choi, G. J. (2021). *In Vitro* and *In Vivo* Antifungal Activity of Sorbicillinoids Produced by *Trichoderma Longibrachiatum*. *J. Fungi* 7, 428. doi: 10.3390/jof7060428

Rateb, M. E. M., and Ebel, R. (2011). Secondary Metabolites of Fungi From Marine Habitats. *Nat. Prod. Rep.* 28, 290. doi: 10.1039/c0np00061b

Soldatou, S., and Baker, B. J. (2017). Cold-Water Marine Natural Products 2006 to 2016. *Nat. Prod. Rep.* 34, 585–626. doi: 10.1039/C6NP00127K

Supratman, U., Suzuki, T., Nakamura, T., Yokoyama, Y., Harneti, D., Maharani, R., et al. (2021). New Metabolites Produced by Endophyte *Clonostachys Rosea* B5-2. *Nat. Prod. Res.* 35, 1525–1531. doi: 10.1080/14786419.2019.1656629

Yoshikawa, K., Ikuta, M., Arihara, S., Matsumura, E., and Katayama, S. (2001). Two New Steroidal Derivatives From the Fruit Body of *Chlorophyllum Molybdites*. *Chem. Pharm. Bull.* 49, 1030–1032. doi: 10.1248/cpb.49.1030

Yuan, X. L., Wang, X. F., Xu, K., Li, W., Chen, D., and Zhang, P. (2020). Characterization of a New Insecticidal Anthraquinone Derivative From an Endophyte of *Acremonium Vitellinum* Against *Helicoverpa Armigera*. *J. Agric. Food Chem.* 68, 11480–11487. doi: 10.1021/acs.jafc.0c05680

Zhai, M. M., Qi, F. M., Li, J., Jiang, C. X., Hou, Y., Shi, Y. P., et al. (2016). Isolation of Secondary Metabolites From the Soil-Derived Fungus *Clonostachys Rosea* YRS-06, a Biological Control Agent, and Evaluation of Antibacterial Activity. *J. Agric. Food Chem.* 64, 2298–2306. doi: 10.1021/acs.jafc.6b00556

Zhang, P., Wei, Q., Yuan, X., and Xu, K. (2020). Newly Reported Alkaloids Produced by Marine-Derived *Penicillium* Species (Covering 2014–2018). *Bioorg. Chem.* 99, 103840. doi: 10.1016/j.bioorg.2020.103840

Zhao, D. L., Han, X. B., Wang, M., Zeng, Y. T., Li, Y. Q., Ma, G. Y., et al. (2020). Herbicidal and Antifungal Xanthone Derivatives From the Alga-Derived Fungus *Aspergillus Versicolor* D5. *J. Agric. Food Chem.* 68, 11207–11214. doi: 10.1021/acs.jafc.0c04265

Zhao, D. L., Yuan, X. L., Du, Y. M., Zhang, Z. F., and Zhang, P. (2018). Benzophenone Derivatives From an Algal-Endophytic Isolate of *Penicillium Chrysogenum* and Their Cytotoxicity. *Molecules* 23, 3378. doi: 10.3390/molecules23123378

Conflict of Interest: The authors declare that the research was conducted in the absence of any commercial or financial relationships that could be construed as a potential conflict of interest.

frontiers | Frontiers in Microbiology

ORIGINAL RESEARCH
published: 09 June 2022
doi: 10.3389/fmicb.2022.890973

Understanding the Variation of Bacteria in Response to Summertime Oxygen Depletion in Water Column of Bohai Sea

Jing Wang[1], Xiaoxiao Guo[1], Yanying Li[1], Guisheng Song[2] and Liang Zhao[3]*

[1] Tianjin Key Laboratory of Animal and Plant Resistance, Tianjin Key Laboratory of Conservation and Utilization of Animal Diversity, Tianjin Normal University, Tianjin, China, [2] School of Marine Science and Technology, Tianjin University, Tianjin, China, [3] College of Marine and Environmental Sciences, Tianjin University of Science and Technology, Tianjin, China

Aiming to reveal the variation in bacteria community under oxygen depletion formed every summer in water column of central Bohai Sea, a time-scenario sampling from June to August in 2018 at a 20-day interval along one inshore–offshore transect was settled. Water samples were collected at the surface, middle, and bottom layer and then analyzed by high-throughput sequencing targeting both 16S rRNA and *nosZ* genes. Compared to the surface and middle water, oxygen depletion occurred at bottom layer in August. In top two layers, Cyanobacteria dominated the bacterial community, whereas heterotrophic bacteria became dominant in bottom water of Bohai Sea. Based on the time scenario, distinct community separation was observed before (June and July) and after (August) oxygen depletion (p = 0.003). Vertically, strict stratification of *nosZ* gene was stably formed along 3 sampling layers. As a response to oxygen depletion, the diversity indices of both total bacteria (16S rRNA) and *nosZ* gene-encoded denitrification bacteria all increased, which indicated the intense potential of nitrogen lose when oxygen depleted. Dissolved oxygen (DO) was the key impacting factor on the community composition of total bacteria in June, whereas nutrients together with DO play the important roles in August for both total and denitrifying bacteria. The biotic impact was revealed further by strong correlations which showed between Cyanobacteria and heterotrophic bacteria in June from co-occurrence network analysis, which became weak in August when DO was depleted. This study discovered the variation in bacteria community in oxygen-depleted water with further effort to understand the potential role of denitrifying bacteria under oxygen depletion in Bohai Sea for the first time, which provided insights into the microbial response to the world-wide expanding oxygen depletion and their contributions in the ocean nitrogen cycling.

Keywords: Bohai Sea, oxygen depletion, bacteria, 16S rRNA, *nosZ* gene, community variation

OPEN ACCESS

Edited by:
Shan He,
Ningbo University, China

Reviewed by:
Yongchao Yin,
Northeastern University, United States
Juan Ling,
South China Sea Institute of Oceanology (CAS), China
Jiayuan Liang,
Guangxi University, China
Cuici Sun,
South China Sea Institute of Oceanology (CAS), China

****Correspondence:***
Jing Wang
jwang_hku@163.com

Specialty section:
This article was submitted to Aquatic Microbiology, a section of the journal Frontiers in Microbiology

Received: *07 March 2022*
Accepted: *05 May 2022*
Published: *09 June 2022*

Citation:
Wang J, Guo X, Li Y, Song G and Zhao L (2022) Understanding the Variation of Bacteria in Response to Summertime Oxygen Depletion in Water Column of Bohai Sea. Front. Microbiol. 13:890973. doi: 10.3389/fmicb.2022.890973

INTRODUCTION

Microbes in marine ecosystem are play the important roles in regulating the biogeochemical cycle and energy transfer, which processes are commonly determined by the diversity and distribution of bacteria functional groups, such as the transformation of nitrogen in world ocean (Voss et al., 2013; Pajares and Ramos, 2019). The ecological interactions between autotrophic bacteria and heterotrophic bacteria are among critical links within global nutrient cycles (Fu et al., 2020).

Typically, the productivity gradient generated by autotrophic bacteria from different locations is ascribed to community composition, which is also one of the explanations for the separation of heterotrophic bacterial communities depending on availability and quality of organic matter from primary production (Fortunato and Crump, 2011). On the other hand, remineralization and catalytic decomposition of organic substrates by heterotrophic bacteria are the keys for the nutrient availability for the primary production as well (Ward, 2013).

Nowadays, with the widespread and rapid changes in biospheric nitrogen concentrations generated by anthropogenic activity, the global impacts on biodiversity and ecosystem productivity have posed an environmental hazard in marine ecosystem (Penuelas et al., 2020; Yu et al., 2020). Therefore, understanding the nitrogen removal pathway mediated by microorganisms is of great importance for alleviating excess nitrogen (Babbin et al., 2014; Wang J. et al., 2019). Denitrification together with anaerobic ammonium oxidation (Anammox) is proved to be two major pathways to remove nitrogen under oxygen-depleted region to oxygen minimum zone (OMZ) (Ward, 2013; Babbin et al., 2014). Before the discovery of Anammox, denitrification mediated by a serial of microorganisms is estimated to account for over 50% of dissolved inorganic nitrogen removal from world ocean (Reyes et al., 2017). There are many reports on nitrogen removal by denitrifying bacteria in OMZs, such as the water column of Arabian Sea (Wyman et al., 2013), the Yangtze River Estuary, and the Pearl River Estuary of China (Wang J. et al., 2019; Li et al., 2020). Understanding the denitrification bacteria and their contribution at each specific steps is critical for estimating the nitrogen budget of the atmosphere and oceans, especially under the changing DO, since oxygen content is a regulating factor in promoting the process of denitrification. At the same time, emission of the greenhouse gas – nitrous oxide (N_2O) is effectively alleviated in the last step of denitrification, in which the enzyme encoded by the *nosZ* gene converts N_2O into N_2 and releases it into the atmosphere (Zumft, 1997). Consumption of oxygen by bacteria respiration leading to the seize of nitrate (NO_3^-) as electron acceptor will eventually increase global warming due to the release of N_2O (Rabalais and Turner, 2019). Among the diverse bacteria that participating in complete denitrification, *nosZ* gene is an accurate and also highly effective biomarker for evaluating denitrifying communities especially with the estimations of greenhouse gas emission in a wide range of environment (Kandeler et al., 2006; Wang J. et al., 2019).

The area of the marine hypoxic zone attributable to climate change varies with depth and emerges a notable expansion trend (Deutsch et al., 2011), resulting in typical OMZs, such as the South Pacific (Sun et al., 2017), northern tropical Indian Ocean (Menezes et al., 2018), North Atlantic (Klar et al., 2018), and Southern Ocean (Levin, 2018), where the increase of N_2 production results in subsequent restriction of global primary production (Deutsch et al., 2011). Dissolved oxygen (DO) is a key parameter for bacteria physiology, and DO gradient has strong correlations with the structure of bacterial community (Spietz et al., 2015). High incidence of oxygen depletion increases denitrification rates, accelerates the recycling of inorganic nitrogen by improving dissimilatory nitrate reduction to ammonium (DNRA), which processes enhance the retention of both organic and inorganic nitrogen, and exacerbates oxygen deficiency further (Jäntti and Hietanen, 2012; Song et al., 2021). Moreover, transcripts of denitrifiers are also confined to the low oxygen level (Suter et al., 2020). Yet, researches on the effects of hypoxia on microbial composition are still limited in inland seas globally, including China. To figure out how individual groups of bacteria respond to decreasing DO functionally, effect of oxygen depletion on microbial communities is crucial to reveal the consequences of outspreading OMZs globally.

Bohai Sea is a semi-enclosed inland sea located in the northeastern part of China (37°07′N–40°56′N, 117°33′E–122°08′E). Due to the continuous nutrients input from the Yellow River and the Haihe River, Bohai Sea is subjected to a high eutrophication level with yearly average loading of nitrogen up to 243.2 mg/L (Peng, 2015; Qiao et al., 2017). Moreover, increasing industrialization and population in surrounding cities also significantly intensifies the degree of eutrophication during the past 60 years (Yang et al., 2011). As a consequence of excessive emission of nutrients and organic pollutants, bottom oxygen depletion occurred every summer in the central Bohai Sea (Zhai et al., 2012), and the oxygen-depleted area had expanded to 1,200 km^2 in August of 2014 (Jiang et al., 2016), covering the Liaodong Bay and the northern part of the Bohai Sea at a greater extent (Wei et al., 2019). Although the biogeochemical cycling driven by microbes has displayed instant or delayed response to oxygen depletion (Bertics et al., 2013; Sinkko et al., 2013), less is known for the microbial communities in the reported oxygen depletion water of Bohai sea. The contribution of denitrifying bacteria in Bohai Sea has been revealed by denitrification rate, relative abundance, and NO_3^-/nitrite (NO_2^-) reductase activity of *nar*/*nir*-encoded denitrifiers in sediments (Wang et al., 2015; Zhang et al., 2019; Chen et al., 2020). However, information on the *nosZ*-type denitrifying bacteria and their metabolism capability in Bohai Sea water column is still unknown, and the potential correlation between denitrifying bacteria and the formation of the bottom water hypoxia is also awaiting to discover.

In this study, surface, middle, and bottom layer water samples were collected along an inshore–offshore transect covering the reported hypoxic zone in Bohai Sea following a time scenario under the formation of oxygen depletion from June to August of 2018. Both 16S rRNA-encoded total bacteria and *nosZ* gene-encoded denitrifying bacteria were fully investigated by high-throughput sequencing with the aim to reveal the impact of oxygen depletion on bacterial community. Based on the variations in bacteria diversity and spatial or temporal distribution patterns, in combination with local environmental parameters, effects of oxygen depletion on variations and distributions of bacteria in Bohai Sea water were evaluated. Moreover, the biotic impact between Cyanobacteria and heterotrophic bacteria was also discussed by co-occurrence network analysis. Contributions of denitrifying bacteria in nitrogen cycle under oxygen depletion in Bohai Sea water were further analyzed by coupling functional prediction by 16S rRNA gene with the distribution of *nosZ* gene in August samples.

MATERIALS AND METHODS

Sample Collection and Physiochemical Parameter Measurement

Cruises were carried out in the Bohai Sea on 11 June, 19 July, and 8 and 26 August of 2018, respectively. A total of three layers (surface, middle, and bottom) of water samples were collected from 6 sites (H2-H7:39.38°–39.69°N, 119.63°–120.55°E) in June and 5 sites (H3-H7:39.62°–39.69°N, 119.84°–120.55°E) in the rest of 3 cruises (site H2 was occupied for aquaculture since July). One additional layer was collected at site H7 between middle and bottom layers in late August for a precise vertical profile of the DO measurement, but this sample was evaluated for geochemical parameter only. Details for the total 62 samples from 4 cruises could be found in **Supplementary Table 1**. The transact was settled from inshore to offshore across the southwest of the bowl-shaped depression area (**Figure 1**), where the oxygen depletion was reported (Zhai et al., 2012). Vertical profiles of physiochemical parameters, including temperature, salinity, depth, DO, and chlorophyll *a* (*Chla*), were acquired using an RBR maestro multi-parameters mounted to the Sea-Bird SBE-911 Plus V2 conductivity–temperature–depth (CTD) system *in situ*. Water samples were collected by 5-L Niskin bottles, and microbes were collected by filtering 1 L of water from each layer through GTTP filters (0.22 μm pore size, 47 mm in diameter, Merck Millipore, Germany) under 0.5 MPa. All the filtrations were accomplished within 0.5 h after the Niskin bottles were on board. The filters were placed into a 2-ml microtube with sterilized tweezers and then frozen in liquid nitrogen immediately. Filters were transported on dry ice to the laboratory and stored at −80°C until DNA extraction. Simultaneously, about 500 ml of each water sample was transported on ice and stored at 4°C for chemical analysis. Concentration of ammonium (NH_4^+), NO_3^-, and NO_2^- was measured in the laboratory using a AA3 HR analyzer (SEAL Analytical, United States).

DNA Extraction and Polymerase Chain Reaction Amplification

Genomic DNA was extracted and purified using lysozyme, proteinase K, and sodium dodecyl sulfate with chloroform extraction and isopropanol precipitation following Kan et al. (2006). Quality and quantity of DNA were reliably ascertained using an ND-2000 nanodrop spectrometer (Thermal Scientific, Wilmington, DE). Primers 338F (ACTCCTACGGGAGGCAGCA) and 806R (GGACTACHVGGGTWTCTAAT) with barcode attached were applied targeting the V3 and V4 regions of bacterial 16S rRNA gene (Dai et al., 2016), and amplification of *nosZ* gene was performed with the primer pairs nosZF (CGCTGTTCITCGACAGYCAG) and nosZR (ATGTGCAKIGCRT-GGCAGAA) after Rich et al. (2003).

The polymerase chain reaction (PCR) was performed in a 20 μl mixture, containing 4 μl of 5× FastPfu Buffer, 2 μl of dNTPs (2.5 mM), 0.8 μl of each primer (5 μM), 0.4 μ of FastPfu polymerase, and 10 ng of template DNA. Amplification and purification of 16S rRNA product followed the protocols in Guo et al. (2022), and protocols for *nosZ* gene were after Wang J. et al. (2019).

High-Throughput Sequencing and Data Processing

Triplicates of the successful PCR products were mixed thoroughly, then purified, quantified, and homogenized to form a sequencing library. High-throughput sequencing was

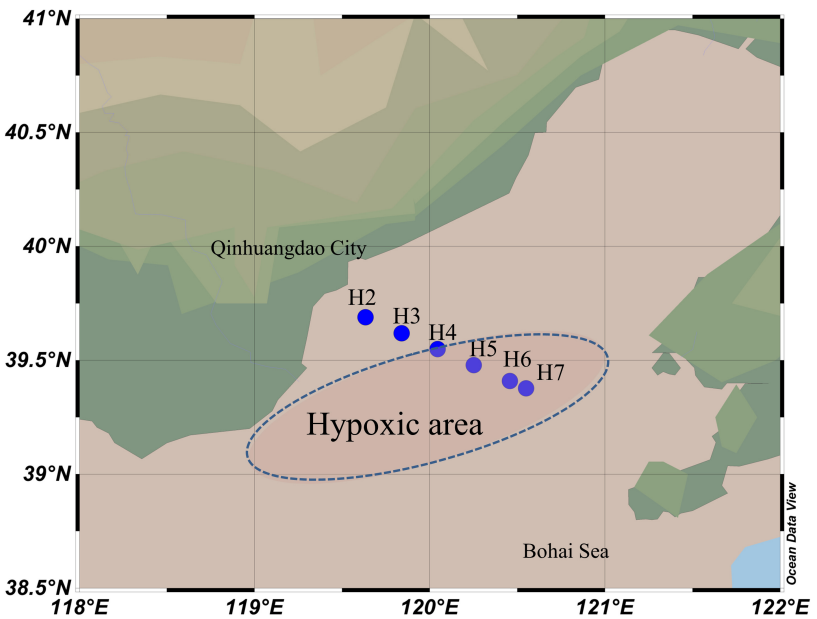

FIGURE 1 | Map showing the sampling sites in Bohai Sea along the inshore–offshore transect. The reported hypoxic area was shown in the blue dash line oval.

performed using Illumina MiSeq System (Illumina MiSeq, United States). The original image data files obtained by high-throughput sequencing were converted into original sequenced reads by base-calling analysis. The results were stored in FASTQ (referred to as "fq") file format. Quality check of sequences was performed using the Quantitative Insights Into Microbial Ecology (QIIME) standard pipeline (Caporaso et al., 2010); the low-quality reads, primers, barcodes, and adaptors were trimmed off correspondingly. The operational taxonomic units (OTUs) were defined by 97% identity for taxonomy assignment by UCLUST method (Edgar, 2010). All the datasets were normalized based on the rarefaction curve, and the following analysis was made based on the flattened data. Taxonomy for each OTU was made by aligning sequences with the database from GeneBank (Release 7.3[1]).

Statistical Analysis

Rarefaction analysis was performed using Mothur (version v.1.30) and R for all the OTUs with the aim to ensure the amount of the sequences was as reasonable as possible (**Supplementary Figure 1**). Mothur software was used to evaluate the species richness and alpha diversity of the samples (accumulated cyclone energy (ACE), Chao1, Simpson, and Shannon indices). Beta diversity at the class level was calculated between the 6 sites using non-metric multidimensional scaling analysis (NMDS) based on binary Jaccard distance. Bacterial community dynamics at generic level along with environmental variables were analyzed using canonical correspondence analysis (CCA) and mapping with R language vegan package. The co-occurrence network was analyzed by R (version 3.6.3), and the Pearson correlation coefficients were used to construct co-occurrence networks. The top 20 abundant OTUs were aligned with OMZ representative sequences to perform phylogenetic analysis, and the phylogenetic tree was generated using Python language tool (version 3.0). Functional potential of microbial communities in water samples was predicted using phylogenetic investigation of communities by reconstruction of unobserved states (PICRUSt2) (Langille et al., 2013).

Nucleotide Sequence Accession Numbers

The annotated nucleotide sequences of 16S rRNA and *nosZ* genes were deposited to National Center for Biotechnology Information (NCBI) under the accession numbers SRR12403482-SRR12403543 and PRJNA815372, respectively.

RESULTS

Biogeochemical Characteristics of Bohai Sea Under Oxygen Depletion

In this study, a clear pattern of environmental parameters was observed. Along sampling time, water temperature increased gradually from June to August, but decreased vertically as the water deepens. The salinity increased from the surface to bottom along the vertical profile, but decreased along sampling time. Other than in June, the maximum Chl*a* was detected all in middle layers, which were the depth of chlorophyll a maximum (DCM) for Bohai Sea; and the observed DO value kept decreasing vertically, with an obvious decline in bottom water ranging from 9.16 (June) to 4.21 mg/L (late August) along the time scenario. The highest and lowest DO values were all observed from the bottom water of H5 (**Figure 2**), which was the deepest site along the transect (**Supplementary Table 1**). Concentrations of NO_3^-, NO_2^-, and NH_4^+ kept increasing from surface to bottom, with that of the NO_3^- which was always greater than NO_2^- for each sample. One exception was observed in late August samples, where the concentration of NH_4^+ was constantly stable along the vertical profile (**Figure 2**).

Diversity of Bacteria in Bohai Sea

In total, 62 samples were sequenced for 16S rRNA gene with 4,919,934 reads that were obtained after sequencing, and 4,573,864 high-quality sequences were generated after paired-end splicing and filtering. After flattening at 25,000 sequences for each sample, in total, 580 OTUs were identified. A rarefaction curve was drawn to confirm that the amount of sequence was sufficient to reflect the species of the samples (**Supplementary Figure 1A**). The OTU numbers ranged from 299 to 488 at a cutoff value of 97% nucleotide similarity, among which, sample H7B808 contained the highest OTU numbers (448 OTUs), and the sample H4M826 contained the lowest OTU numbers (260 OTUs). Vertically, the number of OTUs identified from the bottom layer samples was greater than the surface and middle layers at all sampling time points; horizontally, the OTU numbers displayed an increasing trend from the inshore to offshore. Along the time scenario, the overall OTU numbers showed an increasing trend from June to early August and then decreased at the last sampling time point. The Chao1 and Shannon indices calculated based on the OTU numbers are summarized in **Figure 3**. Shannon indices ranged from 2.38 to 4.74, and Chao1 richness ranged from 311.19 to 539.47. Vertically, the alpha diversity index increased as the water layer deepens. Horizontally, the Chao1 and Shannon indices at the same water layer generally increased from inshore to offshore. Variations among sampling time scenario were displayed by increasing trend in the surface water, but peak in the middle and bottom layers for July and early August samples. Taken all the indices into consideration, samples in August displayed higher diversity, which were represented by 4.74 of Shannon in H3B826 and 539.47 of Chao 1 in H6B808.

Among the 62 samples, successful amplification for *nosZ* gene was only achieved from 15 late August samples, with 1,371,700 sequences that were obtained in total and then flattened with 10,000 sequences. A rarefaction curve was generated by the flattened data to confirm that the number of sequences was sufficient to reflect the species diversity (**Supplementary Figure 1B**). By aligning with the functional gene database from GeneBank (Release 7.3 see text footnote 1), 3351 OTUs were obtained after final annotation. In general, sample H5B826 contained the highest OTU numbers (425 OTUs), and sample H7M826 contained the lowest OTU numbers (50 OTUs). Vertically, the OTU numbers displayed an increasing trend from the surface to bottom layers; horizontally, no regular pattern

[1]http://fungene.cme.msu.edu/

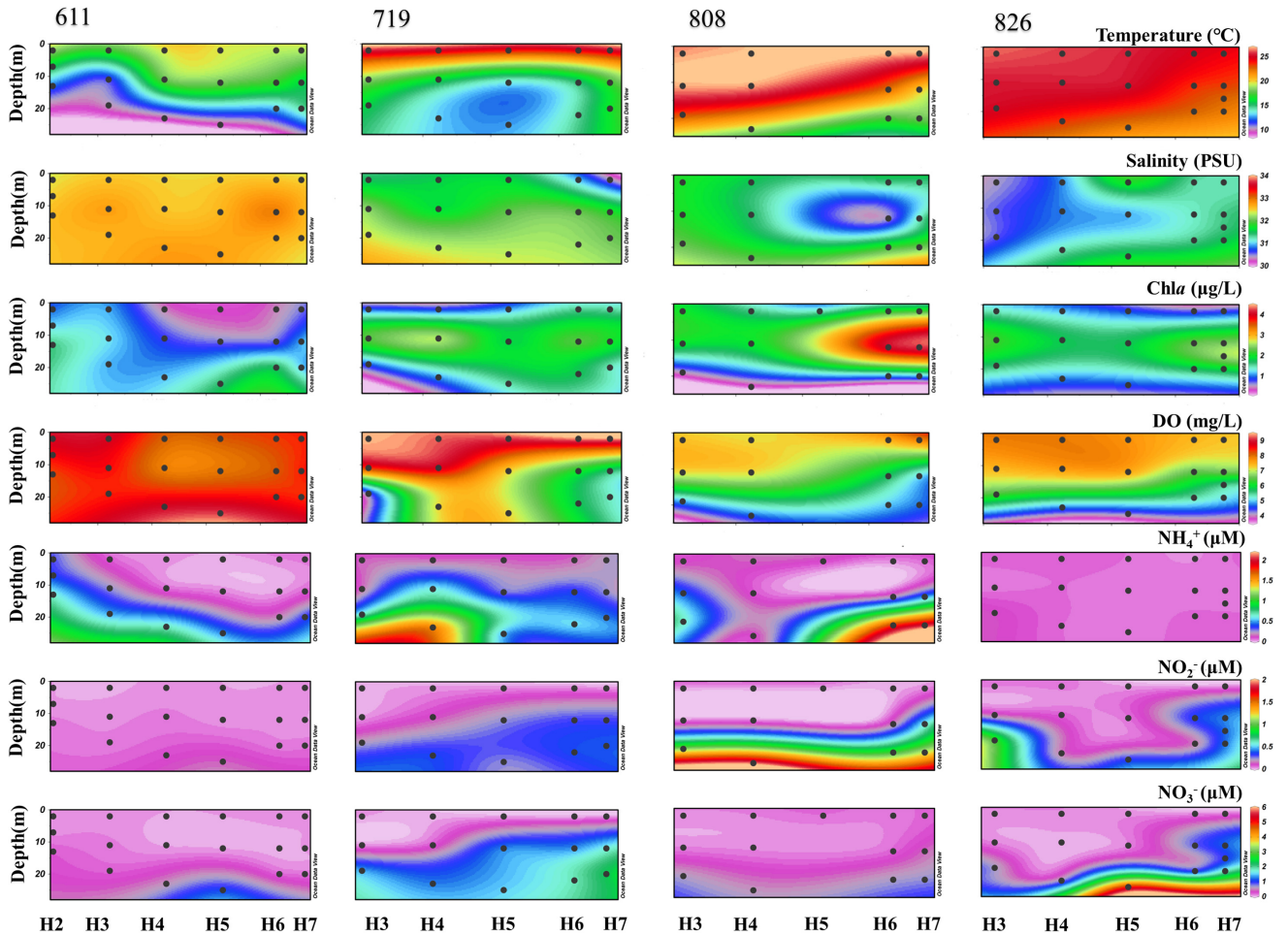

FIGURE 2 | The vertical profile of biogeochemical parameters (temperature, salinity, Chl*a*, DO, NH_4^+, NO_3^-, and NO_2^-) of each water sample.

was observed based on the OTU numbers. As displayed in **Figure 3**. Chao1 richness ranged from 51.50 to 536.98 and Shannon indices ranged from 2.55 to 4.43. Vertically, the Chao1 increased as the water layer deepens. Horizontally, the Chao1 and Shannon indices at the same water layer did not show a regular trend from inshore to offshore, except for samples from site H5 that displayed the highest value. In summary, with the occurrence of oxygen depletion in water, diversity of samples increased, which was represented by 4.03 of Shannon and 536.98 of Chao 1 in H5B826.

Community Composition of 16S rRNA and *nosZ* Gene

The total bacteria revealed by 16S rRNA gene at phylum level showed clear variations in the community both spatially and temporally. In Bohai Sea, the dominant phylum was Cyanobacteria, occupying 22.13% of all the community. Following was Proteobacteria (13.88%), Verrucomicrobia (7.10%), Actinobacteria (6.62%), Firmicutes (5.61%), and Bacteroidetes (5.60%). Phylum of Cyanobacteria was mainly composed of classes Oxyphotobacteria, which was the most dominant class (22%). Vertically, the relative abundance of Cyanobacteria in the surface and middle layer was more than one-third (40.60 and 38.18%, respectively), and their dominance was replaced by the Proteobacteria in the bottom water at all sites. From the top to bottom, the obvious decrease in relative abundance also included phylum Verrucomicrobia and Firmicutes, whereas the increasing trend was observed in Actinobacteria and Bacteroidetes (**Figure 4**). At each layer, the relative abundance of Cyanobacteria kept increasing along the time scenario, whereas the relative proportion of Proteobacteria decreased from June to August, although the absolute OTUs increased in oxygen-depleted August samples. The community composition revealed by *nosZ* gene at genus level is shown in **Figure 4**. The dominant genus was *Ramlibacter*, occupying 18.36% of all the detected communities, followed by *Pseudomonas* (9.71%), *Nitratireductor* (8.06%), *Dinoroseobacter* (5.51%), *Hoeflea* (4.19%), and *Rhodobacter* (3.86%). Denitrifying bacteria showed a stratification preference in each layer with site specification. Vertically, *Ramlibacter*, *Dinoroseobacter*, and *Rhodobacter* tended to distribute in surface layer whereas

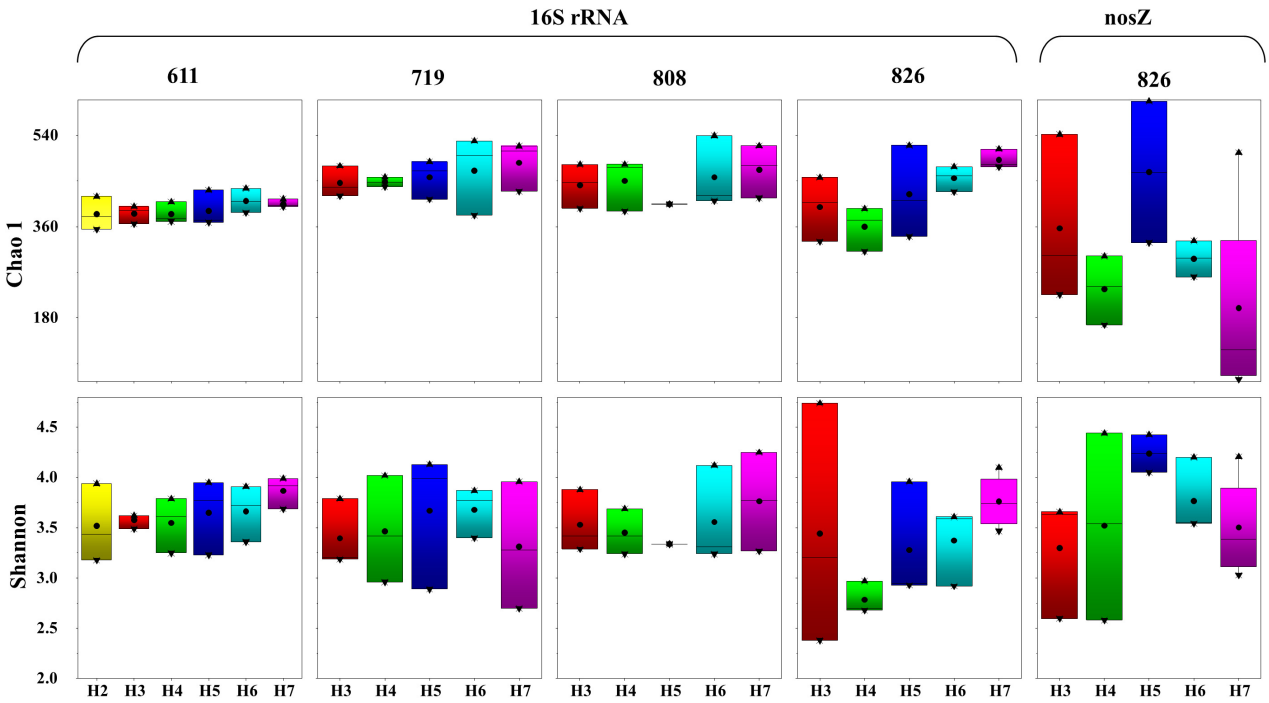

FIGURE 3 | Alpha diversity of 16S rRNA and *nosZ* gene-encoded bacteria at each sampling time. Thick bar represents median, black point represents average, boxes represent the middle 50% of the data, and whiskers represent the upper and lower quartiles.

Pseudomonas, *Nitratireductor*, and *Hoeflea* were abundant in bottom water. Horizontally, *Ramlibacter* and *Rhodobacter* were abundant in coastal sites whereas *Pseudomonas* and *Nitratireductor* preferred to offshore sites. Genus *Aeromonas* replaced *Ramlibacter* and became the dominant group in sample H5B826 when the content of oxygen significantly depleted.

Distribution of Bacterial Communities and Potential Environmental Driver

Spatial (both horizontal and vertical) and temporal distributions of total and denitrifying bacteria were evaluated by non-metric multidimensional scaling (NMDS) analysis based on binary Jaccard distance. The distribution of 16S rRNA gene was well determined by sampling time scenario (stress = 0.154), with clear patterns distinguished by June, July (before oxygen depletion), and August (after oxygen depletion) (p = 0.046–0.003). Samples from early August and late August were grouped together, showing high similarity in community composition within the same month; samples from June were distinctly separated from the rest three sampling time points, showing the distinct community variation with sampling time (**Figure 5A**). Horizontally, there was no clear pattern that could be observed from each month. Vertical distribution of community was displayed by the separation of bottom samples from the surface and middle layers, but except late August. While for *nosZ* gene, vertical distribution showed a very clear pattern separated by water depth (stress = 0.218), with samples from surface, middle and bottom layers that were grouped together, respectively (**Figure 5B**).

Canonical correspondence analysis (CCA) was performed to spot the relationship between the environmental parameter and bacterial community. Identified phylum along with 8 environmental variables (depth, temperature, salinity, Chl*a*, NO_3^-, NO_2^-, NH_4^+, and DO) was analyzed (**Figure 6A**). The length of an environmental parameter arrow in the sorting diagram indicated the strength of the relationship of that variable with community composition. For the first two CCA dimensions, 32.93 and 44.38% of the environmental variables were explained for the total variance, and the results showed that depth, salinity, Chl*a* ($p < 0.01$), and NO_2^- ($p < 0.05$) were the key impact factors shaping the bacterial community composition encoded by 16S rRNA gene. NO_3^-, NO_2^-, and depth were positively correlated with the bottom samples, indicating microbial community from bottom layer was influenced by these parameters strongly. Instead of NO_3^-, NO_2^-, and depth, bacteria communities from surface and middle layers were mostly influenced by temperature, pH, Chl*a*, and DO, among which, temperature was more positively correlated with surface samples. As for the dominant bacterial group, Actinobacteria and Proteobacteria were positively correlated with NO_3^-, NO_2^-, and depth, Bacteroidetes were highly influenced by salinity. Temperature played a key role in Cyanobacteria, especially in surface water layer. Firmicutes and Verrucomicrobia were positively correlated with DO. The results suggested that the distribution of microbial community was affected by multiple environmental factors rather than a single parameter. In addition, correlations of

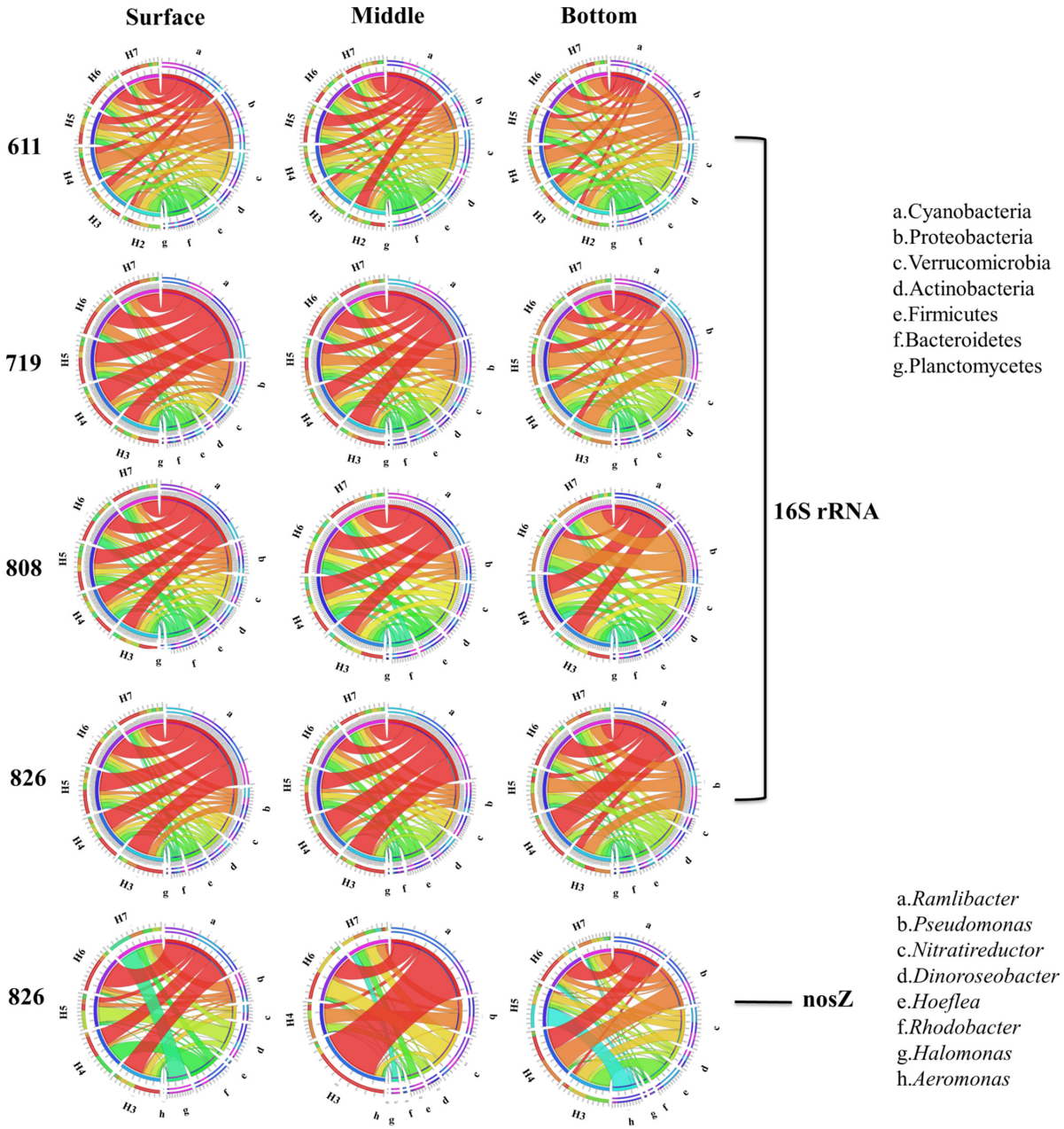

FIGURE 4 | The community composition of 16S rRNA (phylum level) and *nosZ* gene denitrifiers (genus level) was revealed by pyrosequencing.

environmental variables and August samples revealed that DO ($p = 0.002$) was the key impacting factor shaping the community composition in oxygen-depleted water (**Supplementary Table 2**). The CCA analysis for *nosZ*-encoded denitrifying bacteria further confirmed the key role of DO ($p = 0.022$) on the community composition in August. Moreover, pH ($p = 0.048$) and NO_2^- ($p = 0.038$) were also the impacting factors on the denitrifying bacterial community (**Figure 6B**). The correlations between the physicochemical factors and denitrifying bacteria in genus level showed that *Pseudomonas* and *Rhodobacter* were positively correlated with DO and pH. *Nitratireductor* was positively correlated with NO_3^- content whereas *Hoeflea* was positively correlated with concentration of NO_2^-.

The Network Analysis of Total Bacteria Community

The co-occurrence network for 16S rRNA in genus level over different sampling times was summarized in **Figure 7**. Following this, the topological properties of the obtained networks were calculated to distinguish the differences in bacterial correlations. The results showed that the total bacteria

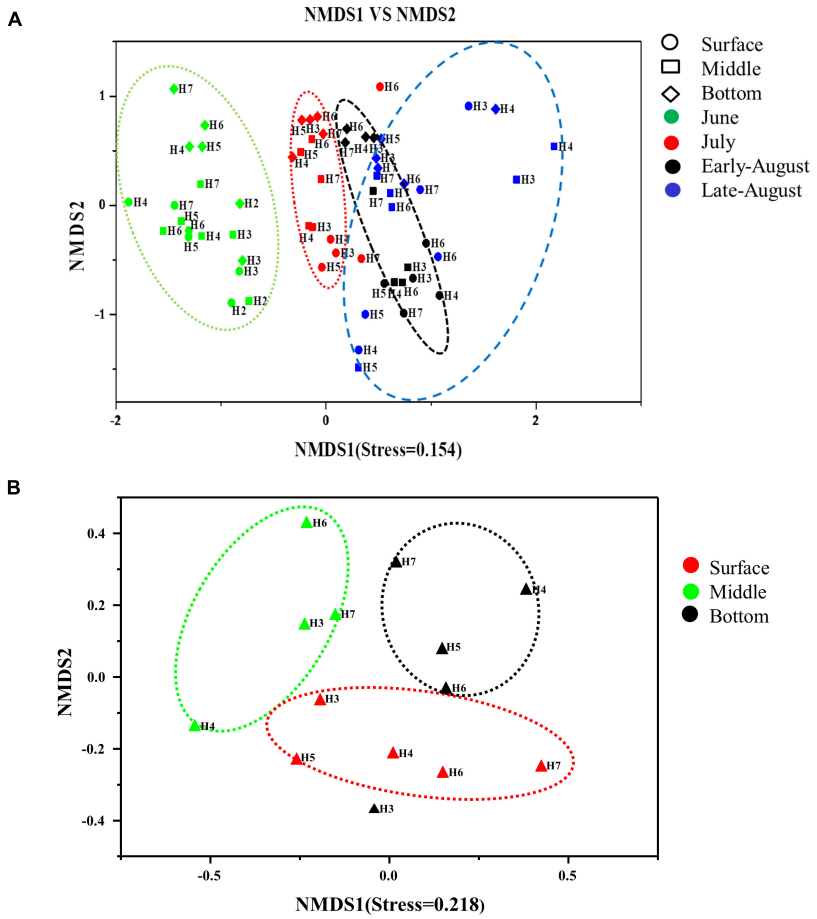

FIGURE 5 | Non-metric multidimensional scaling (NMDS) plot depicting distribution pattern of 16S rRNA **(A)** and *nosZ* gene **(B)** bacteria. Axis defines 2D space that allows the best spatial representation of sample distance, based on binary Jaccard distance with stress = 0.154 **(A)**, stress = 0.218 **(B)**. The points in the figure represent different sampling times, symbols represent different water layers, and the distance between points represents the degree of difference.

in June formed highly connected and more complex networks than the other three sampling time points. The total number of nodes (bacteria identified at the genus level) was 75 for June, 20 for July, 9 for early August, and 8 for late August. Also, the abundance of bacteria (indicated by node size) had a greater value in the network within June sample (584,401). With the passage of sampling time, the number of connections represented by links (edges) first increased and then decreased in late August, and the total links were of 75 for June, 78 for July, 80 for Early August, and 75 for late August. These results indicated that with the procession of oxygen depletion, the co-occurrences between bacterial species became weak gradually. In addition, the group of *Synechococcus*_CC9902 with relatively higher abundance in June samples had a significant difference compared with other sampling times ($p < 0.01$), indicating their unique role under oxygenated environment, which was not strong anymore when DO was depleted. A significant difference was also displayed by Cyanobium_PCC-6307 ($p = 0.004$) in July and August, the same as Akkermansia ($p = 0.014$) between June and July. The connections of these autotrophic with heterotrophic bacteria showed biotic impact on community variation under oxygen depletion.

Predicted Functional Profiling of Seawater Microbiomes

To gain insight into the peculiar functional variations in the microbiota in water column with oxygen deficiency, corresponding metagenomes were inferred from the bacteria profiles using PICRUSt2 to show Kyoto Encyclopedia of Genes and Genomes (KEGG) pathways. A differential abundance analysis was carried out and resulting in 397 MetaCyc pathways. The clustering analysis indicated a distinguished functional profile, characterized by the enrichment in pathways involved in aerobic respiration I (cytochrome c), amino acid biosynthesis [i.e., L-isoleucine biosynthesis II and L-isoleucine biosynthesis I (from threonine)], and nitrogen cycling (i.e., urea cycle, NO_3^- reduction I (denitrification), and nitrifier denitrification). Further investigation of nitrogen metabolism revealed 26 KOs (KEGG orthology) with the predicted gene copy number in the samples. Even if a certain level of dispersions was maintained,

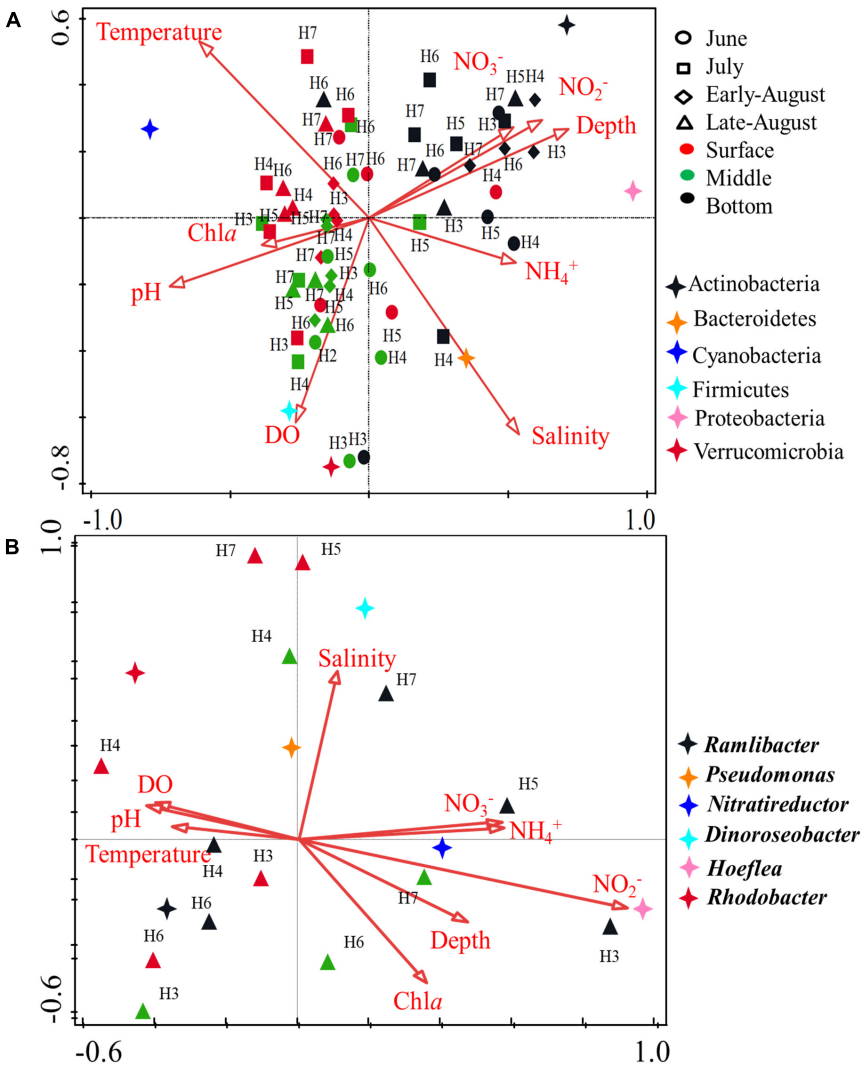

FIGURE 6 | CCA ordination plot showing the relationship of environmental parameters with total bacterial (16S rRNA gene) **(A)** and denitrifying bacteria (*nosZ* gene) **(B)**. Correlations between environmental variables and CCA axes were represented by the length and angle of arrows.

samples showed an overall tendency toward the segregation between water layers, sampling time, and sampling sites. Samples were then clustered according to the abundance profile of the 94 over-abundant pathways (**Figure 8**). Moreover, correlation between KOs related to denitrification and *nosZ* gene abundance was analyzed to reveal the relationship between functional prediction results and distribution of denitrifying bacteria. The results showed that KOs related to denitrification and *nosZ* gene abundance were correlated positively ($p < 0.05$) (**Supplementary Table 3**).

DISCUSSION

Oxygen Depletion in Bohai Sea

Ever since the discovery of periodical occurrence of oxygen depletion in Bohai Sea (Zhai et al., 2012), oxygen-depleted area in Bohai Sea has been widely revealed (Zhao et al., 2017; Zhang et al., 2019). In our study, the variation in DO concentration among the 4 sampling time points is in consistent with previous observations that the intense lower oxygen concentration occurred in August bottom water (Zhai et al., 2012; Liu et al., 2019). The highly stratified and weakly hydrodynamic water column in coastal regions is confirmed to be the primary contributor to the formation of hypoxia (Hamidi et al., 2015; Irby et al., 2016; Wei et al., 2019), which is also proved to be the causes of oxygen depletion in Bohai Sea bottom waters (Zhao et al., 2017; Song et al., 2020). Although the passing of typhoon Yagi (11–16 August 2018) and Rumbia (17–21 August 2018) through the studied area has disturbed the stratification, DO in August bottom water still reaches the lowest value at station H5 (**Figure 2**), which is the deepest site along the transaction. In summer, disturbance also occurs when the southeast wind prevailed, under which the Yellow Sea enters and merges with the water from the

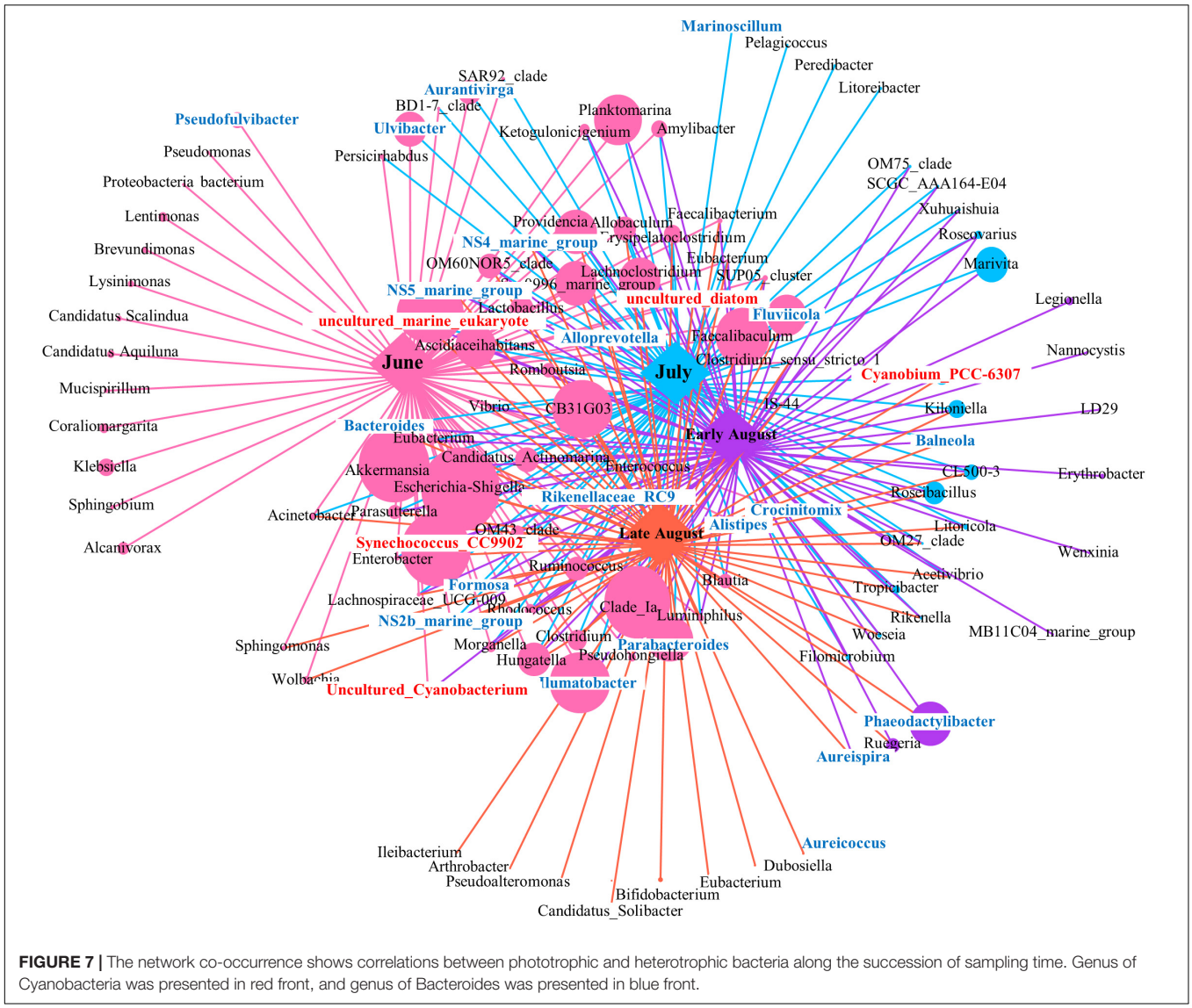

FIGURE 7 | The network co-occurrence shows correlations between phototrophic and heterotrophic bacteria along the succession of sampling time. Genus of Cyanobacteria was presented in red front, and genus of Bacteroides was presented in blue front.

central Bohai Sea and then flows out from the southern Bohai Strait (Zhang et al., 2016). Biological production, atmospheric deposition, water mixing, and release from deep sediment together with terrestrial input are all governing the source of NO_3^- availability and accounting for a high concentration of NO_3^- from inshore waters (Liu et al., 2003). Moreover, transportation or accumulation of nutrients with the help of bacteria decomposition guarantees the concentration when there is a lack of nutrients in seawater (Chu et al., 2010; Amin et al., 2015), which is further in support of growth for Cyanobacteria (Guerrini et al., 1998). Low dissolved inorganic phosphorus (DIP) values at oxygen depletion layer are assumed to make the environment not conducive to biological processes (Noffke et al., 2012). Such condition of low DIP accompanied with low DO is also observed at station H5. Kang et al. (2018) indicated that DIP concentration in the aerobic water column could be two times higher than anoxic environment. Additionally, high NH_4^+ discharge from Yellow River increases the N/P ratio in Bohai Sea, which is a noteworthy factor to shape the phytoplankton as well as the microbial compositions (Yu et al., 2018; Xin et al., 2019).

Variation of Bacteria in Response to Oxygen Depletion in Bohai Sea

To figure out the distribution of bacterial community with the local impact of Bohai Sea, published studies from different locations of Bohai Sea revealed by high-throughput sequencing analysis are summarized in **Table 1** and **Supplementary Figure 3**. Among the 4 studies originated from 2 geographical locations, in total, 3 transections from the coastal of Qinhuangdao city and Tianjin city to the central Bohai Sea are included. It is found that the community composition and dominant species of total bacteria differentiated based on the locations. The two studies from coastal area near Qinhuangdao city reported that the dominant groups were Proteobacteria and Cyanobacteria (He et al., 2017; Wang S. et al., 2019), which is similar to the

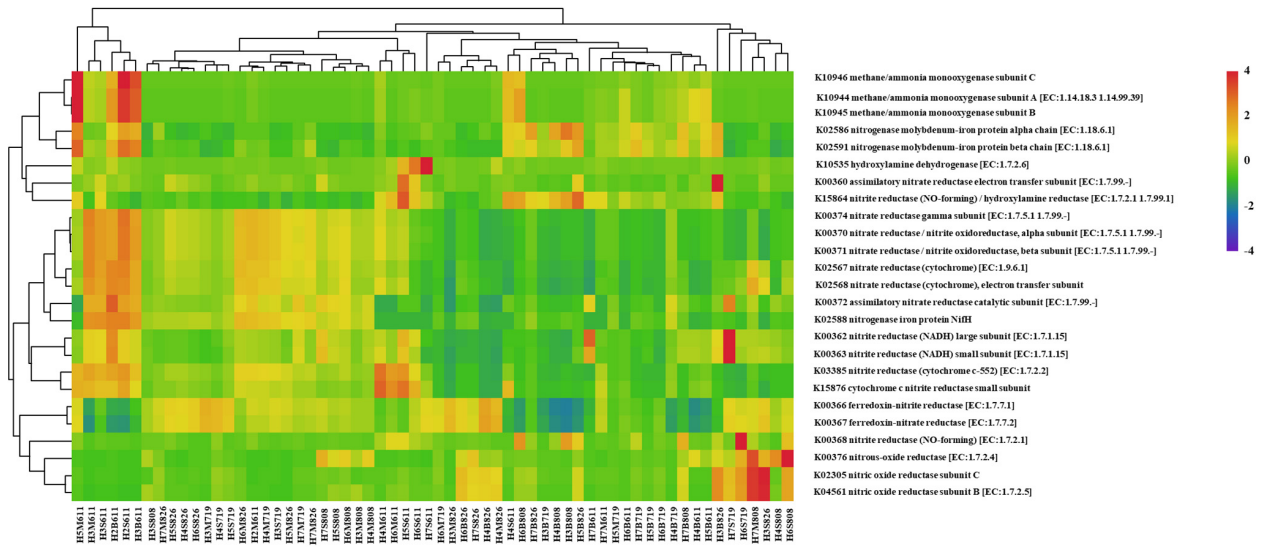

FIGURE 8 | Heatmap profile showing the nitrogen metabolism-related KO based on predicted gene copy in each sample (columns represent the 25 KEGG orthology (KO) functions, rows represent the samples, and the color intensity in the heatmap represents the abundance of the functional genes).

community compositions in this study. The other two studies with locations close to Tianjin city (39.13N, 117.2E) claimed that the dominant group is heterotrophic bacteria solely, even in the surface layer water (Fei et al., 2011; Zhao et al., 2020). Location-based dominance of bacteria species has also been reported by the studies in Pacific Ocean (Li et al., 2018), Atlantic Sea (Guerrero-Feijóo et al., 2017), and Arctic Sea (Rapp et al., 2018) (**Figure 9**). It worth to mention that DO is always a key environmental factor in shaping the composition of bacteria in marine water (Aldunate et al., 2018; De la Iglesia et al., 2020). Concentration of Chl*a* (p = 0.02 in our study) is another key factor in He et al. (2017) and our study (**Supplementary Table 2**). Although Proteobacteria have been widely reported to be dominated in Bohai Sea (**Table 1** and **Supplementary Figure 3**), the predominance of Cyanobacteria in this study is assumed to be attributed to both abiotic environmental factors (**Figure 6**) and biotic impacts (**Figure 7**). Bacterial distributions are susceptible to multiple physiochemical parameters, whereas spatial variability of microbial communities is argued to be subjected to nutrient availability, such as microbial available C (Weitzman et al., 2014), which is fixed by Cyanobacteria. In return, heterotrophic bacteria also promote the primary production, such as denitrification and N_2 fixation. The microbial interactions that could impact the bacterial communities have been confirmed in the stream sediments before (Sienkiewicz et al., 2020). In our study, Cyanobacteria represented by *Synechococcus*_CC9902 and *Cyanobium*_PCC-6307 indeed are closely positively associated with heterotrophic bacteria. On the one hand, extracellular polysaccharides derived from Cyanobacteria can provide a consistent but highly diverse class of molecules to be used exclusively as the substrates for metabolic processes by heterotrophic bacteria (Amin et al., 2015; Smriga et al., 2016); on the other hand, the carbohydrate-active enzyme can catalyze the degradation of algal polysaccharides to achieve this utilization mechanism (Lombard et al., 2014), with high levels that have been detected in Bacteroidetes (Teeling et al., 2016). This assumption is supported not only by the close correlation between Cyanobacteria (represented by red font) and Bacteroides (represented by blue fonts) in network analysis, but also from the abundance variation in Bacteroides after the Cyanobacteria bloom in species composition diagram (**Figure 4**).

In this study, Cyanobacteria dominated at the top two layers before and after oxygen depletion, with a higher preference in coastal sties. Singh and Bhadury (2018) have reported the greater fraction of Cyanobacteria among bacterial composition in summer and higher relative abundances in the coastal ocean than open sea, which is in highly agreement with our results. Nutrient enrichment originated from anthropogenic sources (urban, agricultural, and industrial) as well as water discharge and atmospheric deposition has inspired Cyanobacteria expansion and perseveration (Paerl and Scott, 2010). The significant effect of NO_3^- and NO_2^- on the distribution of Cyanobacteria (**Supplementary Table 4**) in our study is further in consistent with the above conclusions. In addition, persistent vertical stratification, high water temperature (exceeding 20°C) and low flushing rates are all characterized by our study sites and also contribute to the formation and expansion of Cyanobacteria in nutrient-enriched water bodies (Paerl et al., 2001). Among the members of Cyanobacteria, *Synechococcus* lineage is most abundant in all studied sites. Positive correlation of *Synechococcus* lineage with NH_4^+, NO_3^-, and NO_2^- concentrations reflects their preference to nutrients (Zwirglmaier et al., 2008). In our study, NO_2^- concentration is more related to the *Synechococcus* than NO_3^- (**Figure 6**). NO_3^- uptake might be inhibited by NH_4^+ when concentrations >1 μmol L^{-1} (Lindell and Post, 2001). However, *Synechococcus sp.* strain CC9902 is

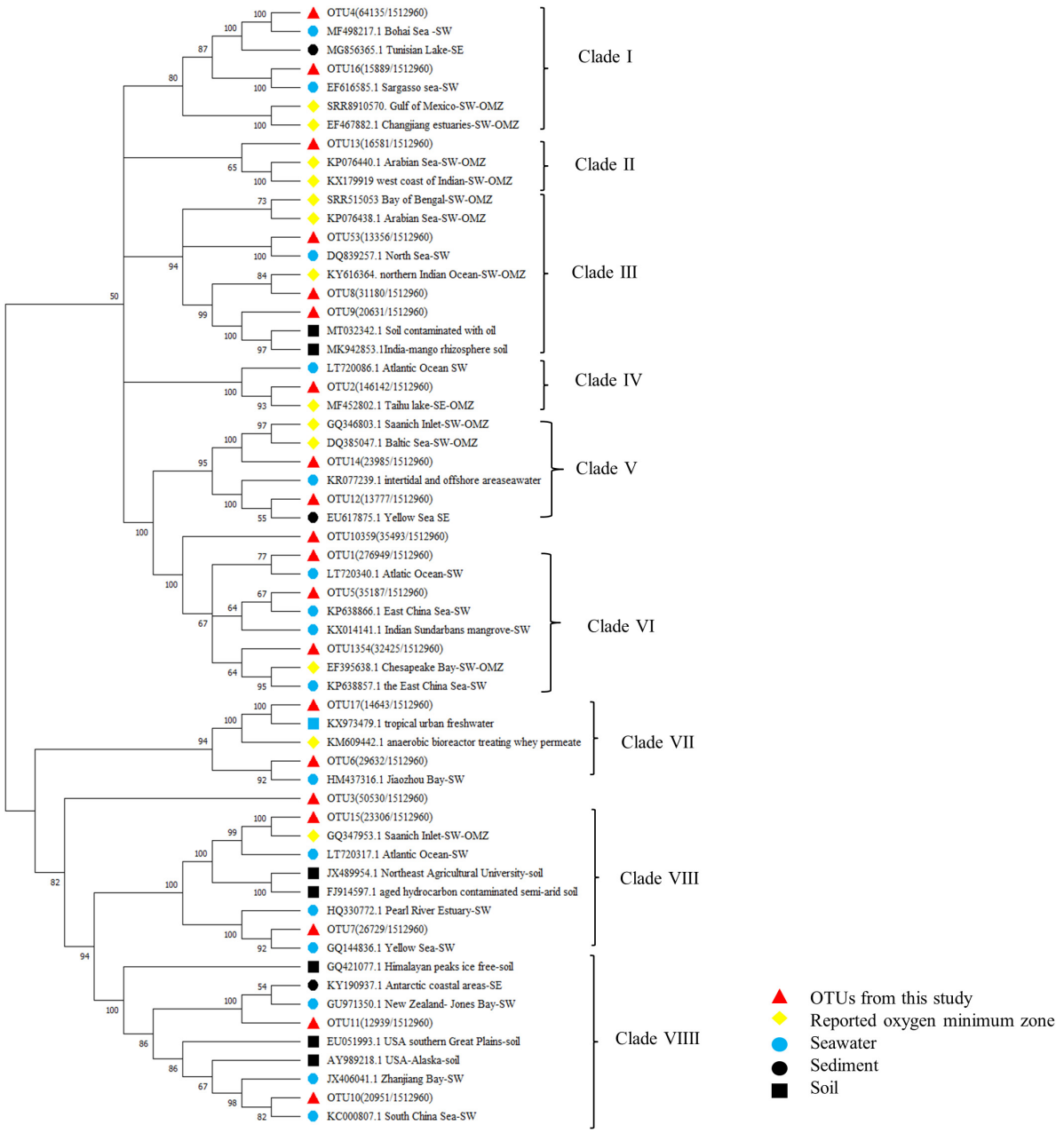

FIGURE 9 | Neighbor-joining phylogenetic tree of the dominant (Top 20 OTUs) OTUs and the reference sequences from typical OMZs. Bootstrap values were 1000 replicates.

capable of assimilating NO_2^- with the presence of high NH_4^+ concentration (Wyman and Bird, 2007). The high concentrations of NH_4^+ (up to 2.34 μmol L^{-1}) in most sites may inhibit the uptake of NO_3^- (**Supplementary Table 4**). Vertically, the close correlation of light and photosynthesis may well explain the dominance of Cyanobacteria in surface layer waters. Surprisingly, the bottom water of oxygen-depleted stie (H4 and H6 in late August) is also dominated by Cyanobacteria (**Figure 4**), which might due to their ability for photosynthesis in the hypoxic zone (Liu et al., 2015). In addition, the vertical mixing caused by typhoons is another assumption for this unexpected distribution, since the community compositions are highly similar between surface and bottom water at these two sites. In addition, *Cyanobium*-PCC-6307 with a relative abundance of 70.29% is identified in the surface water compared to other water layers. The O_2 depleted microzones caused by these cyanobacteria colonies may provide unexpected advantages for reducing nitrogen oxides in surface waters (Wyman et al., 2013).

Intense variations in bacteria community under the impact of oxygen depletion can be clearly observed in Proteobacteria,

TABLE 1 | Summary of studies on bacterial diversity and distribution in Bohai Sea.

Stations	Latitude N	Iongitude E	Sampling time	Sampling depth (m)	Environmental parameters							Impacting factors	Dominant phylum (top 5)	References
					DO (mg/L)	pH	Temp (°C)	Sal (‰)	NO_2^- (μM)	NO_3^- (μM)	NH_4^+ (μM)			
TJ01–TJ28	39.14°–38.63°	118.88°–117.64°	2014/08/17–19	0.5	5.01–8.32	7.92–8.27	23.5–29.4	23.5–29.7	0.13–4.39	1.66–8.61	0.33–12.78	Joint effects of environmental factors	Alphaproteobacteria Gammaproteobacteria Bacteroidetes Actinobacteria Deltaproteobacteria	Zhao et al., 2020
02, 04, 08	38.81°–38.89°	117.72°–117.96°	2006/04/12 2006/07/07 2006/10/23 2007/01/07	5.5 8.5 13.5	–	–	3.5–28.2	30.5–32.3	–	–	–	Temperature, salinity	Proteobacteria Flavobacteria Bacteroides Verrucomicrobia Firmicutes	Fei et al., 2011
S1–S5	39.36°–39.43°	119.31°–119.45°	2016/05/12	0.5 3 5	5.85–9.18	7.99–8.16	12.7–15.1	24.9–26.7	0.06–0.16	0.09–0.59	0.08–1.41	Phosphate	Gammaproteobacteria Alphaproteobacteria Bacteroidetes Verrucomicrobia Cyanobacteria	Wang S. et al., 2019
W1–W6	39.69°–39.90°	119.42°–119.74°	2014/03 2014/07 2014/10 2014/12	1	–	∼11.6	21–25	∼29	0.52–0.76	5.34–7.02	2.28–5.78	Temperature, DO, Chl*a*	Proteobacteria Cyanobacteria Bacteroidetes Actinobacteria Firmicutes	He et al., 2017
H2–H7	39.38°–39.69°	119.63°–120.55°	2018/06/11 2018/07/19 2018/08/08 2018/08/26	2 11–12 19–25	4.21–9.16	7.77–8.27	9.4–27.0	30.08–33.03	0.01–1.98	0.02–5.62	0.01–2.02	Depth, salinity, Chl*a*, NO_2^-, pH	Cyanobacteria Alphaproteobacteria Gammaproteobacteria Deltaproteobacteria Verrucomicrobia	This study

which are functionally related to sulfur, methane, hydroxide, sulfate reduction, and denitrification (Saarenheimo et al., 2015; Jing et al., 2020; Zhou et al., 2020). In this study, relative abundance of Proteobacteria is extremely high in bottom waters, and their dominance increases with the depletion of DO. In bottom water, Rhodobacterales are dominated within the most abundant class of Alphaproteobacteria and are highly correlated with organic particles in marine environment (Dang and Lovell, 2016). Rhodobacterales are active in the pollutant degradation when oxygen is depleted (Loy et al., 2005). SAR11, taxon followed by Rhodobacterales in Alphaproteobacteria has been reported to be ubiquitously dominated in marine surface waters (Kraemer et al., 2020). Their abundant distribution in the bottom layers in this study is most probably due to the intrusions of oligotrophic water from the eastern Bohai Sea (confirmed by CCA with a high correlation with ammonia) (**Figure 6**). Another possible reason is because SAR11 bacteria can catalyze the NO_2^- producing step of denitrification with *nar* gene-encoding proteins, which is vital in NO_3^- reduction in the anoxic zone (Tsementzi et al., 2016). Other than SAR11, the high dependence on the availability of dissolved organic matter by the abundant lineages of SAR86 and Rhodospirillaceae should be the result of accumulated NO_3^- and NO_2^- in the bottom waters when DO began depleted (Freixa et al., 2016). Gammaproteobacteria is the second large class of Proteobacteria in bottom water but overwhelming in top waters, which has been proven to be an adaptive group in some typical hypoxic environments, such as the northern Gulf of Mexico (Devereux et al., 2015), Black Sea (Jessen et al., 2017), and Baltic Sea (Broman et al., 2017). Additionally, SAR406 clade, which is reported particularly abundant in OMZs, also has the ability to reduce NO_3^-, or possibly to oxidize sulfur compounds (Thrash et al., 2017).

Variation after Cyanobacteria blooms has been found in other heterotrophic bacteria. The Eutrophication characteristics and low freshwater input in June are correlated with the high relatively abundance of Bacteroidetes in Bohai Sea, as higher nutrient levels favor their growth (Alonso-Gutiérrez et al., 2009). Bacteroidetes, aerobic bacteria, play an important role in organic matter degradation in eutrophic marine environment, which has been well confirmed by recent genome sequencing (Kabisch et al., 2014). Díez-Vives et al. (2019) describe the distribution of Bacteroidetes within the marine associated NS5 and NS2b clades that are significantly associated with depth. This is in consistent with the relative abundances of NS2b (relative abundance from the surface layer to the bottom layer is 1.5, 2.1, and 7.3%), and NS5 clades (relative from the surface layer to the bottom layer are 3.8, 6.9, and 42.2%) that high in the bottom waters in all sites. Moreover, Bacteroidetes have also been found to be associated with phytoplankton (Arnosti, 2011), but this correlation is weakened with the depletion of oxygen as shown in late August samples (**Figure 7**). Members of Flavobacteria have been reported to have preference with algal organic matter in the surface water partially in help to explain their distribution in studied area (Williams et al., 2013). Additionally, Flavobacterium is able to grow on some algal cells and utilize phytoplankton-derived polysaccharides because of its gliding motion characteristics (Tang et al., 2017). As for Verrucomicrobia, Freitas et al. (2012) find that fraction of Verrucomicrobia is higher in coastal and shallow water, as observed in this study. Together with Planctomycetes, Verrucomicrobia can form the part of a taxonomic super-phylum called PVC and occupying a higher relative abundance in upper waters (Spring et al., 2016). Such distribution of Verrucomicrobia has high possibility relating to their dependence on organic matter and contributing to the carbon cycle (Canfora et al., 2014), but rare has been found in oxygen-depleted deeper water.

Actinobacteria are abundant in coastal and deeper waters especially in August. It is speculated that rainfall and corresponding freshwater input from terrestrial might impact the presence of Actinobacteria since the Actinomycetes are homologous to many soil-originated bacteria from phylogenetic tree (**Figure 8**). Higher abundance of Firmicutes appears mostly in the samples from June, followed by late August. Sun et al. (2017) state that Firmicutes may exploit the denitrification, DNRA, or both the two pathways to remove excess NO_3^- from the environment. Water layers with higher Firmicutes proportion and accordingly low NO_2^- concentration in partial help to understand this distribution.

Nitrogen Removal Under Oxygen Depletion

Nitrate reducing bacteria that utilize and transform NO_3^- to N_2O play the important roles in the nitrogen cycling in spatial variated (both horizontally and vertically) regions where DO reach hypoxic level (Gomes et al., 2020). In our study, diverse and high percentage of NO_3^- reducing bacteria, such as *Nitratireductor*, *Pseudomonas,* and *Halomonas,* are detected in oxygen depletion sites, which potentially provides sufficient substrate for the N_2O reductase encoded by the *nosZ* gene in the reported oxygen depletion area in Bohai Sea. Furthermore, significantly negative correlation of *nosZ* gene out number with DO in August confirms that oxygen depletion can increase the abundance of N_2O consumption bacteria. This is also in consistent with the conventional conclusion that the process of N_2O to N_2 is the least oxygen tolerant anaerobic step in denitrification pathway (Zumft, 1997). N_2O consuming bacteria may be vital in understanding the N_2O flux in OMZ (Arevalo-Martínez et al., 2015). Correlation between N_2O consumption or N_2 generation rate and the abundance of *nosZ* gene showed that in addition to the interference of organic matter or other heterotrophic microorganisms in the environment, the abundance of functional genes was a key factor reflecting the production rate, which indicates the encoded corresponding enzymes that participate and catalyze biochemical processes (Choi et al., 2016; Zhao et al., 2017). In our study, the higher abundance of *nosZ* gene in the oxygen-depleted waters with the ability to convert N_2O into N_2 may help to alleviate the accumulation of the greenhouse gas N_2O from Bohai Sea. Based on the correlations of nitrogen transformation predicted by KEGG pathways from 16S rRNA gene with the relative abundance of *nosZ* gene in this study, the pathways with positive correlations are picked up and successfully sorted back to the corresponding *nosZ* gene-encoded bacteria (**Supplementary Figure 4**) to confirm the processes of

denitrification by bacteria, and the key impacting factor on the double confirmed groups of denitrifying bacteria is also revealed to be DO and NO_2^-. However, in the nearshore sites and the upper water, where the DO content is high, a considerable *nosZ* community has also been identified. The potential active *nosZ* community in these regions might capture N_2O produced in deeper seawater and thus reduce the flux into the atmosphere (Sun et al., 2017).

Ramlibacter is the most abundant denitrification group in all samples, with the preference for surface water. However, there is no *Ramlibacter* identified from surface water at site H7, and *Halomonas* replaced *Ramlibacter* as the dominant group. High salinity in surface water of H5 and H7 possibly provides a preferable habitat for *Halomonas* due to their salt-tolerant properties as one of the halophilic bacteria (Vreeland et al., 1980). Members of *Halomonas* mainly use O_2 or NO_3^- as an electron acceptor, which process competes for the substrate of denitrification process by *Ramlibacter*. *Pseudomonas* is classified as an aerobic denitrifier in the presence of NO_3^- under oxygen limited conditions (Lalucat et al., 2006), which is supposed to be dominant in the reported oxygen depletion zone (Zhai et al., 2012) at our sites H5-H7. Although typhoon disturbance increases the DO level, the high relative abundance of *Pseudomonas* at the bottom water of site H5 just verifies this assumption. *Nitratireductor*, a known denitrifying bacterium under the order *Rhizobiales*, has been identified to be the primary sink for fixed nitrogen in the OMZ of Arabian Sea (Bulow et al., 2010). *Nitratireductor* mainly participates in converting NO_3^- into NO_2^-, which is a key process for N loss. Since oxygen removal will enhance the accumulation of NO_2^- in the OMZ of Bay of Bengal (Bristow et al., 2017), high abundance of *Nitratireductor* (especially in oxygen-depleted bottom water column) and low content of DO together make a significant contribution to the release of N_2 in oxygen-depleted water of Bohai Sea.

CONCLUSION

In Bohai Sea water, Cyanobacteria dominated the bacteria community in the top two layers, whereas heterotrophic bacteria became dominant in the bottom water. Distinct distribution pattern of bacterial community was displayed before (June, July) and after (August) oxygen depletion. Vertically, denitrification bacteria showed a stable stratification when the oxygen depleted in bottom water of Bohai Sea. Distinct variations in specific total bacteria as well as denitrifying bacteria were found as a response to oxygen depletion. Other than location, depth, salinity, Chl*a*, NO_2^-, and pH together played the important roles in shaping the bacterial community. In August, DO was a key factor that determines not only the total bacteria community, but also the denitrifying bacteria composition in the studied area. In addition to environmental parameters, the interaction between microbes also affected the composition of bacteria. Furthermore, our study supplied the evidence on potential contribution of denitrifying bacteria in support of active emission of N_2 as indicated by relative abundances of N_2O reductase genes in Bohai Sea oxygen-depleted water.

DATA AVAILABILITY STATEMENT

The datasets presented in this study can be found in online repositories. The names of the repository/repositories and accession number(s) can be found in the article/ **Supplementary Material**.

AUTHOR CONTRIBUTIONS

JW contributed to the conceptualization. XG and YL contributed to the experimental operation and writing – original draft preparation. JW and GS contributed to the writing – review and editing and funding acquisition. GS and LZ contributed to the field sampling. All authors read and approved the final manuscript.

FUNDING

This study was supported by the National Natural Science Foundation of China (52070143, 42076033, and 41506182) and Natural Science Foundation of Tianjin City (19JCZDJC40300).

ACKNOWLEDGMENTS

We thank the crews for their help and cooperation during the cruises. We are grateful to the reviewers for their constructive comments and suggestions on the earlier version of this manuscript.

SUPPLEMENTARY MATERIAL

The Supplementary Material for this article can be found online at: https://www.frontiersin.org/articles/10.3389/fmicb.2022.890973/full#supplementary-material

REFERENCES

Aldunate, M., De la Iglesia, R., Bertagnolli, A. D., and Ulloa, O. (2018). Oxygen modulates bacterial community composition in the coastal upwelling waters off central Chile. *Deep Sea Res. 2 Top Stud. Oceanogr.* 156, 68–79.

Alonso-Gutiérrez, J., Figueras, A., Albaigés, J., Jiménez, N., Vinas, M., Solanas, A. M., et al. (2009). Bacterial communities from shoreline environments (Costa da Morte. Northwestern Spain) affected by the Prestige oil spill. *Appl. Environ. Microbiol.* 75, 3407–3418. doi: 10.1128/AEM.01776-08

Amin, S. A., Hmelo, L. R., Van Tol, H. M., Durham, B. P., Carlson, L. T., Heal, K. R., et al. (2015). Interaction and signalling between a cosmopolitan phytoplankton and associated bacteria. *Nature* 522, 98–101. doi: 10.1038/nature14488

Arevalo-Martínez, D. L., Kock, A., Schmitz, R. A., and Bange, H. W. (2015). Massive nitrous oxide emissions from the tropical South Pacific Ocean. *Nat. Geosci.* 8, 530–533.

Arnosti, C. (2011). Microbial extracellular enzymes and the marine carbon cycle. *Ann. Rev. Mar. Sci.* 3, 401–425. doi: 10.1146/annurev-marine-120709-142731

Babbin, A. R., Keil, R. G., Devol, A. H., and Ward, B. B. (2014). Organic matter stoichiometry, flux, and oxygen control nitrogen loss in the ocean. *Science* 344, 406–408. doi: 10.1126/science.1248364

Bertics, V. J., Löscher, C. R., Salonen, I., Dale, A. W., Gier, J., Schmitz, R. A., et al. (2013). Occurrence of benthic microbial nitrogen fixation coupled to sulfate reduction in the seasonally hypoxic Eckernförde Bay. *Baltic Sea. Biogeosci.* 10, 1243–1258.

Bristow, L. A., Callbeck, C. M., and Larsen, M. (2017). N2 production rates limited by nitrite availability in the Bay of Bengal oxygen minimum zone. *Nat. Geosci.* 10, 24–29.

Broman, E., Sachpazidou, V., Pinhassi, J., and Dopson, M. (2017). Oxygenation of hypoxic coastal Baltic Sea sediments impacts on chemistry, microbial community composition, and metabolism. *Front. Microbiol.* 8:2453. doi: 10.3389/fmicb.2017.02453

Bulow, S. E., Rich, J. J., Naik, H. S., Pratihary, A. K., and Ward, B. B. (2010). Denitrification exceeds anammox as a nitrogen loss pathway in the Arabian Sea oxygen minimum zone. *Deep Sea Res. 1 Oceanogr. Res. Pap.* 57, 384–393.

Canfora, L., Bacci, G., Pinzari, F., Lo Papa, G., Dazzi, C., and Benedetti, A. (2014). Salinity and bacterial diversity: to what extent does the concentration of salt affect the bacterial community in a saline soil? *PLoS One* 9, e106662. doi: 10.1371/journal.pone.0106662

Caporaso, J. G., Kuczynski, J., Stombaugh, J., Bittinger, K., Bushman, F. D., Costello, E. K., et al. (2010). QIIME allows analysis of high-throughput community sequencing data. *Nat. Methods* 7, 335–336. doi: 10.1038/nmeth.f.303

Chen, Q., Fan, J., Ming, H., Su, J., Wang, Y., and Wang, B. (2020). Effects of environmental factors on denitrifying bacteria and functional genes in sediments of Bohai Sea. *China. Mar. Pollut. Bull.* 160:111621. doi: 10.1016/j.marpolbul.2020.111621

Choi, A., Cho, H., Kim, S. H., Thamdrup, B., Lee, S., and Hyun, J. H. (2016). Rates of N2 production and diversity and abundance of functional genes associated with denitrification and anaerobic ammonium oxidation in the sediment of the Amundsen Sea Polynya. *Antarctica. Deep Sea Res. 2 Top Stud. Oceanogr.* 123, 113–125.

Chu, J., Xia, J., Xu, C., Li, L., and Wang, Z. (2010). Spatial and temporal variability of daily precipitation in Haihe River basin, 1958-2007. *J. Geogr. Sci.* 20, 248–260.

Dai, T., Zhang, Y., Tang, Y., Bai, Y., Tao, Y., Huang, B., et al. (2016). Identifying the key taxonomic categories that characterize microbial community diversity using full-scale classification: a case study of microbial communities in the sediments of Hangzhou Bay. *FEMS Microbiol. Ecol.* 92:fiw150.

Dang, H., and Lovell, C. R. (2016). Microbial surface colonization and biofilm development in marine environments. *Microbiol. Mol. Biol. Rev.* 80, 91–138. doi: 10.1128/MMBR.00037-15

De la Iglesia, R., Echenique-Subiabre, I., Rodríguez-Marconi, S., Espinoza, J. P., von Dassow, P., Ulloa, O., et al. (2020). Distinct oxygen environments shape picoeukaryote assemblages thriving oxygen minimum zone waters off central Chile. *J. Plankton. Res.* 42, 514–529.

Deutsch, C., Brix, H., Ito, T., Frenzel, H., and Thompson, L. (2011). Climate-forced variability of ocean hypoxia. *Science* 333, 336–339. doi: 10.1126/science.1202422

Devereux, R., Mosher, J. J., Vishnivetskaya, T. A., Brown, S. D., Beddick, D. L., Yates, D. F., et al. (2015). Changes in northern Gulf of Mexico sediment bacterial and archaeal communities exposed to hypoxia. *Geobiology* 13, 478–493. doi: 10.1111/gbi.12142

Díez-Vives, C., Nielsen, S., Sánchez, P., Palenzuela, O., Ferrera, I., Sebastián, M., et al. (2019). Delineation of ecologically distinct units of marine Bacteroidetes in the Northwestern Mediterranean Sea. *Mol. Ecol.* 28, 2846–2859. doi: 10.1111/mec.15068

Edgar, R. C. (2010). Search and clustering orders of magnitude faster than BLAST. *Bioinformatics.* 26, 2460–2461. doi: 10.1093/bioinformatics/btq461

Fei, G., Xuyun, G., Junli, W., Xiang, L., and Jingjing, L. (2011). Seasonal changes and diversity of bacteria in Bohai Bay by RFLP analysis of PCR-amplified 16S rDNA gene fragments. *World J. Microbiol. Biotechnol.* 27, 275–284.

Fortunato, C. S., and Crump, B. C. (2011). Bacterioplankton community variation across river to ocean environmental gradients. *Microb. Ecol.* 62, 374–382. doi: 10.1007/s00248-011-9805-z

Freitas, S., Hatosy, S. M., Fuhrman, J. A., Huse, S. M., Welch, D. B., Sogin, M. L., et al. (2012). Global distribution and diversity of marine Verrucomicrobia. *ISME J.* 6, 1499–1505. doi: 10.1038/ismej.2012.3

Freixa, A., Ejarque, E., Crognale, S., Amalfitano, S., Fazi, S., Butturini, A., et al. (2016). Sediment microbial communities rely on different dissolved organic matter sources along a Mediterranean river continuum. *Limnol. Oceanogr.* 61, 1389–1405.

Fu, H., Uchimiya, M., Gore, J., and Moran, M. A. (2020). Ecological drivers of bacterial community assembly in synthetic phycospheres. *PNAS* 117, 3656–3662. doi: 10.1073/pnas.1917265117

Gomes, J., Khandeparker, R., Naik, H., Shenoy, D., Meena, R. M., and Ramaiah, N. (2020). Denitrification rates of culturable bacteria from a coastal location turning temporally hypoxic. *J. Mar. Syst.* 209:103089.

Guerrero-Feijóo, E., Nieto-Cid, M., Sintes, E., Dobal-Amador, V., Hernando-Morales, V., Álvarez, M., et al. (2017). Optical properties of dissolved organic matter relate to different depth-specific patterns of archaeal and bacterial community structure in the North Atlantic Ocean. *FEMS Microbiol. Ecol.* 93:fiw224. doi: 10.1093/femsec/fiw224

Guerrini, F., Mazzotti, A., Boni, L., and Pistocchi, R. (1998). Bacterial-algal interactions in polysaccharide production. *Aquat. Microb. Ecol.* 15, 247–253.

Guo, X., Song, G., Li, Y., Zhao, L., and Wang, J. (2022). Switch of bacteria community under oxygen depletion in sediment of Bohai Sea. *Front. Mar. Sci* 9:833513. doi: 10.3389/fmars.2022.833513

Hamidi, S. A., Bravo, H. R., Klump, J. V., and Waples, J. T. (2015). The role of circulation and heat fluxes in the formation of stratification leading to hypoxia in Green Bay. *Lake Michigan. J. Great. Lakes. Res.* 41, 1024–1036.

He, Y., Sen, B., Zhou, S., Xie, N., Zhang, Y., Zhang, J., et al. (2017).). Distinct seasonal patterns of bacterioplankton abundance and dominance of phyla α-*Proteobacteria* and cyanobacteria in Qinhuangdao coastal waters off the Bohai sea. *Front. Microbiol.* 8:1579. doi: 10.3389/fmicb.2017.01579

Irby, I. D., Friedrichs, M. A., Friedrichs, C. T., Bever, A., Hood, R. R., Lanerolle, L. W., et al. (2016). Challenges associated with modeling low-oxygen waters in Chesapeake Bay: a multiple model comparison. *Biogeosciences* 13:2011.

Jäntti, H., and Hietanen, S. (2012). The effects of hypoxia on sediment nitrogen cycling in the Baltic Sea. *Ambio* 41, 161–169. doi: 10.1007/s13280-011-0233-6

Jessen, G. L., Lichtschlag, A., Ramette, A., Pantoja, S., Rossel, P. E., Schubert, C., et al. (2017). Hypoxia causes preservation of labile organic matter and changes seafloor microbial community composition (Black Sea). *Sci. Adv.* 3:e1601897. doi: 10.1126/sciadv.1601897

Jiang, T., Xu, Y., Liu, C., Zhang, Y., Ding, D., Sun, X., et al. (2016). Report on the occurrence of hypoxia in the central Bohai Sea. *Prog. Fish. Sci.* 37, 1–6.

Jing, H., Wang, R., Jiang, Q., Zhang, Y., and Peng, X. (2020). Anaerobic methane oxidation coupled to denitrification is an important potential methane sink in deep-sea cold seeps. *Sci. Total Environ.* 748:142459. doi: 10.1016/j.scitotenv.2020.142459

Kabisch, A., Otto, A., König, S., Becher, D., Albrecht, D., Schüler, M., et al. (2014). Functional characterization of polysaccharide utilization loci in the marine Bacteroidetes 'Gramella forsetii'KT0803. *ISME J.* 8, 1492–1502. doi: 10.1038/ismej.2014.4

Kan, J., Crump, B. C., Wang, K., and Chen, F. (2006). Bacterioplankton community in Chesapeake Bay: predictable or random assemblages. *Limnol. Oceanogr.* 51, 2157–2169.

Kandeler, E., Deiglmayr, K., Tscherko, D., Bru, D., and Philippot, L. (2006). Abundance of narG, nirS, nirK, and nosZ genes of denitrifying bacteria during primary successions of a glacier foreland. *Appl. Environ. Microbiol.* 72, 5957–5962.

Kang, M., Peng, S., Tian, Y., and Zhang, H. (2018). Effects of dissolved oxygen and nutrient loading on phosphorus fluxes at the sediment-water interface in the Hai River Estuary. *China. Mar. pollut. Bull.* 130, 132–139. doi: 10.1016/j.marpolbul.2018.03.029

Klar, J. K., Schlosser, C., Milton, J. A., Woodward, E. M. S., Lacan, F., Parkinson, I. J., et al. (2018). Sources of dissolved iron to oxygen minimum zone waters on the Senegalese continental margin in the tropical North Atlantic Ocean: insights from iron isotopes. *Geochim. Cosmochim. Ac.* 236, 60–78.

Kraemer, S., Ramachandran, A., Colatriano, D., Lovejoy, C., and Walsh, D. A. (2020). Diversity and biogeography of SAR11 bacteria from the Arctic Ocean. *ISME J.* 14, 79–90. doi: 10.1038/s41396-019-0499-4

Lalucat, J., Bennasar, A., Bosch, R., García-Valdés, E., and Palleroni, N. J. (2006). Biology of *Pseudomonas* stutzeri. *Microbiol. Mol. Biol. Rev.* 70, 510–547.

Langille, M. G. I., Zaneveld, J., Caporaso, J. G., McDonald, D., Knights, D., Reyes, J. A., et al. (2013). Predictive functional profiling of microbial communities using 16S rRNA marker gene sequences. *Nat. Biotechnol.* 31, 814–821. doi: 10.1038/nbt.2676

Levin, L. A. (2018). Manifestation, drivers, and emergence of open ocean deoxygenation. *Ann. Rev. Mar. Sci.* 10, 229–260. doi: 10.1146/annurev-marine-121916-063359

Li, Y., Jing, H., and Kao, S. J. (2020). Metabolic response of prokaryotic microbes to sporadic hypoxia in a eutrophic subtropical estuary. *Mar. Pollut. Bull.* 154:111064. doi: 10.1016/j.marpolbul.2020.111064

Li, Y. Y., Chen, X. H., Xie, Z. X., Li, D. X., Wu, P. F., Kong, L. F., et al. (2018). Bacterial diversity and nitrogen utilization strategies in the upper layer of the northwestern Pacific Ocean. *Front. Microbiol.* 9:797. doi: 10.3389/fmicb.2018.00797

Lindell, D., and Post, A. F. (2001). Ecological aspects of ntcA gene expression and its use as an indicator of the nitrogen status of marine Synechococcus spp. *Appl. Environ. Microbiol.* 67, 3340–3349. doi: 10.1128/AEM.67.8.3340-3349.2001

Liu, J., Fu, B., Yang, H., Zhao, M., He, B., and Zhang, X. (2015). Phylogenetic shifts of bacterioplankton community composition along the Pearl Estuary: the potential impact of hypoxia and nutrients. *Front. Microbiol.* 6:64. doi: 10.3389/fmicb.2015.00064

Liu, S. M., Zhang, J., and Jiang, W. S. (2003). Pore water nutrient regeneration in shallow coastal Bohai Sea. *China. J. Oceanogr.* 59, 377–385.

Liu, X., Liu, D., Wang, Y., Shi, Y., Wang, Y., and Sun, X. (2019). Temporal and spatial variations and impact factors of nutrients in Bohai Bay. *China. Mar. Pollut. Bull.* 140, 549–562. doi: 10.1016/j.marpolbul.2019.02.011

Lombard, V., Ramulu, H. G., Drula, E., Coutinho, P. M., and Henrissat, B. (2014). The carbohydrate-active enzymes database (CAZy) in 2013. *Nucleic. Acids. Res.* 42, 490–495. doi: 10.1093/nar/gkt1178

Loy, A., Schulz, C., Lucker, S., Schopfer-Wendels, A., Stoecker, K., Baranyi, C., et al. (2005). 16S rRNA gene-based oligonucleotide microarray for environmental monitoring of the beta*proteobacteria*l order "Rhodocyclales". *Appl. Environ. Microbiol.* 71, 1373–1386.

Menezes, L. D., Fernandes, G. L., Mulla, A. B., Meena, R. M., and Damare, S. R. (2018). Diversity of culturable Sulphur-oxidising bacteria in the oxygen minimum zones of the northern Indian Ocean. *J. Mar. Syst.* 209:103085.

Noffke, A., Hensen, C., Sommer, S., Scholz, F., Bohlen, L., Mosch, T., et al. (2012). Benthic iron and phosphorus fluxes across the Peruvian oxygen minimum zone. *Limnol. Oceanogr.* 57, 851–867.

Paerl, H. W., Fulton, R. S., Moisander, P. H., and Dyble, J. (2001). Harmful freshwater algal blooms, with an emphasis on cyanobacteria. *Scienti. Wor. J.* 1, 76–113. doi: 10.1100/tsw.2001.16

Paerl, H. W., and Scott, J. T. (2010). Throwing fuel on the fire: synergistic effects of excessive nitrogen inputs and global warming on harmful algal blooms. *Environ. Sci. Technol.* 44, 7756–7758. doi: 10.1021/es102665e

Pajares, S., and Ramos, R. (2019). Processes and microorganisms involved in the marine nitrogen cycle: knowledge and gaps. *Front. Mar. Sci.* 6:739.

Peng, S. (2015). The nutrient, total petroleum hydrocarbon and heavy metal contents in the seawater of Bohai Bay. *China: temporal–spatial variations, sources, pollution statuses, and ecological risks. Mar. Pollut. Bull.* 95, 445–451. doi: 10.1016/j.marpolbul.2015.03.032

Penuelas, J., Janssens, I. A., Ciais, P., Obersteiner, M., and Sardans, J. (2020). Anthropogenic global shifts in biospheric N and P concentrations and ratios and their impacts on biodiversity, ecosystem productivity, food security, and human health. *Glob. Change. Biol.* 26, 1962–1985 doi: 10.1111/gcb.14981

Qiao, Y., Feng, J., Cui, S., and Zhu, L. (2017). Long-term changes in nutrients, chlorophyll a and their relationships in a semi-enclosed eutrophic ecosystem. *Bohai Bay, China. Mar. Pollut. Bull.* 117, 222–228. doi: 10.1016/j.marpolbul.2017.02.002

Rabalais, N. N., and Turner, R. E. (2019). Gulf of Mexico hypoxia: past, present, and future. *Limnol. Oceanogr. Bull.* 28, 117–124.

Rapp, J. Z., Fernández-Méndez, M., Bienhold, C., and Boetius, A. (2018). Effects of ice-algal aggregate export on the connectivity of bacterial communities in the central Arctic Ocean. *Front. Microbiol.* 9:1035. doi: 10.3389/fmicb.2018.01035

Reyes, C., Schneider, D., Lipka, M., Thürmer, A., Böttcher, M. E., and Friedrich, M. W. (2017). Nitrogen metabolism genes from temperate marine sediments. *Mar. Biotechnol.* 19, 175–190. doi: 10.1007/s10126-017-9741-0

Rich, J. J., Heichen, R. S., Bottomley, P. J., Cromack, K. Jr., and Myrold, D. D. (2003). Community composition and functioning of denitrifying bacteria from adjacent meadow and forest soils. *Appl. Environ. Microbiol.* 69, 5974–5982. doi: 10.1128/AEM.69.10.5974-5982.2003

Saarenheimo, J., Tiirola, M. A., and Rissanen, A. J. (2015). Functional gene pyrosequencing reveals core *proteobacteria*l denitrifiers in boreal lakes. *Front. Microbiol.* 6:674. doi: 10.3389/fmicb.2015.00674

Sienkiewicz, N., Bier, R. L., Wang, J., Zgleszewski, L., Lutgen, A., Jiang, G., et al. (2020). Bacterial communities and nitrogen transformation genes in streambank legacy sediments and implications for biogeochemical processing. *Biogeochemistry* 148, 271–290.

Singh, T., and Bhadury, P. (2018). Distribution patterns of marine planktonic cyanobacterial assemblages in transitional marine habitats using 16S rRNA phylogeny. *Phycol. Res.* 66, 189–198.

Sinkko, H., Lukkari, K., Sihvonen, L. M., Sivonen, K., Leivuori, M., Rantanen, M., et al. (2013). Bacteria contribute to sediment nutrient release and reflect progressed eutrophication-driven hypoxia in an organic-rich continental sea. *PLoS One* 8:e67061. doi: 10.1371/journal.pone.0067061

Smriga, S., Fernandez, V. I., Mitchell, J. G., and Stocker, R. (2016). Chemotaxis toward phytoplankton drives organic matter partitioning among marine bacteria. *Proc. Natl. Acad. Sci.* 113, 1576–1581. doi: 10.1073/pnas.1512307113

Song, G., Liu, S., Zhang, J., Zhu, Z., Zhang, G., Marchant, H. K., et al. (2021). Response of benthic nitrogen cycling to estuarine hypoxia. *Limnol. Oceanogr.* 66, 652–666. doi: 10.1016/j.cbpa.2020.110657

Song, G., Zhao, L., Chai, F., Liu, F., Li, M., and Xie, H. (2020). Summertime oxygen depletion and acidification in Bohai Sea. *China. Front. Mar. Sci.* 7:25.

Spietz, R. L., Williams, C. M., Rocap, G., and Horner-Devine, M. C. (2015). A dissolved oxygen threshold for shifts in bacterial community structure in a seasonally hypoxic estuary. *PLoS One* 10, e0135731. doi: 10.1371/journal.pone.0135731

Spring, S., Bunk, B., Spröer, C., Schumann, P., Rohde, M., Tindall, B. J., et al. (2016). Characterization of the first cultured representative of Verrucomicrobia subdivision 5 indicates the proposal of a novel phylum. *ISME J.* 10, 2801–2816. doi: 10.1038/ismej.2016.84

Sun, X., Jayakumar, A., and Ward, B. B. (2017). Community composition of nitrous oxide consuming bacteria in the oxygen minimum zone of the Eastern Tropical South Pacific. *Front. Microbiol.* 8:1183. doi: 10.3389/fmicb.2017.01183

Suter, E. A., Pachiadaki, M. G., Montes, E., Edgcomb, V. P., Scranton, M. I., Taylor, C. D., et al. (2020). Diverse nitrogen cycling pathways across a marine oxygen gradient indicate nitrogen loss coupled to chemoautotrophic activity. *Environ. Microbiol.* 23, 2747–2764. doi: 10.1111/1462-2920.15187

Tang, K., Lin, Y., Han, Yu, and Jiao, N. (2017). Characterization of potential polysaccharide utilization systems in the marine Bacteroidetes gramella flava JLT2011 using a multi-omics approach. *Front. Microbiol* 8:220. doi: 10.3389/fmicb.2017.00220

Teeling, H., Fuchs, B. M., Bennke, C. M., Kruger, K., Chafee, M., Kappelmann, L., et al. (2016). Recurring patterns in bacterioplankton dynamics during coastal spring algae blooms. eLife. 5, 1–31. doi: 10.7554/eLife.11888

Thrash, J. C., Seitz, K. W., Baker, B. J., Temperton, B., Gillies, L. E., Rabalais, N. N., et al. (2017). Metabolic roles of uncultivated bacterioplankton lineages in the northern Gulf of Mexico "dead zone". *mBio* 8, e1017–e1017. doi: 10.1128/mBio.01017-17

Tsementzi, D., Wu, J., Deutsch, S., Nath, S., Rodriguez-R, L. M., Burns, A. S., et al. (2016). SAR11 bacteria linked to ocean anoxia and nitrogen loss. *Nature.* 536, 179–183. doi: 10.1038/nature19068

Voss, M., Bange, H. W., Dippner, J. W., Middelburg, J. J., Montoya, J. P., and Ward, B. B. (2013). The marine nitrogen cycle: recent discoveries, uncertainties and the potential relevance of climate change. *Philos. Trans. R. Soc. B* 368:20130121. doi: 10.1098/rstb.2013.0121

Vreeland, R. H., Litchfield, C. D., Martin, E. L., and Elliot, E. (1980). Halomonas elongata, a new genus and species of extremely salt-tolerant bacteria. *Int. J. Syst. Evol. Microbiol.* 30, 485–495. doi: 10.1007/s11274-012-1020-7

Wang, J., Kan, J., Qian, G., Chen, J., Xia, Z., Zhang, X., et al. (2019). Denitrification and anammox: understanding nitrogen loss from Yangtze Estuary to the east

China sea (ECS). *Environ. Pollut.* 252, 1659–1670. doi: 10.1016/j.envpol.2019.06.025

Wang, S., Zhang, Y., He, J., Jia, X., Lin, J., Li, M., et al. (2019). Molecular analyses of bacterioplankton communities with highly abundant Vibrio clades: a case study in Bohai Sea coastal waters. *J. Oceanol. Limnol.* 37, 1638–1648.

Wang, L., Zheng, B., and Lei, K. (2015). Diversity and distribution of bacterial community in the coastal sediments of Bohai Bay. *China. Acta Oceanol. Sin.* 34, 122–131.

Ward, B. B. (2013). How nitrogen is lost. *Science.* 341, 352–353.

Wei, Q., Wang, B., Yao, Q., Xue, L., Sun, J., Xin, M., et al. (2019). Spatiotemporal variations in the summer hypoxia in the Bohai Sea (China) and controlling mechanisms. *Mar. Pollut. Bull.* 138, 125–134. doi: 10.1016/j.marpolbul.2018.11.041

Weitzman, J. N., Forshay, K. J., Kaye, J. P., Mayer, P. M., Koval, J. C., and Walter, R. C. (2014). Potential nitrogen and carbon processing in a landscape rich in milldam legacy sediments. *Biogeochemistry* 120, 337–357.

Williams, T. J., Wilkins, D., Long, E., Evans, F., DeMaere, M. Z., Raftery, M. J., et al. (2013). The role of planktonic Flavobacteria in processing algal organic matter in coastal East Antarctica revealed using metagenomics and metaproteomics. *Environ. Microbiol.* 15, 1302–1317. doi: 10.1111/1462-2920.12017

Wyman, M., and Bird, C. (2007). Lack of control of nitrite assimilation by ammonium in an oceanic picocyanobacterium. *Synechococcus sp. strain WH 8103*. *Appl. Environ. Microbiol.* 73, 3028–3033. doi: 10.1128/AEM.02606-06

Wyman, M., Hodgson, S., and Bird, C. (2013). Denitrifying alpha*proteobacteria* from the Arabian Sea that express nosZ, the gene encoding nitrous oxide reductase, in oxic and suboxic waters. *Appl. Environ. Microbio.* 79, 2670–2681. doi: 10.1128/AEM.03705-12

Xin, M., Wang, B., Xie, L., Sun, X., Wei, Q., and Liang, S. (2019). Long-term changes in nutrient regimes and their ecological effects in the Bohai Sea. *China. Mar. Pollut. Bull.* 146, 562–573. doi: 10.1016/j.marpolbul.2019.07.011

Yang, L., Li, Z., and Zhang, X. (2011). Distribution characteristics of dissolved oxygen and mechanism of hypoxia in the upper estuarine zone of the Daliaohe River. *Environ. Sci.* 32, 51–57.

Yu, F., Xue, S., Zhao, Y., and Chen, G. (2018). Risk assessment of oil spills in the Chinese Bohai Sea for prevention and readiness. *Mar. Pollut. Bull.* 135, 915–922. doi: 10.1016/j.marpolbul.2018.07.029

Yu, L., Ma, X., Gao, H., Zong, H., Yao, X., Lin, Z., et al. (2020). Distribution and source identification of nitrogen and phosphorus in aerosols in the Qinhuangdao coast, north China. *Atmos. Environ.* 234: 117475.

Zhai, W., Zhao, H., Zheng, N., and Xu, Y. (2012). Coastal acidification in summer bottom oxygen-depleted waters in northwestern-northern Bohai Sea from June to August in 2011. *Chin. Sci. Bull.* 57, 1062–1068.

Zhang, H., Li, Y., Tang, C., Zou, T., Yu, J., and Guo, K. (2016). Spatial characteristics and formation mechanisms of bottom hypoxia zone in the Bohai Sea during summer. *Chin. Sci. Bull.* 61, 1612–1620.

Zhang, Y., Ji, G., Wang, C., Zhang, X., and Xu, M. (2019). Importance of denitrification driven by the relative abundances of microbial communities in coastal wetlands. *Environ. Pollut.* 244, 47–54. doi: 10.1016/j.envpol.2018.10.016

Zhao, H. D., Kao, S. J., Zhai, W. D., Zang, K. P., Zheng, N., Xu, X. M., et al. (2017). Effects of stratification, organic matter remineralization and bathymetry on summertime oxygen distribution in the Bohai Sea. *China. Cont. Shelf. Res.* 134, 15–25.

Zhao, W., Wang, J., Xu, S., Lei, Y., Yang, R., Shi, L., et al. (2020). Bacterioplankton community variation in Bohai Bay (China) is explained by joint effects of environmental and spatial factors. *Microbiol. Open* 9:e997. doi: 10.1002/mbo3.997

Zhou, Z., Tran, P. Q., Kieft, K., and Anantharaman, K. (2020). Genome diversification in globally distributed novel marine *Proteobacteria* is linked to environmental adaptation. *ISME J.* 14, 2060–2077. doi: 10.1038/s41396-020-0669-4

Zumft, W. G. (1997). Cell biology and molecular basis of denitrification. *Microbiol. Mol. Biol. Rev.* 61, 533–616. doi: 10.1128/mmbr.61.4.533-616.1997

Zwirglmaier, K., Jardillier, L., Ostrowski, M., Mazard, S., Garczarek, L., Vaulot, D., et al. (2008). Global phylogeography of marine Synechococcus and Prochlorococcus reveals a distinct partitioning of lineages among oceanic biomes. *Environ. Microbiol.* 10, 147–161. doi: 10.1111/j.1462-2920.2007.01440.x

Conflict of Interest: The authors declare that the research was conducted in the absence of any commercial or financial relationships that could be construed as a potential conflict of interest.

Publisher's Note: All claims expressed in this article are solely those of the authors and do not necessarily represent those of their affiliated organizations, or those of the publisher, the editors and the reviewers. Any product that may be evaluated in this article, or claim that may be made by its manufacturer, is not guaranteed or endorsed by the publisher.

frontiers | Frontiers in Microbiology

ORIGINAL RESEARCH
published: 13 June 2022
doi: 10.3389/fmicb.2022.901741

Seagrass Colonization Alters Diversity, Abundance, Taxonomic, and Functional Community Structure of Benthic Microbial Eukaryotes

Ying Pan[1], Guihao Li[2], Lei Su[3], Pengfei Zheng[3], Yaping Wang[2], Zhuo Shen[2], Zigui Chen[4], Qiuying Han[5] and Jun Gong[2,6,7]**

[1] School of Ecology, Sun Yat-sen University, Shenzhen, China, [2] Laboratory of Microbial Ecology and Matter Cycle, School of Marine Sciences, Sun Yat-sen University, Zhuhai, China, [3] Yantai Institute of Coastal Zone Research, Chinese Academy of Sciences, Yantai, China, [4] Department of Microbiology, The Chinese University of Hong Kong, Hong Kong, China, [5] College of Ecology and Environment, Hainan Tropical Ocean University, Sanya, China, [6] Southern Marine Science and Engineering Guangdong Laboratory, Zhuhai, China, [7] Guangdong Provincial Key Laboratory of Marine Resources and Coastal Engineering, Guangzhou, China

OPEN ACCESS

Edited by:
Shan He,
Ningbo University, China

Reviewed by:
Gao Chen,
The University of Tennessee, Knoxville, United States
Yabing Li,
Michigan State University, United States

***Correspondence:**
Jun Gong
gongj27@mail.sysu.edu.cn
Zhuo Shen
shenzhuo@mail.sysu.edu.cn

Specialty section:
This article was submitted to Aquatic Microbiology, a section of the journal Frontiers in Microbiology

Received: 22 March 2022
Accepted: 03 May 2022
Published: 13 June 2022

Citation:
Pan Y, Li G, Su L, Zheng P, Wang Y, Shen Z, Chen Z, Han Q and Gong J (2022) Seagrass Colonization Alters Diversity, Abundance, Taxonomic, and Functional Community Structure of Benthic Microbial Eukaryotes. Front. Microbiol. 13:901741. doi: 10.3389/fmicb.2022.901741

Seagrass form high productive ecosystems in coastal environments. However, the effects of these coastal plants on the structure and function of the belowground eukaryotic microbiome remain elusive. In this study, we characterized the community of microbial eukaryotes (microeukaryotes) in both vegetated and unvegetated sediments using 18S rRNA gene amplicon sequencing and quantitative PCR. Analysis of sequencing data showed that the eelgrass (*Zostera marina*) colonization decreased the alpha diversity indices of benthic microeukaryotes. Apicomplexa represented an average of 83% of reads across all samples, with a higher proportion at the vegetated sites. The taxonomic community structure was significantly different between these two types of sediments, for which the concentration of NH_4^+ in sediment porewater and salinity could account. Phylogenetic analyses of long 18S rRNA genes (around 1,030 bp) indicated these apicomplexan parasites are closely related to gregarine *Lecudina polymorpha.* Determination of 18S rRNA gene abundances provided evidence that the eelgrass markedly promoted the biomass of the gregarine and all microeukaryotes in the seagrass-colonized sediments and confirmed that the gregarine was hosted by a polychaete species. Significantly higher gene abundances of heterotrophs and mixotrophs were found at the vegetated sites, which could be explained by the finer sediments and short supply of dissolved inorganic nitrogen, respectively. The pigmented protists were more abundant in 18S rRNA gene copies at the lower and higher pH levels than at the intermediate. Nevertheless, the fractions of heterotrophs and phototrophs in the community were significantly related to porewater N:P ratio. These results indicate that seagrass colonization significantly induces an increase in overall biomass and a decrease in diversity of benthic microeukaryotes, making them more heterotrophic. This study also highlights that the hotspot of eukaryotic parasites could be linked with the high productivity of a natural ecosystem.

Keywords: community structure, belowground diversity, protist, parasite, high throughput sequencing, functional composition

INTRODUCTION

Seagrass meadows in shallow estuarine and coastal environments are globally important ecosystems that provide habitats for thousands of fish, bird, and invertebrate species (Han et al., 2017; McKenzie et al., 2020). Seagrass trap particulates from the overlying water, deposit and bury tissue detritus, release dissolved organic matter and dissolved oxygen through roots, which fuel macro- and microorganisms, and modify geochemical characteristics of the sediments they colonize (Garcias-Bonet et al., 2012). Seagrass colonization has been demonstrated to not only enhance the abundance of microbes such as bacteria, archaea, and some specific prokaryotic lineages, but also their diversity in the sediments (Sun et al., 2015; Zheng et al., 2019; Lin et al., 2021). The microbial communities in vegetated sediments could in turn support seagrass productivity and maintain health *via* mediating carbon, nitrogen, and sulfur cycling, and oxidizing potentially toxic sulfides (Ikenaga et al., 2010; Sun et al., 2015; Wang et al., 2021). Nevertheless, recent advances in studying seagrass-associated microbial diversity are mainly restricted to prokaryotes, and little is known about the microbial eukaryotes (microeukaryotes).

The effects of seagrass on quantity and community structure of microeukaryotes in the sediments they colonize are perceivable, but remain to be experimentally investigated. From a functional point of view, seagrass colonization may lead to a more heterotrophic microeukaryotic community because seagrass leaves shelter surface sediment from light, which could limit the growth and biomass of microalgae (microphytobenthos) on the sediment surface (MacIntyre et al., 1996). Furthermore, the higher prokaryotic abundance in vegetated sediments supplies more food for bacterivorous protists (Zheng et al., 2019), thus promoting the proportions and biomass of heterotrophs, such as flagellates, ciliates, and amoebae (Fenchel, 1969). Using molecular approaches, recent surveys on diversity of marine microeukaryotes have detected abundant protistan parasites in productive systems, such as deep-sea hydrothermal vents (Moreira and López-García, 2003), neritic oceans (Gong et al., 2015), and polar marine environments (Liu et al., 2021). Given the cryptic nature of these microparasites and the general importance of parasites in trophic interactions affecting food web structure, keystone species, and ecosystem processes (Preston and Johnson, 2010; Fischhoff et al., 2020), the identities of microeukaryotic parasites and their hosts in sedimentary systems remain to be revealed and hypotheses regarding distributional patterns and regulating factors (such as the relationship with local primary productivity) have yet to be tested.

In this study, we aimed to characterize the diversity, taxonomic, and functional composition of benthic microeukaryotes in a seagrass system using sequencing of 18S rRNA genes. By comparing the vegetated and unvegetated sediments, we tested the hypothesis that seagrass colonization enhanced the diversity and quantity of benthic microbial eukaryotes and altered their taxonomic and functional composition. We detected a predominant apicomplexan parasite in these communities, which raised the question of its phylogenetic position, quantity, and distribution across sediment samples. We also assessed whether it was associated with migrating swans or infauna species. Our results support that the microeukaryotic community tends to be more heterotrophic in the seagrass-colonized sediments and that the apicomplexan parasite may be hosted by a polychaete species which tends to be more abundant in seagrass-colonized sediments.

MATERIALS AND METHODS

Study Area, Sampling, and Environmental Parameters

The seagrass system was located at the Swan Lake (Tian'ehu) lagoon (37°21′N, 122°35′E), Rongcheng Bay, Yellow Sea, northern China. This lagoon is a typical temperate habitat with eelgrass (*Zostera marina*) meadows developed properly during both the spring and summer seasons and is known as the largest swan overwintering habitat in Asia (Sun et al., 2015). Owing to the vegetation of seagrass, the lagoon is rich in biological resources such as shellfish, fish, and other benthic macro-organisms, which serve as food sources for ∼10,000 of whooper swans (*Cygnus cygnus*) that overwinter every year (Sun et al., 2020).

The sampling strategy and characterization of physiochemical parameters of water and sediments were described previously as in Sun et al. (2015). Briefly, on a day of May 2013, we sampled five sites (referred to as V1–V5 thereafter) from within an area covered by the eelgrass (*Zostera marina*) meadow, and another five sites (UV1–UV5) ∼20–40 m distant from the vegetated area but not vegetated. The top layer (∼5 cm) of the sediments was collected and stored at −80°C for DNA extraction. The temperature, pH, salinity, and concentrations of dissolved oxygen (DO) and chlorophyll *a* (Chl-*a*) of the overlying water, and the median diameter of the sediment particles, the concentrations of ammonium (NH_4^+), nitrate (NO_3^-), nitrite (NO_2^-), and soluble reactive phosphate (PO_4^{3-}) in the sediment porewater, the total organic carbon (TOC) and total organic nitrogen contents (TON), and the concentrations of metals at each site were characterized and reported in Sun et al. (2015).

After phylogenetically classifying the dominant apicomplexan parasite (*Lecudina*, see below), we were interested in the source hosts of this parasite. Instead of examining a wide range of animal candidates, we focused on two suspect species, the migrating swans, which regularly visit the lagoon every year with high abundance, and a polychaete species (*Lumbrineris latreilli*), since there are records for *Lecudina* isolates from sandworms (Leander et al., 2003). Fresh and undisturbed swan feces were collected at high tidal sites with a clean spade, put on ice, transported to the laboratory, and stored at −80°C. The live specimens of *Lumbrineris latreilli* were isolated from the sediments colonized by the eelgrass. The worms were washed with seawater and then sterilized seawater on site for several times to minimize contamination, put into liquid nitrogen, and then stored at −80°C until DNA extraction.

DNA Extraction and Microeukaryotic 18S rRNA Gene Amplicon Sequencing

The extractions of DNA from 0.5 to 0.7 grams of sediments, swan feces, and *Lumbrineris latreilli* specimens were performed using the FastDNA spin kit for soil (MP Biomedical, USA) according to the manufacturer's instruction. The DNA integrity was verified on a 1.5% agarose gel, and the DNA purity and concentration were determined using an ND-2000C spectrophotometer (NanoDrop, USA). The extracted DNA was stored at −80°C for later use.

For high-throughput sequencing, the DNA of both vegetated (V1–V5) and unvegetated (UV1–UV5) sediment samples was sent to Novogene (Beijing, China) for MiSeq sequencing using the eukaryote-universal primers 82F (5′-GAAACTGCGAATGGCTC-3′, López-García et al., 2001) and 516R (5′-ACCAGACTTGCCCTCC-3′, Amann et al., 1990). Each sample was identified with a specific 6-bp barcode in the reverse primers. Each 30 μL of PCR reaction solution contained 2× Phusion High-Fidelity PCR Master Mix (New England Biolabs), 0.2 μM of each primer, and 10 ng of DNA. The PCR was performed with a T100 Thermal Cycler (Bio-Rad, USA) with an initial denaturation at 98°C for 1 min, followed by 30 cycles of denaturation at 98°C for 10 s, annealing at 50°C for 30 s, and elongation at 72°C for 30 s, with the last extension step at 72°C for 5 min. Paired-end sequencing was performed with an NEB Next Ultra DNA Library Prep Kit for Illumina on the Illumina MiSeq platform (Illumina, USA) by an outside company (Novogene, Beijing, China).

Bioinformatic Analysis of Microeukaryotic 18S rRNA Gene Short Reads

Raw data of MiSeq sequencing were processed and analyzed based on QIIME v.1.9.0 (Caporaso et al., 2010) and Mothur v.1.35.1 (Schloss et al., 2009). Quality filtering was according to the following criteria: quality score > 20; no ambiguous bases; no primer sequence mismatches; and homopolymers ≤6. Chimera checking was run with USEARCH v.61 based on the SILVA database (119 release), and the putative chimeric sequences were removed. After quality filtering of 353,164 raw reads of 18S rRNA genes, a total of 203,339 reads retained were clustered into operational taxonomic units (OTUs) at 97% sequence similarity with UCLUST v.1.2.2 (Edgar, 2010), and representative sequences of the OTUs were extracted to assign taxonomic classification against the PR^2 database (Guillou et al., 2013). Singletons (the OTUs containing a single read across all samples) were excluded prior to further analysis. The reads of macro-organisms were discarded before subsequent analyses (Zhu et al., 2018).

To normalize the sampling effort, datasets were rarefied to the minimal number of reads across the samples (8,710 sequences) for microeukaryotes. We calculated alpha diversity estimators including OTU richness, Chao1, Simpson, and Shannon indices. Bray–Curtis dissimilarity index-based beta diversity was calculated and visualized using non-metric multiple dimensional scaling (nMDS) in the package PRIMER v.6.0 (Clarke and Gorley, 2006). The ANOSIM function within PRIMER was performed to test the hypothesis that microeukaryotic community was different between the vegetated and unvegetated sediment sites. The contributions of taxonomy groups to the community dissimilarity between these two sites were calculated using the function SIMPER. Redundancy analysis (RDA) was used to explore correlations between environmental factors and variations in communities with CANOCO v.4.5 with a Monte Carlo permutation test (999 permutations) (ter Braak and Smilauer, 2002).

Microeukaryotic 18S rRNA Gene Cloning and Sanger Sequencing

Longer 18S rRNA gene fragments (∼1,030 bp) of microeukaryotes, which provide generally finer resolution of taxonomic classification of eukaryotic species, were obtained for sediment and feces samples *via* clone libraries and Sanger's sequencing. The eukaryote-universal primers E528F: 5′-CGGTAATTCCAGCTCC-3′; Edgcomb et al., 2002) and 1391RE (5′-GGGCGGTGTGTACAARGRG-3′; Dawson and Pace, 2002) were used in PCR reactions. Each reaction solution (25 μl) contained 2.5 μl 10× *Taq* buffer, 0.5 μl dNTP (2.5 μM), 1 μl of each primer (10 μM), 0.125 μl *Taq* polymerase (5 U μl^{-1}), 1 μl DNA template, and 18.875 μl ddH_2O (Thermo Scientific, USA). The PCR amplification program was as follows: an initial denaturation at 94°C for 5 min, 30 cycles of denaturation at 94°C for 60 s, annealing at 56°C for 60 s, and elongation at 72°C for 150 s, with a final elongation at 72°C for 10 min. PCR products derived from the five sediment samples were pooled to generate a clone library for the vegetated (V_Clone) and the unvegetated (UV_Clone), respectively. Another library was prepared for the fecal samples of swans. The PCR products were purified using a TIANprep Midi Purification Kit (Tiangen, Beijing, China), and clone libraries were constructed using InsTAclone PCR Cloning Kit (Thermo Scientific, USA). The positive clones were subjected to colony PCR with primers M13F/M13R; the PCR products were further analyzed using restriction fragment length polymorphism (RFLP) with restriction enzymes *Msp*I and *Hal*I (Thermo Scientific, USA). Digestion was conducted on 37°C water bath for 2 h, and the products were checked on 2% agarose gels to identify RFLP types. Several clones of each RFLP type were selected for Sanger sequencing, which was performed in both directions on ABI 3700 sequencer (Sangon, Shanghai). We randomly sequenced 96 and 124 positive clones for vegetated and unvegetated sediment samples, respectively.

Phylogenetic Analysis of 18S rRNA Gene Sequences

Environmental sequences from the sediment and swan feces clone libraries were checked to remove possible chimers using Bellerophon (Huber et al., 2004). For sediment clone library, OTUs were determined at 97% cutoff with the Mothur package. After removing putative chimeric sequences, 77 and 86 sequences were retained for vegetated and unvegetated sediment samples, respectively. Representative sequences of microeukaryote and possible gregarine OTUs identified by BLASTn appended with closely related sequences derived from GenBank were used in

phylogenetic analyses. The sequences were aligned using MAFFT (Katoh and Standley, 2013), and the alignment was manually adjusted. A maximum likelihood (ML) tree was constructed by RaxML v8.2, with an appropriate model GTRGAMMAI and 1,000 bootstrap analysis (Stamatakis, 2014). A Bayesian inference (BI) tree was constructed using MrBayes v. 3.2.6 with a GTR + I +G model (Ronquist et al., 2012). Four MCMC chains were run for 3,000,000 generations and sampled every 100 generations. The first 750,000 generations were discarded as burn-in. For the swan feces clone library, sequences from each RFLP type were identified by BLASTn to get closely related microeukaryote species that were morphologically identified. A pie was drawn according to the proportion of each type by Microsoft Excel to recover the microeukaryote community structure in swan feces.

Quantitative Real-Time PCR (qPCR) of *Lecudina polymorpha*

Specific primers of the species *Lecudina polymorpha* (Apicomplexa, Gregarines), for which the 18S rRNA gene fragments were found to be very abundant in the eukaryotic microbiome in this study, were newly designed and verified as previously described (Su et al., 2018). Briefly, the primers were first evaluated *in silico* using probeCheck and further tested by constructing clone library for seagrass sediment environmental DNA. The PCR program for the primer set 651F/Gre736R was as follows: 94°C for 5 min, 30 cycles of 94°C for 1 min, 57°C (55°C for Gre1138F/Gre1378R) for 1 min, 72°C for 30s, and a final extension at 72°C for 10 min. Clone library screening and Sanger sequencing were as above described. Bellerophon was used to identify chimeras in newly obtained environmental sequences. A maximum likelihood (ML) tree consisting 13 gregarine sequences retrieved from GenBank and the 69 sediment clone sequences used in primer design was built using FastTree (Price et al., 2009) to check the phylogenetic positions of the resulting sequences derived from qPCR assays.

The qPCR assays were performed with SYBR Green Dye on an ABI 7500 Fast Real-Time PCR System (Applied Biosystems, USA) with the new primer set Gre651F/Gre736R to obtain the *L. polymorpha* rRNA gene copy numbers in seagrass sediment and sandworm. All the reactions were performed in triplicate. The *L. polymorpha* rRNA gene copy numbers were calculated using standard curves generated *via* multiple serial dilutions (10^{-1}-10^{-10}) of the plasmid standards with inserted target rRNA gene fragments.

Functional Assignments

The functional structure of microbial eukaryotes was examined using a trait-based approach (Wang et al., 2020). In brief, the functional assignments of community members were transformed from taxonomic assignments by PR2 based on annotations of ecological (functional) traits of relatively higher ranked eukaryotic groups (Adl et al., 2019), with retaining their "abundance" information (i.e., proportions of reads) in a given community. The read proportion of the taxa assigned into a specific functional category in a community was summed to represent the "relative abundance" of that functional group, which allowed to quantitatively examine how eukaryotic functions varied across samples. In this study, three functional categories were assigned: autotrophs, mixotrophs, and heterotrophs, which were further divided into parasites and phagotrophs. To understand how the functional structure of microbial eukaryotes was organized, read proportions and calculated 18S rRNA gene abundances of these functional groups were compared between the two types of sediments and along environmental gradients.

Statistical Analysis

T-test was performed to statistically test the difference in relative and absolute abundances of major taxonomic or functional groups between vegetated and unvegetated samples. Spearman's and Pearson's correlation coefficients were calculated to explore the associations between richness, read proportions and 18S rRNA gene copy numbers of entire microeukaryotic community, individual taxa (including the dominant parasite *Lecudina polymorpha*), functional groups, and environmental factors using the package SPSS v.11.5.

RESULTS

Taxonomic Diversity and Community Composition of Benthic Microbial Eukaryotes

For all 10 samples collected from both sites, macro-organisms such as Metazoa (mainly Nematoda; on average 11.7%) and Streptophyta (mainly the eelgrass *Zostera*; on average 16.5%) accounted for highly variable proportions ranging from 0.1 to 65.4% and from 1.5 to 22.4%, respectively (**Supplementary Figure S1**). To inspect microbial eukaryotes, these reads from metazoan and eelgrass debris were discarded (**Figure 1**), resulting in a total of 472 OTUs for single-celled eukaryotes. Reads of Apicomplexa dominated the communities, accounting for 83.2% of the total sequences, with the proportions ranging from 9.4 to 97% (**Figure 1**). Read proportions of Rhodophyta (0.2–41.5%; mean 7.2%), Ciliophora (0.8–12.6%; mean 3%), Chlorophyta (0.4–7.3%; mean 2.4%), and Dinophyta (0.4–1.9%; mean 1.2%) were followed. Apart from Apicomplexa, a clear dominance of phylum Rhodophyta was observed in samples UV2 and UV4, which reflected large variability of microeukaryotic community among the unvegetated sites. Other groups such as Fungi (0.8%), Mesomycetozoa (0.4%), and Ochrophyta (0.4%) were minor (**Figure 1**).

The alpha diversity estimators of microeukaryotic OTUs (Shannon, Simpson, and Chao1) were significantly higher in the unvegetated sediments than the vegetated ones ($P < 0.05$), except for OTU richness ($P = 0.10$; **Figure 2A**). Among all measured environmental factors, the concentration of metal Cd was most significantly and negatively correlated with OTU richness of microeukaryotes (Pearson's $r = -0.645$, Spearman's $\rho = -0.671$, $P < 0.05$; **Figure 2B**). Negative correlation between the concentration of Arsenic (As) and OTU richness was significant

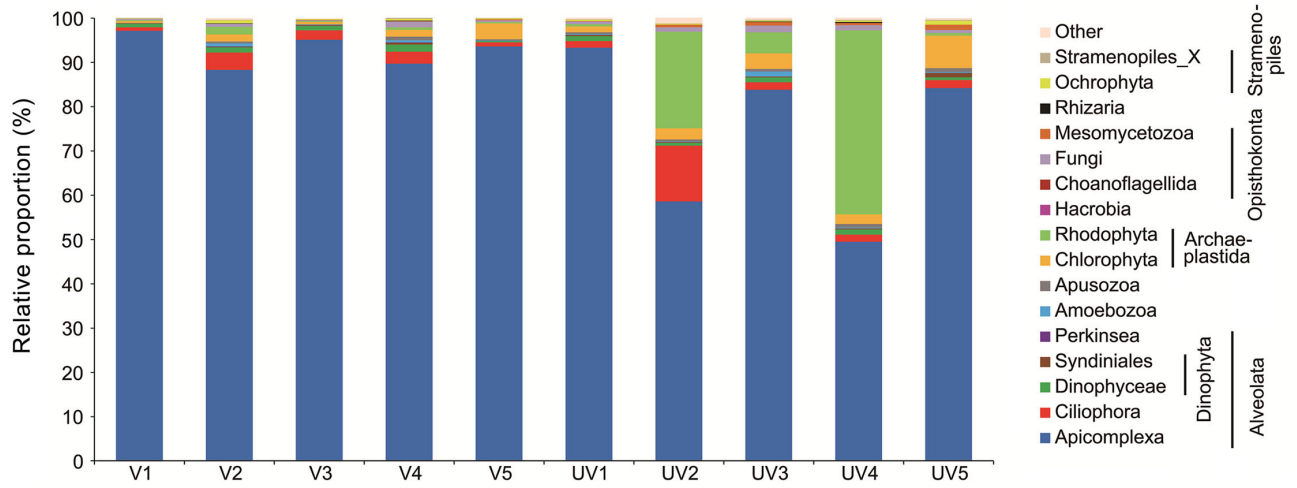

FIGURE 1 | Relative proportions of reads for benthic microbial eukaryotes across vegetated (V1–V5) and unvegetated (UV1–UV5) sites of the seagrass ecosystem.

as well ($r = -0.624$, $P = 0.05$, but $\rho = -0.491$, $P = 0.15$) across all these 10 samples (**Supplementary Figure S2**).

The nMDS plot showed that the microeukaryotic communities in the vegetated sediments were markedly different from those in the unvegetated (**Figure 3A**), which was statistically supported by ANOSIM ($R = 0.39$, $P = 0.048$). The plot of RDA showed that the concentration of NH_4^+ was the most important environmental parameter affecting the microeukaryotic community across seagrass and bare sediments ($P < 0.05$), and salinity was the factor explaining the community heterogeneity within the unvegetated sediment group ($P < 0.05$) (**Figure 3B**).

Differences in Community Structure Between Sediment Types and Contributing Lineages

SIMPER analysis could quantify the contribution of each group of microeukaryote to the community difference (**Supplementary Table S1**). The contribution of fungi to the microeukaryotic community difference between two sediment types reached 16.48%, which was the highest among all taxonomic groups of microeukaryotes, though the average read proportion of all fungi was only about 0.8%. This is likely due to distinct patterns of OTU presence between these two types of sediments as reflected by the high richness of fungi (87, **Supplementary Table S1**). Their presence or absence matters for the community, in particular if some fungal OTUs consistently existed at the vegetated sites, whereas other OTUs were absent, and vice versa. The Chlorophyta, Dinophyta, and Ciliophora, whose read proportions were on average 2.4, 1.2, and 3.0%, were responsible for 14.67, 12.68, and 12.25% of microeukaryotic community differences, respectively. Although the read proportion of Apicomplexa was up to 83.2% in the microeukaryotic communities, their contribution was only about 9.58%.

The read proportions of most eukaryotic lineages showed no substantial differences between these two types of sediments ($P > 0.05$), except for a few subgroups (**Figure 1B**; **Supplementary Table S2**). These included gregarines and tintinnid ciliates, which represented 91.96 and 0.18% reads in the vegetated samples and were significantly higher than their proportions (73.78 and 0.02%) in the unvegetated sediments ($P \leq 0.05$). In contrast, the reads of Trebouxiophyceae (0.26 vs. 0.54%), Opisthokonta (0.66 vs. 1.64%), and Mesomycetozoa (0.08 vs. 0.64%) appeared to be more abundant in the unvegetated sediments ($P < 0.05$).

Eukaryotic Diversity Based on Clone Libraries of 18S rRNA Genes

Both ML and BI trees showed that most (82%) of these non-*Zostera marina* 18S rRNA genes were affiliated to phylum Apicomplexa, whose proportion was higher in the vegetated (98%) than in the unvegetated samples (66%) (**Figures 3C,D**; **Supplementary Figure S3**), which was consistent with the MiSeq dataset (**Figure 1B**). Similarly, other 18S rRNA gene sequences belonging to cercozoans (mainly Plasmodiophoridae and Thaumatomastigidae; 17%) and benthic animals [namely genera *Enoplus* and *Oncholaimus*, family Enchelidiidae (Nematoda), family Polycystididae (Platyhelminthes), and family Loxoconchidae (Arthropoda)] were also highly represented in the unvegetated sediments (17 vs. <2% in the vegetated; **Figures 3C,D**; **Supplementary Figure S3**).

The 18S rRNA genes in swan feces examined using clone library analysis showed a markedly different eukaryotic community from those in sediments (**Figure 3E**). The gut content of swans included the eelgrass (55% in sequence proportion in the library), Metazoa (15%), Fragilariaceae (10%), Philasterida (6%), Achnanthales (4%), Bacillariophyta (3%), Cercozoa (3%), Naviculaceae (2%), and Thraustochytriaceae (2%), but no Apicomplexa (**Figure 3E**). Most of the

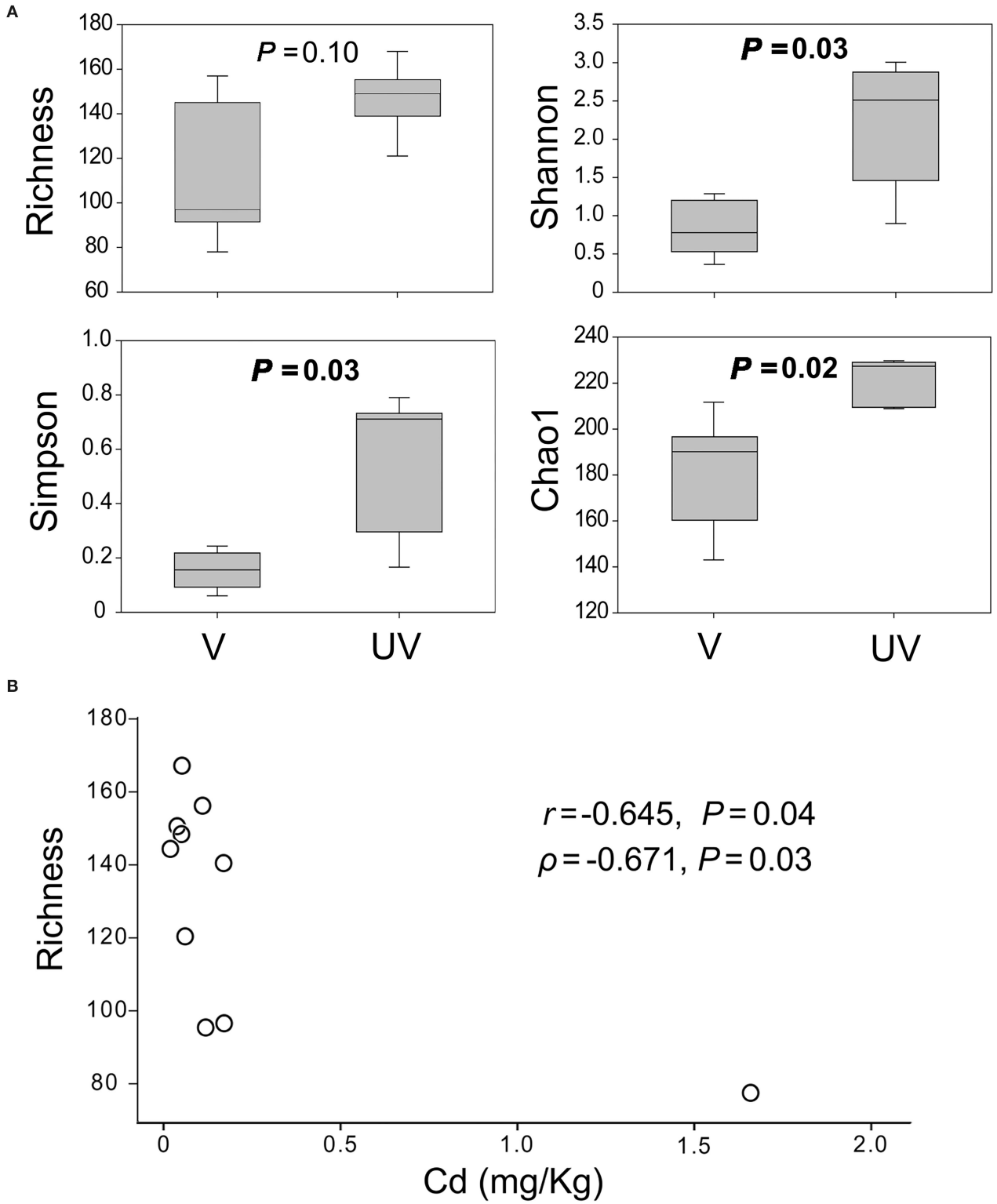

FIGURE 2 | (A) Alpha diversity indices of benthic microeukaryotic OTUs, showing the Shannon, Simpson, and Chao1 estimators of microeukaryotes were significantly higher in the unvegetated than in the seagrass-colonized sites at $P < 0.05$ according to *t*-test; **(B)** a negative correlation between microeukaryotic OTU richness and concentration of Cd.

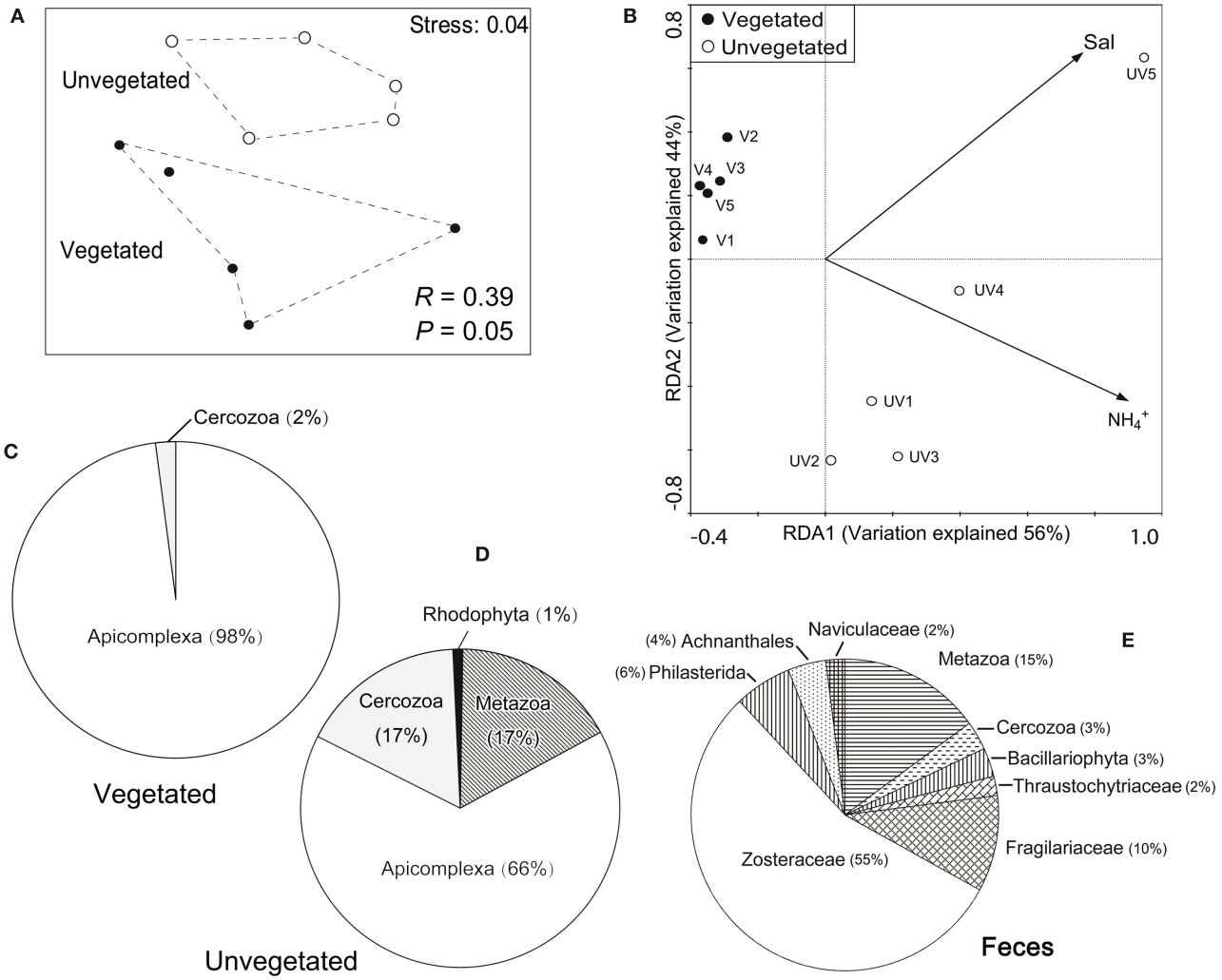

FIGURE 3 | (A) A plot of non-metric multidimensional scaling, showing that the community structure of benthic microeukaryotes was significantly different in the vegetated and unvegetated sediment types; **(B)** a plot of redundancy analysis (RDA), indicating that the changes in microeukaryotic community structure covaried significantly with the concentration of ammonium and salinity across all the 10 sites (Monte Carlo tests, $P < 0.05$); and **(C–E)** pie plots showing the sequence proportions of major eukaryotic taxa based on 18S rRNA gene clone libraries derived from the vegetated **(C)**, unvegetated **(D)**, sediments, and from swan feces **(E)**.

apicomplexan sequences (81%) had high similarities (92–94%) with that of a single described gregarine species, *Lecudina polymorpha* morphotype 2, which belonged to the family Lecudinidae, order Eugregarinorida. Sequences of another gregarine family Selenidiidae (Eugregarinorida) were also detected, but rare in the clone libraries (1%; see **Figure 4**; **Supplementary Figure S3**).

Quantification of *Lecudina polymorpha* Using QPCR

To inspect the "real abundance" of *Lecudina polymorpha*, two species-specific primer pairs, Gre651F–Gre736R and Gre1138F–Gre1378R, were newly designed for quantifying its 18S rRNA genes in environmental samples (**Table 1**; **Supplementary Figure S4**). The specificity of these primers was validated by *in silico* evaluating, cloning, sequencing, and classifying the amplicons using the environmental DNA extracted in this study (**Supplementary Figure S5**).

The qPCR results demonstrated high 18S rRNA gene abundances of *Lecudina polymorpha* in both types of sediment samples (**Figure 5**). There were $(1.65 \pm 0.15) \times 10^7$ copies g^{-1} in the vegetated samples, which was about three times higher than in the unvegetated ones [$(4.7 \pm 1.8) \times 10^6$ copies g^{-1}; $P = 0.001$, $n = 5$]. Application of the qPCR assay for DNA extracted from sandworm tissues succeeded, resulting in $(4.7 \pm 0.1) \times 10^6$ copies g^{-1} (**Figure 5**), indicating the sandworms be the host of this gregarine parasite. According to the read proportions of the apicomplexan and gene abundance obtained using qPCR, the 18S rRNA gene abundances of all microeukaryotes were

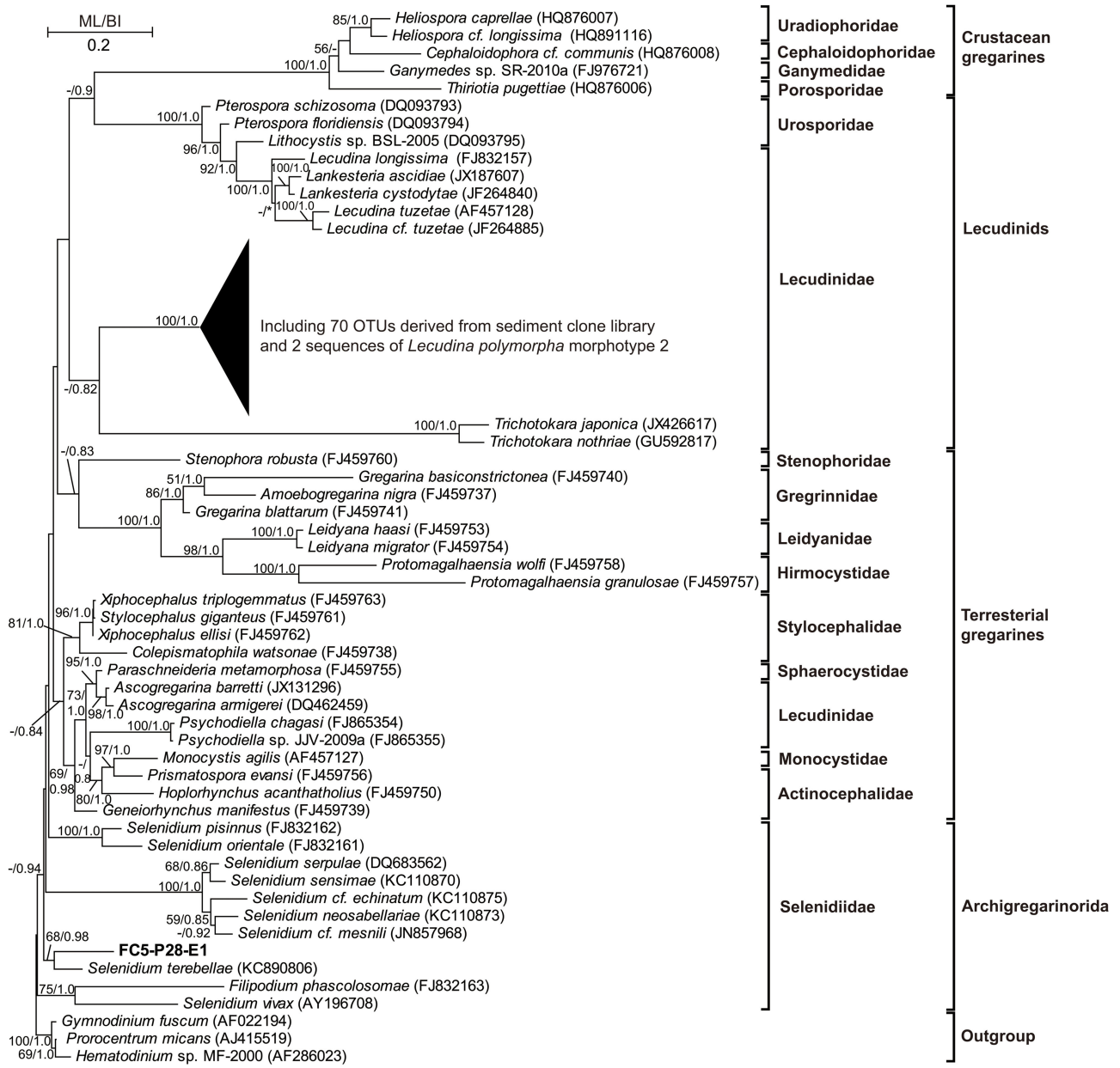

FIGURE 4 | A phylogenetic tree based on 18S rRNA genes and constructed using maximum likelihood (ML) and Bayesian inference (BI) algorithms, showing that most of the gregarine (Apicomplexa) sequences/OTUs obtained from the clone libraries are closely related to that of a described species, *Lecudina polymorpha* morphotype 2 (family Lecudinidae). A few sequences representing a single OTU are affiliated with the genus *Selenidium* (family Selenidiidae). Only bootstrap values >50 and posterior probability >0.8 are shown at the nodes; the lower values are indicated with dashes. Asterisks refer to alternate topologies.

TABLE 1 | Primers newly designed for targeting 18S regions of rRNA genes in gregarines.

Primer name	Sequence (5′-3′)	Length	GC%	Tm (°C)	References
Gre651F	GCATGGAAYACAGAATTGG	19	44.7	48.7–51.9	This study
Gre1138F	TAGGTCATAGTAACTTGGAG	20	40	47.9	This study
Gre736R	GAAACGCTYTCGCATC	16	53.1	48.9–50.8	This study
Gre1378R	CGTATTCATCGSAGACTG	18	50	49.6–50.4	This study

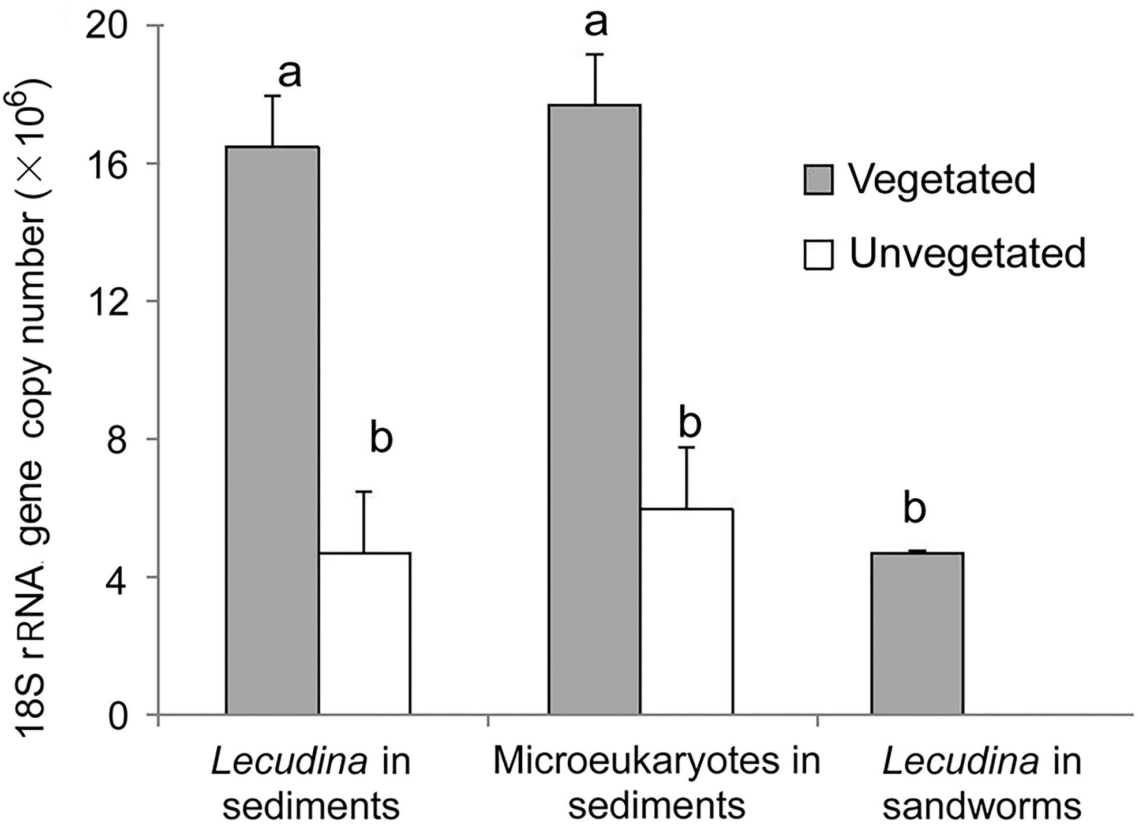

FIGURE 5 | Comparisons of 18S rRNA gene copy numbers of *Lecudina polymorpha* and all microeukaryotes between the vegetated and unvegetated sediments, and in the whole-body tissue mixture of a sandworm species. Different labeling letters (a and b) indicate that the mean values of vegetated and unvegetated samples were significantly different by *t*-test.

calculated, which showed higher abundance in the seagrass-colonized sediments [(17.7 ± 1.5) vs. $(6.0 \pm 2.0) \times 10^6$ copies g^{-1}] as well (**Figure 5**).

Correlation analysis showed that *L. polymorpha* gene abundance was significantly and positively correlated with the concentration of chlorophyll *a* in the overlying water ($r = 0.86$, $\rho = 0.65$, $p < 0.05$) and significantly and negatively with the sediment grain size ($r = -0.84$, $\rho = -0.77$; $p < 0.01$) and the concentration of ammonium in sediments ($r = -0.81$, $\rho = -0.71$; $p < 0.05$) (**Figure 6**).

Shifts in Functional Structure of Microeukaryotic Communities

Both relative proportions and gene abundances of functional groups were statistically tested between habitats and along environmental gradients (**Figure 7**; **Supplementary Figure S6**). Between vegetated and unvegetated sediments, the differences in read proportions were detected for neither parasites, phagotrophs, heterotrophs, phototrophs, nor mixotrophs (all $P < 0.05$; **Figures 7A–E**). However, the gene copy numbers of functional groups (i.e., parasites, heterotrophs, and mixotrophs) were significantly higher in seagrass-colonized sediments than in bare sediments ($P < 0.05$; **Figures 7A,C,E**).

Among all the measured environmental factors, the molar ratio of dissolved inorganic nitrogen (DIN) to phosphate (N:P) was the most significant factor related to the read proportions of phototrophs ($R^2 = 0.684$, $P < 0.05$) and heterotrophs ($R^2 = 0.674$, $P < 0.05$) in the community (**Figure 7F**). Nevertheless, absolute abundance of heterotrophs formed a quadratic relationship with grain size ($R^2 = 0.891$, $P < 0.05$), with the lowest abundance at sediment median grain size of 350 μm (**Figure 7G**). Similarly, both phototrophs ($R^2 = 0.573$, $P < 0.05$) and pigmented eukaryotes (= phototrophs + mixotrophs; $R^2 = 0.424$, $P < 0.05$) had the lowest gene copy numbers at an intermediate pH (8.17; **Figure 7H**). The mixotrophs became the least abundant at an intermediate level of DIN (ca. 1,000 μM; $R^2 = 0.845$, $P = 0.001$; **Figure 7I**).

DISCUSSION

Lower Diversity of Microbial Eukaryotes in Seagrass-Colonized Than in Bare Sediments

To our knowledge, this is the first study to compare eukaryotic microbial communities between seagrass-vegetated

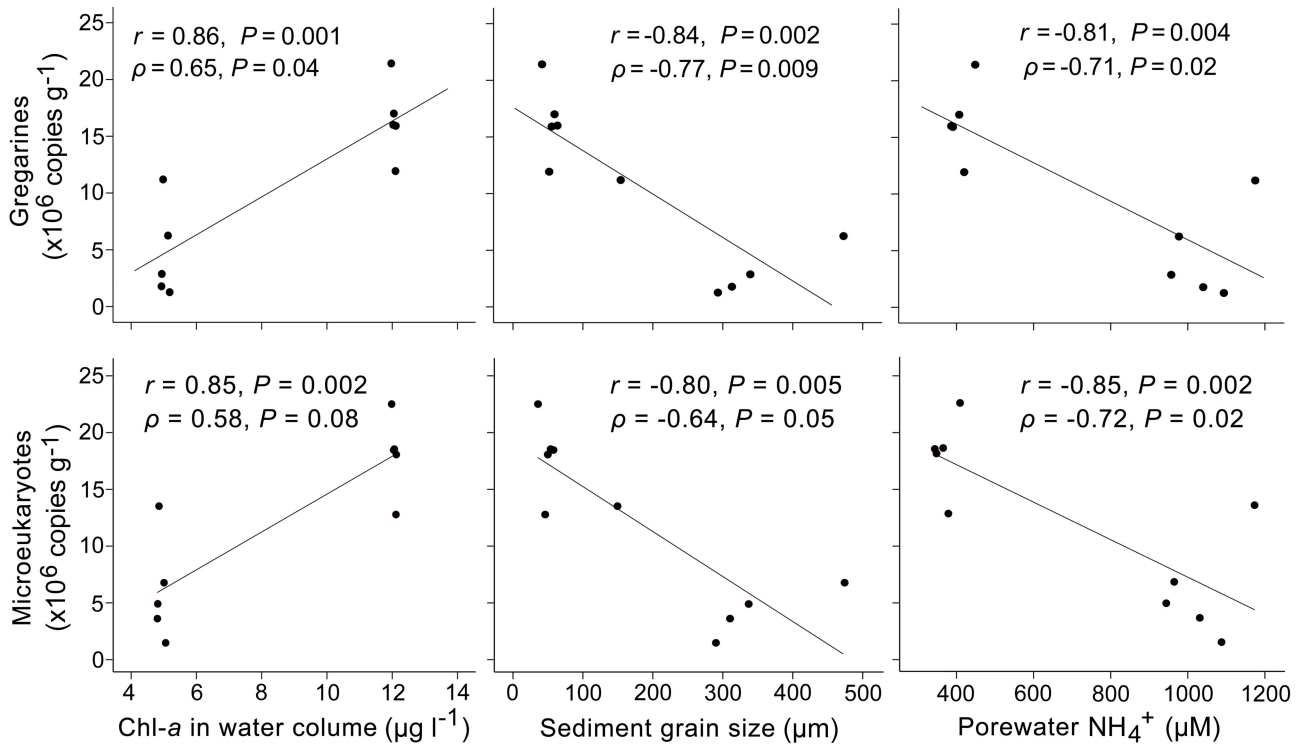

FIGURE 6 | Correlations between the 18S rRNA gene abundances of gregarine apicomplexans, all microeukaryotes, and the measured environmental factors across vegetated and unvegetated sediments. The gene copy number of gregarines was significantly and positively correlated with the concentration of chlorophyll *a* in the overlying water and negatively with the sediment grain size and concentration of ammonium in sediments. Note that the gene copy number of microeukaryotes was estimated based on the gregarine abundance and their read proportion in the community.

and unvegetated sediments using high-throughput sequencing technology. Our results showed that the unvegetated sediment harbored richer microbial eukaryotes than the vegetated one, which is different from the bacterial and archaeal communities, whose alpha diversity was not much different between these two habitats (Sun et al., 2015; Zheng et al., 2019). The different effects of seagrass colonization on alpha diversity of microbes suggest that microbial eukaryotes represent a significant module in benthic microbial food webs in response to environmental turbulence.

We found that the concentrations of several heavy metals (especially Cd) were significantly and negatively correlated with OTU richness of benthic microeukaryotes, suggesting higher concentrations of heavy metals could contribute to lower diversity of microeukaryotes in the vegetated sediments. This could be due to high sensitivity of eukaryotes to metal stress (Corcoll et al., 2019). A previous study on heavy metal pollution in the Swan Lake lagoon showed that the heavy metals (especially Cd) probably come from the use of phosphate fertilizer and corrosion-resistant painting of the fishing boats, as well as from the industrial activities of the adjacent city of Rongcheng Bay (Huang et al., 2013). Apart from this, dissolved oxygen (DO), a chemical factor not measured in this survey, could also be a factor leading to a lower diversity of microeukaryotes in the seagrass-colonized sediment. Due to DO penetration into sediments through seagrass roots at day and exclusive consumption of oxygen at night, there could be larger variability of redox status around the seagrass roots (than in the bare sediments), which may select for fewer protistan species that adapt to wider oxygen tensions (Fenchel and Finlay, 2008). In fact, the sediment near mangrove roots tends to have a lower richness of microbial eukaryotes as well (Zhu et al., 2018). In addition, the markedly higher read proportions of apicomplexan parasite OTUs in this study might have also contributed to the lower diversity of microbial eukaryotes in seagrass-colonized sediments.

Effects of Seagrass on Taxonomic and Functional Composition of Benthic Microbial Eukaryotic Community

We found that seagrass significantly affected the taxonomic composition of microbial eukaryotes in the sediments. The concentration of porewater NH_4^+ was found to be an important abiotic factor explaining the microeukaryotic taxonomic differences between the vegetated and bare sediments. NH_4^+ is known as a dissolved inorganic nitrogen species regenerated from degradation of buried organic matter. Root uptake of NH_4^+ by the seagrass could lower nitrogen availability for epibenthic microalgae (Thornton et al., 1999) and further affect their species richness and composition, which was

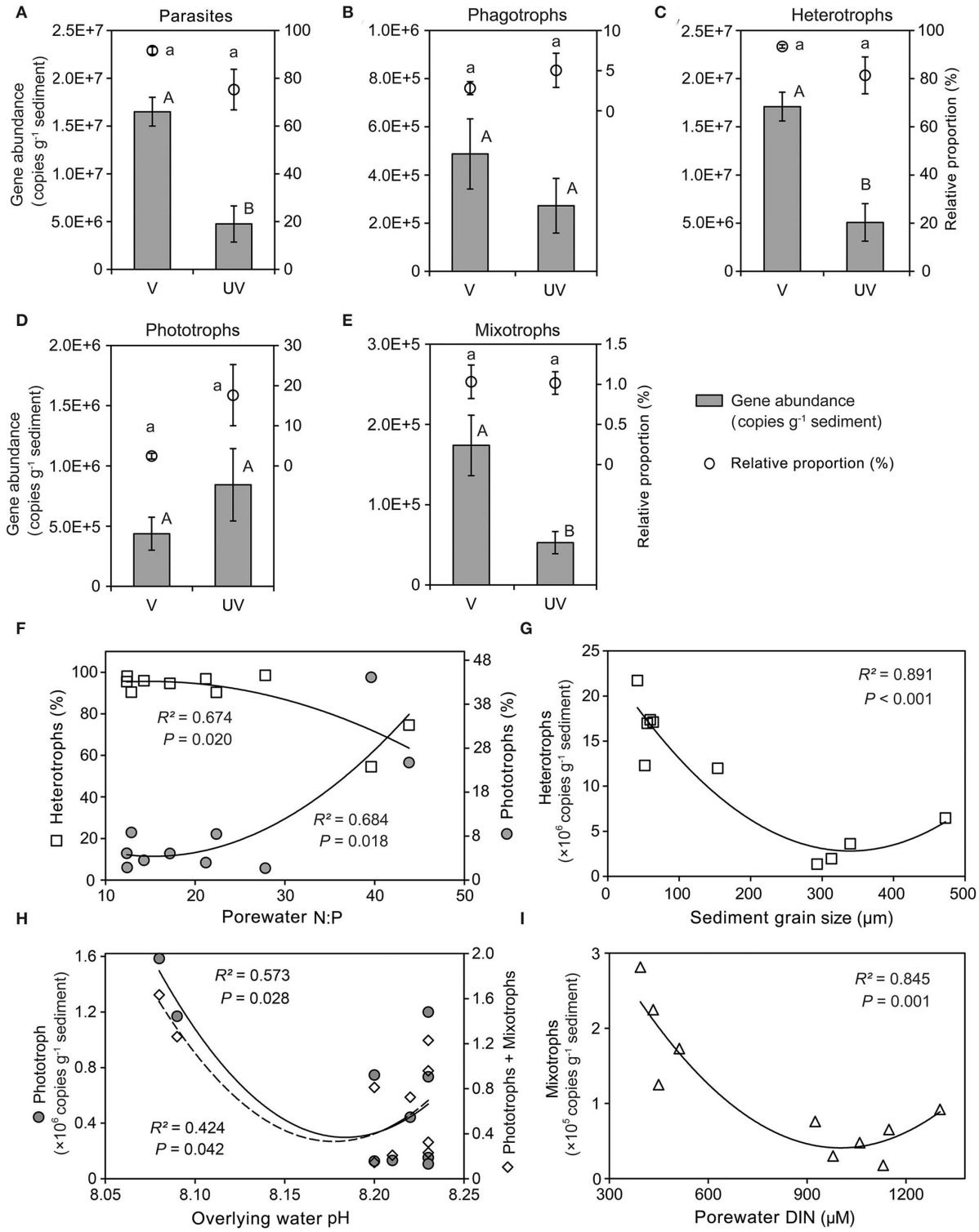

FIGURE 7 | Functional compositions of benthic eukaryotes in sediments of a seagrass system. **(A–E)** Comparison of the relative proportions and gene abundances of parasites **(A)**, phagotrophs **(B)**, heterotrophs **(C)**, phototrophs **(D)**, and mixotrophs **(E)** between vegetated and unvegetated sediments, showing that the read proportions were not significantly different for all the examined functional groups, whereas the total gene copy numbers of parasites, heterotrophs, and mixotrophs were significantly higher in the vegetated sediments; **(F)** the relative proportions of both heterotrophs and phototrophs were related to molar ratio of porewater inorganic nitrogen to phosphate; **(G–I)** the gene abundances of heterotrophs, phototrophs (also pigmented protists), and mixotrophs covaried well with sediment grain size **(G)**, overlaying water pH **(H)**, and concentration of porewater dissolved inorganic nitrogen (DIN) **(I)**, respectively.

partly supported by our result that autotrophic chlorophytes were identified to be a major contributor to the community differences (**Supplementary Table S1**). Another mechanism might be enhancement of ammonia oxidation by nitrifiers in root-associated sediments due to oxygen release through root (Sun et al., 2015; Lin et al., 2021), which resulted in structure shift of nitrogen species (i.e., more nitrate and less ammonium), thus modulating the microalgal composition of different nitrogen assimilatory preference (Dortch, 1990).

From a functionally ecological point of view, we identified significant effects of seagrass colonization on benthic microbial eukaryotes as well. According to recent findings on positive relationships between 18S rRNA gene copy number and protistan biomass (biovolume) (Fu and Gong, 2017; Zou et al., 2021), our comparisons of absolute gene abundances indicate a higher biomass of heterotrophic microeukaryotes (mostly gregarine apicomplexan parasites) in seagrass-colonized (fine) vs. bare (coarse) sediments. This is consistent with previous studies showing higher abundance of benthic animal hosts of these parasites (i.e., polychaetes; see below) at the sites with a higher seagrass biomass and finer sediments (Omena and Creed, 2004; Abrogueña et al., 2021). Apart from the parasites, tintinnid ciliates were identified to have higher biomass at the vegetated sites (**Supplementary Table S2**), indicating that free-living protozoa contributed to the functional shift in microeukaryotic community. Nevertheless, understanding the direct cause of higher planktonic ciliates in seagrass-associated sediments needs more details, for example, whether these ciliates present at an inactive life cycle stage (cysts), relic DNA, and whether they inhabit surface sediments warrant further investigation (Zhu et al., 2018; Zou et al., 2021).

It is interesting to observe that the gene abundance of benthic microphytobenthos (= phototrophs + mixotrophs) forms a U-shaped relationship with pH of overlying waters, instead of nutrient concentrations in waters or sediments (**Figure 7H**). This result is in line with the study of microphytobenthos in seagrass systems in south Florida (Fourqurean et al., 2010). Our previous characterization of environmental variables across the studied sites showed that both chlorophyll *a* concentration (average 12.1 vs. 5.0 μg/L) and pH value (average 8.22 vs. 8.16) in overlying waters were higher in seagrass sites (Sun et al., 2015), suggesting that spatial heterogeneity of seawater pH was shaped by photosynthetic activity and biomass of seagrass and phytoplankton, which increase pH by absorbing dissolved CO_2. The U-shaped relationship suggests that there were different processes controlling the growth of microphytobenthos along the pH gradient. At certain bared sites with a distance from the seagrass bed, there were no seagrass canopy and roots competing for sunlight and regenerated nitrogen, which could promote the growth of microphytobenthos, leading to the highest autotrophic biomass at the lowest pH (left side of the U-shaped curve). At the vegetated sites, microphytobenthos might suffer from competing with abundant seagrass, which corresponded to the upper range of pH. However, epiphytic microalgae detached from seagrass leaves may settle to sediment surface (Bologna and Heck, 1999) and thus supplied and maintained a high level of autotrophic biomass, which explains the right side of the U-shaped curve. The lowest level of benthic autotrophs could be from the bare sites near seagrass or vegetated sites of lower seagrass density.

There were no significant differences in read proportions of functional groups within benthic microeukaryotic communities between vegetated and unvegetated sites, highlighting a degree of functional redundancy of benthic microeukaryotic community across habitat boundaries. This could be partly due to export of particulate (e.g., seagrass leaves, and seagrass-associated and macroalgal detritus) and dissolved organic matter from vegetated to near and distant unvegetated locations (Heck et al., 2008). Furthermore, it has been demonstrated that the effect of seagrass on macrofauna could extend to bare sites at a distance of about 5 m (Han et al., 2017). Therefore, both energy and nutrient transportation and biotic interactions with higher trophic levels could weaken the cross-habitat distinctness in microeukaryotic functionality. Nevertheless, our result indicates that porewater N:P ratio could be a good indicator for the contributions of heterotrophs and autotrophs to benthic microeukaryotic community across vegetated and unvegetated sediments. A mechanistic understanding to this association may involve complicated physical, ecological, and stoichiometric interactions among seagrass, benthic animals, prokaryotes, and the microeukaryotes, which needs further investigation. Recently, a similar result on the importance of nutrients in driving functional composition has been reported for small planktonic eukaryotes (Wang et al., 2020).

Seagrass Bed as a Marine Hotspot of Gregarine Apicomplexans

For the first time, our study demonstrates that the seagrass bed represents a hotspot of Apicomplexa, which represented on average 83% reads across vegetated and unvegetated sediments. Hosts of apicomplexan parasites are known as man, domestic and wild animals, and invertebrates (Levine, 2018). Metabarcoding projects of microeukaryotes or protists in marine ecosystems have generally revealed low proportions of these parasites. For example, Apicomplexa accounted for on average 2.5% and up to 10% reads in surface sediments across Bohai Sea and Yellow Sea (Gong et al., 2015), up to 20% in mangrove sediments (Zhu et al., 2018), and <5% in coastal and oceanic waters (see Mahé et al., 2017). However, in terrestrial ecosystems, moderate amounts of apicomplexans have also been detected in protistan surveys in world's soils (e.g., few to more than 50%, Bates et al., 2013), and comparable abundances (average 84%) in the Neotropical rainforest soils (Mahé et al., 2017). These suggest that, by and large, apicomplexans are widespread in soil and sedimentary habitats, especially highly productive systems. This abundance hotspot is apparently linked to a generally high biomass of their hosts dwelling in these belowground environments (see our discussion above).

Based on phylogenetic analysis and qPCR results, we confirm the apicomplexan phylotypes obtained in this study are closely

related to *Lecudina polymorpha* morphotype 2, a gregarine morphospecies known to parasitize and an unidentified species of *Lumbrineris* (Leander et al., 2003). These results are consistent with existing knowledge, as Polychaeta (including *Lumbrineris latreilli*) dominate the macrobenthic community in the seagrass meadow of Swan Lake (Han et al., 2017), and all *Lecudina* species are known to inhabit intestine of polychaetes (Levine, 2018). In fact, *Lecudina polymorpha* Schrével, 1963 parasitizes the sandworm *Lumbrineris latreilli* (see Levine, 2018), and related *Lecudina* phylotypes have been detected in environmental DNA extracted from mangrove sediments as well (Zhu et al., 2018). These parasites can also be released into the environment with host feces in the form of mature sporocysts (oocyst). Much higher abundance of gregarine 18S rRNA gene was detected in sediment than in sandworm body, suggesting high abundance of Gregarine sporocysts accumulated in the sediment of seagrass bed, and new hosts might get infected when an oocyst is ingested and sporozoites escape into their digestive tract (Solter et al., 2012).

Due to differences in vertebrate and invertebrate diversity and composition of host communities, it is reasonable to detect different groups of apicomplexans across global soils, that is, Eucoccidiorida (Bates et al., 2013) and diverse species of gregarines (Mahé et al., 2017). So far, gregarine apicomplexans have been only reported from 0.32% of invertebrate species (Levine, 2018). There is a well-known high diversity of benthic invertebrates in coastal and deep oceans (Dong et al., 2021), highlighting that a great diversity of gregarines/apicomplexans awaits to be unveiled and linked to their hosts, as we have shown in this study.

In sum, this study demonstrates that there are significant ecological effects of a seagrass on the diversity and community organization of belowground microbial eukaryotes. Seagrass colonization gives rise to a less diverse and more heterotrophic microeukaryotic community. The dominance of gregarine apicomplexan parasites of polychaetes or other macro-organisms in the benthic microeukaryotic community is probably a characteristic for high productivity of those local habitats, reflecting that the belowground microbial diversity is tightly linked with plants and animals through complex food webs in the coastal environment.

DATA AVAILABILITY STATEMENT

The data presented in the study are deposited in the NCBI repository, accession number PRJNA797205, and OM925574 to OM925753.

AUTHOR CONTRIBUTIONS

YP: writing—original draft and editing. GL: data curation and figure plotting. LS: data curation and sample collection. PZ and YW: sample collection. ZS: revision and supervision. ZC: revision. QH: supervision. JG: project administration and writing—review and editing. All authors contributed to the article and approved the submitted version.

FUNDING

This work was supported by the National Natural Science Foundation of China (Nos. 41976128 and 41906113), the Natural Science Foundation of Jiangsu Province (No. BK20190494), the Innovation Group Project of Southern Marine Science and Engineering Guangdong Laboratory (Zhuhai) (No. 311021004), and the CAS Frontiers in Scientific Research Programs, Projects for Young Top-notch Talents (QYZDB-SSW-DQC013).

SUPPLEMENTARY MATERIAL

The Supplementary Material for this article can be found online at: https://www.frontiersin.org/articles/10.3389/fmicb.2022.901741/full#supplementary-material

REFERENCES

Abrogueña, J. B. R., Joydas, T. V., Pappathy, M., Cali, N. A., Alcaria, J., and Shoeb, M. (2021). Structure and composition of the macrobenthic community associated to shallow mangrove-seagrass habitat along the southern Red Sea coast, Saudi Arabia. *Egypt. J. Aquat. Res.* 47, 61–66. doi: 10.1016/j.ejar.2020.10.001

Adl, S.M., Bass, D., Lane, C.E., Lukeš, J., Schoch, C.L., Smirnov, A., et al. (2019). Revisions to the classification, nomenclature, and diversity of eukaryotes. *J. Eukaryot. Microbiol.* 66, 4–119. doi: 10.1111/jeu.12691

Amann, R.I., Binder, B.J., Olson, R.J., Chisholm, S.W., and Stahl, D.A. (1990). Combination of 16s rRNA-targeted oligonucleotide probes with flow cytometry for analyzing mixed microbial populations. *Appl. Environ. Microbiol.* 56, 1919–1925. doi: 10.1128/aem.56.6.1919-1925.1990

Bates, S. T., Clemente, J. C., Flores, G. E., Walters, W. A., Parfrey, L. W., Knight, R., et al. (2013). Global biogeography of highly diverse protistan communities in soil. *ISME J.* 7, 652–659. doi: 10.1038/ismej.2012.147

Bologna, P.A.X., and Heck, K.L. (1999). Macrofaunal associations with seagrass epiphytes: relative importance of trophic and structural characteristics. *J. Exp. Mar. Biol. Ecol.* 242, 21–39. doi: 10.1016/S0022-0981(99)0092-1

Caporaso, J.G., Kuczynski, J., Stombaugh, J., Bittinger, K., Bushman, F.D., Costello, E.K., et al. (2010). QIIME allows analysis of high throughput community sequencing data. *Nat. Methods* 7, 335–336. doi: 10.1038/nmeth.f.303

Clarke, K. R., and Gorley, R. N. (2006). *PRIMER v6: User Manual/Tutorial.* PRIMER-E, Plymouth, UK.

Corcoll, N., Yang, J., Backhaus, T., Zhang, X., and Eriksson, K. (2019). Copper affects composition and functioning of microbial communities in marine biofilms at environmentally relevant concentrations. *Front. Microbiol.* 9, 3248. doi: 10.3389/fmicb.2018.03248

Dawson, S. C., and Pace, N. R. (2002). Novel kingdom-level eukaryotic diversity in anoxic environments. *Proc. Natl. Acad. Sci. U.S.A.* 99, 8324–8329. doi: 10.1073/pnas.062169599

Dong, D., Li, X., Yang, M., Gong, L., Li, Y., Sui, J., et al. (2021). Report of epibenthic macrofauna found from Haima cold seeps and adjacent deep-sea habitats, South China Sea. *Mar. Life Sci. Technol.* 3, 1–12. doi: 10.1007/s42995-020-00073-9

Dortch, Q. (1990). The interaction between ammonium and nitrate uptake in phytoplankton. *Mar. Ecol. Prog. Ser.* 61, 183–201. doi: 10.3354/meps061183

Edgar, R. C. (2010). Search and clustering orders of magnitude faster than BLAST. *Bioinformatics* 26, 2460–2461. doi: 10.1093/bioinformatics/btq461

Edgcomb, V. P., Kysela, D. T., Teske, A., de Vera Gomez, A., and Sogin, M. L. (2002). Benthic eukaryotic diversity in the Guaymas basin hydrothermal vent environment. *Proc. Natl. Acad. Sci. U.S.A.* 99, 7658–7662. doi: 10.1073/pnas.062186399

Fenchel, T. (1969). The ecology of marine microbenthos. IV Structure and function of the benthic ecosystem, its chemical and physical factors and the microfauna communities with special reference to the ciliated protozoa. *Ophelia* 6, 1–182. doi: 10.1080/00785326.1969.10409647

Fenchel, T., and Finlay, B. (2008). Oxygen and the spatial structure of microbial communities. *Biol. Rev.* 83, 553–569. doi: 10.1111/j.1469-185X.2008.00054.x

Fischhoff, I. R., Huang, T., Hamilton, S. K., Han, B. A., LaDeau, S. L., Ostfeld, R. S., et al. (2020). Parasite and pathogen effects on ecosystem processes: a quantitative review. *Ecosphere* 11, 1–12. doi: 10.1002/ecs2.3057

Fourqurean, J. W., Muth, M. F., and Boyer, J. N. (2010). Epiphyte loads on seagrasses and microphytobenthos abundance are not reliable indicators of nutrient availability in oligotrophic coastal ecosystems. *Mar. Pollut. Bull.* 60, 971–983. doi: 10.1016/j.marpolbul.2010.03.003

Fu, R., and Gong, J. (2017). Single cell analysis linking ribosomal (r)DNA and rRNA copy numbers to cell size and growth rate provides insights into molecular protistan ecology. *J. Eukaryot. Microbiol.* 64, 885–896. doi: 10.1111/jeu.12425

Garcias-Bonet, N., Arrieta, J., de Santana, C., Duarte, C., and Marba, N. (2012). Endophytic bacterial community of a Mediterranean marine angiosperm (*Posidonia oceanica*). *Front. Microbiol.* 3, 342. doi: 10.3389/fmicb.2012.00342

Gong, J., Shi, F., Ma, B., Dong, J., Pachiadaki, M., Zhang, X., et al. (2015). Depth shapes alpha- and beta-diversities of microbial eukaryotes in surficial sediments of coastal ecosystems. *Environ. Microbiol.* 17, 3722–3737. doi: 10.1111/1462-2920.12763

Guillou, L., Bachar, D., Audic, S., Bass, D., Berney, C., Bittner, L., et al. (2013). The Protist Ribosomal Reference database (PR2): a catalog of unicellular eukaryote small sub-unit rRNA sequences with curated taxonomy. *Nucleic Acids Res.* 41, D597–D604. doi: 10.1093/nar/gks1160

Han, Q., Han, Q., Zheng, J., and Han, Q. (2017). Macrobenthic assemblages across a gradient of seagrass habitat in Swan Lake, China. *Intl. J. Oceans Oceanogr.* 11, 45–62.

Heck, K. L., Carruthers, T. J. B., Duarte, C. M., Hughes, A. R., Kendrick, G., Orth, R. J., et al. (2008). Trophic transfers from seagrass meadows subsidize diverse marine and terrestrial consumers. *Ecosystems* 11, 1198–1210. doi: 10.1007/s10021-008-9155-y

Huang, L., Pu, X., Pan, J.F., and Wang, B. (2013). Heavy metal pollution status in surface sediments of Swan Lake lagoon and Rongcheng Bay in the northern Yellow Sea. *Chemosphere* 93, 1957–1964. doi: 10.1016/j.chemosphere.2013.06.080

Huber, T., Faulkner, G., and Hugenholtz, P. (2004). Bellerophon: a program to detect chimeric sequences in multiple sequence alignments. *Bioinformatics* 20, 2317–2319. doi: 10.1093/bioinformatics/bth226

Ikenaga, M., Guevara, R., Dean, A., Pisani, C., and Boyer, J. (2010). Changes in community structure of sediment bacteria along the Florida coastal everglades marsh-mangrove-seagrass salinity gradient. *Microb. Ecol.* 59, 284–295. doi: 10.1007/s00248-009-9572-2

Katoh, K., and Standley, D. M. (2013). MAFFT multiple sequence alignment software version 7: improvements in performance and usability. *Mol. Biol. Evol.* 30, 772–780. doi: 10.1093/molbev/mst010

Leander, B.S., Harper, J.T., and Keeling, P.J. (2003). Molecular phylogeny and surface morphology of marine aseptate gregarines (Apicomplexa): *Selenidium* spp. and *Lecudina* spp. *J. Parasitol.* 89, 1191–1205. doi: 10.1645/GE-3155

Levine, N. D. (2018). *The Protozoan phylum Apicomplexa*. Boca Raton, FL: CRC Press.

Lin, X., Zheng, P., Zou, S., Sun, F., Zhang, X., and Gong, J. (2021). Seagrass (*Zostera marina*) promotes nitrification potential and selects specific ammonia oxidizers in coastal sediments. *J. Soils Sediments* 21, 3259–3273. doi: 10.1007/s11368-021-02951-w

Liu, Q., Zhao, Q., McMinn, A., Yang, E. J., and Jiang, Y. (2021). Planktonic microbial eukaryotes in polar surface waters: recent advances in high-throughput sequencing. *Mar. Life Sci. Technol.* 3, 94–102. doi: 10.1007/s42995-020-00062-y

López-García, P., Rodríguez-Valera, F., Pedrós-Alió, C., and Moreira, D. (2001). Unexpected diversity of small eukaryotes in deep-sea Antarctic plankton. *Nature* 409, 603–607. doi: 10.1038/35054537

MacIntyre, H. L., Geider, R. J., and Miller, D. C. (1996). Microphytobenthos: the ecological role of the "secret garden" of unvegetated, shallow-water marine habitats. I. Distribution, abundance and primary production. *Estuaries* 19, 186–201. doi: 10.2307/1352224

Mahé, F., de Vargas, C., Bass, D., Czech, L., Stamatakis, A., Lara, E., et al. (2017). Parasites dominate hyperdiverse soil protist communities in neotropical rainforests. *Nat. Ecol. Evol.* 1, 91. doi: 10.1038/s41559-017-0091

McKenzie, L., Nordlund, L., Jones, B., Cullen-Unsworth, L., Roelfsema, C., and Unsworth, R. (2020). The global distribution of seagrass meadows. *Environ. Res. Lett.*, 15, 74041. doi: 10.1088/1748-9326/ab7d06

Moreira, D., and López-García, P. (2003). Are hydrothermal vents oases for parasitic protists? *Trends Parasitol.* 19, 556–558. doi: 10.1016/j.pt.2003.09.013

Omena, E., and Creed, J.C. (2004). Polychaete fauna of seagrass beds (*Halodule wrightii* Ascherson) along the coast of Rio de Janeiro (Southeast Brazil). *Mar. Ecol.* 25, 273–288. doi: 10.1111/j.1439-0485.2004.00031.x

Preston, D., and Johnson, P. (2010). Ecological consequences of parasitism. *Nat. Educ. Knowl.* 3, 47.

Price, M. N., Dehal, P. S., and Arkin, A. P. (2009). FastTree: computing large minimum-evolution trees with profiles instead of a distance matrix. *Mol. Biol. Evol.* 26, 1641–1650. doi: 10.1093/molbev/msp077

Ronquist, F., Teslenko, M., van der Mark, P., Ayres, D. L., Darling, A., Höhna, S., et al. (2012). MrBayes 3.2: efficient Bayesian phylogenetic inference and model choice across a large model space. *Syst. Biol.* 61, 539–542. doi: 10.1093/sysbio/sys029

Schloss, P. D., Westcott, S. L., Ryabin, T., Hall, J. R., Hartmann, M., Hollister, E. B., et al. (2009). Introducing Mothur: open-source, platform independent, community supported software for describing and comparing microbial communities. *Appl. Environ. Microbiol.* 75, 7537–7541. doi: 10.1128/AEM.01541-09

Solter, L. F., Becnel, J. J., and Vávra, J. (2012). "Research methods for entomopathogenic microsporidia and other protists," in *Manual of Techniques in Invertebrate Pathology*. ed L. Lawrence (Elsevier Ltd), 329–371.

Stamatakis, A. (2014). RAxML version 8: a tool for phylogenetic analysis and post-analysis of large phylogenies. *Bioinformatics* 30, 1312–1313. doi: 10.1093/bioinformatics/btu033

Su, L., Zhang, Q., and Gong, J. (2018). Development and evaluation of specific PCR primers targeting the ribosomal DNA-internal transcribed spacer (ITS) region of peritrich ciliates in environmental samples. *J. Oceanol. Limnol.* 36, 818–826. doi: 10.1007/s00343-018-6326-3

Sun, F., Zhang, X., Zhang, Q., Liu, F., Zhang, J., and Gong, J. (2015). Seagrass (*Zostera marina*) colonization promotes the accumulation of diazotrophic bacteria and alters the relative abundances of specific bacterial lineages involved in benthic carbon and sulfur cycling. *Appl. Environ. Microbiol.* 81, 6901–6914. doi: 10.1128/AEM.01382-15

Sun, Y., Song, Z., Zhang, H., Liu, P., and Hu, X. (2020). Seagrass vegetation affect the vertical organization of microbial communities in sediment. *Mar. Environ. Res.* 162, 105174. doi: 10.1016/j.marenvres.2020.105174

ter Braak, C. J. F., and Smilauer, P. (2002). *CANOCO Reference Manual and CanoDraw for Windows User's Guide: Software for Canonical Ordination, Version 4.5*. Ithaca: Microcomputer Power.

Thornton, D. C. O., Underwood, G. J. C., and Nedwell, D. B. (1999). Effect of illumination and emersion period on the exchange of ammonium across the estuarine sediment-water interface. *Mar. Ecol. Prog. Ser.* 184, 11–20. doi: 10.3354/meps184011

Wang, B., Zheng, X., Zhang, H., Yu, X., Lian, Y., Yang, X., et al. (2021). Metagenomic insights into the effects of submerged plants on functional potential of microbial communities in wetland sediments. *Mar. Life Sci. Technol.* 3, 405–415. doi: 10.1007/s42995-021-00100-3

Wang, Y., Li, G., Shi, F., Dong, J., Gentekaki, E., Zou, S., et al. (2020). Taxonomic diversity of pico-/nanoeukaryotes is related to dissolved oxygen and productivity, but functional composition is shaped by limiting nutrients in eutrophic coastal oceans. *Front. Microbiol.* 11, 601037. doi: 10.3389/fmicb.2020.601037

Zheng, P., Wang, C., Zhang, X., and Gong, J. (2019). Community structure and abundance of Archaea in a *Zostera marina* meadow: a comparison between seagrass-colonized and bare sediment sites. *Archaea* 2019, 5108012. doi: 10.1155/2019/5108012

Zhu, P., Wang, Y., Shi, T., Huang, G., and Gong, J. (2018). Genetic diversity of benthic microbial eukaryotes in response to spatial heterogeneity of sediment geochemistry in a mangrove ecosystem. *Estuar. Coast.* 41, 751–764. doi: 10.1007/s12237-017-0317-z

Zou, S., Fu, R., Deng, H., Zhang, Q., Gentekaki, E., Gong, J., et al. (2021). Coupling between ribotypic and phenotypic traits of protists across life cycle stages and temperatures. *Microbiol. Spectr.* 9, e01738-21. doi: 10.1128/Spectrum.01738-21

Conflict of Interest: The authors declare that the research was conducted in the absence of any commercial or financial relationships that could be construed as a potential conflict of interest.

Publisher's Note: All claims expressed in this article are solely those of the authors and do not necessarily represent those of their affiliated organizations, or those of the publisher, the editors and the reviewers. Any product that may be evaluated in this article, or claim that may be made by its manufacturer, is not guaranteed or endorsed by the publisher.

frontiers | Frontiers in Marine Science

ORIGINAL RESEARCH
published: 20 June 2022
doi: 10.3389/fmars.2022.919253

Characterization of *Kordiimonas marina* sp. nov. and *Kordiimonas laminariae* sp. nov. and Comparative Genomic Analysis of the Genus *Kordiimonas*, A Marine-Adapted Taxon

Yu-Qi Ye[1], *Zhi-Peng Hao*[1], *Yu-Yan Yue*[1], *Lu Ma*[1], *Meng-Qi Ye*[1]* *and Zong-Jun Du*[1,2]*

[1] Marine College, Shandong University, Weihai, China, [2] State Key Laboratory of Microbial Technology, Shandong University, Qingdao, China

OPEN ACCESS

Edited by:
Shan He,
Ningbo University, China

Reviewed by:
Jian He,
Nanjing Agricultural University, China
Zhe-Xue Quan,
Fudan University, China
Weiyan Zhang,
Ningbo University, China

***Correspondence:**
Meng-Qi Ye
yemengqi@126.com
Zong-Jun Du
duzongjun@sdu.edu.cn

Specialty section:
This article was submitted to Aquatic Microbiology, a section of the journal Frontiers in Marine Science

Received: 13 April 2022
Accepted: 19 May 2022
Published: 20 June 2022

Citation:
Ye Y-Q, Hao Z-P, Yue Y-Y, Ma L, Ye M-Q and Du Z-J (2022) Characterization of Kordiimonas marina sp. nov. and Kordiimonas laminariae sp. nov. and Comparative Genomic Analysis of the Genus Kordiimonas, A Marine-Adapted Taxon. Front. Mar. Sci. 9:919253. doi: 10.3389/fmars.2022.919253

Two novel rod-shaped and Gram-negative bacterial strains, designated A6E486^T and 5E331^T, were isolated from a coastal sediment sample taken from Xiaoshi Island, Weihai, China, and a fresh kelp sample collected from a kelp culture area, Rongcheng, China, respectively. Growth of strain A6E486^T occurred at 20°C–43°C (optimum, 33°C–35°C) at pH 5.5–7.5 (optimum, 6.5) and in the presence of 1.0%–5.5% (w/v) NaCl (optimum, 2.5%–3.0%). Strain 5E331^T grew with 1.5%–5.0% (w/v) NaCl (optimum, 3.0%) at 15°C–40°C (optimum, 33°) and pH 6.0–8.5 (optimum, 7.0). The similarity of 16S rRNA gene sequence between the two strains was 95.2%. The phylogenetic analysis based on 16S rRNA gene sequence showed that strains A6E486^T and 5E331^T belong to the genus *Kordiimonas*, sharing the highest similarity to the genus *Kordiimonas* (94.6%–96.8%, 94.9%–96.1%, respectively). Strains A6E486^T and 5E331^T had percentage of conserved protein (POCP) values of 56.0%–67.3% and average nucleotide identity (ANI) values of 68.8%–73.1% to members of the genus *Kordiimonas*. The major polar lipids detected in the two strains were phosphatidylethanolamine (PE), phosphatidylglycerol (PG), diphosphatidylglycerol (DPG), and unidentified glycolipids, aminolipids, and lipids. The predominant respiratory quinone of the two strains was Q-10. Based upon the results presented in this study, strains A6E486^T and 5E331^T represent two novel species of the genus *Kordiimonas*, for which the names *Kordiimonas marina* and *Kordiimonas laminariae* are proposed with the type strains A6E486^T (= KCTC 82758^T = MCCC 1H00470^T) and 5E331^T (= KCTC 92199^T = MCCC 1H00515^T), respectively. Comparative genomic analysis showed that seven species of the genus *Kordiimonas* shared 1,258 core genes and had differences in carbohydrate metabolism, energy metabolism, and cofactor and vitamin metabolism. The pan-genome of the genus *Kordiimonas* was open. The prediction of secondary metabolites showed that most strains of the genus *Kordiimonas* had the ability to produce homoserine lactones, one of the most important

signal molecules in the quorum-sensing system of Gram-negative bacteria. Additionally, numerous genes involved in bacterial defense, motility and chemotaxis, cold adaptation, and environment stress response were found in the genus *Kordiimonas*, indicating the marine-adapted lifestyle of members of the genus *Kordiimonas*.

Keywords: *Kordiimonas*, polyphasic taxonomy, comparative genomic analysis, metabolic pathways, homoserine lactone, marine-adapted lifestyle

1 INTRODUCTION

The genus *Kordiimonas* was firstly proposed as a member of the order *Kordiimonadales* in the class *Alphaproteobacteria* by Kwon et al. (2005), with *Kordiimonas gwangyangensis* being the type species. At the time of writing, the genus *Kordiimonas* consists of seven validly published species according to the List of Prokaryotic names with Standing in Nomenclature[1], including *K. gwangyangensis*, *Kordiimonas lacus*, *Kordiimonas aestuarii*, *Kordiimonas aquimaris*, *Kordiimonas lipolytica*, *Kordiimonas sediminis*, and *Kordiimonas pumila*. All members of the genus *Kordiimonas* are aerobic, oxidase- and catalase-positive, except *K. sediminis* (facultatively anaerobic, oxidase- and catalase-negative) (Zhang et al., 2016). All of the type strains of the genus *Kordiimonas* are isolated from marine environments and habitats, such as marine sediment (Kwon et al., 2005; Xu X. et al., 2011; Math et al., 2012; Zhao et al., 2018), seawater (Yang et al., 2013; Wu et al., 2016), and sea cucumber culture pond sediments (Zhang et al., 2016), and have Q-10 as the predominant respiratory quinone. In this study, we describe two bacterial strains, A6E486^T isolated from a coastal sediment sample and 5E331^T isolated from a fresh kelp sample. Polyphasic investigations showed that the two strains represent two novel species affiliated with the genus *Kordiimonas*. Comparative genomic analyses of these two strains and the related species are contributed to understand the marine-adapted lifestyle of the genus *Kordiimonas*.[1]

2 MATERIALS AND METHODS

2.1 Bacterial Isolation and Cultivation

Strain A6E486^T was isolated from an intertidal sediment sample collected from Xiaoshi Island (37°32'30"N, 122°6'20"E), one of the largest continuous ecosystems in Weihai, China. The sediment sample was treated with an enrichment culture technique at 33°C for 30 days (Mu et al., 2018), and 100-μl enrichment cultures were spread on marine agar 2216 (MA; BD) by using the standard 10-fold dilution plating technique. After incubation at 33°C for 7 days, a beige colony designated A6E486^T was picked and pure cultures were obtained using purification procedures. Strain 5E331^T was obtained from fresh kelp samples, which were taken from a kelp culture area (37°15'96"N, 122° 36'49"E) in Rongcheng, China. Here, 10 g of fresh kelps were cut into small squares with sides of 1.5 cm under sterile conditions. Then, treated samples were placed in a conical flask containing glass beads and 100 ml seawater and shaken at 300 rpm for 1.5 h. Subsequently, the kelp treatment fluid was serially diluted to 10^{-3} with sterile seawater, and 100 μl aliquot was spread on MA. The incubation was performed at 28°C for 2 weeks. Strains A6E486^T and 5E331^T were stored at −80°C in sterile 1% (w/v) saline supplemented with 15% (v/v) glycerol. The type strains *K. gwangyangensis* JCM 12864^T and *K. lipolytica* JCM 30877^T obtained from the Japan Collection of Microorganisms were used as experiment control strains and cultured under optimum conditions.

2.2 Morphological, Physiological, and Biochemical Characteristics

The morphological and physiological features of strains A6E486^T and 5E331^T were examined after incubation at 33°C for 3 days on MA medium. The Gram staining reaction was determined according to the method described previously (Dong and Cai, 2001). Cell morphology and size were examined employing optical microscopy (E600, Nikon), transmission electron microscopy (JEM-1200, Jeol), and scanning electron microscopy (model Nova NanoSEM450, FEI). Growth ranges and optima of temperature were determined on MA at 0°C, 4°C, 15°C, 20°C, 25°C, 28°C, 30°C, 33°C, 35°C, 37°C, 40°C, 43°C, 45°C. The pH range for growth was tested in marine broth 2216 (MB; BD) by adding the appropriate buffers (20 mM), including 2-Morpholinoethanesulfonic acid (MES) (pH 5.5–6.0), 1,4-Piperazinediethanesulfonic acid (PIPES) (pH 6.5–7.0), N-(2-Hydroxyethyl) piperazine-N'-2-ethanesulfonic acid (HEPES) (pH 7.5–8.0), Tricine (pH 8.5), and 3-(Cyclohexylamino)-2-hydroxy-1-propanesulfonic acid (CAPSO) (pH 9.0–9.5). The optimal condition with NaCl for growth was tested in the following medium (0.1% yeast extract, 0.5% peptone), prepared with artificial seawater (per liter: 3.2 g $MgSO_4$, 2.2 g $MgCl_2$, 1.2 g $CaCl_2$, 0.7 g KCl, 0.2 g $NaHCO_3$) containing NaCl at concentrations from 0% to 10% (w/v, in 0.5% intervals). The strains were incubated at optimum temperature for 7 days. Growth experiments with leucine as sole carbon source were tested in the following liquid media, artificial seawater with inorganic carbon ($NaHCO_3$) removed was supplemented with

Abbreviations: ANI, average nucleotide identity; POCP, percentage of conserved proteins; KEGG, Kyoto Encyclopedia of Genes and Genomes; MCCC, Marine Culture Collection of China; KCTC, Korean Collection for Type Cultures; JCM, Japan Collection of Microorganisms; NCBI, National Center for Biotechnology Information; PGAP, Prokaryotic Genome Annotation Pipeline; HPLC, high-performance liquid chromatography; NJ, neighbor-joining; ML, maximum-likelihood; MP, maximum-parsimony; Pfam, Protein Families Database; GO, Gene Ontology; RAST, Rapid Annotation using Subsystem Technology; BPGA, Bacterial Pan Genome Analysis.

[1] https://www.bacterio.net/species

0.1% NH_4Cl as a nitrogen source with or without leucine. Leucine solution was sterilized with 0.22-μm filters. The final concentration of leucine in the medium was 1 g/L. The strains were incubated at optimum temperature for 11 days. Bacterial growth was monitored using a spectrophotometer at 600 nm.

Catalase activity was tested by adding 3% (v/v) H_2O_2 solution to the plate with fresh colonies. Oxidase activity was determined using an oxidase test reagent (bioMérieux). Anaerobic growth was determined by incubating strains on MA with or without 0.1% (w/v) KNO_3 in an AnaeroPack for 14 days. Hydrolysis tests of Tweens (20, 40, 60, and 80), alginate, casein, CM-cellulose, DNA, and starch were carried out according to methods described previously (Dong and Cai, 2001). The API 50CH and API 20E kits (bioMérieux) were employed to investigate acid production and additional biochemical characteristics, respectively. Additional enzyme activities were checked using API ZYM kit (bioMérieux), and carbon source oxidation was tested employing BIOLOG GEN III MicroPlates. All of the API and BIOLOG tests were carried out according to the manufacturer's instructions, except for the modification of adjusting salinity to 3% (w/v). Antibiotic susceptibility was determined on MA at 33°C for 7 days using the disc diffusion method (Jorgensen and Turnidge, 2015).

2.3 Chemotaxonomic Properties

Strains A6E486^T and 5E331^T and experiment control strains were cultured in MB under optimum conditions, and the cells at the late stage of exponential growth phase were harvested and freeze-dried in order to investigate chemotaxonomic characterizations. Fatty acids were extracted from freeze-dried cell biomasses (10 mg) and then analyzed using a gas chromatograph (model 6890N, Agilent) and the Microbial Identification System (MIDI database: TSBA40) (Sasser, 1990). Isoprenoid quinones were obtained from freeze-dried cell biomasses (300 mg) and identified by high-performance liquid chromatography (HPLC), as described previously (Minnikin et al., 1984). Total lipids were extracted with chloroform/methanol/water system (2.5:5:2, v/v/v) and analyzed by two-dimensional TLC according to the modified method described previously (Komagata and Suzuki, 1987).

2.4 16S rRNA Gene Sequence and Phylogenetic Analysis

The 16S rRNA gene was amplified employing PCR technology with the primer pair 27F and 1492R (Lane, 1991) and was sequenced by RuiBiotech (Qingdao, China). To obtain nearly complete 16S rRNA genes, purified PCR products were ligated into the pMD18-T vector (Takara), and ligation products were transferred into *Escherichia coli* DH5a receptor cells according to the manufacturer's instructions. For comparative analysis, the 16S rRNA gene sequences of strains A6E486^T and 5E331^T were submitted to the National Center for Biotechnology Information (NCBI) database[2] and the EzBioCloud server.[3]

The 16S rRNA gene sequences of strains A6E486^T, 5E331^T, and relatives were aligned using MUSCLE (Edgar, 2004), and then the trimmed sequences were used to reconstruct phylogenetic trees employing the neighbor-joining (NJ) and maximum-parsimony (MP) algorithm implemented in the software MEGA X (Felsenstein, 1981; Saitou and Nei, 1987; Kumar et al., 2018). The maximum-likelihood (ML) tree was reconstructed using the best-fit substitution model GTR+G+I. Bootstrap analysis was performed with 1,000 replications to provide confidence estimates for tree topologies.

2.5 Genomic Analysis

Genomic DNA of strains A6E486^T and 5E331^T was extracted using a bacteria genomic DNA kit (Takara), and the draft genomes were determined by Beijing Novogene Bioinformatics Technology Co. Ltd. (Beijing, China). Sequencing was performed on the Illumina NovaSeq 6000 platform (Illumina Inc., San Diego, CA, USA) using the paired-end 150-bp sequencing protocol. Raw sequencing data were generated by Illumina base-calling software CASAVA v1.8.2[4], and the sequenced reads were assembled using SOAPdenovo software (Li et al., 2009). Other relevant genomes in this study were obtained from the NCBI Prokaryotic reference genome database.

The completeness values of the used genomes were estimated based on the method of lineage-specific CheckM v1.1.3 (Parks et al., 2015). Gene content was annotated using the NCBI Prokaryotic Genome Annotation Pipeline (PGAP). The average nucleotide identity (ANI) was calculated using the online ANI calculator[5]. The percentage of conserved protein (POCP) value was calculated as described by Qin et al. (2014).[6] The ribosomal protein phylogenetic tree was reconstructed by FastTree (Price et al., 2009) using JTT+ CAT parameters and IQ-TREE (Nguyen et al., 2015; Chernomor et al., 2016) using the LG +F+I+G4 model. The 15 ribosomal proteins (L2, L3, L4, L5, L6, L14, L15, L16, L22, L24, S3, S8, S10, S17, and S19) were obtained and aligned using Python script[6] with the methods described by Wiegand et al. (2020). All genomes were predicted using Prodigal Server for uniformity (Hyatt et al., 2010). The analysis of core and unique genes was performed using the Bacterial Pan Genome Analysis (BPGA) tool, an ultrafast pan-genome analysis pipeline, with a threshold of 50% amino acid sequence identity (Chaudhari et al., 2016). Metabolic pathways were analyzed in detail by using the Kyoto Encyclopedia of Genes and Genomes (KEGG) database (Kanehisa et al., 2016), and the presence of gene clusters encoding secondary metabolites was predicted by antiSMASH server[7]. Carbohydrate-active enzymes of the genus *Kordiimonas* were annotated employing the online dbCAN2[8], a meta server for automated carbohydrate-active enzyme annotation (Zhang et al., 2018). The analysis of marine adaptation metabolic features was performed by Rapid Annotation using Subsystem Technology (RAST) version 2.0 (Aziz et al., 2008) and the KEGG database (Kanehisa et al., 2016).

[2] https://blast.ncbi.nlm.nih.gov/Blast.cgi
[3] http://www.ezbiocloud.net/
[4] http://support.illumina.com/
[6] https://github.com/2015qyliang/BGAStudio
[7] https://antismash.secondarymetabolites.org/#!/start

3 RESULTS AND DISCUSSION

3.1 Morphological, Physiological, and Biochemical Characteristics

Morphological observations by transmission electron microscopy and scanning electron microscopy showed that cells of strains A6E486^T (with widths of 0.5–0.7 μm and lengths of 1.0–2.5 μm) and 5E331^T (with widths of 0.2–0.5 μm and lengths of 0.8–2.7 μm) were both short rod-shaped (**Supplementary Figure S1**). For strain A6E486^T, the oxidations of the sole carbon source were positive for D-maltose, D-trehalose, D-fructose, glycyl-L-proline, L-glutamic acid, L-galactonic acid lactone, and D-glucuronic acid, which was consistent with *K. gwangyangensis* JCM 12864^T, while that of strain 5E331^T was negative as *K. lipolytica* JCM 30877^T (**Supplementary Table S1**). Strains A6E486^T and 5E331^T exhibited some similarities to *K. gwangyangensis* and *K. lipolytica* JCM 30877^T, including their abilities to hydrolyze Tweens (20, 40, and 60). The differential characteristics of strains A6E486^T and 5E331^T and experiment control strains were summarized in **Table 1** and **Supplementary Table S1**. Both strains A6E486^T and 5E331^T were susceptible to (μg per disc) penicillin (10), chloramphenicol (30), norfloxacin (30), cefotaxime sodium (30), gentamycin (10), ofloxacin (5), clarithromycin (15), carbenicillin (100), and ceftriaxone (30) but resistant to tetracycline (30) and kanamycin (30).

3.2 Chemotaxonomic Properties

The major cellular fatty acids (>10%) of strain A6E486^T consisted of iso-$C_{15:0}$, iso-$C_{17:0}$, iso-$C_{17:1}$ ω9c, and summed feature 3 (comprising $C_{16:1}$ ω6c and/or $C_{16:1}$ ω7c) while those of strain 5E331^T were iso-$C_{15:0}$, iso-$C_{17:1}$ ω9c, and summed feature 3 (**Table 2**). The fatty acid compositions of the two strains were similar to experiment control strains but with differences in the proportions of some fatty acids. For example, iso-$C_{17:0}$ was one of the major fatty acids in strains A6E486^T and *K. gwangyangensis* JCM 12864^T but not in strains 5E331^T and *K. lipolytica* JCM 30877^T. Strains A6E486^T and 5E331^T had Q-10 as

TABLE 1 | Differential characteristics between strains A6E486^T and 5E331^T and experiment control strains.

Characteristic	1	2	3	4
Colony color	Beige	Beige and brown	Cream–white	Beige
Temperature range (°C)	20–43	15–40	17–44 [a]	15–45 [b]
NaCl range (%, w/v)	1.0–5.5	1.5–5.0	0.5–4.0 [a]	0.5–10 [b]
pH range	5.5–7.5	6.0–8.5	6.0–8.5 [a]	5.5–9.5 [b]
Voges–Proskauer reaction	+	+	+	–
Enzyme activity:				
Catalase	w	+	+	+
Gelatinase	–	+	–	+
Lipase (C14)	w	+	–	–
α-chymotrypsin	w	–	+	+
Hydrolysis of:				
Tween 80	w	+	+	++
Starch	–	+	+	–
Casein	+	+	+	–
Acid production from:				
Glycerol	–	–	w	+
L-xylose	+	w	–	–
D-glucose	+	–	+	+
D-fructose	+	+	–	+
D-mannose	–	–	+	+
Inositol	w	–	+	–
N-acetyl glucosamine	–	–	+	+
D-maltose	w	–	+	+
D-trehalose	+	–	+	–
L-rhamnose	–	–	–	+
Oxidation of:				
D-cellobiose	–	–	+	–
Sucrose	+	–	+	–
Glycerol	–	–	+	–
D-fructose-6-PO_4	+	w	–	–
Gelatin	+	–	+	–
L-histidine	+	w	+	–
α-keto-glutaric acid	+	+	+	–
Sodium butyrate	w	+	–	–

Strains: 1, A6E486^T; 2, 5E331^T; 3, K. gwangyangensis JCM 12864^T; 4, K. lipolytica JCM 30877^T. All data were from this study unless indicated otherwise. +, Positive; –, negative; w, weakly positive. All strains were positive for the following characteristics: alkaline phosphatase, esterase (C4), esterase lipase (C8), leucine arylamidase, acid phosphatase, naphthol-AS-BI-phosphohydrolase, esculin ferric citrate, and potassium 5-ketogluconate.

Data from: a, Kwon et al. (2005); b, Wu et al. (2016).

TABLE 2 | Cellular fatty acid composition (%) of strains A6E486^T and 5E331^T and experiment control strains.

Fatty acid	1	2	3	4
Saturated				
$C_{12:0}$	TR	TR	2.0	1.0
$C_{16:0}$	6.4	4.1	5.3	3.2
$C_{17:0}$	1.9	TR	1.2	TR
Unsaturated				
$C_{15:1}$8c	1.7	1.4	–	1.8
$C_{15:1}$ w6c	TR	TR	–	1.0
$C_{17:1}$ w8c	3.7	3.1	1.4	4.5
$C_{17:1}$ w6c	6.5	4.5	1.2	6.8
Branched				
iso-$C_{15:1}$ F	1.2	2.1	TR	1.6
iso-$C_{15:0}$	**16.8**	**27.0**	**15.1**	**17.8**
iso-$C_{16:0}$	TR	1.5	TR	2.3
iso-$C_{17:0}$	**10.3**	2.5	**19.2**	3.2
iso-$C_{17:0}$ 3–OH	1.5	TR	1.02	TR
iso-$C_{17:1}$ w9c	**22.9**	**27.7**	**34.4**	**23.8**
Summed Feature				
3[a]	**16.2**	**17.3**	7.3	**23.2**
8[a]	3.9	1.5	5.1	TR

Strains: 1, A6E486^T; 2, 5E331^T; 3, K. gwangyangensis JCM 12864^T; 4, K. lipolytica JCM 30877^T. All data listed in the table are from this study. TR, trace (<1.0%); –, Not detected; Fatty acids present at >10% are indicated in bold.

[a]Summed features are groups of two or three fatty acids that cannot be separated by GLC using the MIDI system. Summed feature 3 comprises $C_{16:1}$ ω6c and/or $C_{16:1}$ ω7c, and summed feature 8 comprises $C_{18:1}$ ω6c and/or $C_{18:1}$ ω7c.

the predominant respiratory quinone, which was consistent with the quinone type of the genus *Kordiimonas*. The major polar lipids detected in the two strains were phosphatidylethanolamine (PE), phosphatidylglycerol (PG), diphosphatidylglycerol (DPG), and unidentified glycolipids, aminolipids, and lipids. PE, PG, DPG, and unidentified glycolipids were detected in all tested *Kordiimonas* species (**Supplementary Figure S2**).

3.3 16S rRNA Gene Sequence and Phylogenetic Analysis

Nearly complete 16S rRNA gene sequences of strains A6E486^T (1,461 bp; GenBank accession number: MZ901372) and 5E331^T (1,462 bp; GenBank accession number: OM663707) were obtained according to the methods described in the *Materials and Methods* section. Comparative analysis results using EzBioCloud databases showed that strains A6E486^T and 5E331^T shared the highest 16S rRNA gene sequence similarity values of 96.8% and 96.1%, respectively, with *K. lipolytica* JCM 30877^T. NJ phylogenetic tree based on 16S rRNA gene indicated that strains A6E486^T and 5E331^T were affiliated with the genus *Kordiimonas* (**Figure 1**). Similar tree topologies were also obtained with the ML and MP algorithms.

3.4 Comparative Genomic Analysis of the Genus *Kordiimonas*

3.4.1 Comparison of Genomic Properties and Genetic Relatedness

The genome lengths of the seven species of the genus *Kordiimonas* (strains A6E486^T, 5E331^T, *K. gwangyangensis* JCM 30877^T, *K. lipolytica* JCM 12864^T, *K. lacus* CGMCC 1.9109^T, *K. pumila* N18^T, and *K. sediminis* KCTC 42590^T) were 3,243,597–4,557,767 bp with a mean size of 3,894,463 bp. The completeness values of these genomes were 99.6%–100.0%. Among them, strain 5E331^T had the minimum DNA G+C content (46.2%), while strain A6E486^T possessed the maximum content (59.9%). The NCBI PGAP results showed that a total of 3,436 genes were predicted for strain A6E486^T, including 3,381 protein-coding genes and 53 RNA genes (46 tRNA genes, 3 rRNA genes, and 4 ncRNA genes), while strain 5E331^T had 3,505 predicted genes. The detailed PGAP results of the seven species were shown in **Table 3**.

The POCP and ANI values were calculated to identify the genomic similarities of strains A6E486^T and 5E331^T with some members of the genus *Kordiimonas* (**Figure 2**). The POCP and ANI values between strain A6E486^T (strain 5E331^T) and some species of the genus *Kordiimonas* were 56.3%–67.3% (56.0%–61.5%) and 68.6%–73.1% (68.8%–69.9%), respectively. The POCP values were higher than the genus delineation threshold (50%) (Qin et al., 2014a), and the ANI values were lower than the species delineation threshold (95%) (Yoon et al., 2017), which indicated that strains A6E486^T and 5E331^T represented two novel species of the genus *Kordiimonas*. The ribosomal protein phylogenetic tree showed the evolutionary relationships of some members of genus *Kordiimonas* (**Figure 2**).

3.4.2 Pan-Genome Analysis of the Genus *Kordiimonas*

Pan-genome analysis using BPGA was performed to identify orthologous groups among strains A6E486^T, 5E331^T, *K. gwangyangensis* JCM 30877^T, *K. lipolytica* JCM 12864^T, *K. lacus* CGMCC 1.9109^T, *K. pumila* N18^T, and *K. sediminis* KCTC 42590^T. Comparative analysis based on orthologous groups of proteins revealed that 1,258 core genes were shared by the seven species (**Figure 3A**). The percentages of core genes

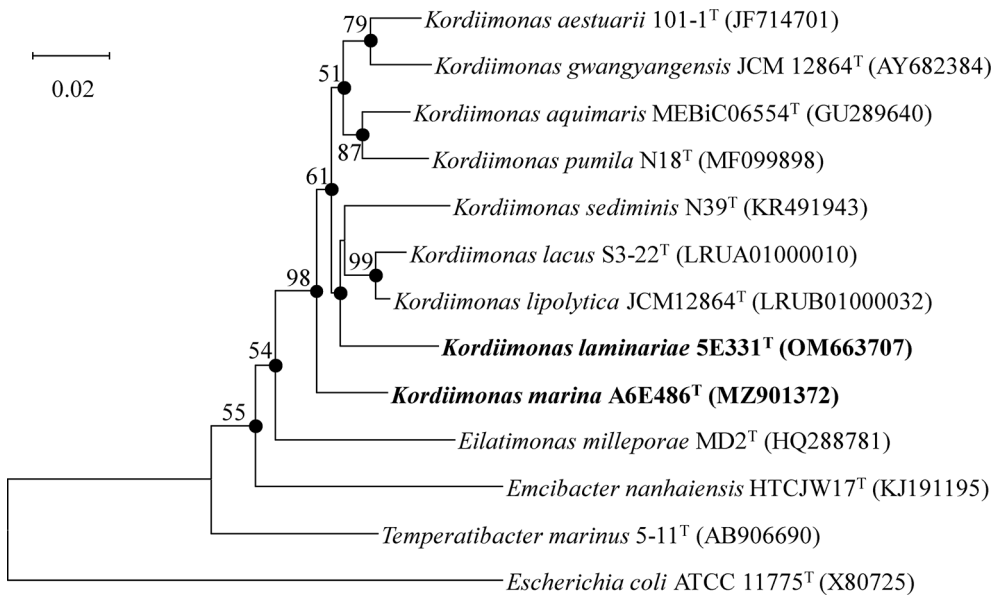

FIGURE 1 | Neighbor-joining phylogenetic tree based on 16S rRNA gene sequences of strains A6E486^T and 5E331^T and other closely related species. Filled circles indicate branches that were recovered with all three methods (neighbor-joining, maximum-likelihood, and maximum-parsimony). Percentage bootstrap values above 50% (1,000 replicates) are shown at branch nodes. *Escherichia coli* ATCC 11775^T was used as the out-group. Bar, 0.02 substitutions per nucleotide position.

in each genome ranged from 34.3% to 44.1% (**Figure 3B**), and compared with unique genes and accessory genes, core genes contributed more to energy metabolism, nucleotide metabolism, replication and repair, and translation (**Supplementary Figure S3**). The proportion of accessory genes and unique genes in the seven genomes varied greatly (**Figure 3B**). Accessory genes and unique genes were more distributed than core genes in amino acid metabolism, carbohydrate metabolism, signal transduction, and xenobiotic biodegradation and metabolism (**Supplementary Figure S3**), which indicated that these genes conferred metabolic diversity and marine environment adaptability to the members of the genus *Kordiimonas* (Innamorati et al., 2020). Results of the core pan-genome prediction model showed that the pan-genome increased with the addition of new strains and was far from saturation (**Supplementary Figure S4**), which indicated that the pan-genome of the genus *Kordiimonas* was open. Compared with a previous study (Geng et al., 2022), the complement of strains A6E486^T and 5E331^T in this study reduced the number of shared core genes of the genus *Kordiimonas*, showing that core genes decreased with the increase of species (**Supplementary Figure S4**).

3.4.3 Metabolic Pathway Analysis

Metabolic pathways were analyzed using KEGG's BlastKOALA service. The results showed that the seven species of the genus *Kordiimonas* had the most genes in gene information processing, followed by signaling and cellular processes and carbohydrate metabolism (**Supplementary Figure S5**). In addition, the metabolic pathways of the seven species were compared and analyzed, including carbohydrate metabolism, energy

TABLE 3 | Genome statistics of strains A6E486^T and 5E331^T and five members of the genus *Kordiimonas*.

	1	2	3	4	5	6	7
Genome size (bp)	3,684,098	3,651,059	4,082,245	4,557,767	4,000,817	4,041,658	3,243,597
Completeness (%)	99.9	100.0	100.0	100.0	99.6	100.0	100.0
Contigs	25	27	13	36	12	1	12
N_{50} length (bp)	603,855	474,336	686,379	229,908	482,103	4,041,658	1,727,258
G+C content (mol %)	59.9	46.2	57.5	56.3	57.2	47.4	49.6
Genes	3,436	3,505	3,727	4,286	3,688	3,608	2,908
Protein-coding genes	3,381	3,434	3,667	4,169	3,623	3,517	2,842
tRNA genes	46	47	43	51	42	42	43
rRNA genes	3	3	5	9	5	6	5
ncRNA genes	4	3	4	4	3	4	4
GenBank ID	JAINDF 000000000	JAKQZA 000000000	AQXF 01000000	LRUB 01000000	FNAK 01000000	CP061205	BNCI 01000000

Strains: 1, A6E486^T; 2, 5E331^T; 3, K. gwangyangensis JCM 30877^T; 4, K. lipolytica JCM 12864^T; 5, K. lacus CGMCC 1.9109^T; 6, K. pumila N18^T; 7, K. sediminis KCTC 42590^T.

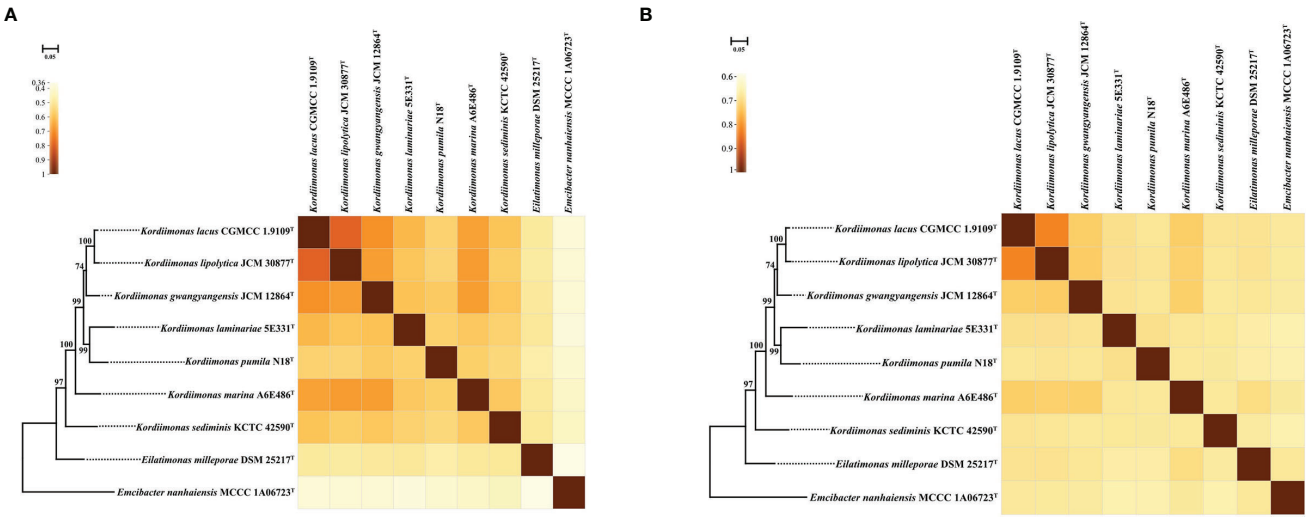

FIGURE 2 | Heat maps showing POCP and ANI values among A6E486^T, 5E331^T, and members of the family *Temperatibacteraceae*. **(A)** Heat map based on POCP values. **(B)** Heat map based on ANI values. IQ-TREE based on ribosomal protein sequences shows the phylogenetic relationships among these strains. Percentage bootstrap values (1,000 replicates) are shown at branch nodes. *Emcibacter nanhaiensis* MCCC 1A06723^T was used as the out-group. Bar, 0.05 substitutions per nucleotide position. Same tree topology was also obtained using FastTree. ANI, average nucleotide identity; POCP, percentage of conserved proteins.

metabolism, lipid metabolism, amino acid metabolism, and metabolism of cofactors and vitamins. Among the seven *Kordiimonas* species, all strains have complete pathways of gluconeogenesis (M00003), pyruvate oxidation (M00307), citrate cycle (M00009), pentose phosphate pathway (M00007), and glyoxylate cycle (M00012), whereas only strains A6E486^T and *K. lipolytica* JCM 30877^T possess a complete glycolysis pathway (M00001) (**Figure 4**). The seven species also have similarities and differences in other metabolic pathways. For example, a complete PE biosynthesis pathway (M00093) was found in all strains, which was consistent with the polar lipid results of the genus *Kordiimonas*. The initiation pathways of fatty acid synthesis (M00082) and cobalamin biosynthesis (M00122) are complete only in strain 5E331^T, while the cytochrome o ubiquinol oxidase (M00417) and betaine biosynthesis (M00555) pathways are complete only in strain A6E486^T (**Figure 4**). Considering that the incomplete glycolysis pathway in most *Kordiimonas* strains leads to pyruvate deficiency and thus to the decrease of acetyl-CoA from the pyruvate oxidation pathway, the leucine degradation pathway is important due to the production of acetyl-CoA (**Figure 5A**). It was proven that strains A6E486^T, 5E331^T, *K. gwangyangensis* JCM 30877^T, and *K. lipolytica* JCM 12864^T could grow slowly in the medium with leucine as the solo carbon source (**Supplementary Figure S6**). In addition, dTDP-L-rhamnose biosynthesis pathway (M00793) was completely annotated in the genomes of the seven *Kordiimonas* species (**Figure 5B**).

3.4.4 Prediction of Secondary Metabolites

AntiSMASH server was used to predict the secondary metabolites of the seven species. Results showed that all of the seven species contained gene clusters encoding RiPP-like (Other unspecified ribosomally synthesized and posttranslationally modified peptide product). Except for *K. gwangyangensis* JCM 12864^T and *K. pumila* N18^T, the genomes of the remaining five strains contained terpene gene clusters. The gene clusters encoding hserlactone (homoserine lactone) were found in genomes of the six strains except *K. pumila* N18^T, which had β-lactone (β-lactone containing protease inhibitor) gene clusters (**Supplementary Table S2**). Homoserine lactones, as one of the most important signal molecules in the quorum-sensing system of Gram-negative bacteria, regulate the expression of many physiological characteristics (Parsek and Greenberg, 2000; Qin et al., 2020). Cluster Pfam (Protein Families Database) analysis and Pfam-based GO (Gene Ontology) term annotation results showed that the core biosynthetic genes in all of the hserlactone gene clusters encoded autoinducer synthase, and there were additional biosynthetic genes encoding luxR family regulatory proteins upstream and downstream of the core genes (**Supplementary Figure S7**). The luxR regulators are important components of the quorum-sensing system, which are distributed to sense and respond to N-acyl homoserine lactone by autoinducer-binding domain (Subramoni and Venturi, 2009; Santos et al., 2012).

3.4.5 Comparative Analysis of Carbohydrate-Active Enzymes

Considering that the strains had differences in acid production and oxidation with different carbohydrates as substrates (**Table 1**; **Supplementary Table S1**), carbohydrate-active enzymes of the genus *Kordiimonas* were annotated and analyzed. The results showed that *K. sediminis* KCTC 42590^T had the least carbohydrate-active enzymes (86), while *K. gwangyangensis* JCM 30877^T had the most (137). Among

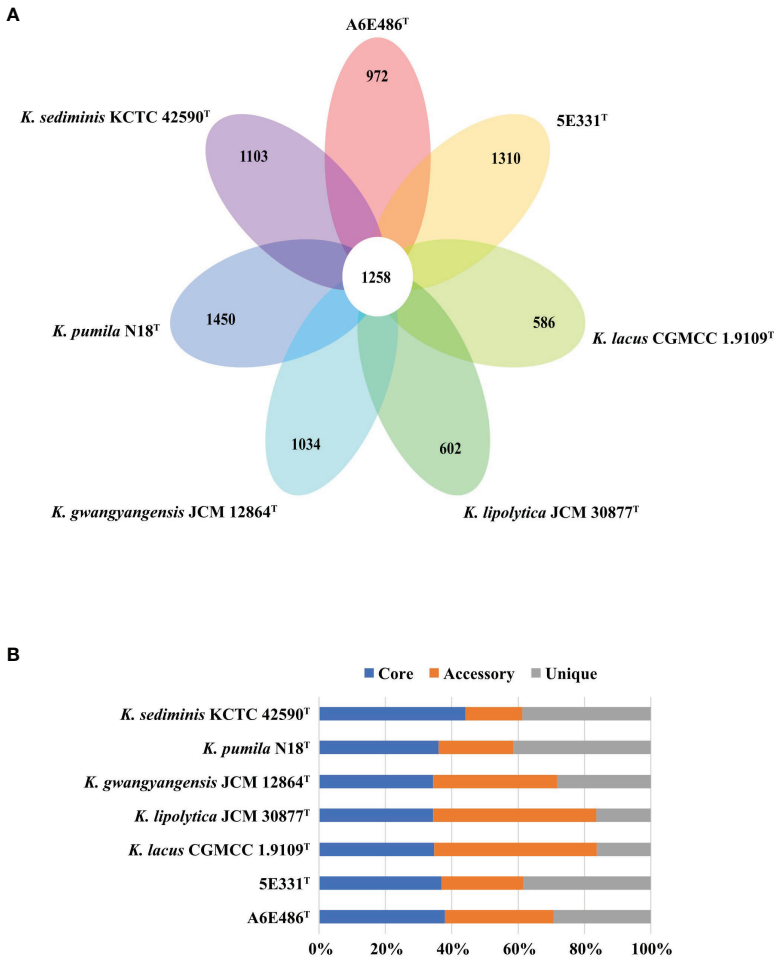

FIGURE 3 | Comparisons of *Kordiimonas* orthologous protein groups in the seven *Kordiimonas* genomes. **(A)** Venn diagram displaying the numbers of core gene families and unique genes for each of the seven *Kordiimonas* strains. **(B)** Percentage of core, accessory, and unique genes in each of the seven genomes.

these carbohydrate-active enzymes, most enzymes in the genomes of the seven species were assigned to the glycosyltransferase (GT) family and glycoside hydrolase (GH) family, which was consistent with a previous study (Geng et al., 2022); however, polysaccharide lyases (PLs) were found in parts of the *Kordiimonas* species (**Figure 6**). Strain A6E486^T had 53 GTs and 50 GHs, which were more than those in strain 5E331^T, *K. lipolytica* JCM 12864^T, *K. lacus* CGMCC 1.9109^T, *K. pumila* N18^T, and *K. sediminis* KCTC 42590^T. Strain 5E331^T harbored 107 carbohydrate-active enzymes, including 42 GTs, 36 GHs, 16 carbohydrate esterases (CEs), 6 carbohydrate-binding modules (CBMs), and 7 auxiliary activities (AAs). Detailed comparison results were shown in **Figure 6**.

3.4.6 Analysis of Marine Environment Adaptability

Considering that members of the genus *Kordiimonas* were all isolated from marine environments and habitats, metabolic features related to functional categories were analyzed to investigate the marine-adapted lifestyle of the genus *Kordiimonas* (**Table 4**). In the first place, 26–51 genes associated with "Virulence, Disease and Defense" were found in the genomes of members of the genus *Kordiimonas*, which may be crucial for bacteria to resist marine environment pollutants including heavy-metal ions, antibiotics, and other toxic compounds. Secondly, flagellar motility and bacterial chemotaxis genes were found, and there were differences in the number of the related genes. Most of the marine environments are oligotrophic; flagellar motility and bacterial chemotaxis genes, which assist marine bacteria in the acquisition of nutrients, may play an important role in the marine sediment-adapted lifestyle (Qin et al., 2011). Thirdly, there were different numbers of genes related to capsular and extracellular polysaccharides and polysaccharide export proteins in the genomes. Exopolysaccharides (EPSs) are essential for the survival of bacteria in marine environments, as EPSs assist them to endure extremes of temperature, salinity, and nutrient availability (Nichols et al., 2005). The existence of genes related to EPS synthesis and export suggested that members of the genus

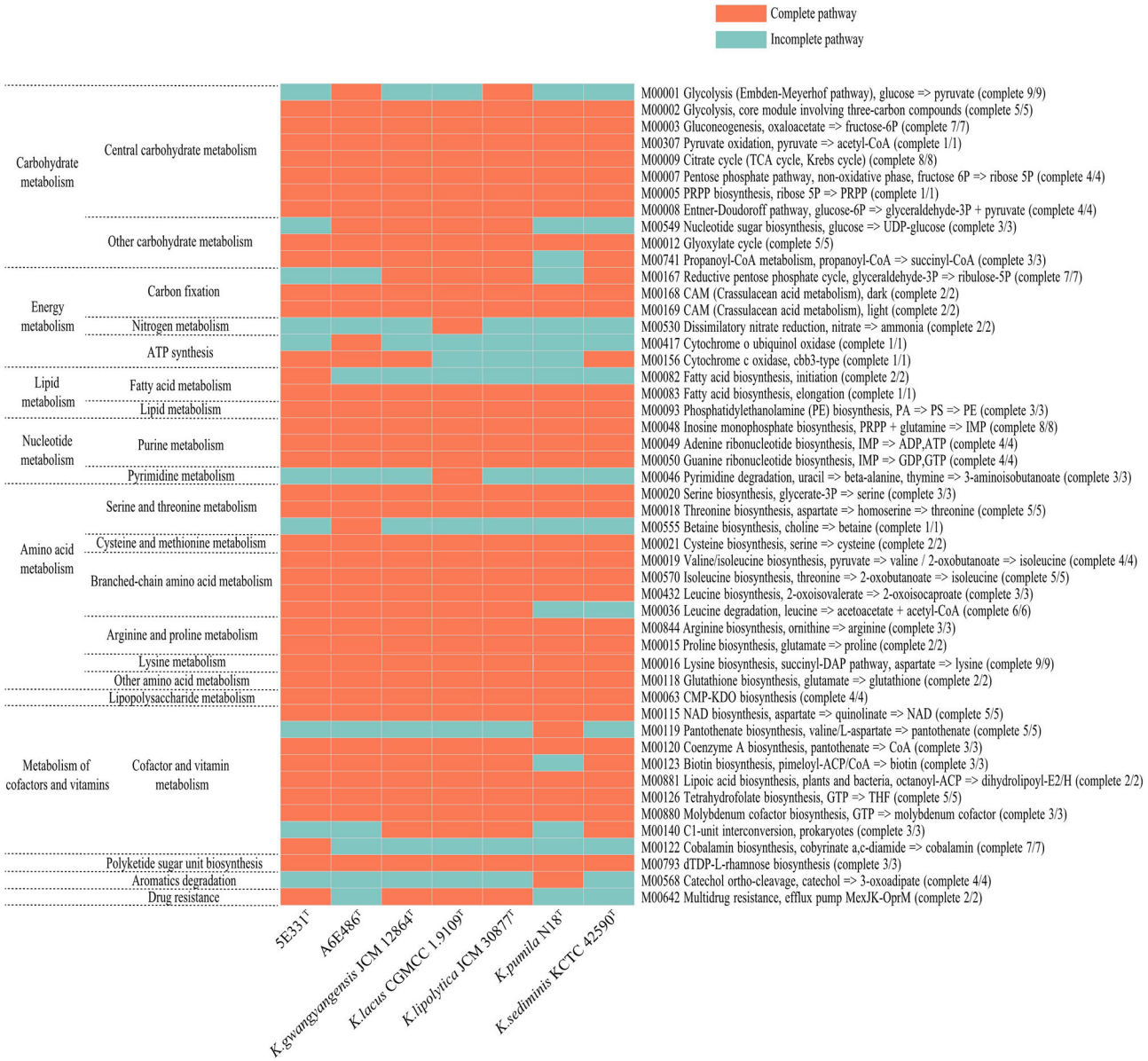

FIGURE 4 | Heat maps of complete and incomplete metabolic pathways in the genomes of strains A6E486^T, 5E331^T, *K. gwangyangensis* JCM 30877^T, *K. lipolytica* JCM 12864^T, *K. lacus* CGMCC 1.9109^T, *K. pumila* N18^T, and *K. sediminis* KCTC 42590^T.

Kordiimonas may be able to resist low temperature through EPS secretion. Additionally, cold-shock proteins and tRNA-dihydrouridine synthase play roles in the cold-adapted lifestyle of marine bacteria by helping protein folding and increasing tRNA flexibility at low temperatures, respectively (Qin et al., 2014b). Fourthly, all members of the genus *Kordiimonas* had numerous genes involved in the "stress response," which may give these species the ability to cope with pressures such as oxygen and temperature in marine environments.

Considering the high osmotic pressure of marine environments and the protective effect of compatible solutes on microorganisms under high osmotic condition (Da et al., 1998; Wood et al., 2001), compatible solute synthesis and transport of the genus *Kordiimonas* were analyzed using the KEGG database. The results showed that only strain A4E486^T had a complete betaine synthesis pathway (M00555) among the seven species of the genus *Kordiimonas* (**Figure 4**). Strains 5E331^T, *K. gwangyangensis* JCM 30877^T, *K. lipolytica* JCM 12864^T, *K. lacus* CGMCC 1.9109^T, *K. pumila* N18^T, and *K. sediminis* KCTC 42590^T encode choline dehydrogenase (CHDH), which converts choline to betaine aldehyde (Zou et al., 2016). The genes encoding glycine betaine transporter were found only in the genome of strain A4E486^T. In

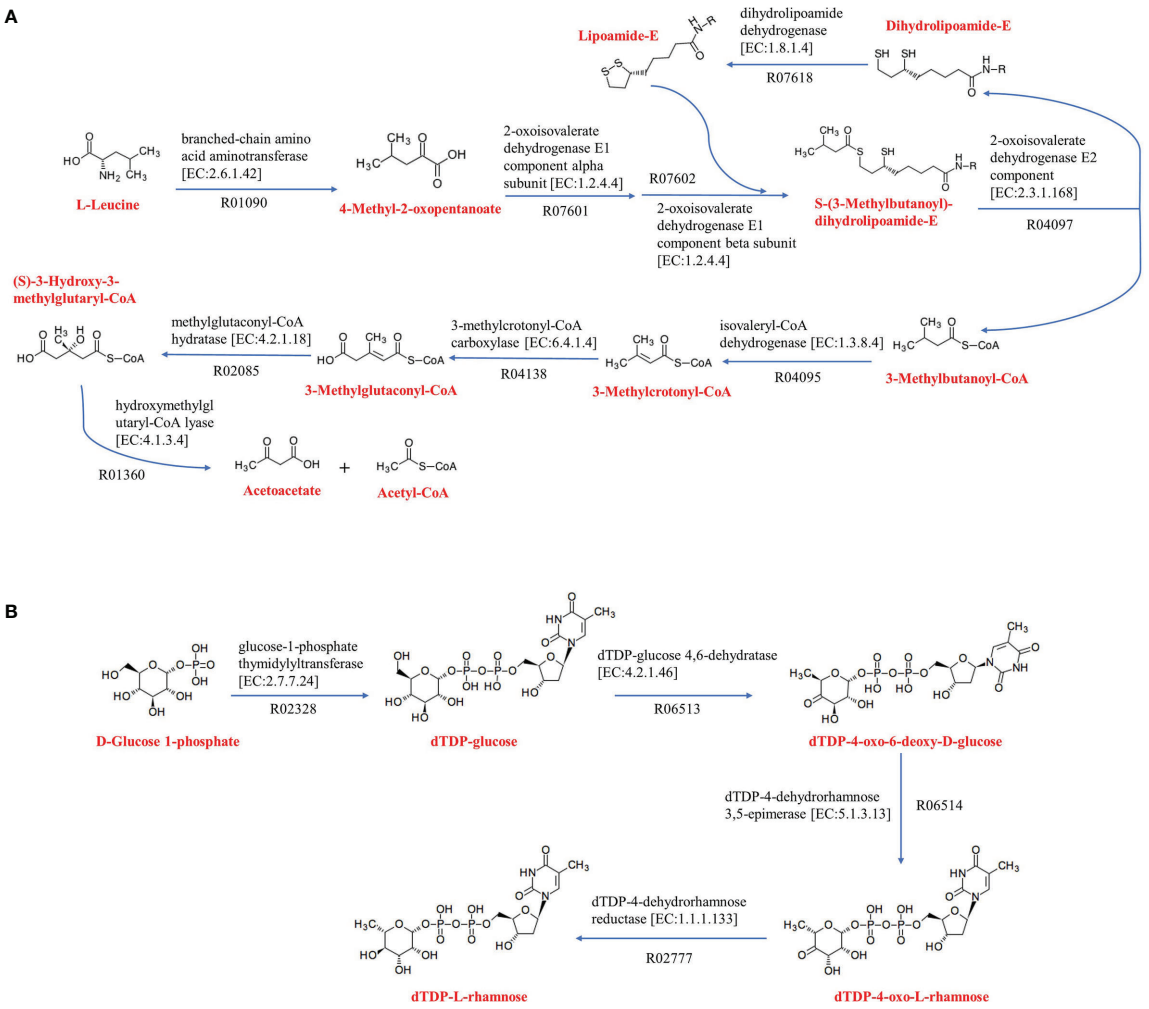

FIGURE 5 | Amino acid metabolism and polyketide sugar unit biosynthesis of *Kordiimonas* strains. **(A)** Leucine degradation. **(B)** dTDP-L-rhamnose biosynthesis. The metabolic pathway maps are based on the KEGG analysis. Other reactants and products have been omitted.

the hypertonic environment, the accumulation of amino acids in cells, such as proline (Hoffmann et al., 2012) and arginine (Xu S. et al., 2011), also plays a positive role in the anti-osmotic ability of microorganisms (Da et al., 1998; Roesser and Muller, 2001). The seven genomes had the proline biosynthesis pathway (M00015) and arginine biosynthesis pathway (M00844) identified by the KEGG database (**Figure 4**). Numerous complete amino acid synthesis pathways in members of the genus *Kordiimonas* may help to resist cell damage caused by high osmotic pressure in marine environments. Finally, the antioxidant systems used to scavenge free radicals were analyzed. The antioxidant system mainly includes superoxide dismutase, catalase, glutathione, and cytochrome oxidase (Pomposiello and Demple, 2002). The analysis showed that all seven species of the genus *Kordiimonas* encoded superoxide dismutase (Fe-Mn family) and catalase-peroxidase. Strains 5E331^T and *K. pumila* N18^T had genes that encoded catalase. The genes encoding cytochrome c peroxidase were found in strains 5E331^T, *K. gwangyangensis* JCM 30877^T, *K. lipolytica* JCM 12864^T, *K. lacus* CGMCC 1.9109^T, and *K. sediminis* KCTC 42590^T. Additionally, all seven members of the genus *Kordiimonas* had a complete glutathione synthesis pathway (M00118) (**Figure 4**).

The analysis of metabolic features and related genes revealed the genetic basis of the genus *Kordiimonas* to adapt to the marine environment.

4 DESCRIPTION OF *KORDIIMONAS MARINA* SP. NOV.

Kordiimonas marina (ma.ri'na. L. fem. adj. marina, pertaining to the isolation of the type strain from the marine environment).

Cells are Gram-negative and facultatively anaerobic with rod shape. Growth is observed at pH 5.5–7.5 (optimum, 6.5) and temperatures of 20°C–43°C (optimum, 33°C–35°C) and with 1.0%–5.5% (w/v, optimum, 2.5%–3.0%) NaCl. Growth occurs

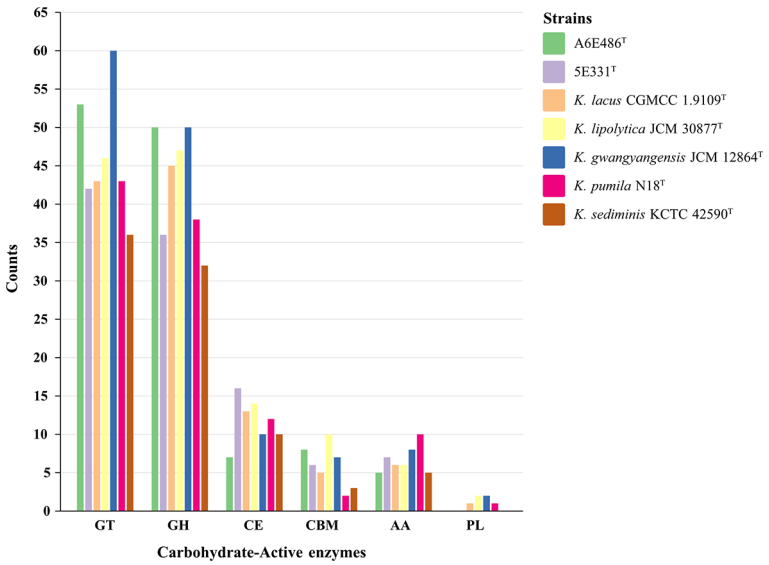

FIGURE 6 | Histogram of predicted carbohydrate-active enzymes in strains A6E486^T, 5E331^T, *K. gwangyangensis* JCM 30877^T, *K. lipolytica* JCM 12864^T, *K. lacus* CGMCC 1.9109^T, *K. pumila* N18^T, and *K. sediminis* KCTC 42590^T. Numbers of each enzyme detected in the genomes were shown in the map. GT, glycosyltransferase; GH, glycoside hydrolase; CE, carbohydrate esterase; CBM, carbohydrate-binding module; AA, auxiliary activity; PL, polysaccharide lyase.

under anaerobic conditions, and nitrate is reduced to nitrite. The activities of trypsin and oxidase are positive, and the activities of α-chymotrypsin, α-galactosidase, α-glucosidase, α-mannosidase, and α-fucosidase are weakly positive. Acids are produced from D-arabinose, D-ribose, D-xylose, L-sorbose, D-tagatose, and potassium 5-ketogluconate. The major cellular fatty acids (>10%) are iso-$C_{15:0}$, iso-$C_{17:0}$, iso-$C_{17:1}$ ω9c, and summed feature 3 (comprising $C_{16:1}$ ω6c and/or $C_{16:1}$ ω7c). The predominant respiratory quinone is Q-10. The major polar lipids consist of PE, PG, DPG, and unidentified glycolipids, aminolipids, and lipids. The DNA G+C content of type strain is 59.9 mol%.

The type strain is A6E486^T (= KCTC 82758^T = MCCC 1H00470^T), which was isolated from coastal sediments collected off the coast of Weihai, China.

5 DESCRIPTION OF *KORDIIMONAS LAMINARIAE* SP. NOV.

Kordiimonas laminariae (la.mi.na'ri.ae. N.L. gen. fem. n. laminariae, pertaining to the kelp Laminaria, from which the type strain was isolated).

TABLE 4 | Metabolic features and selected genes related to the adaptation to marine environments.

Categories	Metabolic features	Gene Count						
		1	2	3	4	5	6	7
Virulence, disease, and defense	*Mycobacterium* virulence operon	18	16	15	15	15	13	14
	Copper resistance	9	9	8	12	9	9	7
	Cobalt-zinc-cadmium resistance	4	10	4	11	7	8	2
	Fluoroquinolones resistance	2	2	2	2	2	2	2
	β-lactamase	1	2	1	2	2	1	1
Motility and chemotaxis	Flagellar motility	65	33	70	84	72	47	24
	Bacterial chemotaxis	17	22	26	30	19	21	15
Cold adaptation	Capsular and extracellular polysaccharides	14	17	28	18	20	27	11
	Polysaccharide export proteins	4	5	2	5	5	2	3
	Cold-shock proteins	4	3	3	4	1	3	1
	tRNA-dihydrouridine synthase	1	1	1	1	1	1	1
Stress response	Osmotic stress	4	0	1	2	2	2	1
	Oxidative stress	33	36	43	41	38	30	29
	Detoxification	9	7	8	7	6	6	7
	Phage shock protein operons	4	5	4	8	4	4	4
	Heat-shock proteins	7	5	6	5	7	5	2

Strains: 1, A6E486^T; 2, 5E331^T; 3, K. gwangyangensis JCM 30877^T; 4, K. lipolytica JCM 12864^T; 5, K. lacus CGMCC 1.9109^T; 6, K. pumila N18^T; 7, K. sediminis KCTC 42590^T.

Cells are Gram-negative and aerobic with rod shape. Growth is observed at pH 6.0–8.5 (optimum,7.0) and temperatures of 15°C–40°C (optimum, 33°C) and with 1.5%–5.0% (w/v, optimum, 3.0%) NaCl. Growth does not occur under anaerobic condition, and nitrate is not reduced to nitrite. The activities of trypsin and oxidase are positive, but the activities of α-chymotrypsin, α-galactosidase, α-glucosidase, α-mannosidase, and α-fucosidase are negative. Acids are produced from D-ribose, L-sorbose, D-turanose, D-lyxose, D-tagatose, and potassium 5-ketogluconate. The major cellular fatty acids (>10%) are iso-$C_{15:0}$, iso-$C_{17:1}$ ω9c, and summed feature 3 (comprising $C_{16:1}$ ω6c and/or $C_{16:1}$ ω7c). The predominant respiratory quinone is Q-10. The major polar lipids consist of PE, PG, DPG, and unidentified glycolipids, aminolipids, and lipids. The DNA G+C content of type strain is 46.2 mol%.

The type strain is 5E331^T (= KCTC 92199^T = MCCC 1H00515^T), which was isolated from fresh kelps collected from a kelp culture area, Rongcheng, China.

DATA AVAILABILITY STATEMENT

The data presented in this study are deposited in the GenBank. The accession number for the 16S rRNA gene sequence of strains A6E486^T and 5E331^T are MZ901372 and OM663707, respectively. The accession number for the whole genome shotgun project of strains A6E486^T and 5E331^T are JAINDF000000000 and JAKQZA000000000, respectively.

AUTHOR CONTRIBUTIONS

Y-QY and Z-PH isolated the strain A6E486^T and performed material preparation, experimental operation, and data collection and analysis. Y-YY helped process cell samples and photograph cell morphology. LM isolated the strain 5E331^T, and Y-QY finished the experiment and article. Z-JD and M-QY offered experiment guidance and critical revision of the article. All authors contributed to the article and approved the submitted version.

FUNDING

This work was supported by the National Natural Science Foundation of China (32070002) and the National Science and Technology Fundamental Resources Investigation Program of China (2019FY100700).

ACKNOWLEDGMENTS

The implementation of scanning electron microscope was supported by the Physical-Chemical Materials Analytical and Testing Center of Shandong University at Weihai.

SUPPLEMENTARY MATERIAL

The Supplementary Material for this article can be found online at: https://www.frontiersin.org/articles/10.3389/fmars.2022.919253/full#supplementary-material

REFERENCES

Aziz, R. K., Bartels, D., Best, A. A., Dejongh, M., Disz, T., Edwards, R. A., et al. (2008). The RAST Server: Rapid Annotations Using Subsystems Technology. *BMC Genomics* 9, 75. doi: 10.1186/1471-2164-9-75

Chaudhari, N. M., Gupta, V. K., and Dutta, C. (2016). BPGA- an Ultra-Fast Pan-Genome Analysis Pipeline. *Sci. Rep.* 6, 24373. doi: 10.1038/srep24373

Chernomor, O., von Haeseler, A., and Minh, B. Q. (2016). Terrace Aware Data Structure for Phylogenomic Inference From Supermatrices. *Syst. Biol.* 65 (6), 997–1008. doi: 10.1093/sysbio/syw037

Da, C. M., Santos, H., and Galinski, E. A. (1998). An Overview of the Role and Diversity of Compatible Solutes in Bacteria and Archaea. *Adv. Biochem. Eng. Biotechnol.* 61, 117–153. doi: 10.1007/BFb0102291

Dong, X. Z., and Cai, M. Y. (2001). ""Determination of Biochemical Characteristics,"," in *Manual for the Systematic Identification of General Bacteria*. Eds. X. Z. Dong and M. Y. Cai (Beijing: Science Press), 370–398.

Edgar, R. C. (2004). MUSCLE: Multiple Sequence Alignment With High Accuracy and High Throughput. *Nucleic Acids Res.* 32 (5), 1792–1797. doi: 10.1093/nar/gkh340

Felsenstein, J. (1981). Evolutionary Trees From DNA Sequences: A Maximum Likelihood Approach. *J. Mol. Evol.* 17 (6), 368–376. doi: 10.1007/BF01734359

Geng, N., Yang, D., Hua, J., Huang, L. J., Dong, H., Sun, C., et al. (2022). Complete Genome Sequence of *Kordiimonas Pumila* N18^T Sheds Light on Biogeochemical Roles of the Genus *Kordiimonas*. *Mar. Genomics* 62, 100930. doi: 10.1016/j.margen.2022.100930

Hoffmann, T., von Blohn, C., Stanek, A., Moses, S., Barzantny, H., and Bremer, E. (2012). Synthesis, Release, and Recapture of Compatible Solute Proline by Osmotically Stressed *Bacillus Subtilis* Cells. *Appl. Environ. Microbiol.* 78 (16), 5753–5762. doi: 10.1128/AEM.01040-12

Hyatt, D., Chen, G. L., Locascio, P. F., Land, M. L., Larimer, F. W., and Hauser, L. J. (2010). Prodigal: Prokaryotic Gene Recognition and Translation Initiation Site Identification. *BMC Bioinf.* 11, 119. doi: 10.1186/1471-2105-11-119

Innamorati, K. A., Earl, J. P., Aggarwal, S. D., Ehrlich, G. D., and Hiller, N. L. (2020). ""The Bacterial Guide to Designing a Diversified Gene Portfolio,"," in *The Pangenome: Diversity, Dynamics and Evolution of Genomes*. Eds. H. Tettelin and D. Medini (Cham, CH: Springer), 51–87.

Jorgensen, J. H., and Turnidge, J. D. (2015). ""Susceptibility Test Methods: Dilution and Disk Diffusion Methods,"," in *Manual of Clinical Microbiology*. Eds. J. H. Jorgensen, K. C. Carroll, G. Funke, M. A. Pfaller, M. L. Landry, S. S. Richter and D. W. Warnock (New York, NY: Wiley), 1253–1273.

Kanehisa, M., Sato, Y., Kawashima, M., Furumichi, M., and Tanabe, M. (2016). KEGG as a Reference Resource for Gene and Protein Annotation. *Nucleic Acids Res.* 44 (D1), 457–462. doi: 10.1093/nar/gkv1070

Komagata, K., and Suzuki, K. (1987). Lipid and Cell-Wall Analysis in Bacterial Systematics. *Methods Microbiol.* 19, 161–207. doi: 10.1016/S0580-9517(08)70410-0

Kumar, S., Stecher, G., Li, M., Knyaz, C., and Tamura, K. (2018). MEGA X: Molecular Evolutionary Genetics Analysis Across Computing Platforms. *Mol. Biol. Evol.* 35 (6), 1547–1549. doi: 10.1093/molbev/msy096

Kwon, K. K., Lee, H. S., Yang, S. H., and Kim, S. J. (2005). *Kordiimonas Gwangyangensis* Gen. Nov., Sp. Nov., a Marine Bacterium Isolated From

Marine Sediments That Forms a Distinct Phyletic Lineage (*Kordiimonadales* Ord. Nov.) in the '*Alphaproteobacteria*'. *Int. J. Syst. Evol. Microbiol.* 55 (5), 2033–2037. doi: 10.1099/ijs.0.63684-0

Lane, D. J. (1991). ""16s/23s rRNA Sequencing,"," in *Nucleic Acid Techniques in Bacterial Systematics*. Eds. E. Stackebrandt and M. Goodfellow (New York, NY: Wiley), 115–175.

Li, R. Q., Yu, C., Li, Y. R., Lam, T., Yiu, S. M., Kristiansen, K., et al. (2009). SOAP2: An Improved Ultrafast Tool for Short Read Alignment. *Bioinformatics* 25 (15), 1966–1967. doi: 10.1093/bioinformatics/btp336

Math, R. K., Jeong, S. H., Jin, H. M., Park, M. S., Kim, J. M., and Jeon, C. O. (2012). *Kordiimonas Aestuarii* Sp. Nov., a Marine Bacterium Isolated From a Tidal Flat. *Int. J. Syst. Evol. Microbiol.* 62 (Pt 12), 3049–3054. doi: 10.1099/ijs.0.038943-0

Minnikin, D. E., O'Donnell, A. G., Goodfellow, M., Alderson, G., Athalye, M., Schaal, A., et al. (1984). An Integrated Procedure for the Extraction of Bacterial Isoprenoid Quinones and Polar Lipids. *J. Microbiol. Meth.* 2 (5), 233–241. doi: 10.1016/0167-7012(84)90018-6

Mu, D. S., Liang, Q. Y., Wang, X. M., Lu, D. C., Shi, M. J., Chen, G. J., et al. (2018). Metatranscriptomic and Comparative Genomic Insights Into Resuscitation Mechanisms During Enrichment Culturing. *Microbiome* 6 (1), 230. doi: 10.1186/s40168-018-0613-2

Nguyen, L. T., Schmidt, H. A., von Haeseler, A., and Minh, B. Q. (2015). IQ-TREE: A Fast and Effective Stochastic Algorithm for Estimating Maximum-Likelihood Phylogenies. *Mol. Biol. Evol.* 32 (1), 268–274. doi: 10.1093/molbev/msu300

Nichols, C. A., Guezennec, J., and Bowman, J. P. (2005). Bacterial Exopolysaccharides From Extreme Marine Environments With Special Consideration of the Southern Ocean, Sea Ice, and Deep-Sea Hydrothermal Vents: A Review. *Mar. Biotechnol. (NY).* 7 (4), 253–271. doi: 10.1007/s10126-004-5118-2

Parks, D. H., Imelfort, M., Skennerton, C. T., Hugenholtz, P., and Tyson, G. W. (2015). CheckM: Assessing the Quality of Microbial Genomes Recovered From Isolates, Single Cells, and Metagenomes. *Genome Res.* 25 (7), 1043–1055. doi: 10.1101/gr.186072.114

Parsek, M. R., and Greenberg, E. P. (2000). Acyl-Homoserine Lactone Quorum Sensing in Gram-Negative Bacteria: A Signaling Mechanism Involved in Associations With Higher Organisms. *Proc. Natl. Acad. Sci. U. S. A.* 97 (16), 8789–8793. doi: 10.1073/pnas.97.16.8789

Pomposiello, P. J., and Demple, B. (2002). Global Adjustment of Microbial Physiology During Free Radical Stress. *Adv. Microb. Physiol.* 46, 319–341. doi: 10.1016/s0065-2911(02)46007-9

Price, M. N., Dehal, P. S., and Arkin, A. P. (2009). FastTree: Computing Large Minimum Evolution Trees With Profiles Instead of a Distance Matrix. *Mol. Biol. Evol.* 26 (7), 1641–1650. doi: 10.1093/molbev/msp077

Qin, Q. L., Li, Y., Zhang, Y. J., Zhou, Z. M., Zhang, W. X., Chen, X. L., et al. (2011). Comparative Genomics Reveals a Deep-Sea Sediment-Adapted Life Style of Pseudoalteromonas Sp. SM9913. *ISME J.* 5 (2), 274–284. doi: 10.1038/ismej.2010.103

Qin, X., Thota, G. K., Singh, R., Balamurugan, R., and Goycoolea, F. M. (2020). Synthetic Homoserine Lactone Analogues as Antagonists of Bacterial Quorum Sensing. *Bioorg Chem.* 98, 103698. doi: 10.1016/j.bioorg.2020.103698

Qin, Q. L., Xie, B. B., Yu, Y., Shu, Y. L., Rong, J. C., Zhang, Y. J., et al. (2014b). Comparative Genomics of the Marine Bacterial Genus *Glaciecola* Reveals the High Degree of Genomic Diversity and Genomic Characteristic for Cold Adaptation. *Environ. Microbiol.* 16 (6), 1642–1653. doi: 10.1111/1462-2920.12318

Qin, Q. L., Xie, B. B., Zhang, X. Y., Chen, X. L., Zhou, B. C., Zhou, J., et al. (2014a). A Proposed Genus Boundary for the Prokaryotes Based on Genomic Insights. *J. Bacteriol.* 196 (12), 2210–2215. doi: 10.1128/JB.01688-14

Roesser, M., and Muller, V. (2001). Osmoadaptation in Bacteria and Archaea: Common Principles and Differences. *Environ. Microbiol.* 3 (12), 743–754. doi: 10.1046/j.1462-2920.2001.00252.x

Saitou, N., and Nei, M. (1987). The Neighbor-Joining Method: A New Method for Reconstructing Phylogenetic Trees. *Mol. Biol. Evol.* 4 (4), 406–425. doi: 10.1093/oxfordjournals.molbev.a040454

Santos, C. L., Correia-Neves, M., Moradas-Ferreira, P., and Mendes, M. V. (2012). A Walk Into the LuxR Regulators of Actinobacteria: Phylogenomic Distribution and Functional Diversity. *PLos One* 7 (10), e46758. doi: 10.1371/journal.pone.0046758

Sasser, M. (1990). "Identification of Bacteria by Gas Chromatography of Cellular Fatty Acids," in *MIDI Technical Note 101* (Newark, DE: MIDI Inc).

Subramoni, S., and Venturi, V. (2009). LuxR-Family 'Solos': Bachelor Sensors/Regulators of Signalling Molecules. *Microbiol. (Reading England).* 155 (5), 1377–1385. doi: 10.1099/mic.0.026849-0

Wiegand, S., Jogler, M., Boedeker, C., Pinto, D., Vollmers, J., Rivas-Marin, E., et al. (2020). Cultivation and Functional Characterization of 79 Planctomycetes Uncovers Their Unique Biology. *Nat. Microbiol.* 5 (1), 126–140. doi: 10.1038/s41564-019-0588-1

Wood, J. M., Bremer, E., Csonka, L. N., Kraemer, R., Poolman, B., van der Heide, T., et al. (2001). Osmosensing and Osmoregulatory Compatible Solute Accumulation by Bacteria. *Comp. Biochem. Physiol. A Mol. Integr. Physiol.* 130 (3), 437–460. doi: 10.1016/s1095-6433(01)00442-1

Wu, Y. H., Jian, S. L., Meng, F. X., Maripatay,, Tohty, D., Wang, C. S., et al. (2016). *Kordiimonas Lipolytica* Sp. Nov., Isolated From Seawater. *Int. J. Syst. Evol. Microbiol.* 66 (6), 2198–2204. doi: 10.1099/ijsem.0.001007

Xu, X. W., Huo, Y. Y., Bai, X. D., Wang, C. S., Oren, A., Li, S. Y., et al. (2011). *Kordiimonas Lacus* Sp. Nov., Isolated From a Ballast Water Tank, and Emended Description of the Genus *Kordiimonas*. *Int. J. Syst. Evol. Microbiol.* 61 (Pt 2), 422–426. doi: 10.1099/ijs.0.018200-0

Xu, S., Zhou, J. W., Liu, L. M., and Chen, J. (2011). Arginine: A Novel Compatible Solute to Protect *Candida Glabrata* Against Hyperosmotic Stress. *Process Biochem.* 46 (6), 1230–1235. doi: 10.1016/j.procbio.2011.01.026

Yang, S. H., Kim, M. R., Seo, H. S., Lee, S. H., Lee, J. H., Kim, S. J., et al. (2013). Description of Kordiimonas Aquimaris Sp. Nov., Isolated From Seawater, and Emended Descriptions of the Genus *Kordiimonas* Kwon Et Al. 2005 Emend. Xu Et Al. 2011 and of its Existing Species. *Int. J. Syst. Evol. Microbiol.* 63 (Pt 1), 298–302. doi: 10.1099/ijs.0.038893-0

Yoon, S. H., Ha, S. M., Lim, J., Kwon, S., and Chun, J. (2017). A Large-Scale Evaluation of Algorithms to Calculate Average Nucleotide Identity. *Antonie Van Leeuwenhoek.* 110 (10), 1281–1286. doi: 10.1007/s10482-017-0844-4

Zhang, H., Yohe, T., Huang, L., Entwistle, S., Wu, P., Yang, Z., et al. (2018). Dbcan2: A Meta Server for Automated Carbohydrate-Active Enzyme Annotation. *Nucleic Acids Res.* 46 (W1), W95–W101. doi: 10.1093/nar/gky418

Zhang, H. X., Zhao, J. X., Chen, G. J., and Du, Z. J. (2016). *Kordiimonas Sediminis* Sp. Nov., Isolated From a Sea Cucumber Culture Pond. *Antonie Van Leeuwenhoek.* 109 (5), 705–711. doi: 10.1007/s10482-016-0671-z

Zhao, J., Zhang, R., Hou, X. J., Han, S. B., Li, Y., Cong, S., et al. (2018). *Kordiimonas Pumila* Sp. Nov., Isolated From Coastal Sediment. *Int. J. Syst. Evol. Microbiol.* 68 (5), 1743–1748. doi: 10.1099/ijsem.0.002740

Zou, H. B., Chen, N. N., Shi, M. X., Xian, M., Song, Y. M., and Liu, J. H. (2016). The Metabolism and Biotechnological Application of Betaine in Microorganism. *Appl. Microbiol. Biotechnol.* 100 (9), 3865–3876. doi: 10.1007/s00253-016-7462-3

Conflict of Interest: The authors declare that the research was conducted in the absence of any commercial or financial relationships that could be construed as a potential conflict of interest.

frontiers | Frontiers in Microbiology

ORIGINAL RESEARCH
published: 07 July 2022
doi: 10.3389/fmicb.2022.950857

Indole Diketopiperazine Alkaloids Isolated From the Marine-Derived Fungus *Aspergillus chevalieri* MCCC M23426

Dongli Lv[1†], Jinmei Xia[2†], Xiaoqing Guan[3†], Qiliang Lai[2†], Beibei Zhang[2], Jianhui Lin[2], Zongze Shao[2], Sulan Luo[1], Dongting Zhangsun[1], Jiang-Jiang Qin[3]* and Weiyi Wang[2]**

[1] Key Laboratory of Tropical Biological Resources of Ministry of Education, School of Pharmaceutical Sciences, Hainan University, Haikou, China, [2] Key Laboratory of Marine Biogenetic Resources, Third Institute of Oceanography, Ministry of Natural Resources, Xiamen, China, [3] The Cancer Hospital of the University of Chinese Academy of Sciences (Zhejiang Cancer Hospital), Institute of Basic Medicine and Cancer, Chinese Academy of Sciences, Hangzhou, China

OPEN ACCESS

Edited by:
Shan He,
Ningbo University, China

Reviewed by:
Haifeng Wang,
Shenyang Pharmaceutical University, China
Caijuan Zheng,
Hainan Normal University, China

***Correspondence:**
Dongting Zhangsun
zhangsundt@163.com
Jiang-Jiang Qin
jqin@ucas.ac.cn
Weiyi Wang
wywang@tio.org.cn

[†] These authors have contributed equally to this work

Specialty section:
This article was submitted to Aquatic Microbiology, a section of the journal Frontiers in Microbiology

Received: 23 May 2022
Accepted: 08 June 2022
Published: 07 July 2022

Citation:
Lv D, Xia J, Guan X, Lai Q, Zhang B, Lin J, Shao Z, Luo S, Zhangsun D, Qin J-J and Wang W (2022) Indole Diketopiperazine Alkaloids Isolated From the Marine-Derived Fungus Aspergillus chevalieri MCCC M23426. Front. Microbiol. 13:950857. doi: 10.3389/fmicb.2022.950857

Two new indole diketopiperazines (**1–2**) obtained from the fermentation culture of a deep-sea-derived fungus *Aspergillus chevalieri* MCCC M23426, were characterized, together with nine biogenetic related compounds (**3–11**). The structures of **1–2** were assigned based on NMR, MS, NMR calculation, DP4+ analysis, and ECD calculation. The bioactive assay showed that compounds **1**, **5**–**7** significantly inhibited the growth of *Staphylococcus aureus*. Meanwhile, compound **8** potently reduced the cell viability of gastric cancer cell MKN1 with an IC_{50} value of 4.6 μM.

Keywords: *Aspergillus*, cytotoxic, antibacterial, NMR, indole diketopiperazine

INTRODUCTION

Indole diketopiperazines (indole DKPs) are a group of natural products with diketopiperazine backbones. The backbones are formed through the condensation of certain amino acids with L-tryptophan. There are multiple candidates for this amino acid, such as L-valine, L-tryptophan, L-alanine, or L-proline. After being modified by various tailoring enzymes the structures of the products can be very diverse. One family worth mentioning is the echinulin family which usually shared the same structure moiety of a cyclo-L-Trp-L-Ala with a prenyl group attached to C-2. The additional prenyl substituents and the diketopiperazine moiety with diverse oxidative states distinguish the members of this family from each other. Most of the reported echinulins were produced by fungi. Due to their diversity in structures and their broad biological and pharmacological activities, echinulins are of great interest to natural medicinal chemists. Several echinulins were reported to be promising leads. Neoechinulin A, isoechinulin A, and variecolorin G can scavenge free radicals such as DPPH. What is more, neoechinulin A also shows anti-inflammatory activity. It can function as a cytoprotective agent and can protect PC12 cells from peroxynitrite-induced death (Nies and Li, 2021).

Our previous work has shown that marine microorganisms are promising producers of bioactive compounds. The secondary metabolites of a deep-sea-derived *Aspergillus chevalieri* strain were studied in this work. The genus *Aspergillus* is very productive in bioactive compounds. Several bioactive products of *Aspergillus chevalieri* were reported. One new nonadride enantiomer named ent-epiheveadride was recently obtained from the marine-derived fungus *Aspergillus chevalieri* PSU-AMF79, together with five known dioxopiperazine derivatives (Ningsih et al., 2022).

In earlier research, sixteen metabolites were separated from the endolichenic fungus *Aspergillus chevalieri* SQ-8 (Lin et al., 2021). Seven of these compounds are C7-alkylated salicylaldehyde derivatives and nine are prenylated indole alkaloids. Interestingly, two indole DKPs were reported to be generated by the deep-sea cold-seep-derived fungus *Aspergillus chevalieri* CS-122 (Yan et al., 2022).

In this study, the extract of a deep-sea-derived *Aspergillus chevalieri* strain showed great potential in antibacterial and cytotoxic activities. Two new indole DKPs, **1–2**, were obtained from the extract by biological activity-tracking, together with nine biogenetic related compounds (**3–11**) (**Figure 1**). Their structures were determined by multiple spectroscopic methods and their bioactivities were also evaluated.

MATERIALS AND METHODS

General Experimental Procedures

A Chirascan spectrometer (Applied Photophysics) was used to detect optical rotations of new compounds in MeOH. A UV-1800 spectrophotometer (Shimadzu, Kyoto, Japan) was used to collect UV (Ultra Violet) data for new compounds dissolved in MeOH. NMR spectra were collected on a Bruker Avance 850 MHz spectrometer. A Waters Xevo G2 Q-TOF mass spectrometer was utilized to obtain accurate molecular weight. MPLC (Medium Pressure Liquid Chromatography) was undertaken using different packing materials such as silica gel (200–300 mesh, 300–400 mesh, Tsingtao Marine Chemical Co., Ltd., Tsingtao, China), RP-C18 (ODS-A, 50 μm, YMC, Kyoto, Japan), and Sephadex LH-20 (GE Healthcare Bio-Science AB, Pittsburgh, PA, United States). HPLC (High-Performance Liquid Chromatography) was conducted on an Agilent 1260 system using an RP-C18 column (5 μm, 20 × 250 mm, YMC, Kyoto, Japan) with HPLC grade MeOH and MeCN as mobile phases.

Fungal Material

Strain R10-1G1 of *Aspergillus chevalieri* was identified by ITS sequence homology [100% similarity with *Aspergillus chevalieri* NRRL 78 (TYPE material) with a Genbank accession No. NR_135340 (max score 955, e value 0.0, query cover 100%)]. A voucher specimen was deposited at the Marine Culture Collection of China (MCCC) with the preservation number MCCC M23426. The strain was streaked on potato dextrose agar (PDA) slants and stored at 4 °C until use.

Fermentation, Extraction, and Isolation

Details about the fermentation, extraction, and isolation were provided in the supporting information (**Supplementary Material**, "Fermentation, Extraction, and Isolation").

5-prenylcryptoechinulin A (**1**): white amorphous solid; UV λ_{max} (methanol) nm (log ε): 230 (4.71), 275 (4.45); ^{1}H NMR and

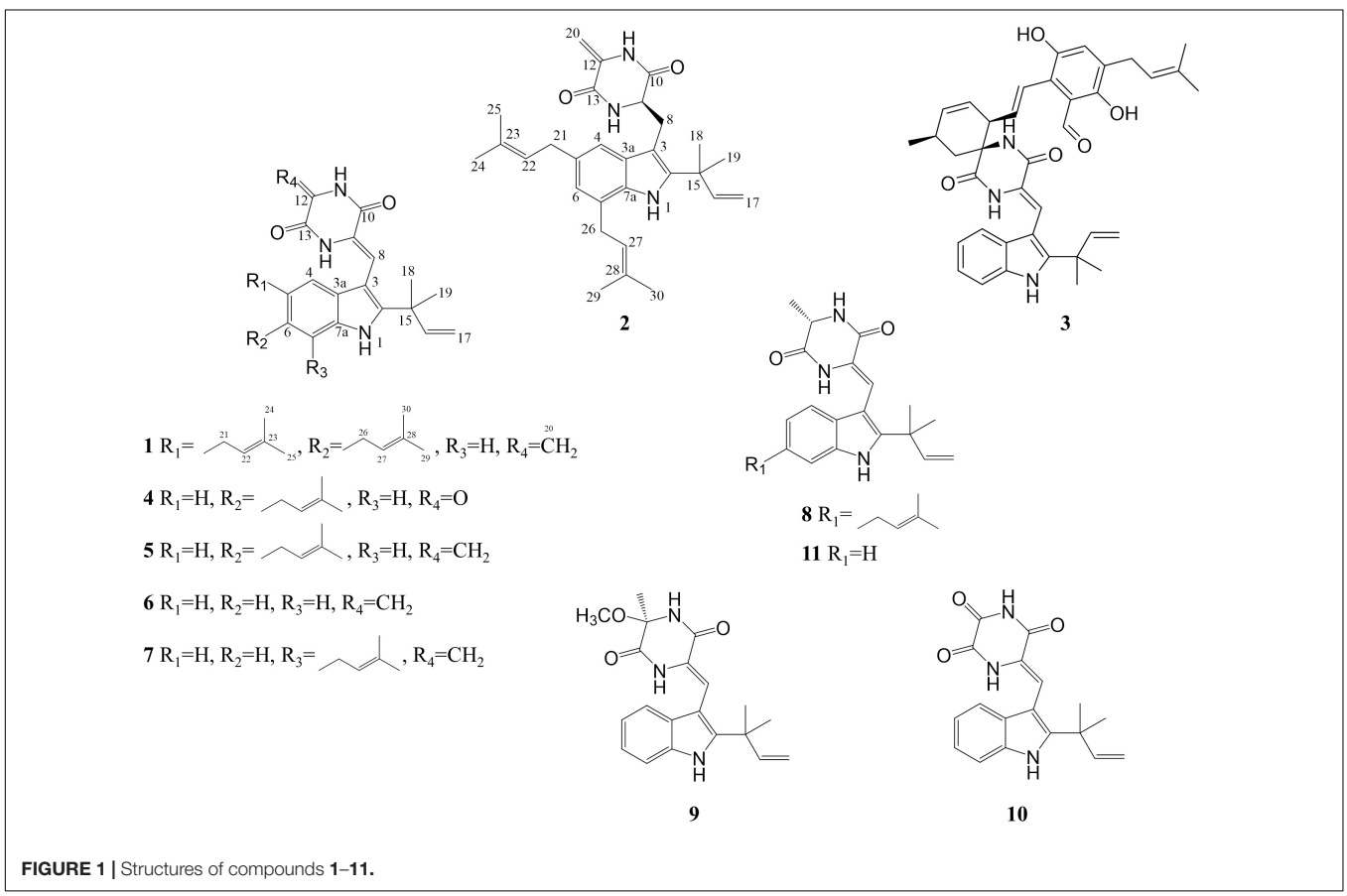

FIGURE 1 | Structures of compounds **1**–**11.**

TABLE 1 | ^{1}H NMR data (850 MHz) and ^{13}C NMR data (214 MHz) for compounds **1–3** (chloroform-*d*).

No.	1		2		3	
	δ_C, type	δ_H Mult. (*J* in Hz)	δ_C, type	δ_H Mult. (*J* in Hz)	δ_C, type	δ_H Mult. (*J* in Hz)
1	NH	8.18 (s, 1H)	NH	8.07 (s, 1H)	NH	8.26 (s, 1H)
2	143.9, C		141.6, C		144.0, C	
3	102.8, C		103.6, C		102.9, C	
4	118.8, CH	7.07 (s, 1H)	115.0, CH	7.14 (d, 1.5 Hz, 1H)	118.7, CH	7.12 (dd, 8.0,1.6 Hz, 1H)
5	133.5, C		134.0, C		121.2, CH	7.10 (ddd, 7.9,6.6,0.9 Hz, 1H)
6	134.9, C		122.9, CH	6.81 (d, 1.5 Hz, 1H)	122.5, CH	7.19 (dd, 6.6,1.6 Hz, 1H)
7	111.1, CH	7.17 (s, 1H)	123.5, C		111.3, CH	7.34 (m, 1H)
8	113.6, CH	7.28 (s, 1H)	30.7, CH_2	3.63 (dd, 14.5,3.8 Hz, 1H)	112.6, CH	7.18 (s, 1H)
8			30.7, CH_2	3.26 (dd, 14.5,12.0 Hz, 1H)		
9	123.7, C		55.6, CH	4.54 (ddd, 12.0,3.9,2.0 Hz, 1H)	124.2, C	
10	157.7, C		166.3, C		167.2, C	
11	NH	7.68 (s, 1H)	NH		NH	7.39 (s, 1H)
12	133.6, C		133.0, C		60.5, C	
13	155.5, C		158.0, C		161.8, C	
14	NH	8.29 (s, 1H)	NH	5.75 (s, 1H)	NH	6.36 (s, 1H)
15	39.3, C		38.9, C		39.1, C	
16	144.3, CH	6.05 (dd, 17.5,10.5 Hz, 1H)	145.7, CH	6.08 (dd, 17.4,10.5 Hz, 1H)	144.1, CH	6.00 (dd, 17.4,10.5 Hz, 1H)
17	113.3, CH_2	5.21 (dd, 10.5,1.0 Hz, 1H)	112.2, CH_2	5.15 (dd, 10.5,1.0 Hz, 1H)	113.5, CH_2	5.19 (dd, 10.5,1.0 Hz, 1H)
17	113.3, CH_2	5.17 (dd, 17.5,1.0 Hz, 1H)		5.13 (dd, 17.1,1.0 Hz, 1H)	113.5, CH_2	5.13 (dd, 17.5,1.0 Hz, 1H)
18	27.5, CH_3	1.51 (s, 3H)	27.7, CH_3	1.50 (s, 3H)	27.3, CH_3	1.40 (d, 4.8 Hz, 3H)
19	27.5, CH_3	1.51 (s, 3H)	27.8, CH_3	1.49 (s, 3H)	27.3, CH_3	1.40 (d, 4.8 Hz, 3H)
20	101.6, CH_2	5.60 (d, 1.2 Hz, 1H)	102.0, CH_2	5.59 (d, 1.2 Hz, 1H)	116.8, C	
20	101.6, CH_2	4.94 (d, 1.2 Hz, 1H)	102.0, CH_2	4.88 (d, 1.2 Hz, 1H)		
21	31.9, CH_2	3.39 (m, 2H)	34.6, CH_2	3.39 (m, 2H)	155.5, C	
22	123.5, CH	5.27 (m, 1H)	124.5, CH	5.35 (m, 1H)	131.0, C	
23	132.4, C		131.6, C		126.8, CH	7.02 (s, 1H)
24	17.8, CH_3	1.69 (s, 3H)	25.8, CH_3	1.74 (s, 3H)	145.5, C	
25	25.6, CH_3	1.72 (s, 3H)	17.9, CH_3	1.75 (s, 3H)	124.3, C	
26	31.7, CH_2	3.40 (m, 2H)	31.4, CH_2	3.54 (m, 2H)	126.7, CH	6.75 (dd, 16.2,0.9 Hz, 1H)
27	123.1, CH	5.31 (m, 1H)	122.9, CH	5.43 (m, 1H)	137.5, CH	5.89 (dd, 16.2,8.0 Hz, 1H)
28	132.6, C		133.0, C		46.1, CH	3.70 (dtd, 7.7,3.3,2.3 Hz, 1H)
29	25.8, CH_3	1.78 (s, 3H)	17.9, CH_3	1.87 (s, 3H)	124.1, CH	5.73 (dt, 10.1,2.6 Hz, 1H)
30	17.9, CH_3	1.71 (s, 3H)	25.7, CH_3	1.81 (s, 3H)	134.4, CH	5.96 (dt, 10.2,2.9 Hz, 1H)
31					27.9, CH	2.71 (dq, 10.9,3.2 Hz, 1H)
32					38.6, CH_2	2.52 (dd, 13.9,7.9 Hz, 1H)
32					38.6, CH_2	1.86 (dd, 13.9,3.5 Hz, 1H)
33					22.0, CH_3	1.26 (d, 7.5 Hz, 3H)
34					196.0, CH	10.06 (s, 1H)
35					27.1, CH_2	3.30 (d, 7.4 Hz, 1H)
36					120.9, CH	5.27 (dddd, 7.4,6.0,2.9,1.4 Hz, 1H)
37					133.9, C	
38					17.8, CH_3	1.68 (m, 3H)
39					25.8, CH_3	1.74 (d, 1.3 Hz, 3H)
7a	133.3, C		132.2, C		134.2, C	
3a	124.1, C		128.8, C		126.0, C	
OH-21					OH	11.80 (s, 1H)

^{13}C NMR data are shown in **Table 1**; HR-ESI-MS: *m*/*z* 456.2650 $[M - H]^-$ (Calcd. 456.2651 for $C_{29}H_{34}N_3O_2$, Δ – 0.2 ppm).

9-*epi*-didehydroechinulin (**2**): white amorphous solid; $[\alpha]_D^{25.0}$−98.9 (*c* 0.1, MeOH); UV λ_{max} (methanol) nm (log ε): 230 (4.56), 275 (4.14); ^{1}H NMR and ^{13}C NMR data are shown in **Table 1**; HR-ESI-MS: *m*/*z* 482.2784 $[M + Na]^+$ (Calcd. 482.2783 for $C_{29}H_{37}N_3O_2Na$, Δ + 0.2 ppm).

NMR Calculation

The conformer rotamer ensemble sampling tool (crest) (Pracht et al., 2020) was utilized to generate candidate conformers and DFT calculations were performed using the Gaussian 16 program (Frisch et al., 2016). The shielding constants were calculated by the GIAO method with TMS (Willoughby et al., 2014). More details about the computations and DP4+ analysis were provided

TABLE 2 | Comparison of the key parameters of (8*Z*)-**1**, (8*E*)-**1,** and **3a–3d** in NMR computations.

	(8*Z*)-1	(8*E*)-1	3a	3b	3c	3d
R^2 (^{13}C)	0.9971	0.9962	0.9969	0.9956	0.9989	0.9985
MAE (^{13}C)	2.4	2.8	3.3	2.6	1.5	1.7
CMAE (^{13}C)	2	2.4	1.9	2.6	1.4	1.7
R^2 (^{1}H)	0.9953	0.9918	0.9454	0.9619	0.9954	0.9847
MAE (^{1}H)	0.15	0.14	0.57	0.57	0.3	0.39
CMAE (^{1}H)	0.1	0.13	0.3	0.28	0.1	0.19
DP4+ (^{13}C)	100.00%	0.00%	NA	NA	NA	NA
DP4+ (^{1}H)	100.00%	0.00%	NA	NA	NA	NA
DP4+ (all data)	100.00%	0.00%	NA	NA	NA	NA

in the supporting information (**Supplementary Material**, "NMR Calculation") (Wang et al., 2018a, 2020a,b).

Antitumor and Antibacterial Assay

The human gastric cancer cell line MKN1 was purchased from American Type Culture Collection (ATCC, LGC Standards SLU, Barcelona, Spain). The *in vitro* assay was carried out to investigate the effects of compounds **1-11** on the gastric cancer cells. The cell viability (CCK8 assays), colony formation, and cell apoptosis (Annexin V-FITC Apoptosis Staining/Detection Kit, BD, United States) were all evaluated and the details were described previously (Wang et al., 2014, 2018c, 2019a). The protocol for antibacterial assay has also been described previously (Wang et al., 2018a,b, 2019b).

RESULTS

Compound **1** was isolated in the form of a colorless amorphous solid. Inspection of the HR-ESI-MS at *m/z* 456.2650 $[M - H]^-$ (calcd. 456.2651 for $C_{29}H_{34}N_3O_2$, Δ − 0.2 ppm, **Supplementary Figure 1**) allowed the establishment of its molecular formula as $C_{29}H_{35}N_3O_2$ with 14 degrees of unsaturation. The HSQC and ^{13}C/DEPT135 spectra evidenced six methyl groups (C-18, 19, 24, 25, 29, and 30), five methylene groups (C-17, 20, 21, and 26), six methine groups (C-4, 7, 8, 16, 22, and 27), and ten quaternary carbons (C-2, 3, 5, 6, 3a, 7a, 9, 10, 12, 13, 15, 23, and 28) (**Supplementary Figures 2, 3**). Interpretation of UV absorptions at λ_{max} 230 and 275 nm delineated the amide and conjugated indole moieties in **1** (**Supplementary Figure 4**). Cross peaks of H-4/C-6 and 7a, NH/C-2, 3, 3a and 7a, and H-7/C-5 and 3a, constructed the indole moiety. Cross peaks of H-8/C-2 and 3a (**Figure 2** and **Supplementary Figure 5**) in HMBC spectra placed the C-8–C-9–C-10 unit at C-3. Detailed inspection of NMR data of **1** proved that **1** might be an indole diketopiperazine, structurally close to cryptoechinulin A (**Supplementary Figures 6, 7**). Additional signals were deduced to be a prenyl group connecting to C-5, based on the apparent single peaks at δ_H 7.07 and 7.17 (coupling constants were small and negligible). This was also supported by the HMBC correlation of H-22/C-5 (**Table 1** and **Supplementary Figure 8**). As the NMR data was insufficient to support the configuration of C-8, NMR calculations at MPW1PW91-SCRF/6–31+G(d,p)//B3LYP/6-31G(d) for two candidate isomers (8*Z*)-**1** and (8*E*)-**1** were carried out. Through the comparison of the key computation parameters, as shown in **Table 2**, the calculated data of (8*Z*)-**1** matched well with their experimental counterparts. In addition, the 100% DP4+ probability of (8*Z*)-**1** (**Table 2**, **Supplementary Tables 1–15**, and **Supplementary Figure 9**) also supported this deduction. The structure of **1** was established and named 5-prenylcryptoechinulin A.

Compound **2** was isolated as a colorless amorphous solid. The UV spectra of **1** and **2** were similar which demonstrated that they shared the same backbone (**Supplementary Figure 10**). The molecular formula $C_{29}H_{37}N_3O_2$ with 13 degrees of unsaturation (**Supplementary Figure 11**) indicated that one double bond was absent in **2** compared to **1,** and **2** was a hydrogenated derivative of **1**. The correlations of H_2-8 to C-2 and C-3a and of H-9 to C-3,

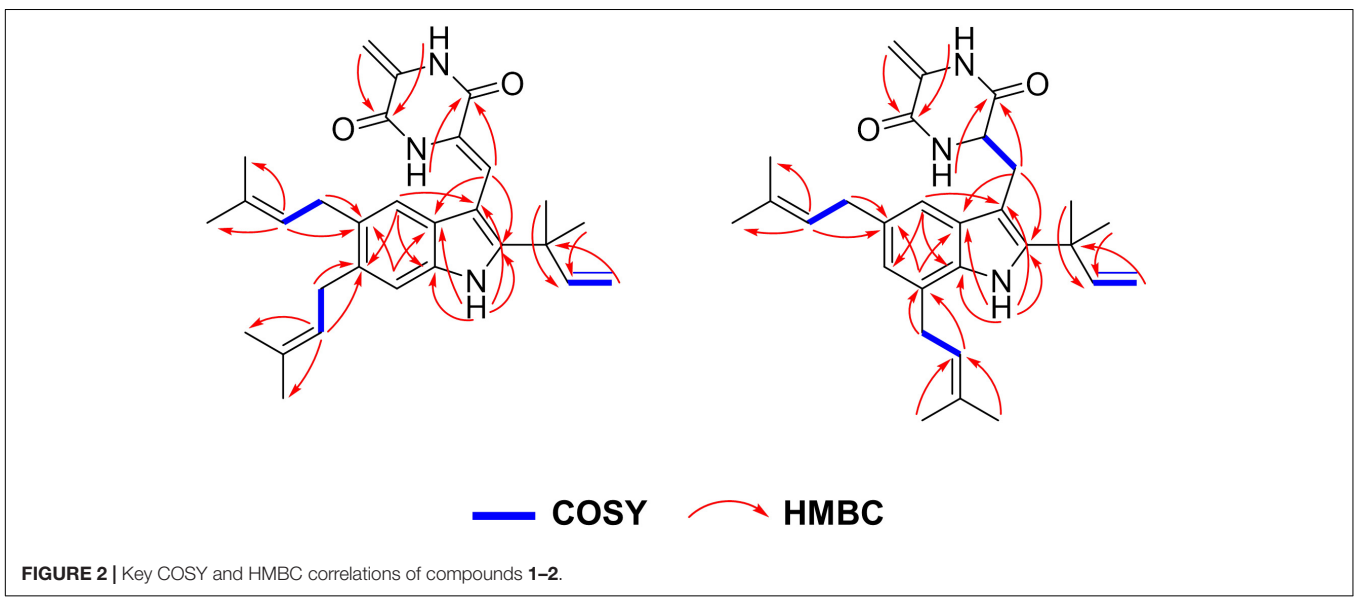

FIGURE 2 | Key COSY and HMBC correlations of compounds **1–2**.

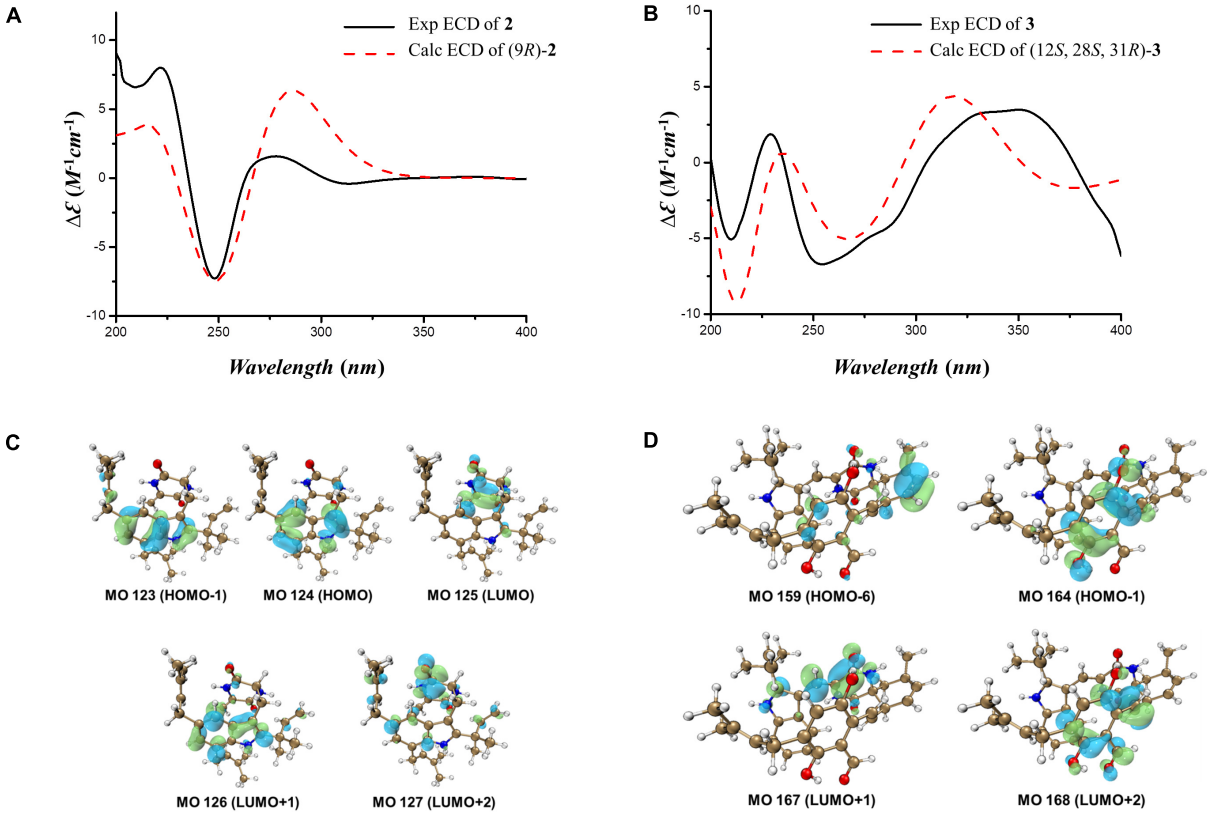

FIGURE 3 | (A,B) Calculated and experimental ECD spectra of **2** and **3**. **(C,D)** Key molecular orbitals (MOs) involved in the important transitions of **2** and **3**.

C-10 and C-13 in the HMBC spectrum allowed the elucidation of the hydrogenated bond C-8-C-9 (**Figure 2** and **Supplementary Figures 12–16**). The ^{1}H-NMR signals at δ 7.14 (d, J = 1.5 Hz) and 6.81 (d, J = 1.5 Hz) indicated the presence of a 4,6 or 5,7 disubstituted benzene moiety (**Table 1** and **Supplementary Figure 17**). The HMBC correlation of H-4/C-3 further placed the two prenyls at C-5 and C-7, respectively (**Figure 2** and **Supplementary Figure 15**), excluding the possibility of 4,6-disubstitution. Next, TDDFT calculation of the ECD spectrum at Cam-B3LYP/Def2SVP (**Supplementary Tables 16–22**) revealed the stereochemistry of C-9 as *R* (**Figure 3A**), as the theoretical ECD curve was in agreement with the experimental one. The molecular orbital (MO) analysis was carried out for the optimal conformer of **2a** (65.2%). The positive Cotton effect (CE) at ∼282 nm of **2** was thus related to electron transition from MO124 (HOMO) to MO125 (LUMO). The negative CE at ∼251 nm could be ascribed to the electron transition from MO124 (HOMO) to MO126 (LUMO+1). The positive CE at ∼219 nm was caused by the electron transition from MO124 (HOMO) to MO127 (LUMO+2) (**Figure 3C**). Finally, compound **2** was assigned as 9-*epi*-didehydroechinulin.

Compound **3** was obtained as a colorless amorphous solid. Detailed analysis of the NMR (**Supplementary Figures 18–23**) and HR-ESI-MS data revealed that **3** shared the same planar structure as the known compound cryptoechinuline D, which was firstly isolated from *Aspergillus amstelodami* in 1976 (Gatti et al., 1976). The relative stereochemistry of cryptoechinuline D was previously determined to be 12*S**, 28*R**, and 31*R** (Gao et al., 2013). In their work, two epimers of cryptoechinuline D were obtained by chiral HPLC and assigned by CD spectra as (12*R*, 28*S*, 31*S*) and (12*S*, 28*R*, 31*R*), respectively. However, after carefully examining the stereochemistry of C-12, 28, and 31 of cryptoechinuline D, we found that the relative stereochemistry reported by Gao (Gao et al., 2013) was wrong and actually should be assigned as 12*S**, 28*S**, 31*R**. To unambiguously establish the relative configuration of compound **3** in the current study, we simplified the candidate structures for DFT calculations as **3a–d** (**Figure 4**) and carried out the NMR calculation. By comparison of the calculated ^{1}H NMR and ^{13}C NMR of C-12, 13, 28, 29, 30, 31, 32, 33, the calculated **3c**, corresponding to (12*S**, 28*S**, 31*R**)-cryptoechinuline D, was found to be in better agreement with the experimental data, as indicated by the correlation coefficient (R^2), the mean absolute error (MAE), and the corrected mean absolute error (CMAE) (**Table 2**). Subsequently, TDDFT ECD calculation at the CAM-B3LYP-SCRF/def2-SVP (IEFPCM) level of theory was performed to elucidate the absolute configuration of compound **3** as 12*S*, 28*S*, 31*R* (**Figure 3B** and **Supplementary Tables 23–27**). The MO analysis of the optimal conformer of (12*S*, 28*S*, 31*R*)-cryptoechinuline D (35.9%) revealed that the negative CE at ∼250 nm in the experimental curve of **3** was related to the electron transition from MO164 (HOMO-1) to MO168 (LUMO+2). The negative CE at ∼206 nm could be

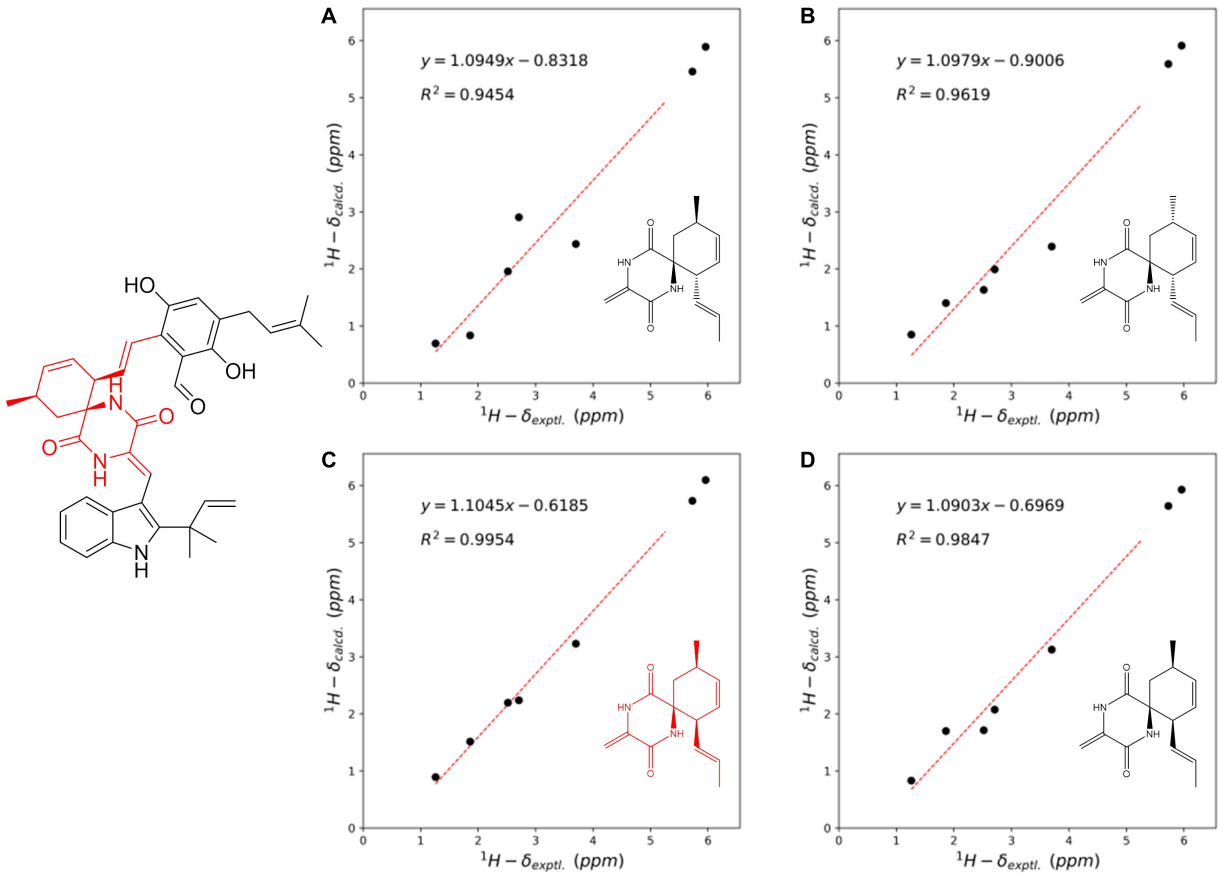

FIGURE 4 | Linear regression analysis between the experimental and calculated NMR data of simplified conformers of **3a–d** at C-12, 13, 28, 29, 30, 31, 32, 33.

ascribed to the electron transition from MO159 (HOMO-6) to MO167 (LUMO+1) (**Figure 3D**). Finally, compound **3** was assigned as (12*S*, 28*S*, 31*R*)-cryptoechinulin D.

The known compounds (**4**–**11**) were identified as neoechinuline (**4**) (Barbetta et al., 1969), cryptoechinulin A (**5**) (Cardillo et al., 1974), neoechinulin B (**6**) (Dossena et al., 1974), 7-prenylneoechinulin B (**7**) (Glisic et al., 2015; Nies and Li, 2021), neoechinulin D (**8**) (Dossena et al., 1975), variecolorin H (**9**) (Wang et al., 2007), cryptoechinulin C (**10**) (Cardillo et al., 1975), and neoechinulin A (**11**) (Cardillo et al., 1975), respectively, by comparing their spectroscopic data with those reported in the literature.

We first evaluated the antibacterial activities of **1**–**11** using strains of *Staphylococcus aureus* CICC 10384, *Vibrio parahaemolyticus* VP-HL, *Vibrio parahaemolyticus* ATCC 17802, and *Escherichia coli* CICC 10302. At the concentration of 250 μM, compounds **1**, **5**–**7** displayed selective antibacterial activities against *Staphylococcus aureus* CICC 10384 with an inhibition rate of over 90%, while compounds **8** and **10** exhibited moderate and weak antibacterial activities with an inhibition rate of 76 and 41%, respectively. Compound **7** showed potent antibacterial activity against *Staphylococcus aureus* CICC 10384 with a MIC value of 62.5 μM (positive control: chloramphenicol, MIC: 15.5 μM). We then evaluated the cytotoxicity of **1**–**11** against the gastric cancer cell line MKN1. Compounds **6** and **8** exhibited growth inhibition effects with IC_{50} values of 20.7 and 4.6 μM, respectively. Other compounds displayed weak cytotoxic activities with IC_{50} values over 100 μM (positive control: cisplatin, IC_{50}: 8.8 μM).

DISCUSSION

Indole DKPs are an important group of bioactive metabolites usually derived from fungi (Ma et al., 2016). *Aspergillus* is the most important genera in producing indole DKPs with great diversity in structures. Seven new prenylated indole DKPs were isolated from *Aspergillus fumigatus* (Wang et al., 2008). Three new indole DKPs were obtained from the *Aspergillus taichungensis* ZHN-7-07 (Cai et al., 2015). Three new indole DKPs were reported to be produced by *Aspergillus ochraceus* (Wen et al., 2018). A pair of enantiomeric indole DKPs were isolated from the mangrove endophytic fungus *Aspergillus* sp. SK-28 (Cai et al., 2019). Three new indole DKPs were generated by a soft coral-associated epiphytic fungus *Aspergillus* sp. EGF 15-0-3 (Wei et al., 2020). New indole DKPs were also obtained from the mangrove rhizosphere soil-derived fungus, *Aspergillus effuses* H1-1 (Gao et al., 2013), the terrestrial-derived endophytic fungus *Aspergillus* sp. (Lhamo et al., 2015), the soil-derived

fungus *Aspergillus ochraceopetaliformis* (Mostafa et al., 2021), the marine-derived fungus *Aspergillus* sp. Z3 (Li et al., 2022), the marine endophytic fungus *Aspergillus* sp. YJ191021 (Yang et al., 2021), the deep-sea-derived fungus *Aspergillus* sp. FS445 (Liu et al., 2021), and so on. In this work, two new indole DKPs were purified from the fermentation of the *Aspergillus chevalieri* MCCC M23426. This further demonstrated that the capacity of the genera *Aspergillus* in producing novel indole DKPs is yet to be fully explored.

In addition to their structural diversity, indole DKPs also exhibit a variety of activities (Jia et al., 2018). The cytotoxic activities of different indole DKPs on MOLT-4, A549, HL-60 (Cai et al., 2015), and BEL-7420 cell lines (Wang et al., 2008), on P388, HL-60, BEL-7402, and A-549 cell lines (Gao et al., 2013), on the prostate cancer PC3 cell line (Li et al., 2022), as well as on the NCI-H1975 gefitinib resistance (NCI-H1975/GR) cell lines (Wei et al., 2020) were evaluated. An indole diketopiperazine named asperthrins A was reported to possess antifungal and antibacterial activities against *Vibrio anguillarum*, *Xanthomonas oryzae* pv. *Oryzicola*, and *Rhizoctonia solani* (Yang et al., 2021). Another indole diketopiperazine named penilline D was assayed for its cytotoxic, antibacterial, and enzyme inhibitory activities against acetylcholinesterase (AChE) and pancreatic lipase (PL) but no significant activity was observed (Hu et al., 2021). Other reported activity assessments include anti-inflammatory effects (Wen et al., 2018), NO production inhibitory activity (Liu et al., 2021), radical scavenging activity against DPPH radicals (Zou et al., 2014), plant growth regulation (Zhang et al., 2013), and antifouling activity against the barnacle *Balanus reticulatus* (Cai et al., 2019). In this study, the inhibition effects of the new indole DKPs on several bacterial strains including the *Staphylococcus aureus*, and their cytotoxic activity against the gastric cancer cell MKN1, were evaluated. Although a variety of models have been applied to evaluate the bioactivities of indole DKPs, the activities observed were usually not significant. In-depth structure-activity relationship studies of these compounds, as well as structural modifications, may bring new chances for finding new structures with better bioactivities.

The cooccurrence of the echinulin family alkaloids also indicated some clues about their biosynthesis. Recent research heterologously expressed the putative echinulin biosynthetic gene cluster from *Aspergillus ruber* in *Aspergillus nidulans* (Nies and Li, 2021). Their work proved that EchPT2 catalyzes the prenylation steps and EchP450 catalyzes the formation of the double bond between C10 and C11. Compound **1** is the prenylated product of compound **5** at C5 whereas compound **7** is the prenylated product of compound **6** at C7. It is possible that these prenylation steps are also catalyzed by EchPT2. It was reported that preechinulin can be converted by the cytochrome P450 enzyme EchP450 to form neoechinulin A with a double bond and it can also be converted by EchPT2 to form prenylated products (Nies and Li, 2021). Here in this work, the obtained compounds **2** and **6** were closely related to a previously reported compound dihydroneochinulin B (Gao et al., 2013). The difference between compound **6** and dihydroneochinulin B lies in the double bond between C8 and C9. Compound **2** can be taken as the bioconversion product of dihydroneochinulin B after two prenylation steps at C5 and C7. It is possible that dihydroneochinulin B can be converted either by EchP450 to form compound **6** or by EchPT2 to produce compound **2**.

CONCLUSION

In the current research, we have isolated two new indole DKPs (**1**–**2**) and nine biogenetically related compounds (**3**–**11**) from the deep-sea-derived *Aspergillus chevalieri* strain. Their structures were elucidated by extensive spectroscopic methods, NMR, and ECD calculations. Compounds **1**, and **5**–**7** selectively inhibited the growth of *Staphylococcus aureus* at the concentration of 250 μM. Meanwhile, compound **8** potently reduced the cell viability of gastric cancer cell MKN1 with an IC_{50} value of 4.6 μM. The present study demonstrates that the fungal indole DKPs are promising candidates for the discovery of new lead compounds for antimicrobial and anticancer therapy.

DATA AVAILABILITY STATEMENT

The datasets presented in this study can be found in online repositories. The names of the repository/repositories and accession number(s) can be found in the article/**Supplementary Material**.

AUTHOR CONTRIBUTIONS

DL, JX, XG, JL, and WW: investigation. QL and ZS: resources. JX, BZ, and WW: data analysis. JX, WW, and J-JQ: writing—original draft preparation. ZS, SL, and DZ: writing-revision. All authors have read and agreed to the published version of the manuscript.

FUNDING

This research was supported by the Natural Science Foundation of Fujian Province (2021J01509), the Scientific Research Foundation of Third Institute of Oceanography SOA (2018021), Deep-Sea Habitats Discovery Project (DY-XZ-04), the National Natural Science Foundation of China (41906104), COMRA program (DY135-B2-01 and DY135-B2-05), and the Scientific Research Foundation of Third Institute of Oceanography MNR (2019021).

ACKNOWLEDGMENTS

We are grateful to all the members of Wang Lab for their contribution to this manuscript.

SUPPLEMENTARY MATERIAL

The Supplementary Material for this article can be found online at: https://www.frontiersin.org/articles/10.3389/fmicb.2022.950857/full#supplementary-material

REFERENCES

Barbetta, M., Casnati, G., Pochini, A., and Selva, A. (1969). Neoechinuline: a new indole metabolite from aspergillus amstelodami. *Tetrahedron Lett.* 10, 4457–4460. doi: 10.1016/S0040-4039(01)88723-2

Cai, R., Jiang, H., Xiao, Z., Cao, W., Yan, T., Liu, Z., et al. (2019). (–)- and (+)-asperginulin A, a pair of indole diketopiperazine alkaloid dimers with a 6/5/4/5/6 pentacyclic skeleton from the mangrove endophytic fungus *Aspergillus* sp. SK-28. *Org. Lett.* 21, 9633–9636. doi: 10.1021/acs.orglett.9b03796

Cai, S., Sun, S., Peng, J., Kong, X., Zhou, H., Zhu, T., et al. (2015). Okaramines S-U, three new indole diketopiperazine alkaloids from *Aspergillus taichungensis* ZHN-7-07. *Tetrahedron* 71, 3715–3719. doi: 10.1016/j.tet.2014.09.019

Cardillo, R., Fuganti, C., Gatti, G., Ghiringhelli, D., and Grasselli, P. (1974). Molecular structure of cryptoechinuline A, a new metabolite of *Aspergillus amstelodami*, isolated during investigations on echinuline biosynthesis. *Tetrahedron Lett.* 15, 3163–3166. doi: 10.1016/S0040-4039(01)91850-7

Cardillo, R., Fuganti, C., Ghiringhelli, D., Grasselli, P., and Gatti, G. (1975). Stereochemical course of the α,β-desaturation of L-tryptophan in the biosynthesis of cryptoechinuline A in *Aspergillus amstelodami*. *J. Chem. Soc. Chem. Commun.* 4, 778–779. doi: 10.1039/C39750000778

Dossena, A., Marchelli, R., and Pochini, A. (1974). New metabolites of *Aspergillus amstelodami* related to the biogenesis of neoechinulin. *J. Chem. Soc. Chem. Commun.* 3, 771–772. doi: 10.1039/c39740000771

Dossena, A., Marchelli, R., and Pochini, A. (1975). Neoechinulin D, a new isoprenylated dehydrotryptophyl metabolite from *Aspergillus amstelodami*. *Experientia* 31, 1249.

Frisch, M. J., Trucks, G. W., Schlegel, H. B., Scuseria, G. E., Robb, M. A., Cheeseman, J. R., et al. (2016). *Gaussian 16 Rev. C.01*. Wallingford, CT.

Gao, H., Zhu, T., Li, D., Gu, Q., and Liu, W. (2013). Prenylated indole diketopiperazine alkaloids from a mangrove rhizosphere soil-derived fungus *Aspergillus effuses* H1-1. *Arch. Pharm. Res.* 36, 952–956. doi: 10.1007/s12272-013-0107-5

Gatti, G., Cardillo, R., Fuganti, C., and Ghiringhelli, D. (1976). Structure determination of two extractives from *Aspergillus amstelodami* by nuclear magnetic resonance spectroscopy. *J. Chem. Soc. Chem. Commun.* 5, 435–436.

Glisic, S., Veljkovic, N., Stanojevic, M., Gemovic, B., Perovic, V., Radosevic, D., et al. (2015). Natural products as promising therapeutics for treatment of influenza disease. *Curr. Pharm. Des.* 21, 5573–5588. doi: 10.2174/1381612821666151002113426

Hu, Y.-W., Chen, W.-H., Song, M.-M., Pang, X.-Y., Tian, X.-P., Wang, F.-Z., et al. (2021). Indole diketopiperazine alkaloids and aromatic polyketides from the Antarctic fungus *Penicillium* sp. SCSIO 05705. *Nat. Prod. Res.* doi: 10.1080/14786419.2021.1973460 [Epub ahead of print].

Jia, B., Ma, Y., Chen, D., Chen, P., and Hu, Y. (2018). Studies on structure and biological activity of indole diketopiperazine alkaloids. *Prog. Chem.* 30, 1067–1081. doi: 10.7536/PC171231

Lhamo, S., Wang, X.-B., Li, T.-X., Wang, Y., Li, Z.-R., Shi, Y.-M., et al. (2015). Three unusual indole diketopiperazine alkaloids from a terrestrial-derived endophytic fungus, *Aspergillus* sp. *Tetrahedron Lett.* 56, 2823–2826. doi: 10.1016/j.tetlet.2015.04.058

Li, X., Xu, J., Wang, P., and Ding, W. (2022). Novel indole diketopiperazine stereoisomers from a marine-derived fungus *Aspergillus* sp. Mycology-Intern. *J. Fung. Bio.* doi: 10.1080/21501203.2022.2069173 [Epub ahead of print].

Lin, L.-B., Gao, Y.-Q., Han, R., Xiao, J., Wang, Y.-M., Zhang, Q., et al. (2021). Alkylated salicylaldehydes and prenylated indole alkaloids from the endolichenic fungus *Aspergillus chevalieri* and their bioactivities. *J. Agric. Food Chem.* 69, 6524–6534. doi: 10.1021/acs.jafc.1c01148

Liu, Z., Chen, Y., Li, S., Hu, C., Liu, H., and Zhang, W. (2021). Indole diketopiperazine alkaloids from the deep-sea-derived fungus *Aspergillus* sp. FS445. *Nat. Prod. Res.* doi: 10.1080/14786419.2021.1925271 [Epub ahead of print].

Ma, Y. M., Liang, X. A., Kong, Y., and Jia, B. (2016). Structural diversity and biological activities of indole diketopiperazine alkaloids from fungi. *J. Agric. Food Chem.* 64, 6659–6671. doi: 10.1021/acs.jafc.6b01772

Mostafa, A. A., Dennis, A., Ahmed, A.-R. S., Ioanna, C., Nikolas, F., Mohamed, S., et al. (2021). New indole diketopiperazine alkaloids from a soil-derived fungus *Aspergillus ochraceopetaliformis*. *Planta Med.* 87, 1316–1317. doi: 10.1055/s-0041-1736992

Nies, J., and Li, S. M. (2021). Prenylation and dehydrogenation of a C2-reversely prenylated diketopiperazine as a branching point in the biosynthesis of echinulin family alkaloids in *Aspergillus ruber*. *ACS Chem. Biol.* 16, 185–192. doi: 10.1021/acschembio.0c00874

Ningsih, B. N. S., Rukachaisirikul, V., Phongpaichit, S., Preedanon, S., Sakayaroj, J., and Muanprasat, C. (2022). A nonadride derivative from the marine-derived fungus *Aspergillus chevalieri* PSU-AMF79. *Nat. Prod. Res.* doi: 10.1080/14786419.2022.2039651 [Epub ahead of print].

Pracht, P., Bohle, F., and Grimme, S. (2020). Automated exploration of the low-energy chemical space with fast quantum chemical methods. *Phys. Chem. Chem. Phys.* 22, 7169–7192. doi: 10.1039/c9cp06869d

Wang, F., Fang, Y., Zhu, T., Zhang, M., Lin, A., Gu, Q., et al. (2008). Seven new prenylated indole diketopiperazine alkaloids from holothurian-derived fungus *Aspergillus fumigatus*. *Tetrahedron* 64, 7986–7991. doi: 10.1016/j.tet.2008.06.013

Wang, W., Chen, R., Luo, Z., Wang, W., and Chen, J. (2018a). Antimicrobial activity and molecular docking studies of a novel anthraquinone from a marine-derived fungus *Aspergillus versicolor*. *Nat. Prod. Res.* 32, 558–563. doi: 10.1080/14786419.2017.1329732

Wang, W., Cheng, J. W., Qin, J. J., Hu, B., Li, X., Nijampatnam, B., et al. (2019a). MDM2-NFAT1 dual inhibitor, MA242: effective against hepatocellular carcinoma, independent of p53. *Cancer Lett.* 459, 156–167. doi: 10.1016/j.canlet.2019.114429

Wang, W., Liao, Y., Chen, R., Hou, Y., Ke, W., Zhang, B., et al. (2018b). Chlorinated azaphilone pigments with antimicrobial and cytotoxic activities isolated from the deep sea derived fungus *Chaetomium* sp. NA-S01-R1. *Mar. Drugs* 16:61. doi: 10.3390/md16020061

Wang, W., Liao, Y., Zhang, B., Gao, M., Ke, W., Li, F., et al. (2019b). Citrinin monomer and dimer derivatives with antibacterial and cytotoxic activities isolated from the deep sea-derived fungus *Penicillium citrinum* NLG-S01-P1. *Mar. Drugs* 17:46. doi: 10.3390/md17010046

Wang, W., Qin, J. J., Voruganti, S., Nijampatnam, B., Velu, S. E., Ruan, K. H., et al. (2018c). Discovery and characterization of dual inhibitors of MDM2 and NFAT1 for pancreatic cancer therapy. *Cancer Res.* 78, 5656–5667. doi: 10.1158/0008-5472.CAN-17-3939

Wang, W., Qin, J. J., Voruganti, S., Wang, M. H., Sharma, H., Patil, S., et al. (2014). Identification of a new class of MDM2 inhibitor that inhibits growth of orthotopic pancreatic tumors in mice. *Gastroenterol.* 147, 893–902.e2. doi: 10.1053/j.gastro.2014.07.001

Wang, W., Yang, J., Liao, Y. Y., Cheng, G., Chen, J., Cheng, X. D., et al. (2020a). Cytotoxic nitrogenated azaphilones from the deep-sea-derived fungus *Chaetomium globosum* MP4-S01-7. *J. Nat. Prod.* 83, 1157–1166. doi: 10.1021/acs.jnatprod.9b01165

Wang, W., Yang, J., Liao, Y. Y., Cheng, G., Chen, J., Mo, S., et al. (2020b). Aspeterreurone A, a cytotoxic dihydrobenzofuran-phenyl acrylate hybrid from the deep-sea-derived fungus *Aspergillus terreus* CC-S06-18. *J. Nat. Prod.* 83, 1998–2003. doi: 10.1021/acs.jnatprod.0c00189

Wang, W.-L., Lu, Z.-Y., Tao, H.-W., Zhu, T.-J., Fang, Y.-C., Gu, Q.-Q., et al. (2007). Isoechinulin-type alkaloids, variecolorins A-L, from halotolerant *Aspergillus variecolor*. *J. Nat. Prod.* 70, 1558–1564. doi: 10.1021/np070208z

Wei, X., Feng, C., Wang, S.-Y., Zhang, D.-M., Li, X.-H., and Zhang, C.-X. (2020). New indole diketopiperazine alkaloids from soft coral-associated epiphytic fungus *Aspergillus* sp. EGF 15-0-3. *Chem. Biodivers.* 17:e2000106. doi: 10.1002/cbdv.202000106

Wen, H., Liu, X., Zhang, Q., Deng, Y., Zang, Y., Wang, J., et al. (2018). Three new indole diketopiperazine alkaloids from *Aspergillus ochraceus*. *Chem. Biodivers.* 15:e1700550. doi: 10.1002/cbdv.201700550

Willoughby, P. H., Jansma, M. J., and Hoye, T. R. (2014). A guide to small-molecule structure assignment through computation of ((1)H and (1)(3)C) NMR chemical shifts. *Nat. Protoc.* 9, 643–660. doi: 10.1038/nprot.2014.042

Yan, L.-H., Li, P.-H., Li, X.-M., Yang, S.-Q., Liu, K.-C., Wang, B.-G., et al. (2022). Chevalinulins A and B, proangiogenic alkaloids with a spiro[bicyclo[2.2.2]octane-diketopiperazine] skeleton from deep-sea cold-seep-derived fungus *Aspergillus chevalieri* CS-122. *Org. Lett.* 24, 2684–2688. doi: 10.1021/acs.orglett.2c00781

Yang, J., Gong, L., Guo, M., Jiang, Y., Ding, Y., Wang, Z., et al. (2021). Bioactive indole diketopiperazine alkaloids from the marine endophytic

fungus *Aspergillus* sp. YJ191021. *Mar. Drugs* 19:157. doi: 10.3390/md19030157

Zhang, Q., Wang, S.-Q., Tang, H.-Y., Li, X.-J., Zhang, L., Xiao, J., et al. (2013). Potential allelopathic indole diketopiperazines produced by the plant endophytic aspergillus fumigatus using OSMAC method. *J. Agric. Food Chem.* 61, 11447–11452. doi: 10.1021/jf403200g

Zou, X., Li, Y., Zhang, X., Li, Q., Liu, X., Huang, Y., et al. (2014). A new prenylated indole diketopiperazine alkaloid from *Eurotium cristatum*. *Molecules* 19, 17839–17847. doi: 10.3390/molecules191117839

Conflict of Interest: The authors declare that the research was conducted in the absence of any commercial or financial relationships that could be construed as a potential conflict of interest.

Publisher's Note: All claims expressed in this article are solely those of the authors and do not necessarily represent those of their affiliated organizations, or those of the publisher, the editors and the reviewers. Any product that may be evaluated in this article, or claim that may be made by its manufacturer, is not guaranteed or endorsed by the publisher.

frontiers | Frontiers in Marine Science

PERSPECTIVE
published: 11 July 2022
doi: 10.3389/fmars.2022.921451

Pathogen Filtration: An Untapped Ecosystem Service

C. A. Klohmann[*†] **and** *J. L. Padilla-Gamiño*[†]

School of Aquatic and Fishery Sciences, University of Washington, Seattle, WA, United States

Marine pathogens present serious challenges to aquaculture, fisheries productivity, and marine conservation requiring novel solutions to identify, control, and mitigate their effects. Several ecological habitats, such as mangroves and wetlands can recycle waste and serve as aquatic filtration systems. While nutrient cycling and other ecosystem services of these habitats have been well-studied, their potential to remove pathogens and mechanisms of filtration remain largely unstudied. Here, we review how mangroves, shellfish beds, seagrasses, and constructed wetlands can reduce pathogen pressure in coastal ecosystems. Mangroves may inhibit bacterial growth through phytochemicals in their leaves and remove viruses through desalination in their roots. Some bivalves remove pathogens by excreting pathogens through their pseudofeces and others concentrate pathogens within their tissues. Seagrasses slow flow rates, increase sedimentation rates and may reduce pathogens through allelopathy. Constructed wetlands decrease pathogens through a combination of mechanical, biological, and chemical filtration mechanisms. Protecting and restoring coastal ecosystems is key to maintaining pathogen filtration capacity, benefiting conservation efforts of threatened host populations, and mitigating large disease outbreaks.

Keywords: parasite, disease ecology, coastal ecosystems and habitats, health, water quality, zoonotic

OPEN ACCESS

Edited by:
Shan He,
Ningbo University, China

Reviewed by:
Jenny R. Hillman,
The University of Auckland, New Zealand
Lydia Jeanne Baker,
University of Miami, United States
Yanchen Sun,
The University of Tennessee, Knoxville, United States

****Correspondence:***
C. A. Klohmann
cak268@uw.edu

†These authors have contributed equally to this work and share first authorship

Specialty section:
This article was submitted to Aquatic Microbiology, a section of the journal Frontiers in Marine Science

Received: *15 April 2022*
Accepted: *14 June 2022*
Published: *11 July 2022*

Citation:
Klohmann CA and Padilla-Gamiño JL (2022) Pathogen Filtration: An Untapped Ecosystem Service. Front. Mar. Sci. 9:921451. doi: 10.3389/fmars.2022.921451

INTRODUCTION

Diseases, ubiquitous in the marine environment, are vital for healthy ecosystems but can be damaging when they impact fisheries, aquaculture, and ecosystem engineers (Burge and Hershberger, 2020). Pathogens can influence the structure, function, and stability of food webs (Selakovic et al., 2014) and they are critical to ecosystem dynamics as they play an important role in controlling host population densities and nutrient cycling (Lafferty et al., 2008; Carlson et al., 2020). At the Channel Islands National Park in California, sea urchin pathogens drove a community shift from desolate urchin-barrens toward biodiverse kelp forest assemblages (Behrens and Lafferty, 2004). Pathogens can have a positive role in mitigating and controlling algal blooms (Bigalke et al., 2019). Algicidal bacteria limited the growth of three phytoplankton species, allowing other species to increase in abundance and thus have the potential to shift phytoplankton community structure (Bigalke et al., 2019). In New Zealand, nematode, trematode, and acanthocephalan parasites increased biodiversity on mudflats (Thompson et al., 2005).

High pathogen abundance can cause host population declines with implications for community structure, ecosystem dynamics, and fisheries and aquaculture production (Groner et al., 2016). This can be especially damaging in keystone and economically important species such as the long-spined sea urchin (*Diadema antillarum*) that declined by almost 98% in the 1980's in the Caribbean (Behrens and Lafferty, 2004). The decline of this ecologically important grazer decreased herbivory of algae,

contributing to coral reef deterioration in the region (Onufryk et al., 2018). Pathogens have the potential to severely compromise fisheries. Epizootic shell disease, caused by bacterial dysbiosis (Groner et al., 2016) (**Figure 1A**) substantially contributed to the decline of one of the most profitable fisheries in the United States (US): the Southern New England lobster stock (Castro et al., 2012; Hoenig et al., 2017). The disease impact was two-fold in that it reduced the abundance of lobsters, with ovigerous females having somewhat higher mortality rates, and rendered the surviving lobsters unappealing for market sale (Lafferty et al., 2015). Another fishery impacted by disease is the black abalone (*Haliotis cracherodii)* along the West coast of the US (Raimondi et al., 2002). This population suffered major die-offs since the 1980's, accounting for total population losses of over 90%. These die-offs were caused by abalone withering syndrome, a chronic condition caused by a Rickettsiales-like organism (WS-RLO) that shrinks the mollusk's foot, preventing the animal from attaching to substrates (Raimondi et al., 2002) (**Figure 1A***)*. While efforts were made to rebuild the population, disease remains a hurdle to restoration and conservation efforts. Similarly, sea star wasting disease, hypothesized to be caused by a densovirus (SSaDV), caused a continental collapse of the sunflower star (*Pycnopodia helianthoides*), a keystone species, and impacted the abundance of 20 asteroid species along the West coast of the US (Lamb et al., 2017; Harvell et al., 2019). Warming ocean temperatures put additional physiological stress on sea stars, decimating wild populations and leading to unprecedented sea star mortality from Alaska to California (**Figure 1A**) (Harvell et al., 2019). Warming events, especially El Niño can trigger disease outbreaks such as the novel ulcerative skin disease that reduced ring-tailed damselfish (*Stegastees beebei)* and king angelfish (*Holacanthus passer*) populations by 78% and 86%, respectively in the Galapagos (Lamb et al., 2018).

Large die-offs of seagrass species over the last hundred years have also been attributed to pathogens. Eelgrass wasting disease, likely caused by the etiological agent *Labyrinthula zosterae*, created a large-scale blight in the Eelgrass (*Zostera marina*) population along the Atlantic coast of the US in the 1930s that has still not fully recovered (**Figure 1A**) (Rasmussen, 1977). *L. zosterae* is causing outbreaks of disease in eelgrass from Europe to western North America (Bockelmann et al., 2013; Groner et al., 2021).

Pathogen pressure is an issue for human health. Humans can experience infections, gastrointestinal and respiratory diseases, and other health effects when exposed to viral and bacterial pathogens in the ocean (Griffin et al., 2003; Graciaa et al., 2018). We must look to innovative, sustainable, and creative solutions to manage ocean pathogens to limit their spread and effects. Filtration is an important ecosystem service to consider for removing and containing pathogens in the coastal environment. Filtration is defined as the reduction of pathogens in the water column by a variety of means including the reduction of water speed (i.e., flow rate), particle interception, biochemical transformation of nutrients and contaminants, absorption of

FIGURE 1 | (A) Marine diseases known to severely impact host species including keystone species and ecosystem engineers. (Pictures courtesy of C. Harvell, NOAA Fisheries, AccessScience, O Graham and C Klohmann). Marine ecosystems with pathogen filtration capacity **(B)**. Mangroves (left), seagrasses (middle), and shellfish beds (right). Pictures courtesy of Vecteezy, NOAA Photo Library, and Wikimedia commons.

water and nutrients, and sedimentation (Kuehn and Mueller, 2000; "Constructed Treatment Wetlands", 2004; Brauman et al., 2007; Wu et al., 2016).

Natural filtration in coastal environments can occur by vegetation (i.e., *via* seagrass, salt marshes and mangroves) and shellfish beds (Burge et al., 2016; J. Lamb et al., 2017). However, these natural filtration services may be in danger as coastal ecosystems are threatened by habitat loss (Halpern et al., 2008), climate change (Harley et al., 2006), and disease (Rasmussen, 1977). The planet has lost about 50% of its wetlands since 1900 (Davidson, 2014) and seagrasses, salt marshes and mangroves are all declining globally (Halpern et al., 2008). Recent estimates indicate that mangroves and seagrass beds are declining annually by 0.13% and 7%, respectively (Evans et al., 2018; Goldberg et al., 2020). Bivalve populations tend to be more intensely managed since they are important source of protein; however, it was estimated that globally, 85% of oysters reefs have been lost (Beck et al., 2011). Since the 1970's mussel (*Mytilus edulis*) populations declined by more than 60% in the gulf of Maine, USA (Sorte et al., 2017) and mussel bed communities declined by 58.9% along the West coast of the United States (Smith et al., 2006). Bivalve populations have declined in Europe but are increasing in Asia (Wijsman et al., 2019).

New research seeks to bolster natural filtration systems to decrease pathogen pressure and improve human health. Investing in natural filtration systems is an affordable and low-maintenance option when compared to wastewater treatment facilities, which cost between $250,000-$10,000,000 USD for installation in the United States ("How Much Does an Industrial Water Treatment System Cost?", 2017). Restoring and protecting wetlands can sustainably reduce pathogen pressure in coastal ecosystems by supplementing existing wastewater treatment strategies. In terrestrial systems, forest cover and proximity to forested areas can decrease childhood diarrheal infections (Herrera et al., 2017), suggesting that conserving forests and riparian vegetation has the potential to limit disease. In Germany, riverbank filtration (water passed through the bank of the river) has been used for over 100 years to purify drinking water, providing approximately 16% of all German drinking water (Kuehn and Mueller, 2000).

Despite recent efforts to better understand pathogen pressure in the ocean (Tracy et al., 2019; Harvell and Lamb, 2020) we still have an incomplete understanding of how these pathogens are controlled in marine systems, and how they will impact marine and human health. So far studies suggest that disease is increasing in certain systems like corals reefs but may be declining in fishes and elasmobranchs (Tracy et al., 2019). It is also unclear whether the systems severely impacted by disease outbreak are lacking a filtration system or have one that has been impaired in some way. Here, we examine the role that coastal marine species, namely (1) mangroves, (2) shellfish beds (mussels and oysters), (3) seagrasses, and (4) constructed wetlands, play in pathogen filtration and the mechanisms that decrease pathogen loads.

MANGROVES

Mangrove forests are coastal ecosystems widespread in the intertidal zone in tropical and subtropical areas, covering 136,000 km^2 globally (**Figure 1B**) (Spalding and Maricé, 2021). These forests provide key ecosystem services such as carbon sequestration, nursery habitat for fish, and coastal protection. Mangroves reduce excess nutrients in coastal waters, including nitrogen and phosphorous (Lin and Dushoff, 2004), and are resilient plants capable of exuding and expelling salts, enabling them to thrive in highly saline environments (Spalding and Maricé, 2021). Tropical shrimp farms utilize mangroves' natural biofiltration properties to efficiently remove excess nutrients (Buhmann and Papenbrock, 2013). They are also the largest store of carbon in the coastal zone and can reduce ocean acidification (Lin and Dushoff, 2004; Sippo et al., 2016). Mangrove trees buffer against acidic water using their roots by metabolizing organic matter from their carbon-rich and oxygen-poor soils and releasing alkaline water in return (Sippo et al., 2016). Mangroves are so efficient at this process that waters within mangrove forests can have a pH as high as 8.1, whereas the seawater measured outside of the forest usually has a pH of 7.3 (Sippo et al., 2016).

Human and fish pathogens are filtered by mangroves. The phytochemicals within mangrove leaves and fungi found in their root sediments may assist in killing bacterial pathogens (Sahoo et al., 2012; Thatoi et al., 2013). Organic solvent extracts of leaves from five mangrove species in the Philippines inhibited growth of pathogenic fish bacteria (Choudhury et al., 2005). These extracts could be used in aquaculture facilities to reduce disease in fish (Choudhury et al., 2005). Mangrove leaf extracts inhibit the growth of human pathogens such as *Staphylococcus* and *Salmonella* (Sahoo et al., 2012). Another study inoculated compost with fungi isolated from mangrove sediments and found that plants grown in the fungal mangrove soil had higher disease defenses than plants without the fungi (Ameen and Ali, 2021). Mangroves have also been referred to as "natural wastewater wetlands" (Wu et al., 2008) and considered as secondary wastewater treatment systems in China due to their filtration capabilities (Palacios et al., 2021)

Mangrove roots, may reduce viral pathogens as they are efficient desalinators, removing up to 90% of sodium ions from seawater (Kim et al., 2016). The outermost root layer has a negative surface potential, attracting the positively charged sodium ions and repelling the negatively charged chlorine ions. These root potentials trap sodium ions in the first (outer) root layer, enabling fresh water to enter the inner roots (Kim et al., 2016) (**Figure 2C**). Mangrove desalination may be an important mechanism for pathogen filtration, as salts promote viral absorption due to the their negative charge (Lukasik et al., 2000). This charge is hypothesized to increase hydrophobic interactions between viruses and the roots, which may lead to viral absorption by the mangroves (Lukasik et al., 2000).

For centuries, mangrove extracts were used to treat a variety of human health issues, and microbial compounds found in mangrove leaves and roots can kill antibiotic-resistant bacteria (Abeysinghe, 2010; Saad et al., 2011; Durai and Radhakrishnan, 2016; Alizadeh Behbahani et al., 2018; Audah, 2020). These services could make mangrove forests very efficient pathogen filtration systems; however, more research is needed to better understand how we can best utilize mangroves to remove pathogens from coastal waters.

SHELLFISH BEDS

Bivalves (Phylum Mollusca) are favorable pathogen filtration specialists due to their high filtration capacity, ubiquity in many ecosystems, tolerance for poor water quality, and abundance. An individual filter-feeding bivalve can filter 10-100 gallons of water a day using their gills (Burge et al., 2016). Bivalves feed by capturing particles from the water column, primarily phyto- and zooplankton, but they can also consume bacteria, viruses, and other organic matter in the process. Bivalves are selective feeders and particle capture depends on size, density and surface chemical compounds (Burge et al., 2016). Some pathogens may be killed within bivalve gills and gut tissue during ingestion and digestion, but most are likely expelled as feces or pseudofeces (**Figure 2**). These feces and pseudofeces remove pathogens through sedimentation, sinking out of the water column along with attached bacteria and viruses (Burge et al., 2016). For example, eelgrass plants had fewer lesions from wasting disease (*Labyrinthula zosterae)* when cocultured with oysters (Groner et al., 2018). Bivalves may also inhibit microbial growth through the production of peptides and polypeptides (Zannella et al., 2017). Additionally, mussels are used at aquaculture facilities to reduce bacterial and eukaryotic pathogen abundance in fish farms (Voudanta et al., 2016).

While bivalves may remove pathogens due to their filtration efficiency, they could also store them in their tissues. Some studies found concentrated pathogens within filter-feeder gill tissues, implicating bivalves as reservoirs for pathogens, and in some cases, amplification (Ben-Horin et al., 2015; Harvell and Lamb, 2020). Accumulation occurs when pathogens do not degrade and instead build up inside the bivalve and can lead to transmission to species that consume the filter feeder (Burge et al., 2016). Specifically, clams and mussels can accumulate and transmit *Vibrio haemolyticus* to humans (Harvell and Lamb, 2020). Mussels off the coast of California have tested positive for *Toxoplasma gondii*, the causative agent of toxoplasmosis, the same strain known to infect sea otters in the region (Miller et al., 2008). This potential transmission renders bivalves a less sustainable option for natural filtration, as shellfish beds present an infection risk to their predators. However, recent research has shown that oyster aquaculture may reduce pathogens for wild oyster populations as long as aquaculture stocks are harvested before they can spread disease (Ben-Horin et al., 2018).

Bivalves grow in very dense clusters, potentially increasing their filtration ability (**Figure 1B**). Mussels (*Mytilus trossulus*) can reach densities of 35 individuals per 100 cm^2 in the intertidal zone and up to 90 individuals per 100 cm^2 at aquaculture facilities (Kirk et al., 2007). Given the large distribution of bivalves, their

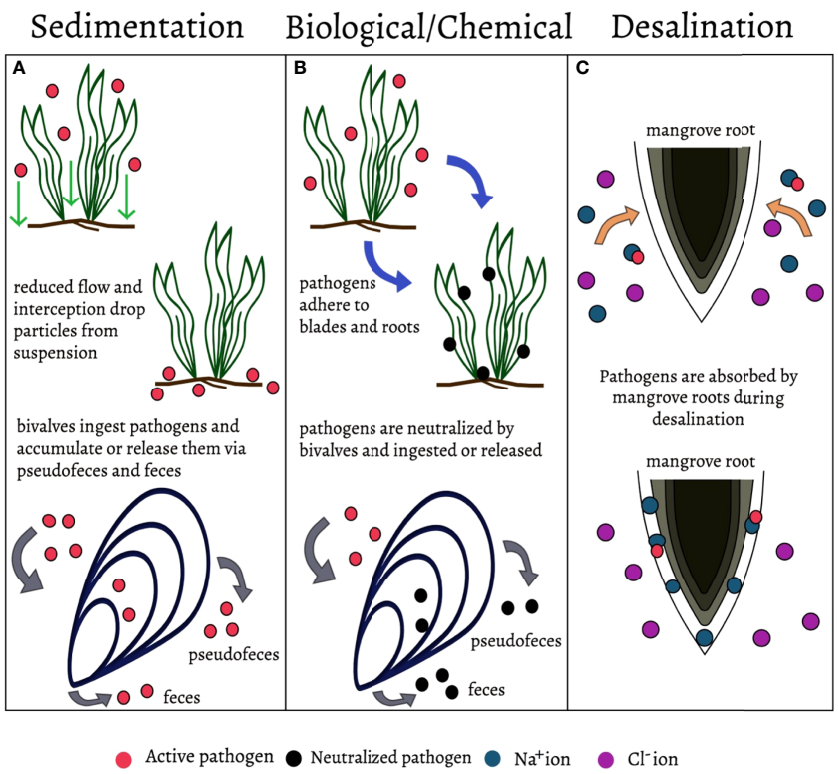

FIGURE 2 | Mechanisms involved in natural pathogen filtration. **(A)** Sedimentation - The removal of pathogens from suspension. This mechanism does not neutralize pathogens but removes them from the environment, it is utilized in seagrasses, bivalves, and constructed wetlands. **(B)** Biological/Chemical filtration - the removal of pathogens through adhesion, consumption, and inhibition (allelopathy). Neutralizes pathogens and/or removes them from the environment. Utilized in seagrasses, bivalves, constructed wetlands, and mangroves. **(C)** Desalination- The removal of sodium ions from salt water. Salts may promote viral absorption due to their negative charge, potentially removing viruses from the seawater. This mechanism is utilized by mangrove roots.

filtration efficiency, and high densities, shellfish beds have the potential to reduce pathogen loads in coastal waters (Ben-Horin et al., 2015). Bivalves could also be used to monitor pathogens and have been used to monitor pollutants. In Poznan, Poland, clams are used as bioindicators to assess water quality: In the presence of even small concentrations of pollutants, the clams will close their shells as a defense mechanism to prevent ingesting harmful or lethal items. Sensors glued to clams are triggered when the bivalves close, which initiates a shutoff of the water supply. This biological sensor system provides a remarkable means of monitoring environmental pollutants at very little cost (Micu, 2020). The National Oceanic and Atmospheric Administration (NOAA) used bivalves as environmental indicators by establishing oysters in the Chesapeake Bay, Maryland to monitor environmental contamination. Scientists tested oyster tissues for pharmaceutical products, pesticides, and other contaminants, detecting 98 different contaminants using this ecosystem-based monitoring approach (Apeti et al., 2018). Complementary monitoring methods can be developed with bivalves to filter, monitor and detect pathogens in the natural environment. One example is an oyster fishery in Myanmar that detected pathogenic bacterial in bivalve tissues, illustrating the impacts of agricultural runoff on coastal ecosystems (Littman et al., 2020)

SEAGRASS BEDS

Seagrass beds are another ecosystem hypothesized to remove pathogens and are one of the most important coastal ecosystems, providing $1.9 trillion USD in nutrient cycling services annually (Waycott et al., 2009) (**Figure 1B**). Additionally, seagrasses act as a "nutrient pump" by absorbing nutrients from the soil and releasing these nutrients through their leaves (Fourqurean, 2002). Seagrasses are estimated to cover 600,000 km^2 of the coastal floor from the Arctic circle to the tropics, and some beds are large enough to be seen from space, earning them the name "forests of the sea" (Cullen-Unsworth and Unsworth, 2013).

While seagrasses are well studied, their ability to filter pathogens from the water column was only recently identified. In the tropics, researchers found that seagrass beds are associated with reduced abundances of human, fish, and invertebrate pathogens (Lamb et al., 2017). This reduction of pathogens not only improves human health but also benefits corals that have fewer diseases in seagrass beds (Lamb et al., 2017). To date, little is known about the underlying mechanisms involved in the reduction of these pathogens. However, it is likely that a combination of sedimentation, a decrease in water flow rate, and mechanical and chemical filtration contribute to seagrasses' reduction of pathogens (S. Wu et al., 2016) (**Figures 2A, B**). Ocean flow rates are reduced by up to 40% within seagrass meadows, which may lead to pathogen particles dropping out of suspension (Lamb et al., 2017). In the South China Sea researchers found that one seagrass species, *Enhalus acroides*, trapped pathogens within its beds thus removing bacteria from the water (Deng et al., 2021). Phytochemicals within the seagrass plants may also kill pathogens, but this mechanism is still unclear (Babuselvam et al., 2017). *Thalassia hemprichii*, likely inhibited pathogens using antimicrobial chemical compounds such as phenol, flavonoid, and tannins (Deng et al., 2021).

Eelgrass (*Zostera marina*), a temperate seagrass that provides $87,000 of ecosystem services per hectare annually (Babuselvam et al., 2017), has been shown to exclude harmful dinoflagellates (Jacobs-Palmer et al., 2020). Researchers discovered significantly lower dinoflagellate abundances inside and around the *Z. marina* bed, such that *Z. marina* can form a 'halo' of dinoflagellate exclusion, up to 16 meters beyond the extent of the meadow (Jacobs-Palmer et al., 2020). Other studies found reduced algal growth due to seagrass phenolic compounds (DellaGreca et al., 2000) and antilarval and antibacterial properties from ethanol extract from a seagrass species in the South China Sea (Qi et al., 2008). Allelopathic activity in seagrasses, the defensive release of chemicals, and biological interactions of the micro and macro epibionts may also play a role in pathogen filtration services in this important ecosystem (Jacobs-Palmer et al., 2020). The outbreaks of the unicellular protist *L. zosterae* (Sullivan et al., 2018) in eelgrass beds (M. Bockelmann et al., 2013; Groner et al., 2021) suggest that seagrass pathogens may also accumulate within the beds and that biological filtration may not only apply to pathogens that are non-infectious to seagrass. It is important to note that the decline of seagrass beds worldwide is attributed to both pathogens and anthropogenic factors such as ocean warming and eutrophication. More research is needed to fully understand the vulnerability and potential of these filtration mechanisms (Jacobs-Palmer et al., 2020) (**Figure 2**).

PATHOGEN REDUCTION USING CONSTRUCTED WETLANDS

Constructed wetlands are defined as treatment systems that improve water quality through natural processes involving wetland vegetation, soils, and associated microbial assemblages ("Constructed Treatment Wetlands", 2004). In the 1950s, constructed wetlands were developed to expand on the services that naturally-occurring wetlands provided, such as improving water quality from stormwater runoff, greywater, and wastewater (Wu et al., 2016). Constructed wetlands can vary in their design but are meant to remove heavy metals, nitrogen, phosphorous, and chemical pollutants from runoff and remove harmful pathogens (Wu et al., 2016).

Constructed wetlands are utilized in a wide variety of industries to filter wastes, such as in textiles, paper milling, agriculture, and mining (Buhmann and Papenbrock, 2013). Recently, constructed wetlands were integrated into the aquaculture industry and have successfully been used to remove nutrients from catfish and rainbow trout aquaculture facilities (Buhmann and Papenbrock, 2013). Vegetation in the constructed wetland removes excess nutrients and also reduce water flow, allowing solids to be taken up by their root systems (Buhmann and Papenbrock, 2013). Constructed wetlands are excellent effluent removal options for land-locked aquaculture facilities because they can be implemented in both fresh and saline environments (Buhmann and Papenbrock, 2013). Additionally, constructed wetlands decrease human pathogens from wastewater without the use of

chlorine, which is a more sustainable and less damaging process than traditional chemical practices (Wu et al., 2016). Some constructed wetlands reduce water flow, allowing viruses in suspension to be killed by UV radiation (Wu et al., 2016).

Pathogens are removed from constructed wetlands by multiple mechanisms. The reduction of nutrients and pathogens depends on wetland type, size, and design and a combination of physical, chemical, and biological mechanisms (Wu et al., 2016). Some physical factors include mechanical filtration, sedimentation, and absorption of organic matter as well as CW design. Sedimentation, the removal of particles from suspension, is most effective against bacteria and coliforms such as fecal streptococcus due to these pathogens' larger size and faster settling rate (Wu et al., 2016). Mechanical filtration (i.e., passing the water through a filter), included in some constructed wetlands, can effectively remove pathogenic microorganisms, particularly protozoans (Wu et al., 2016). One study in a constructed wetland (Redder et al., 2010) noted a 100-fold reduction in protozoan pathogens when using mechanical filtration. Mechanical filtration is also effective at removing fecal indicator bacteria such as *Enterococcus* and *E. coli* (Wu et al., 2016). Predation activity of nematodes, rotifers, protozoa, bacterivorous bacteria, and phages is also an important factor affecting the bacterial removal in CWs (Wu et al., 2016). Artificial and vegetative oxygenation increase dissolved oxygen in CWs and are correlated with pathogen die-offs, especially bacteria (Wu et al., 2016).

The need for sustainable and affordable wastewater treatment systems, such as CWs, will only continue to grow along with the global population and wastewater discharge (Wu et al., 2016). CWs are an excellent example of a sustainable investment that will lower the abundance and risk of pathogens. These systems may also provide some insight into the mechanisms associated with pathogen removal in natural ecosystems.

DISCUSSION

Marine diseases are challenging to manage because pathogen transmission is impacted by water chemistry, currents, and ecological dynamics. We need creative solutions to reduce pathogen pressure to limit catastrophic host population die-offs and other negative downstream impacts. Natural filtration systems are an appealing solution to reduce pathogen loads and supplement wastewater treatment due to (1) their cost compared to artificial filtration systems and/or water treatment plants and (2) because pathogen reduction is not contingent upon pathogen isolation. These benefits make natural filtration systems an excellent investment to reduce novel, zoonotic diseases in marine environments with important consequences for human health (Sutton-Grier and Sandifer, 2019).

Natural pathogen filtration has several inherent limitations. Natural filtration only has the potential to reduce infectious disease when transmission is a rate-limiting step for the epidemiology. Some marine pathogens are so ubiquitous that exposure and transmission are almost guaranteed. In other cases, such as epizootic shell disease in lobsters, many of the bacteria associated with this disease are found on the shell of healthy lobsters, but their role switches from commensal to pathogenic. Natural filtration may be unable to prevent or mitigate the effects of such pathogens on an ecologically significant scale.

In mangroves and seagrasses, filtration mechanisms are not fully understood; likewise, in shellfish beds, it is not clear which pathogens are removed and which pathogens concentrate within bivalve tissues. Similarly, the extent of pathogen removal is still being explored in constructed wetlands. Important aspects of each system need to be explored to take full advantage of their filtration properties, including optimal densities in filtering bivalve populations, the role of microbiomes and epiphytes on seagrasses and mangroves, allelopathic interactions, and climate change on filtration capability. Additionally, it is unclear what the impact of filtration is on the host organism and if it can affect its productivity, physiological performance and/or quality. Future work is needed to examine the interactions between pathogen and host in ecosystems with filtration potential and to answer the following questions: Can natural filters fail due to pathogen overload? How can we test and monitor filtration performance? How often do we need to replace natural filtration systems to maintain pathogen filtration efficiency? What are the impacts of extracellular and intracellular pathogens in filtration performance? These are important questions as we consider the use of natural filtration systems to reduce pathogens in the coastal zone.

Coastal wetland ecosystems create habitats that facilitate high biodiversity, which may lead to lower pathogen pressure (Johnson et al., 2013; Duffy et al., 2015; Rahman et al., 2021). Despite the critical roles these ecosystems play, they are increasingly threatened by climate change, pollution, and anthropogenic activities. It is essential to protect them to maintain the services they provide. Conserving these natural areas may decrease pathogen transmission between wildlife and humans, leading to fewer zoonotic events (Keesing and Ostfeld, 2021). We require further understanding of the mechanisms involved in pathogen filtration, its relation to other ecosystem services, and the role that other ecological factors play in pathogen reduction to implement these systems at their full potential.

AUTHOR CONTRIBUTIONS

All authors listed have made a substantial, direct, and intellectual contribution to the work and approved it for publication.

FUNDING

This work was supported by the National Science Foundation Graduate Research Fellowship Program awarded to Corinne Klohmann and the Alfred Sloan Research Fellowship and National Science Foundation-CAREER awarded to Dr. Padilla-Gamiño.

ACKNOWLEDGMENTS

We would like to thank Dr. Drew Harvell, Dr. Jennifer Ruesink, Dr. Chelsea Wood, and Dr. Maya Groner for expert feedback on the manuscript. We would also like to thank the members of the Padilla-Gamiño laboratory, Núria Viladrich, Miranda Roethler, and Callum Backstrom for their review of this manuscript.

REFERENCES

Abeysinghe, P. D. (2010). Antibacterial Activity of Some Medicinal Mangroves Against Antibiotic Resistant Pathogenic Bacteria. *Indian J. Pharm. Sci.* 72 (2), 167–172. doi: 10.4103/0250-474X.65019

Alizadeh Behbahani, B., Farideh Tabatabaei, Y., Fakhri, S., Hamid, N., Alireza, V. and Ali, A. (2018). Phytochemical Analysis and Antibacterial Activities Extracts of Mangrove Leaf Against the Growth of Some Pathogenic Bacteria. *Microb. Pathog.* 114, 225–232. doi: 10.1016/j.micpath.2017.12.004

Ameen, F. and Ali, A. A.-H. (2021). Compost Inoculated With Fungi From a Mangrove Habitat Improved the Growth and Disease Defense of Vegetable Plants. *Sustainability* 13 (1), 1245. doi: 10.3390/su13010124

Apeti, D., Wirth, E., Leight, A. K., Mason, A. and Pisarski, E. (2018). *An Assessment of Contaminants of Emerging Concern in Chesapeake Bay, MD and Charleston Harbor, SC* (NOAA Technical Memorandum NOS NCCOS 240: Silver Spring, MD), 104. Available at: https://coastalscience.noaa.gov/project/mussel-watch-program-assessment-chesapeake-bay-charleston-harbor/. doi: 10.25923/p4nc-7m71

Audah, K. A. (2020). Antibacterial Screening of Mangrove Extract Library Showed Potential Activity Against *Escherichia Coli* and *Staphylococcus Aureus*. *Journal of Tropical Life Science.*(10),105–111. doi: 10.11594/jtls.10.02.03

(2017). *How Much Does an Industrial Water Treatment System Cost?* (Samco Tech (blog). Available at: https://www.samcotech.com/how-much-does-an-industrial-water-treatment-system-cost/.

Micu, A (2020). *In Poznan, Poland, Eight Clams Get to Decide If People in the City Get Water or Not* (ZME Science (blog). Available at: https://www.zmescience.com/science/poznan-mussel-water-plants-892524/.

EPA(2004). *Constructed Treatment Wetlands* (United States Environmental Protection Agency, EPA). Available at: https://www.epa.gov/wetlands/constructed-wetlands.

Babuselvam,M.,Panneerselvam,A.,Kanimozhi,K.andKavitha,G.(2017)*Antibacterial Potential of Actinomycetes From Seagrass Against Human and Aquaculture Pathogens*. Available at: https://www.semanticscholar.org/paper/Antibacterial-potential-of-actinomycetes-from-human-Babuselvam-Panneerselvam/e2bb6e6ac37c81b256547d86e50f527a1291e06b.

Beck, M. W., Brumbaugh, R. D., Airoldi, L., Carranza, A., Coen, L. D., Crawford, C., et al. (2011). Oyster Reefs at Risk and Recommendations for Conservation, Restoration, and Management. *BioScience* 61 (2), 107–116. doi: 10.1525/bio.2011.61.2.5

Behrens, M. and Lafferty, K. (2004). Effects of Marine Reserves and Urchin Disease on Southern Californian Rocky Reef Communities. *Mar. Ecology-Progress Ser. - Mar. ECOL-PROGR Ser.* 279, 129–139. doi: 10.3354/meps279129

Ben-Horin, T., Bidegain, G., Huey, L., Narvaez, D. A. and Bushek, D. (2015). Parasite Transmission Through Suspension Feeding. *J. Invertebr. Pathol.* 131, 155–176. doi: 10.1016/j.jip.2015.07.006

Ben-Horin, T., Burge, C. A., Bushek, D., Groner, M. L., Proestou, D. A., Huey, L. I., et al. (2018). Intensive Oyster Aquaculture Can Reduce Disease Impacts on Sympatric Wild Oysters. *Aquacult. Environ. Interact.* 10, 557–567. doi: 10.3354/aei00290

Bigalke, A., Meyer, N., Alkistis Papanikolopoulou, L., Helen Wiltshire, K. and Pohnert, G. (2019). The Algicidal Bacterium *Kordia Algicida* Shapes a Natural Plankton Community. *Appl. Environ. Microbiol.* 85 (7), e02779–e02718. doi: 10.1128/AEM.02779-18

Bockelmann, A.-C., Tams, V., Ploog, J., Schubert, P. R. and Reusch, T. B. H. (2013). Quantitative PCR Reveals Strong Spatial and Temporal Variation of the Wasting Disease Pathogen, *Labyrinthula Zosterae* in Northern European Eelgrass (*Zostera Marina*) Beds. *PloS One* 8 (5), e62169. doi: 10.1371/journal.pone.0062169

Brauman, K. A., Daily, G. C., Duarte, T. K. and Mooney, H. A. (2007). The Nature and Value of Ecosystem Services: An Overview Highlighting Hydrologic Services. *Annu. Rev. Environ. Resour.* 32 (1), 67–98. doi: 10.1146/annurev.energy.32.031306.102758

Buhmann, A. and Papenbrock, J. (2013). Biofiltering of Aquaculture Effluents by Halophytic Plants: Basic Principles, Current Uses and Future Perspectives. *Environ. Exp. Bot.* 92, 122–133. doi: 10.1016/j.envexpbot.2012.07.005. Sustainable cultivation and exploitation of halophyte crops in a salinizing world.

Burge, C. A., Closek, C. J., Friedman, C. S., Groner, M. L., Jenkins, C. M., Shore-Maggio, A., et al. (2016). The Use of Filter-Feeders to Manage Disease in a Changing World. *Integr. Comp. Biol.* 56 (4), 573–587. doi: 10.1093/icb/icw048

Burge, C. A. and Hershberger, P. K. (2020). "Climate Change Can Drive Marine Diseases," in *Marine Disease Ecology* (Oxford: Oxford University Press). doi: 10.1093/oso/9780198821632.003.0005

Carlson, C. J., Hopkins, S., Bell, K. C., Doña, J., Godfrey, S. S., Kwak, M. L., et al. (2020). A Global Parasite Conservation Plan. *Biol. Conserv.* 250, 108596. doi: 10.1016/j.biocon.2020.108596

Castro, K. M., Stanley Cobb, J., Gomez-Chiarri, M. and Tlusty, M. (2012). Epizootic Shell Disease in American Lobsters *Homarus Americanus* in Southern New England: Past, Present and Future. *Dis. Aquat. Organisms* 100 (2), 149–158. doi: 10.3354/dao02507

Choudhury, S., Sree, A., Mukherjee, S., Pattnaik, P. and Maringanti, B. (2005). *In Vitro* Antibacterial Activity of Extracts of Selected Marine Algae and Mangroves Against Fish Pathogens. *Asian Fish. Sci.* 18 (2005), 285–294. doi: 10.33997/j.afs.2005.18.3.009

Cullen-Unsworth, L. and Unsworth, R. (2013). Seagrass Meadows, Ecosystem Services, and Sustainability. *Environ. Sci. Policy Sustain. Dev.* 55, 14–28. doi: 10.1080/00139157.2013.785864

Davidson, N. (2014). How Much Wetland Has the World Lost? Long-Term and Recent Trends in Global Wetland Area. *Mar. Freshw. Res.* 65, 936–941. doi: 10.1071/MF14173

DellaGreca, M., Fiorentino, A., Isidori, M., Monaco, P. and Zarrelli, A. (2000). Antialgal Ent-*Labdane Diterpene*s From *Ruppia Maritima*. *Phytochemistry* 55 (8), 909–913. doi: 10.1016/S0031-9422(00)00253-3

Deng, Y., Liu, S., Feng, J., Wu, Y. and Mao, C. (2021). What Drives Putative Bacterial Pathogens Removal Within Seagrass Meadows? *Mar. pollut. Bull.* 166, 112229. doi: 10.1016/j.marpolbul.2021.112229

Duffy, J. E., Reynolds, P. L., Boström, C., Coyer, J. A., Cusson, M., Donadi, S., et al. (2015). Biodiversity Mediates Top–down Control in Eelgrass Ecosystems: A Global Comparative-Experimental Approach. *Ecol. Lett.* 18 (7), 696–705. doi: 10.1111/ele.12448

Durai, S. and Radhakrishnan, M. (2016). *Antimicrobial Activity of Mangrove Leaves Against Drug Resistant Pathogens*, : International Journal of PharmaTech Research in India Vol. 9. 141–146.

Evans, S. M., Griffin, K. J., Blick, R. A. J., Poore, A. G. B. and Vergés, A. (2018). Seagrass on the Brink: Decline of Threatened Seagrass *Posidonia Australis* Continues Following Protection. *PLoS One* 13 (4), e0190370. doi: 10.1371/journal.pone.0190370

Fourqurean, J. W. (2002). HEMMINGA, M. A., AND C. M. DUARTE. 2000. Seagrass Ecology. Cambridge University Press. Xi+298 P. US$80. ISBN 0-521-66184-6. *Limnol. Oceanogr.* 47 (2), 611–611. doi: 10.4319/lo.2002.47.2.0611

Goldberg, L., Lagomasino, D., Thomas, N. and Fatoyinbo, T. (2020). Global Declines in Human-Driven Mangrove Loss. *Global Change Biol.* 26 (10), 5844–5855. doi: 10.1111/gcb.15275

Graciaa, D. S., Cope, J. R., Roberts, V. A., Cikesh, B. L., Kahler, A. M., Vigar, M., et al. (2018). Outbreaks Associated With Untreated Recreational Water - United States 2000-2014. *MMWR. Morb. Mortal. Wkly. Rep.* 67 (25), 701–706. doi: 10.15585/mmwr.mm6725a1

Griffin, D. W., Donaldson, K. A., Paul, J. H. and Rose, J. B. (2003). Pathogenic Human Viruses in Coastal Waters. *Clin. Microbiol. Rev.* 16 (1), 129–143. doi: 10.1128/CMR.16.1.129-143.2003

Groner, M. L., Burge, C. A., Cox, R., Rivlin, N. D., Turner, M., Van Alstyne, K. L., et al. (2018). Oysters and Eelgrass: Potential Partners in a High PCO2 Ocean. *Ecology* 99 (8), 1802–1814. doi: 10.1002/ecy.2393

Groner, Ml, Eisenlord, M. E., Yoshioka, R. M., Fiorenza, E. A., Dawkins, P. D., Graham, O. J., et al. (2021). Warming Sea Surface Temperatures Fuel Summer Epidemics of Eelgrass Wasting Disease. *Mar. Ecol. Prog. Ser.* 679, 47–58. doi: 10.3354/meps13902

Groner, M. L., Maynard, J., Breyta, R., Carnegie, R. B., Dobson, A., Friedman, C. S., et al. (2016). Managing Marine Disease Emergencies in an Era of Rapid Change. *Philos. Trans. R. Soc. B: Biol. Sci.* 371 (1689), 20150364. doi: 10.1098/rstb.2015.0364

Halpern, B. S., Walbridge, S., Selkoe, K. A., Kappel, C. V., Micheli, F., D'Agrosa, C., et al. (2008). A Global Map of Human Impact on Marine Ecosystems. *Science* 319, 948–952. doi: 10.1126/science.1149345

Harley, C. D. G., Randall Hughes, A., Hultgren, K. M., Miner, B. G., Sorte, C. J. B., Thornber, C. S., et al. (2006). The Impacts of Climate Change in Coastal Marine Systems. *Ecol. Lett.* 9 (2), 228–241. doi: 10.1111/j.1461-0248.2005.00871.x

Harvell, C. D. and Lamb, J. B. (2020). Disease Outbreaks Can Threaten Marine Biodiversity. *In Mar. Dis. Ecol. Oxford: Oxford Univ. Press*. doi: 10.1093/oso/9780198821632.003.0008

Harvell, C. D., Montecino-Latorre, D., Caldwell, J. M., Burt, J. M., Bosley, K., Keller, A., et al. (2019). Disease Epidemic and a Marine Heat Wave Are Associated With the Continental-Scale Collapse of a Pivotal Predator (*Pycnopodia Helianthoides*). *Sci. Adv,* 5. doi: 10.1126/sciadv.aau7042

Herrera, D., Ellis, A., Fisher, B., Golden, C. D., Johnson, K., Mulligan, M., et al. (2017). Upstream Watershed Condition Predicts Rural Children's Health Across 35 Developing Countries. *Nat. Commun.* 8 (1), 811. doi: 10.1038/s41467-017-00775-2

Hoenig, J. M., Groner, M. L., Smith, M. W., Vogelbein, W. K., Taylor, D. M., Landers, D. F., Jr., et al. (2017). Impact of Disease on the Survival of Three Commercially Fished Species. *Ecol. Appl.* 27 (7), 2116–2127. doi: 10.1002/eap.1595

Jacobs-Palmer, E., Gallego, R., Ramón-Laca, A., Kunselman, E., Cribari, K., Horwith, M., et al. (2020). A Halo of Reduced Dinoflagellate Abundances in and Around Eelgrass Beds. *PeerJ* 8, e8869. doi: 10.7717/peerj.8869

Johnson, P. T. J., Preston, D. L., Hoverman, J. T. and Richgels, K. L. D. (2013). Biodiversity Decreases Disease Through Predictable Changes in Host Community Competence. *Nature* 494 (7436), 230–233. doi: 10.1038/nature11883

Keesing, F. and Ostfeld, R. S. (2021). Impacts of Biodiversity and Biodiversity Loss on Zoonotic Diseases. *Proc. Natl. Acad. Sci.* 118 (17). doi: 10.1073/pnas.2023540118

Kim, K., Kim, H., Hong Lim, J. and Joon Lee, S. (2016). Development of a Desalination Membrane Bioinspired by Mangrove Roots for Spontaneous Filtration of Sodium Ions. *ACS Nano* 10 (12), 11428–11433. doi: 10.1021/acsnano.6b07001

Kirk, M., Esler, D. and Sean Boyd, W. (2007). Morphology and Density of Mussels on Natural and Aquaculture Structure Habitats: Implications for Sea Duck Predators. *Mar. Ecol. Prog. Ser.* 346, 179–187. doi: 10.3354/meps07046

Kuehn, W. and Mueller, U. (2000). Riverbank Filtration: An Overview. *J. AWWA* 92 (12), 60–69. doi: 10.1002/j.1551-8833.2000.tb09071.x

Lafferty, K. D., Allesina, S., Arim, M., Briggs, C. J., De Leo, G., Dobson, A. P., et al. (2008). Parasites in Food Webs: The Ultimate Missing Links. *Ecol. Lett.* 11 (6), 533–546. doi: 10.1111/j.1461-0248.2008.01174.x

Lafferty, K. D., Harvell, C. D., Conrad, J. M., Friedman, C. S., Kent, M. L., Kuris, A. M., et al. (2015). Infectious Diseases Affect Marine Fisheries and Aquaculture Economics. *Annu. Rev. Mar. Sci.* 7, 471–496. doi: 10.1146/annurev-marine-010814-015646

Lamb, R. W., Smith, F., Aued, A. W., Salinas-de-León, P., Suarez, J., Gomez-Chiarri, M., et al. (2018). El Niño Drives a Widespread Ulcerative Skin Disease Outbreak in Galapagos Marine Fishes. *Sci. Rep.* 8 (1), 16602. doi: 10.1038/s41598-018-34929-z

Lamb, J., Van de Water, J., Bourne, D., Altier, C., Hein, M., Fiorenza, E., et al. (2017). Seagrass Ecosystems Reduce Exposure to Bacterial Pathogens of Humans, Fishes, and Invertebrates. *Science* 355, 731. doi: 10.1126/science.aal1956

Lin, B. and Dushoff, J. (2004). Mangrove Filtration of Anthropogenic Nutrients in the Rio Coco Solo, Panama. *Manage. Environ. Quality: Int. J.* 15, 131–142. doi: 10.1108/14777830410523071

Littman, R. A., Fiorenza, E. A., Wenger, A. S., Berry, K. L. E., van de Water, J. A. J. M., Nguyen, L., et al. (2020). Coastal Urbanization Influences Human Pathogens and Microdebris Contamination in Seafood. *Sci. Total Environ.* 736, 139081. doi: 10.1016/j.scitotenv.2020.139081

Lukasik, J., Scott, T. M., Andryshak, D. and Farrah, S. R. (2000). Influence of Salts on Virus Adsorption to Microporous Filters. *Appl. Environ. Microbiol.* 66 (7), 2914–2920. doi: 10.1128/AEM.66.7.2914-2920.2000

Miller, M. A., Miller, W. A., Conrad, P. A., James, E. R., Melli, A. C., Leutenegger, C. M., et al. (2008). Type X *Toxoplasma Gondii* in a Wild Mussel and Terrestrial Carnivores From Coastal California: New Linkages Between Terrestrial Mammals, Runoff and Toxoplasmosis of Sea Otters. *Int. J. Parasitol.* 38 (11), 1319–1328. doi: 10.1016/j.ijpara.2008.02.005

Onufryk, J., Ebersole, J., Defilippo, J. and Beck, G. (2018). *Diadema Antillarum* on St. Croix, USVI: Current Status and Interactions With Herbivorous Fishes. *Yale J. Biol. Med.* 91, 1. PMID: 30588206 PMCID: PMC6302631

Palacios, O. A., Raúl Adame-Gallegos, J., Estela Rivera-Chavira, B. and Nevarez-Moorillon, G. V. (2021). Antibiotics, Multidrug-Resistant Bacteria, and Antibiotic Resistance Genes: Indicators of Contamination in Mangroves? *Antibiotics* 10 (9):1103. doi: 10.3390/antibiotics10091103

Qi, S.-H., Zhang, S., Qian, P.-Y. and Wang, B.-G. (2008). Antifeedant, Antibacterial, and Antilarval Compounds From the South China Sea Seagrass *Enhalus Acoroides* 51, 5, 441–447. doi: 10.1515/BOT.2008.054

Rahman, M. M., Zimmer, M., Ahmed, I., Donato, D., Kanzaki, M. and Xu, M. (2021). Co-Benefits of Protecting Mangroves for Biodiversity Conservation and Carbon Storage. *Nat. Commun.* 12 (1), 3875. doi: 10.1038/s41467-021-24207-4

Raimondi, P. T., Miner, C., Ambrose, R., Engle, J. M. and Minchinton, T. E. (2002). Continued Declines of Black Abalone Along the Coast of California: Are Mass Mortalities Related to El Niño Events? *Mar. Ecology-Progress Ser. - Mar. ECOL-PROGR Ser.* 242, 143–152. doi: 10.3354/meps242143

Rasmussen, E. (1977). *Seagrass Ecosystems: A Scientific Perspective* (New York: Marcel Dekker, Inc).

Redder, A., Dürr, M., Daeschlein, G., Baeder-Bederski, O., Koch, C., Müller, R., et al. (2010). Constructed Wetlands–Are They Safe in Reducing Protozoan Parasites? *Int. J. Hyg. Environ. Health* 213 (1), 72–77. doi: 10.1016/j.ijheh.2009.12.001

Saad, S., Muhammad, T., Susanti, D., Qaralleh, H. and Afifah Binti Abdul Rahim, N. (2011). Antimicrobial Activity of Mangrove Plant (*Lumnitzera Littorea*). *Asian Pacific J. Trop. Med.* 4 (7), 523–525. doi: 10.1016/S1995-7645(11)60138-7

Sahoo, G., Mulla, N. S. S., Ansari, Z. A. and Mohandass, C. (2012). Antibacterial Activity of Mangrove Leaf Extracts Against Human Pathogens. *Indian J. Pharm. Sci.* 74 (4), 348–351. doi: 10.4103/0250-474X.107068

Selakovic, S., de Ruiter, P. C. and Heesterbeek, H. (2014). Infectious Disease Agents Mediate Interaction in Food Webs and Ecosystems. *Proc. R. Soc. B: Biol. Sci.* 281 (1777), 20132709. doi: 10.1098/rspb.2013.2709

Sippo, J. Z., Maher, D. T., Tait, D. R., Holloway, C. and Santos, I. R. (2016). Are Mangroves Drivers or Buffers of Coastal Acidification? Insights From Alkalinity and Dissolved Inorganic Carbon Export Estimates Across a Latitudinal Transect. *Global Biogeochem. Cycles* 30 (5), 753–766. doi: 10.1002/2015GB005324

Smith, J. R., Fong, P. and Ambrose, R. F. (2006). Dramatic Declines in Mussel Bed Community Diversity: Response to Climate Change? *Ecology* 87 (5), 1153–1161. doi: 10.1890/0012-9658(2006)87[1153:DDIMBC]2.0.CO;2

Sorte, C. J. B., Davidson, V. E., Franklin, M. C., Benes, K. M., Doellman, M. M., Etter, R. J., et al. (2017). Long-Term Declines in an Intertidal Foundation Species Parallel Shifts in Community Composition. *Global Change Biol.* 23 (1), 341–352. doi: 10.1111/gcb.13425

Spalding, M. D. and Maricé, L. (2021). *The State of the World's Mangroves 2021* (Global Mangrove Alliance).

Sullivan, B. K., Trevathan-Tackett, S. M., Neuhauser, S. and Govers, L. L. (2018). Review: Host-Pathogen Dynamics of Seagrass Diseases Under

Future Global Change. *Mar. pollut. Bulletin Securing Future Seagrass* 134, 75–88. doi: 10.1016/j.marpolbul.2017.09.030

Sutton-Grier, A. E. and Sandifer, P. A. (2019). Conservation of Wetlands and Other Coastal Ecosystems: A Commentary on Their Value to Protect Biodiversity, Reduce Disaster Impacts, and Promote Human Health and Well-Being. *Wetlands* 39 (6), 1295–1302. doi: 10.1007/s13157-018-1039-0

Thatoi, H., Behera, B. C. and Mishra, R. R. (2013). Ecological Role and Biotechnological Potential of Mangrove Fungi: A Review. *Mycology* 4 (1), 54–71. doi: 10.1080/21501203.2013.785448

Thompson, R. M., Mouritsen, K. N. and Poulin, R. (2005). Importance of Parasites and Their Life Cycle Characteristics in Determining the Structure of a Large Marine Food Web. *J. Anim. Ecol.* 74 (1), 77–85. doi: 10.1111/j.1365-2656.2004.00899.x

Tracy, A. M., Pielmeier, M. L., Yoshioka, R. M., Heron, S. F. and Harvell, C. D. (2019). Increases and Decreases in Marine Disease Reports in an Era of Global Change. *Proc. R. Soc. B: Biol. Sci.* 286 (1912), 20191718. doi: 10.1098/rspb.2019.1718

Voudanta, E., Ar Kormas, K., Monchy, S., Delegrange, A., Vincent, D., Genitsaris, S., et al. (2016). Mussel Biofiltration Effects on Attached Bacteria and Unicellular Eukaryotes in Fish-Rearing Seawater. *PeerJ* 4, e1829. doi: 10.7717/peerj.1829

Waycott, M., Duarte, C. M., Carruthers, T. J. B., Orth, R. J., Dennison, W. C., Olyarnik, S., et al. (2009). Accelerating Loss of Seagrasses Across the Globe Threatens Coastal Ecosystems. *Proc. Natl. Acad. Sci.* 106 (30), 12377–12381. doi: 10.1073/pnas.0905620106

Wijsman, J. W. M., Troost, K., Fang, J. and Roncarati, A. (2019). "Global Production of Marine Bivalves. Trends and Challenges," in *Goods and Services of Marine Bivalves*. Eds. Smaal, A. C., Ferreira, J. G., Grant, J., Petersen, J. K. and Strand, Ø (Cham: Springer International Publishing), 7–26. doi: 10.1007/978-3-319-96776-9_2

Wu, S., Carvalho, P. N., Müller, J. A., Remony Manoj, V. and Dong, R. (2016). Sanitation in Constructed Wetlands: A Review on the Removal of Human Pathogens and Fecal Indicators. *Sci. Total Environ.* 541, 8–22. doi: 10.1016/j.scitotenv.2015.09.047

Wu, Y., Chung, A., Tam, N. F. Y., Pi, N. and Wong, M. H. (2008). Constructed Mangrove Wetland as Secondary Treatment System for Municipal Wastewater. *Ecol. Eng.* 34 (2), 137–146. doi: 10.1016/j.ecoleng.2008.07.010

Zannella, C., Mosca, F., Mariani, F., Franci, G., Folliero, V., Galdiero, M., et al. (2017). Microbial Diseases of Bivalve Mollusks: Infections, Immunology and Antimicrobial Defense. *Mar. Drugs* 15 (6), 182. doi: 10.3390/md15060182

Conflict of Interest: The authors declare that the research was conducted in the absence of any commercial or financial relationships that could be construed as a potential conflict of interest.

frontiers | Frontiers in Microbiology

TYPE Original Research
PUBLISHED 22 July 2022
DOI 10.3389/fmicb.2022.957397

OPEN ACCESS

EDITED BY
Ming Ma,
Peking University, China

REVIEWED BY
Peng Zhang,
Tobacco Research Institute, Chinese Academy of Agricultural Sciences (CAAS), China
Zong-Jun Du,
Shandong University, China

*CORRESPONDENCE
Weiyan Zhang
zhangweiyan13@126.com

SPECIALTY SECTION
This article was submitted to Aquatic Microbiology, a section of the journal Frontiers in Microbiology

RECEIVED 31 May 2022
ACCEPTED 27 June 2022
PUBLISHED 22 July 2022

CITATION
Ding H, Liu J, Yang C, Guo C, Ding L, Jung D and Zhang W (2022) *Hanstruepera marina* sp. nov. and *Hanstruepera flava* sp. nov., two novel species in the family *Flavobacteriaceae* isolated by a modified *in situ* cultivation technique from marine sediment. *Front. Microbiol.* 13:957397. doi: 10.3389/fmicb.2022.957397

Hanstruepera marina sp. nov. and *Hanstruepera flava* sp. nov., two novel species in the family *Flavobacteriaceae* isolated by a modified *in situ* cultivation technique from marine sediment

Hong Ding, Jiahui Liu, Chen Yang, Chaobo Guo, Lijian Ding, Dawoon Jung and Weiyan Zhang*

Li Dak Sum Yip Yio Chin Kenneth Li Marine Biopharmaceutical Research Center, College of Food and Pharmaceutical Sciences, Ningbo University, Ningbo, China

A modified *in situ* cultivation technique was developed and applied to resource mining of uncultured microbes from marine sediments of Meishan Island in the East China Sea. Two novel strains NBU2968^T and NBU2984^T were isolated by this method but not standard Petri dish, which indicated the modified technique was more effective compared to conventional approaches for isolating uncultured microbes and could be popularized and applied to other aquatic environments. The two novel strains were identified by the polyphasic taxonomic approach. Cells of both strains were observed to be Gram-staining-negative, rod-shaped, nonmotile, aerobic, and yellow-pigmented. Catalase and oxidase activities and hydrolysis of Tweens 40, 60, and 80 of two novel strains were positive. Methyl red reaction, H_2S production, and hydrolysis of Tween 20 were negative. According to 16S rRNA gene sequence analysis, two novel strains shared the highest similarities (96.4–97.7%) to the species with a validated name in the genus *Hanstruepera*, while shared lower sequence similarities (<95.6%) to all other genera. Phylogenetic analysis revealed that strains NBU2968^T and NBU2984^T were affiliated with the genus *Hanstruepera*. ANI and dDDH values between the two novel strains and *Hanstruepera* species were 77.4–78.3% and 20.4–20.9%, respectively, which were below the thresholds for species delineation. The 16S rRNA gene sequence similarity, ANI, and dDDH values between the two novel strains were 99.3, 88.9, and 36.3%, respectively, indicating that the two strains represent different species. The genomes of NBU2968^T and NBU2984^T were 3.28 Mbp with a G+C content of 34.2% and 3.09 Mbp with a G+C content of 34.4%, respectively. The only respiratory quinone was menaquinone-6 (MK-6). The major cellular fatty acids were iso-$C_{15:0}$, iso-$C_{15:1}$G, and iso-$C_{17:0}$ 3-OH. The major polar lipids of the two strains were phosphatidylethanolamine, unidentified amino lipids, and unidentified lipids. Based on the above polyphasic characteristics, strains NBU2968^T and

NBU2984^T represent two novel species within the genus *Hanstruepera*, for which the names *Hanstruepera marina* sp. nov. and *Hanstruepera flava* sp. nov. are proposed. The type strains are NBU2968^T (= MCCC 1K06392^T = KCTC 82913^T) and NBU2984^T (= MCCC 1K07472^T= KCTC 92511^T), respectively.

KEYWORDS

in situ cultivation, modified ichip, *Hanstruepera*, polyphasic taxonomy, marine sediment

Introduction

The overwhelming majority of microbial species do not grow on synthetic media and remain unexplored (Zengler et al., 2002; Epstein, 2013; Jung et al., 2021a), which are known as "uncultivable" microorganisms. In recent years, novel cultivation methods have been advanced to access previously uncultivated microbes. A high-throughput *in situ* cultivation technique of ichip (isolation chip) was developed by Nichols et al. (2010), with highly efficient in terms of both microbial recovery and the novelty of isolated species. *In situ* cultivation techniques could better simulate natural conditions, and provide access to nutrients from the natural environment and critical growth factors supplied by neighboring species. Dormant microbes are able to stochastically wake into activity *in situ* if they detect suitable environmental factors or quorum sensing. Once the dormant cells become recovery, they tend to grow on artificial media (Buerger et al., 2012; Mu et al., 2018; Jung et al., 2021b). However, the original ichip device needs to use a gelling agent like agar to prepare a solid medium, it has two limitations: (1) the gelling agent like agar may inhibit the growth of part microbes or select to isolate some species; (2) the gelling agent act as a sieve, which can reduce the diffusion of nutrients and molecules. To overcome these shortcomings, we propose a modified *in situ* technique to combine the ichip and liquid dilution to extinction cultivation (Rappé et al., 2002; Yang et al., 2016; Oueriaghli et al., 2018) to isolate uncultured microorganisms. In this study, a modified ichip device was designed and applied to isolate uncultured microorganisms from marine sediments of Meishan Island in the East China Sea. Two novel strains NBU2968^T and NBU2984^T were isolated and studied, which belonged to the genus *Hanstruepera*.

The genus *Hanstruepera*, as a member of the family *Flavobacteriaceae*, was first reported by Hameed et al. (2015), to accommodate strictly aerobic, rod-shaped, nonmotile, and zeaxanthin-producing bacteria. It contained menaquinone-6 (MK-6) as the sole respiratory quinone and iso-$C_{15:0}$, iso-$C_{15:1}$ G, and iso-$C_{17:0}$ 3-OH as predominant cellular fatty acids. At the time of writing, the genus *Hanstruepera* has only two recognized species (https://www.bacterio.net/genus/Hanstruepera:) *Hanstruepera neustonica* (type species), isolated from a surface water sample collected from an estuary (Hameed et al., 2015) and *Hanstruepera crassostreae*, isolated from an oyster sample collected from the coast (He et al., 2018). "*Hanstruepera ponticola*" renamed by Huang et al. (Huang et al., 2022), transferred from *Pseudobizionia ponticola* (Park et al., 2018) and isolated from seawater, was a heterotypic synonym of *Hanstruepera crassostreae* (Pei et al., 2021; Huang et al., 2022). In this article, we describe two novel strains NBU2968^T and NBU2984^T following the polyphasic taxonomic approach and propose that they represent two novel species of the genus *Hanstruepera*.

Materials and methods

Design of the modified ichip device

The modified ichip device shares a similar concept and principle with the original one (Nichols et al., 2010; Berdy et al., 2017), which uses the dilution of bacteria of up to one to ten cells per well in microplates, but its incubation is performed in liquid media. The liquid medium potentially provides easier conditions for bacteria to adapt and promotes greater reproduction and growth compared to the solid medium containing the same nutrients. The modified ichip device consists of a central plate for cultivating bacterial cells, polycarbonate membranes with a 0.03 μm pore size on both the top and bottom of the plate, and side panels holding all other parts (Figure 1). Polytetrafluoroethylene (PTFE) is selected to be used as the material for the central plate, which is commercially produced,

Abbreviations: MA, marine agar 2216; MB, marine broth 2216; MCCC, Marine Culture Collection of China; KCTC, Korean Collection for Type Cultures; JCM, Japan Collection of Microorganisms; HPLC, high-performance liquid chromatography; MIDI, Microbial Identification System; TLC, thin layer chromatography; PE, phosphatidylethanolamine; AL, unidentified aminolipid; L, unidentified lipid; NCBI, National Center for Biotechnology Information; MEGA, Molecular Evolutionary Genetics Analysis; NJ, neighbor-joining; ML, maximum-likelihood; MP, maximum parsimony; RAST, Rapid Annotation using Subsystem Technology; KEGG, Kyoto Encyclopedia of Genes and Genomes; ANI, average nucleotide identity; dDDH, digital DNA-DNA hybridization.

cheap and autoclavable. A total of 384 holes (in the original ichip device) are changed to 96 holes in the central plate, which correspond to wells of standard 96-well plates. The volume of holes increases from 1.25 to 50 μl, which prevents the medium inside the holes from drying out. Silicon glue is used to glue the polycarbonate membranes to each side of the central plate. It helps to ensure good sealing of the device and avoid microbial contamination from the outside or between holes. To protect polycarbonate membranes, nylon mesh and stainless steel mesh are, respectively, added on both sides of the plate, which are fixed with splints and screws. The assembled modified ichip device can be cultivated *in situ* environment (This method requires a substantial amount of moisture in the environment to prevent the liquid culture inside the ichip from drying out. Aquatic habitats are appropriate environments for the modified ichip application, but arid and semiarid systems are not.).

Application of modified ichip device for isolation

Sediment samples were collected from the Meishan Island located in the East China Sea, Ningbo, China (121°56'E, 29°46'N) in December 2020. About 3.0 g sediment sample was vortexed and serially diluted to 1–10 cells/50 μl with 1/10 marine broth 2216 (MB). One polycarbonate membrane was glued to one side of the central plate, creating a 96-well plate with a membranous bottom. The cell suspension was aliquoted into the holes of modified ichip, and then the second membrane was glued to the top exposed part of the device. Leaving some compartments unoccupied and filled with sterile 1/10 MB as a control to detect the quality of the seal. Nylon mesh and stainless steel mesh helped to complete the assembly of the device. The assembled modified ichips were returned to the original sample environment for *in situ* cultivation, which helped the recovery and domestication of dormant microbes. After incubation of 4 weeks, the devices were retrieved to the lab. The modified ichips were washed with sterilized water to remove the microorganisms on the outer surfaces of the device. Sterile toothpicks were used to tear one side membrane, and the culture in the holes was transferred to 1/10 marine agar 2216 (MA). Colonies growing on 1/10 MA were picked and purified, and two novel isolates NBU2968^T and NBU2984^T were obtained. Standard Petri dish cultivation was used as control (about 3.0 g sediment sample was serially diluted to 10^{-6} with 1/10 MB, and 200 μl of each diluted sample was spread onto 1/10 MA plates), but these two novel strains were not isolated by this traditional method. These two strains were selected to be identified by the polyphasic taxonomic approach. *Hanstruepera crassostreae* MCCC 1H00246^T and *Hanstruepera neustonica* JCM 19743^T were selected as experimental control strains, which were obtained from the Marine Culture Collection of China (MCCC) and Japan Collection of Microorganisms (JCM), respectively. Both related type strains were cultured under the identical experimental conditions as strains NBU2968^T and NBU2984^T for comparative analysis.

Phenotypic properties

Cell morphology was observed by using an optical microscope (BX40; Olympus) and transmission electron microscopy (JEM-1230; JEOL). Exponentially growing cells incubated on MA plates were suspended and stained with uranyl acetate and then fixed on the copper mesh before being observed with transmission electron microscopy. Gram staining was performed according to Dong and Cai (Dong and Cai, 2001). Motility was examined by microscopic observation and inoculation on semisolid MB medium with 0.5% agar (w/v). The presence of flexirubin-type pigments was investigated as described previously (Bernardet et al., 2002). To determine the growth conditions of strains NBU2968^T and NBU2984^T, the temperature range for growth was determined in MB at 4, 10, 15, 20, 25, 28, 30, 35, 37, 40, 45, 50, and 55°C. The pH range for growth was determined at pH 4.0–10.0 (at intervals of 0.5) in MB supplemented with the following buffers: ammonium acetate (pH 4.0–5.0), MES (pH 5.5–6.0), PIPES (pH 6.5–7.0), Tricine (pH 7.5–8.5), and CAPSO (pH 9.0–10.0) at a concentration of 30 mM. The tolerance to NaCl was determined after cultivation at 32°C, pH 7.0 in modified MB medium with original Na^+ and Cl^- removed (final NaCl concentration 0–10.0%, using increments of 1.0%, w/v). All tests of growth conditions were performed in quadruplicate and OD_{600} measurements were taken after 24-h incubation at 32°C with shaking at 140 rpm.

The following biochemical and physiological tests were carried out on strains NBU2968^T, NBU2984^T, *H. crassostreae* MCCC 1H00246^T, and *H. neustonica* JCM 19743^T in MB, unless otherwise indicated. Catalase activity was detected *via* bubble production in a 3% (v/v) H_2O_2 solution. Oxidase activity was assessed by oxidation of 1% *p*-aminodimethylaniline oxalate. Indole production, methyl red, Voges–Proskauer test, H_2S production, hydrolysis of starch, casein, and Tweens 20, 40, 60, and 80 were tested as described by Zhu et al. (2011). Other enzyme activities, physiological and biochemical properties, and acid production tests were determined by using API ZYM, API 20NE, and API 50CH strips (bioMérieux) according to the manufacturer's instructions. For the API 50CH test, we used modified MB in which yeast extract and peptone were replaced by 0.02 g/l yeast extract and 0.01 g/l phenol red. Anaerobic growth was determined with an AnaeroPack-MicroAero (2.5 l; MGC, Japan) anaerobic system by using sodium thiosulfate (20 mM), sodium sulfite (5 mM), sodium sulfate (20 mM), sodium nitrite (5 mM), or sodium nitrate (20 mM) as electron acceptors, respectively. Same media under aerobic condition were used as control. Susceptibility

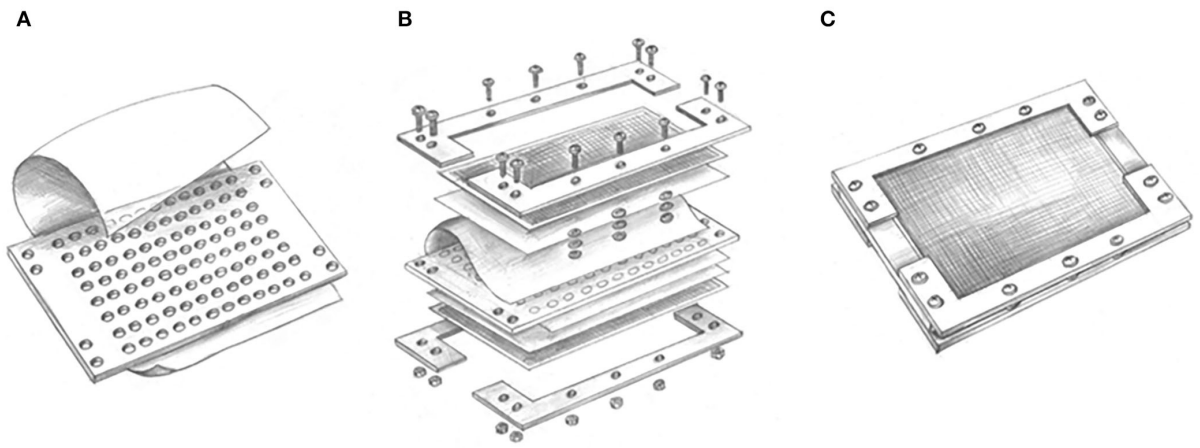

FIGURE 1
Conceptual design of modified ichip device: **(A)** A central plate including 96 through holes has added a suspension containing microbial cells in each hole and glued with the polycarbonate membranes by silicon glue; **(B)** nylon mesh and stainless steel mesh are, respectively, added on both sides of the plate, which are fixed with splints and screws; and **(C)** the assembled modified ichip device can be cultivated *in situ* environment.

to antibiotics was investigated on MA using the disc diffusion method and considered susceptible when the diameter of the inhibition zone was over 1.2 cm (Sheu et al., 2020). The tested antibiotics were (μg per disc, unless indicated): amikacin (30), amoxicillin (20), ampicillin (10), bacitracin (0.04 IU), carbenicillin (100), cefamezin (30), cefoxitin (30), cefradine (30), cephalexin (30), chloramphenicol (30), ciprofloxacin (5), clindamycin (2), doxycycline (30), erythromycin (15), gentamicin (10), kanamycin (30), lincomycin (2), minocycline (30), nalidixic acid (30), neomycin (30), norfloxacin (10), novobiocin (30), nystatin (100), ofloxacin (5), oxacillin (1), penicillin G (10 IU), polymyxin B (300 IU), rifampicin (5), streptomycin (10), tetracycline (30), and vancomycin (30).

Chemotaxonomic characteristic

Biomass for chemotaxonomic and molecular studies was obtained by cultivation in MB at 32°C for 24 h, with shaking at 140 rpm. All the following tests for chemotaxonomic characterization were performed on strains NBU2968^T, NBU2984^T, *H. crassostreae* MCCC 1H00246^T, and *H. neustonica* JCM 19743^T unless otherwise indicated. For fatty acid methyl esters (FAMEs) analysis, late exponential-phase cells were harvested from MB. The identification and quantification of FAMEs were performed using the Sherlock Microbial Identification System (MIDI) with the standard MIS Library Generation Software version 6.1 according to the manufacturer's instructions. Respiratory quinones were extracted and analyzed by using reversed-phase HPLC as described by Minnikin et al. (1984). Total lipids were extracted as described by Kates (1986) and detected by two-dimensional TLC silica-gel 60 F_{254} aluminum-backed thin-layer plates (10 × 10 cm, Merck 5554), and further analyzed as described by Minnikin et al. (1984). The TLC plates were sprayed with phosphomolybdic acid with 5% ethanol to reveal total lipids and ninhydrin to reveal amino lipids (Zhang et al., 2015).

Phylogeny analysis based on 16S rRNA gene sequences

The 16S rRNA gene was amplified by PCR using universal bacterial primers 27F (5'-AGAGTTTGATCCTGGCTCAG-3') and 1492R (5'-GGTTACCTTGTTACGACTT-3') (Sun et al., 2017). Purified PCR products were cloned into the vector pMD19-T (TaKaRa). The recombinant plasmid was transformed into *Escherichia coli* DH5α and then commercially sequenced. The almost-complete 16S rRNA gene sequences (1,487 nt) were compared with those of closely related species by EzBioCloud's Identify Service (http://www.ezbiocloud.net/identify) (Yoon et al., 2017a) and BLAST (https://blast.ncbi.nlm.nih.gov/Blast.cgi). Multiple sequence alignments and phylogenetic tree reconstructions were performed by using MEGA version 7.0 (Kumar et al., 2016). Phylogenetic trees were reconstructed by using three different methods: neighbor-joining (Saitou and Nei, 1987), maximum-likelihood (Felsenstein, 1981), and maximum-parsimony methods (Fitch, 1971). Evolutionary distances were calculated using the Kimura 2-parameter model (Kimura, 1980) for the neighbor-joining method. The topology of the phylogenetic trees was evaluated by using the bootstrap values based on 1,000 resamplings. *Crocinitomix catalasitica* NBRC 15977^T was selected as an outgroup.

TABLE 1 Differential characteristics of strain NBU2968^T, strain NBU2984^T, and related type strains of the genus *Hanstruepera*.

Characteristic	1	2	3	4
Habitat	Marine sediment	Marine sediment	Marine oyster[a]	Estuarine water[b]
Cell size (μm)	0.50–0.8 × 0.8–3.0	0.4–0.6 × 1.0–2.4	0.2–0.4 × 1.0–2.5[a]	0.4–0.5 × 1.0–2.0[b]
Pigmentation	Yellow	Yellow	Orange[a]	Yellowish-orange[b]
Temperature range (optimum, °C)	10–40 (37)	15–37 (32)	4–40 (33)[a]	20–40 (30)[b]
pH range (optimum)	5.5–8.0 (7.0)	6.0–8.5 (7.0)	6.5–8.0 (7.5)[a]	6.0–8.0 (7.0)[b]
NaCl range (optimum) (%, w/v)	0–6.0 (2.0)	0–10.0 (2.0)	1.0–7.0 (3.0)[a]	2.0–4.0 (3.0)[b]
Voges-Proskauer	+	-	-	-
Hydrolysis of:				
Casein	-	+	+	+
Tween 20	-	-	+	+
Tween 80	+	+	-	-
API 20NE test results:				
Fermentation of D-glucose	+	+	+	-
Nitrate reduction, aesculin hydrolysis	-	+	-	-
API ZYM test results:				
Trypsin, α-chymotrypsin	-	+	+	+
N-acetyl-β-D-glucosaminidase, β-glucosidase	-	+	-	-
Lipase (C14)	+	-	-	-
Cystine arylamidase	+	+	-	+
API 50CH test results:				
D-Glucose	+	+	+	-
α-Methyl-D-mannopyranoside, α-methyl-D-glucopyranoside, amygdaline	+	-	+	-
L-Arabinose, arbutin, D-galactose, gentiobiose, β-methyl-D-xylopyranoside, salicine, sucrose	+	-	+	+
Aesculin, 5-ketogluconate	-	+	-	-
Inositol, D-tagatose	-	-	+	+
Cellobiose, D-xylose	+	-	-	+
Susceptibility to				
Tetracycline	S	R	R	S
Novobiocin	R	R	S	S
Ciprofloxacin, streptomycin	S	S	R	S

Taxa: 1, strain NBU2968^T; 2, strain NBU2984^T; 3, *H. crassostreae* MCCC 1H00246^T; 4. *H. neustonica* JCM 19743^T. All data were taken from this study unless otherwise indicated. Data marked with [a] and [b] were taken from He et al. (2018) and Hameed et al. (2015), respectively. -, negative; +, positive; R, resistant; S, susceptible. The same characteristics shared by these four strains were listed in Supplementary Table 1.

Genome sequencing and gene annotation

The whole genomes of strains NBU2968^{T}and NBU2984^T were sequenced using an Illumina HiSeq 4000 system (Illumina) at the Beijing Genomics Institute (Shenzhen, China). The paired-end fragment libraries were sequenced according to the Illumina HiSeq 4000 system's protocol. Raw reads of low quality from paired-end sequencing (those with consecutive bases covered by fewer than five reads) were discarded. The sequenced reads were assembled using SOAPdenovo v1.05 software (Li et al., 2008). The open reading frames (ORFs) and the functional annotation of translated ORFs were predicted by using the RAST server online (Overbeek et al., 2014). The RNA genes were identified through tRNAscan-SE 2.0 (http://lowelab.ucsc.edu/tRNAscan-SE/, Lowe and Chan, 2016) and RNAmmer 1.2 server (http://www.cbs.dtu.dk/services/RNAmmer/, Lagesen et al., 2007). Metabolic pathways were analyzed by using the KEGG's BlastKOALA service (Kanehisa et al., 2016). Genome data publicly available of related *Hanstruepera* species were retrieved from the NCBI Genome database. The average nucleotide identity (ANI) values between strains NBU2968^T, NBU2984^T, and related species were calculated using the ANI calculator online service (Yoon et al., 2017b). Digital DNA-DNA hybridization (dDDH) values were calculated by the genome-to-genome distance calculator (GGDC) server version 2.1 (Meier-Kolthoff et al., 2013). Phylogenomic analysis was performed online by Type (strain) Genome Server (TYGS) (Meier-Kolthoff and Goeker, 2019).

Results and discussion

Phenotypic properties

Cells of strains NBU2968^T and NBU2984^T were Gram-negative, rod-shaped, and nonsporulating with no flagellum (Supplementary Figure 1). Colonies of two strains on MA incubated for 24 h were 1.0 mm in diameter, opaque, yellow-pigmented, and convex with a smooth surface. Flexirubin-type pigments are produced by two strains. Strain NBU2968^T grew at 0–6.0% (w/v) NaCl (optimum 2.0%, w/v), 10–40°C (optimum 37°C), and pH 5.5–8.0 (optimum pH 7.0), while strain NBU2984^T grew at NaCl 0–8.0% (w/v) (optimum, 2.0%), 15–37°C (optimum, 32°C), and pH 6.0–8.5 (optimum, pH 7.0) (Table 1). No growth occurred under the anaerobic condition on MA with the addition of different electron acceptors even after

TABLE 2 Cellular fatty acids for strains NBU2968^T, NBU2984^T, and related type strains of the genus *Hanstruepera*.

Fatty acid	1	2	3	4
Saturated				
$C_{10:0}$	tr	-	2.4	-
$C_{16:0}$	2.0	2.0	3.6	2.9
Unsaturated				
$C_{14:1}$ *ω5c*	tr	tr	1.3	tr
$C_{15:1}$ *ω8c*	-	-	2.0	-
Branched				
iso-$C_{14:0}$	1.0	1.1	1.3	tr
iso-$C_{15:0}$	**23.8**	**14.2**	**28.6**	**30.0**
iso-$C_{15:1}$ G	**27.1**	**25.0**	**25.4**	**28.4**
anteiso-$C_{15:0}$	2.0	1.9	-	tr
anteiso-$C_{15:1}$ A	1.0	1.3	-	-
iso-$C_{16:0}$	1.1	tr	-	tr
iso-$C_{16:1}$ G	2.1	1.2	-	tr
Hydroxy				
$C_{15:0}$ 2-OH	tr	2.3	-	tr
iso-$C_{15:0}$ 3-OH	5.0	6.0	5.7	4.8
iso-$C_{16:0}$ 3-OH	1.5	2.0	-	tr
iso-$C_{17:0}$ 3-OH	**20.2**	**17.5**	**20.2**	**19.3**
Summed feature 3*	9.4	**19.7**	6.7	6.3
Summed feature 9*	-	-	2.9	-

Taxa: 1, strain NBU2968^T; 2, strain NBU2984^T; 3, *H. crassostreae* MCCC 1H00246^T; 4, *H. neustonica* JCM19743^T. All data were taken from this study. Values are percentages of the total fatty acid content. Fatty acids that represented <1% in all columns were omitted. Abbreviations: tr, trace component (<1%); -, not detected. Fatty acids present at >10% are indicated in bold.

*Summed feature 3 contained $C_{16:1}$ *ω7c* and/or $C_{16:1}$ *ω6c*; Summed feature 9 contained iso-$C_{17:1}$ *ω9c*.and/or $C_{16:0}$ 10-methyl.

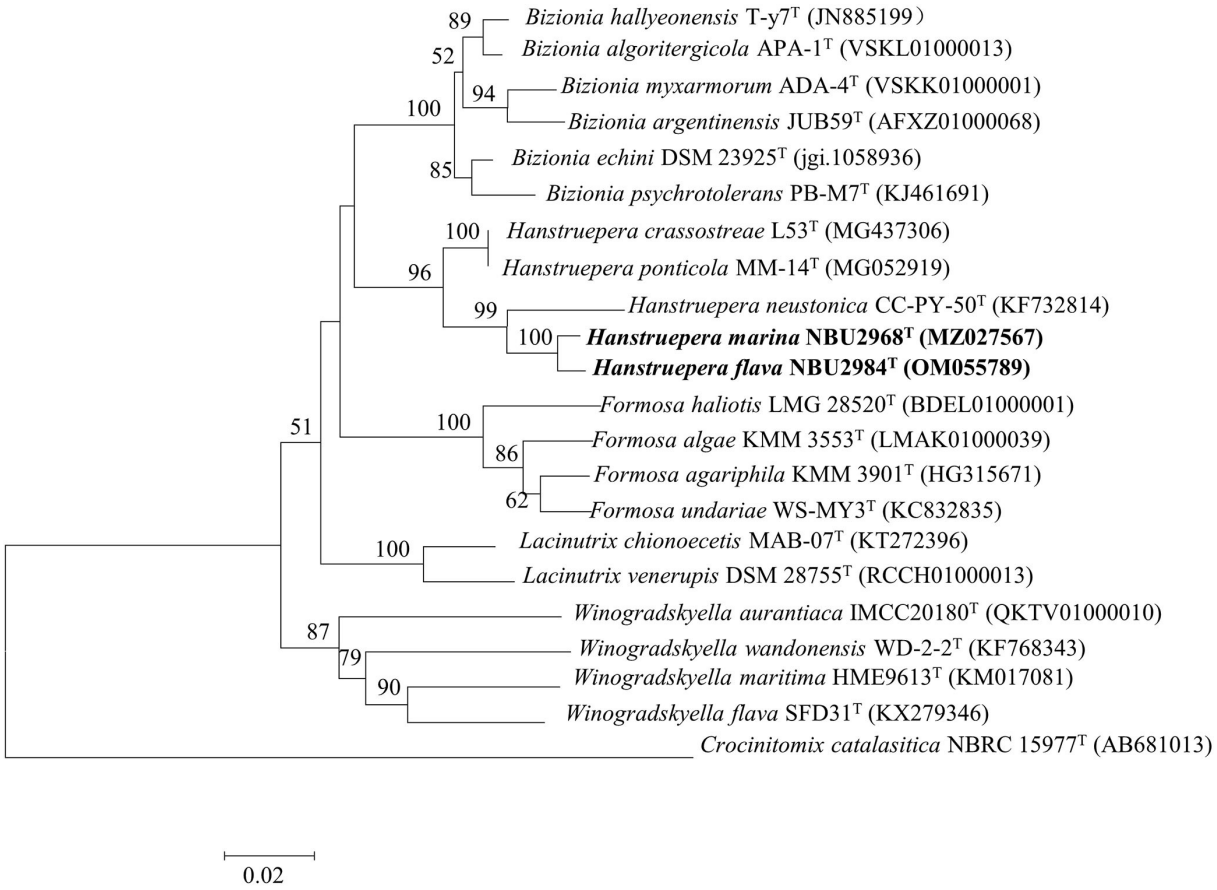

FIGURE 2
Neighbor-joining phylogenetic tree based on the 16S rRNA gene sequences, showing the phylogenetic relationships of strains NBU2968^T, NBU2984^T, and related taxa. Bootstrap values are based on 1,000 resamplings. Bootstrap values higher than 50% are indicated at branch points. Bar, 0.02 substitutions per nucleotide position.

2 weeks. Both strains were sensitive to amoxicillin, ampicillin, carbenicillin, cefamezin, cefoxitin, cefradine, cephalexin, chloramphenicol, ciprofloxacin, clindamycin, doxycycline, erythromycin, lincomycin, minocycline, norfloxacin, ofloxacin, penicillin G, rifampicin, streptomycin, and vancomycin. Strain NBU2968^T was sensitive to tetracycline but not for strain NBU2984^T. Compared to two related type strains, strains NBU2968^T and NBU2984^T could grow without NaCl and hydrolyze Tween 80. Nitrate reduction was positive only for strain NBU2984^T (Table 1). Other physiological and biochemical characteristics are given in the species description (Table 1 and Supplementary Table 1).

Chemotaxonomic properties

The predominant cellular fatty acids (>10%) of strain NBU2968^T were iso-$C_{15:1}$ G (27.1%), iso-$C_{15:0}$ (23.8%), and iso-$C_{17:0}$ 3-OH (20.2%) and that of strain NBU2984^T consisted of iso-$C_{15:1}$ G (25.0%), summed feature 3 (19.7%), iso-$C_{17:0}$ 3-OH (17.5%), and iso-$C_{15:0}$ (14.2%). The major fatty acids of two novel strains were similar to two related type strains (iso-$C_{15:1}$ G, iso-$C_{15:0}$, and iso-$C_{17:0}$ 3-OH). The detailed fatty acid profile showed some differences among the four strains. For example, strain NBU2984^T possessed a higher amount of summed feature 3 but a lower amount of iso-$C_{15:0}$ than the other three strains. Anteiso-$C_{15:1}$ A was detected in strains NBU2968^T and NBU2984^T, but not in two related type strains. Anteiso-$C_{15:0}$, iso-$C_{16:0}$, iso-$C_{16:1}$ G, $C_{15:0}$ 2-OH, and iso-$C_{16:0}$ 3-OH were detected in strains NBU2968^T, NBU2984^T, and *H. neustonica* JCM19743^T but lacked in *H. crassostreae* MCCC 1H00246^T, while $C_{15:1}$ ω8*c* and summed feature 9 were only present in *H. crassostreae* MCCC 1H00246^T (Table 2). The only detected respiratory quinone in two novel strains was menaquinone-6 (MK-6), which was in common with the quinone type of the genus *Hanstruepera*. The major polar lipids were phosphatidylethanolamine (PE), unidentified amino lipids (ALs), and unidentified lipids (Ls), which were

also in accordance with two related type species. The detailed polar lipid profile showed that strain NBU2984^T lacked L1, while the other three strains contained it. AL2 and AL3 were detected in two novel strains but not in two related type strains. AL5 was only present in *H. neustonica* JCM19743^T (Supplementary Figure 2).

Phylogeny of 16S rRNA gene sequences

The almost complete 16S rRNA gene sequences of strains NBU2968^T (1,487 bp, GenBank accession number: MZ027567) and NBU2984^T (1,487 bp, GenBank accession number: OM055789) were obtained through PCR amplification and sequencing. They shared 99.3% sequence similarity with each other. Sequence similarity searching in databases revealed that strains NBU2968^T and NBU2984^T shared the highest 16S rRNA gene sequence similarities (97.7%) with *H. crassostreae* L53^T and "*H. ponticola* MM-14^T" (heterotypic synonym of *H. crassostreae* L53^T), followed by *H. neustonica* CC-PY-50^T (96.4–96.6%), and shared low similarities (<95.6%) to other valid species. Phylogenetic analysis revealed that strains NBU2968^T and NBU2984^T were affiliated with species in the genus *Hanstruepera*, and closely related to *H. neustonica* CC-PY-50^T, *H. crassostreae* L53^T, and "*H. ponticola* MM-14^T" on the different phylogenetic trees (Figure 2) and (Supplementary Figures 3, 4).

Genomic characteristics

The draft genome sequence of strain NBU2968^T is composed of 13 contigs with the size of 3,282,034 bp, containing 3,065 protein-coding genes and 54 RNA genes. The draft genome sequence of strain NBU2984^T is composed of 23 contigs with the size of 3,094,910 bp, containing 2,880 protein-coding genes and 55 RNA genes. A total of 1,321 and 1,290 genes were assigned to KEGG for strains NBU2968^T and NBU2984^T, respectively (Table 3). KEGG's analysis showed the major metabolic pathways of strains NBU2968^T, NBU2984^T, *H. crassostreae* L53^T, and *H. neustonica* JCM19743^T were similar. They possessed the most genes in gene information processing, amino acid metabolism, and carbohydrate metabolism. All strains had complete pathways of gluconeogenesis (M00003), pyruvate oxidation (M00307), citrate cycle (M00009), pentose phosphate pathway (M00007), and phosphoribosyl diphosphate (PRPP) biosynthesis (M00005), whereas only strain NBU2984^T contained a complete glyoxylate cycle (M00012) (Table 4). In other metabolic pathways, the dTDP-L-rhamnose biosynthesis pathway (M00793) was found in all species. And a complete phosphatidylethanolamine (PE) biosynthesis pathway (M00093) was completely annotated in four strains, which was consistent with the polar lipids results of the genus *Hanstruepera*. In addition, the pathway of histidine biosynthesis (M00026) is complete in strains NBU2968^T, NBU2984^T, and *H. crassostreae* L53^T but not in strain *H. neustonica* JCM19743^T, and only strain *H. crassostreae* L53^T did not possess complete C1-unit interconversion (M00140). Phylogenomic analysis showed that two novel strains were closely related to the genus *Hanstruepera* (Supplementary Figure 5), which was similar to NJ, ML, and MP trees. The genomic DNA G+C contents of NBU2968^T and NBU2984^T were 34.2 and 34.4%, respectively, which were close to two related type strains. The ANI and dDDH values between NBU2968^T and NBU2984^T were 88.9 and 36.3%, respectively, which were below the proposed species cut-off values of 95–96% for ANI and 70% for dDDH (Wayne et al., 1987; Goris et al., 2007), indicating that NBU2968^T and NBU2984^T represent two distinctive species. The ANI and dDDH values between the two strains and closely related *Hanstruepera* species were 77.4–78.3% and 20.4–20.9% (Table 3), respectively, indicating that the two strains represent novel species separated from validly published *Hanstruepera* species.

TABLE 3 The comparison of genomic features among strains NBU2968^T, NBU2984^T, and two species in the genus *Hanstruepera*.

Features	1	2	3	4
Genome size (bp)	3,282,034	3,094,910	3,136,223	3,049,585
Number of contigs	13	23	6	16
N50 length (bp)	569,330	1,585,466	2,516,937	499,047
G+C content (%)	34.2	34.4	33.5	35.4
Total Genes	3,119	2,935	2,931	2,842
Protein coding genes	3,065	2,880	2,875	2,802
RNA genes	54	55	39	40
Genes assigned to KEGG	1,321	1,290	1,269	1,265
GenBank accession no.	JAINVX000000000	JALJCW000000000	POTB01000000	POWF01000000
ANI/dDDH values (%, compared to NBU2968^T)	/	88.9/36.3	77.9/20.8	77.5/20.5
ANI/dDDH values (%, compared to NBU2984^T)	88.9/36.3	/	78.3/20.9	77.4/20.4

Taxa: 1, strain NBU2968^T; 2, strain NBU2984^T; 3, *H. crassostreae* L53^T; 4, *H. neustonica* JCM19743^T.

TABLE 4 The comparison of complete and incomplete metabolic pathways in the genomes of strains NBU2968^T, NBU2984^T, and related type strains of the genus *Hanstruepera*.

	Pathway modules#		1	2	3	4
Carbohydrate metabolism	Central carbohydrate metabolism	M00002	+	+	+	+
		M00003	+	+	+	+
		M00307	+	+	+	+
		M00009	+	+	+	+
		M00010	+	+	+	+
		M00011	+	+	+	+
		M00007	+	+	+	+
		M00005	+	+	+	+
	Other carbohydrate metabolism	**M00012**	-	**+**	-	-
Lipid metabolism	Fatty acid metabolism	M00082	+	+	+	+
		M00083	+	+	+	+
		M00086	+	+	+	+
	Lipid metabolism	M00093	+	+	+	+
Nucleotide metabolism	Purine metabolism	M00048	+	+	+	+
		M00049	+	+	+	+
	Pyrimidine metabolism	M00050	+	+	+	+
		M00052	+	+	+	+
		M00053	+	+	+	+
Amino acid metabolism	Serine and threonine metabolism	M00018	+	+	+	+
		M00338	+	+	+	+
	Cysteine and methionine metabolism	M00035	+	+	+	+
		M00527	+	+	+	+
	Lysine metabolism	**M00026**	**+**	**+**	**+**	-
	Histidine metabolism	M00045	+	+	+	+
		M00023	+	+	+	+
	Aromatic amino acid metabolism	M00038	+	+	+	+
Glycan metabolism	Lipopolysaccharide metabolism	M00063	+	+	+	+
Metabolism of cofactors and vitamins	Cofactor and vitamin metabolism	M00912	+	+	+	+
		M00120	+	+	+	+
		M00123	+	+	+	+
		M00881	+	+	+	+
		M00140	**+**	**+**	-	**+**
		M00121	+	+	+	+
Biosynthesis of terpenoids and polyketides	Terpenoid backbone biosynthesis	M00364	+	+	+	+
	Polyketide sugar unit biosynthesis	M00793	+	+	+	+

Taxa: 1, strain NBU2968^T; 2, strain NBU2984^T; 3, *H. crassostreae* L53^T; 4, *H. neustonica* JCM19743^T. #: The description of pathway module numbers is listed in Supplementary Table 2. The different results of pathway module numbers shown in the table are indicated in bold.

Conclusion

A modified *in situ* technique was developed and applied to resource mining of uncultured microbes from marine sediments of Meishan Island in the East China Sea. Two novel strains NBU2968^T and NBU2984^T were isolated by this method but not standard Petri dish, which indicated the modified *in situ* technique was more effective for isolating uncultured microbes and could be popularized and applied to other aquatic environments. Based on the phenotypic, chemotaxonomic, phylogenetic data, and genome analysis, we conclude that strains NBU2968^T and NBU2984^T represent two novel species of the genus *Hanstruepera*, for which the names *Hanstruepera marina* sp. nov. and *Hanstruepera flava* sp. nov. are proposed, respectively.

Description of *Hanstruepera marina* sp. nov.

Hanstruepera marina (ma.ri'na. L. fem. adj. *marina* of the sea, marine).

Cells are Gram-negative, aerobic, rod-shaped, and non-motile. The cell size is 0.5–0.8 × 0.8–3.0 μm. Colonies on Marine agar 2,216 are 1.0 mm in diameter, convex, smooth, opaque, and yellow-pigmented after 24 h at 32°C. Flexirubin-type pigments are present. The temperature range for growth is 10–40°C (optimum 37°C). Growth occurs at 0–6.0% NaCl and pH 5.5–8.0 (optimum, 2.0% NaCl and pH 7.0). Positive for catalase and oxidase activities, Voges–Proskauer, fermentation of D-glucose, arginine dihydrolase, hydrolysis of starch, gelatin, and Tweens 40, 60, and 80. Negative for methyl red, H_2S production, indole production, β-galactosidase, urease, nitrate reduction, hydrolysis of casein, aesculin, and Tween 20. In the API ZYM kit, positive for activities of alkaline phosphatase, esterase (C4), esterase lipase (C8), lipase (C14), leucine arylamidase, valine arylamidase, cystine arylamidase, acid phosphohydrolase, and naphthol-AS-BI-phosphohydrolase. In the API 50CH kit, positive for D-glucose, glycogen, D-fructose, maltose, D-mannose, *N*-acetyl-β-D-glucosamine, lactose, 2-ketogluconate, starch, D-ribose, α-methyl-D-mannopyranoside, α-methyl-D-glucopyranoside, amygdaline, L-arabinose, arbutin, D-galactose, gentiobiose, β-methyl-D-xylopyranoside, salicin, sucrose, cellobiose, and D-xylose. The major fatty acids are iso-$C_{15:0}$, iso-$C_{15:0}$ G, and iso-$C_{17:0}$ 3-OH. MK-6 is the only detected respiratory quinone. The polar lipids include phosphatidylethanolamine (PE), four unidentified amino lipids (ALs), and four unidentified lipids (Ls). The genomic DNA G+C content of the type strain is 34.2%.

The type strain NBU2968^T (= MCCC 1K06392^T = KCTC 82913^T) was isolated from a marine sediment sample taken from the Meishan Island in the East China Sea, China.

Description of *Hanstruepera flava* sp. nov.

Hanstruepera flava (fla'va. L. fem. adj. flava yellow, the color of the pigment that the bacterium produces).

Cells are Gram-negative, aerobic, rod-shaped, and non-motile. The cell size is 0.4–0.6 × 1.0–2.8 μm. Colonies on MA are 1.0 mm in diameter, convex, smooth, opaque, and yellow-pigmented after 24 h at 32°C. Flexirubin-type pigments are present. The temperature range for growth is 15–37°C (optimum 32°C). Growth occurs at 0–10.0% NaCl and pH 6.0–8.5 (optimum, 2.0% NaCl and pH 7.0). Positive for catalase and oxidase activities, nitrate reduction, fermentation of D-glucose, hydrolysis of casein, starch, gelatin, aesculin, and Tweens 40, 60, and 80. Negative for methyl red, Voges–Proskauer, H_2S production, indole production, arginine dihydrolase, β-galactosidase, urease, and hydrolysis of Tween 20. In the API ZYM kit, positive for activities of alkaline phosphatase, trypsin, α-chymotrypsin, *N*-acetyl-β-glucosaminidase, leucine arylamidase, esterase (C4), esterase lipase (C8), valine arylamidase, cystine arylamidase, acid phosphohydrolase, and naphthol-AS-BI-phosphohydrolase. In the API 50CH kit, positive for D-glucose, glycogen, aesculin, maltose, *N*-acetyl-β-D-glucosamine, D-fructose, lactose, D-ribose, starch, D-mannose, 2-ketogluconate, and 5-ketogluconate. The major fatty acids are iso-$C_{15:0}$, iso-$C_{15:1}$ G, iso-$C_{17:0}$ 3-OH, and summed feature 3 ($C_{16:1}$ ω7*c* and/or $C_{16:1}$ ω6*c*). MK-6 is the only detected respiratory quinone. The polar lipids include phosphatidylethanolamine (PE), four unidentified amino lipids (ALs), and three unidentified lipids (Ls). The genomic DNA G+C content of the type strain is 34.4%. The type strain NBU2984^T (= MCCC 1K07472^T = KCTC 92511^T) was isolated from a marine sediment sample taken from the Meishan Island in the East China Sea, China.

Data availability statement

The datasets presented in this study can be found in online repositories. The names of the repository/repositories and accession number(s) can be found in the article/supplementary material.

Author contributions

WZ conceived the study. HD, JL, CY, and CG performed the experiments. WZ, LD, and DJ analyzed data. HD and CY wrote the manuscript. All authors read and approved the manuscript.

Funding

This work was supported by the Natural Science Foundation of Zhejiang Province (LGF22C010001), the National Natural Science Foundation of China (32100001), the Ningbo Key Science and Technology Development Program (2021Z046), and Li Dak Sum Yip Yio Chin Kenneth Li Marine Biopharmaceutical Development Fund.

Conflict of interest

The authors declare that the research was conducted in the absence of any commercial or financial relationships that could be construed as a potential conflict of interest.

Publisher's note

Supplementary material

The Supplementary Material for this article can be found online at: https://www.frontiersin.org/articles/10.3389/fmicb.2022.957397/full#supplementary-material

References

Berdy, B., Spoering, A. L., Ling, L. L., and Epstein, S. S. (2017). In situ cultivation of previously uncultivable microorganisms using the ichip. *Nat. Protoc.* 12, 2232–2242. doi: 10.1038/nprot.2017.074

Bernardet, J. F., Nakagawa, Y., and Holmes, B. (2002). Proposed minimal standards for describing new taxa of the family *Flavobacteriaceae* and emended description of the family. *Int. J. Syst. Evol. Microbiol.* 52, 1049–1070. doi: 10.1099/ijs.0.02136–0

Buerger, S., Spoering, A., Gavrish, E., Leslin, C., Ling, L., Epstein, S. S., et al. (2012). Microbial scout hypothesis and microbial discovery. *Appl. Environ. Microbiol.* 78, 3229–3233. doi: 10.1128/AEM.07308–11

Dong, X. Z., and Cai, M. Y. (2001). *Determinative Manual for Routine Bacteriology*. 1st ed. Beijing: Science Press. 353–364.

Epstein, S. S. (2013). The phenomenon of microbial uncultivability. *Curr. Opin. Microbiol.* 16, 636–642. doi: 10.1016/j.mib.2013.08.003

Felsenstein, J. (1981). Evolutionary trees from DNA sequences: a maximum likelihood approach. *J. Mol. Evol.* 17, 368–376. doi: 10.1007/BF01734359

Fitch, W. M. (1971). Toward defining the course of evolution: minimum change for a specific tree topology. *Syst. Zool.* 20, 406–416. doi: 10.2307/2412116

Goris, J., Konstantinidis, K. T., Klappenbach, J. A., Coenye, T., Vandamme, P., Tiedje, J. M., et al. (2007). DNA-DNA hybridization values and their relationship to whole-genome sequence similarities. *Int. J. Syst. Evol. Microbiol.* 57, 81–91. doi: 10.1099/ijs.0.64483–0

Hameed, A., Shahina, M., Lai, W. A., Lin, S. Y., Liu, Y. C., Hsu, Y. H., et al. (2015). *Hanstruepera neustonica* gen. nov., sp. nov., a zeaxanthin-producing member of the family *Flavobacteriaceae* isolated from estuarine water, and emendation of *Sediminibacter furfurosus* Khan et al. 2007 emend. Kwon et al. 2014, *Mangrovimonas yunxiaonensis* Li et al. 2013, *Antarcticimonas flava* Yang et al. 2009 and *Hoppeia youngheungensis* Kwon et al. 2014. *Int. J. Syst. Evol. Microbiol.* 65, 336–345. doi: 10.1099/ijs.0.066852–0

He, R. H., Liang, Q. Y., Zhao, J. X., and Du, Z. J. (2018). *Hanstruepera crassostreae* sp nov., a novel marine bacterium of the family *Flavobacteriaceae* isolated from an oyster. *Int. J. Syst. Evol. Microbiol.* 68, 3647–3651. doi: 10.1099/ijsem.0.003053

Huang, Z. B., Du, Y. P., and Lai, Q. L. (2022). *Hanstruepera crassostreae* He et al., 2018 is a later heterotypic synonym of *Pseudobizionia ponticola* Park et al., 2018 and transfer of *Pseudobizionia ponticola* to the genus *Hanstruepera* as *Hanstruepera ponticola* comb. nov. *Int. J. Syst. Evol. Microbiol.* 72, 005257. doi: 10.1099/ijsem.0.005257

Jung, D., Liu, B. Y., He, X. P., Owen, J. S., Liu, L. W., Yuan, Y., et al. (2021a). Accessing previously uncultured marine microbial resources by a combination of alternative cultivation methods. *Microb. Biotechnol.* 14, 1148–1158. doi: 10.1111/1751–7915.13782

Jung, D., Liu, L. W., and He, S. (2021b). Application of in situ cultivation in marine microbial resource mining. *Marine Life Sci. Technol.* 3, 148–161. doi: 10.1007/s42995–020-00063-x

Kanehisa, M., Sato, Y., and Morishima, K. (2016). BlastKOALA and GhostKOALA: KEGG tools for functional characterization of genome and metagenome sequences. *J. Mol. Biol.* 428, 726–731. doi: 10.1016/j.jmb.2015.11.006

Kates, M. (1986). *Techniques of Lipidology. Isolation, Analysis and Identification of Lipids*, 2nd ed. Amsterdam: Elsevier.

Kimura, M. (1980). A simple method for estimating evolutionary rates of base substitutions through comparative studies of nucleotide sequences. *J. Mol. Evol.* 16, 111–120. doi: 10.1007/BF01731581

Kumar, S., Stecher, G., and Tamura, K. (2016). MEGA7: molecular evolutionary genetics analysis version 7.0 for bigger datasets. *Mol. Biol. Evol.* 33, 1870–1874. doi: 10.1093/molbev/msw054

Lagesen, K., Hallin, P., Rodland, E. A., Staerfeldt, H-. H., Rognes, T., Ussery, D. W., et al. (2007). RNAmmer: consistent and rapid annotation of ribosomal RNA genes. *Nucl. Acids Res.* 35, 3100–3108. doi: 10.1093/nar/gkm160

Li, R., Li, Y., Kristiansen, K., and Wang, J. (2008). SOAP: short oligonucleotide alignment program. *Bioinformatics* 24, 713–714. doi: 10.1093/bioinformatics/btn025

Lowe, T. M., and Chan, P. P. (2016). tRNAscan-SE On-line: integrating search and context for analysis of transfer RNA genes. *Nucl. Acids Res.* 44, W54–W57. doi: 10.1093/nar/gkw413

Meier-Kolthoff, J. P., Auch, A. F., Klenk, H. P., and Goeker, M. (2013). Genome sequence-based species delimitation with confidence intervals and improved distance functions. *BMC Bioinf.* 14, 60. doi: 10.1186/1471–2105-14–60

Meier-Kolthoff, J. P., and Goeker, M. (2019). TYGS is an automated high-throughput platform for state-of-the-art genome-based taxonomy. *Nat. Commun.* 10, 2182. doi: 10.1038/s41467–019-10210–3

Minnikin, D. O'donnell, A., Goodfellow, M., Alderson, G., Athalye, M., Schaal, A., et al. (1984). An integrated procedure for the extraction of bacterial isoprenoid quinones and polar lipids. *J. Microbiol. Methods* 2, 233–241. doi: 10.1016/0167–7012(84)90018–6

Mu, D. S., Liang, Q. Y., Wang, X. M., Lu, D. C., Shi, M. J., Chen, G. J., et al. (2018). Metatranscriptomic and comparative genomic insights into resuscitation mechanisms during enrichment culturing. *Microbiome* 6, 230. doi: 10.1186/s40168–018-0613–2

Nichols, D., Cahoon, N., Trakhtenberg, E. M., Pham, L., Mehta, A., Belanger, A., et al. (2010). Use of ichip for high-throughput in situ cultivation of "uncultivable" microbial species. *Appl. Environ. Microbiol.* 76, 2445–2450. doi: 10.1128/AEM.01754–09

Oueriaghli, N., Castro, D. J., Liamas, I., Bejar, V., and Martinez-Checa, F. (2018). Study of bacterial community composition and correlation of environmental variables in Rambla Salada, a Hypersaline environment in South-Eastern Spain. *Front Microbiol.* 9, 1377. doi: 10.3389/fmicb.2018.01377

Overbeek, R., Olson, R., Pusch, G. D., Olsen, G. J., Davis, J. J., Disz, T., et al. (2014). The SEED and the Rapid Annotation of microbial genomes

using Subsystems Technology (RAST). *Nucleic Acids Res.* 42, D206–D214. doi: 10.1093/nar/gkt1226

Park, S., Choi, J., Choi, S. J., and Yoon, J. H. (2018). *Pseudobizionia ponticola* gen. *nov., sp. nov.*, isolated from seawater. *Int. J. Syst. Evol. Microbiol.* 68, 1467–1473. doi: 10.1099/ijsem.0.002691

Pei, J. H., Wu, Y., Gao, Y. X., Li, S. C., Fang, J. S., Wei, Y. L., et al. (2021). *Hanstruepera crassostreae* He et al., 2018 is a later heterotypic synonym of *Pseudobizionia ponticola* Park et al., 2018. *Int. J. Syst. Evol. Microbiol.* 71, 005074. doi: 10.1099/ijsem.0.005074

Rappé, M. S., Connon, S. A., Vergin, K. L., and Giovannoni, S. J. (2002). Cultivation of the ubiquitous SAR11 marine bacterioplankton clade. *Nature* 418, 630–633. doi: 10.1038/nature00917

Saitou, N., and Nei, M. (1987). The neighbor-joining method: a new method for reconstructing phylogenetic trees. *Mol Biol Evol* 4, 406–425.

Sheu, S. Y., Guo, Y. P., Kwon, S. W., and Chen, W. M. (2020). *Sphingobium fluviale* sp. *nov.,* isolated from a river. *Int. J. Syst. Evol. Microbiol.* 70, 827–834. doi: 10.1099/ijsem.0.003835

Sun, C., Wu, C., Su, Y., Wang, R. J., Fu, G. Y., Zhao, Z., et al. (2017). *Hyphococcus flavus gen.* nov., sp nov., a novel alphaproteobacterium isolated from deep seawater. *Int. J. Syst. Evol. Microbiol.* 67, 4024–4031. doi: 10.1099/ijsem.0.002237

Wayne, L., Brenner, D., Colwell, R., Grimont, P., Kandler, O., Krichevsky, M., et al. (1987). Report of the ad hoc committee on reconciliation of approaches to bacterial systematics. *Int. J. Syst. Evol. Microbiol.* 37, 463–464. doi: 10.1099/00207713–37-4–463

Yang, S. J., Kang, I., and Cho, J. C. (2016). Expansion of cultured bacterial diversity by large-scale dilution-to-extinction culturing from a single seawater sample. *Microb. Ecol.* 71, 29–43. doi: 10.1007/s00248–015-0695–3

Yoon, S. H., Ha, S. M., Kwon, S., Lim, J., Kim, Y., Seo, H., et al. (2017a). Introducing EzBioCloud: a taxonomically united database of 16S rRNA gene sequences and whole-genome assemblies. *Int. J. Syst. Evol. Microbiol.* 67, 1613–1617. doi: 10.1099/ijsem.0.001755

Yoon, S. H., and Ha, S. M., Lim, J., Kwon, S., and Chun, J. (2017b). A large-scale evaluation of algorithms to calculate average nucleotide identity. *Antonie Van Leeuwenhoek* 110, 1281–1286. doi: 10.1007/s10482–017-0844–4

Zengler, K., Toledo, G., Rappe, M., Elkins, J., Mathur, E. J., Short, J. M., et al. (2002). Cultivating the uncultured. *Proc. Natl. Acad. Sci. U.S.A.* 99, 15681–15686. doi: 10.1073/pnas.252630999

Zhang, X. Q., Sun, C., Wang, C. S., Zhang, X., Zhou, X., Wu, Y. H., et al. (2015). *Sinimarinibacterium flocculans* gen. nov., sp nov., a gammaproteobacterium from offshore surface seawater. *Int. J. Syst. Evol. Microbiol.* 65, 3541–3546. doi: 10.1099/ijsem.0.000452

Zhu, X. F., Jia, X. M., Zhang, X. Q., Wu, Y. H., and Chen, Z. Y. (2011). *Modern Experimental Technique of Microbiology*. Zhejiang University Press, Hangzhou English translation.

frontiers | Frontiers in Microbiology

TYPE Original Research
PUBLISHED 20 September 2022
DOI 10.3389/fmicb.2022.995699

OPEN ACCESS

EDITED BY
Shan He,
Ningbo University,
China

REVIEWED BY
Ajaya Kumar Rout,
Central Inland Fisheries Research Institute (ICAR), India
Jaejin Lee,
Iowa State University,
United States

*CORRESPONDENCE
Jang-Cheon Cho
chojc@inha.ac.kr

†These authors have contributed equally to this work

SPECIALTY SECTION
This article was submitted to Aquatic Microbiology, a section of the journal Frontiers in Microbiology

RECEIVED 16 July 2022
ACCEPTED 23 August 2022
PUBLISHED 20 September 2022

CITATION
Kim S-K, Song J, Rajeev M, Kim SK, Kang I, Jang I-K and Cho J-C (2022) Exploring bacterioplankton communities and their temporal dynamics in the rearing water of a biofloc-based shrimp (*Litopenaeus vannamei*) aquaculture system. *Front. Microbiol.* 13:995699. doi: 10.3389/fmicb.2022.995699

Exploring bacterioplankton communities and their temporal dynamics in the rearing water of a biofloc-based shrimp (*Litopenaeus vannamei*) aquaculture system

Su-Kyoung Kim[1†], Jaeho Song[2,3†], Meora Rajeev[3†], Su Kyoung Kim[1], Ilnam Kang[3], In-Kwon Jang[1] and Jang-Cheon Cho[3*]

[1]West Sea Mariculture Research Center, National Institute of Fisheries Science, Taean, South Korea, [2]Division of Microbiology, Honam National Institute of Biological Resources, Mokpo, South Korea, [3]Department of Biological Sciences and Bioengineering, Inha University, Incheon, South Korea

Biofloc technology (BFT) has recently gained considerable attention as a sustainable method in shrimp aquaculture. In a successful BFT system, microbial communities are considered a crucial component in their ability to both improve water quality and control microbial pathogens. Yet, bacterioplankton diversity in rearing water and how bacterioplankton community composition changes with shrimp growth are rarely documented. In this study, the Pacific white shrimp, *Litopenaeus vannamei* was cultivated in a greenhouse-enclosed BFT system. Rearing water samples were collected on a weekly basis for 5 months (152 days) and water quality variables such as physicochemical parameters and inorganic nutrients were monitored. In parallel, 16S rRNA gene pyrosequencing was employed to investigate the temporal patterns of rearing-water microbiota. The productivity, survival rate, and feed conversion ratio were 3.2–4.4 kg/m^3, 74%–89%, and 1.2–1.3, respectively, representing successful super-intensive cultures. The metataxonomic results indicated a highly dynamic bacterioplankton community, with two major shifts over the culture. Members of the phylum *Planctomycetes* dominated in rearing water during the early stages, while *Actinobacteria* dominated during the middle stages, and *Chloroflexi* and *TM7* dominated during the late stages of culture. The bacterioplankton community fluctuated more in the beginning but stabilized as the culture progressed. Intriguingly, we observed that certain bacterioplankton groups dominated in a culture-stage-specific manner; these groups include *Rhodobacteraceae*, *Flavobacteriaceae*, *Actinobacteria,* and *Chloroflexi*, which either contribute to water quality regulation or possess probiotic potential. Altogether, our results indicate that an operationally successful BFT-based aquaculture system favors the growth and dynamics of specific microbial communities in rearing water. Our study expands the scientific understanding of the practical utilization of microbes in sustainable aquaculture. A thorough understanding of rearing-water microbiota and

factors influencing their dynamics will help to establish effective management strategies.

KEYWORDS

shrimp aquaculture, biofloc technique, *Litopenaeus vannamei*, bacterioplankton community, rearing water, probiotics

Introduction

The increasing human population necessitates a rapid expansion of aquaculture industries to meet the growing seafood demand (Fan and Li, 2019). Among all aquaculture sectors, shrimp production has been increasing steadily over the past few years and therefore, world's total shrimp production in 2015 was 4.5 million tons, which was about four times higher than production in 2000 (Anderson et al., 2016). It is estimated that about 75% of farmed shrimp is produced in Asia, and most shrimp farms use semi-intensive aquaculture systems that allow flow-through of fresh rearing water to aquaculture ponds. Semi-intensive aquaculture systems encounter several challenges, including infectious diseases due to the exchange of rearing water with massive quantities of pathogen-uncontrolled water (Walker and Winton, 2010). Moreover, these systems discharge a large volume of nutrient-rich effluent, which may bring detrimental consequences (e.g., eutrophication) to the receiving water body (Páez-Osuna et al., 2003). To address these issues, several methods such as recirculating aquaculture systems and biofloc technology (BFT) have been adopted by aquaculture researchers. Though the former method is advantageous in terms of water exchange and productivity, the high operational and maintenance costs have hampered its practical deployment (Losordo and Hobbs, 2000; Gutierrez-Wing and Malone, 2006). Moreover, these systems have been shown to function weakly in terms of eliminating residual nutrients.

BFT, on the other hand, involves little or no water exchange and has recently gained considerable attention as a sustainable, cost-effective, and eco-friendly aquaculture method (Avnimelech, 2007). This method has been successfully introduced in shrimp farming (Crab et al., 2012). In principle, BFT uses a higher carbon-to-nitrogen (C/N) ratio to stimulate dense growth of the heterotrophic bacterial community. Because heterotrophic bacteria generate about 40 times more biomass than autotrophic nitrifying bacteria, aquaculture methods that favor their growth produce more bacterial biomass in the system (Brandão et al., 2021). These heterotrophic bacteria coalesce with dead organic matter as well as other microorganisms (e.g., microalgae, phytoplankton, and zooplankton) and develop flocculated aggregates (bioflocs; De Schryver et al., 2008). The densely grown heterotrophic bacterial populations actively uptake carbohydrates in rearing water and assimilate toxic inorganic nitrogen ions released in water (e.g., ammonia) to meet their nitrogen requirement (Ahmad et al., 2017). Hence, employing BFT offers three major advantages over other conventional aquaculture methods: (i) maintenance of rearing water quality by removing toxic nitrogenous constituents, (ii) minimizing the invasion of external pathogens and thus improving biosecurity, and (iii) bioflocs serve as natural proteinaceous feed for growing animals and thereby reduce the feed conversion ratio (FCR; Wasielesky et al., 2006). Considering these advantages, BFT-based operational systems have been extensively applied to shrimp aquaculture (Samocha et al., 2007).

Litopenaeus vannamei (Boone, 1931), also known as Pacific white shrimp and white-leg shrimp, are considered the most profitable species in the aquaculture industry (Zhang et al., 2019). Several characteristics such as their fast growth rate, high survival rate, wide range of salinity, and temperature adaptability make *L. vannamei* an excellent choice for aquaculture industries (Alfiansah et al., 2018). A study by Anderson et al. (2016) reported that *L. vannamei* alone contributed to more than 75% of the world's shrimp production in 2015, which was about 4.2 million tons. Likewise, as per the report of the Fisheries and Aquaculture Department (FAO, Food Agriculture Organization of the United Nations, 2018), crustaceans represented 11.4% of the total aquaculture production, to which the *L. vannamei* alone contributed more than half. However, the aquaculture application of this species is associated with complications such as increased environmental pollution and frequent incidences of viral- and bacterial-originated diseases including white spot syndrome virus, early mortality syndrome, and acute hepatopancreatic necrosis disease (Huang et al., 2016; Flegel, 2019). To address these issues, BFT has been applied worldwide for *L. vannamei* aquaculture (Krummenauer et al., 2011; Correia et al., 2014). Previous studies by our research group observed that bioflocs have a positive influence on *L. vannamei* growth and upregulate the expression of several immunity-related genes (Kim et al., 2014, 2015).

Bacterioplankton communities and their biological functionalities are critical components of BFT (Zeng et al., 2017). The main motive behind characterizing the complex microbial communities is to develop a method that can maintain a stable microbial community, supporting optimal shrimp health and water quality. In fact, variations in microbial communities are thought to be closely associated with disease outbreaks in aquaculture systems (Xiong et al., 2015). Given that the microbial community determines water quality and the overall functioning of BFT, a number of studies have been conducted so far to describe

the microbiota composition of various components of the BFT system. For example, Cardona et al. (2016) investigated bacterial community composition in the intestine of *Litopenaeus stylirostris* and rearing water of both clear seawater and BFT systems and revealed that bacterial communities of both systems varied considerably. Subsequently, carbon sources and the C/N ratio were demonstrated to influence the bacterial community composition of BFT (Deng et al., 2018). It was also demonstrated that the gut microbiota composition of *L. vannamei* changes dramatically during various growth stages (Kim et al., 2021), and that gut microbiota share a strong resemblance with bacterial communities of large-sized bioflocs (Huang et al., 2020). Overall, sufficient studies demonstrating variation in shrimp intestinal microbiota during various growth stages are available in the literature (Zeng et al., 2017; Xiong et al., 2018). However, studies delineating bacterioplankton community dynamics in rearing water at various culture stages, and its association with prevailing environmental variables in a BFT system, are rather scarce.

Henceforth, in the present study, we attempt to culture the shrimp *L. vannamei* in a greenhouse-enclosed production system, operating based on BFT. The growth pattern of *L. vannamei* and physiochemical properties of rearing water were monitored for five consecutive months. Concurrently, high-throughput amplicon sequencing was used to investigate how the bacterioplankton community of the rearing water changed with shrimp growth to explore the intrinsic association between culture stages, environmental variables, and microbiota composition of rearing water.

Materials and methods

Establishment of indoor shrimp production system and preparation of rearing water

A greenhouse-enclosed biofloc aquaculture system for shrimp production was constructed at the West Sea Mariculture Research Center, National Fisheries Research and Development Institute, Taean, South Korea (Supplementary Figures S1, S2). This prototype system had two 300 m^2 raceways (with a water depth of 0.8 m) enclosed in a 1,000 m^2 greenhouse structure with double-layered translucent sheets for heat insulation. The two raceways (Tank-1 and Tank-2), operating based on the BFT, were enclosed by linear low-density polyethylene sheets and had central longitudinal concrete partitions to facilitate water circulation. Polyvinyl chloride (PVC) pipes (50 mm in diameter) were placed at the bottom of the raceways to provide oxygen-rich water and connected with two 3 hp. water pumps. Another PVC pipe on the bottom had injector nozzles (20 mm in diameter) to suspend particulate matters. Each raceway was equipped with six airlifts (5 cm in size) on each side of the partition and also with a foam fractionator to remove excessive particulates. Rearing water was not exchanged during the 152 days of the trial and was heated by a heat-exchanger using groundwater. Foot basins for disinfection using sodium hypochlorite solution (10%) were placed at each entrance.

For the preparation of rearing water, incoming seawater was first pre-filtered with 100-μm-pore filters, then filtered with 10-μm-pore cartridge filters. The filtered seawater was then chlorinated with sodium hypochlorite solution to achieve 20 mg/L of active chlorine concentration and neutralized with sodium thiosulfate after 24 h of chlorination. Prior to stocking shrimp, the rearing water had been fertilized for a week using 2.3 mg L^{-1} urea, 0.1 mg L^{-1} phosphoric acid, and 1.5 mg L^{-1} sodium silicate and was inoculated with cultured diatoms, including 10^4 cells ml^{-1} of *Chaetoceros* spp.

Nursery culture and stocking juveniles

Pathogen-free *L. vannamei* postlarvae were purchased from SyAqua Sia. Co., Ltd. (Thailand). Nursery culture of the postlarvae (mean body weight 0.0015 g) was performed in two separate circular tanks (28 m^2, 13,214 individuals/m^2) for 16 days. The postlarvae were fed newly hatched *Artemia nauplii* and extruder pellet (EP) diet (crude protein 35%; CJ feed company, Korea) four times daily. During the culture trial, molasses was provided to each tank as an additional carbon source to adjust the C/N ratio to 15, and groundwater was added to offset water losses due to evaporation. Then, a total of 120,000 nursery-cultured juveniles (initial body weight 0.038 g) were stocked in each raceway tank with a stocking density of 320 individuals/m^3.

Feed management and rearing water sampling

Juveniles were fed with newly hatched *A. nauplii* for the first week of raceway culture. Thereafter, *A. nauplii* were replaced by crumble feed and EP diet (crude protein 30%) was provided throughout the experiment until harvest. The feed was supplemented manually three times per day. Daily ratios for the first month were based on 10%–20% of the total shrimp biomass estimated in each raceway. Ratios from the second month were adjusted based on feed consumption, gut fullness, shrimp mean weights, estimated survival, and FCR. Shrimp samples were randomly collected and weighed each week to determine the weekly growth rate (WGR) in each raceway. Feed consumption was monitored prior to each feeding by scooping the bottom of the raceway with a dip net.

To better understand the changes in water quality and bacterioplankton community composition across culture stages, rearing water from both Tank-1 and -2 was sampled for 5 months (152 days) at weekly intervals (Supplementary Tables S1, S2). Thus, sampling was performed on a total of 20 occasions, in which rearing water was sampled at three random locations each time.

Physiochemical parameters of rearing water

Physicochemical parameters of rearing water *viz.*, temperature, salinity, and pH were measured on-site using a YSI85 multi-parameter instrument (YSI Inc., Yellow Springs, OH, United States) on a daily basis. Similarly, dissolved oxygen (DO) was monitored using a real-time DO-monitoring system (Dongmun ENT). The contents of total ammonia nitrogen ($NH4^+$-N, TAN), nitrite-nitrogen (NO_2^--N), nitrate-nitrogen (NO_3^--N), chlorophyll-a (Chl-*a*), total suspended solids (TSS), and volatile suspended solids (VSS) were measured following standard methods (Baird et al., 2012).

Bacterial diversity assessment

Total and *Vibrio*-specific bacterial community analyses

To delineate how growing culture stages influence the bacterioplankton community, 10 rearing water samples, collected from Tank-1 on days 6, 20, 34, 48, 69, 83, 104, 118, 132, and 146, were chosen. These samples were designated as TAS1, TAS2, TAS3, TAS4, TAS5, TAS6, TAS7, TAS8, TAS9, and TAS10 culture stages, respectively, and were subjected to various diversity assessment methods. Firstly, an enumeration of total bacteria and *Vibrio* spp. was performed. Quantification of total bacterial cells followed the previously suggested direct count method (Porter and Feig, 1980). Briefly, 1 ml aliquots of each water sample were fixed with 2% (v/v) formaldehyde solution and stained with 4′, 6-diamidino-2-phenylindole (DAPI, Sigma-Aldrich, United States) for 10 min. The suspensions were then vacuum-filtered through 0.22-μm-pore (47-mm-diameter) black polycarbonate membrane filters (Advantec, Tokyo, Japan). These filters were mounted on glass slides and total bacterial cells were counted under an epifluorescence microscope (Carl Zeiss, Germany) using methods described in our earlier study (Kim et al., 2014).

For determining the load of *Vibrio* spp., serially diluted samples were spread plated on the thiosulfate-citrate-bile salts-sucrose (TCBS, BD Diagnostics) agar medium, which is a well-established and extensively used selective medium to isolate *Vibrio* spp. from aquatic environments (Bolinches et al., 1988). The culture plates were incubated at 30°C for 48 h and the resultant colonies were enumerated as colony-forming units (CFU).

Nucleic acid extraction and 16S rRNA gene pyrosequencing

The selected rearing water samples were further analyzed through high-throughput 16S rRNA gene amplicon sequencing. Here, a 1 L volume of each water sample was filtered through a 0.22-μm polyethersulfone membrane filter (Pall Corp., NY, United States), and the resultant filter membranes were used for nucleic acid extraction using a PowerWater® DNA isolation kit (MoBio Laboratories Inc., CA, United States) in accordance with the manufacturer's instructions. The quality of extracted DNA was ascertained by running extracted DNA on a 1% agarose gel and DNA was quantified using an ND-2000 spectrophotometer (NanoDrop Technologies, DE, United States). Next, PCR amplification of the V1-V3 hypervariable regions of the bacterial 16S rRNA gene was performed using the universal bacteria-specific primer pair: 27F (5′-GAGTTTGATCMTGGCTCAG-3′) and 519R (5′-WTTA CCGCGGCTGCTGG-3′), linked with the unique eight-nucleotide barcode and the 454 FLX titanium adaptor sequences. The prepared libraries were then subjected to a clean-up step and evaluated for size and quality on a Bioanalyzer 2,100 (Agilent, Palo Alto, CA, United States) using a DNA 7500 chip. Finally, pyrosequencing was performed using a 454 GS FLX Titanium platform (Roche-454 Life Sciences, CT, United States) at Chun Lab, Inc. (Seoul, Korea) following standard protocol. The generated pyrosequenced amplicons (pyrotags) were processed further for bacterial diversity analysis.

Processing, clustering, and diversity analyses of pyrotags

The bioinformatics workflow used for bacterioplankton diversity analysis follows the standard protocol detailed in previous studies (Rajeev et al., 2019, 2021). Briefly, the quality of raw pyrotags was assessed using FastQC software (Andrews, 2010) and a standard quality control criterion was applied to discard low-quality sequences. In this step, we removed all adapter sequences, barcode sequences, short-length reads (<200 nucleotides), and base calls having an average Phred quality score of <30 using the Cutadapt program (Martin, 2011). The retained high-quality reads were then processed in the Quantitative Insights into Microbial Ecology (QIIME, version 1.9.0) pipeline (Caporaso et al., 2010). In QIIME, the reads were first clustered into operational taxonomic units (OTUs) using the classical open-reference OTU picking approach with the UCLUST algorithm (version 1.2.22). The representative OTUs were then assigned taxonomies using the Greengenes reference database (release 13_8; DeSantis et al., 2006) at a 97% similarity threshold. Following this step, we removed all remaining OTUs that merely contained a single sequence (singletons) using the filter_otus_from_otu_table.py script. Moreover, because the present study involves comparative microbiome analysis, the influence of uneven sequencing depth was eliminated by randomly rarifying the whole dataset to the lowest number of reads.

The rarified OTU table was finally used in the QIIME environment to determine alpha diversity indices (Shannon, Simpson's, and Chao1) and beta diversity indices (Bray-Curtis and weighted UniFrac) and to classify OTUs at various taxonomic ranks.

Graphical visualization and statistical analyses

All the graphical visualizations, unless otherwise specified, were made in R (version 4.0.5). To determine the overall bacterial

community variation among samples, beta diversity using both non-phylogenetic (Bray-Curtis) and phylogenetic (weighted UniFrac; Lozupone and Knight, 2005) distance metrics were determined, and their clustering pattern was visualized with a principal coordinate analysis (PCoA). To test whether group-specific compositional variations in the bacterioplankton community were statistically significant, an analysis of similarity (ANOSIM, 999 permutations) was conducted in QIIME. Similarly, the linear discriminant analysis (LDA) effect size (LEfSe) method (Segata et al., 2011) was employed to determine discriminatory bacterioplankton communities that varied across different culture stages. The LEfSe analysis was conducted using the online Galaxy interface[1] with default settings (alpha Kruskal–Wallis value, 0.05; LDA threshold score [log10], 3.0) and differentially abundant bacterioplankton groups were represented using histogram and cladogram. The association between dominant bacterioplankton groups and environmental variables was determined and visualized with a canonical correspondence analysis (CCA).

Submission of raw pyrotags in a public repository

The pyrosequencing reads of 16S rRNA gene amplicons supporting the findings of this study were deposited in NCBI's Sequence Read Archive (SRA) under accession numbers SRR20075654–SRR20075663 and BioProject PRJNA857547.

Results

Growth performance and production of shrimp

Results of the *L. vannamei* culture are summarized in Table 1. Beginning when the juveniles were stocked, the bodyweight of shrimp was measured every 2 weeks for 152 days. At the end of the culture, the shrimp's bodyweight was 15.2 and 13.6 g/individual in Tank-1 and -2, respectively. Total production constituted 1,640 and 1,210 kg, referring to 4.4 and 3.2 kg/m^3 of productive yield and 287 and 237 individual/m^3 of the final density. Considering the initial shrimp count, survival rates in the designed BFT systems were estimated to be 89.9% and 73.4% in Tank-1 and -2, respectively. The FCRs ranged from 1.2 to 1.3 in both tanks.

1 http://huttenhower.sph.harvard.edu/galaxy

Rearing water quality changes across the culture stages

The sample-specific details on shrimp bodyweight and physicochemical characteristics of rearing water in both tanks are provided in Supplementary Tables S1, S2. Variation in the important physicochemical parameters *viz.*, body weight, temperature, alkalinity, inorganic nutrients (TAN, nitrite, nitrate), TSS, DO, and salinity is represented in Figures 1A–I. As can be seen, the bodyweight of reared shrimp increased gradually over the culture period, rising from 0.38 to 15.2 g. The rearing water temperature was relatively constant, ranging between 25.0–30.4°C in Tank-1 and 25.6°C–30.2°C in Tank-2; however, the air temperature fluctuated considerably, ranging between 10.1°C and 26.2°C. Over the study's course, the alkalinity gradually declined, from 70 to 155 mg $CaCO_3$/L. DO concentrations were maintained over 5.0 mg/l, except for a few days. The content of TAN and nitrate irregularly fluctuated during the study period. For example, the content of TAN initially increased and decreased abruptly. Thereafter, it gradually climbed again and eventually become stable. Similar to TAN, a sudden increase, followed by a decrease in nitrate concentration was observed initially. After, a gradual increase and decrease occurred until the end of the culture. The values of TSS, VSS, and turbidity increased 4, 6, and 12 times, respectively, compared to the initial concentration, with several fluctuations. Finally, Chl-*a* concentration exhibited dramatic changes, ranging from 14–15 to 356–408 µg/l.

Bacterioplankton diversity and community richness in the rearing water

Total bacterial cell count using DAPI staining showed a fluctuation in the bacterioplankton community over the culture stages (Table 2). Furthermore, we observed a slight upsurge in microbial community abundance along the culture stages; the total bacterial count reached 1.06×10^7 cells ml^{-1} in the culture's middle (culture stage TAS4) and 1.95×10^6 at the end of the culture (TAS10), as compared to starting count of 9.95×10^4 (TAS1). On the other hand, a *Vibrio*-specific assessment, employing a selective medium (TCBS), found a modest abundance of *Vibrio* spp. throughout the sampling campaign. The *Vibrio* population accounted for 9.0×10^1 to 3.4×10^3 CFU ml^{-1} of rearing water.

The details of the pyrosequencing effort employed in this study are provided in Table 2. The pyrosequencing run obtained a

TABLE 1 Summary of *Litopenaeus vannamei* aquaculture reared in BFT system for 152 days.

	Initial BW (g)	Final BW (g)	Stocking (shrimps/m^3)	Yield (kg/m^3)	Total production (kg)	Survival rate (%)	FCR
Tank-1	0.038	15.2	320	4.4	1,640	89	1.2
Tank-2	0.038	13.6	320	3.2	1,210	74	1.3

BW, body weight; FCR, feed conversion rate.

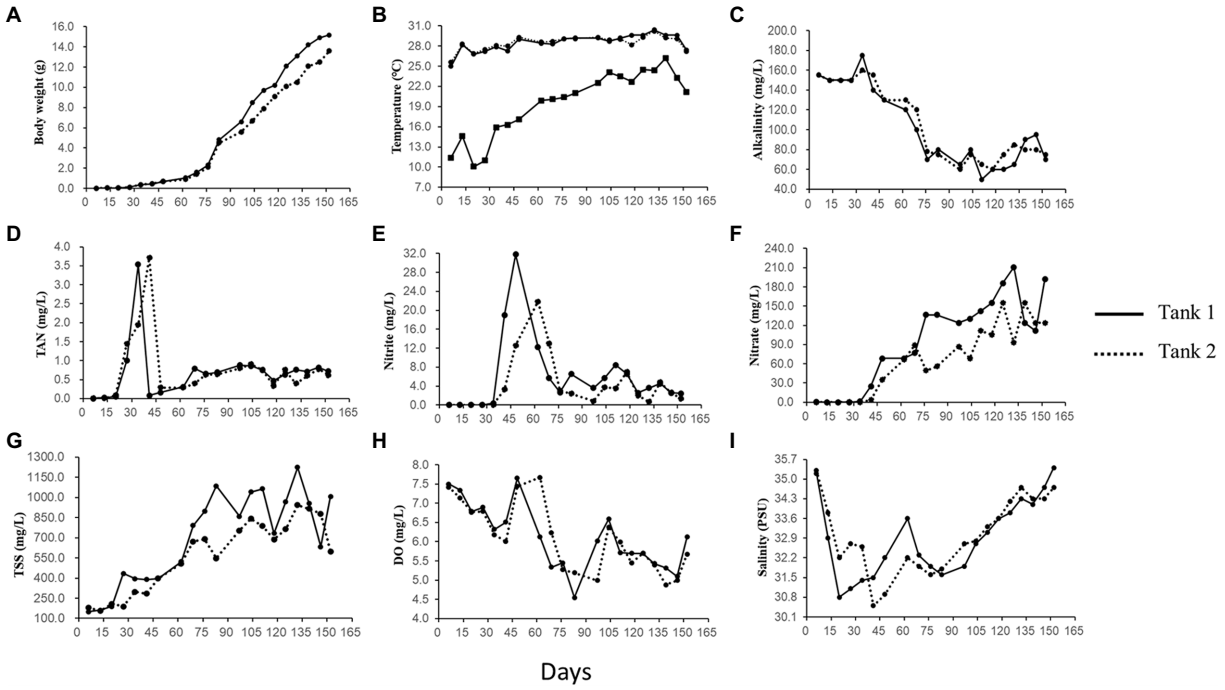

FIGURE 1
Body weight of the reared *Litopenaeus vannamei* and physicochemical parameters of rearing water over 152 growth days in a biofloc aquaculture system. Curves show values of **(A)** body weight, **(B)** temperature of rearing water (upper curves) and air (lower curves), **(C)** alkalinity, **(D)** total ammonia nitrogen (TAN), **(E)** nitrite (NO_2-N), **(F)** nitrate (NO_3-N), **(G)** total suspended solids (TSS), **(H)** dissolved oxygen (DO), and **(I)** salinity in culture Tank-1 and -2.

TABLE 2 Total bacterial counts, *Vibrio* spp. counts and pyrosequencing output of rearing water.

Growth days (culture stages)	Bacterial counts		Overview of pyrosequencing data					
	Total bacterial count	*Vibrio* count (CFU ml^{-1})	No. of raw reads	No. of qualified reads*	No. of OTUs	Shannon	Simpsons	Chao1
6 (TAS1)	9.95×10^4	2.00×10^2	14,218	6,660	596	6.53	0.953	949
20 (TAS2)	5.76×10^5	3.46×10^3	9,054	5,927	452	5.47	0.903	786
34 (TAS3)	3.16×10^6	1.97×10^2	12,099	7,845	614	6.40	0.949	972
48 (TAS4)	1.06×10^7	9.00×10^1	14,326	10,024	739	6.62	0.947	1,485
69 (TAS5)	4.86×10^6	2.40×10^2	7,639	3,545	1,062	9.09	0.994	1,259
83 (TAS6)	9.20×10^5	3.30×10^2	11,169	7,771	606	7.11	0.968	1,053
104 (TAS7)	5.25×10^6	7.50×10^2	14,395	10,329	573	6.14	0.931	1,130
118 (TAS8)	1.15×10^7	2.60×10^3	14,320	10,929	534	6.74	0.969	1,076
132 (TAS9)	3.98×10^6	3.00×10^2	8,729	5,963	651	6.83	0.958	1,307
146 (TAS10)	1.95×10^6	5.13×10^2	12,800	8,857	442	5.64	0.917	819

The alpha diversity indices (Shannon, Simpsons, and Chao1) were calculated at 3% sequence divergence. OTUs, Operational taxonomic units; CFU, Colony-forming units.
*Pyrosequencing reads that passed the quality control criteria.

total of 118,749 raw sequences. After applying quality control criteria, a total of 77,850 high-quality pyrotags (ranging from 3,545 to 10,929) were retained for diversity analyses. The clustering of these high-quality pyrotags at a 97% similarity threshold resulted in a total of 3,918 OTUs with an average of 626 OTUs per sample (ranging from 442 to 1,062). Initially, we plotted the numbers of high-quality sequences against the Chao1 diversity index as a rarefaction curve (Supplementary Figure S3). The Chao1 curves of each analyzed sample grew with increasing sequencing depth and finally reached a saturation stage, indicating that the number of high-quality pyrotags obtained in our study appeared technically adequate to survey most of the phylogenetic information. After random subsampling (rarefaction) of pyrotags in each sample to the shallowest number of sequences (3,545;

TAS5), alpha diversity indices were calculated. These indices were estimated to range from 5.47 to 9.09 for Shannon, 0.903 to 0.969 for Simpson's, and 786 to 1,485 for Chao1 (Table 2). Though there was no discernible pattern of variation in these indices, their values changed considerably along with the culture stages, with the highest increase during TAS5.

Bacterioplankton community composition in rearing water alters across the culture stages

To evaluate the similarity/dissimilarity pattern of bacterioplankton communities along the culture stages, the whole community was compared using beta diversity indices Bray-Curtis and weighted UniFrac (Figures 2A,B). The clustering pattern of these indices in PCoA plots identified a strong influence of the culture stage on rearing water microbiota. Therefore, all samples were grouped into three distinct clusters on both the Bray-Curtis-based PCoA (variation explained by PC1 = 25.6%; PC2 = 15.2%) and the weighted UniFrac-based PCoA (PC1 = 34.7% and PC2 = 22.9%). The first group comprising TAS1–4 culture stages clustered distinctly from the other two groups, which consisted of culture stages TAS5–7 and TAS8–10. Further analysis using ANOSIM indicated that the bacterioplankton community variation based on Bray–Curtis dissimilarity was statistically significant (R value = 0.608, $p = 0.002$).

The pyrotags were next classified into taxonomic ranks. The relative proportion of the most dominant bacterioplankton taxa at the phylum/class level is shown in Figure 3. The bacterioplankton communities of all culture stages were dominated by similar bacterial groups such as *Alphaproteobacteria*, *Gammaproteobacteria*, *Deltaproteobacteria*, *Bacteroidetes*, *Actinobacteria*, and *Planctomycetes* (Figure 3A). However, their proportions varied considerably among the culture stages. Members of the phylum *Cyanobacteria* dominated the bacterioplankton community in the initial culture stages (25.1% and 10.6% in TAS1 and TAS2, respectively). However, their proportion declined in the later stages (<2% during TAS3–TAS10). In contrast to *Cyanobacteria*, several bacterial groups occupied a minor proportion of the community initially but grew to dominate the community in the later culture stages. For example, *Actinobacteria* dominated the community during culture stages TAS5–TAS7 (13.1%, 18.5%, and 29.9%, respectively) and TAS8–TAS10 (12.9%, 11.7%, and 10.7%, respectively) compared to TAS1–TAS4 (0.3%, 6.8%, 0.4%, and 2.2%, respectively). Similarly, *Chloroflexi* were abundantly present during culture stages TAS5–TAS7 (3.7%, 0.5%, and 0.3%, respectively) and TAS8–TAS10 (3.4%, 4.4%, and 2.8%, respectively) but nearly absent during TAS1–TAS4 (0.0%, 0.0%, 0.0%, and 0.03%, respectively). On the other hand, members of the phylum *TM7* were prominent exclusively at the later culture stages (TAS8–TAS10), while they were present in only a minor proportion initially (TAS1–TAS7). It is important to emphasize that temporal variation in the bacterioplankton community was relatively high at the beginning stages (TAS1–TAS4) but became stable at later culture stages (TAS5–TAS10).

Bacterial community variation along the culture stages was more interesting and visible when taxonomic consideration extended to the family level (Figure 3B). As observed previously, each culture stage was dominated by

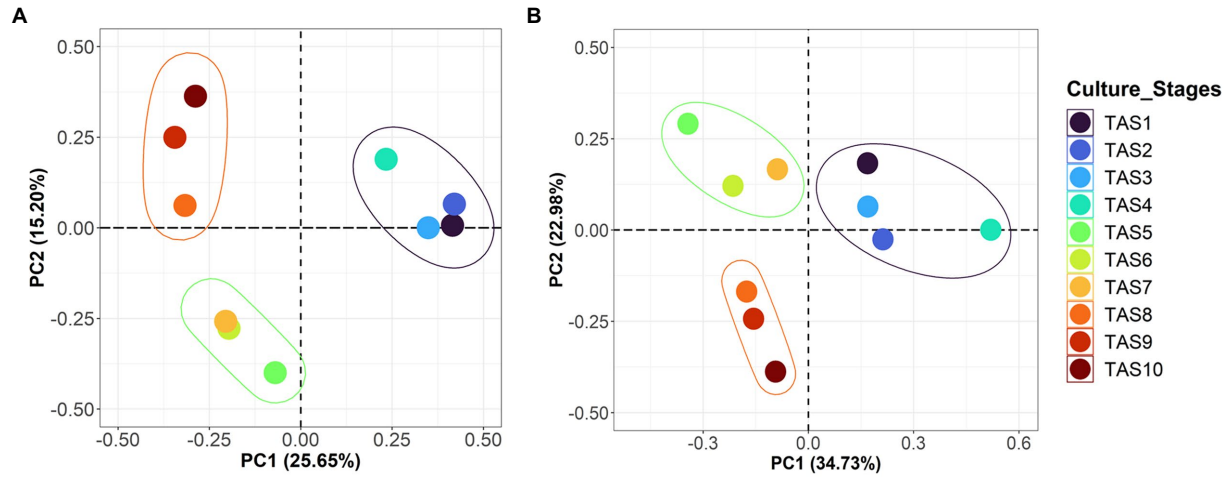

FIGURE 2
Compositional variations of bacterioplankton community in rearing water. Principal coordinate analysis (PCoA) plots represent beta diversity variations based on Bray-Curtis **(A)** weighted UniFrac **(B)** distance metrics in rearing water samples collected across various culture stages from a commercial BFT-based aquaculture system. The designated sample IDs (TAS1 to TAS10) represent shrimp *Litopenaeus vannamei* culture stages in terms of their growth days 6, 20, 34, 48, 69, 83, 104, 118, 132, and 146, respectively, in culture Tank-1.

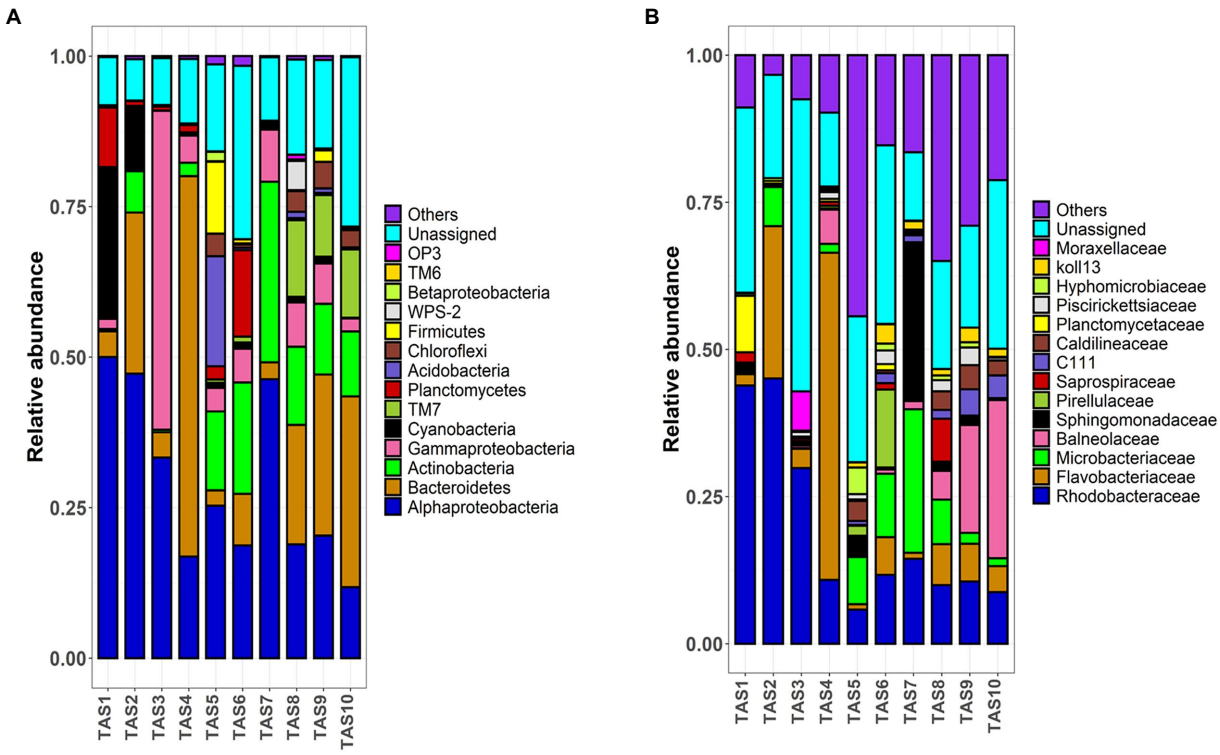

FIGURE 3
Bacterioplankton community dynamic in rearing water of a biofloc aquaculture system. Stacked bar plots depict the relative abundance of top bacterioplankton taxa at **(A)** phylum/class and **(B)** family levels during various culture stages. The proportions of dominant taxa are only shown. "Others" denotes cumulative relative abundances of remaining taxa. The indicated sample identifiers (TAS1 to TAS10) correspond to different shrimp culture stages in culture Tank-1 based on their growth days 6, 20, 34, 48, 69, 83, 104, 118, 132, and 146, respectively.

specific bacterioplankton taxa. For example, *Rhodobacteraceae* represented the most dominant bacterial family (>29%) in culture stages TAS1–TAS3, but it lost that dominance in later culture stages (TAS4–TAS10). In contrast to *Rhodobacteraceae*, members of *Microbacteriaceae* appeared to dominate during TAS5–TAS10, but were absent during TAS1–TAS4 (except for TAS2). Similarly, members of *Balneolaceae* were prominent (>4%) during the later culture stages (TAS7–TAS10) but made up a minor fraction of the community in other stages.

To decipher the impact of culture stages at lower taxonomic ranks, pyrotags were also analyzed at the genus level and the relative abundances of the most abundant genera were visualized in a heatmap (Figure 4). As can be clearly deduced from the hierarchical clustering pattern, several dominant genera exhibited dramatic changes with the culture and therefore investigated culture stages were distinctly grouped into three large clusters. The first cluster, comprising TAS1–4 culture stages (though TAS4 grouped weakly), was dominated by *Planctomyces*, *Marivita*, *Phaeobacter*, *Ruegeria*, *Olleya*, *Octadecabacter*, and *Muricauda*. The bacterial genera *Planctomyces*, *Marivita*, *Novosphingobium*, *Microbacterium*, *Sediminicola*, *Rhodoplanes*, and *Staphylococcus* were predominant in the second cluster (culture stages TAS5–7) and the genera *Polaribacter*, *KSA1*, *Pseudomonas*, and *Microbacterium* dominated in the third cluster (culture stages TAS8–10).

Bacterioplankton community dynamics over the culture stages are marked by specific bacterioplankton taxa

Considering the clear dynamics of the microbiota composition of rearing water, we next sought to identify differentially abundant bacterioplankton taxa during various culture stages using LEfSe. To do so, all of the investigated samples were broadly classified into three groups; the first group (termed "early-stage") includes samples TAS1–TAS4 ($n = 4$), while the second group (termed "middle-stage") includes TAS5–TAS7 ($n = 3$), and the third group (termed "late-stage") includes TAS7–TAS10 ($n = 3$). The sample grouping strategy adopted here is based on the similarity/dissimilarity patterns observed in the PCoA and heatmap (Figures 2, 4). The obtained LEfSe result at phylum to order levels, as illustrated in the cladogram and histogram, identified a number of bacterioplankton group(s) whose abundances were significantly overrepresented (LDA score > 3) in the early-stage, middle-stage, and late-stage of culture

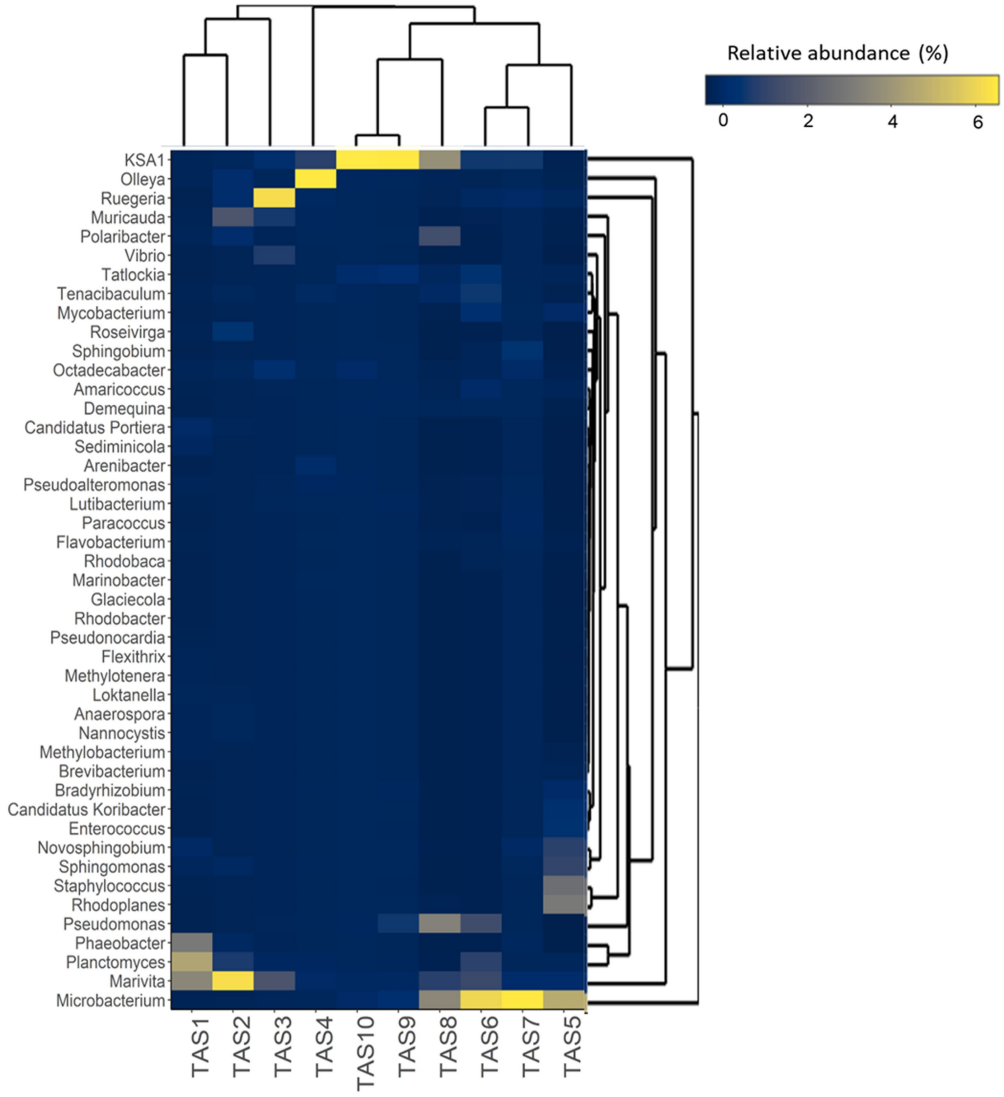

FIGURE 4
Temporal dynamics in bacterioplankton community composition of rearing water at the genus level. The hierarchically clustered heatmap shows the relative abundance of dominant (top 45) bacterioplankton genera in the rearing water during various culture stages. The color intensity in each cell represents the relative abundance of bacterial genera (listed to the left of the figure) at various shrimp culture stages (indicated at the bottom of the figure), according to the color scale at the right. The culture stages (TAS1 to TAS10) represented here denote shrimp *Litopenaeus vannamei* growth days 6, 20, 34, 48, 69, 83, 104, 118, 132, and 146, respectively.

(Figures 5A,B). The abundance of phylum *Planctomycetes* (particularly class *Phycisphaerae*, order *Phycisphaerales*) was especially enriched in the early-stage compared to the other two culture stages. Similarly, the differentially abundant bacterioplankton taxa in the middle-stage belonged to the phyla *Actinobacteria* (class *Actinobacteria*, order *Actinomycetales*) and *Proteobacteria* (class *Alphaproteobacteria*, order *Rhizobiales*), while the late-stage was associated with enrichment of the phyla *Actinobacteria* (classes: *Acidimicrobiia*, and *Thermoleophilia*, and orders: *Acidimicrobiales*, and *Solirubrobacterales*), *Chloroflexi* (class *Anaerolineae*, order *Caldilineales*), and *TM7* (class *TM7*-3, order *I025*). The relative proportions of the identified biomarker taxa (orders) in the categorized culture stages are also represented as box plots (Figure 5C).

Physicochemical parameters responsible for bacterioplankton community variation

To further enhance our understanding of the physicochemical parameters that could contribute to observed bacterioplankton community variation in rearing water, a CCA was performed (Figure 6). Results of the CCA showed a culture stage-specific distribution of the physicochemical characteristics of rearing

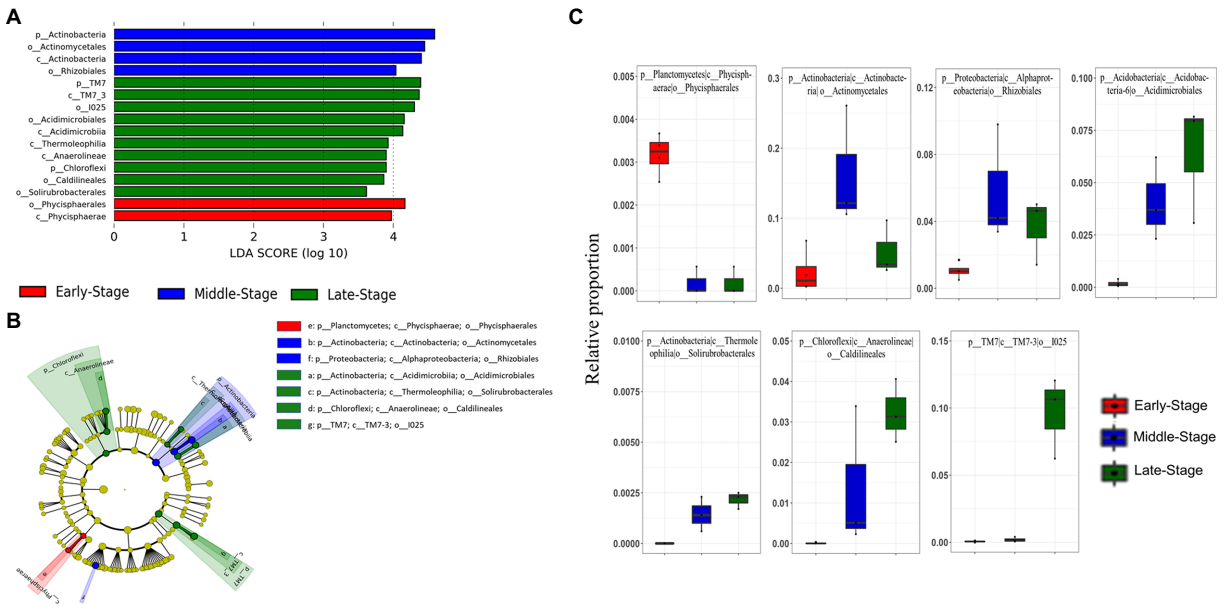

FIGURE 5
Linear discriminant analysis (LDA) effect size (LEfSe) shows the most differentially abundant bacterioplankton groups as a histogram **(A)** and cladogram **(B)** in rearing water of a BFT-based aquaculture system during various culture stages. The relative proportion of the identified bacterioplankton taxa through LEfSe are represented as boxplots **(C)**. Bacterioplankton groups that possess an LDA threshold > 3 are only represented. In the cladogram, each ring indicates a taxonomic level (e.g., center to outermost as phylum, class, order), while each circle indicates a bacterioplankton group. The taxonomic groups highlighted with different colors signify their enrichment in a particular culture stage.

water. A positive correlation existed between salinity, nitrite, nitrate, and DO, whereas a negative correlation existed between these variables and TAN and alkalinity. Concerning the bacterioplankton communities, the class *Gammaproteobacteria* was found to be influenced by TAN and alkalinity. Likewise, temperature, nitrate, nitrate, DO, and salinity jointly structured members of *Chloroflexi*, *Bacteroidetes*, *TM7*, *WPS*-2, and *OP3*. Contrary to these bacterioplankton groups, members of *Alphaproteobacteria*, *Actinobacteria*, *TM6*, *Planctomycetes*, *Cyanobacteria*, *Betaproteobacteria*, *Firmicutes*, and *Acidobacteria*, experienced a negligible impact from any of the investigated physicochemical parameters.

Discussion

Successful implementation of the BFT aquaculture system necessitates the growth of definite microbial communities that are capable of improving water quality, productivity, and biosecurity. There is now mounting evidence that the rearing water microbiota in shrimp aquaculture systems is closely associated with shrimp intestinal microbiota and rearing water microbiota has also been linked to shrimp disease occurrence (Xiong et al., 2018). However, studies remain inconclusive about the bacterioplankton community composition of rearing water and how it changes with shrimp growth.

In the present study, we aimed to understand the changes in physicochemical parameters and bacterioplankton community composition of rearing water during various growth stages of *L. vannamei* in a BFT-based aquaculture system. To promote biofloc formation, we employed a C/N ratio of 15, which is suggested to be the appropriate ratio as compared to other ratios such as 5 and 10 (Panigrahi et al., 2019). Our BFT system yielded an average of 3.6 kg/m^3 *L. vannamei*, matching the 3–6 kg/m^3 *L. vannamei* yield recovered in previous BFT systems (Samocha et al., 2007; Krummenauer et al., 2011). This yield is also substantially higher than the 0.2–0.3 kg/m^3 *L. vannamei* recovered from traditional flow-through culturing systems (Sowers et al., 2006; Krummenauer et al., 2010). Similarly, survival rates (89% and 74% in Tank-1 and -2, respectively) in our systems are within the range of those obtained from other BFT (Samocha et al., 2007; Krummenauer et al., 2011) and traditional flow-through systems (Sowers et al., 2006; Krummenauer et al., 2010). In our study, the poor survival rate (74% in Tank-2) might be explained by shrimp densities, which were higher than the super-intensive density (300 individual/m^3; Ray, 2012). The FCRs were recorded between 1.2 and 1.3, which are similar to those previously reported in a BFT system (Samocha et al., 2007), but considerably lower than those of the traditional flow-through systems (1.9–2.4; Sowers et al., 2006; Krummenauer et al., 2010). Considering the above evidence, the BFT systems designed in this study could be considered successful for *L. vannamei* culture.

Physicochemical parameters have been shown to influence the overall performance of BFT systems. DO is one of the crucial parameters affecting the growth and health of rearing animals. Though DO content decreased as culture stages progressed,

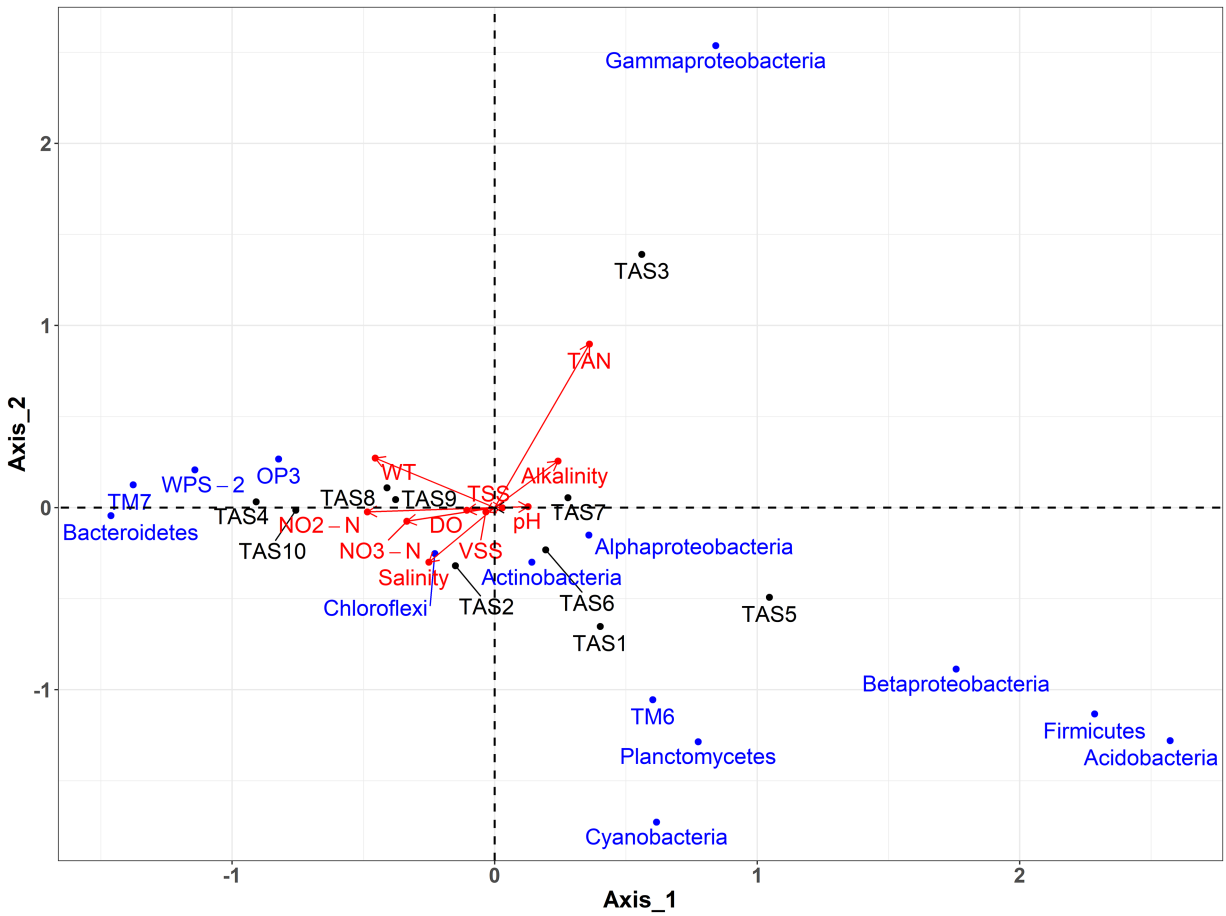

FIGURE 6
Physicochemical parameters of rearing water responsible for bacterioplankton community changes. Canonical correspondence analysis (CCA) shows an association between the dominant bacterioplankton groups (at phylum/class level) and the physicochemical properties of rearing water. WT, water temperature; TAN, Total ammonia nitrogen; TSS, total suspended solid; VSS, volatile suspended solid. The culture stages (TAS1 to TAS10) represent shrimp *Litopenaeus vannamei* growth days 6, 20, 34, 48, 69, 83, 104, 118, 132, and 146, respectively.

values always exceeded the desired requirement for shrimp health of 3.0 ppm (Seidman and Lawrence, 1985). The temperature ranged between 25°C and 30°C, which is generally considered ideal for rapid shrimp growth (Wyban et al., 1995). A study revealed that a pH > 7 may exert a negative influence on *L. vannamei* growth (Wasielesky et al., 2006). Although the pH was greater than 7 after 83 days of rearing, *L. vannamei* sustained a constant increase in growth, suggesting its resistance to a wider pH range. Nitrogenous constituents including TAN, nitrite, and nitrate determine rearing water quality and health of rearing animals, and hence their control has received great attention in aquacultural industries (Boardman et al., 2004). The safe levels of TAN, nitrite, and nitrate, for the healthy *L. vannamei* culture, have been identified as 4.0, 25.7, and 127.6 mg/l, respectively (Lin and Chen, 2003). In our study, TAN and nitrite concentrations were mostly maintained below the recommended levels, whereas the nitrate concentration exceeded its safe level in the last few stages. It seems that the nitrate concentration range that could exert a lethal impact on shrimp health is wide and thus a concentration of even 435 mg/l nitrates did not exert a significant detrimental influence on the survival and growth of *L. vannamei* (Kuhn et al., 2010).

In a BFT system, the two principal nitrogen conversion processes are nitrification and assimilation. Nitrification involves sequential oxidation of ammonia to nitrate *via* nitrite by chemoautotrophic nitrifying bacteria, whereas assimilation involves direct conversion of ammonia to biomass by heterotrophic bacteria (Ebeling et al., 2006). In our BFT system, as expected, a sudden drop of ammonia was observed, which supports the preferred assimilation process by heterotrophic bacteria. However, an equivalent alteration of nitrite and gradually increasing concentration of nitrate implies the existence of a nitrification process. Parallel to our observation, studies have found high levels of nitrate build-up in the BFT system (Nootong et al., 2011), which may be ascribed to heterotrophic nitrification. Recent studies have demonstrated that the nitrification process, to some extent, is also carried out by heterotrophic nitrifiers (Stein, 2011; Rout et al., 2017).

Microbial communities of rearing water in a BFT system are involved in several crucial functions including biofloc formation, maintenance of water quality and shrimp health, and biogeochemical phenomena (Huang et al., 2020). Moreover, several studies investigating the microbiome composition of aquaculture systems have identified a tight link between the microbiomes of shrimp intestines and rearing water (Zheng et al., 2017; Xiong et al., 2018). The speculated association was explained by the constant flow of rearing water through the digestive tract of growing shrimp, which thus influences the composition of gut microflora (Gatesoupe, 1999).

In the present study, we first demonstrated that the bacterioplankton community in rearing water is highly dynamic. A clear change in overall bacterioplankton community composition along the culture growth was observed. The bacterioplankton community exhibited two major shifts during the entire course of the study. The first shift likely occurred between TAS4 and TAS5 (during 48–69 culture days), to which an abruptly increased abundance of *Actinobacteria* might have contributed majorly. Similarly, the second shift began between TAS7 and TAS8 (during 104–118 culture days), which may be partially attributed to the increased proportion of *Chloroflexi* and *TM7* (a candidate phylum, also called *Saccharibacteria*). Similar patterns in the bacterial community of rearing water, along with intestine and sediment, at different culture stages were previously observed in a shrimp aquamimicry system (Zeng et al., 2020).

Further analysis revealed a complex microbial community in rearing water, comprising several bacterioplankton phyla such as *Proteobacteria*, *Actinobacteria*, *Bacteroidetes*, and *Planctomycetes*. *Proteobacteria* was the most dominant phylum throughout the culture stages, which is consistent with several earlier studies (Hou et al., 2017; Zheng et al., 2017). Similarly, *Bacteroidetes* constituted the second most abundant phylum, but showed a wide range of relative abundance, ranging from 2.5% to 63%. This phylum contains some of the dominant bacteria in algal blooms, and is known for degrading macromolecules in aquatic habitats (Buchan et al., 2014). The abundance of some dominant bacterioplankton phyla exhibited an inconsistent pattern during the culture stages. For instance, *Cyanobacteria* dominated the community in the beginning stages, but then diminished in the later culture stages. One possible explanation for such an unusual pattern is that most *Cyanobacteria* are free-floating photosynthetic autotrophs, and the dense turbidity of bioflocs in rearing water might have hampered their photosynthetic efficiency (Kim et al., 2021). In contrast to *Cyanobacteria*, the phylum *Actinobacteria* showed an entirely opposite trend by totally disappearing in the early culture stages. At the class level, rearing water microbiota was predominantly characterized by *Alphaproteobacteria*, *Gammaproteobacteria*, and *Bacteroidetes*. The higher occurrence of these bacterioplankton groups in a BFT system is not surprising considering their principal characteristics, including the requirement of organic material and nitrogen for growth (Cardona et al., 2016).

At the finer taxonomic level, we observed the predominant existence of the family *Rhodobacteraceae* throughout the investigation, which agrees with the findings of an earlier study (Cardona et al., 2016). The observed higher dominance of *Rhodobacteraceae* members might be attributed to carbon supplementation, a key characteristic of BFT systems. A recent study by Huang et al. (2022) observed that the addition of carbohydrates (e.g., glucose) facilitates *Rhodobacteraceae* growth in BFT systems. In our study, the abundance of the *Rhodobacteraceae* family was about 3 times higher (>39% mean abundance) during the initial culture stages (TAS1–TAS3) than in the late stages (<11% mean abundance during TAS4–TAS10), suggesting a potential role of this taxon in shrimp establishment and maintenance of shrimp health. Several *Rhodobacteraceae* members are known to synthesize vitamin B12, which may support shrimp growth (Sañudo-Wilhelmy et al., 2014).

Several characteristics of *Rhodobacteraceae* make this group a suitable candidate for probiotic application in aquaculture systems. For instance, certain *Rhodobacteraceae* members (e.g., genus *Ruegeria* and *Phaeobacter*) produce tropodithietic acid, which has wide-spectrum antagonistic potential against pathogenic *Vibrio* species such as *Vibrio anguillarum* and thus could reduce larval mortality (Porsby et al., 2008). In fact, a member (*Phaeobacter inhibens*) of this group has proven to be a safe-to-use probiotic in aquaculture (Sonnenschein et al., 2020). Besides their probiotic potential, several *Rhodobacteraceae* members have been reported to possess putative ammonia monooxygenase enzymes, which might support heterotrophic ammonia removal (Crossman et al., 1997). Another abundant family, *Flavobacteriaceae*, excels at decomposing diverse macromolecules such as cellulose and chitin (Mann et al., 2013), which may be profitable in degrading excess feed and shrimp excreta and thus improving rearing water quality (Williams et al., 2013).

At the genus level, rearing water contained several halophilic heterotrophic nitrifying bacteria, such as *Halomonas*, *Pseudoalteromonas*, and *Pseudomonas*, which are known to oxidize higher ammonia concentrations in saline environments (Chankaew et al., 2017). The abundance of these genera in our study differed from those detected in *L. vannamei* earthen pond water by Sombatjinda et al. (2011), who observed a higher abundance of several bacterial genera such as *Flavobacterium*, *Synechococcus*, and *Burkholderia*, as well as autotrophic nitrifiers (e.g., *Nitrobacter*, *Nitrosomonas*, and *Nitrosospira*). The observed disparity may be due to the difference in salinity, which varied from 2 to 10 PSU in the earlier study to 30–35 PSU in our study. The rearing water of aquaculture systems has often been shown to contain potentially pathogenic bacterial genera such as *Vibrio*, *Aeromonas*, *Photobacterium*, *Pseudomonas*, *Candidatus Bacilloplasma*, and *Flavobacterium* (Hou et al., 2017). Among these genera, the most notable pathogens are *Vibrio* spp. and thus quantifying their presence was prioritized in the present study. The existence of *Vibrio* spp. was limited (a minor abundance) in

our investigation, which is consistent with earlier similar studies conducted in BFT aquaculture systems (Hoang et al., 2020). The observed low density of *Vibrio* spp. might be due to the water quality and/or higher prevalence of probiotic bacterioplankton taxa that could have restricted their proliferation. Generally, the dominant bacterioplankton members of BFT systems (e.g., *Proteobacteria* and *Bacteroidetes*) compete for food and niche space, limiting the prevalence of pathogens, including *Vibrio* spp. (Wei et al., 2016).

Several antimicrobial agents including antibiotics are being used to control aquaculture pathogens. However, their extensive and indiscriminate use has given rise to the emergence of antibiotic-resistant bacteria and antibiotic-resistant genes in aquaculture production systems (Huang et al., 2015). Due to the higher risk associated with their use, there is growing awareness and strict regulations around the use of antibiotics (Defoirdt et al., 2011). At the same time, this scenario demands effective and environmentally friendly strategies for sustainable aquaculture development. Currently, because of their involvement in shrimp health, water quality, and protection against pathogens, probiotics are considered promising alternatives to antibiotics (Hoseinifar et al., 2018).

Interestingly, we observed a culture stage-specific fluctuation in the abundance of those bacterioplankton groups that could be vital for the effective performance of a BFT system. For instance, *Actinobacteria*, identified as a biomarker taxon during both the middle and late stages of culture, has been frequently described as playing several crucial roles in aquaculture (van der Heul et al., 2018). *Actinobacteria* are recommended as promising candidates for use as probiotics in aquaculture due to several characteristics, such as their ability to degrade macromolecules (e.g., protein and starch) and combat aquaculture pathogens (Das et al., 2008). Previous studies have shown that feed supplemented with members of *Actinobacteria* (e.g., genus *Microbacterium*), could provide health benefits to shrimp by promoting growth and limiting the occurrence of diseases (Das et al., 2008; Skjermo et al., 2015). Additionally, *Actinobacteria* are considered essential for maintaining gut homeostasis (Binda et al., 2018).

Members of the phylum *Chloroflexi* dominated rearing water microbiota in the late-stage of culture. The proportion of *Chloroflexi* members has also been reported to increase with the growth of a commercial fish, *Lateolabrax maculatus* (Duan et al., 2021), indicating that these bacteria might be beneficial in the utilization of accumulated organic matter. Furthermore, certain members of the phylum *Chloroflexi* (e.g., genus *Nitrolancetus*) are known to possess a nitrite oxidoreductase and thus may contribute to the nitrification process by catalyzing nitrite oxidation (Sorokin et al., 2012). Similarly, another biomarker taxon identified during the middle-stage of culture was *Proteobacteria*, whose abundance decreased with increasing culture stages. *Proteobacteria* is a multifunctional phylum in the biofloc-based aquaculture system that possesses the ability to remove nitrogen and degrade organic matter (Cottrell and Kirchman, 2000). In support of our findings, a prior study by Xu et al. (2021) reported that *Planctomycetes* and *Actinobacteria* were biomarker taxa for indoor aquaculture systems. Overall, the LEfSe analysis showed a stage-specific abundance of several beneficial bacterioplankton groups that contribute either to shrimp health or water quality.

In conclusion, we investigated the physicochemical properties and bacterioplankton community of rearing water in a BFT-based *L. vannamei* aquaculture system. Considering the overall performance, the studied BFT system in this study represented a successful and super-intensive *L. vannamei* culture. Our study uncovered the plausible factors shaping the structural composition of the rearing water microbiome, which may help in maintaining rearing water quality and mitigating the occurrence of bacterial diseases in aquaculture systems. Based on our findings, it is reasonable to postulate that shrimp health and production in a BFT-based aquaculture system are largely reliant on rearing water microbiota, besides the shrimp's own intestinal microbiota. In future studies, it would certainly be interesting to illustrate microbial functional processes in aquaculture systems using shotgun metagenomic and transcriptomic approaches.

Data availability statement

The pyrosequencing datasets generated for this study are available in the Sequence Read Archive (SRA) database of the National Center for Biotechnology Information (NCBI) under accession numbers SRR20075654–SRR20075663.

Author contributions

S-KK, JS, SK, and J-CC conceptualized and designed the study. S-KK, JS, SK, and I-KJ collected the rearing water samples and analyzed the physicochemical parameters. S-KK, JS, and SK prepared nucleic acid samples for pyrosequencing. MR and IK performed bioinformatics analyses and interpreted the results. J-CC and IK supervised the study. MR, IK, and J-CC wrote the manuscript. All authors contributed to the article and approved the submitted version.

Funding

This study was supported by Mariculture Technology Development Using Biofloc of the National Institute of Fisheries Science (NIFS), Incheon (R2022014); by Korea Institute of Marine Science and Technology Promotion (KIMST) funded from the Ministry of Oceans and Fisheries (PM62830); and by the Mid-Career Research Program through the National Research Foundation (NRF) funded by the Ministry of Sciences and ICT (NRF-2022R1A2C3008502).

Conflict of interest

The authors declare that the research was conducted in the absence of any commercial or financial relationships that could be construed as a potential conflict of interest.

Publisher's note

All claims expressed in this article are solely those of the authors and do not necessarily represent those of their affiliated organizations, or those of the publisher, the editors and the reviewers. Any product that may be evaluated in this article, or claim that may be made by its manufacturer, is not guaranteed or endorsed by the publisher.

Supplementary material

The Supplementary material for this article can be found online at: https://www.frontiersin.org/articles/10.3389/fmicb.2022.995699/full#supplementary-material

References

Ahmad, I., Rani, A. B., Verma, A. K., and Maqsood, M. (2017). Biofloc technology: an emerging avenue in aquatic animal healthcare and nutrition. *Aquacult. Int.* 25, 1215–1226. doi: 10.1007/s10499-016-0108-8

Alfiansah, Y. R., Hassenrück, C., Kunzmann, A., Taslihan, A., Harder, J., and Gärdes, A. A. M. (2018). Bacterial abundance and community composition in pond water from shrimp aquaculture systems with different stocking densities. *Front. Microbiol.* 9:2457. doi: 10.3389/fmicb.2018.02457

Anderson, J. L., Valderrama, D., and Jory, D. (2016). "Shrimp production review," in *Global Aquaculture Alliance: Presentation Global Aquaculture Production Data and Analysis* (Guangzhou: GOAL), 1–50.

Andrews, S. (2010). FastQC: A quality control tool for high throughput sequence data. Available at: http://www.bioinformatics.babraham.ac.uk/projects/fastqc

Avnimelech, Y. (2007). Feeding with microbial flocs by tilapia in minimal discharge bioflocs technology ponds. *Aquaculture* 264, 140–147. doi: 10.1016/j.aquaculture.2006.11.025

Baird, R. B., Eaton, A. D., and Clesceri, L. S. (2012). *Standard Methods for the Examination of water and Wastewater*. ed. E. W. Rice, *Vol. 10.* (Washington, DC: American public health association).

Binda, C., Lopetuso, L. R., Rizzatti, G., Gibiino, G., Cennamo, V., and Gasbarrini, A. (2018). Actinobacteria: a relevant minority for the maintenance of gut homeostasis. *Dig. Liver Dis.* 50, 421–428. doi: 10.1016/j.dld.2018.02.012

Boardman, G. D., Starbuck, S. M., Hudgins, D. B., Li, X., and Kuhn, D. D. (2004). Toxicity of ammonia to three marine fish and three marine invertebrates. *Environ. Toxicol.* 19, 134–142. doi: 10.1002/tox.20006

Bolinches, J., Romalde, J. L., and Toranzo, A. E. (1988). Evaluation of selective media for isolation and enumeration of *vibrios* from estuarine waters. *J. Microbiol. Methods* 8, 151–160. doi: 10.1016/0167-7012(88)90016-4

Boone, L. (1931). Anomuran, macruran Crustacea from Panama and Canal Zone. *Bull. Am. Mus. Nat. Hist.* 63, 137–189.

Brandão, H., Xavier, Í. V., Santana, G. K. K., Santana, H. J. K., Krummenauer, D., and Wasielesky, W. (2021). Heterotrophic versus mixed BFT system: impacts on water use, suspended solids production and growth performance of *Litopenaeus vannamei*. *Aquac. Eng.* 95:102194. doi: 10.1016/j.aquaeng.2021.102194

Buchan, A., LeCleir, G. R., Gulvik, C. A., and González, J. M. (2014). Master recyclers: features and functions of bacteria associated with phytoplankton blooms. *Nat. Rev. Microbiol.* 12, 686–698. doi: 10.1038/nrmicro3326

Caporaso, J. G., Kuczynski, J., Stombaugh, J., Bittinger, K., Bushman, F. D., Costello, E. K., et al. (2010). QIIME allows analysis of high-throughput community sequencing data. *Nat. Methods* 7, 335–336. doi: 10.1038/nmeth.f.303

Cardona, E., Gueguen, Y., Magré, K., Lorgeoux, B., Piquemal, D., and Pierrat, F. (2016). Bacterial community characterization of water and intestine of the shrimp *Litopenaeus stylirostris* in a biofloc system. *BMC Microbiol.* 16:157. doi: 10.1186/s12866-016-0770-z

Chankaew, S., O-thong, S., and Songnoi, Y. (2017). Nitrogen removal efficiency of salt-tolerant heterotrophic nitrifying bacteria. *Chiang Mai J. Sci.* 44, 1–10.

Correia, E. S., Wilkenfeld, J. S., Morris, T. C., Wei, L., Prangnell, D. I., and Samocha, T. M. (2014). Intensive nursery production of the Pacific white shrimp *Litopenaeus vannamei* using two commercial feeds with high and low protein content in a biofloc-dominated system. *Aquac. Eng.* 59, 48–54. doi: 10.1016/j.aquaeng.2014.02.002

Cottrell, M. T., and Kirchman, D. L. (2000). Natural assemblages of marine proteobacteria and members of the *Cytophaga-Flavobacter* cluster consuming low- and high-molecular-weight dissolved organic matter. *Appl. Environ. Microbiol.* 66, 1692–1697. doi: 10.1128/AEM.66.4.1692-1697.2000

Crab, R., Defoirdt, T., Bossier, P., and Verstraete, W. (2012). Biofloc technology in aquaculture: beneficial effects and future challenges. *Aquaculture* 356-357, 351–356. doi: 10.1016/j.aquaculture.2012.04.046

Crossman, L. C., Moir, J. W., Enticknap, J. J., Richardson, D. J., and Spiro, S. (1997). Heterologous expression of heterotrophic nitrification genes. *Microbiology* 143, 3775–3783. doi: 10.1099/00221287-143-12-3775

Das, S., Ward, L. R., and Burke, C. (2008). Prospects of using marine actinobacteria as probiotics in aquaculture. *Appl. Microbiol. Biotechnol.* 81, 419–429. doi: 10.1007/s00253-008-1731-8

De Schryver, P., Crab, R., Defoirdt, T., Boon, N., and Verstraete, W. (2008). The basics of bioflocs technology: the added value for aquaculture. *Aquaculture* 277, 125–137. doi: 10.1016/j.aquaculture.2008.02.019

Defoirdt, T., Sorgeloos, P., and Bossier, P. (2011). Alternatives to antibiotics for the control of bacterial disease in aquaculture. *Curr. Opin. Microbiol.* 14, 251–258. doi: 10.1016/j.mib.2011.03.004

Deng, M., Chen, J., Gou, J., Hou, J., Li, D., and He, X. (2018). The effect of different carbon sources on water quality, microbial community and structure of biofloc systems. *Aquaculture* 482, 103–110. doi: 10.1016/j.aquaculture.2017.09.030

DeSantis, T. Z., Hugenholtz, P., Larsen, N., Rojas, M., Brodie, E. L., Keller, K., et al. (2006). Greengenes, a chimera-checked 16S rRNA gene database and workbench compatible with ARB. *Appl. Environ. Microbiol.* 72, 5069–5072. doi: 10.1128/AEM.03006-05

Duan, Y., Xiong, D., Li, Y., Ding, X., Dong, H., Wang, W., et al. (2021). Changes in the microbial communities of the rearing water, sediment and gastrointestinal tract of *Lateolabrax maculatus* at two growth stages. *Aquac. Rep.* 20:100742. doi: 10.1016/j.aqrep.2021.100742

Ebeling, J. M., Timmons, M. B., and Bisogni, J. J. (2006). Engineering analysis of the stoichiometry of photoautotrophic, autotrophic and heterotrophic removal of ammonia nitrogen in aquaculture systems. *Aquaculture* 257, 346–358. doi: 10.1016/j.aquaculture.2006.03.019

Fan, L., and Li, Q. X. (2019). Characteristics of intestinal microbiota in the Pacific white shrimp *Litopenaeus vannamei* differing growth performances in the marine cultured environment. *Aquaculture* 505, 450–461. doi: 10.1016/j.aquaculture.2019.02.075

FAO, Food Agriculture Organization of the United Nations (2018) The state of world fisheries and aquaculture 2018—meeting the sustainable development goals. CC BY-NC-SA 3.0 IGO.

Flegel, T. W. (2019). A future vision for disease control in shrimp aquaculture. *World Aquacult. Soc.* 50, 249–266. doi: 10.1111/jwas.12589

Gatesoupe, F. J. (1999). The use of probiotics in aquaculture. *Aquaculture* 180, 147–165. doi: 10.1016/S0044-8486(99)00187-8

Gutierrez-Wing, M. T., and Malone, R. F. (2006). Biological filters in aquaculture: trends and research directions for freshwater and marine applications. *Aquaculture* 34, 163–171. doi: 10.1016/j.aquaeng.2005.08.003

Hoang, M. N., Nguyen, P. N., and Bossier, P. (2020). Water quality, animal performance, nutrient budgets and microbial community in the biofloc-based polyculture system of white shrimp, *Litopenaeus vannamei* and gray mullet, *Mugil cephalus*. *Aquaculture* 515:734610. doi: 10.1016/j.aquaculture.2019.734610

Hoseinifar, S. H., Sun, Y. Z., Wang, A., and Zhou, Z. (2018). Probiotics as means of diseases control in aquaculture, a review of current knowledge and future perspectives. *Front. Microbiol.* 9:2429. doi: 10.3389/fmicb.2018.02429

Hou, D., Huang, Z., Zeng, S., Liu, J., Wei, D., Deng, X., et al. (2017). Environmental factors shape water microbial community structure and function

in shrimp cultural enclosure ecosystems. *Front. Microbiol.* 8:2359. doi: 10.3389/fmicb.2017.02359

Huang, Z., Chen, Y., Weng, S., Lu, X., Zhong, L., Fan, W., et al. (2016). Multiple bacteria species were involved in hepatopancreas necrosis syndrome (HPNS) of *Litopenaeus vannamei*. *Acta Sci. Nat. Univ.* 55, 1–11. doi: 10.13471/j.cnki.acta.snus.2016.01.001

Huang, L., Guo, H., Chen, C., Huang, X., Chen, W., Bao, F., et al. (2020). The bacteria from large-sized bioflocs are more associated with the shrimp gut microbiota in culture system. *Aquaculture* 523:735159. doi: 10.1016/j.aquaculture.2020.735159

Huang, L., Guo, H., Liu, Z., Chen, C., Wang, K., Huang, X., et al. (2022). Contrasting patterns of bacterial communities in the rearing water and gut of *Penaeus vannamei* in response to exogenous glucose addition. *Mar. Life sci. Technol.* 4, 222–236. doi: 10.1007/s42995-021-00124-9

Huang, Y., Zhang, L., Tiu, L., and Wang, H. H. (2015). Characterization of antibiotic resistance in commensal bacteria from an aquaculture ecosystem. *Front. Microbiol.* 6:914. doi: 10.3389/fmicb.2015.00914

Kim, S.-K., Guo, Q., and Jang, I. K. (2015). Effect of biofloc on the survival and growth of the postlarvae of three penaeids (*Litopenaeus vannamei*, *Fenneropenaeus chinensis*, and *Marsupenaeus japonicus*) and their biofloc feeding efficiencies, as related to the morphological structure of the third maxilliped. *J. Crustac. Biol.* 35, 41–50. doi: 10.1163/1937240X-00002304

Kim, Y. S., Kim, S. E., Kim, S. J., Jung, H. K., Park, J., Jeon, Y. J., et al. (2021). Effects of wheat flour and culture period on bacterial community composition in digestive tracts of *Litopenaeus vannamei* and rearing water in biofloc aquaculture system. *Aquaculture* 531:735908. doi: 10.1016/j.aquaculture.2020.735908

Kim, S.-K., Pang, Z., Seo, H. C., Cho, Y. R., Samocha, T., and Jang, I. K. (2014). Effect of bioflocs on growth and immune activity of Pacific white shrimp, *Litopenaeus vannamei* postlarvae. *Aquacult. Res.* 45, 362–371. doi: 10.1111/are.12319

Krummenauer, D., Cavalli, R. O., Ballester, E. L., and Wasielesky, W. Jr. (2010). Feasibility of pacific white shrimp *Litopenaeus vannamei* culture in southern Brazil: effects of stocking density and a single or a double CROP management strategy in earthen ponds. *Aquacult. Res.* 41, 240–248. doi: 10.1111/j.1365-2109.2009.02326.x

Krummenauer, D., Peixoto, S., Cavalli, R. O., Poersch, L. H., and Wasielesky, W. Jr. (2011). Superintensive culture of white shrimp, *Litopenaeus vannamei*, in a biofloc technology system in southern Brazil at different stocking densities. *J. World Aquacult. Soc.* 42, 726–733. doi: 10.1111/j.1749-7345.2011.00507.x

Kuhn, D. D., Smith, S. A., Boardman, G. D., Angier, M. W., Marsh, L., and Flick, G. J. Jr. (2010). Chronic toxicity of nitrate to Pacific white shrimp, *Litopenaeus vannamei*: impacts on survival, growth, antennae length, and pathology. *Aquaculture* 309, 109–114. doi: 10.1016/j.aquaculture.2010.09.014

Lin, Y.-C., and Chen, J. C. (2003). Acute toxicity of nitrite on *Litopenaeus vannamei* (Boone) juveniles at different salinity levels. *Aquaculture* 224, 193–201. doi: 10.1016/S0044-8486(03)00220-5

Losordo, T. M., and Hobbs, A. O. (2000). Using computer spreadsheets for water flow and biofilter sizing in recirculating aquaculture production systems. *Aquac. Eng.* 23, 95–102. doi: 10.1016/S0144-8609(00)00048-0

Lozupone, C., and Knight, R. (2005). UniFrac: a new phylogenetic method for comparing microbial communities. *Appl. Environ. Microbiol.* 71, 8228–8235. doi: 10.1128/AEM.71.12.8228-8235.2005

Mann, A. J., Hahnke, R. L., Huang, S., Werner, J., Xing, P., Barbeyron, T., et al. (2013). The genome of the alga-associated marine flavobacterium *Formosa agariphila* KMM 3901^{T} reveals a broad potential for degradation of algal polysaccharides. *Appl. Environ. Microbiol.* 79, 6813–6822. doi: 10.1128/AEM.01937-13

Martin, M. (2011). Cutadapt removes adapter sequences from high-throughput sequencing reads. *EMBnet J.* 17, 10–12. doi: 10.14806/ej.17.1.200

Nootong, K., Pavasant, P., and Powtongsook, S. (2011). Effects of organic carbon addition in controlling inorganic nitrogen concentrations in a biofloc system. *J. World Aquac. Soc.* 42, 339–346. doi: 10.1111/j.1749-7345.2011.00472.x

Páez-Osuna, F., Gracia, A., Flores-Verdugo, F., Lyle-Fritch, L. P., Alonso-Rodríguez, R., Roque, A., et al. (2003). Shrimp aquaculture development and the environment in the Gulf of California ecoregion. *Mar. Pollut. Bull.* 46, 806–815. doi: 10.1016/S0025-326X(03)00107-3

Panigrahi, A., Sundaram, M., Chakrapani, S., Rajasekar, S., Syama Dayal, J., and Chavali, G. (2019). Effect of carbon and nitrogen ratio (C: N) manipulation on the production performance and immunity of Pacific white shrimp *Litopenaeus vannamei* (Boone, 1931) in a biofloc-based rearing system. *Aquacult. Res.* 50, 29–41. doi: 10.1111/are.13857

Porsby, C. H., Nielsen, K. F., and Gram, L. (2008). *Phaeobacter* and *Ruegeria* species of the *Roseobacter* clade colonize separate niches in a danish turbot (*Scophthalmus maximus*) - rearing farm and antagonize *vibrio anguillarum* under different growth conditions. *Appl. Environ. Microbiol.* 74, 7356–7364. doi: 10.1128/AEM.01738-08

Porter, K. G., and Feig, Y. S. (1980). The use of DAPI for identifying and counting aquatic microflora1. *Limnol. Oceanogr.* 25, 943–948. doi: 10.4319/lo.1980.25.5.0943

Rajeev, M., Sushmitha, T. J., Aravindraja, C., Toleti, S. R., and Pandian, S. K. (2021). Thermal discharge-induced seawater warming alters richness, community composition and interactions of bacterioplankton assemblages in a coastal ecosystem. *Sci. Rep.* 11, 17341–17313. doi: 10.1038/s41598-021-96969-2

Rajeev, M., Sushmitha, T. J., Toleti, S. R., and Pandian, S. K. (2019). Culture dependent and independent analysis and appraisal of early stage biofilm-forming bacterial community composition in the southern coastal seawater of India. *Sci. Total Environ.* 666, 308–320. doi: 10.1016/j.scitotenv.2019.02.171

Ray, A. (2012). "Biofloc technology for super-intensive shrimp culture," in *Biofloc Technology-a Practical guide book*. ed. Y. Avnimelech (Louisiana, USA: The World Aquaculture Society), 167–188.

Rout, P. R., Bhunia, P., and Dash, R. R. (2017). Simultaneous removal of nitrogen and phosphorous from domestic wastewater using Bacillus cereus GS-5 strain exhibiting heterotrophic nitrification, aerobic denitrification and denitrifying phosphorous removal. *Bioresour. Technol.* 244, 484–495. doi: 10.1016/j.biortech.2017.07.186

Samocha, T. M., Patnaik, S., Speed, M., Ali, A. M., Burger, J. M., Almeida, R. V., et al. (2007). Use of molasses as carbon source in limited discharge nursery and grow-out systems for *Litopenaeus vannamei*. *Aquac. Eng.* 36, 184–191. doi: 10.1016/j.aquaeng.2006.10.004

Sañudo-Wilhelmy, S. A., Gómez-Consarnau, L., Suffridge, C., and Webb, E. A. (2014). The role of B vitamins in marine biogeochemistry. *Ann. Rev. Mar. Sci.* 6, 339–367. doi: 10.1146/annurev-marine-120710-100912

Segata, N., Izard, J., Waldron, L., Gevers, D., Miropolsky, L., Garrett, W. S., et al. (2011). Metagenomic biomarker discovery and explanation. *Genome Biol.* 12, R60–R18. doi: 10.1186/gb-2011-12-6-r60

Seidman, E. R., and Lawrence, A. L. (1985). Growth. Feed digestibility, and proximate body composition of juvenile *Penaeus vannamei* and *Penaeus monodon* grown at different dissolved oxygen levels. *J. World Aquac. Soc.* 16, 333–346. doi: 10.1111/j.1749-7345.1985.tb00214.x

Skjermo, J., Bakke, I., Dahle, S. W., and Vadstein, O. (2015). Probiotic strains introduced through live feed and rearing water have low colonizing success in developing Atlantic cod larvae. *Aquaculture* 438, 17–23. doi: 10.1016/j.aquaculture.2014.12.027

Sombatjinda, S., Boonapatcharoen, N., Ruengjitchatchawalya, M., Wantawin, C., Withyachumnarnkul, B., and Techkarnjanaruk, S. (2011). Dynamics of microbial communities in an earthen shrimp pond during the shrimp growing period. *Environ. Nat. Resour. Res.* 1, 171–180. doi: 10.5539/enrr.v1n1p171

Sonnenschein, E. C., Jimenez, G., Castex, M., and Gram, L. (2020). The *Roseobacter*-group bacterium *Phaeobacter* as a safe probiotic solution for aquaculture. *Appl. Environ. Microbiol.* 87:e0258120. doi: 10.1128/AEM.02581-20

Sorokin, D. Y., Lücker, S., Vejmelkova, D., Kostrikina, N. A., Kleerebezem, R., Rijpstra, W. I. C., et al. (2012). Nitrification expanded: discovery, physiology and genomics of a nitrite-oxidizing bacterium from the phylum Chloroflexi. *ISME J.* 6, 2245–2256. doi: 10.1038/ismej.2012.70

Sowers, A. D., Tomasso, J. R. Jr., Browdy, C. L., and Atwood, H. L. (2006). Production characteristics of *Litopenaeus vannamei* in low-salinity water augmented with mixed salts. *J. World Aquacult. Soc.* 37, 214–217. doi: 10.1111/j.1749-7345.2006.00030.x

Stein, L. Y. (2011). "Heterotrophic nitrification and nitrifier denitrification," in *Nitrification*. ed. B. B. Ward (Washington DC: IWA Publishing, ASM press), 95–114.

van der Heul, H. U., Bilyk, B. L., McDowall, K. J., Seipke, R. F., and van Wezel, G. P. (2018). Regulation of antibiotic production in *Actinobacteria*: new perspectives from the post-genomic era. *Nat. Prod. Rep.* 35, 575–604. doi: 10.1039/c8np00012c

Walker, P. J., and Winton, J. R. (2010). Emerging viral diseases of fish and shrimp. *Vet. Res.* 41:51. doi: 10.1051/vetres/2010022

Wasielesky, W., Atwood, H., Stokes, A., and Browdy, C. L. (2006). Effect of natural production in a zero-exchange suspended microbial floc-based super-intensive culture system for white shrimp *Litopenaeus vannamei*. *Aquaculture* 258, 396–403. doi: 10.1016/j.aquaculture.2006.04.030

Wei, Y., Liao, S. A., and Wang, A. L. (2016). The effect of different carbon sources on the nutritional composition, microbial community and structure of bioflocs. *Aquaculture* 465, 88–93. doi: 10.1016/j.aquaculture.2016.08.040

Williams, T. J., Wilkins, D., Long, E., Evans, F., DeMaere, M. Z., Raftery, M. J., et al. (2013). The role of planktonic *Flavobacteria* in processing algal organic matter in coastal East Antarctica revealed using metagenomics and metaproteomics. *Environ. Microbiol.* 15, 1302–1317. doi: 10.1111/1462-2920.12017

Wyban, J., Walsh, W. A., and Godin, D. M. (1995). Temperature effects on growth, feeding rate and feed conversion of the Pacific white shrimp (*Penaeus vannamei*). *Aquaculture* 138, 267–279. doi: 10.1016/0044-8486(95)00032-1

Xiong, J., Dai, W., Qiu, Q., Zhu, J., Yang, W., and Li, C. (2018). Response of host–bacterial colonization in shrimp to developmental stage, environment and disease. *Mol. Ecol.* 27, 3686–3699. doi: 10.1111/mec.14822

Xiong, J., Wang, K., Wu, J., Qiuqian, L., Yang, K., Qian, Y., et al. (2015). Changes in intestinal bacterial communities are closely associated with shrimp disease severity. *Appl. Microbiol. Biotechnol.* 99, 6911–6919. doi: 10.1007/s00253-015-6632-z

Xu, W., Xu, Y., Su, H., Hu, X., Xu, Y., Li, Z., et al. (2021). Production performance, inorganic nitrogen control and bacterial community characteristics in a controlled biofloc-based system for indoor and outdoor super-intensive culture of Litopenaeus vannamei. *Aquaculture* 531, 1–11. doi: 10.1016/j.aquaculture.2020.735749

Zeng, S., Huang, Z., Hou, D., Liu, J., Weng, S., and He, J. (2017). Composition, diversity and function of intestinal microbiota in pacific white shrimp (*Litopenaeus vannamei*) at different culture stages. *PeerJ* 5:e3986. doi: 10.7717/peerj.3986

Zeng, S., Khoruamkid, S., Kongpakdee, W., Wei, D., Yu, L., Wang, H., et al. (2020). Dissimilarity of microbial diversity of pond water, shrimp intestine and sediment in Aquamimicry system. *AMB Express* 10, 1–11. doi: 10.1186/s13568-020-01119-y

Zhang, M., Pan, L., Huang, F., Gao, S., Su, C., Zhang, M., et al. (2019). Metagenomic analysis of composition, function and cycling processes of microbial community in water, sediment and effluent of *Litopenaeus vannamei* farming environments under different culture modes. *Aquaculture* 506, 280–293. doi: 10.1016/j.aquaculture.2019.03.038

Zheng, Y., Yu, M., Liu, J., Qiao, Y., Wang, L., Li, Z., et al. (2017). Bacterial community associated with healthy and diseased Pacific white shrimp (*Litopenaeus vannamei*) larvae and rearing water across different growth stages. *Front. Microbiol.* 8:1362. doi: 10.3389/fmicb.2017.01362

frontiers | Frontiers in Microbiology

TYPE Original Research
PUBLISHED 30 September 2022
DOI 10.3389/fmicb.2022.1016418

OPEN ACCESS

EDITED BY
Shan He,
Ningbo University, China

REVIEWED BY
Songcan Chen,
University of Vienna, Austria
Alexander Galushko,
Agrophysical Research Institute, Russia

*CORRESPONDENCE
Alexis Fonseca
afonseca@bio.au.dk
Victor A. Gallardo
vagallar@udec.cl

SPECIALTY SECTION
This article was submitted to Aquatic Microbiology, a section of the journal Frontiers in Microbiology

RECEIVED 10 August 2022
ACCEPTED 16 September 2022
PUBLISHED 30 September 2022

CITATION
Fonseca A, Espinoza C, Nielsen LP, Marshall IPG and Gallardo VA (2022) Bacterial community of sediments under the Eastern Boundary Current System shows high microdiversity and a latitudinal spatial pattern. *Front. Microbiol.* 13:1016418. doi: 10.3389/fmicb.2022.1016418

Bacterial community of sediments under the Eastern Boundary Current System shows high microdiversity and a latitudinal spatial pattern

Alexis Fonseca[1]*, Carola Espinoza[2], Lars Peter Nielsen[1], Ian P. G. Marshall[1] and Victor A. Gallardo[2]*

[1]Center for Electromicrobiology, Department of Biology, Aarhus University, Aarhus, Denmark, [2]Department of Oceanography, University of Concepción, Concepción, Chile

The sediments under the Oxygen Minimum Zone of the Eastern Boundary Current System (EBCS) along Central-South Peru and North-Central Chile, known as Humboldt Sulfuretum (HS), is an organic-matter-rich benthic habitat, where bacteria process a variety of sulfur compounds under low dissolved-oxygen concentrations, and high sulfide and nitrate levels. This study addressed the structure, diversity and spatial distribution patterns of the HS bacterial community along Northern and South-Central Chile using 16S rRNA gene amplicon sequencing. The results show that during the field study period, the community was dominated by sulfur-associated bacteria. Indeed, the most abundant phylum was *Desulfobacterota*, while Sva0081 sedimentary group, of the family *Desulfosarcinaceae* (the most abundant family), which includes sulfate-reducer and H_2 scavenger bacteria, was the most abundant genus. Furthermore, a spatial pattern was unveiled along the study area to which the family *Desulfobulbaceae* contributed the most to the spatial variance, which encompasses 42 uncharacterized amplicon sequence variants (ASVs), three assigned to *Ca*. Electrothrix and two to *Desulfobulbus*. Moreover, a very high microdiversity was found, since only 3.7% of the ASVs were shared among localities, reflecting a highly diverse and mature community.

KEYWORDS

sulfur bacteria, sulfuretum, OMZ, anoxic sediments, microdiversity, bacterial community, *Desulfobulbaceae*, amplicon sequencing

Introduction

In the Eastern Boundary Current System (EBCS) off the coasts of Chile and Peru, one of the world's largest subsurface sulfidic benthic system occurs: the "Humboldt Sulfuretum"' (HS) (Gallardo et al., 2016). While likely quite widespread in primeval oceans, *ca*. 3.5 Ga ago (Van Kranendonk et al., 2003; Ueno et al., 2008; Wacey et al., 2011; Schopf et al., 2017), these systems are rare and of limited extent in today's Earth oceans. However, notwithstanding their reduced extension, *ca*. 1.15 million km^2 (Helly and Levin, 2004), their contribution to the productivity of the world's oceans is disproportionately high. In this thus rather rare, nonetheless significant biome, benthic bacteria process a variety of sulfur compounds under the absence or very low levels of dissolved oxygen, but rather high levels of reduced sulfur compounds, nitrate, and phosphate (Fossing et al., 1995; Høgslund et al., 2008; Gallardo et al., 2013a).

In similar settings, i.e., sulfide-rich/oxygen-deficient seafloor and subsea sediments, bacterial communities are characterized by anaerobic bacteria, such as sulfate-reducing anaerobic forms and fermenters of *Chloroflexi*, *Proteobacteria*, *Firmicutes*, or *Candidatus* Atribacteria as well as methanogenic, and methanotrophic archaea (Orsi, 2018). These communities are thus well-differentiated from those living in oxic sediments (Zinger et al., 2011; Bienhold et al., 2016). Under sulfidic conditions, the availability of electron donors and acceptors, geochemical and sedimentological properties control the structure of bacterial communities (Fry et al., 2008; Hoshino et al., 2020). Furthermore, lithotrophic, and mostly autotrophic, sulfur-oxidizing bacteria (SOB) are conspicuous inhabitants of these environments, i.e., the "megabacteria" *Cand*. Marithioploca araucae (Salman et al., 2011), and the "macrobacteria" *Cand*. Venteria Ishoeyi (Fonseca et al., 2017), which generate extensive mats in the HS (Gallardo, 1977; Maier and Gallardo, 1984; Schulz et al., 1996; Ferdelman et al., 1997).

Previous work in the HS, using 16S rRNA amplicon sequencing, focused on the diversity of the bacterial community in selected areas of this system. Thereby, following a combination of the principles that sustain the Thienemann-Sanders time-stability hypothesis, Gallardo et al. (2016) suggested that the HS sublitoral bacterial community inhabiting the Central-South distribution area (~36°s), corresponds to an evolutionarily mature, "biologically accommodated" community, a condition that is characterized by the lack of statistically dominant species (OTUs). Moreover, recent work in the Northern Mejillones Bay, located in the permanent mid-water oxygen-deficient upwelling system off Northern Chile, reports that members of *Anaerolineaceae*, *Thiotrichaceae*, *Desulfobulbaceae*, *Desulfarculaceae*, and *Bacteroidales* play an important role in the differentiation of sampling points in this area (Zárate et al., 2021).

The present work is a contribution to the knowledge on the structure and diversity of the HS bacterial community through sediment samples obtained off the coast of Chile from five localities distributed between *ca*. −20 and −36.10′, using 16S rRNA gene amplicon sequencing.

Materials and methods

Sediment core samples

Off the coast of Chile sediment core samples were collected at approximately 50 and 100 m depth at five latitudes from −20 to −36 (**Table 1**), namely off Iquique (IQQ), Antofagasta (ANTF), Caldera (CAL), Valparaíso (VLP), and Concepcion (CCP) (**Figure 1A**). During samplings, the Northern IQQ, CAL, ANTF, and VLP substrates were evidently reduced and devoid of macrofauna, while at the Southern CCP station the scattered presence of polychetes and bivalves was noticeable.

Sampling was carried out from the small motorboats "Otilia" (CCP), "Antares" (IQQ), and various fishing boats (ANTF, CAL, and VLP), with a small handy gravity mono-corer. Samples were sub-sampled on board with the upper 5 cm of sediment transferred to sterile tubes and kept at 4°C until DNA extraction (<12 h later). In addition, dissolved oxygen, from overlying water, sediment redox potential (**Figures 1B,C**), overlying water redox potential (using Ag/AgCl as reference electrode), and temperature, were immediately measured with an Oakton P650 multi-parameter instrument. Porosity and total organic matter (TOM) (**Figure 1D**) were determined by the ignition method (Mook and Hoskin, 1982).

DNA extraction and sequencing

DNA extraction was carried out (in triplicate) from 0.5 g of the upper 5 cm of sediments using the Fast DNA Spin Kit for Soil (MP laboratories) and quantified using a Nanodrop ND1000. Next, at the Marine Biological Laboratory (BPC-MBL), Woods Hole, MA, USA, the v4v6 region of the 16S rRNA gene was amplified and sequenced using a 454 GS FLX Titanium sequencing platform, Details of sequencing technology are described in Huber et al. (2007) and Huse et al. (2008). Data and experiments are available under project code PRJNA251688 in the NCBI database. Reads were demultiplexed and barcodes were removed for submission.

Quality control and filtering reads

After sequencing, the single-end raw reads were assessed for quality control using the FastQC package version 0.11.9,[1]

1 https://www.bioinformatics.babraham.ac.uk/projects/fastqc/

TABLE 1 Metadata for the sampling points included in the study.

Season	Samples	Date*	Lat(S-)	Long (W-)	Depth (m)	Temp. °C	DO ml/L	Sediment** redox	Water redox	TOM%
Fall	S10_iqq50	14/05/2012	20°10,933	70°09,313	72	14	0.81	−300	−110	15.3
Fall	S9_iqq100	15/05/2012	20°10,531	70°10,964	97	13	0.96	−160	−8	20.2
Summer	S5_iqq50	13/01/2012	20°10,933	70°09,313	50	14.5	0.63	−280	−120	12.2
Summer	S6_iqq100	14/01/2012	20°10,531	70°10,964	100	14.1	0.4	−290	−135	21.5
Summer	S7_antf100	19/01/2012	23°37,489	70°25,481	100	16	0.16	−270	−77	25.8
Fall	S11_cal100	17/05/2012	27°01,753	70°50,921	105	13	0.54	−270	−65	15.8
Fall	S14_vlp100	12/05/2012	33°00,921	71°37,333	100	10	1.2	−118	165	12.7
Summer	S3_vlp50	09/01/2012	33°01,485	71°37,325	65	13.5	0.83	−100	80	11.1
Summer	S4_vlp100	10/01/2012	33°00,921	71°37,333	80	14.2	0.97	−100	34	11.6
Summer	S1_ccp50	14/12/2011	36°30,783	73°01,083	50	13.4	1.09	−85	18.4	14
Summer	S2_ccp100	15/12/2011	36°30,866	73°07,750	90	13.8	0.39	−120	10	7.6
Spring	S13_ccp50	29/09/2012	36°30,783	73°01,083	50	9	1.8	−96	8	17.5
Spring	S12_ccp100	29/09/2012	36°30,866	73°07,750	90	10	0.8	−78	37	19.2

Sampling points are as iqq, Iquique; antf, Antofagasta; cal, caldera; vlp, Valparaíso; ccp, Concepción, where the prefix is sample(S)-number and the suffix is depth (50/100). A total of 50 and 100 mean the depth in meters of the samples points. TOM is total organic matter. The redox potential of water and sediment were measured in millivolts (mV). *Date (d/m/y/). **The type of sediment in all samples was fine mud.

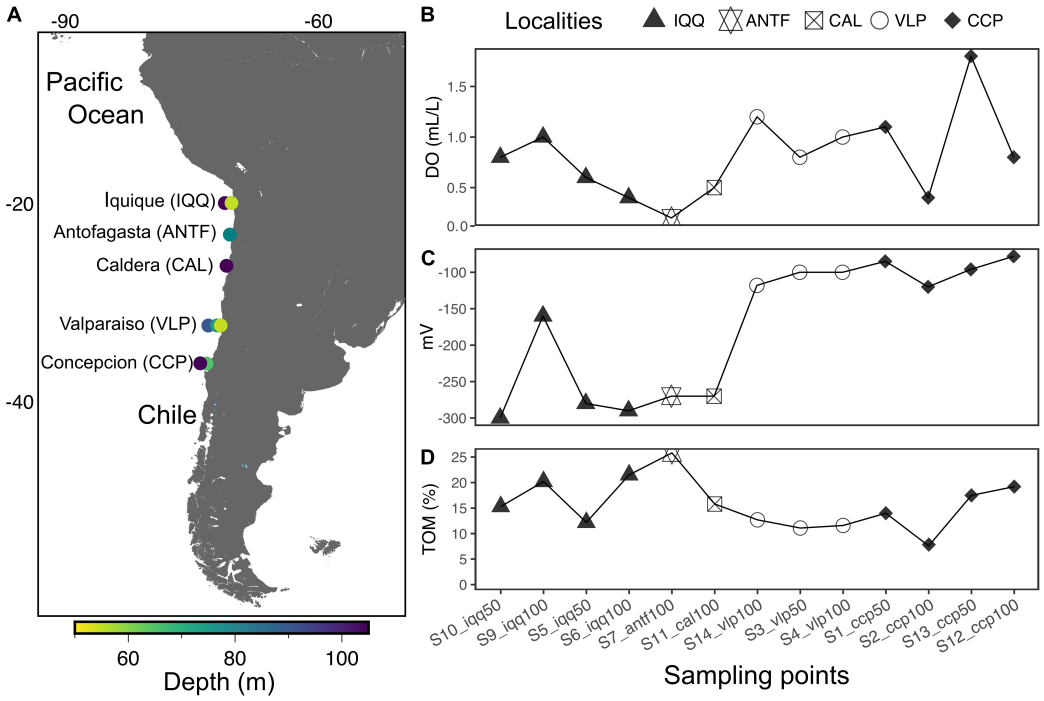

FIGURE 1
(A) Map of sampling points. **(B)** Dissolved oxygen (DO) of bottom water in ml/L. **(C)** Average redox potential of the first 5 cm of sediment, measured in millivolts (mV). **(D)** Average total organic matter (TOM) in percentage of the first 5 cm of sediment.

while the filtering and trimming were performed through the package PRINSEQ-lite version 0.20.4 (Schmieder and Edwards, 2011). Next, reads were subjected to denoising/chimera removal and clustering into amplicon sequence variants (ASVs) using the *denoise-single* method of the DADA2 package, version 1.14 (Callahan et al., 2016), as a plugin through the bioinformatics platform QIIME2, version 2019.10 (Bolyen et al., 2019). The ASV taxonomy assignment was performed through the feature-classifier classify-consensus-vsearch method in QIIME2, using the SILVA database 138.1 as

reference (Quast et al., 2012). Singletons were removed from the final ASV table.

Data analyses

The main data analysis was performed using the R software environment version 3.6.3. Thereby, the bacteria abundance table was rarefied to the smallest sample size (8,000 reads per sample), to perform diversity and ordering analysis, using the function rarefy_even_depth of the Phyloseq package (R package), version 1.30.0 (McMurdie and Holmes, 2013). This function uses the standard R sample function to resample from the abundance values in the ASVs table so that all samples have the same size.

The NMDS ordination analysis was performed using the function ordinate of the package Phyloseq version 1.30.0, using the unifrac and Bray-Curtis distance indices on the ASV abundance table. In particular, unifrac accesses the abundance table, but also to a phylogenetic tree, previously built using the representative reads through QIIME2 and the *de novo* phylogenetic tree creation method, phylogeny fasttree.

The Shannon diversity index and observed ASVs were obtained using the R package Vegan version 2.5-7 (Oksanen et al., 2013). The Analysis of Similarity (ANOSIM) test was used to validate the ordination results using the Vegan function anosim, which statistically tests whether there is a significant difference between two or more groups of sampling units. The statistical comparisons between factors and groups were performed through the Vegan function Adonis statistical test (Permutational Multivariate Analysis of Variance) and the R package ALDEx2 version 1.22.0 (Fernandes et al., 2014). In addition, the correlation and statistical significance between the environmental variables and the Bray-Curtis dissimilarity matrix of the abundance table were performed using a combination of the bioEnv function and the Vegan package's Mantel test. To evaluate the average percentage contribution of individual bacteria to the dissimilarity between groups in the Bray-Curtis dissimilarity matrices, the Vegan method of similarity percentage decomposition (SIMPER) was performed. The graphical representation of the data was achieved using ggplot2 version 3.3.3 (R package), Circos version 0.69-8 (Krzywinski et al., 2009), library Matplotlib from Python version 3.6, and the R package Metacoder version 0.3.4 (Foster et al., 2017).

Results

Community structure and diversity

The thirteen preprocessed libraries rendered 202,779 reads and 3,614 ASVs. The ASVs were distributed among 55 phyla, where the phylum *Desulfobacterota* (formerly the class *Deltaproteobacteria* within the phylum *Proteobacteria*) dominates with 22.7% of the total abundance, including several sulfur-associated bacteria. Next come the phyla *Proteobacteria* (18.4%), *Bacteroidota* (formerly the class *Bacteroidetes*), (15.8%), and *Chloroflexi* (9.4%) (**Figure 2A**). In this connection, there were no statistically significant differences between the most abundant phyla (>2% in abundance) and localities (p-value > 0.05), evaluated through the ALDEx2 statistical package.

A total of 328 families were identified, where *Desulfosarcinaceae* (11%), in the phylum *Desulfobacterota*, is the most abundant; followed by an uncultured-unlabeled cluster (6.1%), and *Anaerolineaceae* (5.4%), of the phylum *Chloroflexi* (**Figure 2A**). According to ALDEx2, the family *Desulfobulbaceae* (3.2%) presents statistically significant differences in the abundances between IQQ and VLP-CCP localities (p-value < 0.05). On the other hand, although there were not statistically significant differences, the family *Flavobacteriaceae* (5.3%) presented greater abundance in IQQ than in VLP and CCP, while the *Halieaceae* family abundance was greater in VLP and CCP than in IQQ (see **Supplementary Figures 2A,B** for the ranking of the most abundant classes and orders). It is worth mentioning that although the *Thiotrichaceae* family is not among the ten most abundant families, it had 1.4% of the total abundance, ranking among the 20 most abundant and appearing with an average of 1.9% in CCP. This family harbors some of the most conspicuous large filamentous sulfur bacteria in the area, such as *Ca*. Marithioploca araucae, of the *Gammaproteobacteria* class.

Continuing with the taxonomic assignment, 397 different genera were retrieved (including one cluster for the uncultured and another for the unassigned). The most abundant genus was the Sva0081 sediment group (4.2%), in the family *Desulfosarcinaceae* (**Supplementary Figure 2C**). In this regard, it should be mentioned that after the Sva0081 sediment group, the genera SEEP-SRB1 (2.25%), LCP-80 (1.19%) and *Desulfosarcina* (0.86%) were identified in the family *Desulfosarcinaceae* (**Supplementary Figure 3**). While in the family *Anaerolineaceae* (5.4%), six genera were identified, of which *Pelolinea* (3.1%) was the most abundant and cosmopolitan. Furthermore, IQQ presented the largest diversity and abundance within that family (**Supplementary Figure 3**). Moreover, going down to the ASV ranking, the most frequent ASV was assigned to the genus *Lutimonas* (1.5%) in the phylum *Bacteroidota*, and the second in the frequency ranking (1.4%), to the order *Syntrophobacterales*, phylum *Desulfobacterota* (the graphical distribution of the most frequent thousand ASVs is in **Supplementary Figure 1**).

Compared with the rest of the sampling stations ANTF presented some different taxa with opposite abundances. Thus, the maximum abundance of *Desulfobacterota* and its family *Desulfosarcinaceae* was found in ANTF, while the abundance of

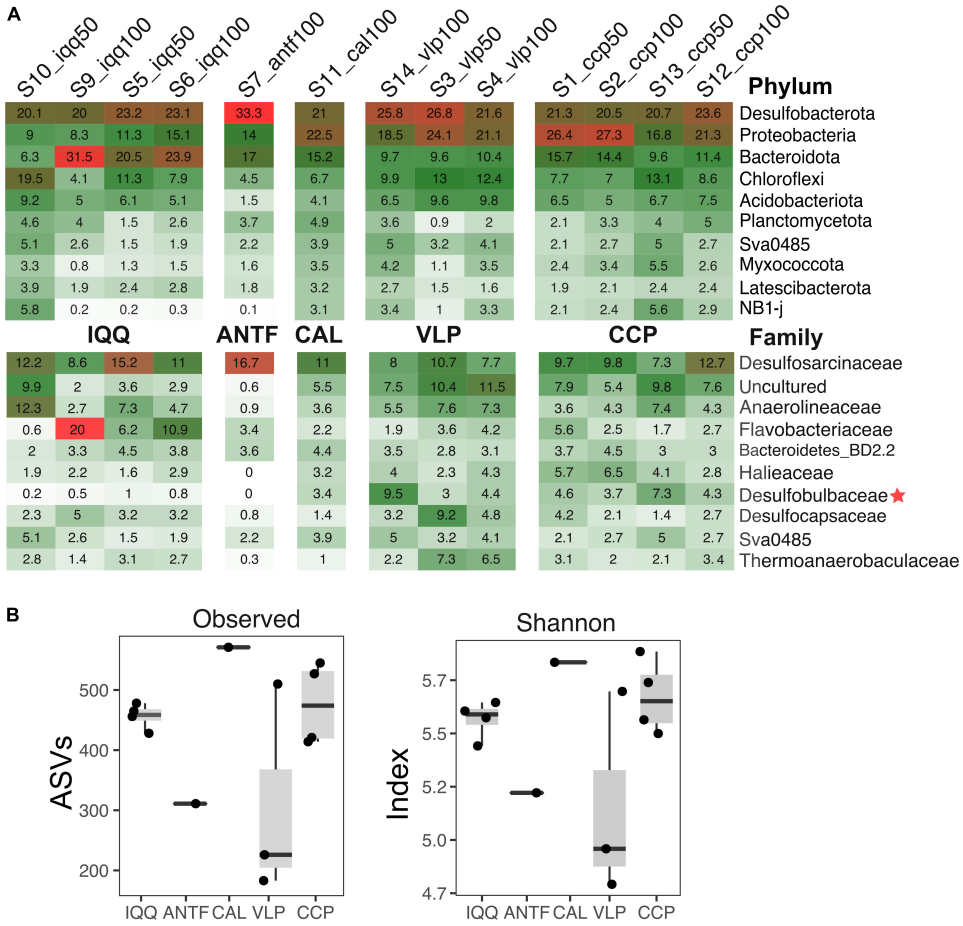

FIGURE 2
(A) Abundance of the ten most abundant phyla and families. The numbers in tiles represent the relative abundance in percent. The red star highlights taxa with statistically significant differences in abundance according to Aldex 2. **(B)** Number of observed ASVs and Shannon diversity index.

families such as *Anaerolineaceae* (5.4%) was very low (0.9%), and others, such as *Halieaceae* and *Desulfobulbaceae* (which were present in IQQ, CAL, VLP, and CCP), were absent.

Regarding diversity indexes (Figure 2B), no statistically significant differences were found between the sampling stations (p-value > 0.05), although VLP had the lowest number of ASVs and Shannon diversity index, in which the sample s14_vlp100 was notably higher than s3_vlp100 and s4_vlp50, increasing the variance in the VLP locality. Furthermore, in terms of numbers of ASVs and Shannon diversity index, the localities of IQQ, CAL, and CCP, were very similar.

Spatial pattern

The NMDS analysis of the unifrac and Bray-Curtis distance matrix revealed a spatial pattern, in which the sampling points of IQQ, VLP, and CCP generated separate clusters (Figure 3). Although only localities with replicate samples (IQQ, VLP, and CCP) were considered valid for *post-hoc* analysis, it should be noted that the ANTF sampling point appeared distant from the complementary sampling points, while CAL appeared close to CCP. The *post-hoc* ANOSIM test confirmed that the clusters observed in the NMDS were statistically significant ($R = 0.56$, p-value = 0.0017), validating the spatial pattern.

Regarding the influence of environmental measures on the Bray-Curtis dissimilarity of the microbial community, the percentage of TOM appeared as the most relevant variable (Supplementary Table 1), as is shown in the adjusted NMDS ordination analysis, built through the envfit method and the metaNMDS function from R (Figure 3). Furthermore, the bioEnv and Mantel test confirmed that TOM has a statistically significant positive correlation with bacterial abundance ($r = 0.36$, p-value = 0.02) as well as redox potential ($r = 0.27$, p-value; $p = 0.02$) (Supplementary Table 2).

To assess how taxa and, in particular, how families influenced the spatial pattern, the ten most abundant families (48% accumulated abundance) were evaluated

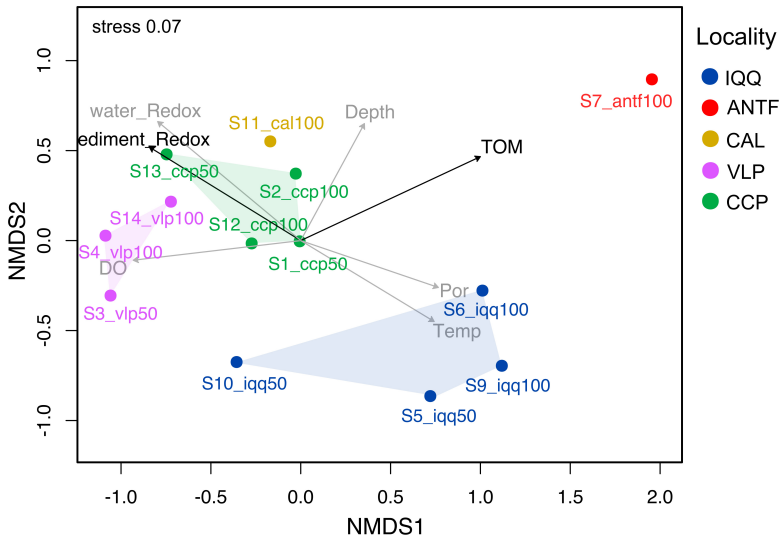

FIGURE 3
Non-metric multidimensional scaling (NMDS) plot of the Bray-Curtis distance of the bacterial community with environmental parameters added using envfit. The NMDS was constructed over the Bray-Curtis dissimilarity matrix. The data was rarefied at 8,000 sequences per sample. The black arrows represent a statistically significant relationship ($p < 0.05$) measured through the Mantel or envfit test. The added parameters were the redox potential of sediment and water, the percentage of total organic matter (TOM), depth, temperature (Temp), and porosity (Por).

through the Adonis statistical test, including the IQQ, VLP, and CCP localities as factors. The result showed that the family *Desulfobulbaceae* was the most important explanatory variable (**Supplementary Table 3**) for spatial pattern between the localities ($R^2 = 0.61$; p-value < 0.01). Moreover, the second most important explanatory variable was *Bacteroidetes* BD2-2 ($R^2 = 0.58$; p-value < 0.01), followed by *Thermoanaerobaculaceae* ($R^2 = 0.57$; p-value < 0.01), and *Desulfocapsaceae* ($R^2 = 0.55$; p-value < 0.01). Besides, at the ASV level, the SIMPER analysis showed that the greatest contribution to the dissimilarity pattern between IQQ and CCP was generated by a couple of ASVs assigned to the genus *Lutimonas*, one ASV assigned to *Syntrophobacterales*, one to the genera *Desulfonema* and *Sulfurovum*, which made 13.6% of the total contribution to dissimilarity. Differentially, between IQQ-VLP and CCP-VLP the greatest contribution was made by an ASV assigned to the genera B2M28 (class *Gammaproteobacteria*) (**Supplementary Table 4**).

The family *Desulfobulbaceae*

Since the family *Desulfobulbaceae* appeared as the most important taxonomic explanatory variable for the spatial pattern between localities, we investigated the distribution of the representatives of this family identified throughout the localities under study.

With 3.2% of the total abundance and 47 ASVs, the family *Desulfobulbaceae* contained three ASVs assigned to the genus *Ca*. Electrothrix, in the cable bacteria functional group, and two others, to the genus *Desulfobulbus*; the complement of 43 ASVs are uncharacterized forms (uncultured). In this regard, the phylogenetic relationship based on the ASV sequences showed four uncultured ASVs in the *Ca*. Electrothrix clade, seven in the *Desulfobulbus* clade, and the rest in a separate clade (**Figure 4A**). The *Ca*. Electrothrix-assigned ASVs were present in four samples from IQQ, CAL, and CCP, while *Desulfobulbus* was present in eleven samples from IQQ, VLP, and CCP, thus more ubiquitous and abundant than *Ca*. Electrothrix (**Figure 4B**). The uncultured genus ASVs were present in the CAL, VLP, and CCP sampling sites, and remarkably, IQQ was characterized by the almost exclusive presence of *Desulfobulbus*. Thus, the distribution pattern of *Desulfobulbaceae* emphasizes the general spatial pattern while further separating the IQQ cluster (**Figure 4C**). Sampling locality differences become more obvious when the numbers of shared and unique ASVs are considered, since only one *Desulfobulbus* assigned ASV (2.1%), is shared among IQQ, VLP, and CCP (**Supplementary Figure 4**). Concerning the influence of environmental variables on the abundance pattern of *Desulfobulbaceae*, the redox potential resulted in a statistically significant positive correlation ($r = 0.41$; p-value $= 0.001$).

Shared and unique amplicon sequence variants

The latitudinal spatial pattern observed at the ASV level in the *Desulfobulbaceae* family, especially in IQQ, led to evaluating

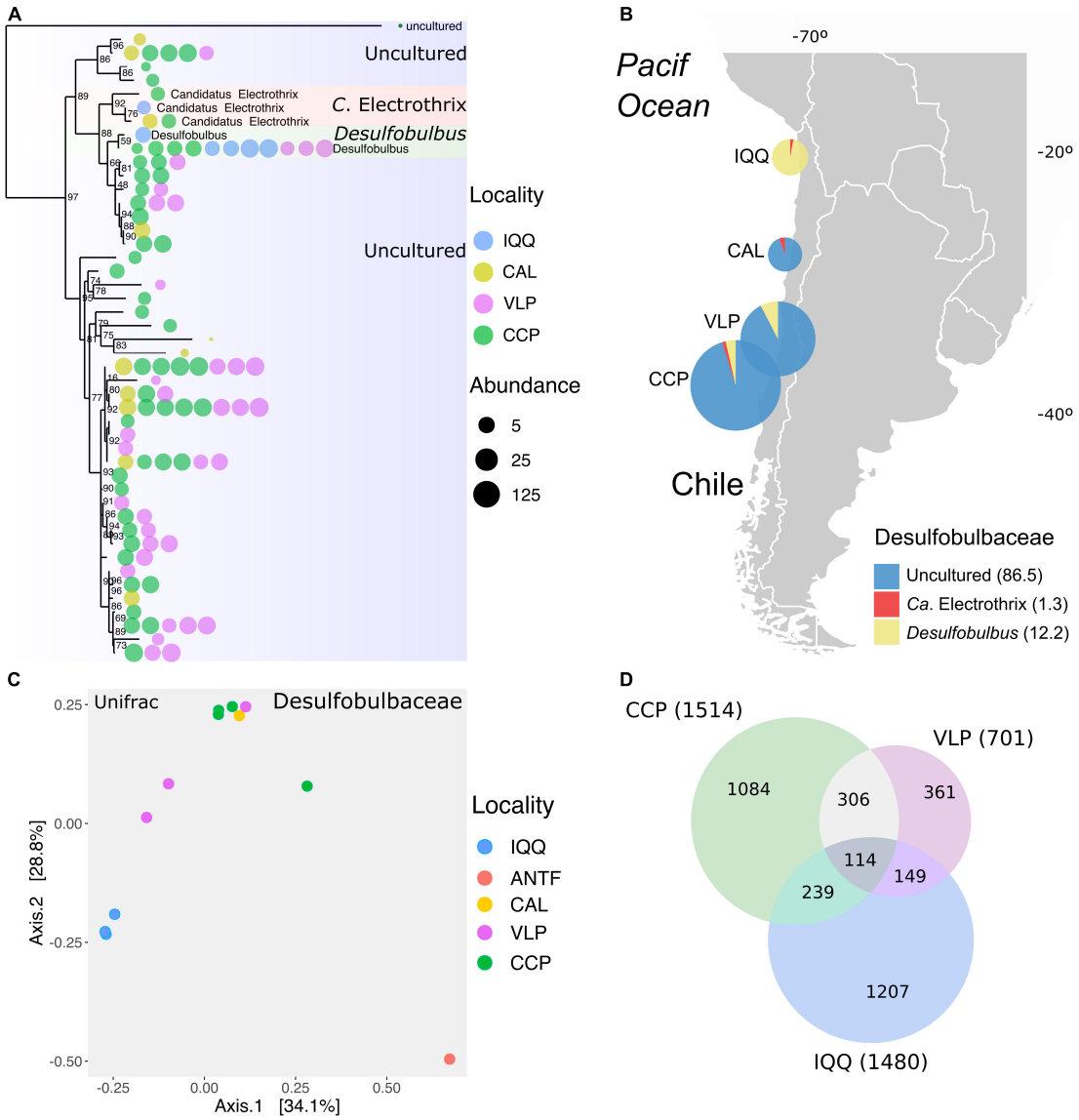

FIGURE 4
(A) Phylogenetic tree of the representatives of the family *Desulfobulbaceae* identified across the data. The color and size of the bubbles indicate the presence and abundance of taxa by locality. **(B)** Distribution of genera of the family *Desulfobulbaceae* by locality in percentage **(C)** Non-metric multidimensional scaling (NMDS) based on the unifrac matrix distance of the abundance in the *Desulfobulbaceae* family (Stress = 0.0005). **(D)** Venn chart of shared and unique ASVs across all data by locality. The number in parentheses is the total ASVs.

the shared and unique ASVs among IQQ, VLP, and CCP across the whole data. Removing the ANT and CAL data the ASVs shared among IQQ, VLP, and CCP were only 113 out of the total of 3,017 ASVs, which represent only 3.7% of the total ASVs (Figure 4D), and 26% of the total reads. Taxonomically, the phylum *Desulfobacterota* (23.5%) dominated among shared ASVs, followed by *Bacteroidota* (19.4%) and *Proteobacteria* (16.2%). Moreover, at the individual level, the first and third most abundant shared ASVs were assigned to the genus *Lutimonas* of the phylum Bacteroidota, and the second, to the phylum *Desulfobacterota* (order *Syntrophobacterales*).

From the uniqueness perspective, IQQ had the highest proportion of unique ASVs (Figure 5) (40%), closely followed by CCP with 36% and, both distant from VLP with 12%. Taxonomically, the phylum *Desulfobacterota* (20.8%) contained the larger number of unique ASVs in IQQ, while in CCP was *Proteobacteria* (21%), and in VLP *Chloroflexi* (16.6%).

At the family level, and without considering the uncultured and the unassigned, the *Desulfosarcinaceae* and *Anaerolineaceae* contained the larger number of unique ASVs. After them, the family *Flavobacteriaceae* (5.5%) in IQQ; *Halieaceae* (3.8%) in CCP, and Sva0485 (formerly

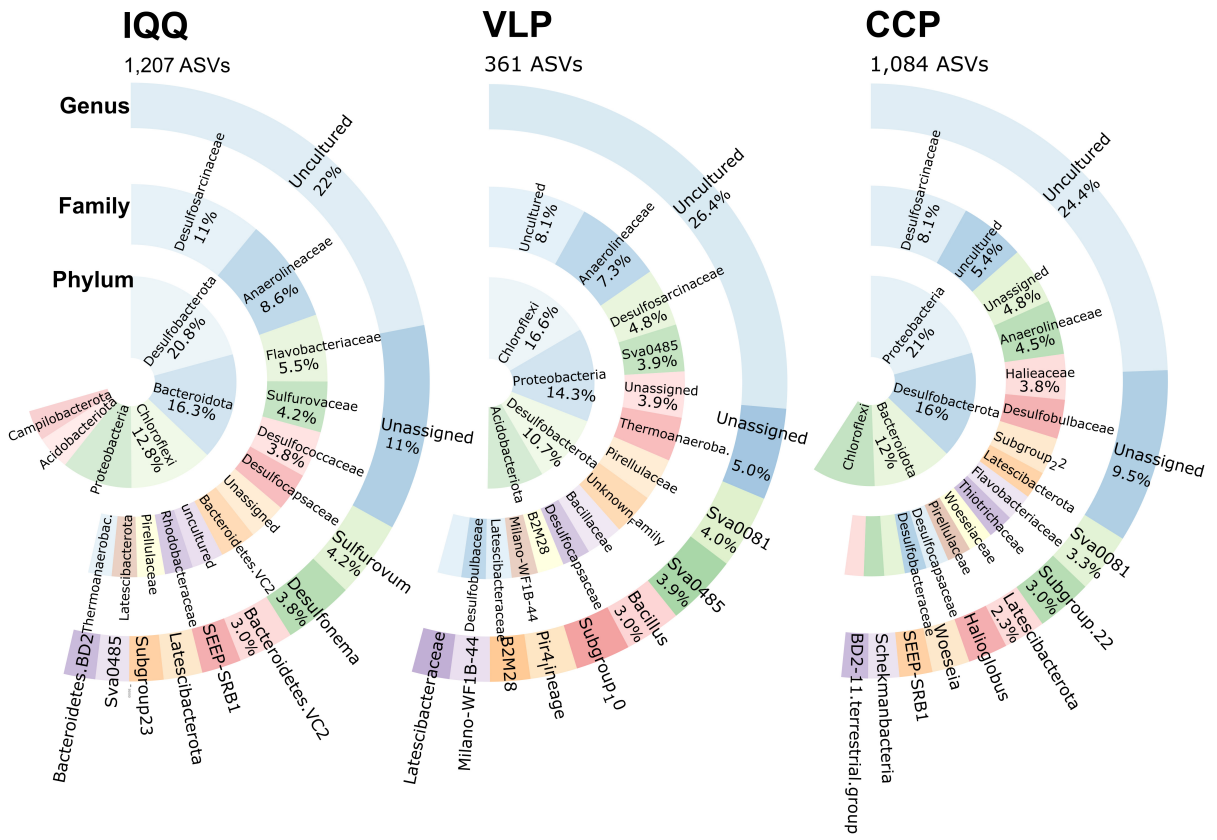

FIGURE 5
Relative abundance of the most frequent unique ASVs and its taxonomic assignment at the phyla, family, and genus levels by locality.

Deltaproteobacteria Candidate Sva0485 clade) in VLP appeared as the most abundant.

At the genus level and on the basis of unique ASVs, samples from IQQ, VLP, and CCP have a prominent sulfidic profile, with the presence of *Sulfurovum* (4.2%) (SOB) and *Desulfonema* (3.8%) (SRB) at the top of the abundance in IQQ, while, VLP and CCP coincide with the genus Sva0081 sediment group (SRB) as top taxa (after the unassigned and uncultured) (**Figure 5**). Conversely, in IQQ the genus Sva008 sediment group presented low abundance. In this sense, uncultured and unassigned assignments, ranging 31–35% of the accumulated abundance, leaves 65–69% of the sequences with known taxonomic affiliation at the genus level.

Discussion

Community structure and diversity

This study shows that the best represented bacteria phyla were *Desulfobacterota* (23%) (formerly the class *Deltaproteobacteria*), *Proteobacteria* (18%), *Bacteroidota* (16%) (the former phylum *Bacteroidetes*), and *Chloroflexi* (9%), a distribution that differs with descriptions of similar environments, such as the superficial anoxic OMZ sediments of the Arabian Sea and the Bay of Bengal (Lincy and Manohar, 2020), where *Firmicutes* (33.08%), *Proteobacteria* (32.59%), *Bacteroidetes* (17.48%), and *Chloroflexi* (5.52%) were the most abundant phyla. The *Firmicutes* phylum appears with only 1.5% of the total abundance in the present study, which may be attributable to patchy distribution or, as Cupit et al. (2019) posits, the fact that a wide range of *Firmicutes* species are not captured by conventional culture-independent DNA extraction methods, primarily due to the non-germinative state of *Firmicutes* endospores.

Global studies on the deeper anoxic layers, i.e., the subseafloor (Hoshino et al., 2020) have reported *Chloroflexi*, *Planctomycetes*, and *Ca.* Atribacteria (*Ca.* Caldatribacteriota or OP9/JS1) as the most frequent phyla. Indeed, in anoxic subseafloor sediments, *Ca.* Atribacteria is described as one of the most abundant bacterial taxa (Orsi, 2018; Hoshino et al., 2020), although it was scarcely present in the HS surface sediment samples. The most likely reason is that *Ca.* Atribacteria were distributed deeper in the sediments, whereas this study covers the first 5 cm of sediment.

In the HS the dominant classes were similar to those reported by Zinger et al. (2011) in their study of coastal sediments, where the most abundant classes were *Gammaproteobacteria* and *Deltaproteobacteria*, which are equivalent to the most abundant classes identified in the HS, taking into account that *Desulfobacteria* is the former *Deltaproteobacteria* class. Therefore, the HS community presents distinctive features at the phylum level with respect to similar environments, while at the class level it seems to agree with previous reports.

The two most abundant families in the HS, the *Desulfosarcinaceae* (10.9%) and *Anaerolineaceae* (5.4%) appear to thrive relatively well in this primeval sulfidic (anoxic) type of environment, a factor that supports the micropaleontological claim relating to the findings of filamentous microfossils in the Hadean (3,235 and 3,465 Ma ago) (Rasmussen, 2000; Schopf et al., 2018). The novel family *Desulfosarcinaceae* includes genera such as *Desulfosarcina*, *Desulfatitalea*, SEEP-SRB1, and Sva0081 sediment group, all of them sulfate-reducing bacteria (SRB). Further, the Sva0081 sediment group was the HS's most abundant genus. According to previous studies, this uncultured genus is an important sink for acetate (Dyksma et al., 2018a) and for H_2 in coastal marine sediments (Dyksma et al., 2018b). It proliferates fast in microaerobic conditions using the H_2 that diffuses from fermentation deeper in the sediment (Dyksma et al., 2018a). Therefore, the dominant presence of Sva0081 sediment group in the HS suggests that H_2 consumption would be an important metabolic pathway for energy, supporting populations like the Sva0081 sediment group.

As mentioned above, in the HS, the family *Anaerolineaceae* (5.4%) in the phylum *Chloroflexi*, was the second most abundant family after the *Desulfosarcinaceae*, with six genera. Among these, *Pelolinea* (3.1%), an anaerobic, cosmopolitan, filamentous genus (Imachi et al., 2014), was the most common. Most of the *Anaerolineaceae* reads (90.3%) are unknown and are assigned as uncultured bacteria. In general terms, this family is defined as consisting of strictly anaerobic and chemoheterotrophic multicellular filamentous bacteria, mostly using sugars and protein for fermentation (Yamada and Sekiguchi, 2018). In this connection, *Anaerolineaceae* could be playing an important role in the HS by generating organic acids, such as acetate (Liang et al., 2015). The latter molecule has been indicated as one of the most important energy substrates for sulfate-reducing bacteria in marine sediments (e.g., Parkes et al., 1989).

At the ASV level, the most frequent in the HS was assigned to the genus *Lutimonas*, which is an interesting coincidence with the Black Sea sediment bacterial community where it has been reported as the most abundant OTU (Jessen et al., 2017). Moreover, the genus *Lutimonas* is defined as symbiont, first isolated from the polychete *Periserrula leucophryna* (Yang et al., 2007), with variable capacity for nitrate reduction (Kim et al., 2014), and presumably also, nitrogen fixation (Petersen et al., 2016). Although the dominant presence of the symbiont genus *Lutimonas* in different sediments has been reported (Quero et al., 2015), its high abundance in the HS suggests that this local taxon is a free-living bacterium, not yet characterized.

This study further shows that the diversity and species richness in both the IQQ and CCP sampling stations are similar, while the VLP station presented the lowest diversity and relative abundances. This feature might be explained by the narrow shelf and thus of the sublittoral zone at this point, as compared with that off Concepcion and off Valparaiso (Völker et al., 2012) which in turn may be related to the quality and levels of available TOM. As suggested by Orsi (2018), these variables generally correlate with the number of cells and diversity in the sediments which depends on the lower or greater availability of electron donors in higher organic carbon fluxes.

Geographic patterns

The NMDS and ANOSIM analyses showed a spatial pattern that separated the sampling localities. Thereby, IQQ and CCP on one side and VLP on the other. In this regard, TOM and redox potential were statistically significantly correlated with bacterial abundance, in this case favoring the former two locations which shared productivity-enhancing factors, i.e., primary productivity-enhancing upwelling in IQQ. In addition to this factor, the nutrient input from the regional rivers (most important, the Bio-Bio and Itata rivers) may play a key factor at Concepcion. It is argued that productivity regimes, especially the content of organic matter in sediments, as well as the presence of oxygen, are key in shaping the structure and diversity of bacterial communities (Bienhold et al., 2016; Hoshino et al., 2020), changing spatially, even at microscales as a result of aggregation, creating very complex communities (Zorz et al., 2019).

Regarding spatial distribution patterns and taxa, the family *Desulfobulbaceae* turned out to be the most influential taxon in explaining the spatial pattern of the HS bacterial community, while it is the seventh most abundant family (3.2%). Indeed, this family presented statistically significant differences in abundance, where its presence is scarce in the locality of IQQ compared to VLP and CCP. In this regard, it has been shown that, as expected, the family *Desulfobulbaceae* tend to enhance their relative abundance toward anoxic conditions, especially those groups affiliated with sulfate-reducing bacteria, since the reduction of sulfates dominated the remineralization of organic matter with increasing hypoxia (Thamdrup and Canfield, 1996; Jessen et al., 2017). It is noteworthy mentioned that the family *Thermoanaerobaculaceae*, containing thermophilic bacteria, is present in all the sampling points of this study, and is the

third most influential taxon in explaining the spatial pattern. In this regard, three uncultured genera were identified across the data; Subgroup 10, Subgroup 23 and TPD-58. According to Dedysh and Yilmaz (2020), sequences that share similarities with the 16S rRNA gene sequence of *Thermoanaerobaculum aquaticum* MP-01^T, the only described member of the family, have been recovered from a variety of habitats including hot springs, saturated soils of water and sediment. The family *Thermoanaerobaculaceae* appears as ubiquitous in all localities and represent an interesting future focus of study in this environment.

The family *Desulfobulbaceae*

The family *Desulfobulbaceae*, in the phylum *Desulfobacterota*, includes SRBs and SOBs, and it has recently been suggested that it maintains important H_2 scavengers subgroups (Dyksma et al., 2018b). Members of this family are commonly found in marine sediments at different latitudes, i.e., the Baltic Sea (Marzocchi et al., 2014; Marshall et al., 2019; Dam et al., 2021), and off the coast of Chile, e.g., in the coastal ecosystem off the Atacama desert, where between some points the *Desulfobulbaceae* is one of the dominant and key families (Zárate et al., 2021).

The data corresponding to *Desulfobulbaceae* contains ASVs assigned to the genera *Desulfobulbus*, *Ca*. Electrothrix (Trojan et al., 2016), and uncultured forms. The genus *Desulfobulbus* is strictly anaerobic, having both a respiratory and fermentative metabolism, with several ways to get energy, i.e., chemoorganoheterotrophic or chemolithoheterotrophic growth. Moreover, sulfate, sulfite, and often thiosulfate serve as terminal electron acceptors and are reduced to H_2S (Galushko and Kuever, 2019). On the other hand, the genus *Ca*. Electrothrix corresponds to filamentous SOB, within the cable bacteria functional group, capable of conducting electrons over centimeter-long distances, coupling sediment electrogenic sulfur oxidation (e-SOx) to dissolved oxygen (Nielsen et al., 2010; Pfeffer et al., 2012), nitrate and nitrite reductions (Marzocchi et al., 2014). Cable bacteria have been found in different oceanographic settings and climate zones, and, in several different coastal habitats (Burdorf et al., 2017), and are a topic of increasing interest. Its presence in the HS system suggests that e-SOx could be occurring in this system, mostly sustained by high levels of nitrate (>20 μM) in both sediments Ahumada et al., 1983), and water column (see also Annexes in Gallardo et al., 2013b).

The relative abundance of *Desulfobulbaceae* in IQQ is low compared to those in VLP and CCP localities. Since *Desulfobulbus* represents 95% of the abundance of *Desulfobulbaceae*, along with a small abundance of *Ca*. Electrothrix (1 ASV; 5% of the abundance) in IQQ. Furthermore, unknown ASVs, assigned as uncultured *Desulfobulbaceae*, were not present in IQQ. Beyond that fact, the uncultured *Desulfobulbaceae* groups represent a "black box," probably new species, close to *Desulfobulbus* and *Ca*. Electrothrix (**Figure 4A**).

The spatial pattern that separates IQQ, VLP, and CCP is clear in the family *Desulfobulbaceae*, where the redox potential appeared positively correlated. In fact, the redox potential is more negative in the northernmost locations (IQQ and ANTF) than in the Central-Southern locations. Therefore, the representatives of the *Desulfobulbaceae* family thrived better in more oxidized sediments in the HS.

The degree of shared *Desulfobulbaceae* ASVs was very low, thus only one ASV (*Desulfobulbus*) is shared between IQQ, VLP, and CCP localities, representing a large latitudinal fragmentation of the group among sites.

Sharing and uniqueness in the community

The spatial fragmentation of the community is clearer at the finer grain phylogenetic level as represented by the ASV clusters, which theoretically span species and subspecies layers. Therefore, the ANOSIM value for the spatial pattern is maximum at the ASV level (**Supplementary Figure 5**), supporting the idea that the spatial pattern is a better fit at this deep phylogenetic level.

This fine spatial pattern, at the ASV level, is probably an extended and general rule for sediment microbial communities, better reflecting environmental changes in microscales. In the Baltic Sea, for example, each site contained distinct ASV signatures of unique sulfate-reducing microorganisms in each family (Marshall et al., 2019). Along the same lines, the percentage of shared ASVs among IQQ, VLP, and CCP is very low, i.e., 3.7% (26% of the reads). This level is even lower than the shared ASVs (16.8%), between anaerobic and aerobic bacterial communities in subseafloor sediments (Hoshino et al., 2020), and those for the Bay of Bengal OMZ and Arabian Sea OMZ sediment bacterial community, with 30% shared OTUs (Lincy and Manohar, 2020). Thus, this result suggests the HS contains a high level of microdiversity, consistent with the Thienemann-Sander temporal stability hypothesis (Gallardo et al., 2016), but with microscale spatial changes, which drive the high microdiversity in a general context of stability, characterized by high abundance of sulfur species, nitrate and very low or no oxygen concentration.

The unique-shared perspective allows distinguishing those ASVs under the same taxonomic assignment, but present and absent in specific locations, revealing intraspecies variation, reflecting high microdiversity across the community. In this regard, IQQ was the locality with the highest proportion of unique ASVs (40%) and, although in a different order, they appeared predominantly assigned to *Desulfobacterota*,

Proteobacteria, and *Chloroflexi*, and further, the most frequent families were *Desulfosarcinaceae*, and *Anaerolineaceae* (in the phylum *Chloroflexi*). Thus, at each site, there is a strong selection for taxonomically lower-level bacteria into the same groups (micro niches). Moreover, at the genus level, in the IQQ site, the most abundant unique ASVs were assigned to the genera *Sulfurovum* and *Desulfonema*, a facultative anaerobic SOB (hydrogen-oxidizing, thiosulfate-reducing), and SRB, respectively. In the VLP sampling site, the anaerobic SRB genera Sva0081 sediment group and Sva0485 (*Candidatus* Acidulodesulfobacterales), a facultatively anaerobic, sulfate/iron reducer, probably a sulfur oxidant under aerobic respiration (Tan et al., 2019), dominated the unique ASVs. In the CCP site, the Sva0081 sediment group was the most frequent, while poorly represented in IQQ suggesting different biogeochemical processes than those at VLP and CCP. Thus, according to these observations, both sulfur-reducing and sulfide-oxidzing processes occur simultaneously.

Conclusion

According to this study *Desulfobacterota* and *Desulfosarcinaceae* dominate in the HS, especially by SRB, reflected by the most abundant genus: the uncultivated genus Sva0081 sediment group. The revealed spatial pattern along the Chilean coast indicates changes at the bacteria community level, positively correlated with the percentage of TOM and redox potential.

Despite the fact that the *Desulfobulbaceae* species are still not properly characterized, they appeared as a key taxon with significant differences in their distribution influencing the general spatial pattern. Moreover, the spatial pattern is influenced by a large microdiversity, since a very small number of ASVs are shared (3.4%) among the localities included in the comparison, reflecting a diverse, mature and stable HS bacterial community.

Data availability statement

The datasets presented in this study can be found in online repositories. The names of the repository/repositories and accession number(s) can be found below: https://www.ncbi.nlm.nih.gov/bioproject/PRJNA251688.

Author contributions

AF, VAG, and IPGM: conceptualization. AF: formal analysis. VAG, CE, and LN: resources. LPN, IPGM, and VAG: funding acquisition and supervision. AF, CE, and VAG: experimental studies and writing—original draft. AF, VAG, IPGM, and LPN: wrote and finalized the manuscript. All authors have read and approved the final version of the manuscript.

Funding

This study was financed by the National Research and Development Agency (ANID) of Chile, in particular through the Conicyt Project 1110786 and a doctoral grant to AF. Besides, the Center for Electromicrobiology (CEM), Department of Biology at Aarhus University.

Acknowledgments

We sincerely appreciate the support of the National Agency for Research and Development of Chile (ANID–former Conicyt). In addition, we thank the Department of Marine Sciences, Universidad Arturo Prat, Iquique, Chile, the crew of the R/V "Kay Kay," the Department of Oceanography, University of Concepción, Chile, and the Census of Marine Life (CoML) project with its program "International Census of Marine Microbes" (ICoML).

Conflict of interest

The authors declare that the research was conducted in the absence of any commercial or financial relationships that could be construed as a potential conflict of interest.

Publisher's note

Supplementary material

The Supplementary Material for this article can be found online at: https://www.frontiersin.org/articles/10.3389/fmicb.2022.1016418/full#supplementary-material

References

Ahumada, R., Anny, R. G., and Victorino, M. M. (1983). Circulation and fertility of waters in Concepción Bay. *Estuar. Coast. Shelf Sci.* 16, 95–105. doi: 10.1016/0272-7714(83)90096-3

Bienhold, C., Zinger, L., Boetius, A., and Ramette, A. (2016). Diversity and biogeography of bathyal and abyssal seafloor bacteria. *PLoS One* 11:e0148016. doi: 10.1371/journal.pone.0148016

Bolyen, E., Rideout, J. R., Dillon, M. R., Bokulich, N. A., Abnet, C. C., Al-Ghalith, G. A., et al. (2019). Reproducible, interactive, scalable and extensible microbiome data science using QIIME 2. *Nat. Biotechnol.* 37, 852–857. doi: 10.1038/s41587-019-0209-9

Burdorf, L. D., Tramper, A., Seitaj, D., Meire, L., Hidalgo-Martinez, S., Zetsche, E. M., et al. (2017). Long-distance electron transport occurs globally in marine sediments. *Biogeosciences* 14, 683–701. doi: 10.5194/bg-14-683-2017

Callahan, B. J., McMurdie, P. J., Rosen, M. J., Han, A. W., Johnson, A. J. A., and Holmes, S. P. (2016). DADA2: High-resolution sample inference from Illumina amplicon data. *Nat. Methods* 13, 581–583. doi: 10.1038/nmeth.3869

Cupit, C., Lomstein, B. A., and Kjeldsen, K. U. (2019). Contrasting community composition of endospores and vegetative firmicutes in a marine sediment suggests both endogenous and exogenous sources of endospore accumulation. *Environ. Microbiol. Rep.* 11, 352–360. doi: 10.1111/1758-2229.12679

Dam, A. S., Marshall, I. P., Risgaard-Petersen, N., Burdorf, L. D., and Marzocchi, U. (2021). Effect of salinity on cable bacteria species composition and diversity. *Environ. Microbiol.* 23, 2605–2616. doi: 10.1111/1462-2920.15484

Dedysh, S. N., and Yilmaz, P. (2020). *Thermoanaerobaculaceae. Bergey's manual of systematics of archaea and bacteria*. Hoboken, NJ: John Wiley & Sons. doi: 10.1002/9781118960608.fbm00358

Dyksma, S., Lenk, S., Sawicka, J. E., and Mußmann, M. (2018a). Uncultured gammaproteobacteria and desulfobacteraceae account for major acetate assimilation in a coastal marine sediment. *Front. Microbiol.* 9:3124. doi: 10.3389/fmicb.2018.03124

Dyksma, S., Pjevac, P., Ovanesov, K., and Mussmann, M. (2018b). Evidence for H2 consumption by uncultured desulfobacterales in coastal sediments. *Environ. Microbiol.* 20, 450–461. doi: 10.1111/1462-2920.13880

Ferdelman, T. G., Lee, C., Pantoja, S., Harder, J., Bebout, B. M., and Fossing, H. (1997). Sulfate reduction and methanogenesis in a *Thioploca*-dominated sediment off the coast of Chile. *Geochim. Cosmochim. Acta* 61, 3065–3079. doi: 10.1016/S0016-7037(97)00158-0

Fernandes, A. D., Reid, J. N., Macklaim, J. M., McMurrough, T. A., Edgell, D. R., and Gloor, G. B. (2014). Unifying the analysis of high-throughput sequencing datasets: Characterizing RNA-seq, 16S rRNA gene sequencing and selective growth experiments by compositional data analysis. *Microbiome* 2:15. doi: 10.1186/2049-2618-2-15

Fonseca, A., Ishoey, T., Espinoza, C., Perez-Pantoja, D., Manghisi, A., Morabito, M., et al. (2017). Genomic features of "candidatus venteria ishoeyi", a new sulfur-oxidizing macrobacterium from the humboldt sulfuretum off Chile. *PLoS One* 12:e0188371. doi: 10.1371/journal.pone.0188371

Fossing, H., Gallardo, V. A., Jørgensen, B. B., Hüttel, M., Nielsen, L. P., Schulz, H., et al. (1995). Concentration and transport of nitrate by the mat-forming sulphur bacterium *Thioploca*. *Nature* 374, 713–715. doi: 10.1038/374713a0

Foster, Z. S., Sharpton, T. J., and Grünwald, N. J. (2017). Metacoder: An R package for visualization and manipulation of community taxonomic diversity data. *PLoS Comput. Biol.* 13:e1005404. doi: 10.1371/journal.pcbi.1005404

Fry, J. C., Parkes, R. J., Cragg, B. A., Weightman, A. J., and Webster, G. (2008). Prokaryotic biodiversity and activity in the deep subseafloor biosphere. *FEMS Microbiol. Ecol.* 66, 181–196. doi: 10.1111/j.1574-6941.2008.00566.x

Gallardo, V. A. (1977). Large benthic microbial communities in sulphide biota under Peru–Chile subsurface countercurrent. *Nature* 268, 331–332. doi: 10.1038/268331a0

Gallardo, V. A., Espinoza, C., Fonseca, A., and Musleh, S. (2013a). Las grandes bacterias del sulfureto de humboldt. *Gayana (Concepción)* 77, 136–170. doi: 10.4067/S0717-65382013000200008

Gallardo, V. A., Fonseca, A., Espinoza, C., Ruiz-Tagle, N., and Musleh, S. (2016). Bacteria of the humboldt sulfuretum comply with unifying macroecological principles. *Mar. Biodivers.* 46, 399–406. doi: 10.1007/s12526-015-0377-x

Gallardo, V. A., Fonseca, A., Musleh, S. S., and Espinoza, C. (2013b). Extrapolations of standing-stocks of big bacteria in humboldt eastern boundary current ecosystem (HEBCE). *Oceanography* 1:110. doi: 10.4172/2332-2632.1000110

Galushko, A., and Kuever, J. (2019). *Desulfobulbus. Bergey's manual of systematics of archaea and bacteria*. Hoboken, NJ: John Wiley and Sons. doi: 10.1002/9781118960608.gbm01023.pub2

Helly, J. J., and Levin, L. A. (2004). Global distribution of naturally occurring marine hypoxia on continental margins. *Deep Sea Res. Part I Oceanogr. Res. Pap.* 51, 1159–1168. doi: 10.1016/j.dsr.2004.03.009

Høgslund, S., Revsbech, N. P., Cedhagen, T., Nielsen, L. P., and Gallardo, V. A. (2008). Denitrification, nitrate turnover, and aerobic respiration by benthic foraminiferans in the oxygen minimum zone off Chile. *J. Exp. Mar. Biol. Ecol.* 359, 85–91. doi: 10.1016/j.jembe.2008.02.015

Hoshino, T., Doi, H., Uramoto, G. I., Wörmer, L., Adhikari, R. R., Xiao, N., et al. (2020). Global diversity of microbial communities in marine sediment. *Proc. Natl. Acad. Sci. U.S.A.* 117, 27587–27597. doi: 10.1073/pnas.1919139117

Huber, J. A., Mark Welch, D. B., Morrison, H. G., Huse, S. M., Neal, P. R., Butterfield, D. A., et al. (2007). Microbial population structures in the deep marine biosphere. *Science* 318, 97–100. doi: 10.1126/science.1146689

Huse, S. M., Dethlefsen, L., Huber, J. A., Welch, D. M., Relman, D. A., and Sogin, M. L. (2008). Exploring microbial diversity and taxonomy using SSU rRNA hypervariable tag sequencing. *PLoS Genet.* 4:e1000255. doi: 10.1371/journal.pgen.1000255

Imachi, H., Sakai, S., Lipp, J. S., Miyazaki, M., Saito, Y., Yamanaka, Y., et al. (2014). *Pelolinea submarina* gen. nov., sp. nov., an anaerobic, filamentous bacterium of the phylum Chloroflexi isolated from subseafloor sediment. *Int. J. Syst. Evol. Microbiol.* 64, 812–818. doi: 10.1099/ijs.0.057547-0

Jessen, G. L., Lichtschlag, A., Ramette, A., Pantoja, S., Rossel, P. E., Schubert, C. J., et al. (2017). Hypoxia causes preservation of labile organic matter and changes seafloor microbial community composition (Black Sea). *Sci. Adv.* 3:e1601897. doi: 10.1126/sciadv.1601897

Kim, E., Lin, Y., Kerney, R., Blumenberg, L., and Bishop, C. (2014). Phylogenetic analysis of algal symbionts associated with four North American amphibian egg masses. *PLoS One* 9:e108915. doi: 10.1371/journal.pone.0108915

Krzywinski, M., Schein, J., Birol, I., Connors, J., Gascoyne, R., Horsman, D., et al. (2009). Circos: An information aesthetic for comparative genomics. *Genome Res.* 19, 1639–1645. doi: 10.1101/gr.092759.109

Liang, B., Wang, L. Y., Mbadinga, S. M., Liu, J. F., Yang, S. Z., Gu, J. D., et al. (2015). Anaerolineaceae and *Methanosaeta* turned to be the dominant microorganisms in alkanes-dependent methanogenic culture after long-term of incubation. *AMB Express* 5:117. doi: 10.1186/s13568-015-0117-4

Lincy, J., and Manohar, C. S. (2020). A comparison of bacterial communities from OMZ sediments in the Arabian Sea and the Bay of Bengal reveals major differences in nitrogen turnover and carbon recycling potential. *Mar. Biol. Res.* 16, 656–673. doi: 10.1080/17451000.2020.1840593

Maier, S., and Gallardo, V. A. (1984). *Thioploca araucae* sp. nov. and *Thioploca chileae* sp. nov. *Int. J. Syst. Evol. Microbiol.* 34, 414–418. doi: 10.1099/00207713-34-4-414

Marshall, I. P., Ren, G., Jaussi, M., Lomstein, B. A., Jørgensen, B. B., Røy, H., et al. (2019). Environmental filtering determines family-level structure of sulfate-reducing microbial communities in subsurface marine sediments. *ISME J.* 13, 1920–1932. doi: 10.1038/s41396-019-0387-y

Marzocchi, U., Trojan, D., Larsen, S., Louise Meyer, R., Peter Revsbech, N., Schramm, A., et al. (2014). Electric coupling between distant nitrate reduction and sulfide oxidation in marine sediment. *ISME J.* 8, 1682–1690. doi: 10.1038/ismej.2014.19

McMurdie, P. J., and Holmes, S. (2013). Phyloseq: An R package for reproducible interactive analysis and graphics of microbiome census data. *PLoS One* 8:e61217. doi: 10.1371/journal.pone.0061217

Mook, D. H., and Hoskin, C. M. (1982). Organic determinations by ignition: Caution advised. *Estuar. Coast. Shelf Sci.* 15, 697–699. doi: 10.1016/0272-7714(82)90080-4

Nielsen, L. P., Risgaard-Petersen, N., Fossing, H., Christensen, P. B., and Sayama, M. (2010). Electric currents couple spatially separated biogeochemical processes in marine sediment. *Nature* 463, 1071–1074. doi: 10.1038/nature08790

Oksanen, J., Blanchet, F. G., Kindt, R., Legendre, P., Minchin, P. R., O'hara, R., et al. (2013). *Package 'vegan'. Community ecology package, version. 2.*

Orsi, W. D. (2018). Ecology and evolution of seafloor and subseafloor microbial communities. *Nat. Rev. Microbiol.* 16, 671–683. doi: 10.1038/s41579-018-0046-8

Parkes, R. J., Gibson, G. R., Mueller-Harvey, I., Buckingham, W. J., and Herbert, R. A. (1989). Determination of the substrates for sulphate-reducing bacteria

within marine and esturaine sediments with different rates of sulphate reduction. *Microbiology* 135, 175–187. doi: 10.1099/00221287-135-1-175

Petersen, J. M., Kemper, A., Gruber-Vodicka, H., Cardini, U., Van Der Geest, M., Kleiner, M., et al. (2016). Chemosynthetic symbionts of marine invertebrate animals are capable of nitrogen fixation. *Nat. Microbiol.* 2:16195. doi: 10.1038/nmicrobiol.2016.195

Pfeffer, C., Larsen, S., Song, J., Dong, M., Besenbacher, F., Meyer, R. L., et al. (2012). Filamentous bacteria transport electrons over centimetre distances. *Nature* 491, 218–221. doi: 10.1038/nature11586

Quast, C., Pruesse, E., Yilmaz, P., Gerken, J., Schweer, T., Yarza, P., et al. (2012). The SILVA ribosomal RNA gene database project: Improved data processing and web-based tools. *Nucleic Acids Res.* 41, 590–596. doi: 10.1093/nar/gks1219

Quero, G. M., Cassin, D., Botter, M., Perini, L., and Luna, G. M. (2015). Patterns of benthic bacterial diversity in coastal areas contaminated by heavy metals, polycyclic aromatic hydrocarbons (PAHs) and polychlorinated biphenyls (PCBs). *Front. Microbiol.* 6:1053. doi: 10.3389/fmicb.2015.01053

Rasmussen, B. (2000). Filamentous microfossils in a 3,235-million-year-old volcanogenic massive sulphide deposit. *Nature* 405, 676–679. doi: 10.1038/35015063

Salman, V., Amann, R., Girnth, A. C., Polerecky, L., Bailey, J. V., Høgslund, S., et al. (2011). A single-cell sequencing approach to the classification of large, vacuolated sulfur bacteria. *Syst. Appl. Microbiol.* 34, 243–259. doi: 10.1016/j.syapm.2011.02.001

Schmieder, R., and Edwards, R. (2011). Quality control and preprocessing of metagenomic datasets. *Bioinformatics* 27, 863–864. doi: 10.1093/bioinformatics/btr026

Schopf, J. W., Kitajima, K., Spicuzza, M. J., Kudryavtsev, A. B., and Valley, J. W. (2018). SIMS analyses of the oldest known assemblage of microfossils document their taxon-correlated carbon isotope compositions. *Proc. Natl. Acad. Sci. U.S.A.* 115, 53–58. doi: 10.1073/pnas.1718063115

Schopf, J. W., Kudryavtsev, A. B., Osterhout, J. T., Williford, K. H., Kitajima, K., Valley, J. W., et al. (2017). An anaerobic ca. 3400 Ma shallow-water microbial consortium: Presumptive evidence of Earth's Paleoarchean anoxic atmosphere. *Precambrian Res.* 299, 309–318. doi: 10.1016/j.precamres.2017.07.021

Schulz, H. N., Jorgensen, B. B., Fossing, H. A., and Ramsing, N. B. (1996). Community structure of filamentous, sheath-building sulfur bacteria, *Thioploca* spp., off the coast of Chile. *Appl. Environ. Microbiol.* 62, 1855–1862. doi: 10.1128/aem.62.6.1855-1862.1996

Tan, S., Liu, J., Fang, Y., Hedlund, B. P., Lian, Z. H., Huang, L. Y., et al. (2019). Insights into ecological role of a new deltaproteobacterial order Candidatus Acidulodesulfobacterales by metagenomics and metatranscriptomics. *ISME J.* 13, 2044–2057. doi: 10.1038/s41396-019-0415-y

Thamdrup, B. O., and Canfield, D. E. (1996). Pathways of carbon oxidation in continental margin sediments off central Chile. *Limnol. Oceanogr.* 41, 1629–1650. doi: 10.4319/lo.1996.41.8.1629

Trojan, D., Schreiber, L., Bjerg, J. T., Bøggild, A., Yang, T., Kjeldsen, K. U., et al. (2016). A taxonomic framework for cable bacteria and proposal of the candidate genera Electrothrix and Electronema. *Syst. Appl. Microbiol.* 39, 297–306. doi: 10.1016/j.syapm.2016.05.006

Ueno, Y., Ono, S., Rumble, D., and Maruyama, S. (2008). Quadruple sulfur isotope analysis of ca. 3.5 Ga dresser formation: New evidence for microbial sulfate reduction in the early Archean. *Geochim. Cosmochim. Acta* 72, 5675–5691. doi: 10.1016/j.gca.2008.08.026

Van Kranendonk, M. J., Webb, G. E., and Kamber, B. S. (2003). Geological and trace element evidence for a marine sedimentary environment of deposition and biogenicity of 3.45 Ga stromatolitic carbonates in the Pilbara Craton, and support for a reducing Archaean ocean. *Geobiology* 1, 91–108. doi: 10.1046/j.1472-4669.2003.00014.x

Völker, D., Geersen, J., Behrmann, J. H., and Weinrebe, W. R. (2012). "Submarine mass wasting off Southern Central Chile: Distribution and possible mechanisms of slope failure at an active continental margin," in *Submarine mass movements and their consequences*, eds Y. Yamada, et al. (Dordrecht, NL: Springer), 379–389. doi: 10.1007/978-94-007-2162-3_34

Wacey, D., Kilburn, M. R., Saunders, M., Cliff, J., and Brasier, M. D. (2011). Microfossils of sulphur-metabolizing cells in 3.4-billion-year-old rocks of Western Australia. *Nat. Geosci.* 4, 698–702. doi: 10.1038/ngeo1238

Yamada, T., and Sekiguchi, Y. (2018). "Anaerolineae," in *Bergey's manual of systematics of archaea and bacteria*, ed. W. B. Whitman (Hoboken, NJ: John Wiley & Sons). doi: 10.1002/9781118960608.fbm00301

Yang, S. J., Choo, Y. J., and Cho, J. C. (2007). Lutimonas vermicola gen. nov., sp. nov., a member of the family Flavobacteriaceae isolated from the marine polychaete *Periserrula leucophryna*. *Int. J. Syst. Evol. Microbiol.* 57, 1679–1684. doi: 10.1099/ijs.0.65060-0

Zárate, A., Dorador, C., Valdés, J., Molina, V., Icaza, G., Pacheco, A. S., et al. (2021). Benthic microbial diversity trends in response to heavy metals in an oxygen-deficient eutrophic bay of the Humboldt current system offshore the Atacama Desert. *Environ. Pollut.* 286:117281. doi: 10.1016/j.envpol.2021.117281

Zinger, L., Amaral-Zettler, L. A., Fuhrman, J. A., Horner-Devine, M. C., Huse, S. M., Welch, D. B. M., et al. (2011). Global patterns of bacterial beta-diversity in seafloor and seawater ecosystems. *PLoS One* 6:e24570. doi: 10.1371/journal.pone.0024570

Zorz, J., Willis, C., Comeau, A. M., Langille, M. G., Johnson, C. L., Li, W. K., et al. (2019). Drivers of regional bacterial community structure and diversity in the Northwest Atlantic Ocean. *Front. Microbiol.* 10:281. doi: 10.3389/fmicb.2019.00281

frontiers | Frontiers in Marine Science

TYPE Original Research
PUBLISHED 18 October 2022
DOI 10.3389/fmars.2022.1017136

OPEN ACCESS

EDITED BY
Shan He,
Ningbo University, China

REVIEWED BY
Erin Field,
East Carolina University, United States
Rajeev Meora,
Inha University, South Korea

*CORRESPONDENCE
Nico Boon
Nico.Boon@UGent.be

SPECIALTY SECTION
This article was submitted to Aquatic Microbiology, a section of the journal Frontiers in Marine Science

RECEIVED 11 August 2022
ACCEPTED 15 September 2022
PUBLISHED 18 October 2022

CITATION
Van Landuyt J, Kundu K, Van Haelst S, Neyts M, Parmentier K, De Rijcke M and Boon N (2022) 80 years later: Marine sediments still influenced by an old war ship.
Front. Mar. Sci. 9:1017136.
doi: 10.3389/fmars.2022.1017136

80 years later: Marine sediments still influenced by an old war ship

Josefien Van Landuyt[1], Kankana Kundu[1], Sven Van Haelst[2], Marijke Neyts[3], Koen Parmentier[3], Maarten De Rijcke[2] and Nico Boon[1,4]*

[1]Center for Microbial Ecology and Technology (CMET), Bioscience Engineering, Universiteit Gent, Gent, Belgium, [2]Vlaams Instituut van de Zee (VLIZ), InnovOcean Site, Oostende, Belgium, [3]Fysico-Chemie van Ecosystemen (ECOCHEM), Koninklijk Belgisch Instituut voor Natuurwetenschappen (KBIN), Oostende, Belgium, [4]Centre for Advanced Process Technology for Urban Resource Recovery (CAPTURE), Gent, Belgium

Historic shipwrecks form an anthropogenic landmark in marine environment, yet their influence on the local geochemistry and microbiology remains largely unexplored. In this study, sediment and steel hull samples were taken around the V-1302 *John Mahn*, a World War II shipwreck, at increasing distance from the wreck, in different directions. Polycyclic aromatic hydrocarbons (PAH's), explosives, and heavy metal levels were determined and related to the microbial composition. Benz(a)anthracene and fluoranthene remain present at the mg kg^{-1} level, probably originating from the coal bunker. These PAH's indicate that the wreck is still influencing the surrounding sediments however the effects are very dependent on which side of the wreck is being studied. Known PAH degrading taxa like *Rhodobacteraceae* and *Chromatiaceae* were more abundant in samples with high aromatic pollutant content. Moreover, sulphate reducing bacteria (such as *Desulfobulbia*), proven to be involved in steel corrosion, were found present in the biofilm. This study shows that even after 80 years, a historic shipwreck can still significantly steer the surrounding sediment chemistry and microbial ecology.

KEYWORDS

microbial ecology, shipwreck microbiome, heavy metal contamination, aromatic hydrocarbon, microalgal chloroplasts

1 Introduction

On the 12th of February 1942 *Vorpostenboot* V-1302 of the German Kriegsmarine sank to the bottom of the Belgian part of the North Sea (BPNS) during Operation Cerberus (The Channel Dash). The 48 m long ship was built in 1927 by the *Reiherstieg Schiffwerke* (Hamburg) as the fishing boat "*John Mahn*". During World War II (WWII),

the steam trawler was requisitioned by the German Navy and adapted to warfare. At 15h53 that day in February, V-1302 was attacked by six British Royal AirForce Hawker Hurricanes in front of the Belgian coast. Despite successfully downing one of the aircrafts, she was struck by two aerial bombs. The first bomb hit the funnel amidships and detonated in the boiler room, the second hit the aft section and destroyed the propeller shaft tunnel. V-1302 sank rapidly, heeling over after only half a minute, taking 11 sailors and all remaining munitions and coal reserves with her. Today the wreck lies slightly askew at the bottom of the BPNS, with a large hole on the port side due to the first bomb hit.

Shipwrecks on the seafloor worldwide contain hazardous substances such as explosives and petroleum products that, if released, may harm the marine environment. In contrast to artificial reefs (*i.e.* intentionally sunk vessels and structures), wartime shipwrecks were sunk without being stripped of hazardous substances, often having reserves of crude oil or other petroleum derivatives and unexploded munitions still on board. Even today, it is estimated that World War I and II shipwrecks around the globe, collectively, contain 2.5 to 20.4 million tonnes of petroleum products (Landquist et al., 2017). Rogowska et al. (2015) showed that latent, historic (WWII shipwreck) contamination with fossil fuels from point sources can influence the chemical composition of the marine sediment to this day. The risk that petroleum products and its derivatives pose to marine wildlife has been studied extensively, showing they can affect feeding, growth, reproduction and causes irreversible tissue damage in many marine organisms (Martínez-Gómez et al., 2010). In addition, up to 1.6 million tonnes of ammunition of all types (both attached to and separate from ships) were sunk or dumped in the Northern seas of Europe after both World Wars (Sternheim et al., 2019). The few studies performed on the subject suggest explosive compounds such as trinitrotoluene (TNT) and its derivatives (Koske et al., 2020), as well as chemical warfare agents (Czub et al., 2020), can have toxic effects on aquatic wildlife. However, the influence of these compounds on an ecological level remains unclear. Historic shipwrecks could also significantly affect the surrounding fauna and flora when leaching heavy metals and metalloids due to (biological) corrosion (Kelly et al., 2012). While wrecks are often considered biodiversity hotspots, the overall environmental impact on the seafloor of historic shipwrecks from the World Wars has only recently sparked interest (Landquist et al., 2013; Thomas et al., 2021).

As solid heterogeneous substrates, shipwrecks are rapidly colonized by microorganisms which allow other organisms to attach and form an assemblage with dynamic community interactions (Price et al., 2020). A recent study on historic (sunk >50 years ago) shipwrecks in shallow water performed by (Price et al., 2020) has shown that the hull microbiome composition differs even on the phylum level compared to the close-surrounding sediments. Another recent study, performed by Hamdan et al. (2018), showed a similar result in deep water. Where sediments are high in *Deltaproteobacteria*, the shipwrecks and sediments closer to the ships will show higher abundances in *Alphaproteobacteria* and *Gammaproteobacteria*. Several bacteria have been collected or identified from the hull of a shipwreck and marine steel fragments and proven to be involved in microbial induced corrosion (MIC) (Smith et al., 2019; Price et al., 2020). These bacteria were shown to be either members of the iron-oxidising bacterial groups like *Mariprofundus ferrooxydans* or sulphate-reducing/sulphur-oxidising bacteria (SRB/SOB) like *Desulfobulbus propionicus*. Sulphur cyclers such as *Desulfovibrionaceae* and *Desulfobulbaceae* combined made up 30 to 75% of mooring chain surface corrosion products formed after 10 years at 2 km deep (Rajala et al., 2022).

Not only prokaryotes, but also microalgae play a role in the structure and function of marine sediment (Baustian et al., 2011; Lake and Brush, 2011). The microphytobenthos and its microalgal community structure can be shaped and changed by disturbances due to anthropogenic, polluting compounds ranging from polycyclic aromatic hydrocarbons (PAH's) to pesticides (Chapman et al., 2010; Sundbäck et al., 2010; Magnusson et al., 2013; Pinckney et al., 2013; Cibic et al., 2019). Sundbäck et al. (2010) showed that the effect of pyrene (a PAH) on the benthic microalgae in a microcosm study was two-fold. On the one hand, grazers were affected which resulted in higher benthic microalgae in total, while on the other hand the pyrene caused a shift in biodiversity, with the main structural differences found in the *Bacillariophyceae* (diatoms). Little to no research has been done to investigate the microalgal contribution to shipwreck microbial ecology. Investigating the shipwreck's microbiome, both bacterial as well as microalgal, can give us a deeper insight into the corrosion (Price et al., 2020), the potential presence, and biodegradation of contaminants, as well as the micro biodiversity and macro biodiversity potential through biofilm-mediated settlement clues (Whalan and Webster, 2014).

This study investigates the microbial community composition of the biofilm on steel fragments of the historic World War II shipwreck V-1302 *John Mahn* and in the surrounding seabed to identify species related to bio-corrosion and PAH biodegradation. The bacterial and microalgal chloroplast diversity was determined using 16S rRNA gene sequencing. At the same time, the top layer (up to 15 cm deep) of the sediment surrounding the shipwreck was analysed for PAH's, explosives and heavy metals using gas chromatography combined with mass spectrometry for the organics and inductively coupled plasma atomic emission spectroscopy for the metals. With this integrative study of the sediment chemistry and the microbial community we provide insights into the microbial ecology of historic artificial features in coastal waters which contributes to a deeper understanding of the effect of potentially polluting shipwrecks on the (local) microbiology at the bottom of the sea.

2 Results

2.1 Chemical content of the sediment

Chemical analysis in samples taken in four axial directions from the shipwreck was performed (Figure 1) to see whether pollution increased upon approaching the *John Mahn* shipwreck from any direction. Figures 1A, B show the gradients based on the heavy metal content. From bow to stern, we observe higher concentrations when approaching the ship. The highest metal and metalloid concentrations were found in the sample closest to the coal bunker, with specifically a high nickel, copper, and arsenic content. There is less of a trend on the starboard-port side axis when approaching the shipwreck. Most notably, the freshly deposited sediment in the wake of the wreck has a high metal content, which could be due to the deposition of metal flakes peeling off the wreck along with sediment particles. We also observed that the heavy metal signature is different in the fresh sediment relative to the other samples on the port-starboard axis, as it has a considerably higher nickel content and considerably lower chromium content. This freshly deposited sediment on the starboard side is being deposited by a dead zone in the underwater current. PAH concentrations tended to be inversely related to the distance to the ship on both the port and bow side (Figure 1C). The stern side samples, taken closest to the damaged coal bunker, show the highest PAH concentrations. Samples from the starboard side, where fresh sediment is deposited in the wake of the ship due to scour along the predominant direction of the tidal currents (Figure 1D), have a much lower aromatic compound content. Low concentrations (µg/kg) of explosive compounds were detected in mainly the port and stern side sediment samples. Both TNT and 1,3-dinitrobenzene (1,3-DNB), a biodegradation product of TNT (Supplementary Figure S1), were detected, however, only TNT data are shown in Figures 1E, F as 1,3-DNB was found in some of the blanks as well. When plotting the diversity based on the chemical content in a PCA plot (Figure 2A), it shows that the chemical composition determines some clustering of the stern side samples whereas the fresh sediment sample presents a clear outlier away from all important polluting drivers.

2.2 The sediment shipwreck microbiome

The number of microbial cells in the sediment were on average the same across all samples, namely around 10^6 cells per g wet sediment (Figures 3A, B). A biological analysis in four axial directions from the shipwreck of the study area was also made based on the bacterial and algal chloroplast composition in the sediment (Figures 3C–F) based on 16S rRNA gene analysis.

Algal chloroplast 16S rRNA gene sequences were used to identify the relative abundance of eukaryotic microalgae in the samples (Figures 3C, D). The analysis based on the algal chloroplast content shows a different composition of the samples taken closest to the coal bunker (stern side) with relatively more *Pycnococcaceae* (27.6 ± 7.4% *vs.* 19.5 ± 14.7%) as well as unidentified chloroplasts (*Eukaryota* kingdom) and relatively less *Navicula* (1.4 ± 1.9% *vs.* 4.9 ± 1.6%), *Thallassiosira* (4.3 ± 3.0% *vs.* 20.2 ± 5.0%) and chloroplasts from the *Bacillariophyta* order (2.5 ± 1.5% *vs.* 4.1 ± 1.9%) compared to the port and bow side. The freshly deposited sediment also appears to have a different microalgal composition, with relatively more *Pycnococcaceae* (33.0 ± 4.7%) and unidentified chloroplasts (*Eukaryota* kingdom) and relatively less *Thallassiosira* (11.7 ± 4.5%) compared to the port and bow side samples.

The relative abundances of the different bacterial taxonomic groups are different in the freshly deposited sediment (starboard sample at 20m) compared to the other sediment samples (Figures 3E, F); among others, there is relatively more *Flavobacteriaceae* (18.9 ± 1.8% *vs.* 9.1 ± 3.1%) and relatively less *Halieaceae* (0.5 ± 0.9% *vs.* 3.2 ± 1.6%). A representative of the *Desulfobulbales* (8.6 ± 14.2%) order is highly abundant in the sample closest to the coal bunker that is almost non-existent in the other samples (on average 0.2 ± 0.4%).

Flow cytometry data were used to plot a non-metric dimension scaling (NMDS) figure of the phenotypic microbial Bray-Curtis beta-diversity (Figure 2B). This plot revealed a slight grouping per sampling side. Mainly the stern side samples are most dissimilar from the other samples. When looking at the Bray-Curtis dissimilarity of the 16S rRNA gene sequencing data (Figures 2C, D), most samples are similarly based on the bacterial taxonomy. However, the freshly deposited sediment at the starboard side is an outlier. The samples with higher PAH content from the stern and bow side tend to cluster together. The micro algal taxonomy shows a similar pattern, with the higher PAH polluted (points with bigger size on the figure) stern and bow side samples clustering more clearly away from the other samples.

Comparing the lowest chemically contaminated samples (low: total PAH below 25 µg/kg, high: total PAH over 75 µg/kg) versus the highest contaminated samples, there are several bacterial amplicon sequence variants (ASV's) significantly more abundant. Most of these ASV's could be attributed to the following families: *Rhodobacteraceae*, *Flavobacteriaceae* and *Chromatiaceae*. From the top 100 most abundant bacterial ASV's there are two ASV's, one belonging to the *Desulfobulbales* order and one to the *Marinilabiliaceae* family (Figure 4A). With the 16S rRNA gene sequencing and the chemical data, a canonical component analysis (CCA) was performed to indicate what chemistry and which bacterial ASV's contributed to the variance of the bacterial alpha and beta diversity amongst all locations (Figure 4B). The CCA visualisation shows that the PAH concentration drives the bacterial differences between the fresh sediment and exposed/aged sediments. For the bacterial ASV's contributing most to the variance (based on the CCA), a Pearson's correlation matrix was made (Supplementary Figure S2) to investigate whether the abundancy of these ASV's was

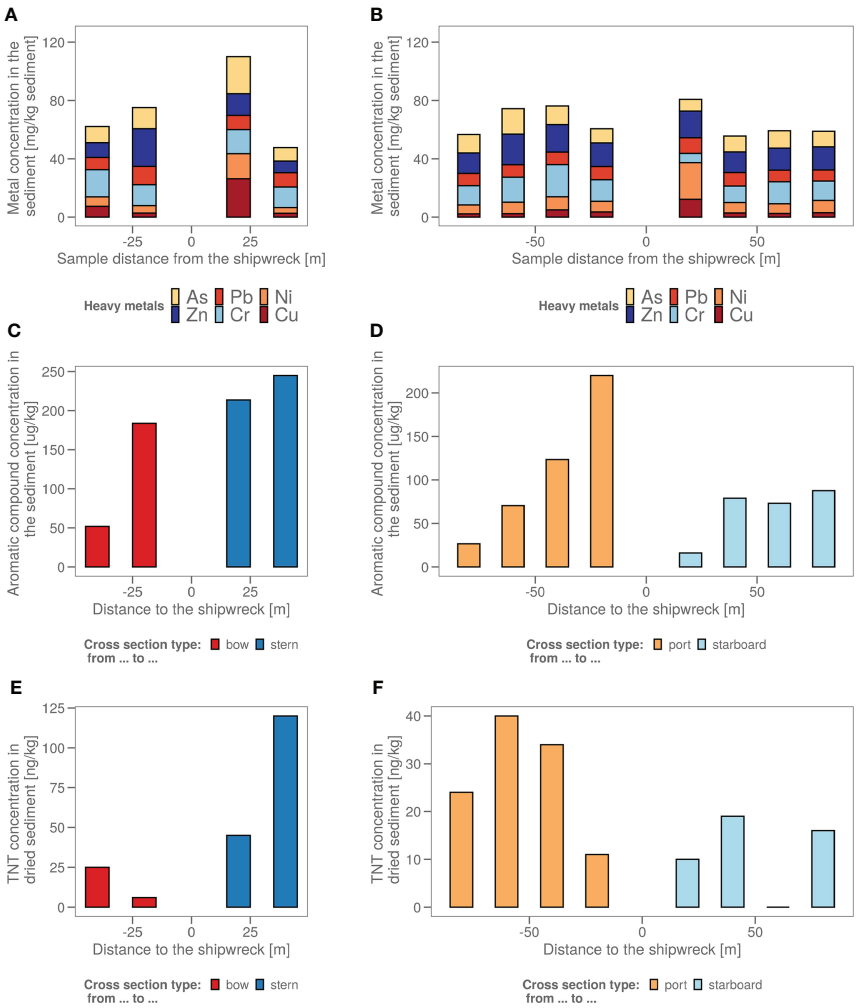

FIGURE 1
(A) The sediment samples from bow to stern and **(B)** from port side to starboard side with their total heavy metal content in mg heavy metals/kg wet sediment. The sample taken in the dead zone of the ship wreck, with freshly deposited sediment is indicated with a red arrow. **(C)** The sediment samples from bow to stern and **(D)** from port side to starboard side with their polycyclic aromatic hydrocarbon (PAH) content in µg aromatics/kg wet sediment. The sample taken in the dead zone of the ship wreck, with freshly deposited sediment is indicated with a red arrow. **(E)** The sediment samples from bow to stern and **(F)** from port side to starboard side with their total explosive content in ng TNT/kg dry sediment. (All values <17 are estimations as 17 ng/kg is the LOQ).

significantly correlated to the heavy metals, metalloids and aromatic compound concentrations measured in the samples. Bacterial ASV's with the highest positive correlation to aromatic compound content and heavy metal concentrations were identified as representatives of the *Woeseia*, *Thiotrichaceae*, *Ilumatobacter*, *Arenicella* and *Rhodobacteraceae* (red dots on the figure). Bacterial ASV's with negative correlations included members of *Sulfurimonas* and *Woeseia* (blue dots on the figure). A similar correlation matrix analysis (Supplementary Figure S3) was performed on the ASV's that were identified as chloroplasts of algae. In red, we can see some algal chloroplast ASV's correlated positively to the presence of PAH, similar to the chloroplasts of the families *Pycnoccaceae* and *Thoracospharaceae*. In blue, we marked a single negatively correlated algal chloroplast ASV that could not be identified beyond the *Chlorophyta* taxon.

2.3 The steel shipwreck microbiome

The biofilm on the shipwreck contained >40% of sulphur cycling bacteria from families including *Desulfocapsaceae*, *Desulfosarcinaceae*, *Sulfurimonadaceae*, *Sulfurovaceae*, *Thiomicrospinaceae* and *Thiotrichaceae* (Figure 5A). Total relative abundance of sulphur cyclers was on average almost 6 times more abundant in steel samples (>40%) compared to sediment samples (7%) (Figure 5A). Comparing the specific bacterial families found in

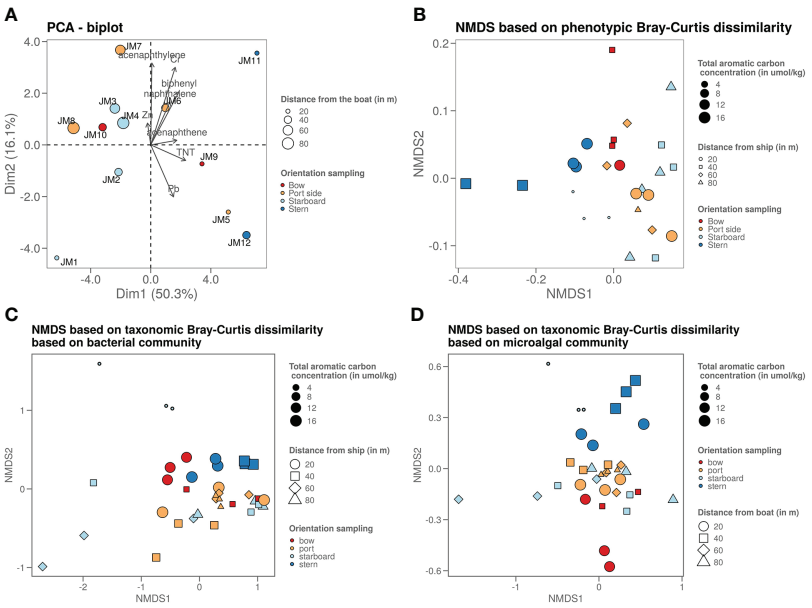

FIGURE 2
(A) Graph shows a PCA plot of the chemistry data where it shows that the samples taken on the stern side are the ones strongest polluted (highest chemical content). The sample closest to the ship on the starboard side is least polluted, as it is freshly deposited due to the dead zone. **(B)** Graph shows an NMDS visualisation of the microorganisms phenotypic betadiversity, **(C)** graph shows an NMDS visualisation of the bacterial taxonomic betadiversity and **(D)** graph shows an NMDS visualisation of the microalgal taxonomic betadiversity.

sediment versus shipwreck biofilm samples using Analysis of Compositions of Microbiomes with Bias Correction (ancombc) confirmed a significantly higher abundance of families with members involved in sulphur cycling (Figure 5B). When looking at the taxonomic families composing the community structure of the samples, average relative abundance showed that about 2% of the families present in the shipwreck microbiome were specific to the shipwreck niche (*i.e.* not native to the sediment microbiome (<10-10%)). Alpha diversity analysis (Hill numbers, D2) showed a significantly lower bacterial biodiversity on the biofilm compared to the sediment samples (Wilcoxon Rank Sum test; $p<0.05$) (Figure 5C). Moreover, there did not seem to be a trend of higher diversity in the sediment closer to the shipwreck, and lower diversity when moving further away from the wreck, for some sampling directions an opposite trend may even be seen, as for bow and stern the diversity decreases closer to the wreck (Figure 5D).

3 Discussion

3.1 Chemical characterisation of the sediments suggests slow leaching

To the best of our knowledge, the present study is the first to combine a chemical and microbial characterization of a potentially polluting wreck in the Belgian part of the North Sea. The *John Mahn* shipwreck, even after almost 80 years on the seafloor, seems to still leach micropollutants into the sediment, both from the coal bunker (aromatic compound content) as well as munition (still) present on the wreck (TNT content) and the wreck itself (heavy metals). In comparison to the total PAH concentrations found around the s/s *Stuttgart* of the Polish coast in the Baltic Sea (Rogowska et al., 2010), *i.e.* from 16.05 mg/kg to 244.90 mg/kg sediment, the concentrations found around the V-1302 *John Mahn* are about 100 to 1000 times lower (µg/kg *vs.* mg/kg), which is in the same range as the concentrations found around the HMS *Royal Oak* in Scotland (Thomas et al., 2021) (closest samples taken 50 m from the HMS) and within background concentration levels for sediments in the OSPAR (Oslo/Paris convention for the Protection of the Marine Environment of the North-East Atlantic) marine area (Dataset Commission, O, 2017). Our sampling pattern revealed increasing concentrations when approaching the shipwreck (Figures 1C, D). The PAH composition showed a higher pyrogenic than petrogenic content, which is more indicative of exhaust pollution rather than un-burnt hydrocarbons leaching from a tank, contrasting with the concentration profiles that do suggest leaching from the wreck. However, leaching from ashes in the boiler, a flash fire from the bomb hit, and burned coal tar potentially used to preheat the boilers could also explain the higher pyrogenic rather than petrogenic PAH content. The heavy metal concentrations surrounding the V-1302 *John*

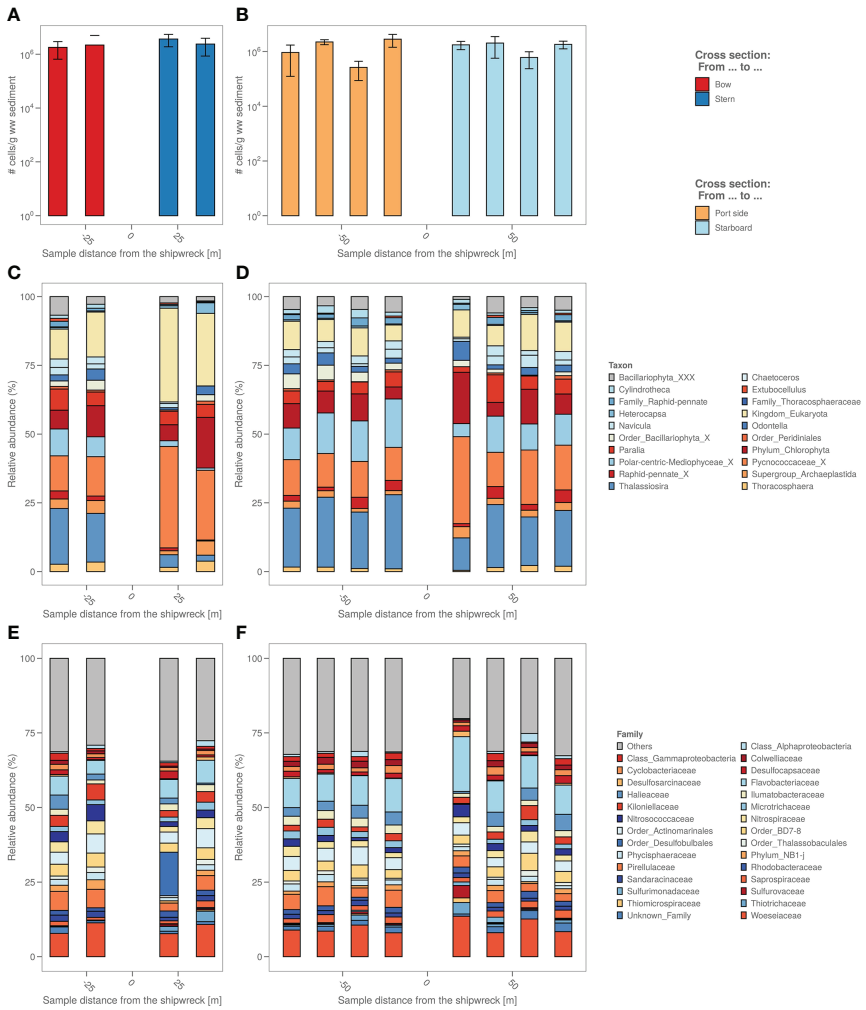

FIGURE 3
(A) The sediment samples from bow to stern and **(B)** from port side to starboard side with total number of cells per g wet weight sediment. **(C)** The sediment samples from bow to stern and **(D)** from port side to starboard side with their relative micro-algal abundances per sample site coloured by top 9 most abundant microalgae genus. "_X" and "_XXX" were added when classification could not be performed down to genus level, i.e. "unclassified". **(E)** The sediment samples from bow to stern and **(F)** from port side to starboard side with their relative bacterial abundances per sample site coloured by top 19 most abundant bacterial family.

Mahn, are in the same range as the ones found by Gwizdala et al. (2018) in the gulf of Gdańsk surrounding the small World War II shipwrecks, Munin and Abille, where samples were taken at 100 m from both wrecks. The higher arsenic combined with higher PAH content in the samples closest to the coal bunker suggests the arsenic might originate from the coal. Arsenic and copper could also be leaching from antifouling agents, as the paints used in that time period commonly contained arsenic, mercury or copper (Almeida et al., 2007). The TNT concentrations found in this study (up to 120 ng TNT/kg dry sediment) were 5 to 10 times lower than what was detected in sediments close to sunken artillery shells in Halifax, Canada, where they found concentrations ranging from 0.5 to >100 ug/kg (Rodacy et al., 2001), although, to compare the values of TNT in these different sediments in-depth, normalisation of the organic matter content should be performed. These results suggest either the remnants of a strong historic contamination or continuous slow leaching. The half-life in marine sediments of recalcitrant PAH components can range from several days up to decades (Marini and Frapiccini, 2013; Mandić and Vrančić, 2017) which means some of the components could be historic contamination however others, such as naphthalene (with a half-life up to 13 days according to Marini and Frapiccini (2013)) has probably been slowly leaching more recently.

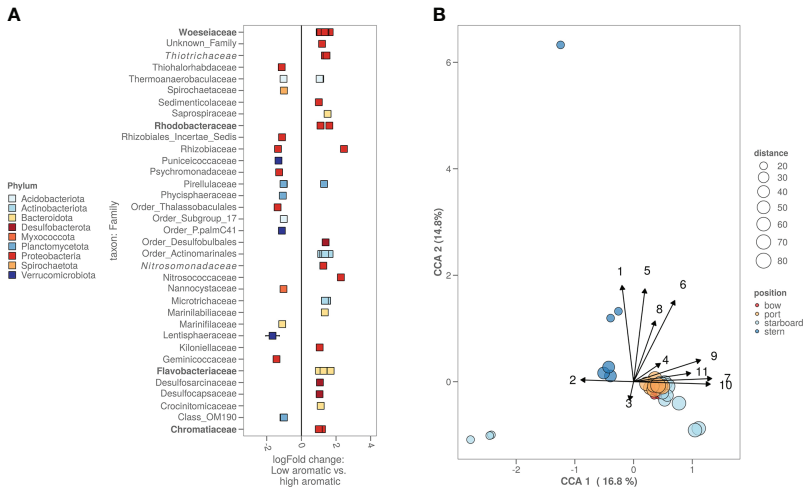

FIGURE 4
(A) High versus low polluted sediment based on the bacterial ASV's. Cut-off for high polycyclic aromatic hydrocarbon (PAH) content was >75 PAH µg kg-1 sediment while cut-off for low was <25 µg kg-1 sediment. Families with known biodegradation pathways were highlighted in bold. Families with known enrichment in PAH polluted sediments were highlighted in italic. **(B)** CCA plot combining chemistry, bacterial and algal information. Starboard samples closest to the ship were freshly deposited sediment. Numbers on the arrows stand for the following chemicals: 1. methylphenanthrene, 2. Pb, 3. Zn, 4. acenaphthene, 5. fluorene, 6. dimethylnaphthalene, 7. organic carbon content in µg kg-1, 8. total PAH in umol kg-1, 9. biphenyl, 10. naphthalene and 11. acenaphthylene.

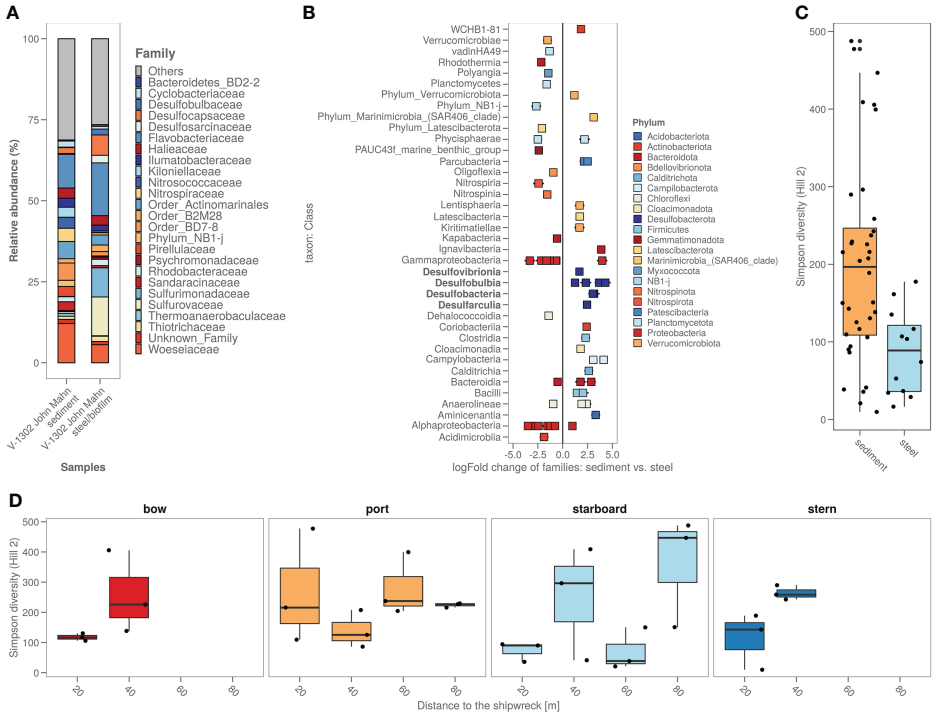

FIGURE 5
(A) Sediment around the shipwreck and the steel their bacterial composition (ASV's) based on top 25 taxa based on family; **(B)** Steel versus sediment based on the bacterial families. Classes with known corrosion members were highlighted in bold; **(C)** Alpha diversity (as Simpson diversity calculated by Hill number q=2) of the sediment and steel samples; **(D)** Alpha diversity (as Simpson diversity calculated by Hill number q=2) per sampling direction and distance from the ship.

3.2 The sediment microbiome shows indication of shipwreck influence

Although not the most prevalent (only 2 bacterial ASV's from the top 100 most abundant ones), several bacterial ASV's were more dominant in the more contaminated sediments (Figure 4A). These ASV's belong to families which include members that are known to be able to degrade aromatic compounds, *e.g. Rhodobacteraceae* (Buchan et al., 2019), *Flavobacteraceae* (Trzesicka-Mlynarz and Ward, 1995), *Chromataciaceae* (Rochman et al., 2017) and *Woeseiaceae* (Bacosa et al., 2018), while others belonged to families previously shown to be enriched in PAH contaminated sediments, *e.g. Thiotrichaceae* (Dell'Anno et al., 2021) and *Nitrosomonadaceae* (Jiao et al., 2016). Specific (relatively low abundant) ASV's belonging to the genus *Woeseia* and to the families *Thiotrichaceae* and *Rhodobacteraceae* showed a strong positive correlation with the PAH concentrations (Supplementary Figure S2). It is also suggested from both the algal and bacterial beta-diversity that the freshly deposited sediment is different from sediment surrounding the shipwreck (Figure 3). Overall, our results indicate that both the shipwreck itself and the PAH which are presumably leaching from the wreck to the sediment, despite the low concentrations, drive at least part of the bacterial community structure in the surrounding sediment.

3.3 Comparing two World War II shipwrecks indicate similar higher taxonomic level composition but clear differences at lower levels

The effects of the shipwreck on both chemical and microbial composition of the sediment are in contrast with the study performed by Thomas et al. (2021) on sediments surrounding the HMS *Royal Oak*. Although similar in time spent on/in the sediment (John Mahn: sank in 1942 *vs*. Royal Oak: sank in 1939), similar in depth (21-35 m *vs*. 12-33 m), similar in climate (both in between 50-60° N and between 3° W and 3° E, both in a sheltered Sea (BPNS *vs*. Scapa Flow), and similar in how far the samples were taken from the ship (40 m *vs*. 50 m), Thomas et al. (2021) found no leaching nor any clear bacterial enrichment due to PAH's. The bacterial composition of sediment samples of the HMS *Royal Oak* showed similar higher taxonomic groups as reported here. *Acidimicrobiia*, *Alphaproteobacteria*, *Bacteroidia*, *Gammaproteobacteria*, *Desulfobulbia*, *Nitrospira*, *Phycispaerae* and *Polyangia* were the most significant contributors in both cases (Supplementary Figure S4). However, when looking into a lower taxonomic level, there was a clear difference based on relative abundances of families present, with *Flavobacteriaceae*, *Desulfosarcinaceae*, and *Sulfurovaceae* dominating the Royal Oak sediment while *Woeseiaceae*, *Flavobacteriaceae*, and BD-7-8 group dominated the John Mahn sediment. Although similar research aims were pursued, a big difference with the HMS Royal Oak study is that Thomas et al. (2021) focused on sediment further from the shipwreck (50 - 1000 m), whereas here the samples were taken close to and on the shipwreck (0 to 80 m). This could suggest that the effect of World War II shipwrecks (<50 m deep) in the North Sea sediment are limited to a small area around the wreck due to the dynamic nature of the BPNS, with strong currents from diverse directions. In addition, sandy sediment often lacks a high carrying capacity for contaminants. Furthermore, the Royal Oak contained fuel oil rather than coal, which was demonstrated to leak a lot during the 1960s and the 1990s and was partially cleaned during the 2000s, while to our knowledge the V-1302 John Mahn's remaining coal reserves are mostly still in place, seemingly slow but continuously leaching to this date.

3.4 Steel shipwreck microbiome shows a selection of corroders

Phycisphaerae, *Verrucomicrobia* and *Bacteroidetes* were reported by Price et al. (2020) to be at a higher abundance on shipwreck samples compared to sediment. In this study, the abundance of *Verrucomicrobia* and *Bacteroidetes* are also generally higher on the shipwreck steel (Supplementary Figure S4). Upon closer look, several families have significantly higher abundances while other families from these phyla show a significantly lower abundance (Figure 4B).

A clear difference found in this study was the higher abundance of sulphur cyclers in the steel samples. The classes, highlighted in bold in Figure 5B, shown to be significantly more abundant on the steel fragments, are sulphate reducing bacteria (SRB) and sulphur-oxidising bacteria (SOB). When looking at solely the *Zetaproteobacteria* (main iron-oxidising bacterial group) only one ASV from the *Mariprofundus* genus is present, and only on the steel fragment samples (0.076% *vs*. 0%). Colonization of steel in marine sediments starts with an increase in abundance of iron-oxidizers, and as the biofilm matures, bacteria and other microbes, involved in speeding up the corrosion process, appear (McBeth and Emerson, 2016). Smith et al. (2019) performed a thorough analysis of marine steel fragments, obtained from a corroded steel surface in the UK, showing the involvement of both SRB and SOB in marine steel bio-corrosion. Iron sulphides are formed by reaction with hydrogen sulphide produced by the SRB causing primary corrosion. These iron sulphides are subsequently being oxidised through a series of sulphur oxidation states by the SOB, forming acid at all stages, causing even more corrosion. Enning et al. (2012) have suggested that some bacteria (such as SRB and SOB) are able to take up external electrons from abiotic sources like shipwreck steel, explaining the enrichment of both SRB and SOB and other heterotrophic bacteria on shipwreck steel. SRB and SOB would thus be expected in a mature steel hull bacterial biofilm.

Two genera from the algal class *Bacillariophyta* were more abundant in the steel samples compared to the sediment samples (Supplementary Figure S5), moreover, if we look at the total average % of diatoms in the samples, it shows that more diatoms were present on the steel fragments (57.2% ± 15.1% *vs*. 49.9% ± 18.6%) suggesting a role in settlement on/in the biofilm and ultimately a potential (in)direct effect on corrosion. Smith et al. (2019) showed diatomaceous algae cemented within the corrosion biofilm and iron oxide nodules as well, showing diatoms could be involved in the mechanism at some level. However, more research into what specific functional mechanism these microalgae contribute to corrosion is still needed.

4 Conclusions

In conclusion, this study demonstrated that the local microbiology and geochemistry on and around this World War II ship is still influenced by the wreck even after having been down there for almost 80 years. Both local bacteria as well as microalgae are influenced by the chemistry and structure this shipwreck provides.

5 Materials and methods

5.1 Wreck selection and sampling

Based on literature and incidental reports by recreational divers, an estimated 35 wrecks in the Belgian Part of the North Sea may still contain munitions. From this list, the V-1302 was selected for this study based on the known presence of pollutants (coal reserves, depth charges) and its favourable conditions for diving (depth, current speeds, average turbidity). When built, the ship was 48 m long and weighed 292 tonnes. As the ship was built in 1927, it was most likely built with *Schiffbaustahl type I*, which had a yield strength of 360-430 MPa and a 20% strain. It consisted of 0.25-0.3% carbon, 0.3-0.5% manganese and 0.3% silicon (Bauer et al., 1925). During adaptation from shipping boat to warfare, an 88mm naval gun, 20mm c/38 light anti-air artillery pieces, and multiple anti-submarine depth charges were added. Documents from the German Military Records in the Bundesarchiv in Freiburg revealed the fate of this vessel. The ship was hit twice after which it sank within 35 minutes. The ship wreck lies slightly askew with a large hole on the port side (due to the first bomb blast) at 51°28,937' N and 2°41,339' E between 21m and 35m of depth (Supplementary Figure S6). Visual inspections by scientific divers have shown that various munitions (88mm shells, 20mm cartridges, and at least six depth charges) are still present on the wreck, but the leakage of polyaromatic hydrocarbons (PAH's), munition compounds or heavy metals had not been investigated to date.

To investigate whether pollutants (organic aromatic compounds, heavy metals and explosives) are (still) present in the sediment surrounding the wreck, samples were taken in a cross-shaped sampling pattern around the V-1302 John Mahn. Eight sampling points were decided upon on the port/starboard axis, four on each side. Four sampling points were decided upon on the bow/stern axis, two on each side. Sampling points were chosen approximately 20 m apart, as shown in Figure 6. At each sampling point, a Van Veen grab with a sampling surface of 0.1 m^2, and a sampling depth of approximately 15 cm was lowered. Once aboard, the sediment of each point was homogenised by hand before the sample was split into four, providing ample sample for each of the different analyses. Two small pieces of loose wreckage were also recovered by divers during the sampling campaign. Before the microbial analysis, all the sub-samples for this analysis (sediment and wreckage pieces) were frozen at -20°C on board.

5.2 Aromatic compound analysis

A broad-spectrum analysis of 23 PAHs was used to compare the chemical composition and pollution of various sampling stations. The analysis included naphthalene, 1-methylnaphthalene, 2,6-dimethylnaphthalene, 2,3,5-trimethylnaphthalene, biphenyl, acenaphthylene, acenaphthene, fluorene, fluoranthene, phenanthrene, 1-methylphenanthrene, anthracene, pyrene, chrysene, benz(a)anthracene, dibenz(a,h) anthracene, benzo(b)fluoranthene, benzo(k)fluoranthene, benzo (e)pyrene, benzo(a)pyrene, perylene, benzo(ghi)perylene, and indeno(1,2,3-cd)pyrene. First, PAHs were extracted from the sediment with dichloromethane in an Accelerated solvent extractor at a pressure of 13.8 MPa. Gel permeation chromatography (columns used: ENVIROGEL 19X300MM and ENVIROGEL 19X150MM) was then used for the clean-up. The analysis was done by gas chromatography with mass spectrometry (GC-MS; Thermo TSQ8000) with the conditions for the column (Rxi-5silMS 20 m, 0.18 mm diameter, 0.18 µm internal diameter) as follows: 35°C for 2 min, heat to 250°C at 25° min^{-1}, hold for 0 min, heat to 300°C at 10°C min^{-1}, and a final hold for 10 min; The GC-MS is equipped with a programmable temperature vaporising (PTV) injector, using helium as a carrier gas in the constant flow mode (1 mL min^{-1}). The conditions of the PTV were 40°C for 0.01 min, heating to 300°C at 14.5°C s^{-1}, holding for 2 min. A split flow of 20 ml min^{-1} was used. Explosives were extracted in the same way as the PAHs with an additional clean-up with aluminium oxide (10% deactivated) and a limited pressure (10.3 MPa). The analysis was done by GC-MS (Thermo TSQ8000). The conditions for the column (Rxi-5silMS 20 m, 0.18 mm diameter, 0.18 µm internal diameter) were as follows: 30°C for 4 min, heat to 120°C at 20°C min^{-1}, heat to 150°C at 7°C min^{-1}, heat to 300°C at 20°C min^{-1} heat to 300°C at 10°C min^{-1}, and a final hold for 1 min; Large volume PTV injection

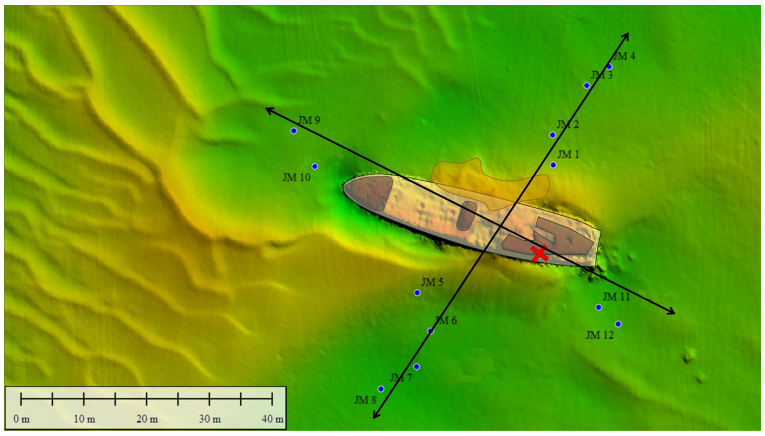

FIGURE 6
Sediment (JM xx) samples were taken around the John Mahn shipwreck on the four transects radiating Northeast (four sediment samples and one water sample), Southeast (two sediment samples and one water sample), Southwest (four sediment samples and one water sample) and Northwest (two sediment samples and one water sample) from the ship's centre. The coal bunker was located in the back of the ship on the port/stern side indicated by the red cross. The bombs the ship was equipped with were predominantly found at the front and back of the vessel.

carrier gas helium in constant flow mode (1 mL min^{-1}). The conditions of the PTV were 40°C for 0.30 min with a pressure of 20 kPa at a flow of 70 ml mincript-1. The heating to 260°C was performed at 1.3°C sec^{-1} and at a pressure of 250 kPa. Final hold was for 1 min. A split flow of 20 ml min^{-1} was used.

5.3 Microbial analysis

During flow cytometry analysis, the samples were first diluted in 0.22 µm-filtered Instant Ocean® artificial seawater and stained with 1 vol% SYBR® Green I (SG, 100x concentrate in 0.22 µm-filtered DMSO, Invitrogen) for total cell analysis. Staining was performed as described previously, with an incubation period of 20 min at 37°C in the dark (Chatzigiannidou et al., 2018). Samples were analysed immediately after incubation on an Attune NXT (Thermo Fisher Scientific, Waltham, MA, USA) flow cytometer, equipped with a blue (488 nm) and red (637 nm) laser with Focusing Fluid (Thermo Fisher Scientific, Waltham, MA, USA) as sheath fluid. The instrument performance was verified daily using Attune™ Performance Tracking Beads (Thermo Fisher Scientific, Waltham, MA, USA). The gating strategy can be found in Supplementary Figure S7.

For 16S rRNA gene sequencing, triplicate subsamples of approximately 100 mg were taken from the -20°C frozen sediment samples. Two swabs per -20°C frozen iron piece of the wreckage were taken for 16S rRNA gene sequencing as well. Subsequent DNA extraction was performed by adding about 1 mL Tris/HCl (100 mM, pH 8) lysis buffer and 200 mg glass beads (0.11 mm Sartorius, Göttingen, Germany) to each swab after which cells were mechanically lysed by multidirectional beating for 5 mins at 4500 rpm in a PowerLyzer instrument (Mo Bio laboratories). Glass beads were removed by centrifugation for 5 min at 18 000 g, DNA was purified by a phenol-chloroform extraction and precipitated by adding 1 volume ice-cold isopropyl alcohol and 1:10 volume 3 M sodium acetate for at least 1 hr at -20°C, followed by centrifugation for 30 min at 18 000 g. The supernatant was discarded and the DNA pellet was dried and suspended in 100 µL 1× TE buffer (10 mM Tris, 1 mM EDTA). A DNA Clean and Concentrator kit (Zymo Research, BaseClear, Netherlands) was used according to the producer's protocol to remove any contaminants able to interfere with PCR and sequencing.

For subsequent DNA extract quality control, the 16S rRNA gene V3-V4 hypervariable regions were amplified by PCR with Taq DNA Polymerase and the Fermentas PCR Master Mix Kit according to the manufacturers' specifications (Thermo Fisher Scientific, Waltham, MA, USA) using primers 341F (5'-CCT ACG GGN GGC WGC AG -3') and 785Rmod (5'-GAC TAC HVG GGT ATC TAA KCC-3'). The reverse primer was adapted from Klindworth et al. (2013), to increase coverage. The V3-V4 hypervariable region of the 16SrRNA gene was chosen as these regions have the best "*environments*" for the best pick-up rate during 2 x 250 base pair Illumina Miseq sequencing Klindworth et al. (2013). The obtained PCR product was run along with the DNA extract as well as a GeneRuler DNA Ladder Mix (Thermo Fisher Scientific, Waltham, MA, USA) on a 2% agarose gel for 30 minutes at 100 V as a control. The genomic DNA of the samples was then sent out to LGC genomics GmbH (Berlin, Germany) for library preparation and sequencing on an Illumina Miseq platform with V3 chemistry. The microbial data from the HMS Royal Oak sediments were downloaded from the European Nucleotide Archive database under accession number PRJEB37440, these data were obtained by Thomas et al. (2021).

5.4 Heavy metal analysis

The sediment subsamples of each 3-4 grams sediment were dried for 48 h at 55°C and weighed again. Metal content analysis was performed according to the official 2010 VITO (Dataset VITO, 2010; Dataset VITO, 2020) destruction method for solid material (CMA/2/II/A.3). In short, 0.5 g of dried sediment was digested and metals were extracted with a mixture of HCl, HF and HNO3 in a 20 min during temperature cycle with a microwave, followed by the addition of a Hipt3BO3 microwaved for another 3 minutes. Samples were subsequently filtered and run on an inductively coupled plasma-optical emission spectroscopy (Thermo Fisher iCap Q). The accuracy of the analysis was verified using BCR-277R estuarine sediment (certified reference material, European Commission).

5.5 Data analysis

5.5.1 Bacterial amplicon sequencing

All data analysis was performed in R (version 4.0.3). The DADA2 R package was used to process the amplicon sequence data according to the pipeline tutorial (Callahan et al., 2016). In a first quality control step, the primer sequences were removed and reads were truncated at a quality score cut-off (truncQ = 2). Besides trimming, additional filtering was performed to eliminate reads containing any ambiguous base calls or reads with high expected errors (maxEE = 2,2). After dereplication, unique reads were further denoised using the Divisive Amplicon Denoising Algorithm (DADA) error estimation algorithm and the selfConsist sample inference algorithm (with the option pooling = TRUE). The obtained error rates were inspected and after approval, the denoised reads were merged. Subsequently, the amplicon sequence variant (ASV) table obtained after chimera removal was used for taxonomy assignment using the Naive Bayesian Classifier and the DADA2 formatted Silva v138 (Quast et al., 2013). ASV's mapping back to anything other than 'Bacteria' were filtered out as they were considered technical noise. Singletons, reads occurring only once in all samples were considered noise and were removed (McMurdie and Holmes, 2014). In all analyses of bacteria, we removed chloroplast/mitochondria sequences. In analyses of phytoplankton, we only used chloroplast/mitochondria sequences. All the 'chloroplast' ASV's were separately reassigned using the 16S rRNA sequence taxonomy from the plastid, apicoplast, chromatophore and mitochondrion part of the pr2 database (Decelle et al., 2015; Derelle et al., 2016; Gaonkar et al., 2018; Adl et al., 2019) to identify the chloroplasts present in the sample as a proxy of photosynthetic eukaryotes as performed in a similar workflow by both Fuentes et al. (2019) and Tamayo-Leiva et al. (2021).

5.5.2 Statistical data analysis

Further data analysis was performed using statistical packages like Phenoflow (v1.1.2) (Props et al., 2016) for flow cytometric data analysis, Phyloseq (v1.22.3) (McMurdie and Holmes, 2013) for ASV's data handling, vegan (v2.5.6) (Dixon, 2003) and betapart for diversity analysis of ASV's, ancombc (v2) (Lin and Peddada, 2020) for significant higher/lower abundance of ASV's. To assess significant changes due to the imposed environmental conditions, (PERM)ANOVA analysis was used, using a cut-off of (adjusted) p-value<0.05. Furthermore, a Pearson's correlation was performed in R to correlate environmental conditions (heavy metal concentration, organic pollutant concentration) with the abundance of specific ASV's.

Data availability statement

The datasets presented in this study can be found in online repositories. The names of the repository/repositories and accession number(s) can be found below: BioProject number PRJNA800643 in the NCBI database (https://www.ncbi.nlm.nih.gov/).

Author contributions

JV: Formal analysis, Investigation, Writing - original draft, Visualization. KK: Methodology, Writing - review and editing, Supervision. SV: Methodology, Investigation. MN: Methodology, Investigation. KP: Methodology, Writing - review and editing, Supervision. MD: Conceptualization, Methodology, Writing - review and editing, Supervision, Project administration, Funding acquisition. NB: Conceptualization, Methodology, Writing - review and editing, Supervision, Project administration, Funding acquisition. All authors contributed to the article and approved the submitted version.

Funding

The research leading to the results presented in this publication was carried out with infrastructure funded by the BOF.GOA.2015.0002.01 BOF15/GOA/006 project awarded by BOF and the "North Sea Wrecks" project awarded by the EU Interreg North Sea Region Programme.

Acknowledgments

Dr. Ruth Plets for her help in the acquisition and processing of multibeam imagery. Volunteers of the VLIZ Scientific diving

team (Marjan Steppe, Jessica Vandevelde). The crew of the RV Simon Stevin. Uwe Wilchert for providing eye-witness reports on the sinking of V-1302 from the German Military Records in the Bundesarchiv in Freiburg, Germany. The EU Interreg North Sea Region programme for their financial support of the "North Sea Wrecks" project. Dr. Karel Folens for his help with the metal analysis. Dr. Frederiek-Maarten Kerckhof for his suggestions and his help on the microbial data analysis.

Conflict of interest

The authors declare that the research was conducted in the absence of any commercial or financial relationships that could be construed as a potential conflict of interest.

Publisher's note

All claims expressed in this article are solely those of the authors and do not necessarily represent those of their affiliated organizations, or those of the publisher, the editors and the reviewers. Any product that may be evaluated in this article, or claim that may be made by its manufacturer, is not guaranteed or endorsed by the publisher.

Supplementary material

The Supplementary Material for this article can be found online at: https://www.frontiersin.org/articles/10.3389/fmars.2022.1017136/full#supplementary-material

References

Adl, S. M., Bass, D., Lane, C. E., Lukeš, J., Schoch, C. L., Smirnov, A., et al. (2019). Revisions to the classification, nomenclature, and diversity of eukaryotes. *J. Eukaryotic Microbiol.* 66, 4–119. doi: 10.1111/jeu.12691

Almeida, E., Diamantino, T. C., and de Sousa, O. (2007). Marine paints: The particular case of antifouling paints. *Prog. Organic Coatings* 59, 2–20. doi: 10.1016/j.porgcoat.2007.01.017

Bacosa, H. P., Erdner, D. L., Rosenheim, B. E., Shetty, P., Seitz, K. W., Baker, B. J., et al. (2018). Hydrocarbon degradation and response of seafloor sediment bacterial community in the northern gulf of Mexico to light Louisiana sweet crude oil. *ISME J.* 12, 2532–2543. doi: 10.1038/s41396-018-0190-1

Bauer, B., Buzek, C., Daeves, D., Cremer, T, Daeves, K, Dornhecker, K, et al. (1925). "Handbuch der eisen- und stahlgießerei," in *Erster band grundlagen* (Berlin, Heidelberg: Springer Berlin Heidelberg). zweite, erweiterte auflage edn.

Baustian, M. M., Rabalais, N. N., Morrison, W. L., and Turner, R. E. (2011). Seasonal microphytobenthos on the hypoxic northern gulf of Mexico continental shelf. *Mar. Ecol. Prog. Ser.* 436, 51–66. doi: 10.3354/meps09262

Buchan, A., González, J. M., and Chua, M. J. (2019). "Aerobic hydrocarbon-degrading alphaproteobacteria: Rhodobacteraceae (Roseobacter)," in *Taxonomy, genomics and ecophysiology of hydrocarbon-degrading microbes*. Ed. T. J. McGenity (Cham: Springer International Publishing), 93–104. doi: 10.1007/978-3-030-14796-9_8

Callahan, B. J., McMurdie, P. J., Rosen, M. J., Han, A. W., Johnson, A. J. A., and Holmes, S. P. (2016). DADA2: High-resolution sample inference from illumina amplicon data. *Nat. Methods* 13, 581–583. doi: 10.1038/nmeth.3869

Chapman, M., Tolhurst, T., Murphy, R., and Underwood, A. (2010). Complex and inconsistent patterns of variation in benthos, micro-algae and sediment over multiple spatial scales. *Mar. Ecol. Prog. Ser.* 398, 33–47. doi: 10.3354/meps08328

Chatzigiannidou, I., Props, R., and Boon, N. (2018). Drinking water bacterial communities exhibit specific and selective necrotrophic growth. *NPJ Clean Water* 1, 1–4. doi: 10.1038/s41545-018-0023-9

Cibic, T., Fazi, S., Nasi, F., Pin, L., Alvisi, F., Berto, D., et al. (2019). Natural and anthropogenic disturbances shape benthic phototrophic and heterotrophic microbial communities in the po river delta system. *Estuarine Coast. Shelf Sci.* 222, 168–182. doi: 10.1016/j.ecss.2019.04.009

Czub, M., Nawała, J., Popiel, S., Dziedzic, D., Brzeziński, T., Maszczyk, P., et al. (2020). Acute aquatic toxicity of sulfur mustard and its degradation products to daphnia magna. *Mar. Environ. Res.* 161, 105077. doi: 10.1016/j.marenvres.2020.105077

Dataset Commission, O (2017). Status and trends in the concentrations of polycyclic aromatic hydrocarbons (PAHs) in sediment.

Dataset VITO (2010). Gesloten en semi-open microgolfoven destructiemethode met salpeterzuur, zoutzuur en waterstoffluoride.

Dataset VITO (2020). Compendium voor monsterneming en analyses van afvalstoffen en bodem (CMA). *EMIS*.

Decelle, J., Romac, S., Stern, R. F., Bendif, E. M., Zingone, A., Audic, S., et al. (2015). PhytoREF: a reference database of the plastidial 16S rRNA gene of photosynthetic eukaryotes with curated taxonomy. *Mol. Ecol. Resour.* 15, 1435–1445. doi: 10.1111/1755-0998.12401

Dell'Anno, F., Rastelli, E., Tangherlini, M., Corinaldesi, C., Sansone, C., Brunet, C., et al. (2021). Highly contaminated marine sediments can host rare bacterial taxa potentially useful for bioremediation. *Front. Microbiol.* 12. doi: 10.3389/fmicb.2021.584850

Derelle, R., López-García, P., Timpano, H., and Moreira, D. (2016). A phylogenomic framework to study the diversity and evolution of stramenopiles (=Heterokonts). *Mol. Biol. Evol.* 33, 2890–2898. doi: 10.1093/molbev/msw168

Dixon, P. (2003). VEGAN, a package of r functions for community ecology. *J. Vegetation Sci.* 14, 927–930. doi: 10.1111/j.1654-1103.2003.tb02228.x

Enning, D., Venzlaff, H., Garrelfs, J., Dinh, H. T., Meyer, V., Mayrhofer, K., et al. (2012). Marine sulfate-reducing bacteria cause serious corrosion of iron under electroconductive biogenic mineral crust. *Environ. Microbiol.* 14, 1772–1787. doi: 10.1111/j.1462-2920.2012.02778.x

Fuentes, S., Arroyo, J. I., Rodríguez-Marconi, S., Masotti, I., Alarcón-Schumacher, T., Polz, M. F., et al. (2019). Summer phyto- and bacterioplankton communities during low and high productivity scenarios in the Western Antarctic peninsula. *Polar Biol.* 42, 159–169. doi: 10.1007/s00300-018-2411-5

Gaonkar, C. C., Piredda, R., Minucci, C., Mann, D. G., Montresor, M., Sarno, D., et al. (2018). Annotated 18S and 28S rDNA reference sequences of taxa in the planktonic diatom family chaetocerotaceae. *PLoS One* 13, e0208929. doi: 10.1371/journal.pone.0208929

Gwizdala, M., Jelenska, M., and Leczynski, L. (2018). "Surface sediments pollution around small shipwrecks (Munin and abille) in the gulf of gdańsk: Magnetic and heavy metals study," in *Magnetometry in environmental sciences: Studying environmental structure changes and environmental pollution*. Eds. M. Jelenska, L. Leczynski and T. Ossowski (Cham: Springer International Publishing), 37–50. GeoPlanet: Earth and Planetary Sciences. doi: 10.1007/978-3-319-60213-4_3

Hamdan, L. J., Salerno, J. L., Reed, A., Joye, S. B., and Damour, M. (2018). The impact of the deepwater horizon blowout on historic shipwreck-associated sediment microbiomes in the northern gulf of Mexico. *Sci. Rep.* 8, 9057. doi: 10.1038/s41598-018-27350-z

Jiao, S., Chen, W., Wang, E., Wang, J., Liu, Z., Li, Y., et al. (2016). Microbial succession in response to pollutants in batch-enrichment culture. *Sci. Rep.* 6, 21791. doi: 10.1038/srep21791

Kelly, L. W., Barott, K. L., Dinsdale, E., Friedlander, A. M., Nosrat, B., Obura, D., et al. (2012). Black reefs: iron-induced phase shifts on coral reefs. *ISME J.* 6, 638–649. doi: 10.1038/ismej.2011.114

Klindworth, A., Pruesse, E., Schweer, T., Peplies, J., Quast, C., Horn, M., et al. (2013). Evaluation of general 16S ribosomal RNA gene PCR primers for classical and next-generation sequencing-based diversity studies. *Nucleic Acids Res.* 41, e1. doi: 10.1093/nar/gks808

Koske, D., Goldenstein, N. I., Rosenberger, T., Machulik, U., Hanel, R., and Kammann, U. (2020). Dumped munitions: New insights into the metabolization of

2,4,6-trinitrotoluene in Baltic flatfish. *Mar. Environ. Res.* 160, 104992. doi: 10.1016/j.marenvres.2020.104992

Lake, S. J., and Brush, M. J. (2011). The contribution of microphytobenthos to total productivity in upper Narragansett bay, Rhode island. *Estuarine Coast. Shelf Sci.* 95, 289–297. doi: 10.1016/j.ecss.2011.09.005

Landquist, H., Hassellöv, I. M., Rosén, L., Lindgren, J. F., and Dahllöf, I. (2013). Evaluating the needs of risk assessment methods of potentially polluting shipwrecks. *J. Environ. Manage.* 119, 85–92. doi: 10.1016/j.jenvman.2012.12.036

Landquist, H., Norrman, J., Lindhe, A., Norberg, T., Hassellöv, I. M., Lindgren, J. F., et al. (2017). Expert elicitation for deriving input data for probabilistic risk assessment of shipwrecks. *Mar. Pollut. Bull.* 125, 399–415. doi: 10.1016/j.marpolbul.2017.09.043

Lin, H., and Peddada, S. D. (2020). Analysis of compositions of microbiomes with bias correction. *Nat. Commun.* 11, 3514. doi: 10.1038/s41467-020-17041-7

Magnusson, M., Heimann, K., Ridd, M., and Negri, A. P. (2013). Pesticide contamination and phytotoxicity of sediment interstitial water to tropical benthic microalgae. *Water Res.* 47, 5211–5221. doi: 10.1016/j.watres.2013.06.003

Mandić, J., and Vrančić, M. P. (2017). Concentrations and origin of polycyclic aromatic hydrocarbons in sediments of the middle Adriatic Sea. *Acta Adriatica* 58, 3–24. doi: 10.32582/aa.58.1.1

Marini, M., and Frapiccini, E. (2013). Persistence of polycyclic aromatic hydrocarbons in sediments in the deeper area of the northern Adriatic Sea (Mediterranean Sea). *Chemosphere* 90, 1839–1846. doi: 10.1016/j.chemosphere.2012.09.080

Martínez-Gómez, C., Vethaak, A. D., Hylland, K., Burgeot, T., Köhler, A., Lyons, B. P., et al. (2010). A guide to toxicity assessment and monitoring effects at lower levels of biological organization following marine oil spills in European waters. *ICES J. Mar. Sci.* 67, 1105–1118. doi: 10.1093/icesjms/fsq017

McBeth, J. M., and Emerson, D. (2016). In situ microbial community succession on mild steel in estuarine and marine environments: Exploring the role of iron-oxidizing bacteria. *Front. Microbiol.* 7. doi: 10.3389/fmicb.2016.00767

McMurdie, P. J., and Holmes, S. (2013). Phyloseq: An r package for reproducible interactive analysis and graphics of microbiome census data. *PLoS One* 8, e61217. doi: 10.1371/journal.pone.0061217

McMurdie, P. J., and Holmes, S. (2014). Waste not, want not: Why rarefying microbiome data is inadmissible. *PLoS Comput. Biol.* 10, e1003531. doi: 10.1371/journal.pcbi.1003531

Pinckney, J. L., Hagenbuch, I. M., Long, R. A., and Lovell, C. R. (2013). Sublethal effects of the antibiotic tylosin on estuarine benthic microalgal communities. *Mar. pollut. Bull.* 68, 8–12. doi: 10.1016/j.marpolbul.2013.01.006

Price, K. A., Garrison, C. E., Richards, N., and Field, E. K. (2020). A shallow water ferrous-hulled shipwreck reveals a distinct microbial community. *Front. Microbiol.* 11. doi: 10.3389/fmicb.2020.01897

Props, R., Monsieurs, P., Mysara, M., Clement, L., and Boon, N. (2016). Measuring the biodiversity of microbial communities by flow cytometry. *Methods Ecol. Evol.* 7, 1376–1385. doi: 10.1111/2041-210X.12607

Quast, C., Pruesse, E., Yilmaz, P., Gerken, J., Schweer, T., Yarza, P., et al. (2013). The SILVA ribosomal RNA gene database project: Improved data processing and web-based tools. *Nucleic Acids Res.* 41, D590–D596. doi: 10.1093/nar/gks1219

Rajala, P., Cheng, D.-Q., Rice, S. A., and Lauro, F. M. (2022). Sulfate-dependant microbially induced corrosion of mild steel in the deep sea: A 10-year microbiome study. *Microbiome* 10, 4. doi: 10.1186/s40168-021-01196-6

Rochman, F. F., Sheremet, A., Tamas, I., Saidi-Mehrabad, A., Kim, J.-J., Dong, X., et al. (2017). Benzene and naphthalene degrading bacterial communities in an oil sands tailings pond. *Front. Microbiol.* 8. doi: 10.3389/fmicb.2017.01845

Rodacy, P., Reber, S., Walker, P., and Andre, J. (2001). Chemical sensing of explosive targets in the Bedford basin, Halifax, Nova Scotia. *Tech. Rep.* SAND2001-3569, 789594. doi: 10.2172/789594

Rogowska, J., Kudłak, B., Tsakovski, S., Gałuszka, A., Bajger-Nowak, G., Simeonov, V., et al. (2015). Surface sediments pollution due to shipwreck s/s "Stuttgart": a multidisciplinary approach. *Stoch Environ. Res. Risk Assess.* 29, 1797–1807. doi: 10.1007/s00477-015-1054-0

Rogowska, J., Wolska, L., and Namieśnik, J. (2010). Impacts of pollution derived from ship wrecks on the marine environment on the basis of s/s "Stuttgart" (Polish coast, Europe). *Sci. Total Environ.* 408, 5775–5783. doi: 10.1016/j.scitotenv.2010.07.031

Smith, M., Bardiau, M., Brennan, R., Burgess, H., Caplin, J., Ray, S., et al. (2019). Accelerated low water corrosion: the microbial sulfur cycle in microcosm. *NPJ Mater Degrad* 3, 1–11. doi: 10.1038/s41529-019-0099-9

Sternheim, J., Rytkönen, J., and Helavuori, M.. (2019). *SUBMERGED – HELCOM: Warfare materials in the Baltic Sea*. Finland: techreport. pp. 141. Available at: https://portal.helcom.fi/meetings/RESPONSE%2028-2020-743/MeetingDocuments/9-2%20Att.2%20Comments%20on%20the%20draft%20Submerged%20Assessment.pdf

Sundbäck, K., Alsterberg, C., and Larson, F. (2010). Effects of multiple stressors on marine shallow-water sediments: Response of microalgae and meiofauna to nutrient–toxicant exposure. *J. Exp. Mar. Biol. Ecol.* 388, 39–50. doi: 10.1016/j.jembe.2010.03.007

Tamayo-Leiva, J., Cifuentes-Anticevic, J., Aparicio-Rizzo, P., Arroyo, J. I., Masotti, I., and Díez, B. (2021). Influence of estuarine water on the microbial community structure of Patagonian fjords. *Front. Mar. Sci.*, 8. doi: 10.3389/fmars.2021.611981

Thomas, G. E., Bolam, S. G., Brant, J. L., Brash, R., Goodsir, F., Hynes, C., et al. (2021). Evaluation of polycyclic aromatic hydrocarbon pollution from the HMS royal oak shipwreck and effects on sediment microbial community structure. *Front. Mar. Sci.* 8. doi: 10.3389/fmars.2021.650139

Trzesicka-Mlynarz, D., and Ward, O. P. (1995). Degradation of polycyclic aromatic hydrocarbons (PAHs) by a mixed culture and its component pure cultures, obtained from PAH-contaminated soil. *Can. J. Microbiol.* 41, 470–476. doi: 10.1139/m95-063

Whalan, S., and Webster, N. S. (2014). Sponge larval settlement cues: The role of microbial biofilms in a warming ocean. *Sci. Rep.* 4, 4072. doi: 10.1038/srep04072

frontiers | Frontiers in Microbiology

TYPE Original Research
PUBLISHED 02 November 2022
DOI 10.3389/fmicb.2022.1041521

OPEN ACCESS

EDITED BY
Shan He,
Ningbo University, China

REVIEWED BY
Zenghu Zhang,
Chinese Academy of Sciences (CAS), China
Yunyun Zhuang,
Ocean University of China, China
Liqiang Yang,
Ocean University of China, China

*CORRESPONDENCE
Feng Zhou
zhoufeng@sio.org.cn
Pengbin Wang
algae@sio.org.cn

SPECIALTY SECTION
This article was submitted to Aquatic Microbiology, a section of the journal Frontiers in Microbiology

RECEIVED 11 September 2022
ACCEPTED 29 September 2022
PUBLISHED 02 November 2022

CITATION
Guo R, Ma X, Zhang J, Liu C, Thu CA, Win TN, Aung NL, Win HS, Naing S, Li H, Zhou F and Wang P (2022) Microbial community structures and important taxa across oxygen gradients in the Andaman Sea and eastern Bay of Bengal epipelagic waters.
Front. Microbiol. 13:1041521.
doi: 10.3389/fmicb.2022.1041521

Microbial community structures and important taxa across oxygen gradients in the Andaman Sea and eastern Bay of Bengal epipelagic waters

Ruoyu Guo[1,2], Xiao Ma[2,3], Jingjing Zhang[1], Chenggang Liu[1], Chit Aung Thu[4], Tun Naing Win[5], Nyan Lin Aung[6], Hlaing Swe Win[7], Sanda Naing[8], Hongliang Li[1], Feng Zhou[2,3]* and Pengbin Wang[1,2]*

[1]Key Laboratory of Marine Ecosystem Dynamics, Second Institute of Oceanography, Ministry of Natural Resources, Hangzhou, China, [2]Observation and Research Station of Yangtze River Delta Marine Ecosystems, Ministry of Natural Resources, Zhoushan, China, [3]State Key Laboratory of Satellite Ocean Environment Dynamics, Second Institute of Oceanography, Ministry of Natural Resources, Hangzhou, China, [4]Research and Development Section, Department of Fisheries, Naypyidaw, Myanmar, [5]Department of Meteorology and Hydrology, Ministry of Transport and Communication, Naypyidaw, Myanmar, [6]Environmental Conservation Department, Ministry of Natural Resources and Environmental Conservation, Naypyidaw, Myanmar, [7]National Analytical Laboratory, Department of Research in Innovation, Ministry of Education, Naypyidaw, Myanmar, [8]Port and Harbour Engineering Department, Myanmar Maritime University, Thanlyin, Myanmar

In oceanic oxygen minimum zones (OMZs), the abundances of aerobic organisms significantly decrease and energy shifts from higher trophic levels to microorganisms, while the microbial communities become critical drivers of marine biogeochemical cycling activities. However, little is known of the microbial ecology of the Andaman Sea and eastern Bay of Bengal (BoB) OMZs. In the present study, a total of 131 samples which from the Andaman Sea and eastern BoB epipelagic waters were analyzed. The microbial community distribution patterns across oxygen gradients, including oxygenic zones (OZs, dissolved oxygen [DO] $\geq$ 2 mg/L), oxygen limited zones (OLZs, 0.7 mg/L $<$ DO $<$ 2 mg/L), and OMZs (DO $\leq$ 0.7 mg/L), were investigated. Mantel tests and Spearman's correlation analysis revealed that DO was the most important driver of microbial community structures among several environmental factors. Microbial diversity, richness, and evenness were highest in the OLZs and lowest in the OZs. The microbial community compositions of OZ and OMZ waters were significantly different. Random forest analysis revealed 24 bioindicator taxa that differentiated OZ, OLZ, and OMZ water communities. These bioindicator taxa included Burkholderiaceae, HOC36, SAR11 Clade IV, Thioglobaceae, Nitrospinaceae, SAR86, and UBA10353. Further, co-occurrence network analysis revealed that SAR202, AEGEAN-169, UBA10353, SAR406, and Rhodobacteraceae were keystone taxa among the entire interaction network of the microbial communities. Functional prediction further indicated that the relative

abundances of microbial populations involved in nitrogen and sulfur cycling were higher in OMZs. Several microbial taxa, including the Thioglobaceae, Nitrospinaceae, SAR202, SAR406, WPS-2, UBA10353, and Woeseiaceae, may be involved in nitrogen and/or sulfur cycling, while also contributing to oxygen consumption in these waters. This study consequently provides new insights into the microbial community structures and potentially important taxa that contribute to oxygen consumption in the Andaman Sea and eastern BoB OMZ.

KEYWORDS

oxygen minimum zone, keystone taxa, bioindicator taxa, Andaman Sea, Bay of Bengal

Introduction

Dissolved oxygen (DO) concentration is one of most important factors that shapes community structures and functions in marine ecosystems (Vaquer-Sunyer and Duarte, 2008; Beman and Carolan, 2013). As deoxygenation intensifies in marine ecosystems, aerobic organism abundances significantly decrease and biogeochemical processes are altered, leading to energetic shifts from higher trophic levels to microorganisms (Diaz and Rosenberg, 2008; Wright et al., 2012). Ocean regions where oxygen decreases to very low concentrations and then rises again with increasing depth are termed oxygen minimum zones (OMZs) (Paulmier and Ruiz-Pino, 2009). Previous studies have revealed numerous microbial taxa and microbial-mediated biogeochemical cycling patterns associated with global OMZs (Walsh et al., 2009; Wright et al., 2012; Padilla et al., 2016; Long et al., 2021). Indeed, OMZs harbor unique microbial taxa and community compositions (Beman and Carolan, 2013; Bush et al., 2017). Hence, microbial communities that mediate biogeochemical cycling in OMZs are distinct from those in oxygenic regions (Beman and Carolan, 2013; Bertagnolli and Stewart, 2018). Nitrogen and/or sulfur cycling activities generally increase in OMZs (Ulloa et al., 2012; Wright et al., 2012; Penn et al., 2019). Moreover, microbial communities mediate numerous biogeochemical feedbacks in OMZs that can exacerbate or ameliorate deoxygenation by participating in nitrogen, sulfur, and carbon cycles (Levin, 2018). In recent years, microbial studies have significantly improved our understanding of the ecology and biogeochemical cycling within OMZs.

Oxygen minimum zones typically occur at water depths of 100–1500 m underlying surface waters. Four permanent OMZs have been identified globally including the eastern tropical North Pacific (ETNP), the eastern tropical South Pacific (ETSP), the Arabian Sea, and the Bay of Bengal (BoB) (Diaz and Rosenberg, 2008; Paulmier and Ruiz-Pino, 2009; Lam and Kuypers, 2011; Breitburg et al., 2018). However, coastal eutrophication and climate change have led to OMZs expanding and shoaling in past decades, and these processes remain ongoing (Diaz and Rosenberg, 2008; Deutsch et al., 2011; Schmidtko et al., 2017; Breitburg et al., 2018; Oschlies, 2021). The expansion and shoaling of OMZs can potentially alter the microbial communities and microbially-mediated biogeochemical cycling activities in these regions (Gilly et al., 2013; Bertagnolli and Stewart, 2018).

The Andaman Sea, located in the northeastern Indian Ocean, is a semi-closed marginal sea, and is bounded by Myanmar to the north, in addition to Thailand and Malaysia in the east, while being partly isolated by the Andaman and Nicobar Islands from the BoB (Dutta et al., 2007). The Andaman Sea is connected to the eastern BoB through shallow passages including the Preparis Channel in the north, the Ten Degree Channel, and the Great Channel in the south (Jithin and Francis, 2020). A large freshwater influx and seasonal monsoon winds lead to the region containing the Andaman Sea and BoB being distinct from other water bodies in tropical regions (Han and Mccreary, 2001; Mahadevan, 2016). However, investigations of the microbial ecology in the Andaman Sea and BoB in addition to its associations with oxygen concentration effects remain limited. A few microbial diversity studies have been conducted focusing on the BoB OMZ (Rajpathak et al., 2018; Fernandes et al., 2020; Vijayan et al., 2020; Gu et al., 2022). Specifically, 16S rRNA gene sequencing investigations, analysis of specific functional genes, culture-based methods, and metagenomic analyses have been used to evaluate BoB OMZ microbial communities (Bristow et al., 2016; Rajpathak et al., 2018; Fernandes et al., 2020; Vijayan et al., 2020; Gu et al., 2022). Microbial taxa that potentially function in nitrogen and/or sulfur cycling in the BoB OMZs include the SAR11, Pelagibacteraceae, and Caulobacteraceae groups (Rajpathak et al., 2018; Fernandes et al., 2020; Gu et al., 2022). Nevertheless, investigating the microbial diversity and composition within the BoB OMZs and their interactive relationships will help improve our understanding of ecosystem and biogeochemical cycling processes in this area.

In the present study, the microbial diversity and compositional structures and their interactive patterns were investigated between 90.04°E–97.26°E and 12.94°N–16.10°N, ranging from the Andaman Sea to the eastern BoB. High-throughput sequencing was used to evaluate the microbial

composition of 131 water samples from the region. Further, the microbial diversity from oxygenic zones (OZs) to OMZs at depths of up to 200 m were characterized and their potential functions were evaluated.

Materials and methods

Sampling and geochemical analyses

Sampling was conducted at 23 stations across the Andaman Sea and the eastern BoB spanning water depths from 2 to 200 m through the international cooperation cruise, namely Joint Advanced Marine and Ecological Studies (JAMES) between China and Myanmar, during December 2019 to January 2020 (**Supplementary Figure 1** and **Supplementary Table 1**). Seawater samples were collected with Niskin bottles mounted to a Sea-bird conductivity, temperature, and depth (CTD) sensor (SBE 911, Sea-Bird Co., WA, USA). A total of 2 L of seawater was filtered from each layer using 0.2-μm pore-size membrane filters (Millipore, Tullagreen, Carrigtwohill, Ireland). The collected filter samples were immediately frozen in liquid nitrogen and maintained at −20°C on board the ship. At the end of the cruise, the filters were moved to storage at −80°C in the lab until subsequent DNA extraction. Environmental parameters (i.e., depth, temperature, and salinity) were measured using a CTD sensor (SBE 911, Sea-Bird Co., WA, USA). Nutrient and DO levels were analyzed following previously described protocols (Grasshoff et al., 1999).

Oceanic OMZ region boundaries are fluid and their definitions have considerably varied, depending on oxygen concentration demands of marine organisms and varying thresholds for hypoxia among ocean regions (Karstensen et al., 2008; Vaquer-Sunyer and Duarte, 2008; Gilly et al., 2012, 2013). Further, the units used to define OMZ or hypoxic conditions are variable, and criteria have not been defined to identify these areas. In this study, the hypoxia threshold was defined as 0.7 mg/L and these samples were considered as OMZs, while mild hypoxia was defined at concentrations of 0.7–2 mg/L and considered as oxygen limited zones (OLZs), while samples with DO $\geq$ 2 mg/L were considered OZs (**Supplementary Table 2**). These definitions were made based on those of previous studies (Karstensen et al., 2008; Vaquer-Sunyer and Duarte, 2008; Gilly et al., 2012, 2013).

Sequencing, data processing, and operational taxonomic unit assignments

DNA extraction and sequencing was conducted following previously described methods (Guo et al., 2020). The universal primer pair 338F (5′-ACTCCTACGGGAGGCAGCAG-3′) and 806R (5′ GGACTACHVGGGTWTCTAA T-3′) was used to amplify the V3–V4 hypervariable regions of 16S rRNA genes. Sequencing was subsequently conducted at Majorbio Bio-Pharm Technology Co. Ltd. (Shanghai, China). Raw sequences were processed using the QIIME pipeline (Caporaso et al., 2010). Raw data quality filtering and assembly were conducted using Fastp 0.19.6 and FLASH v1.2.11, respectively (Magoč and Salzberg, 2011; Chen et al., 2018). Raw reads were trimmed with a quality score threshold of tailing bases < 20 using moving-window sizes of 50 bp. If the average base pair quality in a window was < 20, sequences were trimmed and reads with length < 50 bp and those that contained ambiguous bases (N's) were removed. Subsequently remaining paired-end reads were assembled with a minimum overlap length of 10 bp and with < 2% mismatches. Singletons were removed from the datasets and the remaining sequences were clustered into operational taxonomic units (OTUs) at a nucleotide similarity level of 97% using Uparse (version 7.0.1090) (Edgar, 2013). Taxonomic classification of each OTU was conducted using the RDP Classifier 2.11.[1] Representative 16S rRNA gene sequences from each OTU were annotated against the SILVA database (silva132/16s_bacteria) using a similarity cutoff value of 0.7. The sequence information was listed in **Supplementary Table 1**. The raw sequence data generated in this study have been deposited in the NCBI Sequence Read Archive database under the accession number PRJNA862716.

Data analysis

Alpha diversity indices including the Chao1 (richness), Heip (evenness), and Shannon (diversity) values were calculated using MOTHUR version 1.30.2 (Schloss et al., 2009). Mantel tests based on Bray–Curtis distances were used to assess the relationships of environmental factors and bacterial communities using the QIIME software package. Principal coordinates analysis (PCoA) was used to evaluate beta diversity patterns. To evaluate co-occurrence networks, the 500 most abundant OTUs were used to construct co-occurrence networks using Spearman's correlation (r) relationships among abundances of OTUs. Correlations with $R \mid \geq \mid 0.8$ and $p < 0.01$ were used for the final network analysis and visualized with the Gephi software program (version 0.9.2; WebAtlas, Paris, France). Module detection and topology parameter analysis was conducted in the Gephi 0.9.2 program. High degree, high closeness centrality, and low betweenness centrality values were used to define keystone taxa (Banerjee et al., 2018). The cutoff value for keystone taxa were 96, 0.477, 0.04 for degree, closeness centrality, and betweenness centrality, respectively. Random Forest analysis was used to identify significant indicator taxa associated with DO concentrations

1 https://sourceforge.net/projects/rdp-classifier/

using the R randomForest package. LEfSe (Segata et al., 2011) analysis was used to identify microbial taxa that distinguished two or more groups using the all-against-all strategy and linear discriminant analysis (LDA) score thresholds of > 4. Heatmaps of environmental factors and important taxa were constructed from Spearman's correlation analyses. Lastly, the functional annotation of prokaryotic taxa software program (FAPROTAX) was used to predict the potential functions of microbial communities. The important taxa were defined as the taxa that assigned to specific taxa, significantly different taxa, keystone taxa, and bioindicator taxa.

Results

Relationships between microbial communities and environmental factors

A total of 5,729 OTUs were generated from 16S rRNA gene sequencing analysis of 131 water samples. The Shannon alpha diversity index values of bacterial communities were negatively correlated with DO and temperature measurements (Table 1; Supplementary Figure 2), but positively correlated with depth, salinity, and NO_3^- concentrations. The regression analysis R^2 indicated that DO was the most correlated environmental factor to the Shannon index, while depth was the least correlated (Table 1). Mantel tests indicated that bacterial community composition was positively associated with environmental factors including DO, temperature, depth, salinity, and NO_3^- concentrations (Table 2). DO exhibited the highest positive relationships with bacterial community composition. Thus, DO was the most important driver shaping the microbial communities in the OMZs of the Andaman Sea and eastern BoB above 200 m depth.

Bacterial community compositions and differences among oxygen zones

Samples were separated into three groups based on DO concentrations including OMZs, OLZs, and OZs. The Shannon, Chao1, and Heip indices of bacterial community diversity were significantly higher in the OMZs and OLZs than in the OZs. Although these index values for OLZ communities were higher than in those of OMZ communities, significant differences were not detected (Figure 1). PCoA analysis (Figure 2, Bray–Curtis distance: $R = 0.811$, $p = 0.001$) was used to assess the distribution of microbial communities at the OTU level. The first PCoA axis explained 42.18% of the total variation and separated the OMZ and OZ communities. However, the microbial communities from OLZ could not be separated from the OMZ and OZ communities based on PCoA ordinations. PERMANOVA results (Supplementary Table 3) indicated that the DO showed the highest R^2 (0.398) compared to other environmental factors. These results were corresponding to Mantel test result (Table 2), it indicated that DO was the most important environmental factors shaping the microbial communities in the Andaman Sea and eastern BoB above 200 m depth.

A total of 79, 89, and 65 classes, in addition to 355, 391, and 312 families were identified in the OMZ, OLZ, and OZ communities, respectively (Supplementary Figure 3). Further, the predominant classes included the Oxyphotobacteria, Alphaproteobacteria, and Actinobacteria within the OZ communities, while the three most abundant classes of the OLZs were the Gammaproteobacteria, Alphaproteobacteria, and Actinobacteria, in addition to the SAR406 group in the OMZs. At the family level, the Cyanobiaceae, Flavobacteriaceae, and Actinomarinaceae dominated the OZ communities, while the SAR406, SAR324 marine group B, and Microtrichaceae families were most dominant in the OLZ and OMZ communities (Figure 3). The relative abundances of Alphaproteobacteria and Gammaproteobacteria were highest in the OMZ and lowest in the OZ (Figure 3). Moreover, the Deltaproteobacteria, SAR406, Dehalococcoidia, and WPS-2 exhibited gradually increased

TABLE 2 Mantel test results for environmental factors and bacterial community composition at the OTU level.

Environmental factor	*R*	*P*
DO	0.795	0.001
Temperature	0.687	0.001
Depth	0.681	0.001
Salinity	0.723	0.001
NO_3^-	0.702	0.001

TABLE 1 Spearman's correlation analysis between Shannon diversity and environmental factors.

Environmental factor	Correlation coefficient	Sig. (2-Tailed)	R^2 of regression analysis	*P*
DO	−0.676	0.000	0.7343	0.000
Temperature	−0.731	0.000	0.5034	0.000
Depth	0.746	0.000	0.4245	0.000
Salinity	0.735	0.000	0.7188	0.000
NO_3^-	0.740	0.000	0.7135	0.000

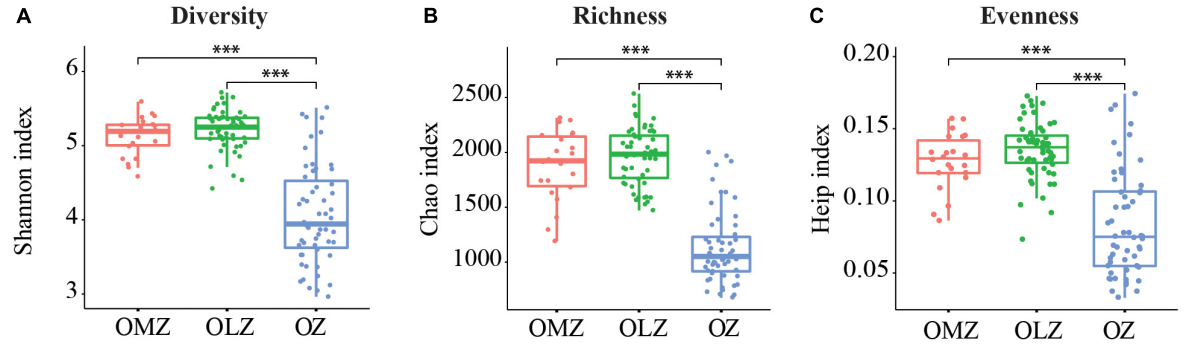

FIGURE 1
Distribution of alpha diversity index values for samples from the OMZ, OLZ, and OZ. **(A)** Diversity; **(B)** richness; and **(C)** evenness values are shown. Horizontal bars within boxes represent medians of each index. ***$p < 0.001$. Welch's *t*-test was used in the statistical analysis.

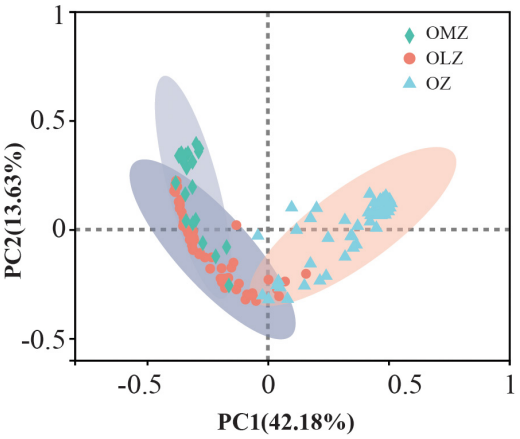

FIGURE 2
Principal coordinate analysis (PCoA) of Bray–Curtis distances among communities from the OMZ, OLZ, and OZ waters. ANOSIM was used in the statistical analysis.

relative abundances with decreasing DO concentrations (from the OZ to the OMZ communities) (Figure 2).

A total of 16, 37, and 9 families were specific to the OMZ, OLZ, and OZ, communities, respectively (Supplementary Figure 3). The top three highest relative abundance specific taxa for the OMZ communities were Latescibacteraceae, MSBL5 (o), and Rhodobiaceae, while the most specific families for the OLZ communities were the Muribaculaceae, Thermodesulfovibrionia (c), and Rhizobiales (o). Lastly, the Bradymonadales (o), type III (Entomoplasmatales), and Pseudanabaenaceae were the top three highest relative abundance specific taxa for the OZ communities (Supplementary Table 4).

LEfSe analysis revealed significant differences of taxa among the OZ, OLZ, and OMZ communities. Specifically, the Thioglobaceae, SAR202, WPS-2 (p), UBA10353, and SAR406 were enriched in the OMZ communities, while the HOC36 and Microtrichaceae were enriched in the OLZ communities (Figure 4). The SAR86, SAR116, Actinomarinaceae, Flavobacteriaceae, and Cyanobiaceae groups were enriched in the OZ communities.

Random forest modeling was used to identify bioindicator taxa that differentiated OZ, OLZ, and OMZ communities at the family level (Figure 5A). Further, 10-fold cross-validation was used to evaluate the importance of bioindicator microbial families. The cross-validation error curve stabilized with an error rate of 0.129 when considering the 24 most relevant families. The 24 families were consequently identified as bioindicator taxa (Figure 5A). The families belong to 11 classes in addition to eight and five families, within the Gammaproteobacteria and Alphaproteobacteria, respectively (Figures 5A,B). Burkholderiaceae was the most important bioindicator taxa and their relative abundances were highest in the OZ communities (Figure 5B; Supplementary Figure 4). In addition, the relative abundances of SAR116, the SAR11 clade IV, and the PS1 clade were highest in the OZ. The HOC36, Nitrospinaceae, OCS116 (o), Woeseiaceae (o), NB1-j (o), Lentimicrobiaceae, RCP2-54, and N9D0 (c) groups exhibited the highest relative abundances in the OLZ (Figure 5B; Supplementary Figure 4). In addition, the Thioglobaceae, UBA10353 (o), Rickettsiales (o), and Chloroflexi (p) groups exhibited the highest relative abundances in the OMZ communities (Figure 5B; Supplementary Figure 4). The S085, TK17, and N9D0 (within the Chloroflexi phylum) were also identified as bioindicator taxa (Figure 5A). The relative abundances of these groups were very low, and they were more abundant in the OMZ and OLZ communities than in the OZ community (Figure 5B; Supplementary Figure 4). All of these taxa clustered into a single clade and exhibited close relationships with the Lentimicrobiaceae (Figure 5B). Unclassified HOC36 were the second most important bioindicator taxa (Figure 5A). OTUs affiliated with the HOC36 or *Candidatus* Thioglobus sp. taxa remain uncultured.

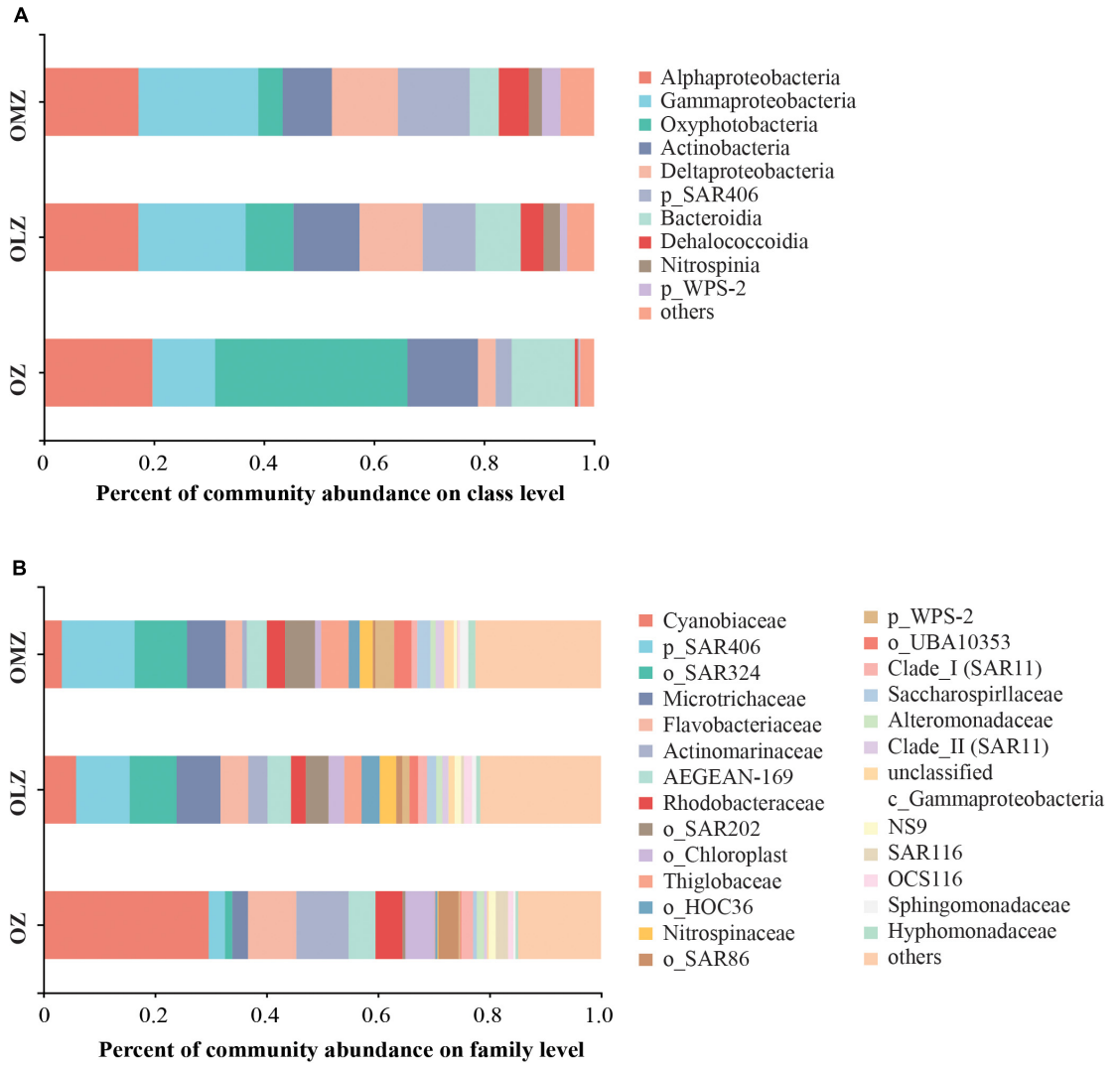

FIGURE 3
Microbial community composition of OMZ, OLZ, and OZ waters at the class and family levels. Taxa are distinguished at the **(A)** class and **(B)** family level. p, phylum; o, order; c, class.

Bacterial community co-occurrence patterns

A co-occurrence network was generated to explore bacterial interactions among bacterial communities (Figure 6A and Table 3). The network exhibited a scale-free degree distribution, suggesting non-random co-occurrence patterns (Supplementary Figure 5). The co-occurrence network comprised 324 nodes and 8,851 edges. A total of 7,191 positive correlations were present in the network in addition to 1,660 negative edges.

The entire network was divided into 14 modules, with modules 0, 1, and 2 respectively accounting for 30.86, 26.23, and 33.95% of the entire network. Module 0 was associated with OMZ communities and predominantly comprised Dehalococcoidia, Gammaproteobacteria, and Alphaproteobacteria that constituted the largest relative abundances of 19.6, 18.6, and 16.5%, respectively, among module 0 (Figure 6B) nodes. Module 1 (Figure 6C) was associated with OZs, wherein Alphaproteobacteria, Bacteroidia, and Gammaproteobacteria contributed 29.4, 23.5, and 22.4% of the module 1 nodes, respectively. Lastly, module 2 (Figure 6D) was associated with OLZs. Alphaproteobacteria, Gammaproteobacteria, and SAR406 accounted for 21.2, 17.7, and 16.8% of the module 2 nodes, respectively.

Keystone taxa considerably influence community networks, in addition to maintaining their structures and functions (Berry and Widder, 2014; Banerjee et al., 2018). High degree, high closeness centrality, and low betweenness

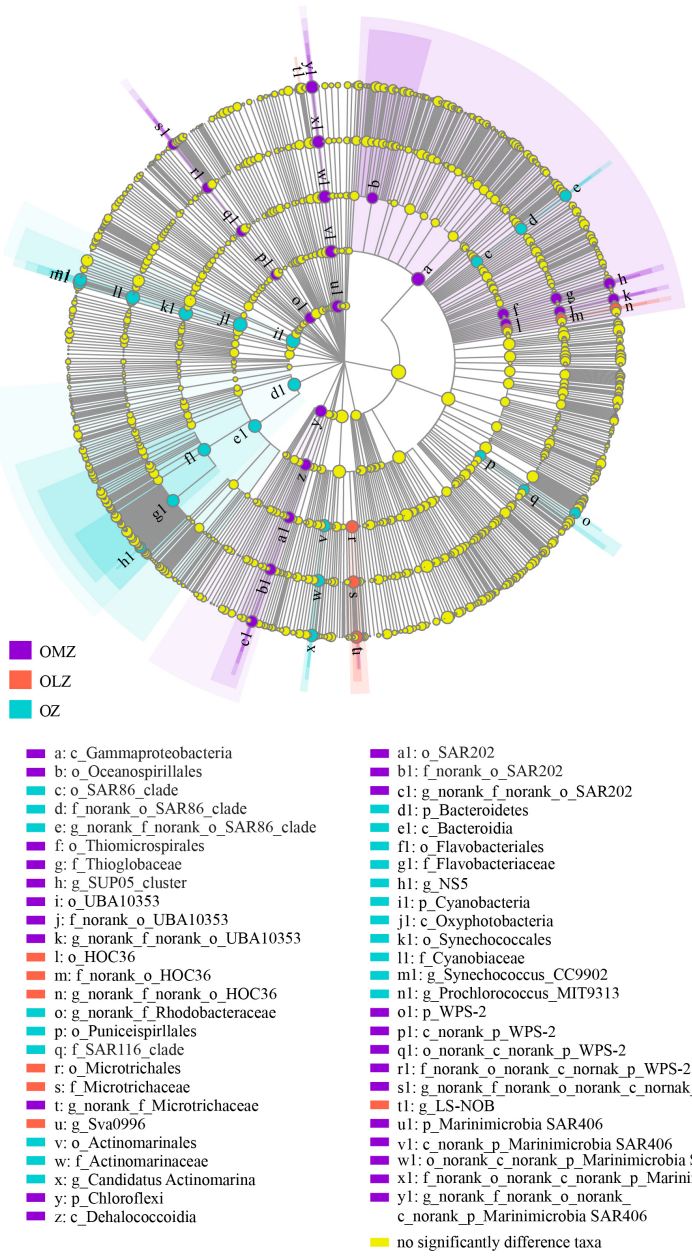

FIGURE 4
Taxonomic cladogram showing distinctive taxa in the OMZ, OLZ, and OZ communities identified by LEfSe analysis. Enlarged colored circles show differentially abundant taxa in each sampling zone. Yellow dots mean the taxa that no significant different between OMZ, OLZ, and OZ waters.

centrality values were used to identify keystone OTUs (**Supplementary Table 5**) that were affiliated with the SAR202, AEGEAN-169, UBA10353, SAR406, and Rhodobacteraceae groups, with most of these OTUs belonging to module 0. OTU6020 was affiliated with the Rhodobacteraceae and was a keystone taxa for module 1. In addition, OTU881 was affiliated with SAR406 and was a keystone taxa for module 2.

Relationships between environmental factors and important taxa

Spearman correlation analysis revealed that the relative abundances of most taxa were significantly correlated with measurements of DO, temperature, depth, salinity, and NO_3^- concentrations (**Figure 7**). SAR86 relative abundances were only significantly positively correlated with DO (**Figure 7**;

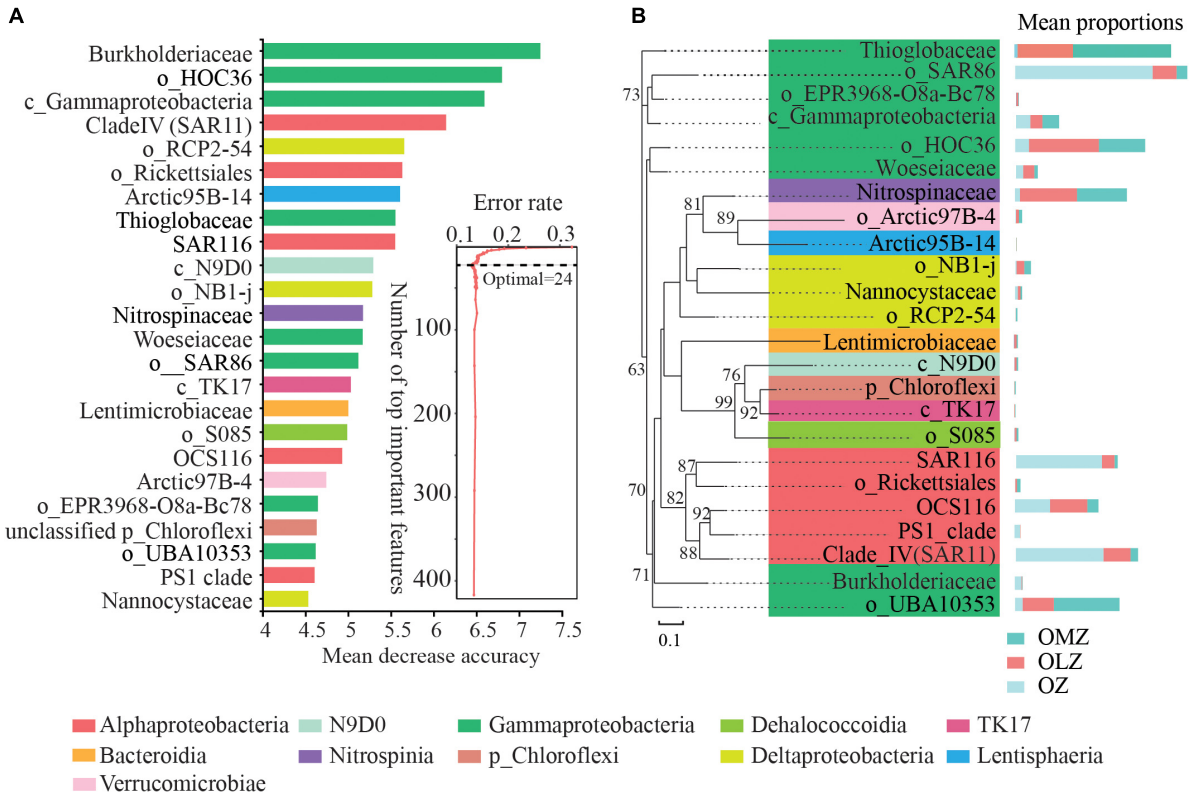

FIGURE 5
Random forest modeling analysis detection of microbial biomarker taxa that significantly differentiate OMZ, OLZ, and OZ communities. **(A)** The 24 most discriminatory microbial families were identified by applying Random Forest classification of the relative abundances of populations in the OMZ, OLZ, and OZ communities. Biomarker taxa are ranked in descending order of importance to the accuracy of the model. **(B)** Phylogenetic analysis of biomarker families. Bars represent the relative abundances of microbial taxa in the OMZ, OLZ, and OZ communities.

Supplementary Table 6). Correlations between AEGEAN-169 relative abundances and temperature were not observed. The relative abundances of Nitrospinaceae, SUP05, SAR406, SAR324, UBA10353, and HOC36 were negatively correlated with DO. Lastly, the relative abundances of Burkholderiaceae, PS1, Woeseiaceae, Clade I, Clade III, and Clade IV were positively correlated with DO.

Functional predictions of bacterial communities

Functional Annotation of Prokaryotic Taxa (FAPROTAX) analysis indicated the presence of various functional processes including chemoheterotrophy, nitrification, denitrification, and dark sulfite/sulfur oxidation that were more abundant in the OMZ and OLZ communities compared with the OZ communities (Figure 8). Denitrification potential was predicted for the communities, but the relative abundances were very low. In contrast, nitrification potential exhibited higher relative abundances than denitrification potential. Furthermore, the phototrophy and oxygenic photoautotrophy were more abundant in the OZ and OLZ compared to OMZ (Figure 8). FAPROTAX functional predictions for bioindicator taxa identified by random forest analysis suggested that bioindicator taxa for the OMZ and OLZ communities exhibited functions in nitrogen and sulfur cycling, including *via* nitrate reduction, nitrification, and dark sulfide/sulfur compound oxidation (Supplementary Figure 6). Among the indicator taxa for the OZ communities, aromatic hydrocarbon degradation, chemoheterotrophy, and ureolysis functions were prominent (Supplementary Figure 6).

Discussion

The expansion and shoaling of OMZs have increased in recent decades and these processes remain ongoing. Microbial communities are important players in biogeochemical processes and feature prominently within OMZ generation and functioning (Bertagnolli and Stewart, 2018). In the present study, samples were collected from the epipelagic zone of the Andaman Sea and eastern BoB to assess the microbial ecology of waters exhibiting different oxygen concentrations across

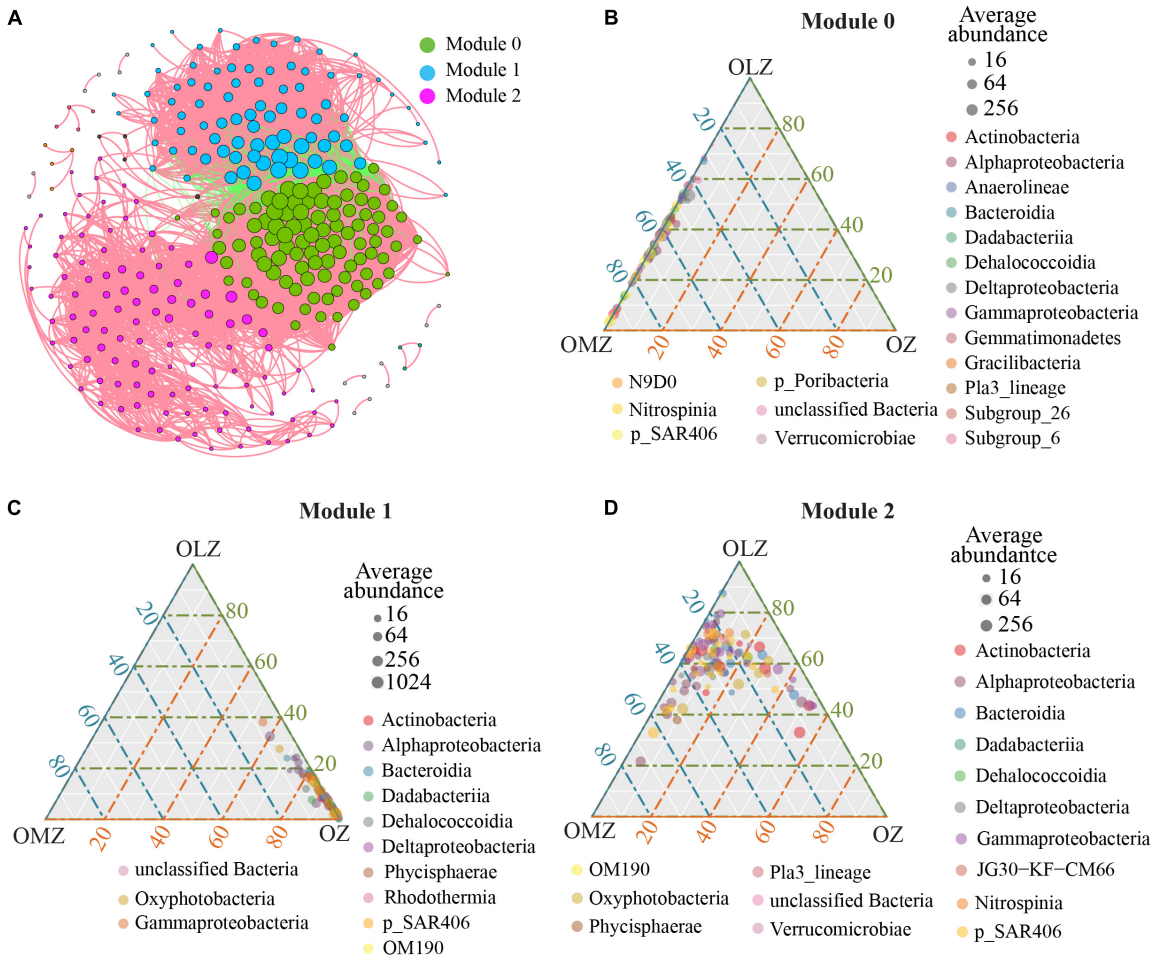

FIGURE 6
Co-occurrence patterns of microbial populations based on Spearman's correlation analysis. **(A)** Co-occurrence network. Network nodes represent OTUs and the size of each node is proportional to the number of its associations (degree). Each node is colored in a module. A connection represents a strong and significant correlation of abundance ($|r| > 0.8$, $p < 0.01$). **(B)** Ternary plot showing the distribution of OTUs from module 0 at the class level. **(C)** Ternary plot showing the distribution of OTUs from module 1 at the class level. **(D)** Ternary plot showing the distribution of OTUs from module 2 at the class level. The gray dots indicate the average abundant of taxa.

TABLE 3 Topological properties of community networks.

Network metric	Value
No. of nodes	324
No. of edges	8,851
Modularity (no of modules)	0.745 (14)
Average clustering coefficient	0.731
Network diameter	9
Average path length	2.61
Average degree	29.778
Density	0.169

OMZs, OLZs, and OZs. The microbial community diversity, composition, bioindicator, and keystone taxa identified here suggest that major biogeochemical processes differ considerably between OZs and OMZs of the Andaman Sea and eastern BoB epipelagic waters.

Environmental factors controlling the diversity and composition of microbial communities

Investigation of relationships between environmental factors with microbial community composition and diversity revealed that DO, depth, temperature, salinity, and NO_3^- concentrations were the significant environment factors that structured microbial communities in the study region. These results indicated that DO, depth, temperature, salinity, and NO_3^- should co-shape microbial communities. Among these, DO was the most highly associated environmental

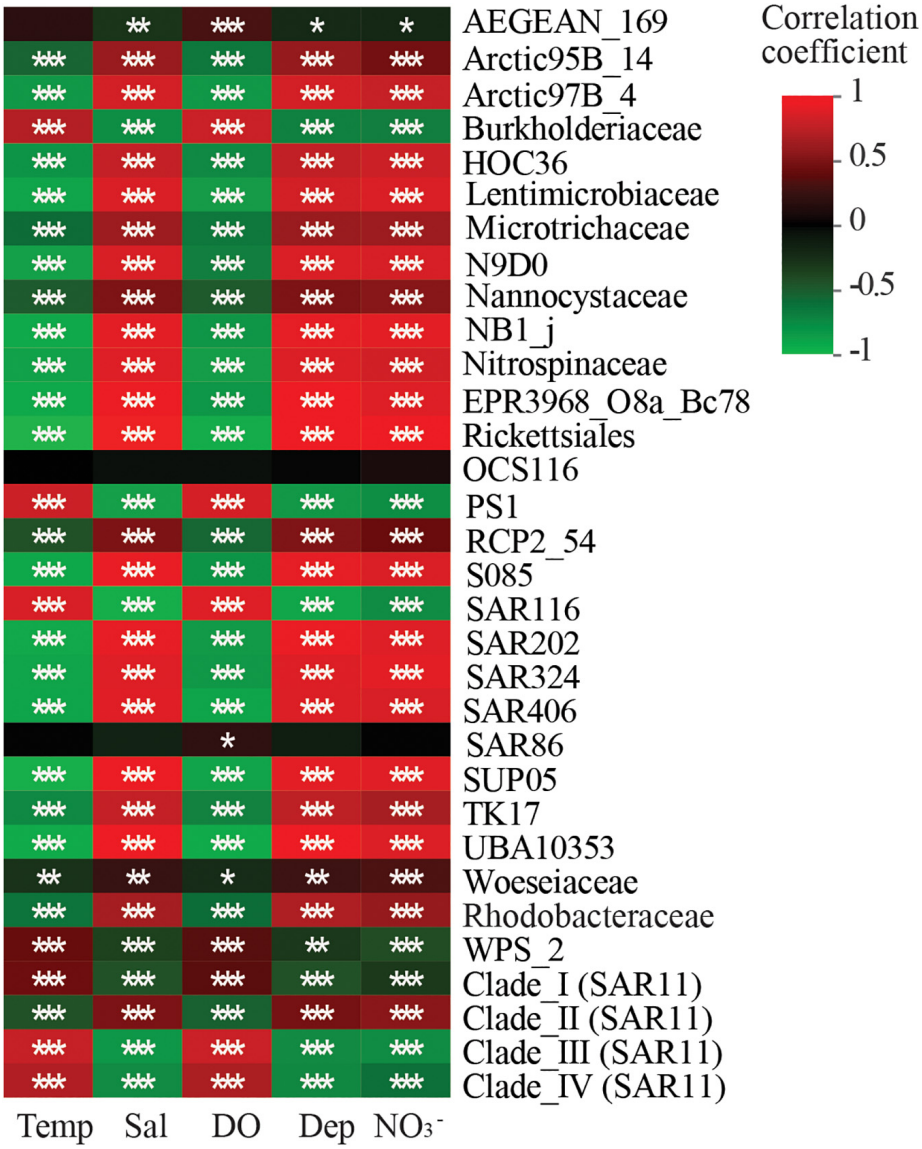

FIGURE 7
Heatmap showing the correlations of biomarker and keystone taxa with environmental factors. Temp, temperature; Sal, salinity; DO, dissolved oxygen; Dep, depth; NO_3^-, Spearman's correlation analysis was employed in the correlation analysis of environmental factors and each taxon. Correlation coefficient value *R* were shown in different colors. *$p < 0.05$; **$p < 0.01$; ***$p < 0.001$.

factor with microbial communities, and also significantly differentiated microbial community types. Thus, although microbial community structures were determined by multiple interacting environmental factors, DO was the most important driver of community structure in the epipelagic zone of the study site, likely due to the oxygen-depleted water column. DO has been similarly detected as an important and strong driver of microbial community diversity and community structure in hypoxic ocean regions like the Gulf of Mexico hypoxic zone and the eastern tropical North Pacific Ocean (ETNP) (Beman and Carolan, 2013; Campbell et al., 2018).

Microbial community composition and important taxa in the Andaman Sea and eastern Bay of Bengal

Alpha diversity index comparisons suggested that microbial communities exhibited increased species richness and evenness in oxygen deficient (OMZ and OLZ) compared with oxygenic (OZ) water column communities. However, significant differences of diversity indices were not detected between OLZ and OMZ communities, indicating that the microbial community composition of OLZs was more similar to OMZ

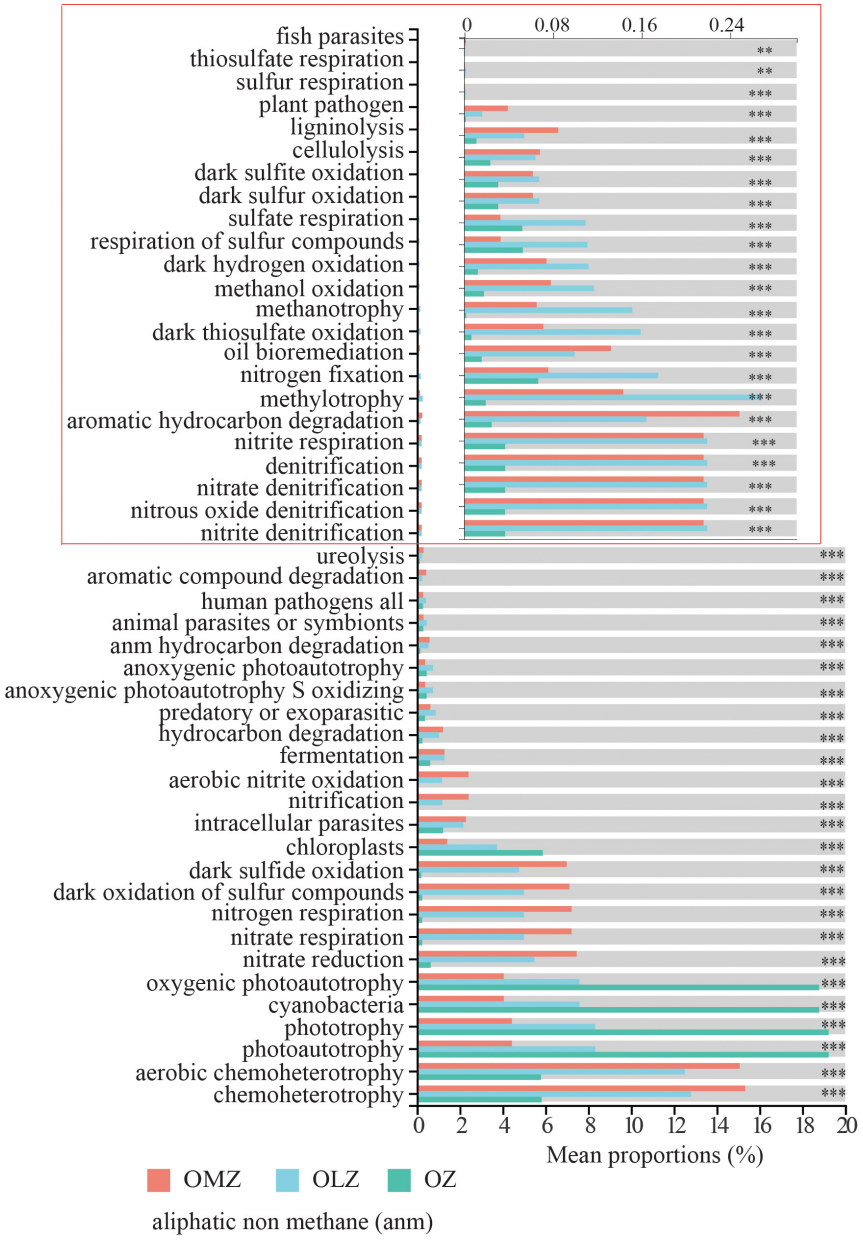

FIGURE 8
Functional Annotation of Prokaryotic Taxa (FAPROTAX) function predication plot showed mean proportions of predicated functions in OMZ, OLZ, and OZ. Games–Howell were used in the statistical test. $^{**}p < 0.01$; $^{***}p < 0.001$. Since the mean proportions of some functions (in red box) is very less, the x-axis was enlarged, and the number marked in the x-axis in red box was still the real mean proportions of each function.

communities than OZ communities. PCoA also indicated that the microbial communities of OMZ and OZ samples were considerably different, while the microbial community compositions of OLZ overlapped with OZ and OMZ communities. OLZs are transition regions adjacent to OZs and OMZs, perhaps accounting for the mixed characteristics of the OLZ microbial communities. These results are consistent with those from the ETNP, wherein bacterial richness exhibited a unimodal distribution with decreasing DO, reaching maximum values at the edge of the OMZ, then decreasing (Beman and Carolan, 2013). These data indicate that the transition region from the OZ to OMZ contained greater types of microbiota (i.e., greater diversity).

The microbial communities analyzed in this study possessed characteristics common to other global OMZs. As previously shown (Wright et al., 2012; Long et al., 2021), the Oxyphotobacteria, Alphaproteobacteria, Actinobacteria, and SAR86 phyla are prevalent in oxygenic water columns overlying

OMZs. Prevalent microbial taxa such as the Nitrospinaceae, SAR202, SAR406, SAR324, Thioglobaceae (primarily the SUP05 group), and UBA10353 previously observed in oxygen-deficient waters (Wright et al., 2012; Pajares et al., 2020; Long et al., 2021) were also identified in the OMZ/OLZ investigated in this study. Relatively high abundances of SAR202, SAR406, SAR324, SUP05, Nitrospinaceae, and UBA10353 have also been detected in many OMZs, including those in the ETNP, Northeast subarctic Pacific Ocean, Arabian Sea, and Black Sea (Fuchsman et al., 2011; Allers et al., 2013; Beman and Carolan, 2013; Lüke et al., 2016; Thrash et al., 2017; Pajares et al., 2020). The family affiliated with the SAR324 was the second most predominant taxa in the OMZ of this study, while the SAR202, SAR406, and UBA10353 groups were not only abundant, but also keystone taxa that maintained the network structure of interactions among the OMZ/OLZ communities of the Andaman Sea and eastern BoB. The SAR324, SAR202, and SAR406 groups ubiquitously inhabit a wide variety of environments, and their abundances are higher in deeper waters or in low-oxygen concentration waters such as OMZs (Giovannoni et al., 1996; Morris et al., 2004; Wright et al., 2012, 2014; Rinke et al., 2013; Sheik et al., 2014; Guerrero-Feijóo et al., 2018). SAR324 possess metabolic flexibility allowing their use of several electron donors including sulfur, hydrocarbons, C1 compounds, and organic carbon, in addition to the use of several electron acceptors such as nitrite or oxygen (Sheik et al., 2014). SAR202 members possess versatile metabolic functions including nitrate/nitrous oxide reduction in addition to the metabolism of complex carbohydrates and organosulfur compounds (Thrash et al., 2017; Mehrshad et al., 2018). Likewise, SAR406 genomes encode genes involved in dissimilatory sulfur oxidation and reduction, dissimilatory nitrite reduction to ammonia, and degradation of complex carbohydrate compounds (Wright et al., 2014; Thrash et al., 2017). Nevertheless, the SAR202 and SAR406 groups contain multiple sub-lineages that may possess distinct metabolic functions in various environmental conditions (Thrash et al., 2017). Moreover, the gene expression of certain nitrogen/sulfur cycling genes were closely correlated to DO concentrations (Thrash et al., 2017).

UBA10353 and AEGEAN-169 were also keystone taxa in the network analysis. Unlike the SAR202 and SAR406 groups, the ecology, genetics, and functions of UBA10353 and AEGEAN-169 have not been well-documented. Indeed, the identification of UBA10353 has only been reported in recent years. However, more abundant populations have been identified in deeper layers of the western Mediterranean Sea and the OMZ core of Tropical Mexican Pacific, and they also have been shown to exhibit the potential ability for carbon fixation and sulfur oxidation (Pajares et al., 2020; Martínez-Pérez et al., 2022; Mena et al., 2022).

The relative abundances of AEGEAN-169 were similar between OMZ, OLZ, and OZ communities, but still exhibited the highest relative abundances in OZ samples of this study. The AEGEAN-169 group is closely related to SAR11 (Alonso-Sáez et al., 2007), and is generally present throughout water columns (Cram et al., 2015a; Reintjes et al., 2019). The group is also particularly abundant in the surface waters of the Ultraoligotrophic South Pacific Gyre and most abundant at 500 m within the San Pedro Channel (Cram et al., 2015a; Reintjes et al., 2019). Several environmental factors, such as oxygen, salinity, NO_3^-, influence the distribution of AEGEAN-169 (Cram et al., 2015b). The correlation of oxygen concentration with AEGEN-169 were different among OTUs, and both negative and positive relationship have been detected (Cram et al., 2015b). The different adaption characteristic for oxygen of AEGEAN-169 ecotypes might contribute to the similar relative abundance between OMZ, OLZ, and OZ communities.

Arctic97B-4 (affiliated with Verrucomicrobia) was identified as a bioindicator taxa in this study and have also been detected in other oxygen-deficient waters, including the OMZs of the Arabian Sea and Cariaco Basin (Lüke et al., 2016; Suter et al., 2018). The ecological roles of Arctic97B-4 remain unclear, but Verrucomicrobia taxa might be capable of surviving under oxygen-depleted conditions and potentially oxidizing methanol or methane (Dalcin Martins et al., 2021). A strong association between Arctic97B-4 and SAR202 was also detected and both were simultaneously present in modules 1 and 2 (**Supplementary Figure 7**). Tight associations of SAR202 and Arctic97B-4 have been detected in coastal waters that are also oxygen deficient water environments (Suter et al., 2018; Chun et al., 2021). Arctic97B-4, SAR202, and SAR406 taxa have been repeatedly shown to be associated in modules related to nutrient compositions, with the taxa exhibiting functions related to nitrate reduction, nitrification, and dark sulfide oxidation (Chun et al., 2021). Arctic97B-4 taxa exhibit unclear functions, but frequently share distribution patterns with SAR202 and SAR406 taxa, implying they share a similar functional role.

The Nitrospinaceae (including *Nitrospina* and *LS-NOB*) and SUP05 groups were significantly abundant in the OLZ and OMZ communities of this study and were also important indicator taxa. *Nitrospina* are aerobes and major nitrite oxidizing bacteria that contribute to nitrification in marine environments (Sun et al., 2019; Beman et al., 2021). Their members are often detected in global OMZs, as in OMZs of the Arabian Sea, ETSP, ETNP, and BoB (Sun et al., 2019; Gu et al., 2022). The relatively higher abundances of *Nitrospina* in the OLZ indicate that they might contribute oxygen-depletion and nitrification functions in the Andaman Sea and eastern BoB. SUP05 is also highly associated with globally distributed OMZs. The group includes known chemolithoautotrophs that have the potential capacity for carbon fixation, sulfur oxidation, and nitrate/nitrite reduction in oxygen-deficient oceanic waters (Walsh et al., 2009; Shah et al., 2017; Mattes et al., 2021). The HOC36 group (including uncultured taxa and *Candidatus* Thioglobus sp.) were the second most important bioindicator taxa. *Candidatus*

Thioglobus sp. belongs to the SUP05 clade (Marshall and Morris, 2013), suggesting that HOC36 might exhibit similar functions as SUP05 (Thioglobaceae). These data suggest that the SAR324, SAR202, SAR406, Nitrospinaceae, SUP05, and UBA10353 taxa could contribute to carbon, nitrogen, or sulfur cycling alongside oxygen depletion in the OMZ and OLZ of the Andaman Sea and eastern BoB epipelagic waters.

Several taxa not previously reported extensively in OMZs, including the WPS-2, Microtrichaceae, and Woeseiaceae, were identified as bioindicator taxa in this study. In particular, the WPS-2 and Microtrichaceae were especially abundant in the OMZ and OLZ communities of this study. WPS-2 exhibits a global distribution and is most often found in cool, acidic, and aerobic environments, contributing to their hypothesized functions as aerobic or microaerobic taxa (Ward et al., 2019) that may also perform chemolithoautotrophy (Sheremet et al., 2020; Ji et al., 2021). However, the WPS-2 have rarely been identified in marine environments. Thus, the identification of higher relative abundances of WPS-2 in OLZs or OMZs might imply that WPS-2 contribute to oxygen depletion in this region. Microtrichaceae have been shown to play roles in nitrification-anammox systems and can hydrolyze and metabolize complex organic matter (Wang et al., 2020; Li et al., 2021). Woeseiaceae is one of the most abundant bacterial families in marine sediments (Mußmann et al., 2017; Moreno-Ulloa et al., 2020; Zhou et al., 2022), and might contribute to sulfur-oxidation (Dyksma et al., 2016; Mußmann et al., 2017). In addition, RCP2-54 might be involved in methane, sulfur, and nitrogen cycling activities in Barents Sea sediments (Begmatov et al., 2021). These data suggest that most of the bioindicator taxa with higher relative abundances in the OMZ and OLZ communities of this study exhibit wide capacities for oxygen depletion, sulfur cycling, and nitrogen cycling.

Burkholderiaceae, Clade IV, SAR116, and SAR86 taxa were also identified as bioindicator taxa that were abundant in the OZ. Burkholderiaceae was the most significant bioindicator taxa identified in this study. Burkholderiaceae are associated with organic contaminants and have been detected in greater abundance in coastal shallow ecosystems such as in the Baltic Sea and south China sea, where they have been partially affected by anthropogenic activities (Iburg et al., 2021; Zhang et al., 2021). Some of the sampling locations in this study included continental shelf seas and near coastal estuaries, which could be impacted by pollutants, leading to anthropogenic influences. Clade IV belongs to the SAR11 group and was the fourth most important bioindicator taxa. SAR11 are prevalent in oxygen-rich surface oceans and are also abundant in OMZs (Wright et al., 2012; Tsementzi et al., 2016). SAR11 members can respond to organic matter produced autochthonously by phytoplankton release or *via* food web production of dissolved organic carbon (Schwalbach et al., 2010; Morris et al., 2012), while possessing the ability to reduce nitrate in anoxic zones (Tsementzi et al., 2016). The group has also been identified as abundant taxa that might be important nitrate reducers in the BoB OMZ (Gu et al., 2022). The SAR11 group contains several subclades including Clade I and Clade II that were also identified in samples of this study, to the exclusion of Clade IV. Similar to Clade IV, Clade I is also more abundant in OZ samples, while Clade II exhibited increased relative abundance with decreasing DO concentrations. Adverse effects from environmental factors on the abundances of Clade I and IV with Clade II were also detected in this study (**Figure 7**). These data suggest that different subclades of SAR11 might differentially contribute to oxygenic zone communities *via* different functions, while also contributing to nitrogen cycling in the Andaman Sea and eastern BoB. SAR86 and SAR116 are ubiquitous and abundant taxa that also differentiated communities in the Andaman Sea and BoB. The functions and ecological characteristics of different SAR86 ecotypes might shape their variable distribution patterns, while the SAR86 are most abundant in surface oceans and are also prevalent in oxygenic waters overlying OMZs (Reintjes et al., 2019; Hoarfrost et al., 2020; Mena et al., 2020). SAR116 exhibited decreased OTU numbers in the OMZ of the ETNP in association with decreasing DO levels (Beman and Carolan, 2013), indicating decreasing ecotype prevalence with decreasing oxygen concentrations. The positive correlation between the relative abundances of SAR116 and SAR86 indicate that they prefer the oxygenic waters of the Andaman Sea and eastern BoB. Cyanobiaceae is one of family that showed highest relative abundance in the OZ, and the relative high abundance were also detected in the OLZ and OMZ waters. These groups should contribute to autotrophy/oxygenic photoautotrophy of predicated function. The cyanobacteria such as *Prochlorococcus* and *Synechococcus* are commonly present with high abundance in the euphotic waters of OMZ regions (Beman and Carolan, 2013; Gu et al., 2022). The activity of cyanobacteria is largely light dependent that could contribute to large percentage of global primary production (Flombaum et al., 2013). However, the low-light clade of *Prochlorococcus* has been detected in ETSP and Arabian Sea, the OMZ shoaling into the euphotic zone may expand the niche of these type cyanobacteria (Goericke et al., 2000; Lavin et al., 2010; Gilly et al., 2013).

Potential biogeochemical cycling functions

Functional prediction revealed potential biogeochemical cycling activities among the taxa in the Andaman Sea and eastern BoB. Functions including nitrate/nitrite respiration/reduction, nitrification, denitrification, chemoheterotrophy, and hydrocarbon degradation exhibited increased predicted proportions in the OMZ and OLZ water samples of the Andaman Sea and eastern BoB. Nitrogen

and sulfur metabolisms are important for nutrient cycling in OMZs (Wright et al., 2012; Long et al., 2021). Nitrogen cycling activities including nitrification and denitrification are extensively present in oxygen-deficient waters such as in OMZs, and OMZs might account for 30–50% of oceanic nitrogen loss (Lam and Kuypers, 2011; Kuypers et al., 2018). In the BoB, low oxygen concentrations could support denitrifier and anammox microbial populations that mediate low, but significant N loss (Bristow et al., 2016). Although potential microbial populations that could be denitrifiers were identified here, the actual *in situ* metabolisms of these populations might closely depend on oxygen concentrations (Lam and Kuypers, 2011; Bristow et al., 2016; Gu et al., 2022). Oxygen concentrations within all samples from the OMZ in this study ranged from 0.27 to 0.7 mg L^{-1}. Within samples exhibiting these concentrations, some microbial groups (e.g., SAR11) encoding genes involved in nitrification exhibited higher levels in the BoB OMZ (Gu et al., 2022). In the present study, predicted denitrification gene abundances were considerably lower than nitrification gene abundances. These data imply that nitrification and denitrification activities might co-exist and that nitrification is a potential major nitrogen cycling activity in the OMZ region of the Andaman Sea and the eastern BoB.

Sulfur cycling–related functional genes such as those involved in dark sulfide/sulfur compound, sulfur, and sulfite oxidation also exhibited higher predicted abundances in OMZ/OLZ water samples than in oxygenic water samples. The OMZ sulfur cycle comprises abiotic and biologically mediated reactions (van Vliet et al., 2021). However, it is difficult to investigate sulfur reactions *in situ*, with the exception sulfide oxidation and sulfate reduction, due to technological difficulties (van Vliet et al., 2021). Nevertheless, investigations of sulfur-based microorganisms have greatly improved our understanding of sulfur cycling in oceanic OMZs (Callbeck et al., 2021; van Vliet et al., 2021). Microorganisms potentially involved in sulfur cycling including the SUP05, SAR324, and SAR406 were detected in the Andaman Sea and eastern BoB communities of the present study. These sulfur cycle–associated bacterial taxa might also potentially couple nitrogen and carbon cycling (Mußmann et al., 2017; Thrash et al., 2017; Callbeck et al., 2018; van Vliet et al., 2021).

Microbial populations that mediate nitrogen and sulfur cycling or other processes such as aerobic chemoheterotrophy also exhibit aerobic and/or anaerobic metabolisms that can coexist and reach stable equilibrium to a certain extent in anoxic marine zones (Zakem et al., 2020). Aerobic metabolisms such as aerobic chemoheterotrophy can consume oxygen in the water column. Thus, microbial communities, and especially bioindicator and keystone taxa identified here, including SAR406, SAR202, Thioglobaceae, and Nitrospinaceae, mediate nitrogen or sulfur cycling and potentially account for oxygen consumption in the OMZ of the Andaman Sea and eastern BoB.

Conclusion

The microbial community profiles of the Andaman Sea and eastern BoB epipelagic waters including oxygenic and oxygen-deficient samples were characterized here. Microbial community diversity and composition were highly correlated with environmental factors including DO, pH, temperature, salinity, and NO_3^- concentrations. DO was the most highly correlated environmental factor with microbial community composition. Microbial diversity, richness, and evenness were highest in the OLZ and lowest in the OZ, while microbial composition was significantly different between the OMZs and OZs of epipelagic waters. LEfSe, random forest modeling, and network analysis revealed significant differences of taxa, bioindicators, and keystone taxa within the OMZ, OLZ, and OZ environments. Taxa such as SUP05, SAR202, SAR406, WPS-2, and UBA10353 were abundant in the OMZ, while SAR202, SAR406, and UBA10353 were also keystone taxa in the microbial interaction network. A total of 24 taxa, including the Burkholderiaceae, HOC36, SAR11 Clade IV, and Nitrospinaceae groups, were identified as bioindicator taxa that differentiated OMZ, OLZ, and OZ communities of the Andaman Sea and eastern BoB epipelagic waters. Furthermore, functional prediction analysis indicated that nitrogen and sulfur cycling taxa potentially increased with decreased DO levels. Several microbial groups, including Nitrospinaceae, WPS-2, SAR324, SAR202, SAR406, SUP05, and UBA10353, might contribute to nitrogen and sulfur cycling, in addition to oxygen consumption in these areas. These results indicate that the core OMZ communities are generally distributed in much deeper waters, microbial community composition and biogeochemical cycling activities of OMZs are significantly different from those in the oxygenic, epipelagic waters.

Data availability statement

The datasets presented in this study can be found in online repositories. The names of the repository/repositories and accession number(s) can be found in the article/**Supplementary material**.

Author contributions

RG conceived the study, carried out the sampling and experiments, conducted data analyses, and wrote the manuscript. XM, HL, and JZ carried out the sampling and conducted data analysis. CT, TW, NA, HW, and CL carried out the sampling. SN revised the manuscript. FZ and PW conceived the study and reviewed and revised the manuscript. All

authors reviewed the manuscript and approved the submitted version.

Funding

This work was supported by the Global Change and Air-Sea Interaction II Program (Grant No. GASI-01-EIND-STwin), National Natural Science Foundation of China (Nos. 41961144013, 41906140, and 42176039), Natural Science Foundation of Zhejiang Province (No. LY20D060004), and the Project of State Key Laboratory of Satellite Ocean Environment Dynamics (No. SOEDZZ2105).

Acknowledgments

We thank all the co-investigators attend the international cooperation cruise of Joint Advanced Marine and Ecological Studies between China and Myanmar, and thank the captain, crew, and marine technicians of the Xiangyanghong 06 during the cruise.

Conflict of interest

The authors declare that the research was conducted in the absence of any commercial or financial relationships that could be construed as a potential conflict of interest.

Publisher's note

Supplementary material

The Supplementary Material for this article can be found online at: https://www.frontiersin.org/articles/10.3389/fmicb.2022.1041521/full#supplementary-material

References

Allers, E., Wright, J. J., Konwar, K. M., Howes, C. G., Beneze, E., Hallam, S. J., et al. (2013). Diversity and population structure of Marine Group A bacteria in the Northeast subarctic Pacific Ocean. *ISME J.* 7, 256–268. doi: 10.1038/ismej.2012.108

Alonso-Sáez, L., Balagué, V., Sà, E. L., Sánchez, O., González, J. M., Pinhassi, J., et al. (2007). Seasonality in bacterial diversity in north-west Mediterranean coastal waters: assessment through clone libraries, fingerprinting and FISH. *FEMS Microbiol. Ecol.* 60, 98–112. doi: 10.1111/j.1574-6941.2006.00276.x

Banerjee, S., Schlaeppi, K., and van der Heijden, M. G. A. (2018). Keystone taxa as drivers of microbiome structure and functioning. *Nat. Rev. Microbiol.* 16, 567–576. doi: 10.1038/s41579-018-0024-1

Begmatov, S., Savvichev, A. S., Kadnikov, V. V., Beletsky, A. V., Rusanov, I. I., Klyuvitkin, A. A., et al. (2021). Microbial communities involved in methane, sulfur, and nitrogen cycling in the Sediments of the Barents Sea. *Microorganisms* 9:2362. doi: 10.3390/microorganisms9112362

Beman, J. M., and Carolan, M. T. (2013). Deoxygenation alters bacterial diversity and community composition in the ocean's largest oxygen minimum zone. *Nat. Commun.* 4:2705. doi: 10.1038/ncomms3705

Beman, J. M., Vargas, S. M., Wilson, J. M., Perez-Coronel, E., Karolewski, J. S., Vazquez, S., et al. (2021). Substantial oxygen consumption by aerobic nitrite oxidation in oceanic oxygen minimum zones. *Nat. Commun.* 12:7043. doi: 10.1038/s41467-021-27381-7

Berry, D., and Widder, S. (2014). Deciphering microbial interactions and detecting keystone species with co-occurrence networks. *Front. Microbiol.* 5:219. doi: 10.3389/fmicb.2014.00219

Bertagnolli, A. D., and Stewart, F. J. (2018). Microbial niches in marine oxygen minimum zones. *Nat. Rev. Microbiol.* 16, 723–729. doi: 10.1038/s41579-018-0087-z

Breitburg, D., Levin, L. A., Oschlies, A., Grégoire, M., Chavez, F. P., Conley, D. J., et al. (2018). Declining oxygen in the global ocean and coastal waters. *Science* 359:eaam7240. doi: 10.1126/science.aam7240

Bristow, L. A., Callbeck, C. M., Larsen, M., Altabet, M. A., Dekaezemacker, J., Forth, M., et al. (2016). N2 production rates limited by nitrite availability in the Bay of Bengal oxygen minimum zone. *Nat. Geosci.* 10, 24–29. doi: 10.1038/NGEO2847

Bush, T., Diao, M., Allen, R. J., Sinnige, R., Muyzer, G., and Huisman, J. (2017). Oxic-anoxic regime shifts mediated by feedbacks between biogeochemical processes and microbial community dynamics. *Nat. Commun.* 8:789. doi: 10.1038/s41467-017-00912-x

Callbeck, C. M., Canfield, D. E., Kuypers, M., Yilmaz, P., and Bristow, L. A. (2021). Sulfur cycling in oceanic oxygen minimum zones. *Limnol. Oceanogr.* 66, 2360–2392. doi: 10.1002/lno.11759

Callbeck, C. M., Lavik, G., Ferdelman, T. G., Fuchs, B., Gruber-Vodicka, H. R., Hach, P. F., et al. (2018). Oxygen minimum zone cryptic sulfur cycling sustained by offshore transport of key sulfur oxidizing bacteria. *Nat. Commun.* 9:1729. doi: 10.1038/s41467-018-04041-x

Campbell, L. G., Thrash, C., Rabalais, N. N., and Mason, O. U. (2018). Extent of the annual Gulf of Mexico hypoxic zone influences microbial community structure. *PLoS One* 14:e0209055. doi: 10.1371/journal.pone.0209055

Caporaso, J. G., Kuczynski, J., Stombaugh, J., Bittinger, K., Bushman, F. D., Costello, E. K., et al. (2010). QIIME allows analysis of high-throughput community sequencing data. *Nat. Methods* 7, 335–336. doi: 10.1038/nmeth.f.303

Chen, S., Zhou, Y., Chen, Y., and Gu, J. (2018). fastp: an ultra-fast all-in-one FASTQ preprocessor. *Bioinformatics* 34, i884–i890. doi: 10.1093/bioinformatics/bty560

Chun, S.-J., Cui, Y., Baek, S. H., Ahn, C.-Y., and Oh, H.-M. (2021). Seasonal succession of microbes in different size-fractions and their modular structures determined by both macro- and micro-environmental filtering in dynamic coastal waters. *Sci. Total. Environ.* 784:147046. doi: 10.1016/j.scitotenv.2021.147046

Cram, J. A., Chow, C. E., Sachdeva, R., Needham, D. M., Parada, A. E., Steele, J. A., et al. (2015a). Seasonal and interannual variability of the marine bacterioplankton community throughout the water column over ten years. *ISME J.* 9, 563–580. doi: 10.1038/ismej.2014.153

Cram, J. A., Xia, L. C., Needham, D. M., Sachdeva, R., Sun, F., and Fuhrman, J. A. (2015b). Cross-depth analysis of marine bacterial networks suggests downward propagation of temporal changes. *ISME J.* 9, 2573–2586. doi: 10.1038/ismej.2015.76

Dalcin Martins, P., de Jong, A., Lenstra, W. K., van Helmond, N., Slomp, C. P., Jetten, M. S. M., et al. (2021). Enrichment of novel Verrucomicrobia,

Bacteroidetes, and Krumholzibacteria in an oxygen-limited methane- and iron-fed bioreactor inoculated with Bothnian Sea sediments. *MicrobiologyOpen* 10:e1175. doi: 10.1002/mbo3.1175

Deutsch, C., Brix, H., Lto, T., Frenzel, H., and Thompson, L. A. (2011). Climate-Forced variability of ocean hypoxia. *Science* 333, 336–339. doi: 10.1126/science.1202422

Diaz, R., and Rosenberg, R. (2008). Spreading dead zones and consequences for marine ecosystems. *Science* 321, 926–929. doi: 10.1126/science.1156401

Dutta, K., Bhushan, R., and Somayajulu, B. L. (2007). Rapid vertical mixing rates in deep waters of the Andaman Basin. *Sci. Total. Environ.* 384, 401–408. doi: 10.1016/j.scitotenv.2007.04.041

Dyksma, S., Bischof, K., Fuchs, B. M., Hoffmann, K., Meier, D., Meyerdierks, A., et al. (2016). Ubiquitous Gammaproteobacteria dominate dark carbon fixation in coastal sediments. *ISME J.* 10, 1939–1953. doi: 10.1038/ismej.2015.257

Edgar, R. C. (2013). UPARSE: highly accurate OTU sequences from microbial amplicon reads. *Nat. Methods* 10, 996–998. doi: 10.1038/nmeth.2604

Fernandes, G. L., Shenoy, B. D., and Damare, S. R. (2020). Diversity of bacterial community in the oxygen minimum zones of Arabian Sea and Bay of Bengal as deduced by illumina sequencing. *Front. Microbiol.* 10:3153. doi: 10.3389/fmicb.2019.03153

Flombaum, P., Gallegos, J. L., Gordillo, R. A., Rincón, J., Zabala, L. L., Jiao, N., et al. (2013). Present and future global distributions of the marine Cyanobacteria *Prochlorococcus* and *Synechococcus*. *Proc. Natl. Acad. Sci. U.S.A.* 110, 9824–9829. doi: 10.1073/pnas.1307701110

Fuchsman, C. A., Kirkpatrick, J. B., Brazelton, W. J., Murray, J. W., and Staley, J. T. (2011). Metabolic strategies of free-living and aggregate-associated bacterial communities inferred from biologic and chemical profiles in the Black Sea suboxic zone. *FEMS Microbiol. Ecol.* 78, 586–603. doi: 10.1111/j.1574-6941.2011.01189.x

Gilly, W. F., Beman, J. M., Litvin, S. Y., and Robison, B. H. (2013). Oceanographic and biological effects of shoaling of the oxygen minimum zone. *Ann. Rev. Mar. Sci.* 5, 393–420. doi: 10.1146/annurev-marine-120710-100849

Gilly, W. F., Zeidberg, L. D., Booth, J., Stewart, J. S., Marshall, G., Abernathy, K., et al. (2012). Locomotion and behavior of Humboldt squid, *Dosidicus gigas*, in relation to natural hypoxia in the Gulf of California, Mexico. *J. Exp. Biol.* 215, 3175–3190. doi: 10.1242/jeb.072538

Giovannoni, S. J., Rappé, M. S., Vergin, K. L., and Adair, N. L. (1996). 16S rRNA genes reveal stratified open ocean bacterioplankton populations related to the Green Non-Sulfur bacteria. *Proc. Natl. Acad. Sci. U.S.A.* 93, 7979–7984. doi: 10.1073/pnas.93.15.7979

Goericke, R., Olson, R. J., and Shalapyonok, A. (2000). A novel niche for *Prochlorococcus* sp. in low-light suboxic environments in the Arabian Sea and the Eastern Tropical North Pacific. *Deep Sea Res. I Oceanogr. Res. Pap.* 47, 1183–1205. doi: 10.1016/S0967-0637(99)00108-9

Grasshoff, K., Kremling, K., and Ehrhardt, M. (1999). *Methods of seawater analysis*. Weinheim: Verlag Chemie Press.

Gu, B., Liu, J., Cheung, S., Ho, N. H. E., Tan, Y., Xia, X., et al. (2022). Insights into prokaryotic community and its potential functions in nitrogen metabolism in the Bay of Bengal, a pronounced Oxygen Minimum Zone. *Microbiol. Spectr.* 10:e00892-21. doi: 10.1128/spectrum.00892-21

Guerrero-Feijóo, E., Sintes, E., Herndl, G. J., and Varela, M. M. (2018). High dark inorganic carbon fixation rates by specific microbial groups in the Atlantic off the Galician coast (NW Iberian margin). *Environ. Microbiol.* 20, 602–611. doi: 10.1111/1462-2920.13984

Guo, R., Wang, P., Lu, D., and Dai, X. (2020). Comparison of bacterial communities associated with *Prorocentrum donghaiense* and *Karenia mikimotoi* strains from Chinese coastal waters. *Mar. Freshw. Res.* 71, 1662–1671. doi: 10.1071/MF20035

Han, W., and Mccreary, J. P. (2001). Modeling salinity distributions in the Indian Ocean. *J. Geophys. Res.* 106, 859–877. doi: 10.1029/2000JC000316

Hoarfrost, A., Nayfach, S., Ladau, J., Yooseph, S., Arnosti, C., Dupont, C. L., et al. (2020). Global ecotypes in the ubiquitous marine clade SAR86. *ISME J.* 14, 178–188. doi: 10.1038/s41396-019-0516-7

Iburg, S., Izabel-Shen, D., Austin, ÅN., Hansen, J. P., Eklöf, J. S., and Nascimento, F. J. A. (2021). Effects of recreational boating on microbial and meiofauna diversity in coastal shallow ecosystems of the Baltic Sea. *mSphere* 6:e00127-21. doi: 10.1128/mSphere.00127-21

Ji, M., Williams, T. J., Montgomery, K., Wong, H. L., Zaugg, J., Berengut, J. F., et al. (2021). *Candidatus* Eremiobacterota, a metabolically and phylogenetically diverse terrestrial phylum with acid-tolerant adaptations. *ISME J.* 15, 2692–2707. doi: 10.1038/s41396-021-00944-8

Jithin, A. K., and Francis, P. A. (2020). Role of internal tide mixing in keeping the deep Andaman Sea warmer than the Bay of Bengal. *Sci. Rep.* 10:11982. doi: 10.1038/s41598-020-68708-6

Karstensen, J., Stramma, L., and Visbeck, M. (2008). Oxygen minimum zones in the eastern tropical Atlantic and Pacific oceans. *Prog. Oceanogr.* 77, 331–350. doi: 10.1016/j.pocean.2007.05.009

Kuypers, M. M. M., Marchant, H. K., and Kartal, B. (2018). The microbial nitrogen-cycling network. *Nat. Rev. Microbiol.* 16, 263–276. doi: 10.1038/nrmicro.2018.9

Lam, P., and Kuypers, M. M. (2011). Microbial nitrogen cycling processes in oxygen minimum zones. *Ann. Rev. Mar. Sci.* 3, 317–345. doi: 10.1146/annurev-marine-120709-142814

Lavin, P., González, B., Santibáñez, J. F., Scanlan, D. J., and Ulloa, O. (2010). Novel lineages of *Prochlorococcus* thrive within the oxygen minimum zone of the eastern tropical South Pacific. *Environ. Microbiol. Rep.* 2, 728–738. doi: 10.1111/j.1758-2229.2010.00167.x

Levin, L. A. (2018). Manifestation, drivers, and emergence of open ocean deoxygenation. *Ann. Rev. Mar. Sci.* 10, 229–260. doi: 10.1146/annurev-marine-121916-063359

Li, J., Zheng, L., Ye, C., Ni, B., Wang, X., and Liu, H. (2021). Evaluation of an intermittent-aeration constructed wetland for removing residual organics and nutrients from secondary effluent: performance and microbial analysis. *Bioresour. Technol.* 329:124897. doi: 10.1016/j.biortech.2021.124897

Long, A. M., Jurgensen, S. K., Petchel, A. R., Savoie, E. R., and Brum, J. R. (2021). Microbial ecology of oxygen minimum zones Amidst Ocean deoxygenation. *Front. Microbiol.* 12:748961. doi: 10.3389/fmicb.2021.748961

Lüke, C., Speth, D. R., Kox, M., Villanueva, L., and Jetten, M. (2016). Metagenomic analysis of nitrogen and methane cycling in the Arabian Sea oxygen minimum zone. *PeerJ* 4:e1924. doi: 10.7717/peerj.1924

Magoč, T., and Salzberg, S. L. (2011). FLASH: fast length adjustment of short reads to improve genome assemblies. *Bioinformatics* 27, 2957–2963. doi: 10.1093/bioinformatics/btr507

Mahadevan, A. (2016). The impact of submesoscale physics on primary productivity of plankton. *Ann. Rev. Mar. Sci.* 8, 161–184. doi: 10.1146/annurev-marine-010814-015912

Marshall, K. T., and Morris, R. M. (2013). Isolation of an aerobic sulfur oxidizer from the SUP05/Arctic96BD-19 clade. *ISME J.* 7, 452–455. doi: 10.1038/ismej.2012.78

Martínez-Pérez, C., Greening, C., Bay, S. K., Lappan, R. J., Zhao, Z., De Corte, D., et al. (2022). Phylogenetically and functionally diverse microorganisms reside under the Ross Ice Shelf. *Nat. Commun.* 13:117. doi: 10.1038/s41467-021-27769-5

Mattes, T. E., Ingalls, A. E., Burke, S., and Morris, R. M. (2021). Metabolic flexibility of SUP05 under low DO growth conditions. *Environ. Microbiol.* 23, 2823–2833. doi: 10.1111/1462-2920.15226

Mehrshad, M., Rodriguez-Valera, F., Amoozegar, M. A., López-García, P., and Ghai, R. (2018). The enigmatic SAR202 cluster up close: shedding light on a globally distributed dark ocean lineage involved in sulfur cycling. *ISME J.* 12, 655–668. doi: 10.1038/s41396-017-0009-5

Mena, C., Reglero, P., Balbín, R., Martín, M., Santiago, R., and Sintes, E. (2020). Seasonal niche partitioning of surface temperate open ocean prokaryotic communities. *Front. Microbiol.* 11:1749. doi: 10.3389/fmicb.2020.01749

Mena, C., Reglero, P., Balbín, R., Martín, M., Santiago, R., and Sintes, E. (2022). Dynamics of actively dividing prokaryotes in the western Mediterranean Sea. *Sci. Rep.* 12:2064. doi: 10.1038/s41598-022-06120-y

Moreno-Ulloa, A., Sicairos Diaz, V., Tejeda-Mora, J. A., Macias Contreras, M. I., Castillo, F. D., Guerrero, A., et al. (2020). Chemical profiling provides insights into the metabolic machinery of hydrocarbon-degrading deep-sea microbes. *mSystems* 5:e00824-20. doi: 10.1128/mSystems.00824-20

Morris, R. M., Frazar, C. D., and Carlson, C. A. (2012). Basin-scale patterns in the abundance of SAR11 subclades, marine *Actinobacteria* (OM1), members of the *Roseobacter clade* and OCS116 in the South Atlantic. *Environ. Microbiol.* 14, 1133–1144. doi: 10.1111/j.1462-2920.2011.02694.x

Morris, R. M., Rappé, M. S., Urbach, E., Connon, S. A., and Giovannoni, S. J. (2004). Prevalence of the Chloroflexi-related SAR202 bacterioplankton cluster throughout the mesopelagic zone and deep ocean. *Appl. Environ. Microbiol.* 70, 2836–2842. doi: 10.1128/aem.70.5.2836-2842.2004

Mußmann, M., Pjevac, P., Krüger, K., and Dyksma, S. (2017). Genomic repertoire of the Woeseiaceae/JTB255, cosmopolitan and abundant core members

of microbial communities in marine sediments. *ISME J.* 11, 1276–1281. doi: 10.1038/ismej.2016.185

Oschlies, A. (2021). A committed fourfold increase in ocean oxygen loss. *Nat. Commun.* 12:2307. doi: 10.1038/s41467-021-22584-4

Padilla, C. C., Bristow, L. A., Sarode, N., Garcia-Robledo, E., Gómez Ramírez, E., Benson, C. R., et al. (2016). NC10 bacteria in marine oxygen minimum zones. *ISME J.* 10, 2067–2071. doi: 10.1038/ismej.2015.262

Pajares, S., Varona-Cordero, F., and Hernández-Becerril, D. U. (2020). Spatial distribution patterns of bacterioplankton in the oxygen minimum zone of the Tropical Mexican Pacific. *Microb. Ecol.* 80, 519–536. doi: 10.1007/s00248-020-01508-7

Paulmier, A., and Ruiz-Pino, D. (2009). Oxygen minimum zones (OMZs) in the modern ocean. *Prog. Oceanogr.* 80, 113–128. doi: 10.1016/j.pocean.2008.08.001

Penn, J. L., Weber, T., Chang, B. X., and Deutsch, C. (2019). Microbial ecosystem dynamics drive fluctuating nitrogen loss in marine anoxic zones. *Proc. Natl. Acad. Sci. U.S.A.* 116, 7220–7225. doi: 10.1073/pnas.1818014116

Rajpathak, S. N., Roumik, B., Mishra, P. G., Khedkar, A. M., Patil, Y. M., Joshi, S. R., et al. (2018). An exploration of microbial and associated functional diversity in the OMZ and non-OMZ areas in the Bay of Bengal. *J. Biosci.* 43, 635–648. doi: 10.1007/s12038-018-9781-2

Reintjes, G., Tegetmeyer, H. E., Bürgisser, M., Orlić, S., Tews, I., Zubkov, M., et al. (2019). On-Site analysis of bacterial communities of the ultraoligotrophic South Pacific Gyre. *Appl. Environ. Microbiol.* 85:e00184-19. doi: 10.1128/AEM.00184-19

Rinke, C., Schwientek, P., Sczyrba, A., Ivanova, N. N., Anderson, I. J., Cheng, J. F., et al. (2013). Insights into the phylogeny and coding potential of microbial dark matter. *Nature* 499, 431–437. doi: 10.1038/nature12352

Schloss, P. D., Westcott, S. L., Ryabin, T., Hall, J. R., Hartmann, M., Hollister, E. B., et al. (2009). Introducing mothur: open-source, platform-independent, community-supported software for describing and comparing microbial communities. *Appl. Environ. Microbiol.* 75, 7537–7541. doi: 10.1128/aem.01541-09

Schmidtko, S., Stramma, L., and Visbeck, M. (2017). Decline in global oceanic oxygen content during the past five decades. *Nature* 542, 335–339. doi: 10.1038/nature21399

Schwalbach, M. S., Tripp, H. J., Steindler, L., Smith, D. P., and Giovannoni, S. J. (2010). The presence of the glycolysis operon in SAR11 genomes is positively correlated with ocean productivity. *Environ. Microbiol.* 12, 490–500. doi: 10.1111/j.1462-2920.2009.02092.x

Segata, N., Izard, J., Waldron, L., Gevers, D., Miropolsky, L., Garrett, W. S., et al. (2011). Metagenomic biomarker discovery and explanation. *Genome Biol.* 12:R60. doi: 10.1186/gb-2011-12-6-r60

Shah, V., Chang, B. X., and Morris, R. M. (2017). Cultivation of a chemoautotroph from the SUP05 clade of marine bacteria that produces nitrite and consumes ammonium. *ISME J.* 11, 263–271. doi: 10.1038/ismej.2016.87

Sheik, C. S., Jain, S., and Dick, G. J. (2014). Metabolic flexibility of enigmatic SAR324 revealed through metagenomics and metatranscriptomics. *Environ. Microbiol.* 16, 304–317. doi: 10.1111/1462-2920.12165

Sheremet, A., Jones, G. M., Jarett, J., Bowers, R. M., Bedard, I., Culham, C., et al. (2020). Ecological and genomic analyses of candidate phylum WPS-2 bacteria in an unvegetated soil. *Environ. Microbiol.* 22, 3143–3157. doi: 10.1111/1462-2920.15054

Sun, X., Kop, L. F. M., Lau, M. C. Y., Frank, J., Jayakumar, A., Lücker, S., et al. (2019). Uncultured Nitrospina-like species are major nitrite oxidizing bacteria in oxygen minimum zones. *ISME J.* 13, 2391–2402. doi: 10.1038/s41396-019-0443-7

Suter, E. A., Pachiadaki, M., Taylor, G. T., Astor, Y., and Edgcomb, V. P. (2018). Free-living chemoautotrophic and particle-attached heterotrophic prokaryotes dominate microbial assemblages along a pelagic redox gradient. *Environ. Microbiol.* 20, 693–712. doi: 10.1111/1462-2920.13997

Thrash, J. C., Seitz, K. W., Baker, B. J., Temperton, B., Gillies, L. E., Rabalais, N. N., et al. (2017). Metabolic roles of uncultivated bacterioplankton lineages in the Northern Gulf of Mexico "Dead Zone". *mBio* 8:e01017-17. doi: 10.1128/mBio.01017-17

Tsementzi, D., Wu, J., Deutsch, S., Nath, S., Rodriguez, R. L., Burns, A. S., et al. (2016). SAR11 bacteria linked to ocean anoxia and nitrogen loss. *Nature* 536, 179–183. doi: 10.1038/nature19068

Ulloa, O., Canfield, D. E., DeLong, E. F., Letelier, R. M., and Stewart, F. J. (2012). Microbial oceanography of anoxic oxygen minimum zones. *Proc. Natl. Acad. Sci. U.S.A.* 109, 15996–16003. doi: 10.1073/pnas.1205009109

van Vliet, D. M., von Meijenfeldt, F. A. B., Dutilh, B. E., Villanueva, L., Sinninghe Damsté, J. S., Stams, A. J. M., et al. (2021). The bacterial sulfur cycle in expanding dysoxic and euxinic marine waters. *Environ. Microbiol.* 23, 2834–2857. doi: 10.1111/1462-2920.15265

Vaquer-Sunyer, R., and Duarte, C. M. (2008). Thresholds of hypoxia for marine biodiversity. *Proc. Natl. Acad. Sci. U.S.A.* 105, 15452–15457. doi: 10.1073/pnas.0803833105

Vijayan, J., Kumar, V., and Ammini, P. (2020). Comparison of bacterial community structure in coastal and offshore waters of the Bay of Bengal, India. *Reg. Stud. Mar. Sci.* 39:101414. doi: 10.1016/j.rsma.2020.101414

Walsh, D., Zaikova, E., Howes, C. G., Song, Y., Wright, J., Tringe, S., et al. (2009). Metagenome of a versatile chemolithoautotroph from expanding oceanic dead zones. *Science* 326, 578–582. doi: 10.1126/science.1175309

Wang, B., Wang, Z., Wang, S., Qiao, X., Gong, X., Gong, Q., et al. (2020). Recovering partial nitritation in a PN/A system during mainstream wastewater treatment by reviving AOB activity after thoroughly inhibiting AOB and NOB with free nitrous acid. *Environ. Int.* 139:105684. doi: 10.1016/j.envint.2020.105684

Ward, L. M., Cardona, T., and Holland-Moritz, H. (2019). Evolutionary implications of anoxygenic phototrophy in the bacterial phylum *Candidatus* Eremiobacterota (WPS-2). *Front. Microbiol.* 10:1658. doi: 10.3389/fmicb.2019.01658

Wright, J. J., Konwar, K. M., and Hallam, S. J. (2012). Microbial ecology of expanding oxygen minimum zones. *Nat. Rev. Microbiol.* 10, 381–394. doi: 10.1038/nrmicro2778

Wright, J. J., Mewis, K., Hanson, N. W., Konwar, K. M., Maas, K. R., and Hallam, S. J. (2014). Genomic properties of Marine Group A bacteria indicate a role in the marine sulfur cycle. *ISME J.* 8, 455–468. doi: 10.1038/ismej.2013.152

Zakem, E. J., Mahadevan, A., Lauderdale, J. M., and Follows, M. J. (2020). Stable aerobic and anaerobic coexistence in anoxic marine zones. *ISME J.* 14, 288–301. doi: 10.1038/s41396-019-0523-8

Zhang, R., Liu, W. C., Liu, Y., Zhang, H. L., Zhao, Z. H., Zou, L. Y., et al. (2021). Impacts of anthropogenic disturbances on microbial community of coastal waters in Shenzhen, South China. *Ecotoxicology* 30, 1652–1661. doi: 10.1007/s10646-020-02297-y

Zhou, Z., Meng, H., Gu, W., Li, J., Deng, M., and Gu, J. D. (2022). High-throughput sequencing reveals the main drivers of niche-differentiation of bacterial community in the surface sediments of the northern South China sea. *Mar. Environ. Res.* 178:105641. doi: 10.1016/j.marenvres.2022.105641

frontiers | Frontiers in Marine Science

TYPE Original Research
PUBLISHED 30 November 2022
DOI 10.3389/fmars.2022.1046808

OPEN ACCESS

EDITED BY
Shan He,
Ningbo University, China

REVIEWED BY
Pengbin Wang,
Ministry of Natural Resources, China
Aibin Zhan,
Research Center for Eco-environmental Sciences, Chinese Academy of Sciences (CAS), China

*CORRESPONDENCE
Yunyun Zhuang
yunyun.zhuang@ouc.edu.cn

SPECIALTY SECTION
This article was submitted to Aquatic Microbiology, a section of the journal Frontiers in Marine Science

RECEIVED 17 September 2022
ACCEPTED 14 November 2022
PUBLISHED 30 November 2022

CITATION
Chen T, Zhuang Y, Chen C, Mao X, Ge R, Chen H, Chen J, Fu L, Yang Z and Liu G (2022) Metabarcoding reveals the differential sensitivity of planktonic microbiome to environmental filtering and biointeraction in Sansha Yongle blue hole.
Front. Mar. Sci. 9:1046808.
doi: 10.3389/fmars.2022.1046808

Metabarcoding reveals the differential sensitivity of planktonic microbiome to environmental filtering and biointeraction in Sansha Yongle blue hole

Tianying Chen[1], Yunyun Zhuang[1,2]*, Chang Chen[1], Xuewei Mao[1], Ruping Ge[1], Hongju Chen[1,2], Jianwei Chen[3,4], Liang Fu[5], Zuosheng Yang[6] and Guangxing Liu[1,2]

[1]Key Laboratory of Marine Environment and Ecology, Ministry of Education, Ocean University of China, Qingdao, China, [2]Laboratory for Marine Ecology and Environmental Science, Pilot National Laboratory for Marine Science and Technology (Qingdao), Qingdao, China, [3]BGI Research-Qingdao, BGI, Qingdao, China, [4]Qingdao-Europe Advanced Institute for Life Sciences, BGI, Qingdao, China, [5]Sansha Trackline Institute of Coral Reef Environment Protection, Sansha, China, [6]College of Marine Geosciences, Ocean University of China, Qingdao, China

The Sansha Yongle blue hole (SYBH) is the world's deepest blue hole known so far and its unique hydrochemical characteristics make it a valuable site for studying biodiversity and ecological processes. Here, we used metabarcoding approach to investigate the diversity, assembly mechanism and co-occurrence pattern of planktonic microbiome in SYBH. Our results revealed the distinct separation of communities from upper oxic, middle oxic and suboxic-anoxic layer and significant day-night difference was detected in the upper-layer community of microeukaryotes, indicating potential diel migration. Stochastic processes played a significant role in the community assembly of microeukaryotes, while deterministic processes dominated in prokaryotes, confirming the stronger environmental filtering on prokaryotes as also suggested by the correlation with environmental variables. Microeukaryotes were less sensitive to environments but significantly affected by cross-domain biointeraction. When comparing the subcommunities of different abundance, we found that abundant taxa were widespread while rare taxa were habitat-specific. In co-occurrence network, over 87% of the interactions and 19 out of 20 keystone OTUs (Operational Taxonomic Units) were affiliated to moderate or rare taxa, suggesting the importance of non-abundant taxa in maintaining community stability. The predominant positive edges in the network pointed to that interspecies cooperation may be one of the ecological strategies in SYBH.

Overall, we highlight the divergent assembly pattern and different driving forces in shaping plankton microbiome in SYBH, which may advance current understanding on diversity and dynamics of marine life in blue hole ecosystems.

KEYWORDS

Sansha Yongle blue hole, planktonic microbiome, microbial diversity, assembly mechanism, rare taxa, microbial interaction

Introduction

Marine blue holes are underwater sinkholes open to the marine environment, which formed in carbonate bank during glacial periods when sea level was below current sea level and were submerged during interglacial periods (Mylroie et al., 1995; Wyrwoll et al., 2006). They have been found on island, coral reef and peninsular coastlines around world's oceans. The geomorphology of blue holes contributes to the special hydrochemical characteristics including low photosynthetic oxygen production, tidally-influenced upper water, stratified water column with limited vertical mixing. Typically, the permanent thermo-halocline and the hypoxic/anoxic layer below are found in blue holes with high level of hydrogen sulfide formed in deep waters (Gonzalez, 2010). Being relatively isolated ecosystems, blue holes are described as time capsules providing evidence of Earth's history regarding past climate change, karst processes, and life evolution (Mylroie et al., 1995; Swart et al., 2010). They are also considered to be extreme environments for life with poor supply of light, nutrient and oxygen (Northup and Lavoie, 2001; Krstulović et al., 2013). In spite of this, highly diverse organisms, new and blue hole-specific species ranging from Arthropoda, Mollusca, Ciliophora, Proteobacteria to Woesearchaeota have been documented (Iliffe and Kornicker, 2009; Ricci et al., 2015; Patin et al., 2021; Kajan et al., 2022). Biodiversity of microbes and benthic fauna in blue holes have been found to be significantly higher than that in ambient waters (Garman et al., 2011). Spatial heterogeneity is one of the reasons that produce major biodiversity pattern, and potentially making blue hole a hotspot of microbial diversity. How the community is structured, how the organisms adapt and thrive, and how these biological evidences reflect the ecosystem stability and functions in blue holes have become hot topics of research. For example, photoheterotroph utilizing a range of rhodopsins has been proposed to be an important lifestyle of microbes in Shark Bay Blue Bole (Kindler et al., 2021).

The Sansha Yongle Blue Hole (SYBH, N16°31.5′, E111°46.1′, Figure 1) located at the eastern end of the Yongle Atoll of the Xisha Islands, South China Sea is the deepest blue hole ever discovered in the world, with the observed deepest portion at 301.19 m (Li et al., 2018). The 3D topography of the SYBH and underwater photography revealed the sinuous underwater structure with two large transitions at 76-78 m and 158 m, and no water or material exchange with the outside open sea (Li et al., 2018). Several investigations detailed the hydrochemical properties in the SYBH (Bi et al., 2018; Yao et al., 2018; Xie et al., 2019), which were different from others with fresh water injection or subsurface connections to the sea (Gonzalez, 2010). Strong vertical stratification in the hole is controlled by temperature gradients and three distinct layers including an oxic layer, a chemocline and an anoxic layer of deep water have been characterized (Xie et al., 2019). Unique hydrochemical characteristics of SYBH, particularly the strong vertical heterogeneity, make it a valuable and challenging site for uncovering the fundamental ecological processes.

In aquatic ecosystems, plankton serve as one of the sensitive indicators of biodiversity and environmental changes, and underpin important ecosystem functions (e.g., Ibarbalz et al., 2019; Sunagawa et al., 2020), thus scientists have started to explore the community composition of plankton and its relationship with environmental variables in SYBH. Prokaryotic plankton including bacteria and archaea community (He et al., 2019; Zhang et al., 2021), microeukaryotic plankton (Liu et al., 2019), microphytoplankton (Ge et al., 2020) and mesozooplankton (Chen et al., 2018) in SYBH have been investigated separately, with some lineages such as a genus of gram-negative bacteria *Vibrio* (Li et al., 2020a) and foraminifera (Li et al., 2020b) being addressed. However, the assembly mechanism of plankton microbiome, the role of subcommunities of different abundance and the potential microbial biointeraction remain elusive, which is crucial for understanding the ecological processes in SYBH.

Metabarcoding approaches have been widely used to study the diversity, assembly mechanism and biological interaction of planktonic microbiomes (e.g., de Vargas et al., 2015; Sunagawa et al., 2020; Burki et al., 2021), but in most studies, prokaryotes and eukaryotes are analyzed separately. Although amplicon libraries for metabarcoding of prokaryotes and eukaryotes have to be prepared separately due to the distinct nucleotide

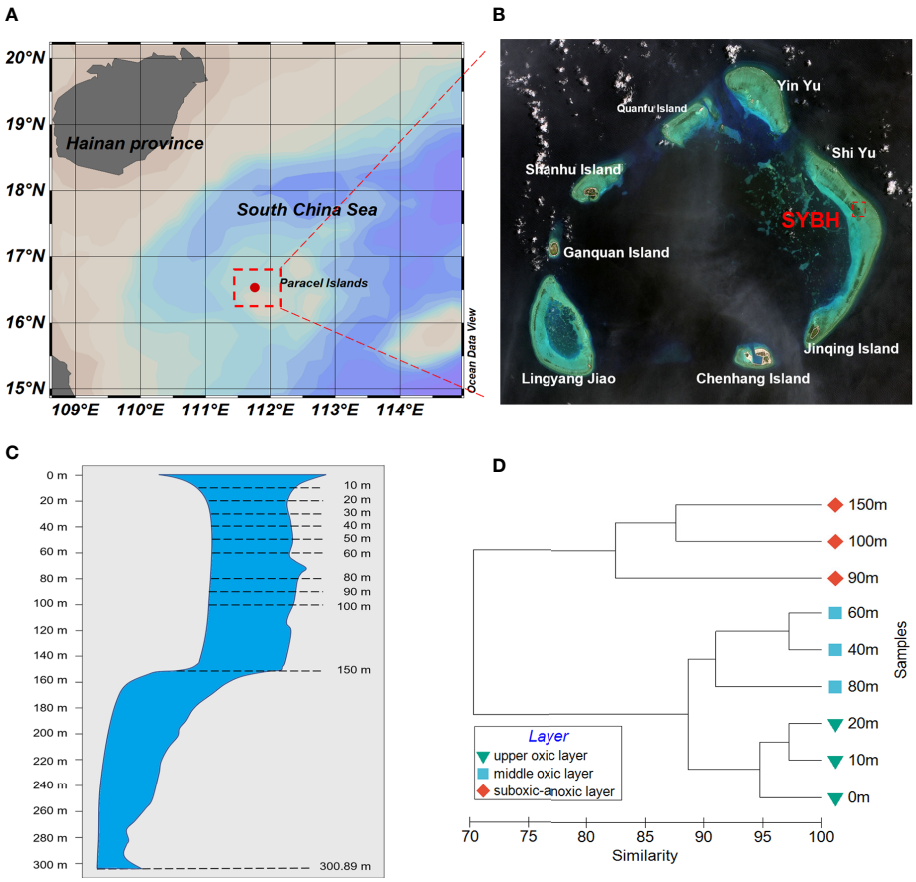

FIGURE 1
(A, B) Location of the Sansha Yongle Blue Hole (SYBH). **(C)** Vertical section through the SYBH and dash lines indicate the sampling depths in this study and the deepest depth of 300.89 m (modified from Li et al.,2018). **(D)** Vertical heterogeneity shown by the dendrogram of cluster analysis based on environmental variables at each depth in the SYBH.

characters, they form microbial assemblage in natural waters and play roles together in ecological processes such a microbial food web. Recently, increasing attention has been paid to joint analysis of microbial prokaryotic and eukaryotic plankton in aquatic ecosystems (Jiang et al., 2018; Wu et al., 2020; Lu et al., 2022; Sun et al., 2022), revealing that the distribution patterns and assembly mechanisms are distinct between domains, and cross-domain interaction plays an important role in shaping the plankton community, even overriding abiotic factor in some cases. Which process contributes more to the community assembly? The answer needs the quantification of the relative influence of 'habitat heterogeneity and environment-induced species sorting' (niche theory) versus 'random demographic fluctuation and disperse' (neutral theory) (Stegen et al., 2013), which may depend on geographic scale and strength of environmental gradients (Hanson et al., 2012; Morrison-Whittle and Goddard, 2015). Moreover, it has been widely accepted that rare biosphere plays important roles in community turnover, driving functions and maintaining stability of ecosystem (Debroas et al., 2015; Lynch and Neufeld et al., 2015; Jia et al., 2018), particularly in extreme environment like deep sea (Sogin et al., 2006). Also, taxa with moderate abundance (also called intermediate subcommunity) have been found to be highly metabolic active and determine the plankton community transition among seasons (Sun et al., 2017). Previous studies on microbial plankton pointed out that the composition, diversity, assembly processes and response to environment of non-abundant subcommunity are different from those of abundant one (Logares et al., 2014; Xue et al., 2018). Removing rare taxa from dataset may neglect some keystone species and hinder the understanding of community dynamics (Gobet et al., 2012).

In this study, based on high-throughput sequencing of 18S rRNA and 16S rRNA genes, we investigated the community composition, diversity, assembly mechanism and co-occurrence network of microbial plankton communities in the SYBH. We hypothesized that (1) microbial plankton community are structured by vertical environmental gradient and day-night

variation in the SYBH; (2) drivers of microeukaryotic and prokayrotic plankton community and their sensitivity to environmental filtering are different; (3) non-dominant subcommunities play a central role in diversity and biological interaction. As the first attempt, we jointly analyzed eukaryotic and prokaryotic microbe, and compared the subcommunities of different abundance in the SYBH. It is hoped that this study will contribute to a deeper understanding on community assembly and drivers of microbial plankton in the SYBH, which may have implication in conservation strategies.

Materials and methods

Sampling and environmental factors analyses

Samples were collected from the SYBH (16°31 '30 "N, 111°46 '05 "E) at the depths of 0-150 m (Figure 1C) on the night of March 14 and the day of March 17, 2017. Temperature, salinity, dissolved oxygen (DO) and depth of all water samples were measured *in situ* using a CTD profiler. Seawater was collected by Niskin bottles mounted on a rosette, equipped with CTD (SeaBird SBE 19 Plus), and then was prefiltered through 200-μm mesh to remove large zooplankton. A subsample (4~6 L) of the prefiltered water was passed successively through 5-μm and 0.45-μm polycarbonate membranes (Millipore, USA), which was then stored in liquid nitrogen until DNA extraction. Another 500 mL subsample was filtered by the manner for the analysis of chlorophyll a. The filter membrane was extracted with 10 mL of 90% v/v acetone aqueous solution for 24 h at 4°C and in darkness, centrifuged at 1500 g for 10 min, and the supernatant was measured with a fluorescence spectrophotometer (Hitachi F-4500, Japan). H_2S was determined in site with a spectrophotometer at 670 nm after color development, and pH was determined with a Mettler-Toledo Delta 320 pH meter. The seawater for nutrient determination was filtered through 0.45-μm acetate filter membranes that were soaked and washed in dilute hydrochloric acid before use, and the filtrates were immediately frozen at -20°C. Nutrients were measured using colorimetric method by AA3 continuous flow analyzer (Seal Analytical Company, UK). The detection limits of NO_3^-, NO_2^-, NH_4^+, PO_4^{3-} and SiO_3^{2-} were 0.02, 0.01, 0.04, 0.02 and 0.01 μmol mL^{-1}, respectively, and the uncertainty of repeated determination was less than 5%-10%. Vertical profiles of multiple hydrochemical parameters in this study was adopted from Bi et al. (2018) and Yao et al. (2018).

DNA extraction, PCR amplification and Illumina sequencing

Membrane filters of different pore sizes from the same depth were pooled together. A total of 18 samples (10 from nighttime and 8 from daytime) were subjected to DNA extraction following the method described by Yuan et al. (2015). Briefly, each membrane filter was cut with sterilizing scissors and immersed in 1 mL DNA extraction buffer (100 mM EDTA, 1% SDS and 10 μg mL^{-1} proteinase K) for 24-h incubation at 56°C. After incubation, DNA was extracted using the CTAB method, further purified using the DNA Clean & Concentrator kit (Zymo Research, USA), and eluted in 25 μL 10mM Tris-HCl. The concentrations and purities of DNA were measured on a NanoDrop 2000 Spectrophotometer (Thermo Scientific, USA). DNA integrity was assessed by gel electrophoresis.

The V4 region of the eukaryotic 18S rDNA gene was amplified with the primers MEG_F (5'- GGCAAG TCTGGTGCCAG -3') and MEG_R (5'- GACTACGACGGT ATCTRATCRTCTTCG -3') (Bråte et al., 2010). The PCR was performed as follows: 95°C for 5 min, followed by 25 cycles of 95°C for 30 s, 60°C for 30 s, and 72°C for 40 s, with a final extension at 72°C for 10 min. The V4 hypervariable region of prokaryotic 16S rDNA was amplified with 515F (5'- GTGYCAGCMGCCGCGGTAA -3') and 806R (5'- GGACTACNVGGGTWTCTAAT -3') (Caporaso et al., 2011). The PCR was performed as follows: 95°C for 5 min, followed by 25 cycles of 95°C for 30 s, 56°C for 30 s, and 72°C for 40 s, with a final extension at 72°C for 10 min. PCR reactions were performed in a total volume of 25 μL using Ex Taq (Takara, China) with 20-300 ng template gDNA. All amplicons were paired-end sequenced (2×300 bp) using Illumina MiSeq platform (GENEWIZ, SuZhou, China).

Quality filtration, clustering and annotation of metabarcodes

Raw reads were subjected to quality filtration by trimming sequencing adaptor, primers, low quality bases and too short reads (<200 bp) with Cutadapt (v1.9.1), Vsearch (v1.9.6) and Qiime (v1.9.1) (Martin 2011; Rognes et al., 2016; Bolyen et al., 2019). The remaining high-quality paired-end reads were assembled into metabarcodes with fastq mergepairs module of Vsearch (v1.9.6) and non-singleton ones were clustered into OTUs (Operational Taxonomic Units) with a 97% identity. Then the rest of metabarcodes were mapped to the OTU representative sequences to generate the OTU abundance profile. For taxonomic annotations, the representative OTU sequences of 18S rRNA genes were taxonomically classified by sintax algorithm (Edgar, 2016) compared with PR2 database (Guillou et al., 2012), and the confidence threshold was set to 0.8. The representative OTU sequences of 16S rRNA gene were taxonomically classified by Bayesian algorithm of the RDP classifier (Ribosomal Database Program, v2.2; Wang et al., 2007) using Silva128 Database (Quast et al., 2012). Taxonomic annotation was further manually checked particularly for highly abundant and ambiguous metabarcodes. The ecological

functions of bacterial communities were further annotated using Functional Annotation of Prokaryotic Taxa (FAPROTAX) (Louca et al., 2016).

In addition to the total community, abundant, moderate, and rare subcommunities were analyzed separately. We defined 'abundant' OTUs as those having relative abundances above 0.1% of total sequences, 'rare' OTUs as those having relative abundances below 0.01% and 'moderate' OTUs as those having relative abundances between 0.01% and 0.1% (Campbell et al., 2011).

Diversity and statistical analyses

For alpha-diversity, richness and Shannon diversity index were calculated for each sample using the 'vegan' package in R (v4.0.3). Significance of the difference in alpha-diversity between groups was tested using the Wilcoxon rank sum test. Non-Metric Multidimensional Scaling (NMDS) ordination of community structure was performed using Bray-Curtis dissimilarity matrices in PRIMER 6 (Clarke and Gorley, 2009). Global and pairwise differences among groupings of samples were further tested by ANOSIM within PRIMER 6. Mantel tests with 9999 permutations were performed using the 'vegan' package in R, to examine the Spearman's correlation between abiotic factors (temperature, salinity, pH, DO, nutrient and etc.), cross-domain biotic factors (PCoA 1 and 2 value of community) and the Bray-Curtis distances of communities. The circos plot are visualized using the 'circlize' package in R.

Community assembly process

To quantify the relative importance of deterministic and stochastic processes in microbial communities and subcommunities with different abundance, the phylogenetic null model of Stegen et al. (2013) was applied. Phylogenetic turnover between communities was first used to determine the effects of selection, followed by OTU turnover to determine the effects of dispersal and drift. Values of βNTI greater than 2 or less than −2 indicate the impact of environmental pressures on heterogeneous and homogeneous selection, respectively. If the |βNTI| is < 2 but with an |RCbray| >0.95, the community assembly is controlled by homogenizing dispersal or dispersal limitation, respectively. In addition, the |βNTI| < 2 and a |RCbray| < 0.95 suggest that the community assembly is not dominated by any single process, consisting of weak selection, weak dispersal, and diversification or drift. (Stegen et al., 2013).

Construction of microbial co-occurrence network

Spearman's correlations between OTU relative abundance were calculated using the 'rcorr' function in the 'Hmisc' package, based on which co-occurrence network analysis was conducted. To reduce false-positive prediction, OTUs present in ≥6 samples with robust correlation (spearman rho > |0.8| and $P<0.01$) were considered for network analysis. Networks were visualized using Gephi (v0.9.2). Topological properties of nodes, including degree, betweenness centrality and modularity, were also calculated in Gephi. A random network with the same number of nodes and edges as a real network is generated in the 'igraph' R package. The topological characteristics of real and random networks, including modularity, clustering coefficient network diameter and average path length, are calculated and compared. Nodes with high degree (>50) and low betweenness centrality (<5000) values were considered to be keystone species in the co-occurrence network.

Results

Environmental parameters

The vertical profiles of several environmental parameters in SYBH showed depth-dependent pattern (Supplementary Figure 1). Temperature, pH and DO decreased with depth. Oxycline appeared around 80-90 m and the water became anoxic below 100 m. Contrastingly, salinity and the concentrations of silicate, phosphate increased with depth, which was more evident at depths below 80 m. Turbidity, the concentration of nitrate and nitrite showed a single-peak pattern with the maxima detected at 100 m, and 90 m, 40 m, respectively. The concentration of chlorophyll a also showed a single-peak pattern, with the maximum found at 40 m and 20 m at daytime and nighttime, respectively. The maximum of H_2S concentration was detected at 150 m, which was the deepest sampling depth of this study, mirroring the anoxic condition. Considering all the measured environmental variables, the vertically heterogeneous environments above 150 m in the SYBH could be categorized into two major clusters: the oxic layer in the top 80 m and the suboxic-anoxic layer below 90 m. The oxic layer could be further divided to upper oxic layer (0-20 m) and middle oxic layer (40-80 m) (Figure 1D).

Taxonomic composition of planktonic microbiome

Microeukaryotic and prokaryotic plankton communities were examined separately in 18 samples collected from nine layers of the SYBH. Rarefaction curves and Shannon-Wiener curves depicted a leveling off with increased sequences for all samples, indicating that sequencing depth was sufficient to identify the majority of OTU richness and community diversity (Supplementary Figure 2). A total of 1,817,031 high-quality 18S rDNA metabarcodes and 1,083,134 high-quality 16S rDNA metabarcodes were obtained, and yielded 6,121 and 2,883 OTUs, respectively (Supplementary Table 1). Among these, 948 (relative abundance 4.29%) eukaryotic OTUs and 160 (relative abundance 1.61%) prokaryotic OTUs did not match any sequence in the reference databases (the 'unclassified' category in Figure 2), pointing to the undocumented genetic diversity in SYBH.

The taxonomic composition of planktonic microbiome in the SYBH was uneven across depths and the sampling times of the day (Figure 2). Microeukaryotic plankton community was dominated by Dinophyceae, Annelida and Fungi (Figure 2A). Dinophyceae and Annelida accounted for 13.55% and 14.02% of the reads within microeukaryotes, respectively, but there was no significant difference between day and night communities, nor among the three layers. Rhodophyta, Radiolaria and Fungi showed the most vertically heterogenous distribution ($P<0.05$) with Rhodophyta and Radiolaria mainly distributed in the upper oxic layer, while Fungi in the middle oxic layer. Such depth

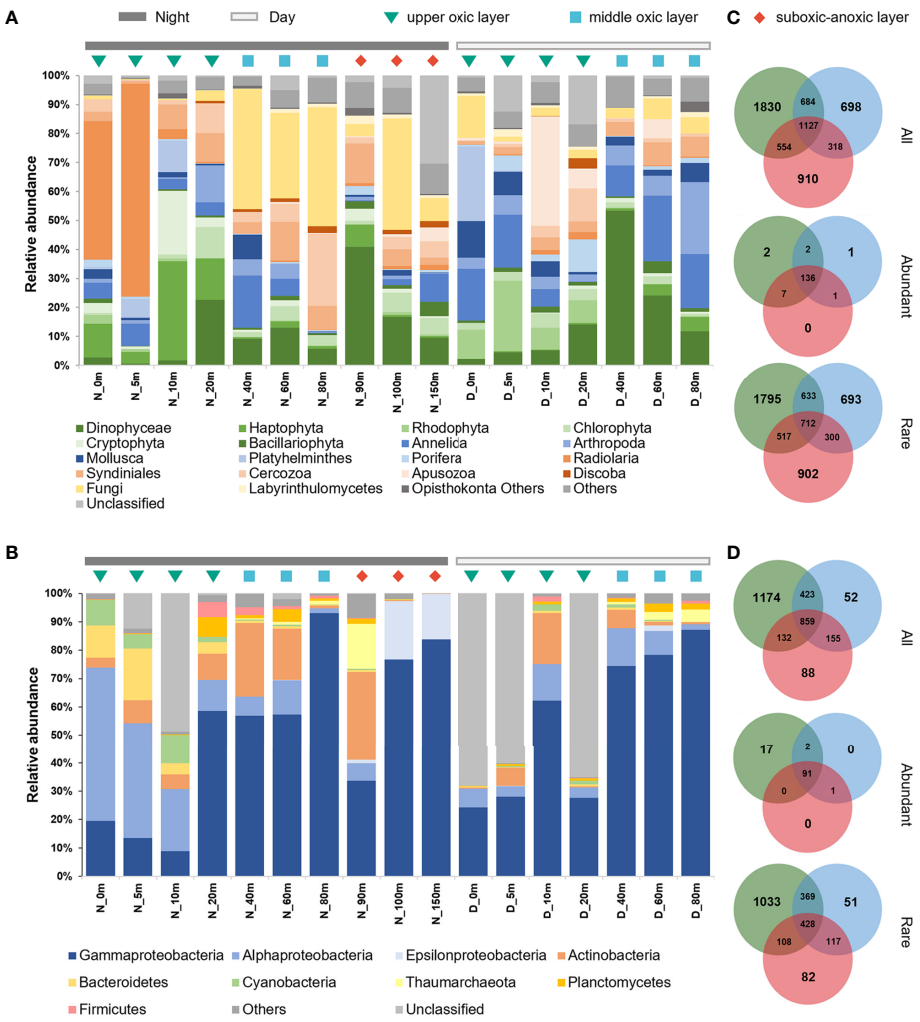

FIGURE 2
Community composition of plankton microbiome in the SYBH. The relative abundances of microeukaryotic **(A)** and prokaryotic **(B)** plankton community across depths and time of the day. D, Day; N, Night. Venn diagrams showing the numbers of unique and shared OTUs of microeukaryotes **(C)** and prokaryotes **(D)** among three layers. All, whole community; Abundant, abundant plankton subcommunities; Rare, rare plankton subcommunities.

partitioning was more pronounced at nighttime (Supplementary Figure 3), leading to the significant day-night difference (P<0.05) in the upper oxic layer community of Haptophyta, Rhodophyta, Radiolaria, Apusozoa and Labyrinthulomycetes.

The prokaryotic plankton community was dominated by Proteobacteria, Actinobacteria, Bacteroidetes, Cyanobacteria, Planctomycetes and Thaumarchaeota, which accounted for over 90% of the total sequences (Figure 2B). Within Proteobacteria, Gammaproteobacteria (average 52.60%) and Alphaproteobacteria (11.72%) dominated across all samples except for those from 100 m and 150 m at nighttime, where Epsilonproteobacteria and Gammaproteobacteria were abundant class (Figure 2B). Although no significant day-night difference was detected for prokaryotic plankton community, Cyanobacteria, Gammaproteobacteria, Epsilonproteobacteria, and Thaumarchaeota showed depth-dependent distribution (P<0.05). Cyanobacteria were mainly distributed in the upper oxic layer, Gammaproteobacteria in the middle oxic layer, while Epsilonproteobacteria and Thaumarchaeota in the suboxic-anoxic layer. Despite the low abundance, the relative abundance of nitrite-oxidizing bacteria (NOB) affiliated with the phylum Nitrospinae peaked at 90 m, where that of ammonium-oxidizing archaea (AOA) of the phylum Thaumarchaeota also peaked (Supplementary Figure 4). Such vertical niche partition was more remarkable when considering the ecological functions of prokaryotes (Supplementary Figure 5). Most of chemoheterotrophs were mainly distributed in the upper and middle oxic layers. Nitrifier and aerobic ammonium oxidizer were enriched at the middle oxic layer and peaked at oxycline of 80-90 m. Contrastingly, lineages responsible for dark oxidation of sulfur and sulfur-containing compounds were mainly found below 100 m.

After categorizing OTUs by relative abundance, we found that both eukaryotic and prokaryotic plankton communities in the SYBH were dominated by few abundant taxa (Supplementary Table 2). Among the total 6121 eukaryotic OTUs, 2.4% of OTUs (149) were classified as abundant taxa and accounted for 82.0% of total sequences. In contrast, 90.7% of OTUs (5552) were classified as rare taxa but only accounted for 5.4% of total sequences. Similar pattern was also observed in prokaryotes, as abundant taxa accounted for 3.9% of OTUs (111) but 77.1% of total sequences, while rare taxa accounted for 75.9% of OTUs (2188) but 5.8% of total sequences. Moreover, 91.28% of abundant 18S rDNA OTUs and 81.98% of abundant 16S rDNA OTUs were commonly found in three layers, accounting for 79.37% and 70.87% of total reads, respectively (Figures 2C, D). Nevertheless, the majority of layer-specific OTUs belonged to rare taxa. Plankton community composition also differed between abundant and rare taxa (Supplementary Figure 6). Abundant subcommunity of microeukaryotic plankton was dominated by Annelida, Dinophyceae and Fungi, while 14 lineages including Phaeophyceae, Hemichordata, *Centroheliozoa* and Perkinsea were exclusively present in rare subcommunity. Both abundant and rare subcommunities of prokaryotic plankton were dominated by Gammaproteobacteria, but Nitrospinae, Betaproteobacteria, Deltaproteobacteria and Acidobacteria was exclusively found in rare subcommunity.

The drivers shaping planktonic microbiome

NMDS ordinations and ANOSIM analysis revealed the distinct separation of microplankton communities from the upper oxic, middle oxic and suboxic-anoxic layer, suggesting that the microbiome assembly was mainly shaped by vertical heterogeneity of environment for both eukaryotic (R=0.592, P=0.001) and prokaryotic communities (R=0.552, P=0.001) (Supplementary Table 3). This was also the case when analyzing abundant, moderate and rare subcommunities separately (Supplementary Figure 7, Supplementary Table 3). The alpha-diversity were also compared between different layers and subcommunities (Figures 3A, B). Rare subcommunities of both microeukaryotic and prokaryotic plankton contained a significantly greater diversity of OTUs than abundant and moderate counterparts (Supplementary Figure 8). The alpha diversity of prokaryotic plankton gradually decreased with depths which was significant in rare subcommunity (P<0.05), while no significant change was detected in that of microeukaryotes across depths (Figures 3A, B). Moreover, significant day-night difference was only detected in the upper layer community of microeukaryotic plankton (R=0.948, P<0.05) (Supplementary Table 3), of which the rare subcommunity at daytime had significantly higher richness and diversity than that at nighttime (Supplementary Figure 9). All these results indicated that rare subcommunities contributed significantly to the biodiversity in the SYBH, and potentially the sensitivity of microeukaryotic and prokaryotic plankton to environment differed.

Mantel test further suggested that prokaryotic plankton had stronger correlation with environmental variables than microeukaryotic plankton did (Figure 4; Supplementary Table 4). Except for the concentrations of inorganic nitrogen and chlorophyll a, all the other physicochemical properties showed a significant positive correlation with overall prokaryotic plankton community and three subcommunities (R=0.251~0.728, P<0.05). Contrastingly, the influence of environmental factors on microeukaryotic community was much weaker (R=0.210~0.474, P<0.05) and varied among subcommunities, of which rare subcommunity was most sensitive to environmental variables with salinity (R=0.657, P<0.001) and temperature (R=0.728, P<0.001) showed the strongest correlation. We also assessed the influence of cross-domain biotic factor on planktonic microbiome (Table 1). Mantel tests revealed that the rare subcommunities of microeukaryotic plankton were more sensitive to the cross-domain biotic factors, and the moderate and rare subcommunity of prokaryotic plankton played significant roles in microeukayotic community variation (R=0.344~0.524, P<0.01).

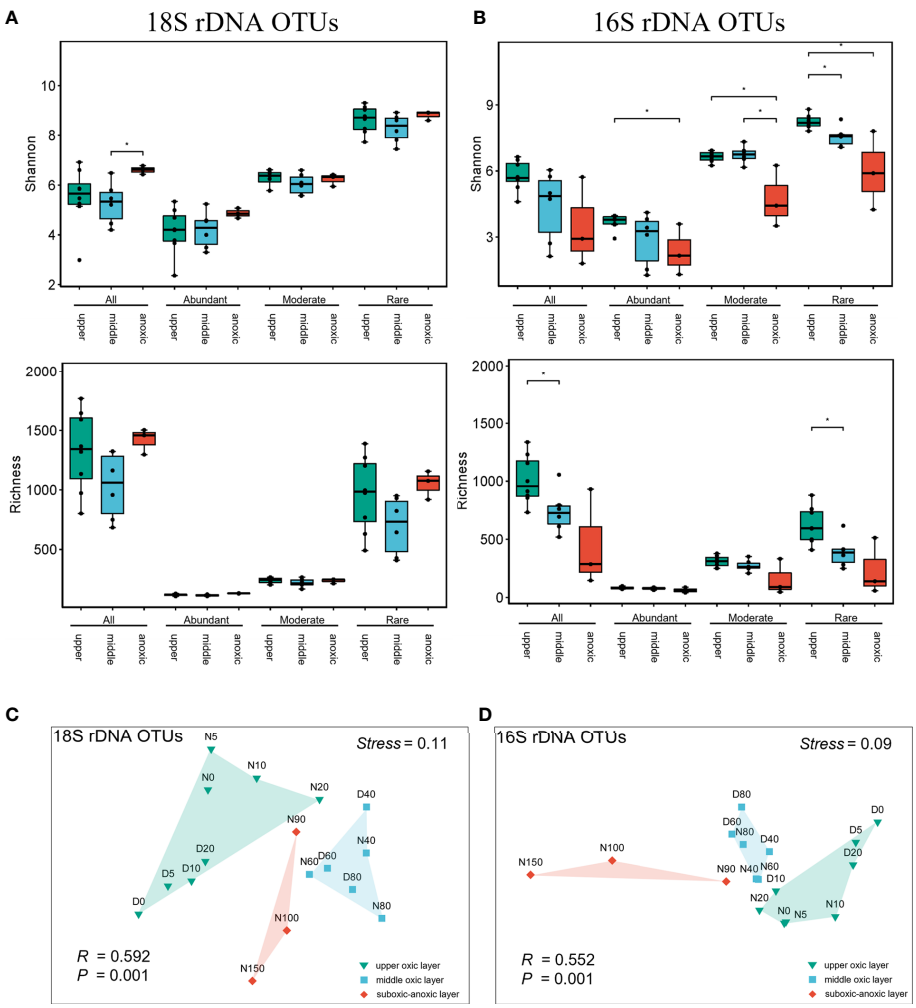

FIGURE 3
Community structuring of microeukaryotic and prokaryotic plankton in the SYBH. The richness and Shannon Index of microeukaryotic **(A)** and prokaryotic **(B)** plankton communities. The error bars indicate SD, and asterisks (*) indicate significant differences at the level of $P<0.05$. **(C, D)** Non-metric multidimensional scaling (NMDS) ordination of plankton communities based on Bray–Curtis distances. upper, upper oxic layer; middle, middle oxic layer; anoxic, suboxic-anoxic layer. All, whole community; Abundant, Moderate and Rare indicate the abundant, moderate and rare plankton subcommunities, respectively.

Co-occurrence network of planktonic microbiome

Given the contribution of rare taxa in the biodiversity of SYBH and potential effect of cross-domain biotic factor on planktonic community, we performed co-occurrence network analysis (Figure 5). All obtained network exhibited a scale-free and non-random distribution with power-law $R^2 = 0.824$ (Supplementary Figure 10, Supplementary Table 5). The network was composed of 9238 positive and 416 negative edges, among which 1,343, 2,360 and 5,951 edges were from microeukaryote-prokaryote, microeukaryote-microeukaryote, and prokaryote-prokaryote connections with 62.74% of the negative edges were found between microeukaryotes and prokaryotes. Nodes linked by cross-domain edges were mainly composed of Gammaproteobacteria, Alphaproteobacteria and Syndiniales (Supplementary Table 7). Among 1629 nodes, the majority (49.54%) was rare OTUs followed by moderate (37.57%) and abundant (12.83%) OTUs (Figure 5A). The interactions with rare taxa were found to be most frequent in the network (Supplementary Table 6). Nodes were mainly represented by Gammaproteobacteria (18.97%), Alphaproteobacteria (13.20%), Syndiniales (6.02%). Eighteen prokaryotic OTUs and 2 eukaryotic OTUs were identified as keystone species with high degree (>50) and low betweenness centrality (<5000), which consisted of 6 rare OTUs, 13 moderate OTUs and 1 abundant OTU belong to Gammaproteobacteria, Alphaproteobacteria, Planctomycetacia, Actinobacteria, Verrucomicrobia, Radiolaria (Figure 5C;

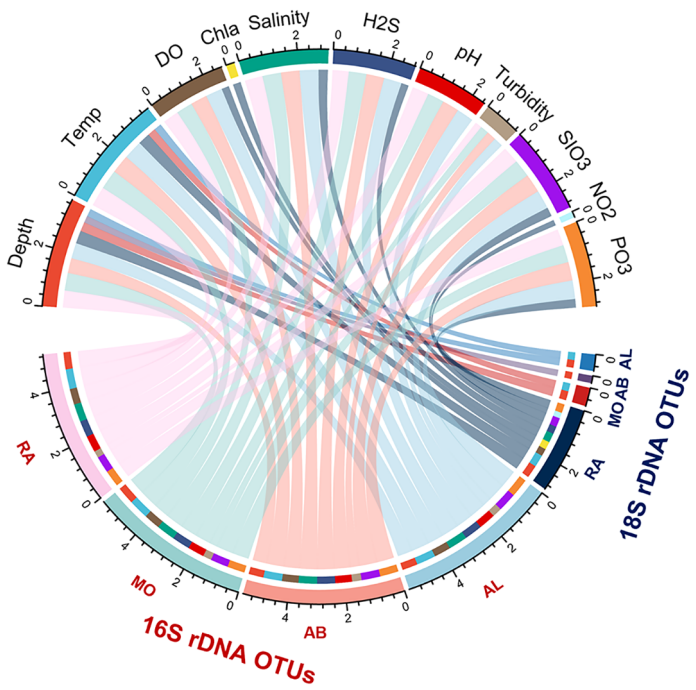

FIGURE 4
The circos plot depicts the effects of environmental variables on the beta diversity of microeukaryotes and prokaryotes plankton communities revealed by Mantel tests. Each environmental variable and subcommunity are depicted by the arcs. The correlation between the relative abundance of community and environmental variable are depicted by the arcs with specific color. The area of ribbons indicate the contribution of each variables with significant positive correlation. Detailed results of Mantel test are shown in Supplementary Table 4. RA, Rare subcommunity; MO, Moderate subcommunity; AB, Abundant subcommunity; AL, whole community.

TABLE 1 Mantel tests showing the effects of cross-domain biotic factors on microeukaryotic and prokaryotic plankton communities.

	18S_All community		18S_Abundant subcommunity		18S_Moderate subcommunity		18S_Rare subcommunity	
16S PCoA 1&2	rho	P	rho	P	rho	P	rho	P
All	0.110	0.183	0.082	0.231	0.169	0.073	**0.328**	**0.002**
Abundant	0.100	0.197	0.071	0.256	0.167	0.082	**0.325**	**0.002**
Moderate	**0.369**	**0.004**	**0.344**	**0.009**	**0.426**	**0.001**	**0.435**	**0.001**
Rare	**0.507**	**0.001**	**0.489**	**0.001**	**0.524**	**0.001**	**0.421**	**0.001**
	16S_All community		**16S_Abundant subcommunity**		**16S_Moderate subcommunity**		**16S_Rare subcommunity**	
18S PCoA 1&2	rho	P	rho	P	rho	P	rho	P
All	0.043	0.338	0.010	0.419	0.176	0.103	0.213	0.069
Abundant	0.039	0.337	0.005	0.433	0.178	0.100	0.216	0.070
Moderate	0.125	0.168	0.089	0.222	**0.260**	**0.036**	**0.304**	**0.023**
Rare	0.070	0.258	0.033	0.356	0.206	0.067	**0.246**	**0.042**

All, whole community; Abundant, abundant subcommunity; Moderate, moderate subcommunity; Rare, rare subcommunity; 18S, 18S rDNA dataset of microeukaryote; 16S, 16S rDNA dataset of prokaryote.
The PCoA1 and PCoA2 denote the first and second axes of the PCoA ordination of community (subcommunity), respectively, which were used as proxy to quantify the effect of cross-domain biotic factor.
Bold font indicates significant correlation ($P<0.05$).

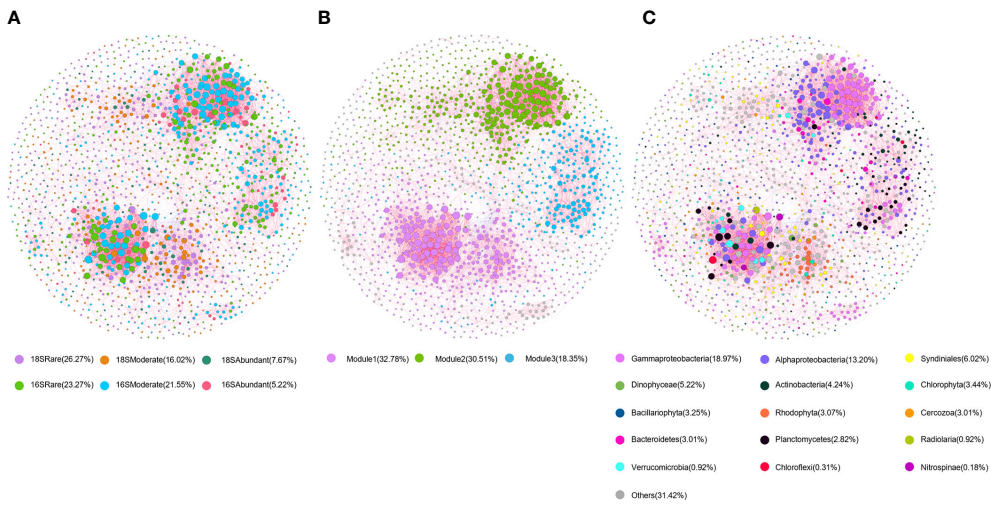

FIGURE 5
Co-occurrence network of planktonic microbiome in SYBH. The network was established by calculating correlations among OTUs. The nodes in the network are colored according to **(A)** subcommunities of different abundance; **(B)** modules and **(C)** taxa. The red and blue lines represent positive and negative correlations, respectively. The sizes of the nodes are scaled to the degree of connection.

Supplementary Table 8). Among these keystone species, the top 2 OTUs with highest degree were affiliated to rare OTUs of Planctomycetes and Alphaproteobacteria.

The co-occurrence network was clustered into three major modules accounting for 81.64% of the total nodes (Figure 5B). All three modules were dominated by rare OTUs affiliated to Alphaproteobacteria and Gammaproteobacteria (Figure 5C). Three modules of prokaryotic OTUs exhibited distinct distribution pattern along the vertical gradient which was not observed for microeukaryotes (Supplementary Figure 11). Most of the prokaryotic OTUs from module I had higher relative abundance in the middle oxic layer, while the relative abundance of OTUs in module II and III was higher in the upper oxic layer (Supplementary Figure 11).

Ecological processes shaping the microeukaryotic and prokaryotic plankton communities

The relative contribution of each ecological process underpinning the assembly of microbial community was quantified by the phylogenetic null model analysis (Figure 6). It was found that stochastic processes, mainly dispersal limitation (83.09%), made crucial contributions to microeukaryotic plankton assembly, while prokaryotic assembly was dominated by deterministic processes consisting of heterogenous (42.65%) and homogenous selection (47.79%). Nevertheless, the effect of ecological drift was minor (<0.74%). The role of different ecological processes varied among subcommunities (Figure 6). Dispersal limitation made a significant contribution to microeukaryotic subcommunities assembly, accounting for 97.06%, 91.91%, 66.18% in abundant, moderate and rare subcommunities, respectively. Homogenous selection was not detected in abundant subcommunity but more diverse processes played a role in rare subcommunity. For prokaryotes, abundant taxa were driven mainly by dispersal limitation (54.41%) and heterogeneous selection (41.18%). The moderate taxa were mainly driven by deterministic processes (70.59%) with heterogeneous and homogeneous selection accounting for 42.65% and 27.94%, respectively, and dispersal limitation also made a significant contribution (27.21%). The effect of deterministic processes was overwhelming (100%) in rare subcommunity with homogenous and heterogenous selection contributed 57.35% and 42.65%, respectively. Generally, the contribution of deterministic processes to the microbial assembly increased with the taxa abundance, while that of stochastic processes showed the opposite trend.

Discussion

Depth partitioning of plankton microbiome in the SYBH

Environmental heterogeneity is regarded as a universal driver of biodiversity (Stein et al., 2014), thus the strong vertically heterogeneous environment in the SYBH explained its higher plankton diversity than that in outer reef slope and

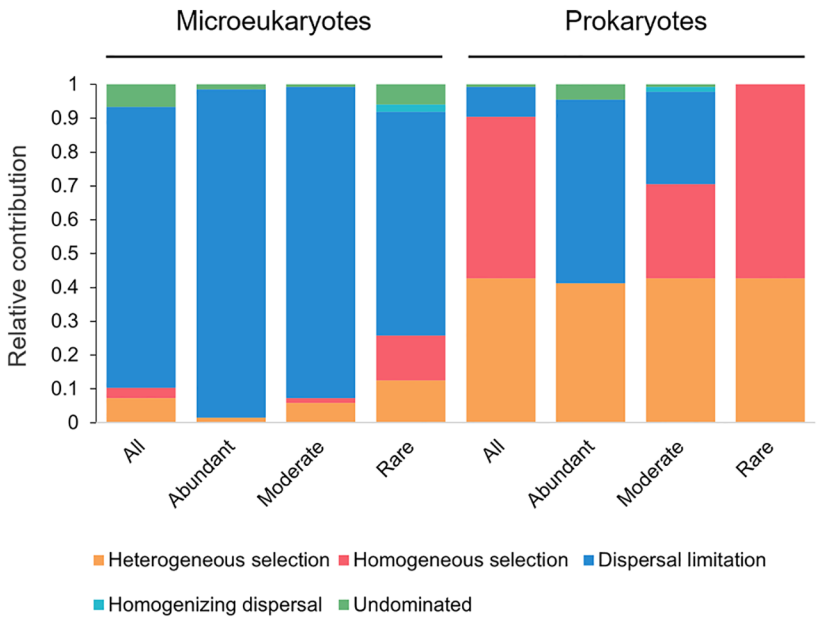

FIGURE 6
The relative contributions of the ecological processes in shaping plankton microbiome. Abundant, Moderate and Rare indicate the abundant, moderate and rare plankton subcommunities, respectively.

other Chinese marginal seas (He et al., 2019; Liu et al., 2019; Li et al., 2020b). In this study, our joint analysis of microeukaryotic and prokaryotic plankton found that planktonic microbiome above 150 m in the SYBH was vertically structured along the abiotic gradients and grouped into three clusters as upper oxic layer (0-20 m), middle oxic layer (40-80 m) and suboxic-anoxic layer (90-150 m) (Figures 1D, 3). This finding is consistent with previous studies on *Vibrio* community (Li et al., 2020a) and overall bacterial communities (Zhang et al., 2021) in the SYBH, and such depth partitioning of microbial community was also found in the Hospital Hole (Davis and Garey, 2018). The decrease of richness and diversity with depths was detected in prokaryotic plankton community in the SYBH (Figure 3B) which is also in concert with previous findings of overall bacterial community (Zhang et al., 2021). Contrastingly, no significant variation of diversity was detected in microeukaryotes across depths (Figure 3A), indicating the different sensitivity of eukaryotic and prokaryotic community to the strong vertical stratification.

The vertical variation of relative abundance was particularly pronounced in some lineages. As expected, the abundance of oxygenic photosynthetic phytoplankton decreases has light decays at the depth of 90 m in the hole (Bi et al., 2018), which explained the greater abundance of Haptophyta, Rhodophyta and Cyanobacteria in the upper oxic layer ($P<0.05$, Supplementary Figure 3). However, no significant vertical variation among three layers was detected in the most dominant phytoplankton Dinophyceae, of which the versatile nutrient utilization and mixotrophy might make Dinophyceae less sensitive to the light availability and nutrient input (Edwards, 2019), and consequently thrive in the bule hole. Fungi dominated by the phylum Ascomycota was enriched (average 21.36%) in the middle oxic layer of the SYBH. The depth-dependent distribution of pelagic Fungi has been characterized to be universal in the global oceans (Morales et al., 2019) and integrated omics analysis pointed to that depth is also a significant factor in structuring the function of Fungi, particularly in carbonhydrate and lipid degradation (Morales et al., 2019; Chrismas and Cunliffe, 2020; Baltar et al., 2021). Thus, given the important roles of pelagic Fungi in marine biogeochemical cycles, the vertical distribution of Fungi in the SYBH suggests a potential variation in organic carbon speciation with depth.

With the increase of depth, the relative abundance of ammonium oxidizer Thaumarchaeota and nitrite oxidizer Nitrospinae increased and peaked at 90 m (Supplementary Figure 4) with a sharp reduction downward. Such vertical profile of nitrifying consortium well matches that of inorganic nitrogen concentrations, indicating that the main biological process below euphotic zone is nitrification and shifts to denitrification and anaerobic ammonium oxidation (annammox) below 90 m as speculated in previous studies (He et al., 2019; Xie et al., 2019). Moreover, increasing evidence has shown that the reciprocal feeding on diverse dissolved organic nitrogen (DON) such as urea and cyanate between Thaumarchaeota and Nitrospinae may fuel the nitrification in

deep ocean (Palatinszky et al., 2015; Pachiadaki et al., 2017; Kitzinger et al., 2019), which might be overlooked in the past. In upper sunlit but N-deplete ocean waters, DON may also play a role in 'regenerated' primary production (Kamennaya et al., 2008). The depth-dependent ecological roles of DON are also mirrored by the distribution and expression of genes related to DON metabolism which differed significantly among surface and mesopelagic zones in the global oceans (Mao et al., 2022). Such vertical pattern could be more pronounced in the strongly stratified SYBH and as the reduced form of nitrogen, DON could be particularly important in structuring the microbial community in suboxic-oxic layer. Although no DON measurement has been so far attempted for SYBH, in the future omic approaches could be utilized to characterizing DON pool as it has been done in other ocean waters (Palatinszky et al., 2015; Pachiadaki et al., 2017; Mao et al., 2022).

The relative abundance of Epsilonproteobacteria sharply increased at the depth of 100 m and retained high (15.99%) down to 150 m. Most members of Epsilonproteobacteria are chemoautotrophs and play crucial roles in biogeochemical cycle of carbon, nitrogen and sulfur in extreme environments such as deep-sea hydrothermal vents (Akerman et al., 2013; Meyer and Huber, 2014). It has been reported to be more abundant in the deep layer of SYBH than those in other caves and other areas of South China Sea (He et al., 2019). The dominancy of Epsilonproteobacteria at suboxic-oxic layer can be attributed to the sulfidic environment below 100 m in SYBH which is totally disconnected from adjacent ocean (Bi et al., 2018; Xie et al., 2019).

Diel pattern of plankton community composition

The diel vertical distribution of mesozooplankton, micro- and nanophytoplankton in the SYBH have been characterized based on morphological analysis (Chen et al., 2018; Ge et al., 2020). Results in these studies showed that diel vertical variation was mainly detected in the oxic layer (<90 m) and the strong thermohalocline around 80-90 m is considered to be the barrier of vertical migration for plankton. In this study, metabarcoding analysis also revealed the significant daytime-nighttime difference of community composition, which was restricted in the upper oxic layer and was mainly detected in microeukaryotic community (Supplementary Figure 3).

Radiolarian was most abundant in the upper oxic layer of nighttime, reaching the highest relative abundance at 5 m (Figure 2A), suggesting their diel periodicity. Hu et al. (2018) reported the significant diel rhythmicity in the field community of Rhizaria including radiolarians and their acantharians relatives in the North Pacific Subtropical Gyre, which had higher metabolic activities at nighttime compared to that at daytime. Diel vertical migration (DVM) was also observed in acantharians in the Atlantic Ocean, but the pattern could vary among different waters (Massera Bottazzi and Andreoli, 1982). Members of Rhizaria are commonly found in the euphotic zone, host algal endosymbionts and prey on a variety of microorganisms (Decelle et al., 2012; Ohtsuka et al., 2015). Their diel rhythmicity could be related to the availability of light and picocyanobacterial prey (Massera Bottazzi and Andreoli, 1982; Hu et al., 2018), which may also explain why the different daily distribution of plankton only found in the upper layer of SYBH. Given the importance of Rhizaria in global plankton biomass and contribution to carbon export (Biard et al., 2016; Caron, 2016; Guidi et al., 2016), further investigation is desired to fully portrait their diversity and distribution in the SYBH.

Besides DVM, we also postulated that diel horizontal migration (DHM) could be a potential factor shaping the distribution of eukaryotic plankton in SYBH: plankton inhabit the walls of SYBH at daytime and horizontally migrate into water column at nighttime. Nocturnal horizontal migration has been observed in both freshwater and marine ecosystems (Webb and Wooldridge, 1990; White, 1998) and is hypothesized to help organisms find prey and avoid predator, like DVM does. It has been suggested that abiotic conditions are less likely to influence DHM than DVM when horizontal gradients of abiotic conditions are weaker relative to the vertical gradients (Burks et al., 2002), which is also the case in the SYBH. This could partly explain that relative to prokaryotes, the day-night difference of community composition was more evident in microbial eukaryotes, who were less sensitive to abiotic environmental factors in the SYBH (Figure 4). Moreover, viable sampling techniques are desired in the future to quantify the DHM organisms and assess the factors influencing DHM.

Distinct patterns and drivers of microeukaryotic and prokaryotic plankton assembly

Analysis of diversity, abiotic and biotic factors, co-occurrence network and assembly mechanism consistently pointed to the divergent assembly pattern and driving forces for prokaryotic and microeukaryotic plankton community in SYBH. Vertical heterogeneity significantly shaped the community composition of microeukaryotic plankton without affecting overall diversity (Figures 3A, B). Abiotic factors played a minor role in shaping microeukaryotic plankton community in SYBH, which is often found to be more influential in other aquatic ecosystems such as the northwestern Pacific Ocean (Wu et al., 2020). Moreover, compared to prokayrotes, microeukaryotic plankton community had less compact network topology with lower average degree and number of intradomain edges. The modularity of microeukaryotes OTUs in

network showed less depth partitioning. Network complexity and connectivity are considered to be associated with sensitivity of microbes to environmental disturbances (Zhou et al., 2010). Weaker network connectivity of microeukaryotic community than bacterial community has been found in previous study, indicating the community assembly is less determined by environmental selection processes (Jiang et al., 2018), which is consistent with our results in assembly mechanism.

Quantifying the relative importance of each ecological process in community assembly highlighted the different roles in shaping the composition of microeukaryotic and prokaryotic plankton community in SYBH. We observed that stochastic processes, mainly dispersal limitation played a significant role in the community assembly of microeukaryotic plankton, which is consistent with previous findings in reservoir, intertidal zone, and costal upwelling system (Xue et al., 2018; Kong et al., 2019; Sun et al., 2022). In comparison to prokaryotic plankton, microeukaryotes were more dispersal limited which has hypothesized to increase with body size in planktonic communities (Finlay, 2002; Soininen et al., 2013; Villarino et al., 2018). Very limited vertical mixing and exchange with adjacent waters in SYBH forms a strong barrier to dispersal for larger planktonic organisms. Such barriers include persistent oceanographic features like thermhalocline and other sharp environmental gradients and the effect of barriers varies across taxa depending on both body size and abundance (Finlay, 2002; Martiny et al., 2006; Jenkins et al., 2007). Furthermore, although the role of ecological drift was minor for both planktonic community assembly, the contribution of it was slightly higher in microeukaryotic plankton. This still could be explained by the generally smaller size of prokaryotic plankton as smaller organisms are expected to have lower demographic stochasticity and ecological drift (Rosindell et al., 2011), thus resulting in higher population density than larger organisms. Ecological drift is also expected to be more significant with decreasing population size and community size (Liu et al., 2018). However, using community snapshots by amplicon sequencing may not fully quantify the random demographic events (Stegen et al., 2015) and effect of size and abundance on ecological drift of natural assemblage remain uncertain with scarce of field data (Liu et al., 2018).

Contrastingly, deterministic processes dominated over the stochastic processes in prokaryotic community but contributed much less to the assembly of microeukaryotic communities, confirming the stronger environmental filtering on prokaryotes in SYBH as shown by mantel test (Figure 4; Supplementary Table 4). The difference of assembly mechanism between prokaryotic and microeukaryotic community in SYBH is consistent with previous research on protist and bacteria in global surface waters (Logares et al., 2020) and upwelling system (Sun et al., 2022), but contradict with that in East China Sea's euphotic zone where protist community is mainly structured by selection processes (Wu et al., 2018). Such inconsistency has been discussed in several studies on microbiomes across different ecosystems (Xue et al., 2018; Xiong et al., 2021; Lu et al., 2022; Sun et al., 2022), supporting that the combined effect of species, straits, habitat type, spatiotemporal scale and environmental gradient determine the relative contribution of determinism and stochasticity in shaping the microbial landscape (Chase and Myers, 2011; Hanson et al., 2012; Morrison-Whittle and Goddard, 2015).

Collectively, our results showed that microeukaryotic plankton community in SYBH was less sensitive to environmental filtering compared with prokaryotes. Their different physiological characteristics, particularly body size, fundamentally determine the community turn over, community size, physiological plasticity, niche breaths and eventually environmental sensitivity (Shade et al., 2012). Despite of weaker environmental sensitivity, the effect of cross-domain biotic factor, i.e. effect of prokaryotic community on microeukaryotic community, was significant, pointing to the importance of bio-interaction in shaping microeukaryotic community in SYBH. In present study of SYBH, there were more positive interactions than negative ones in co-occurrence network, suggesting that interspecies cooperation such as symbiosis (Supplementary Table 5) may play a critical role in supporting ecosystem function and stability in SYBH. Mutual interactions in the form of symbiosis can increase the fitness of hosts and allow them to exploit new ecological niches, which is prevalence in aquatic ecosystem and particularly important in extreme habitats such as hydrothermal vent and anoxic environment (Zehr and Caron, 2022). Obligate symbiosis with the chemoautotrophs including methanogens and sulfur oxidizers might be restricted in anoxic or microoxic environment, and movement of host like ciliate between oxic and anoxic zones may favor the symbiont growth (Dziallas et al., 2012). Denitrification in anoxic environments could be also performed by eukaryotic microbes like foraminifera harboring denitrifying symbionts (Bernhard et al., 2012). Thus, we also expect diverse symbiotic relationships would favor the organisms in blue hole to cope with extreme conditions like anoxia, low light and poor supply of labile organic matter (Northup and Lavoie, 2001; Krstulović et al., 2013).

About 14% of edges in co-occurrence network were between microeukaryotes and prokaryotes, indicating the nonnegligible cross-domain interaction in SYBH planktonic ecosystem. Among these, microeukayotes were most associated with Proteobacteria, and bacteria were most associated with Syndiniales (Supplementary Table 7), which was also found in the euphotic zone of Northwest Pacific Ocean (Wu et al., 2020) and permanently anoxic Cariaco Basin (Suter et al., 2022). Microbial interaction, especially parasitism involving Syndiniales is a very significant factor in structuring the global plankton community (Lima-Mendez et al., 2015) and particularly important in maintaining microbial food web productivity in resources-limited waters (Suter et al., 2022).

Interestingly, although the network possessed a higher proportion of positive correlations than negative ones, 62.74% of negative correlations existed between microeukaryotes and prokaryotes, suggesting their predation or other competition relationship may play an important role in the pelagic food web of SYBH where the supply of nutrient and organic matter is limited (Boenigk and Arndt, 2002; Melanie and Sara, 2016). In comparison to prokaryotic plankton, we expect more complex biotic factors shaping the microeukaryotic assembly in SYBH, including microbe-microbe symbiosis, predation by mesoplankton or micronekton and diel migration at both vertical and horizontal directions. Although it has been pointed out biological interaction based on rDNA-derived OTU correlation may be overestimated due to variable rDNA copy number among some lineage such alveolates, next generation sequencing enables us to discover a vast array of potential biotic interactions in batch (Lima-Mendez et al., 2015), when morphological observation and physiological experiment are impractical.

The important ecological role of non-abundant taxa in SYBH

As normally found in most habitats (Pedros-Alio, 2012; Lynch and Neufeld, 2015), a skewed abundance distribution of plankton was also observed in SYBH, as the community across depths was dominated by a few abundant taxa. The richness of rare subcommunities was 7-fold and 6-fold greater than that of abundant ones for microeukaryotes and prokaryotes, respectively (Supplementary Figure 8), corroborating the well-recognized idea that rare biosphere contribute significantly to the microbial diversity (Debroas et al., 2015; Lynch and Neufeld et al., 2015). The sensitivity to environments also differed between subcommunities as supported by multiple evidence. Firstly, abundant taxa were commonly found in three layers in SYBH while rare taxa were habitat-specific (Figure 2C, D). Secondly, although deterministic processes represented played a minor role in shaping the assembly of microeukaryotic plankton community, the selection effect increased from abundant to rare subcommuniteis and the enhancement was more pronounced in prokaryotic plankton (Figure 6). This indicates that in comparison with abundant taxa, rare taxa were more sensitive to local environmental filtering, which in concert with previous studies on planktonic microbiomes in freshwater ecosystems (Liu et al., 2015; Xue et al., 2018). The high abundance resulted from active growth mirrors that abundant taxa are more competitive in resource acquisition and better adapted to habitats. However, high diversity and functional redundancy of rare taxa make them important in ecosystem resilience (Jousset et al., 2017).

Furthermore, non-abundant taxa are indispensable in maintaining the structure of microbial community as denoted in co-occurrence network with over 87% of significant biological interactions involved non-abundant taxa. Moreover, except for one abundant OTU, all keystone species in co-occurrence network were belonged to moderate and rare taxa. Compared to eukaryotic plankton of reservoir (Xue et al., 2018), the role of moderate taxa was more prominent in SYBH, which has been also found in estuarine ciliate community (Sun et al., 2017). Rare taxa are more likely to be ignored through morphological analysis and low-resolution sampling due to habitat specificity. Although deep sequencing of metabarcodes unveiled the rare biosphere in diverse habitats (Pedros-Alio, 2012), the role of rare taxa in maintaining the microbiome stability has not been addressed in SYBH. Moreover, much less attention has been paid to moderate taxa, which could contribute up to 30% of abundance (Logares et al., 2014) and critical to the dynamics of community (Mangot et al., 2013; Sun et al., 2017). Out of 20 keystone OTUs, 13 were affiliated with moderate taxa which is considered as initiating components in network with longer evolutionary history (Barabási 2009). Future study on temporal variation of microbial community in SYBH could provide precise assessment on the role of non-abundant taxa on microbiome stability and have important implication in conservation strategy.

Limitation and perspective

Metabarcoding approaches come with some limitations. The most common one is the variation in rDNA gene copy number among different taxa, especially in microbial eukaryotes, hinders the directly translation of the rDNA read counts into absolute abundance of organisms (Burki et al., 2021). The rDNA copy number per genome positively correlates to cell size and biovolume (de Vargas et al., 2015). Thus, cautions should be taken when interpreting amplicon sequencing data, especially for organisms of large size or unique genome architecture (e.g., ciliate). Although metabarcoding analysis only provides relative or semiquantitative information, one can assume that such molecular biases would be relatively constant across samples and will allow the comparison between different ecological conditions (Pawlowski et al., 2016). Therefore, rDNA OTUs and reads can still be rough proxies for assessing, respectively, the genetic biodiversity and biovolume of microbial eukaryotic communities with great ecological relevance (de Vargas et al., 2015; Pawlowski et al., 2016).

Since the SYBH has been discovered for only six years, we are still at the stage of preliminary exploration and have to admit the sampling difficulty and technical limitation. SYBH sits on the coral reef and it is impractical to set up a large observation platform equipped with comprehensive and powerful facilities.

Meanwhile, sinuous underwater structure and the slope at the depth about 150 m increase the difficulty of vertically sampling. Although several professional-grade facilities such as underwater remotely operated vehicle (ROV) have been exploited to obtain geomorphological profile of SYBH, more flexible sampler with less disturbance to organism is desired. In the future, portable and autonomous facility or unmanned aerial vehicles (UAV)-based system could provide a promising approach for remote sampling in the SYBH (Horricks et al., 2022).

Although the vertical profile of hydrochemical properties and microbial plankton community structure in the SYBH showed generally similar pattern among multiple investigations (He et al., 2019; Xie et al., 2019; Li et al., 2020a), variation in the depth of Deep Chlorophyll Maximum and community composition are still observed. Whether these inconsistencies are resulted from different sampling time of the day and season, or occasional observation is still unclear. Thus, replicate, high-resolution and time-series samples are needed to fully portrait the spatiotemporal distribution of life in SYBH. Moreover, currently available information about plankton diversity in SYBH are based on morphological identification (Chen et al., 2018; Ge et al., 2020; Fu et al., 2020) and DNA metabarcoding (He et al., 2019; Liu et al., 2019; Li et al., 2020a; Li et al., 2020b) which are impossible to differentiate the dead and live organisms. Thus, profiling the viability, metabolic activity and machinery of organism, particularly for those survive in anoxic conditions, is crucial for unveiling the ecological strategy and evolutionary adaptation of marine life in the SYBH, which could be achieved by viability assessment (Eva-Maria and Meysnan, 2012) and RNA-based approaches. Finally, integrated investigation on organisms from broad size spectrum and multiple habitats (plankton, bentho and neckton) are desired, which is essential for improve our understanding on the nature of bio-interaction and ecological functions in SYBH.

Data availability statement

The data presented in the study are deposited in China National GeneBank DataBase (https://db.cngb.org/), accession number CNP0003459.

Author contributions

YZ and HC conceived and coordinated the project with help from LF, ZY and GL. CC and RG carried out the sampling with help from LF. YZ, CC and XM processed the samples by extracting DNA and preparing the amplicon libraries. TC, YZ and JC analyzed the data. TC and YZ wrote the manuscript with input from all authors. ZY and GL supervised the work. All authors contributed to the article and approved the submitted version.

Funding

This work was supported by the Marine S&T Fund of Shandong Province for Pilot National Laboratory for Marine Science and Technology (Qingdao) (No.LSKJ202202804), the National Natural Science Foundation of China (No. 41876156, No. 42076146), the Fundamental Research Funds for the Central Universities (No. 201762038, No. 201812019) and Research and Development Program for the South China Sea of the Sansha Track Ocean Coral Reef Conservation Research Institute (No. HJLD17-01).

Acknowledgments

We are grateful to the Sansha Track Ocean Coral Reef Conservation Research Institute expedition vessel for their support. We also thank Libao Yang, Honglin Ma and Lin Chen for their assistance in sampling. We also thank Peng Yao and Naishuang Bi for their advice on the manuscript.

Conflict of interest

Author JC is employed by BGI, Qingdao, China.

The remaining authors declare that the research was conducted in the absence of any commercial or financial relationships that could be construed as a potential conflict of interest.

Publisher's note

Supplementary material

The Supplementary Material for this article can be found online at: https://www.frontiersin.org/articles/10.3389/fmars.2022.1046808/full#supplementary-material

References

Akerman, N. H., Butterfield, D. A., and Huber, J. A. (2013). Phylogenetic diversity and functional gene patterns of sulfur-oxidizing subseafloor *Epsilonproteobacteria* in diffuse hydrothermal vent fluids. *Front. Microbiol.* 4. doi: 10.3389/fmicb.2013.00185

Baltar, F., Zhao, Z., and Herndl, G. J. (2021). Potential and expression of carbohydrate utilization by marine fungi in the global ocean. . *Microbiome* 9, 106. doi: 10.1186/s40168-021-01063-4

Barabási, A. L. (2009). Scale-free networks: A decade and beyond. *Science* 325, 412–413. doi: 10.1126/science.1173299

Bernhard, J. M., Edgcomb, V. P., Casciotti, K. L., McIlvin, M. R., and Beaudoin, D. J. (2012). Denitrification likely catalyzed by endobionts in an allogromiid foraminifer. *ISME J.* 6, 951–960. doi: 10.1038/ismej.2011.171

Biard, T., Stemmann, L., Picheral, M., Mayot, N., Vandromme, P., Hauss, H., et al. (2016). *In situ* imaging reveals the biomass of giant protists in the global ocean. *Nature* 532, 504–507. doi: 10.1038/nature17652

Bi, N., Liang, F., Chen, H., Liu, R., Lin, C., Liu, Q., et al. (2018). Hydrographic features of the yongle blue hole in the south China sea and their influential factors. *Chin. Sci. Bulletin* 63, 2184–2186. doi: 10.1360/N972017-01329

Boenigk, J., and Arndt, H. (2002). Bacterivory by heterotrophic flagellates: community structure and feeding strategies. *Antonie van Leeuwenhoek.* 81, 465–480. doi: 10.1023/a:1020509305868

Bolyen, E., Rideout, J. R., Dillon, M. R., Bokulich, N. A., Abnet, C. C., Al-Ghalith, G. A., et al. (2019). Reproducible, interactive, scalable and extensible microbiome data science using QIIME 2. *Nat. Biotechnol.* 37, 852–857. doi: 10.1038/s41587-019-0209-9

Bråte, J., Logares, R., Berney, C., Ree, D. K., Klaveness, D., Jakobsen, K. S., et al. (2010). Freshwater perkinsea and marine-freshwater colonizations revealed by pyrosequencing and phylogeny of environmental rDNA. *ISME J.* 4, 1144–1153. doi: 10.1038/ismej.2010.39

Burki, F., Sandin, M. M., and Jamy, M. (2021). Diversity and ecology of protists revealed by metabarcoding. *Curr. Biol.* 31, R1267–R1280. doi: 10.1016/j.cub.2021.07.066

Burks, R. L., Lodge, D. M., Jeppesen, E., and Lauridsen, T. L. (2002). Diel horizontal migration of zooplankton: Costs and benefits of inhabiting the littoral. *Freshw. Biol.* 47, 343–365. doi: 10.1046/j.1365-2427.2002.00824.x

Campbell, B. J., Yu, L., Heidelberg, J. F., and Kirchman, D. L. (2011). Activity of abundant and rare bacteria in a coastal ocean. *Proc. Natl. Acad. Sci. United States America* 108, 12776–12781. doi: 10.1073/pnas.1101405108

Caporaso, J. G., Lauber, C. L., Walters, W. A., Berg-Lyons, D., Lozupone, C. A., Turnbaugh, P. J., et al. (2011). Global patterns of 16S rRNA diversity at a depth of millions of sequences per sample. *Proc. Natl. Acad. Sci.* 108, 4516–4522. doi: 10.1073/pnas.1000080107

Caron, D. A. (2016). Ocean science: the rise of rhizaria. *Nature* 532, 444–445. doi: 10.1038/nature17892

Chase, J. M., and Myers, J. A. (2011). Disentangling the importance of ecological niches from stochastic processes across scales. *Philos. Trans. R. Soc B* 366, 2351–2363. doi: 10.1098/rstb.2011.0063

Chen, C., Fu, L., Bi, N., Ge, R., Liu, G., Zhuang, Y., et al. (2018). Zooplankton community composition and diel vertical distribution in the yongle blue hole, xisha islands, south China sea. *Oceanologia Limnologia Sinica* 49, 10. doi: 10.11693/hyhz20171200328

Chrismas, N., and Cunliffe, M. (2020). Depth-dependent mycoplankton glycoside hydrolase gene activity in the open ocean–evidence from the *Tara* oceans eukaryote metatranscriptomes. *ISME J.* 14, 2361–2365. doi: 10.1038/s41396-020-0687-2

Clarke, K. R., and Gorley, R. N. (2009). PRIMER v6: User Manual/Tutorial. (Plymouth, PRIMER–E).

Davis, M. C., and Garey, J. R. (2018). Microbial function and hydrochemistry within a stratified anchialine sinkhole: A window into coastal aquifer interactions. *Water* 10, 972–972. doi: 10.3390/w10080972

Debroas, D., Hugoni, M., and Domaizon, I. (2015). Evidence for an active rare biosphere within freshwater protists community. *Mol. Ecol.* 24, 1236–1247. doi: 10.1111/mec.13116

Decelle, J., Siano, R., Probert, I., Poirier, C., and Not, F. (2012). Multiple microalgal partners in symbiosis with the acantharia *Acanthochiasma* sp. (*Radiolaria*). *Symbiosis* 58, 233–244. doi: 10.1007/s13199-012-0195-x

de Vargas, C., Audic, S., Henry, N., Decelle, J., Mahé, F., Logares, R., et al. (2015). Eukaryotic plankton diversity in the sunlit ocean. *Science* 348, 29223618–29223625. doi: 10.1126/science.1261605

Dziallas, C., Allgaier, M., Monaghan, M. T., and Grossart, H.-P. (2012). Act together-implications of symbioses in aquatic ciliates. *Front. Microbio* 3. doi: 10.3389/fmicb.2012.00288

Edgar, R. (2016). SINTAX: A simple non-Bayesian taxonomy classifier for 16S and ITS sequences. *bioRxiv*. doi: 10.1101/074161

Edwards, K. F. (2019). Mixotrophy in nanoflagellates across environmental gradients in the ocean. *Proc. Natl. Acad. Sci.* 116, 6211–6220. doi: 10.1073/pnas.1814860116

Eva-Maria, Z., and Meysman, F. J.R. (2012). Dead or alive? viability assessment of micro- and mesoplankton. *J. Plankton Res.* 34, 493–509. doi: 10.1093/plankt/fbs018

Finlay, B. J. (2002). Global dispersal of free-living microbial eukaryote species. *Science* 296, 1061–1063. doi: 10.1126/science.1070710

Fu, M., Sun, P., Li, Y., Pu, X., Yuan, C., and Zhang, X. (2020). Phytoplankton community structure in sansha yongle blue hole and its adjacent area of the south China Sea. *Adv. Mar. Sci.* 38, 304–316. doi: 10.3969/j.issn.1671-6647.2020.02.010

Garman, K. M., Rubelmann, H., Karlen, D. J., Wu, T., and Garey, J. R. (2011). Comparison of an inactive submarine spring with an active nearshore anchialine spring in Florida. *Hydrobiologia* 677, 65–87. doi: 10.1007/s10750-011-0740-2

Ge, R., Fu, L., Bi, N., Chen, C., Liu, G., Zhuang, Y., et al. (2020). Diel vertical distribution of phytoplanktonin yongle blue hole, xisha islands in spring. *Periodical Ocean Univ. China* 50, 65–73. doi: 10.16441/j.cnki.hdxb.20180428

Gobet, A., Böer, S., Huse, S., Beusekom, J. E. E., Quince, C., Sogin, M. L., et al. (2012). Diversity and dynamics of rare and of resident bacterial populations in coastal sands. *ISME J.* 6, 542–553. doi: 10.1038/ismej.2011.132

Gonzalez, B. C. (2010). *Novel bacterial diversity in an anchialine blue hole on abaco island, bahamas. master's thesis* (College Station, TX, USA: Texas A&M University).

Guidi, L., Chaffron, S., Bittner, L., Eveillard, D., Larhlimi, A., Roux, S., et al. (2016). Plankton networks driving carbon export in the oligotrophic ocean. *Nature* 532, 465–470. doi: 10.1038/nature16942

Guillou, L., Bachar, D., Audic, S., Bass, D., Berney, C., Bittner, L., et al. (2012). Protist ribosomal reference database (PR2): A catalog of unicellular eukaryote small sub-unit rRNA sequences with curated taxonomy. *Nucleic Acids Res.* 41, D597–D604. doi: 10.1093/nar/gks1160

Hanson, C. A., Fuhrman, J. A., Horner-Devine, M. C., and Martiny, J. B. (2012). Beyond biogeographic patterns: Processes shaping the microbial landscape. *Nat. Rev. Microbiol.* 10, 497–506. doi: 10.1038/nrmicro2795

He, H., Fu, L., Liu, Q., Fu, L., Bi, N., Yang, Z., et al. (2019). Community structure, abundance and potential functions of bacteria and archaea in the sansha yongle blue hole, xisha, south China Sea. *Front. Microbiol.* 10. doi: 10.3389/fmicb.2019.02404

Horricks, R. A., Bannister, C., Lewis-McCrea, L. M., Hicks, J., Watson, K., and Reid, G. K. (2022). Comparison of drone and vessel-based collection of microbiological water samples in marine environments. *Environ. Monit Assess.* 194, 439. doi: 10.1007/s10661-022-10095-8

Hu, S. K., Connell, P. E., Mesrop, L. Y., and Caron, D. A. (2018). A hard day's night: diel shifts in microbial eukaryotic activity in the north pacific subtropical gyre. *Front. Mar. Sci.* 5. doi: 10.3389/fmars.2018.00351

Ibarbalz, F. M., Henry, N., Brando, M. C., Martini, S., Busseni, G., Byrne, H., et al. (2019). Global trends in marine plankton diversity across kingdoms of life. *Cell* 179, 1084–1097.e21. doi: 10.1016/j.cell.2019.10.008

Iliffe, T. M., and Kornicker, L. S. (2009). Worldwide diving discoveries of living fossil animals from the depths of anchialine and marine caves. *Smithson Contrib Smithsonian Contributions to Mar. Sci.* 38, 269–280.

Jenkins, D. G., Brescacin, C. R., Duxbury, C. V., Elliott, G. A., Evans, J. A., Grablow, K. R., et al. (2007). Does size matter for dispersal distance? *Glob. Ecol. Biogeogr.* 16, 415–425. doi: 10.1111/j.1466-8238.2007.00312.x

Jia, X., Dini-Andreote, F., and Salles, J. F. (2018). Community assembly processes of the microbial rare biosphere. *Trends Microbiol.* 26, 738–747. doi: 10.1016/j.tim.2018.02.011

Jiang, Y., Lei, Y., Yang, Y., Korpelainen, H., Niinemets, U., and Li, C. (2018). Divergent assemblage patterns and driving forces for bacterial and fungal communities along a glacier forefield chronosequence. *Soil Biol. Biochem.* 118, 207–216. doi: 10.1016/j.soilbio.2017.12.019

Jousset, A., Bienhold, C., Chatzinotas, A., Gallien, L., Gobet, A., Kurm, V., et al. (2017). Where less may be more: how the rare biosphere pulls ecosystems strings. *ISME J.* 11, 853–862. doi: 10.1038/ismej.2016.174

Kajan, K., Cukrov, N., Cukrov, N., Bishop-Pierce, R., and Orlić, S. (2022). Microeukaryotic and prokaryotic diversity of anchialine caves from Eastern Adriatic Sea islands. *Microb. Ecol.* 83, 257–270. doi: 10.1007/s00248-021-01760-5

Kamennaya, N. A., Chernihovsky., M. P., and Anton., F. (2008). The cyanate utilization capacity of marine unicellular cyanobacteria. *Limnology Oceanography* 53, 2485–2494. doi: 10.4319/lo.2008.53.6.2485

Kindler, G. S., Wong, H. L., Larkum, A. W. D., Johnson, M., Macleod, F. I., and Burns, B. P. (2021). Genome-resolved metagenomics provides insights into the functional complexity of microbial mats in blue holes, shark bay. *FEMS Microbiol. Ecol.* 98, fiab158. doi: 10.1093/femsec/fiab158

Kitzinger, K., Padilla, C. C., Marchant, H. K., Hach, P. F., Herbold, C. W., Kidane, A. T., et al. (2019). Cyanate and urea are substrates for nitrification by thaumarchaeota in the marine environment. *Nat. Microbiol.* 4, 234–243. doi: 10.1038/s41564-018-0316-2

Kong, J., Wang, Y., Warren, A., Huang, B., and Sun, P. (2019). Diversity distribution and assembly mechanisms of planktonic and benthic microeukaryote communities in intertidal zones of southeast fujian, China. *Front. Microbiol.* 10. doi: 10.3389/fmicb.2019.02640

Krstulović, N., Šolić, M., Šantić, D., Maršić-Lučić, J., Ordulj, M., and Šestanović, S. (2013). Microbial community structure in two anchialine caves on mljet island (Adriatic Sea). *Acta Adriat* 54, 183–198.

Li, T., Feng, A., Liu, Y., Li, Z., Guo, K., Jiang, W., et al. (2018). Three-dimensional (3D) morphology of sansha yongle blue hole in the south China Sea revealed by underwater remotely operated vehicle. *Sci. Rep.* 8, 17122. doi: 10.1038/s41598-018-35220-x

Li, Q., Lei, Y., Morard, R., Li, T., and Wang, B. (2020b). Diversity hotspot and unique community structure of foraminifera in the world's deepest marine blue hole – sansha yongle blue hole. *Sci. Rep.* 10, 10257. doi: 10.1038/s41598-020-67221-0

Li, B., Liu, J., Zhou, S., Fu, L., Yao, P., Chen, L., et al. (2020a). Vertical variation in *Vibrio* community composition in sansha yongle blue hole and its ability to degrade macromolecules. *Mar. Life Sci. Technol.* 2, 60–72. doi: 10.1007/s42995-019-00003-4

Lima-Mendez, G., Faust, K., Henry, N., Decelle, J., Colin, S., Carcillo, F., et al. (2015). Determinants of community structure in the global plankton interactome. *Science* 348, 1262073. doi: 10.1126/science.1262073

Liu, Y., He, H., Fu, L., Liu, Q., Yang, Z., and Zhen, Y. (2019). Environmental DNA sequencing reveals a highly complex eukaryote community in sansha yongle blue hole, xisha, south China Sea. *Microorganisms* 7, 624. doi: 10.3390/microorganisms7120624

Liu, J., Vellend, M., Wang, Z., and Yu, M. (2018). High beta diversity among small islands is due to environmental heterogeneity rather than ecological drift. *J. Biogeography* 45, 2252–2261. doi: 10.1111/jbi.13404

Liu, L., Yang, J., Yu, Z., and Wilkinson, D. M. (2015). The biogeography of abundant and rare bacterioplankton in the lakes and reservoirs of China. *ISME J.* 9, 2068–2077. doi: 10.1038/ismej.2015.29

Logares, R., Audic, S., Bass, D., Bittner, L., Boutte, C., Christen, R., et al. (2014). Patterns of rare and abundant marine microbial eukaryotes. *Curr. Biol.* 24, 813–821. doi: 10.1016/j.cub.2014.02.050

Logares, R., Deutschmann, I. M., Junger, P. C., Giner, C. R., Krabberød, A. K., Schmidt, T. S. B., et al. (2020). Disentangling the mechanisms shaping the surface ocean microbiota. *Microbiome* 8, 55. doi: 10.1186/s40168-020-00827-8

Louca, S., Parfrey, L. W., and Doebeli, M. (2016). Decoupling function and taxonomy in the global ocean microbiome. *Science* 353, 1272–1277. doi: 10.1126/science.aaf4507

Lu, L., Tang, Q., Li, H., and Li, Z. (2022). Damming river shapes distinct patterns and processes of planktonic bacterial and microeukaryotic communities. *Environ. Microbiol.* 24, 1760–1774. doi: 10.1111/1462-2920.15872

Lynch, M. D. J., and Neufeld, J. D. (2015). Ecology and exploration of the rare biosphere. *Nat. Rev. Microbiol.* 13, 217–229. doi: 10.1038/nrmicro3400

Mangot, J. F., Domaizon, I., Taib, N., Marouni, N., Duffaud, E., Bronner, G., et al. (2013). Short-term dynamics of diversity patterns: evidence of continual reassembly within lacustrine small eukaryotes. *Environ. Microbiol.* 15, 1745–1758. doi: 10.1111/1462-2920.12065

Mao, X., Chen, J., van Oosterhout, C., Zhang, H., Liu, G., Zhuang, Y., et al. (2022). Diversity, prevalence, and expression of cyanase genes (cynS) in planktonic marine microorganisms. *ISME J.* 16, 602–605. doi: 10.1038/s41396-021-01081-y

Martin, M. (2011). Cutadapt removes adapter sequences from high-throughput sequencing reads. *EMBNet J.* 17, 10–12. doi: 10.14806/ej.17.1.200

Martiny, J. B. H., Bohannan, B. J. M., Brown, J. H., Colwell, R. K., Fuhrman, J. A., Green, J. L., et al. (2006). Microbial biogeography: putting microorganisms on the map. *Nat. Rev. Micro* 4, 102–112. doi: 10.1038/nrmicro1341

Massera Bottazzi, E., and Andreoli, M. (1982). Distribution of adult and juvenile acantharia (*Protozoa sarcodina*) in the Atlantic ocean. *J. Plankton Res.* 4, 757–777. doi: 10.1093/plankt/4.4.757

Melanie, G., and Sara, M. (2016). The ecology and evolution of microbial competition. *Trends Microbiol.* 24, 833–845. doi: 10.1016/j.tim.2016.06.011

Meyer, J., and Huber, J. (2014). Strain-level genomic variation in natural populations of *Lebetimonas* from an erupting deep-sea volcano. *ISME J.* 8, 867–880. doi: 10.1038/ismej.2013.206

Morales, S. E., Biswas, A., Herndl, G. J., and Baltar, F. (2019). Global structuring of phylogenetic and functional diversity of pelagic fungi by depth and temperature. *Front. Mar. Sci.* 6. doi: 10.3389/fmars.2019.00131

Morrison-Whittle, P., and Goddard, M. R. (2015). Quantifying the relative roles of selective and neutral processes in defining eukaryotic microbial communities. *ISME J.* 9, 2003–2011. doi: 10.1038/ismej.2015.18

Mylroie, J. E., Carew, J. L., and Moore, A. I. (1995). Blue holes: definition and genesis. *Carbonates Evaporites* 10, 225–233. doi: 10.1007/BF03175407

Northup, D. E., and Lavoie, K. H. (2001). Geomicrobiology of caves: a review. *Geomicrobiol J.* 18, 199–222. doi: 10.1080/01490450152467750

Ohtsuka, S., Suzaki, T., Horiguchi, T., Suzuki, N., and Not, F. (2015). *Marine protists: diversity and dynamics* (Tokyo: Springer Japan).

Pachiadaki, M. G., Sintes., E., Bergauer, K., Brown, J. M., Record, R., Swan, B. K., et al. (2017). Major role of nitrite-oxidizing bacteria in dark ocean carbon fixation. *Science* 358, 1046–1051. doi: 10.1126/science.aan8260

Palatinszky, M., Herbold, C., Jehmlich, N., Pogoda, M., Han, P., Bergen, M., et al. (2015). Cyanate as an energy source for nitrifiers. *Nature* 524, 105–108. doi: 10.1038/nature14856

Patin, N. V., Dietrich, Z. A., Stancil, A., Quinan, M., Beckler, J. S., Hall, E. R., et al. (2021). Gulf of Mexico blue hole harbors high levels of novel microbial lineages. *ISME J.* 15, 2206–2232. doi: 10.1038/s41396-021-00917-x

Pawlowski, J., Lejzerowicz, F., Apotheloz-Perret-Gentil, L., Visco, J., and Esling, P. (2016). Protist metabarcoding and environmental biomonitoring: time for change. *Eur. J. Protisto* 55, 12–25. doi: 10.1016/j.ejop.2016.02.003

Pedros-Alio, C. (2012). The rare bacterial biosphere. *Annu. Rev. Mar. Sci.* 4, 449–466. doi: 10.1146/annurev-marine-120710-100948

Quast, C., Pruesse, E., Yilmaz, P., Gerken, J., Schweer, T., Yarza, P., et al. (2012). The SILVA ribosomal RNA gene database project: Improved data processing and web-based tools. *Nucleic Acids Res.* 41, D590–D596. doi: 10.1093/nar/gks1219

Ricci, S., Sacco Perasso, C., Antonelli, F., and Davidde Petriaggi, B. (2015). Marine bivalves colonizing Roman artefacts recovered in the gulf of pozzuoli and in the blue grotto in Capri (Naples, italy): boring and nestling species. *Int. Biodeterioration Biodegradation* 98, 89–100. doi: 10.1016/j.ibiod.2014.12.001

Rognes, T., Flouri, T., Nichols, B., Quince, C., and Mahé, F. (2016). VSEARCH: a versatile open source tool for metagenomics. *PeerJ* 4, e2584. doi: 10.7717/peerj.2584

Rosindell, J., Hubbell, S. P., and Etienne, R. S. (2011). *The unified neutral theory of biodiversity and biogeography (MPB-32)* (Princeton: Princeton University Press).

Shade, A., Peter, H., Allison, S. D., Baho, D. L., Berga, M., Burgmann, H., et al. (2012). Fundamentals of microbial community resistance and resilience. *Front. Microbiol.* 3. doi: 10.3389/fmicb.2012.00417

Sogin, M., Morrison, H., Huber, J., Welch, D., Huse, S., Neal, P., et al. (2006). Microbial diversity in the deep sea and the underexplored "rare biosphere". *Proc. Natl. Acad. Sci.* 103, 12115–12120. doi: 10.1073/pnas.0605127103

Soininen, J., Korhonen, J. J., and Luoto, M. (2013). Stochastic species distributions are driven by organism size. *Ecology* 94, 660–670. doi: 10.1890/12-0777.1

Stegen, J. C., Lin, X., Fredrickson, J. K., Chen, X., Kennedy, D. W., Murray, C. J., et al. (2013). Quantifying community assembly processes and identifying features that impose them. *ISME J.* 7, 2069–2079. doi: 10.1038/ismej.2013.93

Stegen, J. C., Lin, X., Fredrickson, J. K., and Konopka, A. E. (2015). Estimating and mapping ecological processes influencing microbial community assembly. *Front. Microbiol.* 6. doi: 10.3389/fmicb.2015.00370

Stein, A., Gerstner, K., and Kreft, H. (2014). Environmental heterogeneity as a universal driver of species richness across taxa, biomes and spatial scales. *Ecol. Lett.* 17, 866–880. doi: 10.1111/ele.12277

Sunagawa, S., Acinas, S. G., Bork, P., Bowler, C., Eveillard, D., Gorsky, G., et al. (2020). *Tara* oceans: towards global ocean ecosystems biology. *Nat. Rev. Microbiol.* 18, 428–445. doi: 10.1038/s41579-020-0364-5

Sun, P., Huang, L., Xu, D., Huang, B., Chen, N., and Warren, A. (2017). Marked seasonality and high spatial variation in estuarine ciliates are driven by exchanges between the a'bundant' and 'intermediate' biospheres. *Sci. Rep.* 7, 9494. doi: 10.1038/s41598-017-10308-y

Sun, P., Wang, Y., Huang, X., Huang, B., and Wang, L. (2022). Water masses and their associated temperature and cross-domain biotic factors co-shape upwelling microbial communities. *Water Res.* 215, 118274. doi: 10.1016/j.watres.2022.118274

Suter, E. A., Pachiadaki, M., Taylor, G. T., and Edgcomb, V. P. (2022). Eukaryotic parasites are integral to a productive microbial food web in oxygen-depleted waters. *Front. Microbiol.* 12. doi: 10.3389/fmicb.2021.764605

Swart, P. K., Arienzo, M., Broad, K., Clement, A., and Kakuk, B. (2010). Blue holes in Bahamas: repositories of climate, anthropogenic, and archaeological changes over the past 300 000 years. *J. Earth Sci.* 21, 265. doi: 10.1007/s12583-010-0231-9

Villarino, E., Watson, J. R., Jönsson, B., Gasol, J. M., Salazar, G., Acinas, S. G., et al. (2018). Large-Scale ocean connectivity and planktonic body size. *Nat. Commun.* 9, 142. doi: 10.1038/s41467-017-02535-8

Wang, Q., Garrity, G. M., Tiedje, J. M., and Cole, J. R. (2007). Naive Bayesian classifier for rapid assignment of rRNA sequences into the new bacterial taxonomy. *Appl. Environ. Microbiol.* 73, 5261–5267. doi: 10.1128/AEM.00062-07

Webb, P., and Wooldridge, T. H. (1990). Diel horizontal migration of *Mesopodopsis slabberi* (*Crustacea: Mysidacea*) in algoa bay, southern Africa. . *Mar. Ecol. Progress* 62, 73–77. doi: 10.3354/meps062073

White, M. G. (1998). Horizontal distribution of pelagic zooplankton in relation to predation gradients. *Ecography* 21, 44–62. doi: 10.1111/j.1600-0587.1998.tb00393.x

Wu, P., Li, D., Kong, L., Li, Y., Zhang, H., Xie, Z., et al. (2020). The diversity and biogeography of microeukaryotes in the euphotic zone of the northwestern pacific ocean. *Sci. Total Environ.* 698, 134289. doi: 10.1016/j.scitotenv.2019.134289

Wu, W., Lu, H. P., Sastri, A., Yeh, Y., Gong, G., Chou, W., et al. (2018). Contrasting the relative importance of species sorting and dispersal limitation in shaping marine bacterial versus protist communities. *ISME J.* 12, 485–494. doi: 10.1038/ismej.2017.183

Wyrwoll, K., Zhu, Z., Collins, L. B., and Hatcher, B. G. (2006). Origin of blue hole structures in coral reefs: Houtman abrolhos, Western Australia. *J. Coast. Res.* 22, 202–208. doi: 10.2112/05A-0015.1

Xie, L., Wang, B., Pu, X., Xin, M., He, P., Li, C., et al. (2019). Hydrochemical properties and chemocline of the sansha yongle blue hole in the south China Sea. *Sci. Total Environ.* 649, 1281–1292. doi: 10.1016/j.scitotenv.2018.08.333

Xiong, C., He, J., Singh, B. K., Zhu, Y., Wang, J., Li, P., et al. (2021). Rare taxa maintain the stability of crop mycobiomes and ecosystem functions. *Environ. Microbiol.* 23, 1907–1924. doi: 10.1111/1462-2920.15262

Xue, Y., Chen, H., Yang, J., Liu, M., Huang, B., and Yang, J. (2018). Distinct patterns and processes of abundant and rare eukaryotic plankton communities following a reservoir cyanobacterial bloom. *ISME J. 12*, 2263–2277. doi: 10.1038/s41396-018-0159-0

Yao, P., Chen, L., Fu, L., Zhang, Y., Bi, N., Wang, L., et al. (2018). Controls on vertical nutrient distributions in the sansha yongle blue hole, south China sea. *Chin. Sci. Bulletin* 63, 2393–2402. doi: 10.1360/N972018-00155

Yuan, J., Li, M., and Lin, S. (2015). An improved DNA extraction method for efficient and quantitative recovery of phytoplankton diversity in natural assemblages. *PloS One* 10, e0133060–e0133060. doi: 10.1371/journal.pone.0133060

Zehr, J. P., and Caron, D. A. (2022). "Symbiosis in the ocean microbiome," in *The marine microbiome. the microbiomes of humans, animals, plants, and the environment*, vol. 3 . Eds. L. J. Stal and M. S. Cretoiu (Springer, Cham), 535–577. doi: 10.1007/978-3-030-90383-1_13

Zhang, Y., Xu, H., Wang, L., Liu, R., Fu, L., and Lin, K. (2021). Unique bacterial communities and potential function along the vertical gradient in the deepest marine blue hole. *Environ. Microbiol. Rep.* 13, 911–927. doi: 10.1111/1758-2229.13001

Zhou, J., Deng, Y., Luo, F., He, Z., Tu, Q., and Zhi, X. (2010). Functional molecular ecological networks. *Mbio* 1, e00169–e00110. doi: 10.1128/mbio.00169-10

frontiers | Frontiers in Microbiology

TYPE Original Research
PUBLISHED 30 November 2022
DOI 10.3389/fmicb.2022.992034

OPEN ACCESS

EDITED BY
Shan He,
Ningbo University,
China

REVIEWED BY
Guangyi Wang,
Tianjin University,
China
Xiang Zeng,
Ministry of Natural Resources, China

*CORRESPONDENCE
Li Wang
l-wang@shou.edu.cn.
Rulong Liu
rlliu@shou.edu.cn
Jiasong Fang
jsfang@shou.edu.cn

SPECIALTY SECTION
This article was submitted to Aquatic Microbiology, a section of the journal Frontiers in Microbiology

RECEIVED 12 July 2022
ACCEPTED 31 October 2022
PUBLISHED 30 November 2022

CITATION
Wang L, Shen Z, Cheng X, Hwang J-S, Guo Y, Sun M, Cao J, Liu R and Fang J (2022) Metagenomic insights into the functions of microbial communities in sulfur-rich sediment of a shallow-water hydrothermal vent off Kueishan Island. *Front. Microbiol.* 13:992034. doi: 10.3389/fmicb.2022.992034

Metagenomic insights into the functions of microbial communities in sulfur-rich sediment of a shallow-water hydrothermal vent off Kueishan Island

Li Wang[1]*, Ziyi Shen[1], Xinyi Cheng[1], Jiang-Shiou Hwang[2], Yizhe Guo[1], Mingye Sun[1], Junwei Cao[1], Rulong Liu[1]* and Jiasong Fang[1,3]*

[1]Shanghai Engineering Research Center of Hadal Science and Technology, College of Marine Sciences, Shanghai Ocean University, Shanghai, China, [2]Institute of Marine Biology, National Taiwan Ocean University, Keelung, Taiwan, [3]Laboratory for Marine Biology and Biotechnology, Qingdao National Laboratory for Marine Science and Technology, Qingdao, China

Hydrothermal vent (HTV) systems are important habitats for understanding the biological processes of extremophiles on Earth and their relative contributions to material and energy cycles in the ocean. Current understanding on hydrothermal systems have been primarily focused on deep-sea HTVs, and little is known about the functions and metabolisms of microorganisms in shallow-water HTVs (SW-HTVs), which are distinguished from deep-sea HTVs by a depth limit of 200m. In this study, we analyzed metagenomes of sulfur-rich sediment samples collected from a SW-HTV of Kueishan Island, located in a marginal sea of the western Pacific Ocean. Comparing with a previously published report of pelagic samples from the nearby sampling site, microbial communities in the SW-HTV sediments enriching with genes of both aerobic and anaerobic respiration inferred variable environments in the tested sediments. Abundant genes of energy metabolism encoding sulfur oxidation, H_2 oxidation, and carbon fixation were detected from the sediment samples. Sixty-eight metagenome-assembled-genomes (MAGs) were reconstructed to further understand the metabolism and potential interactions between different microbial taxa in the SW-HTVs sediment. MAGs with the highest abundant were chemolithotrophic sulfur-oxidization bacteria, including *Sulfurovum* represented Campylobacteria involved *sox* multienzyme, sulfide oxidation genes and rTCA cycle, and Gammaproteobacteria involved *dsr* gene and CBB cycle. In addition, Desulfobacterota with the potential to participate in sulfur-disproportionating processes also had higher abundance than the sample's overall mean value. The interaction of these bacterial groups allows the microbial communities to efficiently metabolize a large variety of sulfur compounds. In addition, the potential to use simple organic carbon, such as acetate, was found in chemolithotrophic Campylobacterial MAGs. Collectively, our results revealed the complexity of environmental conditions of the vent sediment and highlight the interactive relationships of the dominant microbial

populations in driving sulfur cycles in the SW-HTV sediments off Kueishan Island.

KEYWORDS

Campylobacteria, shallow-water hydrothermal vent, sulfur cycle, sediment, metagenome-assembled-genomes, Kueishan Island

Introduction

Hydrothermal vents (HTVs) are sites in the seafloor where geothermally heated water is expelled through fissures in Earth's crust. They can be found globally along spreading zones in the mid-ocean ridges or volcanic arcs (Tarasov et al., 2005). Environmental conditions at HTVs, e.g., elevated temperature and enrichment of reduced compounds, gases and heavy metals, are significantly different from those in other marine habitats (Tarasov et al., 2005). Vigorously venting black smokers on the ocean floor can reach temperatures of >400°C at 2 ~ 8 km depth. The same process also supports more subdued, lower-temperature diffuse flow systems that typically emit fluids at 5 ~ 50°C, and white smoker vents with warmer fluids (100 ~ 300°C). Elements (such as Cu, Zn, Fe, Pb, S, and SiO_2), and volatiles (such as CO_2, H_2S, H_2, and CH_4) are incorporated into the fluids through leaching out of the rocks and direct degassing of magma chambers, respectively (Kelley et al., 2002). Since the discovery of deep-sea HTVs (DS-HTVs) in the Pacific Ocean in 1977, they have attracted wide attention. In the deep sea, far away from the sun, chemoautotrophic microbes at the base of the ecosystem derive their carbon and energy from volatile dissolved chemicals, thereby supporting the huge biomass of larger organisms (tube worms, clams, crabs etc.).The unexpectedly abundant microbial inhabitants in HTVs' ecosystems have refined our understanding of extremophiles on Earth and their relative contribution to material and energy cycles.

Shallow-water HTVs (SW-HTVs), another type of vent system locating at depth of <200 m, are more accessible than DS-HTVs. The depth limit of 200 m is set to distinguish between "deep-sea" and "shallow-water" HTVs (Tarasov et al., 2005), coincides with the average depth of the photic zone and with a large change in the slope of the seawater boiling curve. Characteristics such as the types of gas discharges, iron or sulfur component of subsurface, and temperature changed among vents (Price and Giovannelli, 2017), but there are some common traits for SW-HTVs. As the lower pressures in shallow depth, free gas phases present in SW-HTVs, which was called "gasohydrothermal" vents in the past. Enhanced gas exsolution in the form of free gas bubbles or degassing is substantially altered fluid chemistry by mass transfer from gas to aqueous phase. Additionally, due to their shallow nature and proximity to land masses, a significant amount of terrigenous organic carbon and primary production is in direct contact with vent processes. Also, low salinity or nearly salt-free vent fluids derived from the meteoric water can be found off Ambitle Island, Papua New Guinea and Dominica Island (Lesser Antilles). As a result, the presence of light, terrestrial inputs, tidal cycles, and meteoric water inputs give rise to highly diverse and complex microbial communities in SW-HTVs (Tarasov et al., 2005; Price and Giovannelli, 2017). However, the nature of such interactions has only recently begun to be investigated, and much less studies of microbial community have been reported at SW-HTV than its deep-sea cousin.

Kueishan Island (also known as Guishan Island) is a young volcanic island located to the southernmost part of the Okinawa Trough of the western Pacific Ocean (Liu, 1995). A cluster of more than 30 type I and II vents (Giovannelli and Price, 2019) spewing sulfur-rich plumes with temperature up to 112°C and pH of 1.9–4.6 are located at depths between 10 and 80 m off the southeastern tip of Kueishan Island, while more than half of these vents are at depths <20 m (Jeng et al., 2004; Chen et al., 2005b). The hydrothermal fluid and volcanic gases contain high concentrations of CO_2 and H_2S (Yang et al., 2005). Wide distribution of sulfur chimney, sulfur sand, sulfur ball was observed in the seabed (Zeng et al., 2011). The yellow sulfur chimneys are composed of nearly pure sulfur (>99%; Chen et al., 2005a; Zeng et al., 2007) while more than 97% of the native sulfur is present in the form of sulfur balls (Zeng et al., 2011). Comparison with samples out of the vent area, seldom photosynthetic Chromatiales order (Gammaproteobacteria) and eukaryotic were detected in the sediment sample in Kueishan Island area by 16S rRNA gene (Wang et al., 2015). However, bacterial genera *Nautilia* and *Sulfurovum* of class Campylobacteria were reported as the dominant bacteria in low-temperature vent fluids and sediments, respectively (Zhang et al., 2012; Wang et al., 2015, 2017). Chemolithotrophic bacteria of the class Campylobacteria (formerly Epsilonproteobacteria; reclassified as a class of phylum Campylobacterota; Waite et al., 2017) have been found to be one of the most important taxa in diverse biomes of DS-HTVs (Campbell et al., 2006; Dick, 2019) and sulfur-rich shallow-water vents (Price and Giovannelli, 2017). Existing studies consistently indicated Campylobacteria occupying a high-sulfide, low-oxygen and mesophilic temperatures niche (Nakagawa and Takai, 2008; Hügler and Sievert, 2010; Meier et al., 2017; Dick, 2019). The metagenomics and metatranscriptomics studies in Kueishan Island (Tang et al., 2013; Li et al., 2018) showed that the Campylobacteria were involved in carbon fixation, sulfur oxidation, and nitrate reduction in the water column above the vents, similar to their roles in deep-sea

vent systems. In order to know more special traits of these Campylobacteria thrived in SW-HTVs of Kueishan Island, we investigated for the first time the functional potentials of benthic microbial communities in the vent system off Kueishan Island by metagenomic analysis. The genes involving in energy yielding of dominant chemolithotrophic Campylobacteria and other abundant bacterial groups are analyzed based on metagenome-assembled genomes (MAGs). The potential ecological roles and possible interactions of the dominant bacterial taxa will be discussed. The study will advance the knowledge on metabolic mechanisms and ecological functions of microorganisms in SW-HTVs.

Materials and methods

Sample collection

Sediment cores (~10 cm) were collected from site W (121.96232°E, 24.83420°N), located 2 m away from a low-temperature vent (type II) off Kueishan Island, by scuba divers in September 2013. The sampling details and environmental parameter can be found in our previous study (Wang et al., 2015, 2017). Triplicate samples (W1, W2 and W3) were taken and immediately frozen on shipboard. In the laboratory, the samples were stored at −80°C until DNA extraction and other analyses.

DNA extraction and metagenomic sequencing

DNA was extracted from the sediment samples after removal of the top 1 cm using the PowerSoil DNA Isolation Kit (MO BIO Laboratories, Inc., Carlsbad, United States) according to the manufacturer's instructions. Environmental DNA of the samples was break into short fragment around 350 bp and added the adaptor. Then paired-end sequenced on an Illumina HiSeq 4,000 platform (Illumina, San Diego, CA, United States) according to standard protocols by the Beijing Genomics Institute (BGI, Shenzhen, China). Retrieved reads were filtered using an in-house developed program to remove low-quality reads by BGI. The sequencing data have been submitted to the NCBI database (accession number PRJNA851985).

Comparative metagenomic analyses

Raw sequencing reads were submitted to the MG-RAST server (version 3.0) for gene annotation (Meyer et al., 2008).[1] The artificially created duplicate reads (Gomez-Alvarez et al., 2009) were removed automatically by MG-RAST. The putative open reading frames (ORFs) were identified using FragGeneScen (Rho et al., 2010), and their corresponding protein sequences were searched with BLAST against the M5NR non-redundant protein database (Wilke et al., 2012) in the MG-RAST. M5NR is an integration of many databases, including the NCBI GenBank, COG, Kyoto Encyclopedia of Genes and Genomes (KEGG), and SEED. Taxonomic and functional profiles within MG-RAST (hits to IMG, M5NRA, SEED, COG, and KEGG databases) were extracted (an E-value cutoff of less than 1×10^{-5}, a minimum read length of 50 bp and a minimum abundance of 100).

The functional attributes of our three sediment metagenomes from this study (MG-RAST ID: 4716389.3, 4716390.3 and 4716391.3) were compared with the two pelagic metagenomes previously published (Tang et al., 2013) that was stored in MG-RAST database (MG-RAST ID: 4487625.3 and 4487624.3) and hereby referred to as GS4 and GS7. In addition, nine datasets of DS-HTVs (Supplementary Table S1) were also chosen from MG-RAST to compare with the microbial communities in SW-HTVs (Grzymski et al., 2008; Brazelton and Baross, 2009; Anderson et al., 2014; Cerqueira et al., 2018; Namirimu et al., 2022). The files ("MG-RAST ID"0.299.screen.passed.fna) contained all the sequences which were passed the quality control steps in MG-RAST were downloaded to calculate the average coverage for all the collected metagenomic datasets using Nonpareil tool (Rodriguez-R and Konstantinidis, 2014). The taxonomical profile was also used to calculate the alpha-diversity using mothur (Schloss et al., 2009). The resulting profiles from MG-RAST were further analyzed using statistical software STAMP (Parks et al., 2014).

Sequences processing, assembly, binning, and annotation

All raw sequencing reads from the triplicates (W1, W2 and W3) were assembled into contigs employing IDBA-UD algorithm with the optimized kmer 98 (Peng et al., 2012). Metagenomic binning was then conducted for assemblies longer than 2,500 bp using MetaBAT 2 (Kang et al., 2019). Redundant metagenome-assembled-genomes (MAGs) were subsequently dereplicated using dRep v. 2.3.2 (Olm et al., 2017) at 99% average nucleotide identity (ANI), and MAGs with the highest quality was selected from each cluster for downstream analysis. Qualities of the MAGs were assessed by CheckM v1.1.2 (Parks et al., 2015). Only MAGs with more than 60% completeness and less than 5% contamination were selected, all the qualified MAGs were imported into anvi'o v6.2 (Eren et al., 2015) to summary the genomic information of MAGs including abundance. Briefly, metagenomic reads were mapped to contigs using Bowtie2 (Langmead and Salzberg, 2012). The mapping results were converted into sorted and indexed BAM files for each samples (W1, W2 and W3) using samtools (Li et al., 2009). The result file of samtools and MAGs genomes was input to anvi'o to estimate the abundance and other genomics information for all MAGs.

1 http://metagenomics.anl.gov/

Taxonomic and functional annotation of MAGs

Taxonomy of the MAGs were assigned by multiple approaches. In addition to the taxonomic annotations reported by CheckM, detailed taxonomic classification of the MAGs was determined using GTDB-Tk (Chaumeil et al., 2019) based on the phylogenetically calibrated Genome Taxonomy Database (GTDB). For the interested phylum /class, phylophlan (Asnicar et al., 2020) were used to construct phylogenetic tree. As some MAGs cannot get their clear genus information from GTDB or CheckM, the genus level classification of each MAGs was also inferred from the phylogenetic tree. To ascribe functions of the MAGs, coding sequences predicted by Prodigal (Hyatt et al., 2010) were annotated using BlastKOALA against the KEGG database with default parameters (Kanehisa et al., 2016).

Metagenomic fragment recruitment

The distribution of retrieved MAGs was studied *via* reads recruitment against published metagenomes from SW- and DS-HTVs environments (Supplementary Table S1). Raw reads were downloaded from NCBI-SRA or MG-RAST. The procedure of reads recruitment followed Liu et al. (2022). Briefly, rRNA gene sequences in MAGs were first masked to avoid bias in recruitment results. Recruitments were performed using BLASTN, and hits were filtered with a length cut-off of 50 bp, an identity cut-off of 95%, and an e-value cut-off of $1e^{-5}$. Qualified hits were used to compute the RPKG (reads recruited per kilobase of genome per gigabase of metagenome) values, which reflect a normalized abundance of MAGs allowing the comparison across different metagenomes.

Results and discussion

Comparative metagenomic analysis between the sediment and pelagic microbiome in the SW-HTVs

A total of ~40 Gbp unique sequence data was generated for W1, and ~ 5 Gbp for W2 and W3. To eliminate possible impacts of sequencing depth, 5 Gb sequences of W1 was extracted up-loaded to MG-RAST together with the data of W2 and W3. In the MG-RAST pipeline, the three sediment samples (W1, W2 and W3) were analyzed and compared with two previously published metagenomes of pelagic samples, i.e., GS7 and GS4 collected from vent fluid and surface seawater above the vent, respectively (Tang et al., 2013). Taxonomic profile showed that Campylobacteria and Gammaproteobacteria were the dominant class/phylum in all three sediment samples (Figure 1A). Campylobacteria also dominated in vent fluid sample GS7 (Figure 1A), but the compositions of benthic sediment Campylobacteria were apparently different from those in the vent fluid (Figure 1B). Genus *Sulfurovum* was enriched in sediment sample W1, while genera *Nautila*, *Camylobacter* and *Caminibacter* were greatly enriched in vent fluid sample GS7 (Figure 1B). These results are consistent with findings in previous investigations by 16S rRNA gene (Zhang et al., 2012; Wang et al., 2017). It has been reported that the reduced conditions of vent fluids (high concentration of H_2 and other reduced chemicals but out of oxygen) benefited the growth of *Nautilia* which is strictly anaerobic (Nakagawa and Takai, 2014), while the environment in the vent sediments were greatly fluctuated and might facilitate the thriving of facultative aerobic *Sulfurovum* and *Sulfurimonas* (Campbell et al., 2006; Sievert et al., 2008; Yamamoto et al., 2010). Different from the sediment and vent fluid microbiomes, the microbial communities in the surface seawater above vent (sample GS4) were dominated by *Thiomicrospira* of the Gammaproteobacteria (Figures 1A,C). Existing data showed that the genus *Thiomicrospira* mainly contained aerobic, sulfur-oxidizing and mesophilic species, found in hydrothermal environments and sulfide-rich sediment–water interfaces worldwide (Teske, 2009). Comparing with facultative aerobic *Sulfurovum* (Campylobacteria), the Gammaproteobacterial autotrophs (such as *Thiomicrospira*) preferred higher concentrations of dissolved oxygen (Teske, 2009; Dick, 2019). Overall, these results indicated that the composition of the microbial communities in different habitats around the Kueishan Island SW-HTV were greatly controlled by the prevailing redox environments in the vent fluid (GS7), the sediment (W) and the surface water (GS4).

The functional gene profiles also reflected the distinctive patterns related with oxygen availability among the three biomes. In total, about 53–57% of the identified genes were annotated for the analyzed sediment samples. Based on the annotated results of SEED subsystem, the major SEED categories (Supplementary Figures S1–S3), the key genes involving in energy metabolism (Figure 2) and the most abundant genes (Figure 3; Supplementary Figure S4) were further analyzed. Being consistent with the dominance of facultative aerobic *Sulfurovum* in the sediments (Figure 1C), the metagenomes from vent sediments showed genetic features for both anaerobic and aerobic metabolisms. On the one hand, the sediment metagenomes contained more genes related with anaerobic processes than in the surface water (GS4): the category "electron donating/accepting reaction" (level 2) was significantly distinct between the sediment sample W1 and pelagic sample GS4 (Supplementary Figure S2). Their subgroups "anaerobic respiratory reductases" (level 3) was found to be significantly higher in W1 than GS4 (Supplementary Figure S3A). Moreover, the genes related with anaerobic respiration, e.g., *napAB* which encode dissimilatory nitrate reductase and hydrogenase, were higher in sediment samples than GS4 (Figure 2). On the other hand, the sediment metagenomes contained more genes related to aerobic processes than those in the vent fluids. Diverse aerobic processes were identified from the sediment samples, including genes of Sox

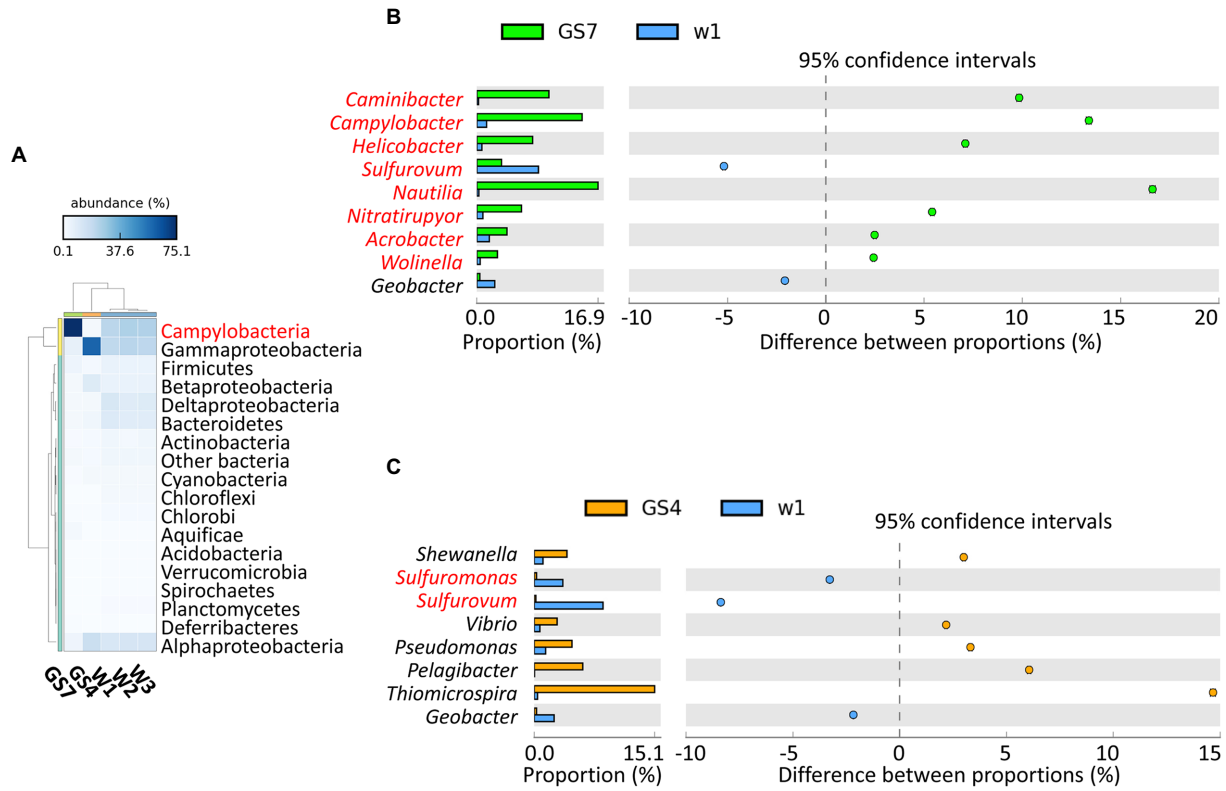

FIGURE 1
The taxonomic profile of typical phyla or classes (for Proteobacteria) **(A)** and extended error bar plot for the bacterial genera that have a difference of at least 2% between the vent fluid (GS7) or surface seawater (GS4) with sediment sample W1 **(B,C)**. "Other bacteria" in the phylogenetic classification include those with abundance<0.5% of total bacteria. The genera in red belonged to Campylobacteria.

(sulfur-oxidation) system (*soxABCDXYZ* encoded), sulfide oxidation (*fccB* encoded), and cbb3-type O_2 metabolism (*ccoNOQP* encoded). The relative abundances of genes involved in the above processes were much higher in sediment metagenomes than in vent fluid sample GS7 (Figure 2). In addition, the sediment metagenomes exhibited the highest ratio of genes involving in dissimilatory sulfate reduction/oxidation (such as *dsrAB*, *sat*), nitrogenase (*nifDK and nifH*) and denitrification (*nirKS* encoding nitrite reductase, *norBC* encoding nitric oxide reductase and *norZ*) among the three biomes compared (sediments, vent fluid, and surface water; Figure 2). As a result, the genes encoding both aerobic and anaerobic respiration, including O_2/nitrate reduction, sulfur oxidation, and H_2 oxidation, were retrieved from the sediment samples, indicating variable environments in the tested samples (W1, W2 and W3).

Genes related with "resistance to antibiotics and toxic compounds" (level 2; Supplementary Figure S2) were greatly enriched in the vent sediments than any of the pelagic samples. In the comparison of 10 most abundant genes among vents, three genes of "resistance to antibiotics and toxic compounds" (level 2) were preferentially enriched in SW- and DS-HTVs' sediment metagenomes (Figure 3), including "cation efflux system protein *CusA*," "copper-translocating P-type ATPase" and "acriflavine resistance protein." The former two genes implicated the role of copper homeostasis in the sediments, while the third gene encodes a kind of multidrug resistance efflux system to protect bacteria by decreasing the intracellular concentration of acriflavine, other dyes and sodium dodecylsulfate (Nakamura, 1968). Acriflavine was used as typical antiseptic for freshwater fish as well as marine fish. The higher ratio of resistant genes of toxic compound and aquaculture drugs may indicate the accumulation of related chemicals in the sediments, which might be sourced from the hydrothermal activities (such as trace metal) or anthropogenic sources (such as aquaculture around the SW-HTVs). Fluid chemistry characteristics present both opportunities and lethal challenges to hydrothermal vent organisms. As the high temperature hydrothermal fluids were rich in heavy metal and reduced chemicals, a common characteristic of vent organisms is their ability to take advantage of the carbon and energy sources provided by hydrothermal processes while evolving mechanisms to counteract the toxic effects of high concentrations of heavy metals or short-term exposure to lethal high temperatures (Kelley et al., 2002). However, in a comparative metagenomics among mangrove, ocean, forest, grassland and agricultural soil samples, acriflavine resistance proteins were found to be highly enriched in all the samples,

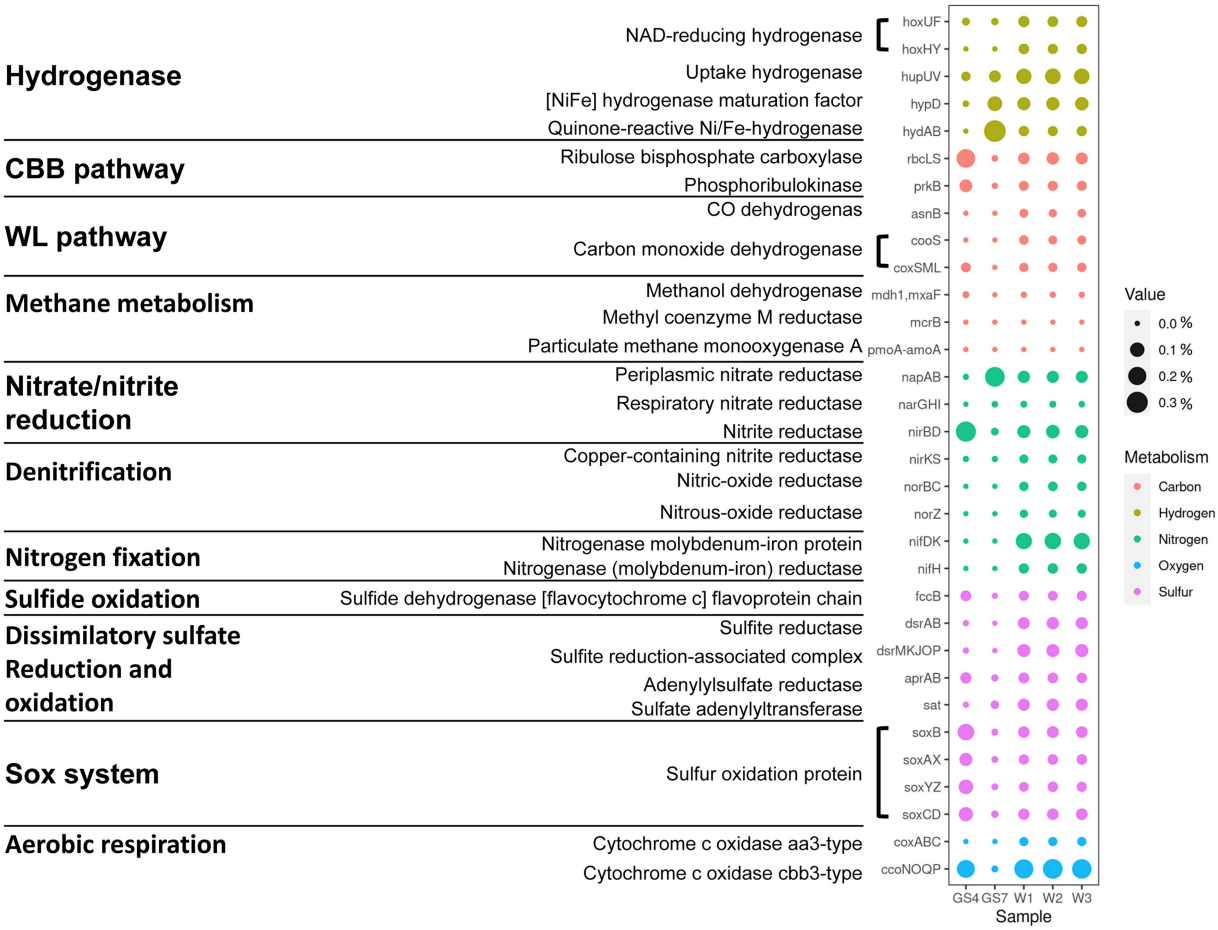

FIGURE 2
Differences in key genes involved in carbon, hydrogen, nitrogen, sulfur and oxygen metabolism among the SW-HTV sediment samples.

irrespective of ecosystem types or anthropogenic activities (Imchen et al., 2018). The exact role of "acriflavine resistance protein" in SW- and DS-HTVs still needs more studies.

Although the three studied sediment samples and two published pelagic samples may not have been taken from the exactly same vent site, the sampling sites were close to each other as they were all located in the eastern vent area of the Kueishan Island with an area of only 0.5 km^2 (Chen et al., 2005b). Furthermore, the sampling sites were all with moderate temperature (49 ~ 30°C), low pH (4.8 ~ 5.9) and shallow depth (0 ~ 21 m; Tang et al., 2013; Wang et al., 2015). Moreover, the different vents were not isolated from each other, and the vent plumes could affect the nearby vents (Han et al., 2014). All of these facts support the validity of the metagenomic comparison conducted in this study. However, our sediment samples were taken in different years from the pelagic samples, and the possible temporal variations might cause uncertainties in the comparison. Nevertheless, our preliminary study presented the first metagenomic comparisons between sediment and pelagic biomes in SW-HTVs systems, lays a foundation for future studies.

Genomes of the dominant taxa revealed the significance of sulfur oxidization in the SW-HTV sediments

To further reveal the metabolic processes and the ecological roles of the microorganisms in the SW-HTV sediments, genomes of the dominant microbial taxa were retrieved from the metagenomes *via* binning. A total of 68 MAGs (> 60% completeness and < 5% contaminations) were retrieved from all the data of three sediment samples, including. 49 from W1, 8 from W2, and 12 from W3 (Figure 4). Within them, 27 MAGs were high quality with more than 90% completeness according to the standards mentioned in Bowers et al. (2017). All the 68 MAGs were accounting for 21.68, 31.01 and 21.60% of all nucleotides in the three metagenomes, respectively. Information of the MAGs, including taxonomy, abundance, completeness, was included in Figure 4. In this study, MAG abundance was defined as its mean coverage divided by that sample's overall mean coverage. MAGs with high abundance values were more represented in that sample than those with low abundance values. A total number of 20 "abundant MAGs" (abundance value >1) were identified, and they

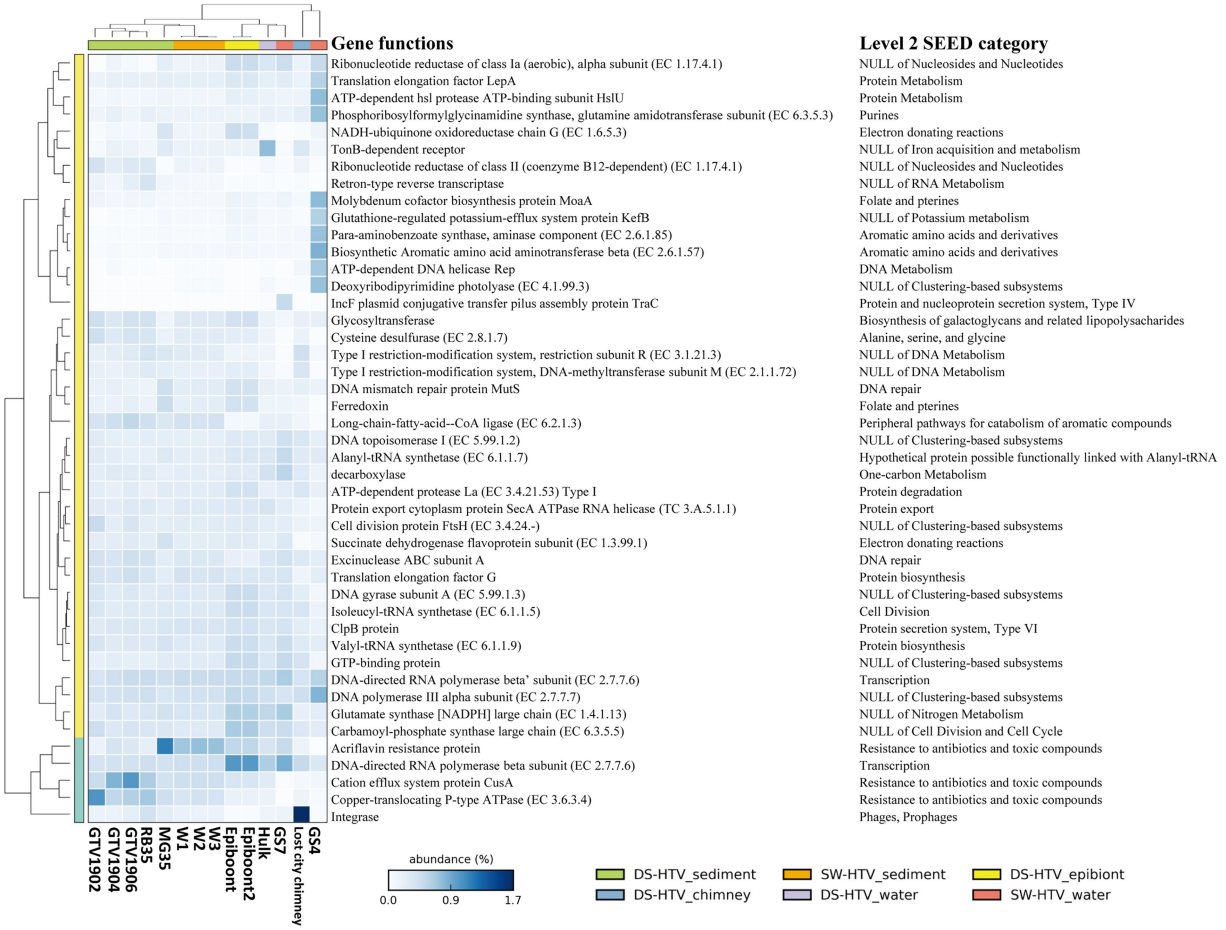

FIGURE 3
The 10 most abundant functions in our data and collected metagenomic datasets form both SW- and DS-HTVs. The dendrogram for the samples (the row) and the function (the column) were cluster by furthest neighbor and average neighbor (UPGMA) method, respectively. The name of level 2 SEED category is also listed for the functional genes.

were belonging to phyla Desulfobulbia (bin10037 and bin100106), Campylobacteria (bin20011, bin1004, bin10034, bin30019 and bin10083), Calditrichia (bin100119 and bin100120), Bacteroidia (bin10020 and 100,117), Acidimicrobiia (bin10049 and bin30015), Chloroflexota (bin10092) and class Gammaproteobacteria (bin10019, bin10026, bin2008, bin30013, bin3008 and bin 20,021).

Functional annotation revealed that genes related with sulfur or sulfide oxidation processes (*soxABCDZY*, *dsrAB*, *aprAB*, *sqr* or *fccB*) were found in nearly all MAGs of Gammaproteobacteria and Campylobacteria (Figure 5), suggesting the significance of sulfur oxidization in the SW-HTV sediments. Two different modes of sulfur oxidation have been previously proposed for bacteria. The first mode involved the reverse dissimilatory sulfite reductase (rDSR, *dsrAB* encoded; Dahl et al., 2005), and the product sulfite is subsequently oxidized to sulfate by adenosine 5′-phosphosulfate (APS) reductase (*aprAB* encoded) with sulfate adenylyltransferase (*sat* encoded), or sulfite:acceptor oxidoreductase (*sor* encoded; Grimm et al., 2010). The second mode was the sulfur oxidation *via* the Sox system, which involves seven *sox* structural genes coding for four periplasmic proteins, SoxXA, SoxYZ, SoxB, and SoxCD, responsible for thiosulfate-, sulfite-, sulfur-, and hydrogen sulfide-dependent cytochrome c reduction (Friedrich et al., 2001, 2005). By these metabolic features, the sulfur-oxidizing bacteria (SOB) can oxidize reduced sulfur compounds (such as sulfide, sulfur, thiosulfide) to intermediate sulfur species (sulfite and thiosulfate) or completely to sulfate.

In our study, the 16 Campylobacterial MAGs were classified into five genera (*Sulfurovum*, *Sulfurimonas*, *Sulfuricurvum*, *Sulfurospirillum*, and *Nitratifractor*; Supplementary Figure S5). All the retrieved Campylobacterial MAGs harbored or partially harbored genes encoding the Sox system (*soxABCDZY*) but not the reverse dissimilatory sulfite reductase (rDSR, *dsrAB* gene), and the bacteria suggesting their potential ability to fix CO_2 through rTCA cylcle (*aclB* and *porA* genes; Figure 5). Genes encoding fructose-1,6-bisphosphatase and phosphoenolpyruvate carboxykinase for gluconeogenesis were also annotated in these MAGs (Supplementary Table S2), suggesting that the fixed carbon can be stored as glucose. Similar processes have been reported in previous studies on deep-sea lineages of Campylobacteria (Waite et al., 2017). Among the Campylobacterial lineages, the genus

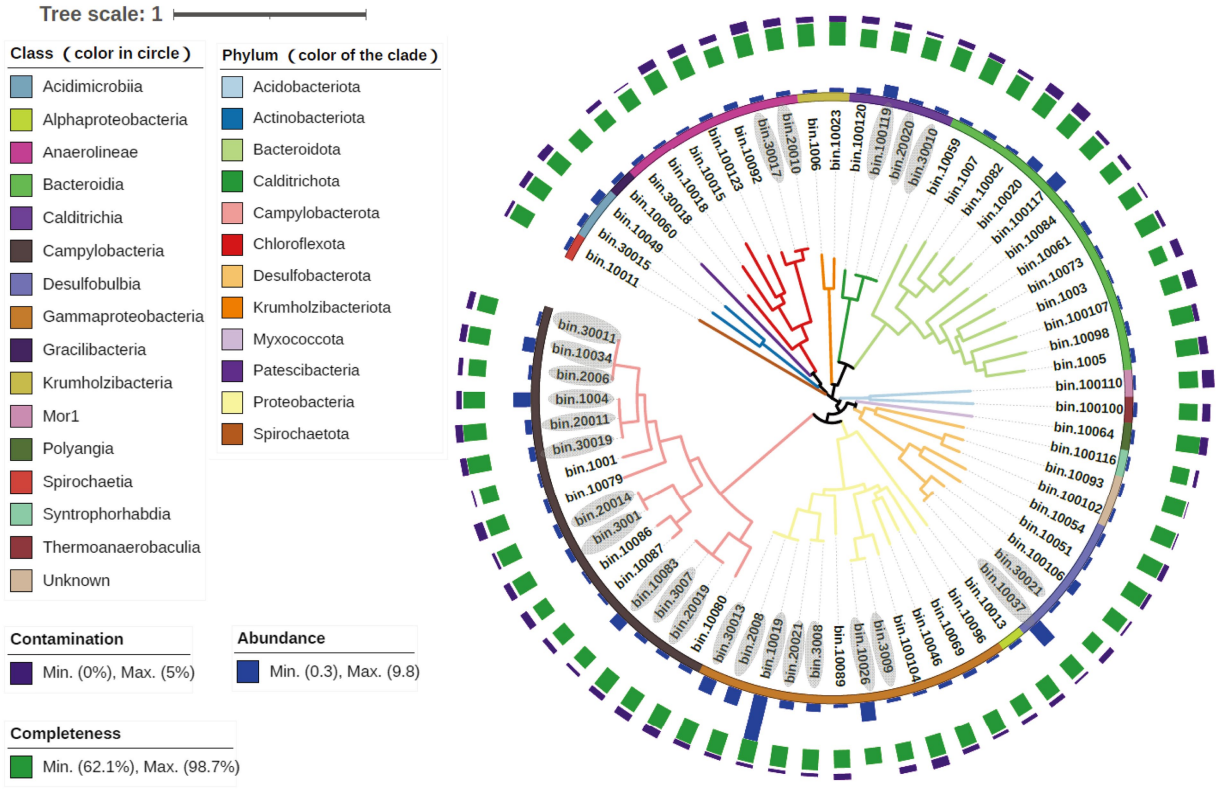

FIGURE 4
Information of all the reconstructed 69 MAGs. The colors of clades were responding to the phyla taxonomic level, while the first circle were family level. MAGs ID stating with "100" were restructed from meatgenomics of W1, "200" from W2 and "300" from W3. As the MAGs ID stands for the source of sample, their abundance referred to the ratio of that MAG's mean coverage to that sample's overall mean coverage. The MAGs ID with grey color own ANI value of 90~99% calculated by dRep.

Sulfurovum was identified as the most dominant taxa, reflected by either the taxonomic profile (Figure 1) or MAG abundance (Figure 4; Supplementary Table S3). Although gene *sqr* was contained in all Campylobacterial MAGs, only MAGs of the *Sulfurovum* (bin20011, bin1004, bin30019, bin10034, bin30011, bin2006, and bin1001, Figure 5) were found to contain the *fcc* gene (Figure 5). Both the membrane-bound Sqr and periplasmic Fcc enzymes catalyzed sulfide oxidation to form S^0. However, Fcc was sensitive for the H_2S concentration since its down-stream cytochrome c oxidase (Cco) enzyme was sensitive to HS^- even at moderate sulfide concentrations (Collman et al., 2009). On the contrary, Sqr was not subjected to sulfide inhibition because it used the non-cytochrome system – the quinone pool for electron transfer (Brune, 1989). The presence of both Fcc and Sqr in *Sulfurovum* enhanced their ability to use sulfide, especially under the conditions of low H_2S concentration and the presence of O_2. Such metabolic features would provide survival advantages for *Sulfurovum* species in the variable environmental conditions of the vent sediments.

Most of the retrieved Gammaproteobacterial MAGs harbored the genes encoding incomplete Sox system lacking of *soxCD* (encoding the sulfur dehydrogenase). These Gammaproteobacterial MAGs also contained gene sets encoding the rDsr pathway, an additional pathway for sulfur oxidation. Moreover, the Gammaproteobacteria in the vent sediments showed the potential for CO_2 fixation *via* the CBB pathway (*rbcLS*; Figure 5). These genomic features were consistent with previous reports of chemotrophic and phototrophic sulfur-oxidizing Gammaproteobacteria (Yamamoto and Takai, 2011). The rDsr enzyme was homologous to, but phylogenetically clearly distinguishable from the dissimilatory sulfite reductase catalysing the energy-conserving reduction of sulfite to sulfide in sulfite/sulfate-reducing prokaryotes (SRP). The paralogous genes *dsrA* and *dsrB*, encoding its α- and β-subunits respectively, were used as phylogenetic markers for SOB capable of sulfur storage (intracellular sulfur globules). In the phylogenetic tree of *dsrAB* gene, Gammaproteobacterial MAGs formed a highly supported monophyletic branch with other SOB, separating from typical sulfite/sulfate-reducing prokaryotes (SRP; Figure 6). Among the other retrieved MAGs, those from the phyla Desulfobacterota (bin10051, bin10054 and bin30021) and Acidobacteria (bin100100 and bin100110; Figure 6) also harbored the *dsrAB* genes (Figure 5), but they clustered with the SRP in the phylogenetic tree (Figure 6), indicating their role in sulfate reduction not sulfur oxidation. Obviously higher abundance of Gammaproteobacterial SOB containing rDsr pathway (as high as 9.81,

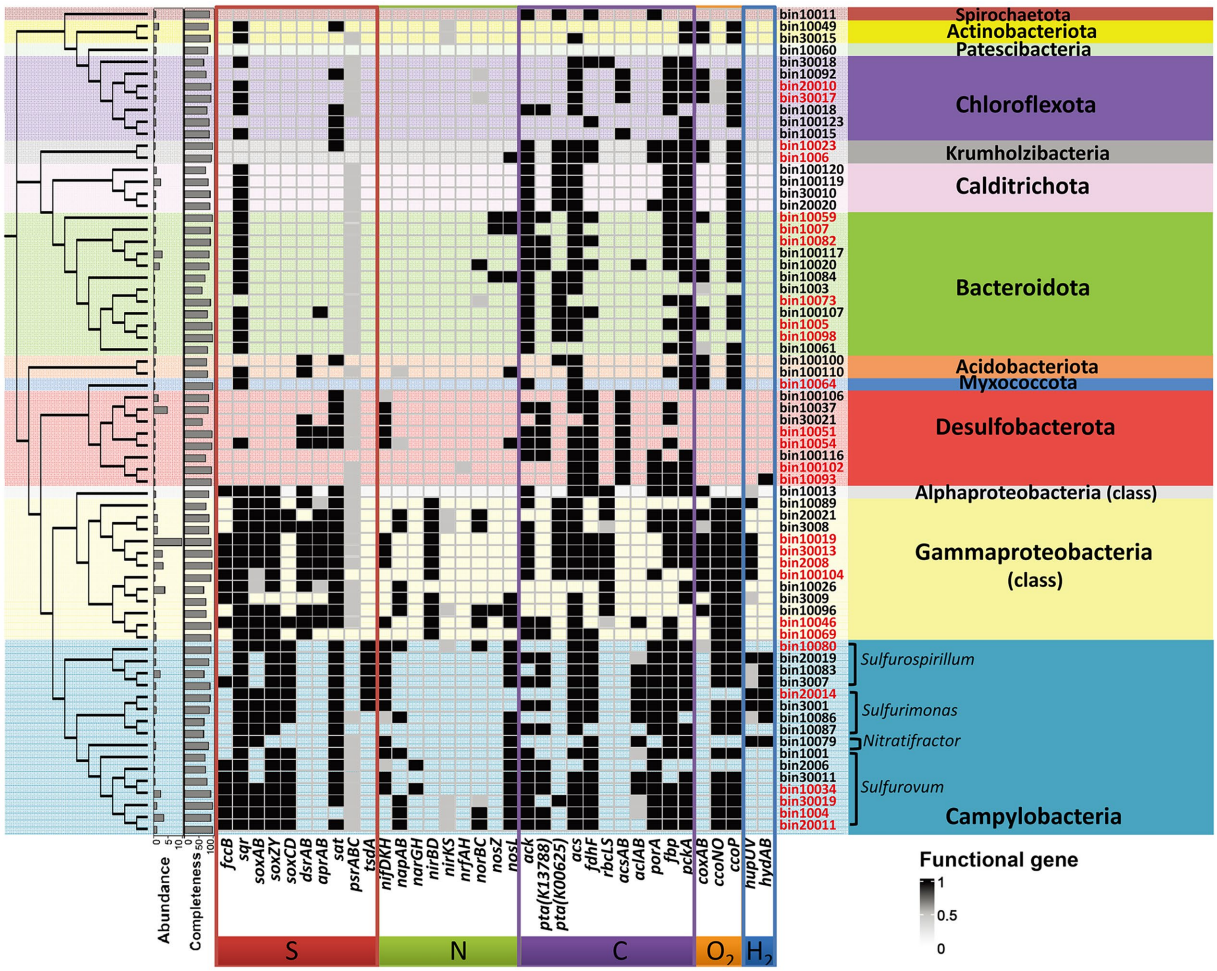

FIGURE 5
Differences in genomic information and key genes involved in carbon, hydrogen, nitrogen, sulfur and oxygen metabolism among 69 MAGs. The name of MAGs colored with red indicate the high quality MAGs with completeness >90%. The dendrogram showing the clusting of MAGs was generated from GTDB-tk. The phylum name was shown for all the MAGs. The identification of genus for the dominant Campylobacteria was inferred from the genomic phylogenetic tree (Supplementary Figure S5).

Supplementary Table S3) than MAGs of SRP (abundance lower than the mean of community at value <0.6; Supplementary Table S3) suggested the predominance of sulfur oxidation process in the vents' sediments of Kueishan Island.

The potential to use simple organic carbon in chemolithotrophic campylobacteria

To date, nearly all of the existing Campylobacterial isolates from deep-sea hydrothermal vents have been described as chemolithoautotrophs (Campbell et al., 2006), fixing carbon *via* the rTCA cycle (Hügler et al., 2005). Except dissimilatory oxidizing inorganic sulfur compounds (sulfide, sulfur or thiosulfate), they gain energy by oxidizing hydrogen/formate (Waite et al., 2017) using hydrogenase and formate dehydrogenase (*fdhF* encoded). Some other simple organic substances such as acetate were also reported to be used in host-associated isolates of Campylobacteria (Campbell et al., 2006), or from the genomes of MAGs in sulfidic hydrocarbon-rich aquifer (Keller et al., 2015), and co-culture Campylobacterial groups of benzene-degrading microbial community (Starke et al., 2016), but were seldom reported in the free living microbes of vent area.

Our result showed for the first time that the Campylobacteria in SW-HTV sediments may have the potential to use acetate and some simple organic carbon, as genes related with the metabolism of acetate and some C4 organic carbon was found in the genomes of our Campylobacterial MAGs (Figure 5; Supplementary Table S2). Firstly, acetate may be absorbed and used by the cells. Acetate kinase (Ack, EC 2.7.2.1, encoded by *ack* gene) and phosphate acetyltransferase (Pta, EC 2.3.1.8, encoded by *pta* gene) presented in nearly all MAGs of *Sulfurovum* and most of other Campylobacteria MAGs (Figure 5). The Ack-Pta pathway not only catalyzes the conversion of acetyl-CoA and ADP to acetate and ATP in most facultative and strictly anaerobic

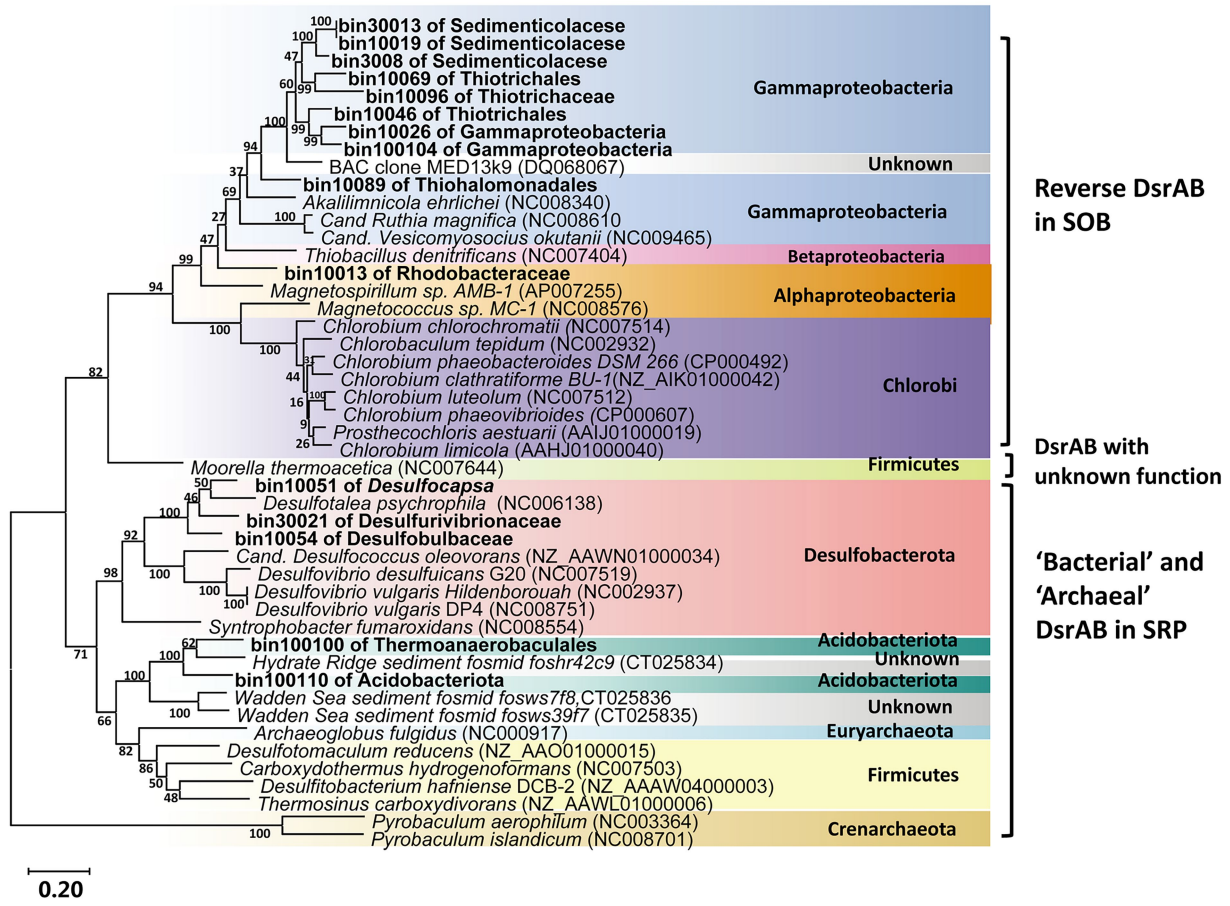

FIGURE 6
Phylogenetic tree of dsrAB amino acid sequences from all related MAGs. The reference gene was from Loy et al. (2009). Scale bar indicates 20% sequences divergence as estimated from distance-matrix analysis. The labelled names of MAGs were the lowest taxonomic level assigned by GTDB (Supplementary Table S3).

microbes, but also reversibly catalyzes the activation of acetate to acetyl-CoA as a first step in the assimilation or dissimilation of acetate in some aerobic and anaerobic bacteria (Preston et al., 1989). The Ack-Pta pathway was able to dissimilate high concentrations of acetate (Kumari et al., 1995), and it also allowed the bacteria to switch from acetate production to consumption rapidly. The presence of *actP* gene encoding acetate permease for acetate absorbing and enhancing the possibility of using extracellular acetate in Campylobacteria, was found in the nearly complete MAGs bin30019 (completeness = 98%) of *Sulfurovum* (data not shown). Secondly, genes related with C4-dicarboxylates sensing and sugar transport was annotated from the MAGs of Campylobacteria. In our study, *dctB* and *dctD* were detected in Campylobacterota-like MAGs (Supplementary Table S2), which were the key genes encoding the C4-dicarboxylate transport system (Dct), a regulatory system to monitor the external concentration of C4-dicarboxylic molecules (Janausch et al., 2002). C4-dicarboxylates (fumarate, succinate, malate, oxaloacetate, aspartate, etc.) were intermediates of central metabolism in most living organisms, serving as important carbon and energy sources for growth. Besides, fumarate also can be used as electron acceptor to performed oxidative phosphorylation with H_2 or formate as electron donors, as revealed from model organism *Wolinella succinogenes* of phylum Campylobacterota (Kröger et al., 2002). Given the great importance of the C4 dicarboxylates, the presence of Dct system would undoubtably benefit the survival of Campylobacteria in nutrient-limited environments. In addition, genes encoding multiple sugar transport system ATP-binding protein (K10112) and phospholipid/cholesterol/gamma-HCH transport system *mlaDEF* (K02065, K02066 and K02067) were annotated from genomes of genus *Nitratrifractor* of Campylobacterota (Supplementary Table S2), indicating the ability to uptake of different types of organic compounds such as disaccharides and/or oligosaccharides as well as lipids. All of these results showed the potential of Campylobacteria to perform heterotrophic metabolisms. Till now, nearly all of the existing Campylobacteria isolates from hydrothermal vents were chemolithotrophic (Campbell et al., 2006), and the mechanisms and ecological implications of their potentials for heterotrophic metabolism in

SW-HTV sediments may need to be further explored in future studies.

Complex relationships among diverse bacteria involving in sulfur metabolism

The SW-HTV sediments we analyzed in this study were rich in sulfur with visible sulfur globules, as seen in our previous study (Wang et al., 2017). Elemental sulfur is widely distributed in the vent sediments of Kueishan island, represented by the extensive distribution of sulfur chimney, sulfur sand etc. (Zeng et al., 2011). However, the natural orthorhombic sulfur (formed abiotically, most in the form of S_8) was hard to be directly used by microbes due to their hydrophobic nature and low aqueous solubility. In contrast, the biologically produced elemental sulfur is hydrophilic and was recognized as the "microbiologically preferred form" (Prange, 2008). For example, chainlike type R-S_n-R with R being H, Cl, Br, SO_3^- and/or organic group were usually found in phototrophs (Kleinjan et al., 2003). For chemotrophs, soluble extracellular S^0 coating with organic envelopes rich in amide and carboxylic groups were also found in *Sulfuricurvum kujiense* (Campylobacteria; Cron et al., 2021). In our study, potential SOBs, i.e., Campylobacteria and Gammaproteobacteria were found to be the dominant bacterial taxa in the vent sediments analyzed, and their genomes harbored multiple types of energy-yielding pathways (Figure 5) allowing the oxidation of different forms of sulfur compounds, with different end products, depending on the redox conditions in the surrounding environments (Figure 7). Particularly, the bio-active element sulfur can be formed under incomplete oxidation of sulfide when the availability of electron acceptor such as oxygen and nitrate is limited, while complete sulfide oxidation to sulphate may be occurred where oxygen or nitrate is sufficient (Lavik et al., 2009).

Except the potential sulfur oxidizing Campylobacteria and Gammaproteobacteria, MAGs of phylum Desulfobacterota were also retrieved in high abundance, such as bin100106 (abundance 1.54, completeness 85.25%) and bin10037 (abundance 4.76, completeness 83.04%; Supplementary Figure S3; Supplementary Table S3). These abundant MAGs were affiliated with genus *Desulfurivibrio* of family Desulfurivibrionaceae (Supplementary Figure S6). Previous study showed that bacteria from genus *Desulfurivibrio* were incapable of driving sulfate or sulfite reduction, but can perform sulfur disproportionation utilizing sulfur compounds as electron acceptor and short-chain fatty acids or hydrogen as electron donors (Sorokin et al., 2008). The high abundance of the sulfur disproportionation bacteria (SDB) affiliated MAGs indicated sufficient substrate for their growth. As the natural orthorhombic sulfur own low aqueous solubility, SDB can use the intermediate products (biotic sulfur) formed by SOB under partial oxidization when the electron acceptor such as oxygen and nitrate is limited (Figure 7). It was also reported that chemoautotrophic strain *Sulfurimonas denitrificans* (Campylobacteria) was able to access cyclooctasulfur (S_8) with a metabolic feature not yet demonstrated (Pjevac et al., 2014). As a result, SDB may also benefit from Campylobacteria during its activating orthorhombic sulfur (Figure 7).

Based on the physical reports of phototrophic SOB, the complete Sox pathway results in sulfate as the sole end product, whereas the incomplete pathway (with SoxCD absent) results in either intra- (Sakurai et al., 2010) or extracellular (Gregersen et al., 2011) accumulation of S^0. However, it was found that Sox system gene clusters split into two major clusters in chemoautotrophic Campylobacteria (Nakagawa et al., 2007). Enzymatic activity measurements and partial protein purification indicated that the Sox enzyme system was constitutively expressed when H_2 or thiosulfate as the electron donor (Yamamoto et al., 2010). As most knowledge of sulfur oxidizing process were originated and reviewed from the studies on phototrophic SOB (Frigaard and Dahl, 2008), further study on the process of sulfur oxidation need to be noticed for chemolithotrophic SOB. The detection of sulfur oxidation process under diver electron donor (H_2, S^0, etc.) with different concentration of electron donors should give deeper studies by transcriptomics or proteomics. Furthermore, the lack of pure cultures of the dominant sulfur oxidizers in deep-sea and shallow-water vents limited the understanding of the mechanisms. As a result, isolate SOB from vent system is needed as the first step.

Comparative metagenomics analysis between DS-HTVs and SW-HEVs

We compared our dataset to a collection of metagenomes derived from the sediments, epibiont, water and chimney biofilm of DS-HTVs (Supplementary Table S1). As shown by the Nonpareil curve (Supplementary Figure S7), the coverage of our samples was as high as 92% when the sequences number reached 50 Gb (Supplementary Figure S7; Supplementary Table S4). Majority of the DS-HTVs sediment samples (except MG35 sediment sample) had higher Nonpareil diversity than the SW-HTVs sediments analyzed in this study (Supplementary Figure S7; Supplementary Table S4), while MG35 had comparable diversity value with ours. The sediment samples of both DS- and SW-HTVs had Shannon diversity above 5.28 except MG35, while the epibionts and GS7 had lower Shannon index (below 3.72; Supplementary Figure S8). Bacteria dominated in all of the compared metagenomes (Supplementary Table S1). Camplylobacteria was the most abundant bacterial phylum in most datasets, with higher relative abundance in GS7 of SW-HTVs, epibiont samples and sediment sample MG35 of DS-HTVs, following by the water sample from "Hulk" DS-HTVs and sediment samples from SW-HTVs (Supplementary Figure S9A). At the genus level, *Sulfurovum* was the most abundant Camplylobacteria group in SW-HTV sediment samples, whose relative abundance was comparable with the epibiont samples, but lower than sediment sample MG35 in DS-HTVs (Supplementary Figures S9B, S10). The dominance of

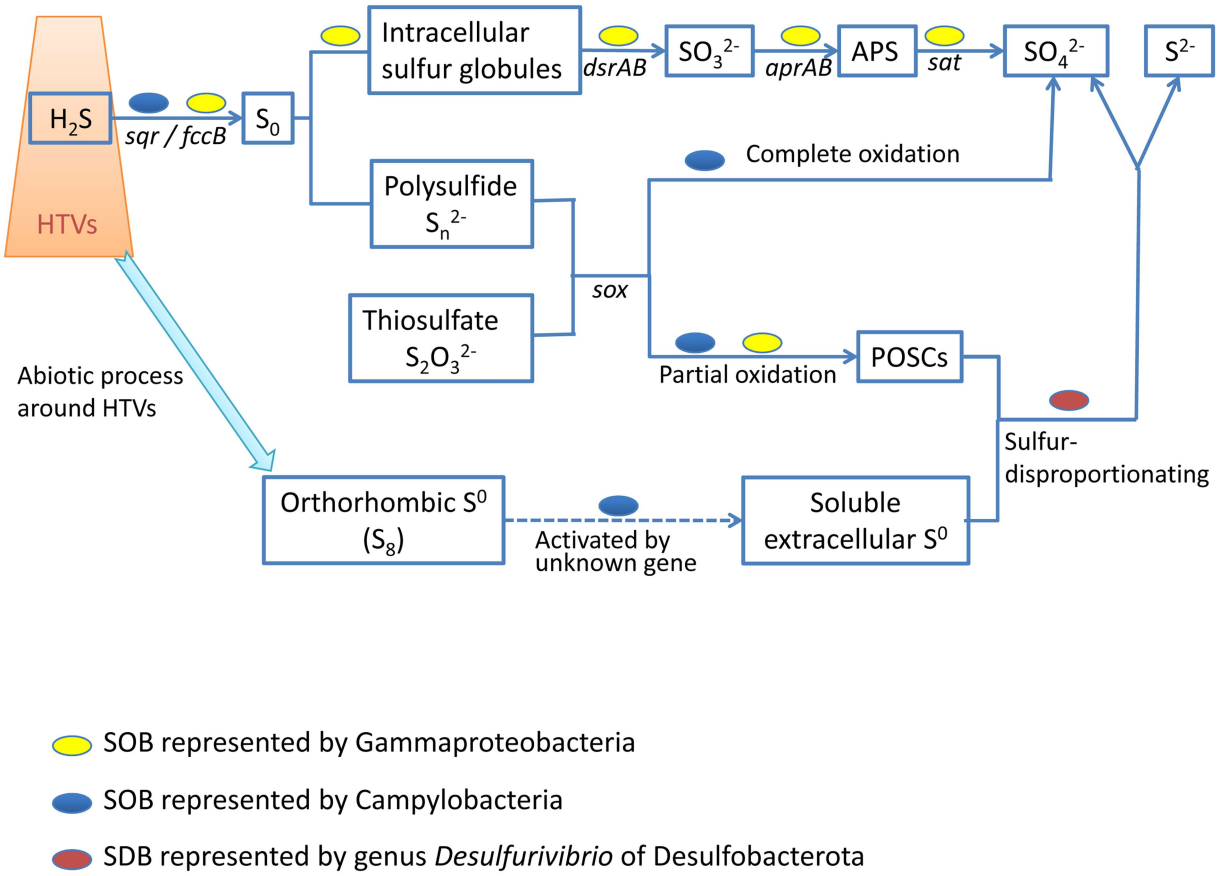

FIGURE 7
Schematic diagram showing relationship of the abundant MAGs involving in the sulfur cycle. Although both Gammaproteobacterial and Campylobacterial SOB can oxidize various sulfur form (H^2S, Sn^{2-}, $S2O3^{2-}$, etc.), their mechanism and processes were different. Gammproteobacteria (colored with yellow) can form intracellular sulfur globules and use reverse dissimilatory sulfite reductase (encoded by dsrAB gene) to form oxidative sulfate, while Campylobacteria (colored with blue) use the Sox multi-enzymes to form sulfate, or partially oxidized sulfur compounds (POSCs) when the availability of electron acceptor such as oxygen and nitrate was limited. The formed POSCs or soluble extracellular S^0 activated by some kind of Campylobacteria can offer growth for SDB (colored with red). SOB: sulfur-oxidizing bacteria; SDB: sulfur disproportionation bacteria.

Sulfurovum in MG35, W1, W2, W3 and epibiont samples (Supplementary Figure S10B) of oxic mixing zone, and with high rate of H_2S and CO_2 indicate the special niche for these bacteria (Cerqueira et al., 2018). For the reconstructed MAGs, their distribution among the collected datasets was shown in Supplementary Figure S11. Most of the MAGs had much higher RPKG value in the SW-HTV sediment samples analyzed in this study, suggesting an endemic distribution of the dominant bacterial species. The heatmap of top 10 abundant functions shown the acriflavin resistance protein and copper homeostasis proteins (including CusA and Copper tanslocating P-type ATPase) were abundant in the sediments of both DS- and SW-HTVs (Figure 3). The resistance of acriflavin was highest in W1, W2 W3 and MG35. The copper homeostasis proteins were higher in GTV1902, GTV1904, GTV1906 and RB35 of DS-HTVs sediments biome than the SW-HTVs, but MG35 of DS-HTVs sediments own comparable ratio with SW-HTVs sediments.

Conclusion

In this study, we report for the first time the sediment microbial community functional potential of a shallow water hydrothermal vent off Kueishan Island. Comparative metagenomic analysis with two published pelagic datasets of the vent revealed the different microbial taxa and functional potentials of biomes in the sediments and the water column above the vent. The microbial community structure was largely controlled by the prevailing redox conditions, with the dominance of facultative aerobic *Sulfurovum* (Camplylobacteria) in the sediments, as oppose to strictly anaerobic *Nautilia* in the vent fluid and aerobic *Thiomicrospira* in seawater above the vent. Chemolithotrophs, implicated in carbon fixation, dissimilatory sulfur oxidation/reducing, dissimilatory nitrate reduction, and hydrogen oxidation were detected in SW-HTVs as their deep-sea cousin. In addition, the dominant MAGs of sulfur-disproportionation bacteria

illustrated the diverse energy-yielding processes related with element sulfur in SW-HTVs. As element sulfur was the most important precipitate from fluids in SH-HTVs of Kueishan Island, the special characteristics to use element sulfur, or interactive cooperation with others to do so, may be an advantage to survive for the microbes there. The details of the sulfur related process could be followed in the future. Furthermore, we also detected the potential to use simple organic carbon from the genomes of chemolithotrophic Camplylobacterial MAGs.

Data availability statement

The data presented in the study are deposited in the NCBI repository, accession number PRJNA851985.

Author contributions

LW, RL, and JF designed the expedition and sampling scheme. LW, XC, and MS conducted experimental procedures including DNA extraction and PCR amplification. LW, ZS, and YG performed bioinformatical analyses including sequence processing, metagenomic comparison, binning, and phylogenetic analysis. LW and RL analyzed and summarized the data and wrote the article. J-SH managed the sampling. JC made comments and suggestions to the text. All authors contributed to the article and approved the submitted version.

Funding

This work was supported by the National Natural Science Foundation of China (grant nos. 41906134 and 91951210), the special developmental project of Shanghai Ocean University (grant no. A2-2006–00-200217), and a direct grant for research from the research committee of The Chinese University of Hong Kong.

Acknowledgments

We thank students and technicians in J-SH laboratory of National Taiwan Ocean University for their assistance with sample collection. We are grateful to Chongkim Wong of Chinese University of HongKong for his advice and support in the progressing of this study. We also thank Sihua Peng and Liangbiao Chen for their kindly supports in the beginning of this study. We thank all the reviewers for their suggestions and advice to improve the manuscript.

Conflict of interest

The authors declare that the research was conducted in the absence of any commercial or financial relationships that could be construed as a potential conflict of interest.

Publisher's note

Supplementary material

The Supplementary material for this article can be found online at: https://www.frontiersin.org/articles/10.3389/fmicb.2022.992034/full#supplementary-material

References

Anderson, R. E., Sogin, M. L., and Baross, J. A. (2014). Evolutionary strategies of viruses, bacteria and archaea in hydrothermal vent ecosystems revealed through metagenomics. *PLoS One* 9:e109696. doi: 10.1371/journal.pone.0109696

Asnicar, F., Thomas, A. M., Beghini, F., Mengoni, C., Manara, S., Manghi, P., et al. (2020). Precise phylogenetic analysis of microbial isolates and genomes from metagenomes using PhyloPhlAn 3.0. *Nat. Commun.* 11:2500. doi: 10.1038/s41467-020-16366-7

Bowers, R. M., Kyrpides, N. C., Stepanauskas, R., Harmon-Smith, M., Doud, D., Reddy, T. B. K., et al. (2017). Minimum information about a single amplified genome (MISAG) and a metagenome-assembled genome (MIMAG) of bacteria and archaea. *Nat. Biotechnol.* 35, 725–731. doi: 10.1038/nbt.3893

Brazelton, W., and Baross, J. (2009). Abundant transposases encoded by the metagenome of a hydrothermal chimney biofilm. *ISME J.* 3, 1420–1424. doi: 10.1038/ismej.2009.79

Brune, D. C. (1989). Sulfur oxidation by phototrophic bacteria. *Biochim. Biophys. Acta* 975, 189–221. doi: 10.1016/S0005-2728(89)80251-8

Campbell, B. J., Engel, A. S., Porter, M. L., and Takai, K. (2006). The versatile epsilon-proteobacteria: key players in sulphidic habitats. *Nat. Rev. Microbiol.* 4, 458–468. doi: 10.1038/nrmicro1414

Cerqueira, T., Barroso, C., Froufe, H., Egas, C., and Bettencourt, R. (2018). Metagenomic signatures of microbial communities in deep-sea hydrothermal sediments of Azores vent fields. *Microb. Ecol.* 76, 387–403. doi: 10.1007/s00248-018-1144-x

Chaumeil, P. A., Mussig, A. J., Hugenholtz, P., and Parks, D. H. (2019). GTDB-Tk: a toolkit to classify genomes with the genome taxonomy database. *Bioinformatics* 36, 1925–1927. doi: 10.1093/bioinformatics/btz848

Chen, C. T. A., Wang, B. Y., Huang, J. F., Lou, J. Y., Kuo, F. W., Tu, Y. Y., et al. (2005b). Investigation into extremely acidic hydrothermal fluids off Kueishan Tao, Taiwan, China. *Acta Oceanol. Sin.* 24, 125–133.

Chen, C. T. A., Zeng, Z., Kuo, F.-W., Yang, T. F., Wang, B.-J., and Tu, Y.-Y. (2005a). Tide-influenced acidic hydrothermal system offshore NE Taiwan. *Chem. Geol.* 224, 69–81. doi: 10.1016/j.chemgeo.2005.07.022

Collman, J. P., Ghosh, S., Dey, A., and Decréau, R. A. (2009). Using a functional enzyme model to understand the chemistry behind hydrogen sulfide induced hibernation. *Proc. Natl. Acad. Sci. U. S. A.* 106, 22090–22095. doi: 10.1073/pnas.0904082106

Cron, B., Macalady, J. L., and Cosmidis, J. (2021). Organic stabilization of extracellular elemental sulfur in a sulfurovum-rich biofilm: a new role for

extracellular polymeric substances? *Front. Microbiol.* 12:720101. doi: 10.3389/fmicb.2021.720101

Dahl, C., Engels, S., Pott-Sperling, A. S., Schulte, A., Sander, J., Lübbe, Y., et al. (2005). Novel genes of the *dsr* gene cluster and evidence for close interaction of Dsr proteins during sulfur oxidation in the phototrophic sulfur bacterium *Allochromatium vinosum*. *J. Bacteriol.* 187, 1392–1404. doi: 10.1128/JB.187.4.1392-1404.2005

Dick, G. J. (2019). The microbiomes of deep-sea hydrothermal vents: distributed globally, shaped locally. *Nat. Rev. Microbiol.* 17, 271–283. doi: 10.1038/s41579-019-0160-2

Eren, A. M., Esen, Ö. C., Quince, C., Vineis, J. H., Morrison, H. G., Sogin, M. L., et al. (2015). Anvi'o: an advanced analysis and visualization platform for 'omics data. *PeerJ.* 3:e1319. doi: 10.7717/peerj.1319

Friedrich, C. G., Bardischewsky, F., Rother, D., and Quentmeier, A. J. (2005). Prokaryotic sulfur oxidation. *Curr. Opin. Microbiol.* 8, 253–259. doi: 10.1016/j.mib.2005.04.005

Friedrich, C. G., Rother, D., Bardischewsky, F., Quentmeier, A., and Fischer, J. (2001). Oxidation of reduced inorganic sulfur compounds by bacteria: emergence of a common mechanism? *Appl. Environ. Microbiol.* 67, 2873–2882. doi: 10.1128/AEM.67.7.2873-2882.2001

Frigaard, N.-U., and Dahl, C. (2008). "Sulfur metabolism in phototrophic sulfur bacteria," in *Advances in microbial physiology*. ed. R. K. Poole (Cham: Springer), 103–200.

Giovannelli, D., and Price, R. E. (2019). "Marine shallow-water hydrothermal vents: microbiology," in *Encyclopedia of ocean sciences*. eds. J. K. Cochran, H. J. Bokuniewicz and P. L. Yager. *Third* ed (Oxford: Academic Press), 353–363.

Gomez-Alvarez, V., Teal, T. K., and Schmidt, T. M. (2009). Systematic artifacts in metagenomes from complex microbial communities. *ISME J.* 3, 1314–1317. doi: 10.1038/ismej.2009.72

Gregersen, L., Bryant, D., and Frigaard, N.-U. (2011). Mechanisms and evolution of oxidative sulfur metabolism in green sulfur bacteria. *Front. Microbiol.* 2:116. doi: 10.3389/fmicb.2011.00116

Grimm, F., Dobler, N., and Dahl, C. (2010). Regulation of dsr genes encoding proteins responsible for the oxidation of stored sulfur in Allochromatium vinosum. *Microbiology* 156, 764–773. doi: 10.1099/mic.0.034645-0

Grzymski, J. J., Murray, A. E., Campbell, B. J., Kaplarevic, M., Gao, G. R., and Lee, C. (2008). Metagenome analysis of an extreme microbial symbiosis reveals eurythermal adaptation and metabolic flexibility. *Proc. Natl. Acad. Sci. U. S. A.* 105, 17516–17521. doi: 10.1073/pnas.0802782105

Han, C. H., Ye, Y., Qin, H. W., Wu, G. H., and Chen, C. T. A. (2014). Spatial distribution pattern of seafloor hydrothermal vents to the southeastern Kueishan Tao offshore Taiwan Island. *Acta Oceanol. Sin.* 33, 37–44. doi: 10.1007/s13131-014-0405-x

Hügler, M., and Sievert, S. M. (2010). Beyond the Calvin cycle: autotrophic carbon fixation in the ocean. *Annu. Rev. Mar. Sci.* 3, 261–289. doi: 10.1146/annurev-marine-120709-142712

Hügler, M., Wirsen, C. O., Fuchs, G., Taylor, C. D., and Sievert, S. M. (2005). Evidence for autotrophic CO_2 fixation via the reductive tricarboxylic acid cycle by members of the epsilon subdivision of proteobacteria. *J. Bacteriol.* 187, 3020–3027. doi: 10.1128/JB.187.9.3020-3027.2005

Hyatt, D., Chen, G. L., Locascio, P. F., Land, M. L., Larimer, F. W., and Hauser, L. J. (2010). Prodigal: prokaryotic gene recognition and translation initiation site identification *BMC Bioinform.* 11:119. doi: 10.1186/1471-2105-11-119

Imchen, M., Kumavath, R., Barh, D., Vaz, A., Góes-Neto, A., Tiwari, S., et al. (2018). Comparative mangrove metagenome reveals global prevalence of heavy metals and antibiotic resistome across different ecosystems. *Sci. Rep.* 8:11187. doi: 10.1038/s41598-018-29521-4

Janausch, I. G., Zientz, E., Tran, Q. H., Kröger, A., and Unden, G. (2002). C_4-dicarboxylate carriers and sensors in bacteria. *Biochim. Biophys. Acta* 1553, 39–56. doi: 10.1016/S0005-2728(01)00233-X

Jeng, M. S., Ng, N. K., and Ng, P. K. L. (2004). Feeding behaviour: hydrothermal vent crabs feast on sea 'snow'. *Nature* 432:969. doi: 10.1038/432969a

Kanehisa, M., Sato, Y., and Morishima, K. (2016). BlastKOALA and GhostKOALA: KEGG tools for functional characterization of genome and metagenome sequences. *J. Mol. Biol.* 428, 726–731. doi: 10.1016/j.jmb.2015.11.006

Kang, D. D., Li, F., and Kirton, E. (2019). MetaBAT 2: an adaptive binning algorithm for robust and efficient genome reconstruction from metagenome assemblies. *PeerJ.* 7:e7359. doi: 10.7717/peerj.7359

Keller, A. H., Schleinitz, K. M., Starke, R., Bertilsson, S., Vogt, C., and Kleinsteuber, S. (2015). Metagenome-based metabolic reconstruction reveals the ecophysiological function of Epsilonproteobacteria in a hydrocarbon-contaminated sulfidic aquifer. *Front. Microbiol.* 6:1396. doi: 10.3389/fmicb.2015.01396

Kelley, D. S., Baross, J. A., and Delaney, J. R. (2002). Volcanoes, fluids, and life at mid-ocean ridge spreading centers. *Annu. Rev. Earth Planet. Sci.* 30, 385–491. doi: 10.1146/annurev.earth.30.091201.141331

Kleinjan, W. E., de Keizer, A., and Janssen, A. J. H. (2003). "Biologically produced sulfur," in *Elemental sulfur and sulfur-rich compounds I*. ed. R. Steudel (Berlin, Heidelberg: Springer Berlin Heidelberg), 167–188.

Kröger, A., Biel, S., Simon, J., Gross, R., Unden, G., and Lancaster, C. R. D. (2002). Fumarate respiration of *wolinella succinogenes*: enzymology, energetics and coupling mechanism. *Biochim. Biophys. Acta* 1553, 23–38. doi: 10.1016/S0005-2728(01)00234-1

Kumari, S., Tishel, R., Eisenbach, M., and Wolfe, A. J. (1995). Cloning, characterization, and functional expression of acs, the gene which encodes acetyl coenzyme a synthetase in *Escherichia coli*. *J. Bacteriol.* 177, 2878–2886. doi: 10.1128/jb.177.10.2878-2886.1995

Langmead, B., and Salzberg, S. L. (2012). Fast gapped-read alignment with bowtie 2. *Nat. Methods* 9, 357–359. doi: 10.1038/nmeth.1923

Lavik, G., Stührmann, T., Brüchert, V., Van der Plas, A., Mohrholz, V., Lam, P., et al. (2009). Detoxification of sulphidic African shelf waters by blooming chemolithotrophs. *Nature* 457, 581–584. doi: 10.1038/nature07588

Li, H., Handsaker, B., Wysoker, A., Fennell, T., Ruan, J., Homer, N., et al. (2009). The sequence alignment/map format and SAMtools. *Bioinformatics* 25, 2078–2079. doi: 10.1093/bioinformatics/btp352

Li, Y., Tang, K., Zhang, L., Zhao, Z., Xie, X., Chen, C.-T. A., et al. (2018). Coupled carbon, sulfur, and nitrogen cycles mediated by microorganisms in the water column of a shallow-water hydrothermal ecosystem. *Front. Microbiol.* 9:2718. doi: 10.3389/fmicb.2018.02718

Liu, C. C. (1995). The Ilan plain and the southwestward extending Okinawa trough. *J. Geol. Soc. China*. 38, 229–242.

Liu, R., Wei, X., Song, W., Wang, L., Cao, J., Wu, J., et al. (2022). Novel Chloroflexi genomes from the deepest ocean reveal metabolic strategies for the adaptation to deep-sea habitats. *Microbiome.* 10:75. doi: 10.1186/s40168-022-01263-6

Loy, A., Duller, S., Baranyi, C., Mussmann, M., Ott, J., Sharon, I., et al. (2009). Reverse dissimilatory sulfite reductase as phylogenetic marker for a subgroup of sulfur-oxidizing prokaryotes. *Environ. Microbiol.* 11, 289–299. doi: 10.1111/j.1462-2920.2008.01760.x

Meier, D. V., Pjevac, P., Bach, W., Hourdez, S., Girguis, P. R., Vidoudez, C., et al. (2017). Niche partitioning of diverse sulfur-oxidizing bacteria at hydrothermal vents. *ISME J.* 11, 1545–1558. doi: 10.1038/ismej.2017.37

Meyer, F., Paarmann, D., D'Souza, M., Olson, R., Glass, E. M., Kubal, M., et al. (2008). The metagenomics RAST server – a public resource for the automatic phylogenetic and functional analysis of metagenomes. *BMC. Bioinformatics.* 9:386. doi: 10.1186/1471-2105-9-386

Nakagawa, S., and Takai, K. (2008). Deep-sea vent chemoautotrophs: diversity, biochemistry and ecological significance. *FEMS Microbiol. Ecol.* 65, 1–14. doi: 10.1111/j.1574-6941.2008.00502.x

Nakagawa, S., and Takai, K. (2014). "The family Nautiliaceae: the genera *Caminibacter*, *Lebetimonas*, and *Nautilia*," in *The prokaryotes: Deltaproteobacteria and Epsilonproteobacteria*. eds. E. Rosenberg, E. F. DeLong, S. Lory, E. Stackebrandt and F. Thompson (Berlin, Heidelberg: Springer Berlin Heidelberg), 393–399.

Nakagawa, S., Takaki, Y., Shimamura, S., Reysenbach, A. L., Takai, K., and Horikoshi, K. (2007). Deep-sea vent epsilon-proteobacterial genomes provide insights into emergence of pathogens. *Proc. Natl. Acad. Sci. U. S. A.* 104, 12146–12150. doi: 10.1073/pnas.0700687104

Nakamura, H. (1968). Genetic determination of resistance to acriflavine, phenethyl alcohol, and sodium dodecyl sulfate in Escherichia coli. *J. Bacteriol.* 96, 987–996. doi: 10.1128/jb.96.4.987-996.1968

Namirimu, T., Kim, Y. J., Park, M. J., Lim, D., Lee, J. H., and Kwon, K. K. (2022). Microbial community structure and functional potential of deep-sea sediments on low activity hydrothermal area in the central Indian ridge. *Front. Mar. Sci.* 9:784807. doi: 10.3389/fmars.2022.784807

Olm, M. R., Brown, C. T., Brooks, B., and Banfield, J. F. (2017). dRep: a tool for fast and accurate genomic comparisons that enables improved genome recovery from metagenomes through de-replication. *ISME J.* 11, 2864–2868. doi: 10.1038/ismej.2017.126

Parks, D. H., Imelfort, M., Skennerton, C. T., Hugenholtz, P., and Tyson, G. W. (2015). CheckM: assessing the quality of microbial genomes recovered from isolates, single cells, and metagenomes. *Genome Res.* 25, 1043–1055. doi: 10.1101/gr.186072.114

Parks, D. H., Tyson, G. W., Hugenholtz, P., and Beiko, R. G. (2014). STAMP: statistical analysis of taxonomic and functional profiles. *Bioinformatics* 30, 3123–3124. doi: 10.1093/bioinformatics/btu494

Peng, Y., Leung, H. C., Yiu, S. M., and Chin, F. Y. (2012). IDBA-UD: a de novo assembler for single-cell and metagenomic sequencing data with highly uneven depth. *Bioinformatics* 28, 1420–1428. doi: 10.1093/bioinformatics/bts174

Pjevac, P., Kamyshny, A. Jr., Dyksma, S., and Mußmann, M. (2014). Microbial consumption of zero-valence sulfur in marine benthic habitats. *Environ. Microbiol.* 16, 3416–3430. doi: 10.1111/1462-2920.12410

Prange, A. (2008). "Speciation analysis of microbiologically produced sulfur by X-ray absorption near edge structure spectroscopy," in *Microbial sulfur metabolism*. eds. C. Dahl and C. G. Friedrich (Berlin: Springer Berlin Heidelberg), 259–272.

Preston, G. G., Zeiher, C., Wall, J. D., and Emerich, D. W. (1989). Acetate-activating enzymes of *bradyrhizobium japonicum* Bacteroids. *Appl. Environ. Microbiol.* 55, 165–170. doi: 10.1128/aem.55.1.165-170.1989

Price, R. E., and Giovannelli, D. (2017). "A review of the geochemistry and microbiology of marine shallow-water hydrothermal vents," in *Reference module in earth systems and environmental sciences.* (Netherlands: Elsevier), 1–9.

Rho, M., Tang, H., and Ye, Y. (2010). FragGeneScan: predicting genes in short and error-prone reads. *Nucleic Acids Res.* 38:e191. doi: 10.1093/nar/gkq747

Rodriguez-R, L., and Konstantinidis, K. (2014). Nonpareil: a redundancy-based approach to assess the level of coverage in metagenomic datasets. *Bioinformatics* 30, 629–635. doi: 10.1093/bioinformatics/btt584

Sakurai, H., Ogawa, T., Shiga, M., and Inoue, K. (2010). Inorganic sulfur oxidizing system in green sulfur bacteria. *Photosynth. Res.* 104, 163–176. doi: 10.1007/s11120-010-9531-2

Schloss, P. D., Westcott, S. L., Ryabin, T., Hall, J. R., Hartmann, M., Hollister, E. B., et al. (2009). Introducing mothur: open-source, platform-independent, community-supported software for describing and comparing microbial communities. *Appl. Environ. Microbiol.* 75, 7537–7541. doi: 10.1128/AEM.01541-09

Sievert, S. M., Scott, K. M., Klotz, M. G., Chain, P. S., Hauser, L. J., Hemp, J., et al. (2008). Genome of the epsilonproteobacterial chemolithoautotroph *Sulfurimonas denitrificans*. *Appl. Environ. Microbiol.* 74, 1145–1156. doi: 10.1128/AEM.01844-07

Sorokin, D. Y., Tourova, T. P., Mußmann, M., and Muyzer, G. (2008). *Dethiobacter alkaliphilus* gen. Nov. sp. nov., and *Desulfurivibrio alkaliphilus* gen. Nov. sp. nov.: two novel representatives of reductive sulfur cycle from soda lakes. *Extremophiles* 12, 431–439. doi: 10.1007/s00792-008-0148-8

Starke, R., Keller, A., Jehmlich, N., Vogt, C., Richnow, H. H., Kleinsteuber, S., et al. (2016). Pulsed $^{13}C_2$-acetate protein-SIP unveils Epsilonproteobacteria as dominant acetate utilizers in a sulfate-Rreducing microbial community mineralizing benzene. *Microb. Ecol.* 71, 901–911. doi: 10.1007/s00248-016-0731-y

Tang, K., Liu, K., Jiao, N., Zhang, Y., and Chen, C.-T. A. (2013). Functional metagenomic investigations of microbial communities in a shallow-sea hydrothermal system. *PLoS One* 8:e72958. doi: 10.1371/journal.pone.0072958

Tarasov, V. G., Gebruk, A. V., Mironov, A. N., and Moskalev, L. I. (2005). Deep-sea and shallow-water hydrothermal vent communities: two different phenomena? *Chem. Geol.* 224, 5–39. doi: 10.1016/j.chemgeo.2005.07.021

Teske, A. (2009). "Deep-sea gydrothermal vents," in *Encyclopedia of microbiology*. ed. M. Schaechter. *Third* ed (Oxford: Academic Press), 80–90.

Waite, D. W., Vanwonterghem, I., Rinke, C., Parks, D. H., Zhang, Y., Takai, K., et al. (2017). Comparative genomic analysis of the class Epsilonproteobacteria and proposed eeclassification to Epsilonbacteraeota (phyl. Nov.). *Front. Microbiol.* 8:682. doi: 10.3389/fmicb.2017.00682

Wang, L., Cheung, M. K., Kwan, H. S., Hwang, J.-S., and Wong, C. K. (2015). Microbial diversity in shallow-water hydrothermal sediments of Kueishan Island, Taiwan as revealed by pyrosequencing. *J. Basic Microbiol.* 55, 1308–1318. doi: 10.1002/jobm.201400811

Wang, L., Cheung, M. K., Liu, R., Wong, C. K., Kwan, H. S., and Hwang, J.-S. (2017). Diversity of total bacterial communities and chemoautotrophic populations in sulfur-rich sediments of shallow-water hydrothermal vents off Kueishan Island. *Taiwan. Microb. Ecol.* 73, 571–582. doi: 10.1007/s00248-016-0898-2

Wilke, A., Harrison, T., Wilkening, J., Field, D., Glass, E. M., Kyrpides, N., et al. (2012). The M5nr: a novel non-redundant database containing protein sequences and annotations from multiple sources and associated tools. *BMC. Bioinformatics.* 13:141. doi: 10.1186/1471-2105-13-141

Yamamoto, M., Nakagawa, S., Shimamura, S., Takai, K., and Horikoshi, K. (2010). Molecular characterization of inorganic sulfur-compound metabolism in the deep-sea Epsilonproteobacterium *Sulfurovum* sp. NBC37-1. *Environ. Microbiol.* 12, 1144–1153. doi: 10.1111/j.1462-2920.2010.02155.x

Yamamoto, M., and Takai, K. (2011). Sulfur metabolisms in epsilon- and gamma-Proteobacteria in deep-sea hydrothermal fields. *Front. Microbiol.* 2:192. doi: 10.3389/fmicb.2011.00192

Yang, T. F., Lan, T. F., Lee, H.-F., Fu, C.-C., Chuang, P.-C., Lo, C.-H., et al. (2005). Gas compositions and helium isotopic ratios of fluid samples around Kueishantao, NE offshore Taiwan and its tectonic implications. *Geochem. J.* 39, 469–480. doi: 10.2343/geochemj.39.469

Zeng, Z., Chen, C.-T. A., Yin, X., Zhang, X., Wang, X., Zhang, G. L., et al. (2011). Origin of native sulfur ball from the Kueishantao hydrothermal field offshore Northeast Taiwan: evidence from trace and rare earth element composition. *J. Asian Earth Sci.* 40, 661–671. doi: 10.1016/j.jseaes.2010.10.019

Zeng, Z., Liu, C., Chen, C. A., Yin, X., Chen, D., Wang, X., et al. (2007). Origin of a native sulfur chimney in the Kueishantao hydrothermal field, offshore Northeast Taiwan. *Sci. China. Ser. D.* 50, 1746–1753. doi: 10.1007/s11430-007-0092-y

Zhang, Y., Zhao, Z., Chen, C.-T. A., Tang, K., Su, J., and Jiao, N. (2012). Sulfur metabolizing microbes dominate microbial communities in andesite-hosted shallow-sea hydrothermal systems. *PLoS One* 7:e44593. doi: 10.1371/journal.pone.0044593

frontiers | Frontiers in Microbiology

TYPE Original Research
PUBLISHED 15 December 2022
DOI 10.3389/fmicb.2022.1059262

OPEN ACCESS

EDITED BY
Shan He,
Ningbo University, China

REVIEWED BY
Jun Sun,
China University of Geosciences Wuhan, China
John Albert Raven,
University of Dundee, United Kingdom
Hualong Wang,
Ocean University of China, China
Meilin Wu,
South China Sea Institute of Oceanology (CAS), China

*CORRESPONDENCE
Da-Zhi Wang
dzwang@xmu.edu.cn

SPECIALTY SECTION
This article was submitted to Aquatic Microbiology, a section of the journal Frontiers in Microbiology

RECEIVED 01 October 2022
ACCEPTED 30 November 2022
PUBLISHED 15 December 2022

CITATION
Liu S-J, Xie Z-X, Wu P-F, Zheng R-W, Liu Y, Lin L, Liu H-P and Wang D-Z (2022) Composition and assembly of the bacterial community in the overlying waters of the coral reef of China's Xisha Islands. *Front. Microbiol.* 13:1059262. doi: 10.3389/fmicb.2022.1059262

Composition and assembly of the bacterial community in the overlying waters of the coral reef of China's Xisha Islands

Si-Jia Liu[1], Zhang-Xian Xie[1,2], Peng-Fei Wu[1], Ru-Wen Zheng[1], Yuan Liu[1], Lin Lin[1,2], Hai-Peng Liu[3] and Da-Zhi Wang[1,2]*

[1]State Key Laboratory of Marine Environmental Science, College of the Environment and Ecology, Xiamen University, Xiamen, China, [2]Southern Marine Science and Engineering Guangdong Laboratory (Zhuhai), Sun Yat-Sen University, Zhuhai, China, [3]State Key Laboratory of Marine Environmental Science, College of Ocean & Earth Science, Xiamen University, Xiamen, China

Coral reef ecosystems are one of the most diverse and productive habitats on Earth. Microbes in the reef-overlying waters are key players in maintaining this ecosystem through regulating biogeochemical and ecological processes. However, the composition structure and assembly mechanism of microbial community in the reef-overlying waters remain largely unknown. In the present study, the bacterial communities from the overlying waters of atolls and fringing reefs as well as the surface waters of the adjacent open ocean of the Xisha Islands in the South China Sea were investigated using 16S rRNA high-throughput sequencing combined with a size-fractionation strategy. The results showed that environments of all sampling stations were similar, characterized by an almost complete lack of inorganic nutrients such as nitrogen and phosphorus. *Proteobacteria*, *Cyanobacteria* and *Bacteroidetes* were the dominant phyla, and *Synechococcus* was most abundant at the genus level in both large fraction (LF; 1.6–200μm) and small fraction (SF; 0.2–1.6μm) communities. Only a slight difference in community composition between LF and SF samples was observed. The bacterial communities among the three habitat types showed noticeable differences, and the bacterial composition among the atoll reefs was more varied than that among the fringing reefs. The similarity of bacterial communities significantly declined with the increasing geographic distance, and stochastic processes were more important than deterministic processes in bacterial community assembly. This study sheds lights on the bacterial biodiversity of coral reefs and the importance of stochastic process in structuring bacterial communities.

KEYWORDS

bacterial community, assembly mechanism, 16S rRNA gene, coral reef, Xisha Islands

Introduction

Coral reefs represent only a small fraction of marine ecosystem, but they support the highest marine biodiversity on earth, harboring 25% of global marine species and approximately one-third of marine fish (Pendleton et al., 2016). Furthermore, coral reefs are extremely important for nutrient cycling in shallow oligotrophic tropical waters. Reef productivity is largely dependent on the capture and recycling of nutrients by reef-associated microbial communities (Bourne and Webster, 2013). Planktonic microorganisms are abundant but invisible members of the coral reef community, which play important roles in the efficient cycling of internal nutrient through their essential functions, including primary production, nitrogen fixation and nutrient recycling (Ainsworth et al., 2010; Rädecker et al., 2015; Brandl et al., 2019). Photoautotrophic phytoplankton are the major contributors to the biomass and primary productivity of oligotrophic reef waters (Charpy, 2005). For example, *Synechococcus* is abundant in many coral reef waters (Charpy et al., 2012; Furby et al., 2014; Ke et al., 2018). Meanwhile, bacterioplankton generally account for a large fraction of carbon biomass and are responsible for high organic matter recycling rates within coral reefs (Ferrier-Pagès and Gattuso, 1998; Nelson et al., 2011). Furthermore, benthic coral reef communities exhibit strong dependency on bacterioplankton of the overlying waters as an important source of nutrition (Sorokin and Sorokin, 2010).

Research efforts have been devoted to comparing the bacterial composition of reef seawater with host-associated microbes, and the composition of coral-associated microbes have showed them to be distinct from microbial communities in surrounding seawater (de Voogd et al., 2015; Webster et al., 2016; Cleary et al., 2018; van Oppen et al., 2018). However, few studies have been directly assessed the diversity and phylogenetic composition of bacteria in coral reef seawater. The stability of both coral-associated microbial communities and habitat seawater microbial communities affects environmental adaptation and ecological function of corals, nevertheless, we know little about the diversity, composition, and geographic patterns of bacteria in coral reef waters as well as the assembly mechanism of bacterial communities, especially in South China Sea because of the rigorous protection of coral habitats.

Community similarity versus geographic distance displays a distance–decay relationship for microbial communities in many habitats (Soininen et al., 2007; Hanson et al., 2012; Wang et al., 2017), and both deterministic and stochastic processes could give rise to such a negative pattern (Sloan et al., 2006; Zhang et al., 2014; Wu et al., 2020). The deterministic processes, including species traits, interspecies interactions (e.g., competition, predation, mutualisms, and trade-offs), and environmental conditions (e.g., pH, temperature, salt, and moisture), largely control the patterns of species composition, abundance and distribution (Chesson, 2000). However, the stochastic processes including dispersal limitation, water mass effect and random demographics also regulate assembly of bacterial communities (Chave, 2004; Zhou and Ning, 2017). The relative importance of different deterministic and stochastic processes always shows different trends in mediating communities, and the environmental selection tends to produce a distance–decay relationship while dispersal counteracts it (Hanson et al., 2012). Therefore, understanding community assembly process can enable us to explore the underlying mechanisms shaping microbial biogeographic patterns.

Microbial communities are also structured over much smaller spatial scales, and the composition of microbial assemblages exhibit differences among different size fractions in different marine ecosystems (Ganesh et al., 2014, 2015; Liu et al., 2018; Suter et al., 2018). The large size fraction ranging from 1.6 to 200 μm retains a wide range of microorganisms, including particle-attached prokaryotes, microeukaryotes and zooplankton, while the small size fraction ranging from 0.2 to 1.6 μm predominantly contains free-living prokaryotes and picoeukaryotes (Ganesh et al., 2014; Chen et al., 2021). Furthermore, they have different dispersal potential, metabolic capability and ecological roles in marine ecosystems. Although much effort has been devoted to bacterial communities from different size fractions of marine plankton (Rusch et al., 2007; Sunagawa et al., 2015; Salazar et al., 2016), our knowledge on bacterial diversity and biogeographic patterns of different size fractions in the coral reefs is limited.

The Xisha Islands in the central South China Sea consist of different types of coral reefs with important ecological and biodiversity value (Wang et al., 2011; Yang et al., 2015; Zuo et al., 2017), providing an ideal area to study microbial biodiversity. Previous studies have shown that many coral reefs of the Xisha Islands are being threatened or have already degraded over the past few decades (Shi et al., 2012; Hughes et al., 2013; Ding et al., 2019). However, the diversity and composition of bacteria are generally understudied in the Xisha Islands, which greatly impedes our understanding, protection and remediation of coral reefs. With the aim of gaining a more comprehensive understanding of microbial biodiversity in the coral reefs of the Xisha Islands, in the present study, we adopted a size fractionation strategy to collect both large fraction (1.6–200 μm) and small fraction (0.2–1.6 μm) of bacterial communities living in the overlying waters of the coral reefs, and investigated the composition and structure of bacterial communities using high-throughput sequencing of the 16S rRNA gene. This study therefore provides new insights into the bacterial diversity and composition of different coral reef habitats, offering guidance for further exploring the mechanisms shaping the bacterial community structure and geographic distribution in the Xisha Islands.

Materials and methods

Sample collection

The survey was conducted in the Xisha Islands of the South China Sea from May 13th to 24th in 2019. Three atolls (Beijiao, BJ;

Yuzhuojiao, YZJ; Huaguangjiao, HGJ) which usually contain a central open lagoon, three fringing reefs (Beidao, BD; Zhaoshudao, ZSD; Jinqingdao, JQD) which grow directly from a shore of island, and three open ocean stations (O1; O2; O3) were selected for the study. Duplicate biological samples were collected from the surface layer (approximately 0.5 m depth) in locations of lagoon, reef flat and outer reef in three atolls (BJ, YZJ and HGJ); reef flat and outer reef in three fringing reefs (BD, ZSD and JQD), and three open ocean stations (O1; O2; O3).Surface seawater samples (100 l) were collected from each location using Niskin bottles, each sample was pre-filtered through a 200-μm polyethylene sieve to remove large-sized plankton, then was sequentially filtered through a GF/A membrane (pore-size of 1.6 μm, Waterman) and a polyethersulfone membrane (pore-size of 0.2 μm, Millipore) to collect the large-fraction (LF) and small-fraction (SF) bacterial samples, respectively. All samples were immediately frozen with liquid nitrogen and stored at −80°C for further processing.

Environmental parameters measurement

The latitude and longitude of the sampling stations were determined by a portable global positioning system (GPS Jisibao G330, Beijing, China). Salinity, temperature and dissolved oxygen were measured using a SeaBird 911 plus CTD instrument. Chlorophyll a concentration was determined using a Turner TrilogyVR fluorometer. Nutrients, including silicate, phosphate, ammonium, nitrate and nitrite were analyzed using a continuous flow analyzer (SAN11, Skalar, The Netherlands). Filtrate passing through GF/A filter was fixed with 2% glutaraldehyde for bacterial cell numeration. After staining with SYBR Green I (Invitrogen, Thermo Fisher Scientific, Waltham, MA, USA), bacterial abundance was estimated using a BD FACSAria Flow Cytometer (Becton Dickinson, Franklin Lanes, NJ, USA) (Marie et al., 1999).

DNA extraction, PCR analysis and Illumina sequencing

For each sample, DNA was extracted from the membranes using FastDNA SPIN extraction kit (MP Biomedicals, Santa Ana, USA), following the manufacturer's instructions. The concentrations and purity of extracted DNA were examined using a Scientific Nano Drop2000 spectrophotometer (NanoDrop Technologies Wilmington, USA). The V4 hypervariable region of prokaryotic 16S rDNA was amplified with primers of 515FmodF (5'-GTGYCAGCMGCCGCGGTAA-3′) and 806RmodR (5'-GGACTACNVGGGTWTCTAAT −3′) (Parada et al., 2016). All PCR reactions were performed in a 30 μl volume with 15 μl of Phusion® High-Fidelity PCR Master Mix (New England Biolabs); 0.2 μM of forward and reverse primers, and approximately 10 ng template DNA. The PCR thermal cycle was performed as follows: denaturation at 95°C for 5 min, 34 cycles of 94°C for 1 min, 57°C for 45 s, 72°C for 1 min, and a final extension at 72°C for 10 min. PCR products were purified using a GeneJET Gel Extraction Kit (Thermo Fisher Scientific, USA) and paired-end sequenced (2 × 250 bp) on an Illumina® MiSeq (PE300) platform.

Low-quality raw reads were filtered using fastp (v.0.23.1, Chen et al., 2018) with following criteria: (1) reads were truncated at any site with an average quality score < 20 over a 50 bp sliding window, and reads shorter than 50 bp after truncated, reads containing ambiguous characters were removed; (2) 1 or more mismatch in barcode; (3) > 2 nucleotide mismatch in primers. Paired-end reads were merged using FLASH (v.1.2.11, Magoč and Salzberg, 2011) with the parameter that overlap was longer than 10 bp and its mismatch rate was lower than 0.2. Paired-end reads were then sorted by sample-specific barcodes and clustered into operational taxonomic units (OTUs) using Uparse (v.7.1, Edgar, 2013) at 97% identity. The phylogenetic classification was analyzed by RDP Classifier with confidence threshold of 70% based on the Silva (SSU r138) database (Cole et al., 2009; Quast et al., 2013). The sequencing data are available in the China National GeneBank DataBase[1] with project number CNP0002755.

Statistical analysis

To reduce the bias of sequencing coverage and ensure inter-sample comparability for our taxonomic diversity, the singleton OTUs were discarded and only the reads belonging to bacteria were retained for analysis. All samples were normalized based on the minimum of the sequencing depth (39,588 reads), and the taxa with relative abundance < 0.01 in all samples were classified as "others." For alpha-diversity analysis, indices of Sobs, Shannon, Simpson, ACE, Chao1 and coverage were calculated with the vegan R package (Oksanen et al., 2020), and the subsequent computations were also performed using *R* (v.4.0.2, R Core Team, 2014). For beta-diversity analysis, Bray–Curtis dissimilarity matrices were calculated and non-metric multidimensional scaling (NMDS) analysis was applied based on Bray–Curtis dissimilarity using the Vegan package. Analysis of similarities (ANOSIM) was used to evaluate the difference between groups. The Mantel test was used to determine correlations between environmental factors and the bacterial community (based on Bray-Cutis distance).

The Spearman's rank correlations were used to determine the relationship between the Bray–Curtis similarity of bacterial community and the geographical distance of sampling stations. To explore the potential factors regulating the community composition, the phylogenetic bin-based null model analysis (iCAMP) was selected to reveal the ecological drivers of bacterial community assembly (Ning et al., 2020), and quantify the contribution of each ecological process to microbial community assembly, including homogeneous selection (HoS), heterogeneous selection (HeS), dispersal limitation (DL),

1 https://db.cngb.org/

homogenizing dispersal (HD), drift and others (DR). HoS and HeS belong to deterministic processes, whereas DL, HD, and DR are classified as stochastic processes. Furthermore, the neutral community model (NCM) was used to predict the relationship between OTU detection frequency and their relative abundance across the wider metacommunity to determine the potential importance of stochastic processes on community assembly (Sloan et al., 2006; Stegen et al., 2013), the R code used for the NCM was obtained from Chen et al. (2019). In this model, R^2 indicates the fit to the neutral model; when R^2 is close to 1, the community assembly is considered to be fully consistent with stochastic processes. Dispersal between communities was estimated by the Nm value, representing the metacommunity size (N) multiplied by the immigration rate (m).

Results

Overview of the investigation area

Surface seawater samples were collected from six coral reef sites and three adjacent open ocean stations in the Xisha Islands (Figure 1). The spatial variations of physical environments among the sampling locations were very small, with temperatures ranging from 30.4°C to 31.9°C, salinity from 33.2 to 34.29 PSU, and dissolved oxygen from 4.63 to 5.68 mg/l (Supplementary Table S1). The concentrations of inorganic nitrogen were less than 2.48 μmol/l and phosphorus was below the detection limit of the analyzer in most of the sampled locations. The primary production and bacterial biomass indicated by chlorophyll a concentration (0.07–0.28 μg/l) and bacterial cell density ($1.42–5.38 \times 10^8$ cells/ L) were also similar among locations.

Diversity and distribution of bacterial communities

A total of 11,118,121 sequences were generated and were clustered into 13,734 OTUs. To minimize the bias caused by the sequencing depth and allow for comparison of sequencing results among samples, the sequences were normalized by minimum sample sequence numbers (39,588 reads) respectively, and the rarefaction curves of all samples were showed in Supplementary Figure S1. Shannon index did not vary across different habitats (Figure 2A), with the lowest index observed in the samples of BJ. The Shannon index of each reef region in the atoll was quite different, whereas the differences among the fringing reefs were small in both LF and SF samples (Figure 2B). To explore whether the difference of bacterial structure and composition was correlate with sampling location, we computed the sample diversity using Bray-Curtis distance (Figure 2C). The close clustering of samples indicated similar community composition. Although the stress values were below 0.2, indicating an acceptable fit of the data to the clusters in the NMDS ordinations, the samples from different reef habitats and open ocean surface waters showed different patterns. Comparison of the atoll and open ocean samples showed that the atoll samples formed well-defined groups in both LF and SF samples, while the fringing reef and open ocean samples were clearly distinct, which were generally clustered together and even some samples of the different stations showed overlapping (Figure 2C). ANOSIM results also indicated that the communities of the atoll and open ocean samples were significantly separated, while there were small R values among the fringing reef and open ocean samples. Thus, the bacterial community presented greater difference between the atoll and open ocean samples than that between the fringing reef and open ocean samples.

Venn diagram displaying the OTU richness distribution among habitats and sites showed that the unique OTU numbers in coral reef surface waters were higher than that in adjacent open ocean surface waters, and the highest unique OTU numbers were detected in YZJ (Supplementary Figure S2). Relatively abundant bacterial phyla in the adjacent coral seawater included *Proteobacteria* (49.72%), *Cyanobacteria* (22.11%) and *Bacteroidetes* (19.79%) (Figure 3). Highly abundant *Proteobacteria* groups were concentrated in *Alphaproteobacteria* and *Gammaproteobacteria*. In the LF samples, *Alphaproteobacteria* was most abundant (50.48%) in the reef flat of JQD and the lowest (11.93%) in the lagoon of BJ, while *Gammaproteobacteria* had the highest proportion (40.83%) in the reef flat of YZJ. In the SF samples, *Alphaproteobacteria* showed the highest abundance (57.89%) in the reef flat of JQD and *Gammaproteobacteria* was abundant in the reef flat of YZJ, accounting for 63.73%. *Cyanobacteria* was abundant in the LF samples in the reef flat of BJ (50.20%) and in the SF samples in the lagoon of BJ (55.13%). At the genus level, the most abundant group was *Synechococcus* in both LF and SF samples (Supplementary Figure S3). Only a weak but significant variance was found between the LF and SF samples by ANOSIM analysis ($R = 0.09$, $p < 0.001$; Supplementary Figure S4), but the bacterial communities among the three habitat types showed more noticeable differences ($R = 0.23$, $p < 0.001$; Supplementary Figure S5). Furthermore, the difference of bacterial community composition among three atoll reefs (BJ, HGJ, and YZJ) was significantly larger than that in the fringing reefs (BD, JQD, and ZSD; Table 1), displaying a consistent trend with the NMDS results. Therefore, the samples were distributed according to the sampling location rather than according to the sample size fractions in the following analysis.

Spatial and environmental factors influencing bacterial community composition

Community similarity versus geographic distance for each pairwise set of samples displayed a significant distance–decay

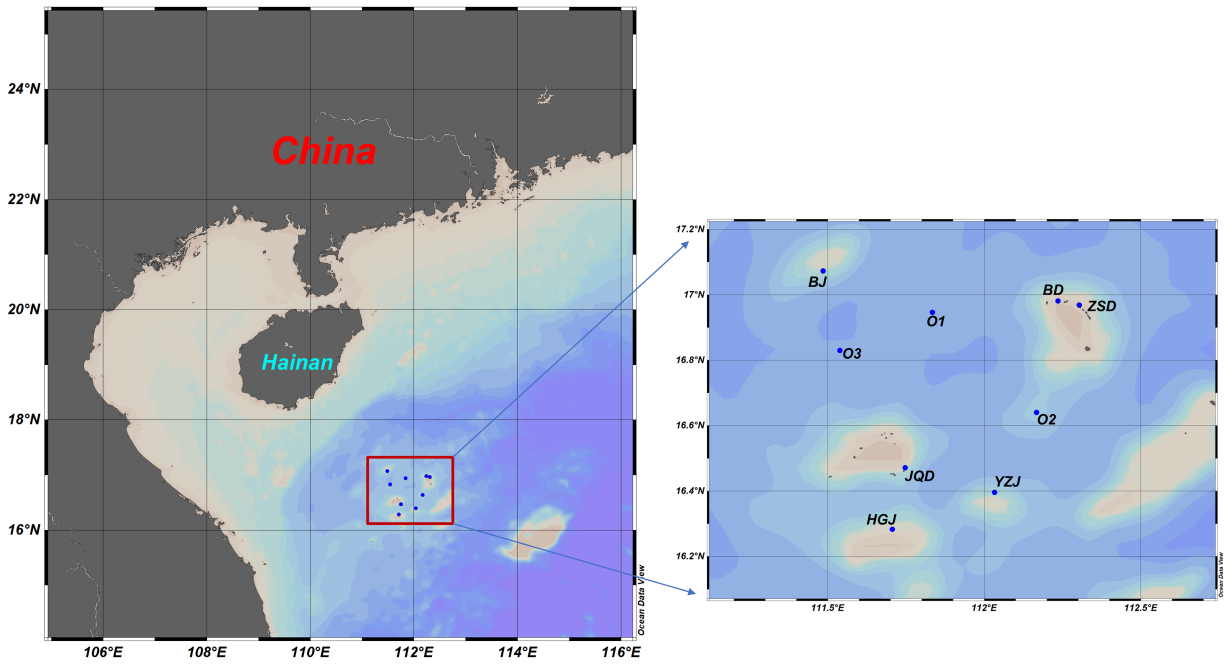

FIGURE 1
Investigation region and sampling sites in the Xisha coral reef areas.

relationship for bacterial communities. Although our investigation was conducted over a small geographic scale, a significant negative correlation was observed between Bray-Cutis community similarity and geographic distance ($p < 0.01$; Figure 4). Furthermore, the results based on the iCAMP analysis implied contributions of different ecological processes to the assembly of bacterial community. For example, HoS processes accounted for more than 20% in each habitat, while stochastic process of DL and DR contributed approximately 50% to the community assembly (Figure 5; Supplementary Figure S6). The neutral community model that is particularly useful for quantifying the importance of neutral processes, successfully estimated a large fraction of the relationship between the occurrence frequency of OTUs and their relative abundance variations, explaining 66.8, 64.3, 55.9, and 71.8% of the community variance for the entire survey region, atoll, fringing reef and open ocean surface seawaters, respectively (Figure 6). The Nm-value for bacterial taxa was higher in the open ocean than in the coral habitats, indicating that species dispersal of bacteria was higher in the open ocean than in the coral habitats. These results indicated that neutral process played important roles in the bacterial assembly in each habitat, especially driving the variations of community compositions between atoll and open ocean or between fringing reef and open ocean (Supplementary Figure S7). However, bacterial community variation between atoll and open ocean were significantly driven by environmental factors ($p < 0.01$), but not to the significantly variation between the fringing reef and open ocean communities (Supplementary Table S3).

Discussion

Physicochemical and microbial features of the over-lying waters in the Xisha Islands

Nutrient concentrations of the over-lying waters in the coral reefs were very low and even undetectable, which is consistent with the results reported in other coral reef areas, suggesting rapid nutrient turnover by microorganisms (Kleypas et al., 1999; Weber et al., 2020). The bacteria of local over-lying waters are closely related to the diversity and adaptation of reef corals, and play an important role in nutrient cycling (Ferrier-Pagès and Gattuso, 1998; Nelson et al., 2011; Brandl et al., 2019). In this study, the bacterial communities of the over-lying waters in the Xisha Islands had high diversity and were dominated by *Proteobacteria*, *Cyanobacteria* and *Bacteroidetes*, consistent with other coral reef environments (Somboonna et al., 2014; Kemp et al., 2015). Although the major compositions of bacterial community were similar at phylum level among samples collected from water areas with a small environmental gradient, but we could still observe a high variation in the reef overlying waters across regions at the OTU level (Supplementary Figure S2). The number of unique OTUs in the reef-overlying waters was higher than that in the open ocean surface waters, indicating the presence of differences in term of bacterial diversity between coral reef ecosystem and the open ocean. Previous studies have shown that the microbial community richness of the surface-waters varies significantly among reef categories (Nelson et al., 2011; Frade et al., 2020; Laas

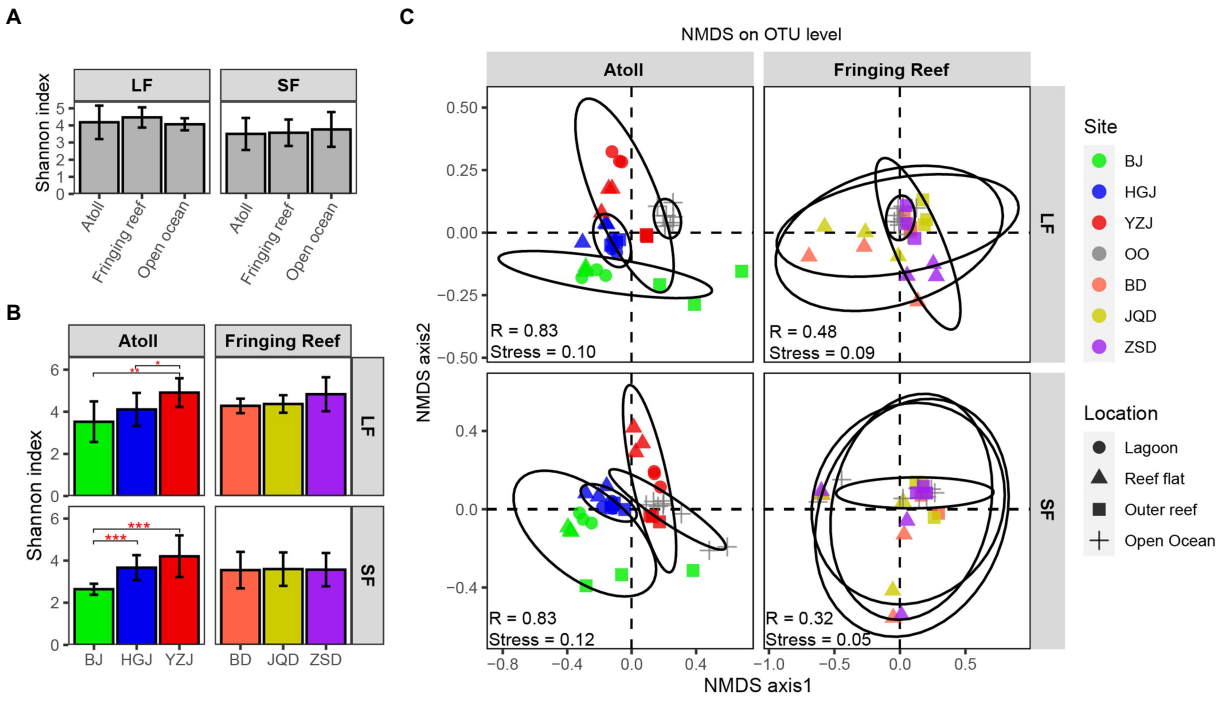

FIGURE 2
Alpha and beta diversity analyzes of bacterial composition. **(A)** Difference significance of average Shannon index among habitat types in each size fraction, **(B)** Shannon index difference of different reefs and different fraction sizes. Error bars represent±SD. **(C)** Non-metric multidimensional scaling ordinations (NMDS) for bacterial communities (The statistic R represents the separation degree of between-group mean rank similarities used the ANOSIM method.).

et al., 2021). A distinctly different pattern observed among samples from different habitats in both LF and SF samples (Figure 2), indicating that a noticeable dissimilarity among community composition of different reef. Both the bacterial community diversity and composition of the over-lying waters in three atolls differed obviously, but there was no notable difference in the over-lying waters of three fringing reefs. Only a weak but significant difference existed between the LF and SF samples, small bacteria could be retained in the LF samples as a consequence of blocking during the filtration (Padilla et al., 2015).

It is reported that annual mean Chlorophyll a concentration in the lower range (< 0.3 μg/l) has been shown to be beneficial to maintain the operation of coral reef ecosystems (Bell, 2010). The low concentrations of nutrients and the low range of Chlorophyll a in the Xisha Islands surface waters indicated that the stability of the system was not markedly disturbed. The maintenance of complex coral reef shared ecosystems might result from the interactions between the autotrophs (e.g., planktonic and benthic algae) and associated heterotrophs. *Synechococcus* and *Prochlorococcus* showed relatively high abundance in both LF and SF samples, which are known to constitute a substantial proportion of planktonic biomass and primary production (Ferrier-Pages and Furla, 2001; Flombaum et al., 2013). Furthermore, *Synechococcus* had the highest abundance in the lagoon of BJ, and was more abundant than *Prochlorococcus* in most of the atoll stations sampled, which were characterized by relatively high nutrients. This supports the previous findings that *Synechococcus* is abundant in a relatively more nutrient-enriched condition such as the coral reef lagoonal environment while *Prochlorococcus* dominates more nutrient-depleted environments (Campbell et al., 1994; Crosbie and Furnas, 2001; Charpy, 2005). These results indicated that bacteria communities of the over-lying waters presented a habitat-specific distribution pattern in the Xisha Islands.

The key processes shaping bacterial community assembly

The environmental heterogeneity and dispersal limitation can generate a negative correlation between community similarity and geographic distance (Tuomisto et al., 2003; Soininen et al., 2007), and the biogeographic patterns are mainly dictated by the spatial scale of the investigation (Rahbek, 2005; Clark et al., 2021). Although our investigation was performed over a relatively small geographic scale and the environmental parameters were similar across sampling sites, we still found a clear and significant distance–decay relationship between the bacterial community similarity and geographic distance for each pairwise set of samples. Deterministic and stochastic processes are important in structuring bacterial communities, and

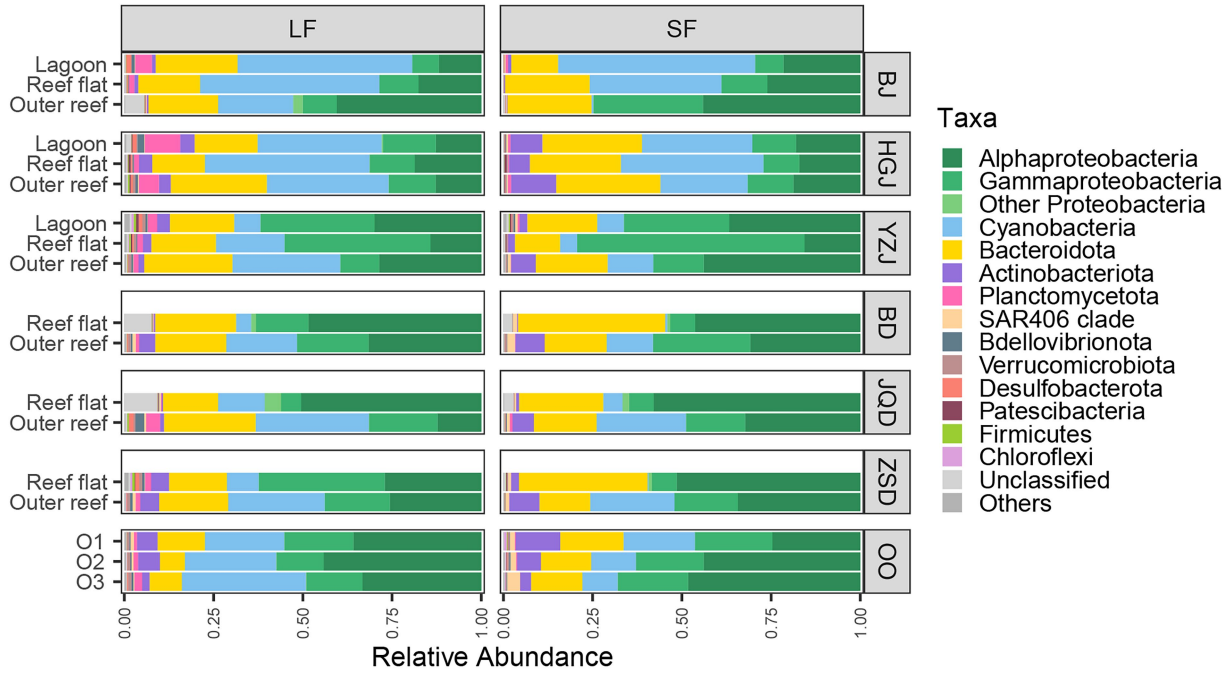

FIGURE 3
Community composition of bacterial groups that are specific to a given number of samples.

TABLE 1 ANOSIM of bacterial communities among different type reefs.

	LF		SF	
	R	*P*	*R*	*P*
Atoll	0.416	0.001	0.633	0.001
Fringing reef	0.063	0.191	0.079	0.859

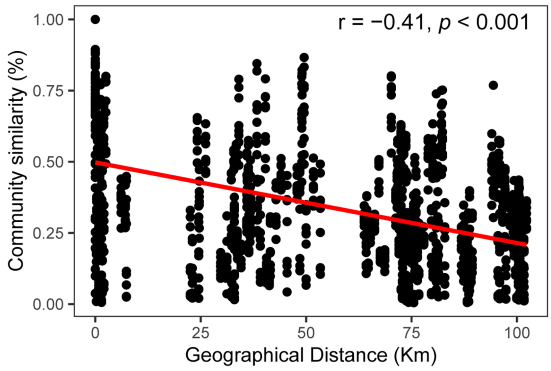

FIGURE 4
Distance-decay patterns based on the Bray–Curtis similarity for the bacterial communities.

we found that stochastic process appeared to be more important than the deterministic process in the Xisha Islands surface waters. Our results indicated that both DR and DL processes, which are stochastic assembly mechanisms, played more important roles than other ecological processes either in a single habitat type, or in different habitat types (Figure 5). Furthermore, the bacterial community had a good fit to the neutral community model which further confirmed the important role of stochastic process. These findings are consistent with the previous conclusions that the stochasticity is the dominant process under stable local-scale conditions (Dini-Andreote et al., 2015; Bahram et al., 2016).

Drift, homogenizing dispersal and homogeneous selection can result in community differences and counteract the distance–decay relationship (Ning et al., 2020), and these three ecological processes showed large relative importance contributions to the bacterial community of each habitat sampled in this study (Figure 5). The surface water in the Xisha Islands is very dynamic, facilitating high dispersal and homogenization of the bacterial communities. The bacterial community structure of the surface layer at different sampling sites within the same reef region was similar, which might be caused by the limited dispersal, resulting in individuals tending to disperse to nearby regions. However, the community difference was greater between the atoll and open ocean samples than that between the fringing reef and open ocean samples, suggesting roles for both the dispersal limitation and environmental selection. Studies have demonstrated that both environmental factors and geographical distance play important roles in driving community structure on a small scale (Horner-Devine et al., 2004; Bell, 2010). Inorganic nutrients are essential for the growth and development of microbes and are considered to be important factors in shaping the microbial community (Follows and Dutkiewicz, 2011). The

Mantel test showed that the influence of inorganic nutrients was relatively small when stochastic processes played the dominant role in the homogeneous surface waters. The temperature of Xisha Island surface waters ranged from 30.4°C to 31.9°C in this study, even a small rise in temperature can lead to coral bleaching and death because the majority of coral reefs are surviving at their

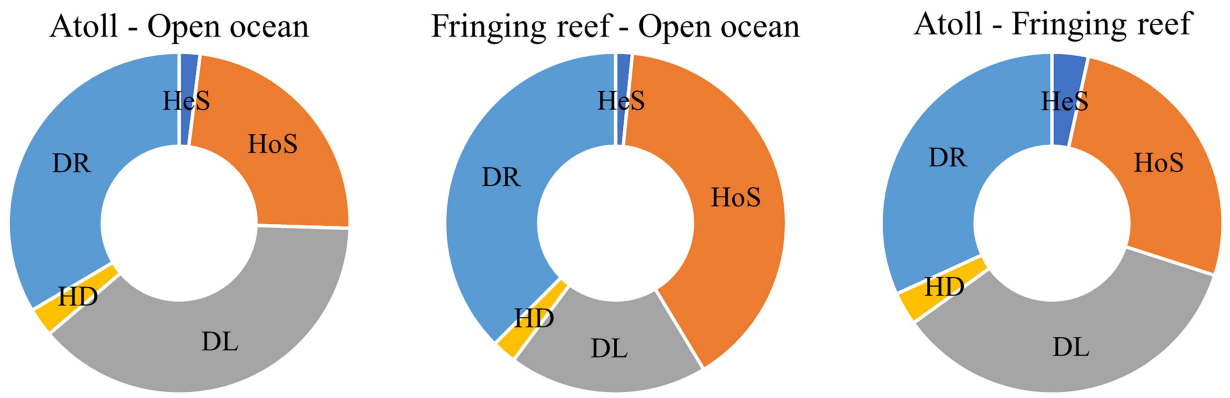

FIGURE 5
Relative importance of different ecological processes in different habitat types. HeS, Heterogeneous selection; HoS, Homogeneous selection; DL, Dispersal limitation; HD, Homogenizing dispersal; DR, Drift and others.

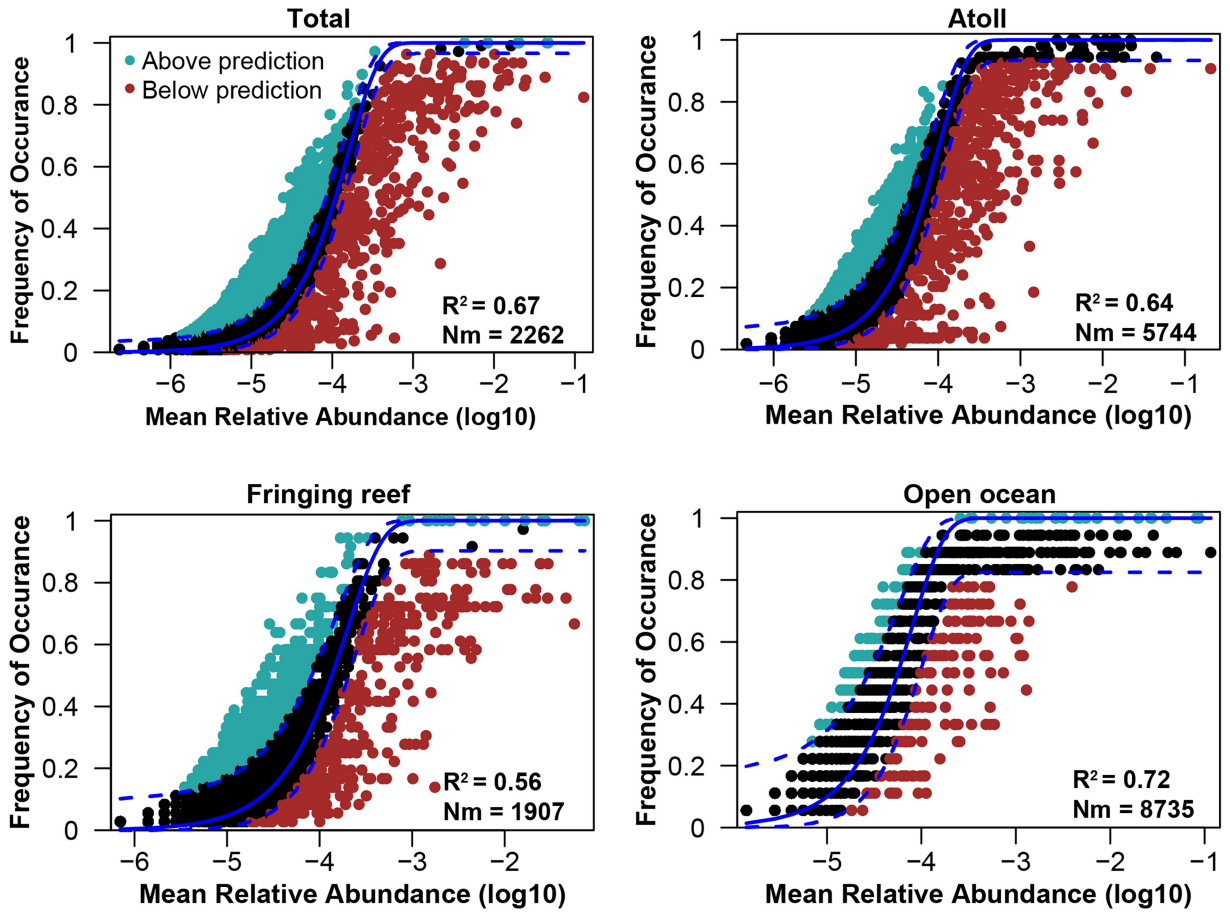

FIGURE 6
Fitting of the neutral model of bacterial community. R^2 indicates the fit to this model, Nm indicates the metacommunity size times immigration.

upper thermal limit (Frieler et al., 2013; Hughes et al., 2017). Temperature is an important factor that may alter community composition and diversity and is also a stronger driver than other environmental factors in shaping microbial community composition (Fuhrman et al., 2008; Sunagawa et al., 2015). The high abundance group *Cyanobacteria* which has a high optimal growth temperature, a major contributors to the primary productivity that enters the food web through microbial consumption processes (Sorokin and Sorokin, 2010; Visser et al., 2016). Thus, understanding the interactions between bacterioplankton and other microorganisms (e.g., microeukaryotes) is a longstanding challenge in microbial community ecology. It is noteworthy that environmental factors explained a significant portion of the community variance in the atoll and open ocean samples (Supplementary Table S3), and the variation of community turnover might also be strongly related to the variability of spatial structure between habitat types and dispersal limitation (Soininen et al., 2007). Environmental differences increase with the increasing geographical distance, and the difference of the community composition will enlarge with environmental changes (Huber et al., 2020).

It is important to note that other uninvestigated environmental and biological factors, such as tides, upwelling, surface wind and biotic interactions, along with different methodology, might lead to variations in microbial communities (Stachowicz, 2001; Monismith and Genin, 2004; Hancock et al., 2006; Falter et al., 2013; Payet et al., 2014). Previous studies suggest that the deterministic process is stronger at a larger scale and various environmental factors can influence bacterial diversity and communities (Shi et al., 2018; Huber et al., 2020; Wu et al., 2020). Microbes in adjacent sea areas are an indispensable part of the coral reef shared ecosystems, their species composition, richness, evenness, and interactions influence ecosystem properties (Hooper et al., 2005). Overall, to comprehensively understand bacterial community assembly mechanisms, the sampling scale effects (spatial extent and time scale), other potentially important explanatory deterministic factors (e.g., unmeasured environmental factors and species interactions), and other possible stochastic factors should be considered in future studies (Chen et al., 2019).

Conclusion

Our study showed that the photoautotrophic bacteria *Synechococcus* and *Prochlorococcus* were relatively abundant in the overlying water of the coral reef in the Xisha Islands, indicating their importance in the coral reef ecosystem. A distance-decay relationship for bacterial communities was observed in the study area, and the larger difference among atoll sites indicated that each atoll had its own individual characteristics even in bacterial community. Stochasticity played a more important role in bacterial community assembly in high homogeneous surface waters in the Xisha Islands. Collectively, the findings from this study contribute to gaining a deeper understanding of bacterial diversity and assembly in the coral reefs, and provide a valuable reference for further investigation of microbial biodiversity in coral reefs. In the future, state-of-the-art techniques—such as metagenomics, metaproteomics, as well as other meta-omics approaches—should be applied to investigate coral reef microbes to comprehensively explore species, genetic, and functional biodiversity. Such approaches will help to further advance our understanding of coral reef systems to enable their appropriate protection and remediation.

Data availability statement

The datasets presented in this study can be found in online repositories. The names of the repository/repositories and accession number(s) can be found in the article/Supplementary material.

Author contributions

D-ZW and H-PL developed the original research plan and revised the manuscript. P-FW, R-WZ, and YL implemented sampling, DNA extraction, and 16S rDNA sequencing. S-JL conducted the analyzes and drafted the manuscript with the help from Z-XX and LL. D-ZW and S-JL finalized the manuscript. All authors contributed to the article and approved the submitted version.

Funding

This work was supported by the Ministry of Science and Technology of the People's Republic of China (No. 2018YFC1406501).

Acknowledgments

We thank Jun Yang and his team members from the Institute of Urban Environment to help statistical analysis of this study as well as constructive comments and suggestions.

Conflict of interest

The authors declare that the research was conducted in the absence of any commercial or financial relationships that could be construed as a potential conflict of interest.

Publisher's note

All claims expressed in this article are solely those of the authors and do not necessarily represent those of their

affiliated organizations, or those of the publisher, the editors and the reviewers. Any product that may be evaluated in this article, or claim that may be made by its manufacturer, is not guaranteed or endorsed by the publisher.

Supplementary material

The Supplementary material for this article can be found online at: https://www.frontiersin.org/articles/10.3389/fmicb.2022.1059262/full#supplementary-material

References

Ainsworth, T. D., Thurber, R. V., and Gates, R. D. (2010). The future of coral reefs: a microbial perspective. *Trends Ecol. Evol.* 25, 233–240. doi: 10.1016/j.tree.2009.11.001

Bahram, M., Kohout, P., Anslan, S., Harend, H., Abarenkov, K., and Tedersoo, L. (2016). Stochastic distribution of small soil eukaryotes resulting from high dispersal and drift in a local environment. *ISME J.* 10, 885–896. doi: 10.1038/ismej.2015.164

Bell, T. (2010). Experimental tests of the bacterial distance-decay relationship. *ISME J.* 4, 1357–1365. doi: 10.1038/ismej.2010.77

Bourne, D. G., and Webster, N. S. (2013). "Coral reef bacterial communities" in *The prokaryotes*. eds. E. Rosenberg, E. F. Delong, S. Lory, E. Stackebrandt and F. Thompson (Berlin, Heidelberg: Springer Berlin Heidelberg), 163–187.

Brandl, S. J., Rasher, D. B., Côté, I. M., Casey, J. M., Darling, E. S., Lefcheck, J. S., et al. (2019). Coral reef ecosystem functioning: eight core processes and the role of biodiversity. *Front. Ecol. Environ.* 17, 445–454. doi: 10.1002/fee.2088

Campbell, L., Nolla, H. A., and Vaulot, D. (1994). The importance of *Prochlorococcus* to community structure in the central North Pacific Ocean. *Limnol. Oceanogr.* 39, 954–961. doi: 10.4319/lo.1994.39.4.0954

Charpy, L. (2005). Importance of photosynthetic picoplankton in coral reef ecosystems. *Vie Milieu* 55, 217–223.

Charpy, L., Casareto, B. E., Langlade, M. J., and Yoshimi, S. (2012). Cyanobacteria in coral reef ecosystems: a review. *J. Mar. Biol.* 2012, 1–9. doi: 10.1155/2012/259571

Chave, J. (2004). Neutral theory and community ecology. *Ecol. Lett.* 7, 241–253. doi: 10.1111/j.1461-0248.2003.00566.x

Chen, S., He, Y. B., Xie, Z. X., Kong, L. F., Yan, K. Q., Li, D. X., et al. (2021). Metaproteomics reveals nutrient availability shaping distinct microbial community and metabolic niche in the nutrient-depleted and replete layers of an oligotrophic euphotic zone. *Sci. Total Environ.* 774:145123. doi: 10.1016/j.scitotenv.2021.145123

Chen, W., Ren, K., Isabwe, A., Chen, H., Liu, M., and Yang, J. (2019). Stochastic processes shape microeukaryotic community assembly in a subtropical river across wet and dry seasons. *Microbiome* 7:138. doi: 10.1186/s40168-019-0749-8

Chen, S., Zhou, Y., Chen, Y., and Gu, J. (2018). Fastp: an ultra-fast all-in-one FASTQ preprocessor. *Bioinform.* 34, i884–i890. doi: 10.1093/bioinformatics/bty560

Chesson, P. (2000). Mechanisms of maintenance of species diversity. *Annu. Rev. Ecol. Syst.* 31, 343–366. doi: 10.1146/annurev.ecolsys.31.1.343

Clark, D. R., Underwood, G. J. C., McGenity, T. J., and Dumbrell, A. J. (2021). What drives study-dependent differences in distance–decay relationships of microbial communities? *Glob. Ecol. Biogeogr.* 30, 811–825. doi: 10.1111/geb.13266

Cleary, D. F. R., Polónia, A. R. M., Becking, L. E., de Voogd, N. J., Gomes, H., and Gomes, N. C. M. (2018). Compositional analysis of bacterial communities in seawater, sediment, and sponges in the Misool coral reef system. *Indones. Mar. Biodivers.* 48, 1889–1901. doi: 10.1007/s12526-017-0697-0

Cole, J. R., Wang, Q., Cardenas, E., Fish, J., Chai, B., Farris, R. J., et al. (2009). The ribosomal database project: improved alignments and new tools for rRNA analysis. *Nucleic Acids Res.* 37, D141–D145. doi: 10.1093/nar/gkn879

Crosbie, N. D., and Furnas, M. J. (2001). Abundance, distribution and flow-cytometric characterization of picophytoprokaryote populations in central (17°S) and southern (20°S) shelf waters of the great barrier reef. *J. Plankton Res.* 23, 809–828. doi: 10.1093/plankt/23.8.809

de Voogd, N. J., Cleary, D. F. R., Polónia, A. R. M., and Gomes, N. C. M. (2015). Bacterial community composition and predicted functional ecology of sponges, sediment and seawater from the thousand islands reef complex, West Java. *Indones. FEMS Microbiol. Ecol.* 91. doi: 10.1093/femsec/fiv019

Ding, J., Jiang, F., Li, J., Wang, Z., Sun, C., Wang, Z., et al. (2019). Microplastics in the coral reef systems from Xisha Islands of South China Sea. *Environ. Sci. Technol.* 53, 8036–8046. doi: 10.1021/acs.est.9b01452

Dini-Andreote, F., Stegen, J. C., van Elsas, J. D., and Salles, J. F. (2015). Disentangling mechanisms that mediate the balance between stochastic and deterministic processes in microbial succession. *Proc. Natl. Acad. Sci. U. S. A.* 112, E1326–E1332. doi: 10.1073/pnas.1414261112

Edgar, R. C. (2013). UPARSE: highly accurate OTU sequences from microbial amplicon reads. *Nat. Methods* 10, 996–998. doi: 10.1038/nmeth.2604

Falter, J. L., Lowe, R. J., Zhang, Z., and McCulloch, M. (2013). Physical and biological controls on the carbonate chemistry of coral reef waters: effects of metabolism, wave forcing, sea level, and geomorphology. *PLoS One* 8:e53303. doi: 10.1371/journal.pone.0053303

Ferrier-Pages, C., and Furla, P. (2001). Pico- and nanoplankton biomass and production in the two largest atoll lagoons of French Polynesia. *Mar. Ecol. Prog. Ser.* 211, 63–76. doi: 10.3354/meps211063

Ferrier-Pagès, C., and Gattuso, J. P. (1998). Biomass, production and grazing rates of pico-and nanoplankton in coral reef waters (Miyako Island. Japan). *Microb. Ecol.* 35, 46–57. doi: 10.1007/s002489900059

Flombaum, P., Gallegos, J. L., Gordillo, R. A., Rincón, J., Zabala, L. L., Jiao, N., et al. (2013). Present and future global distributions of the marine cyanobacteria *Prochlorococcus* and *Synechococcus*. *Proc. Natl. Acad. Sci. U. S. A.* 110, 9824–9829. doi: 10.1073/pnas.1307701110

Follows, M. J., and Dutkiewicz, S. (2011). Modeling diverse communities of marine microbes. *Annu. Rev. Mar. Sci.* 3, 427–451. doi: 10.1146/annurev-marine-120709-142848

Frade, P. R., Glasl, B., Matthews, S. A., Mellin, C., Serrão, E. A., Wolfe, K., et al. (2020). Spatial patterns of microbial communities across surface waters of the great barrier reef. *Commun. Biol.* 3:442. doi: 10.1038/s42003-020-01166-y

Frieler, K., Meinshausen, M., Golly, A., Mengel, M., Lebek, K., Donner, S. D., et al. (2013). Limiting global warming to 2 degrees C is unlikely to save most coral reefs. *Nat. Clim. Chang.* 3, 165–170. doi: 10.1038/nclimate1674

Fuhrman, J. A., Steele, J. A., Hewson, I., Schwalbach, M. S., Brown, M. V., Green, J. L., et al. (2008). A latitudinal diversity gradient in planktonic marine bacteria. *Proc. Natl. Acad. Sci. U. S. A.* 105, 7774–7778. doi: 10.1073/pnas.0803070105

Furby, K. A., Apprill, A., Cervino, J. M., Ossolinski, J. E., and Hughen, K. A. (2014). Incidence of lesions on Fungiidae corals in the eastern Red Sea is related to water temperature and coastal pollution. *Mar. Environ. Res.* 98, 29–38. doi: 10.1016/j.marenvres.2014.04.002

Ganesh, S., Bristow, L. A., Larsen, M., Sarode, N., Thamdrup, B., and Stewart, F. J. (2015). Size-fraction partitioning of community gene transcription and nitrogen metabolism in a marine oxygen minimum zone. *ISME J.* 9, 2682–2696. doi: 10.1038/ismej.2015.44

Ganesh, S., Parris, D. J., DeLong, E. F., and Stewart, F. J. (2014). Metagenomic analysis of size-fractionated picoplankton in a marine oxygen minimum zone. *ISME J.* 8, 187–211. doi: 10.1038/ismej.2013.144

Hancock, G. J., Webster, I. T., and Stieglitz, T. C. (2006). Horizontal mixing of great barrier reef waters: offshore diffusivity determined from radium isotope distribution. *J. Geophys. Res.* 111:C12019. doi: 10.1029/2006JC003608

Hanson, C. A., Fuhrman, J. A., Horner-Devine, M. C., and Martiny, J. B. (2012). Beyond biogeographic patterns: processes shaping the microbial landscape. *Nat. Rev. Microbiol.* 10, 497–506. doi: 10.1038/nrmicro2795

Hooper, D. U., Chapin Iii, F. S., Ewel, J. J., Hector, A., Inchausti, P., Lavorel, S., et al. (2005). Effects of biodiversity on ecosystem functioning: a consensus of current knowledge. *Ecol. Monogr.* 75, 3–35. doi: 10.1890/04-0922

Horner-Devine, M. C., Lage, M., Hughes, J. B., and Bohannan, B. J. M. (2004). A taxa–area relationship for bacteria. *Nature* 432, 750–753. doi: 10.1038/nature03073

Huber, P., Metz, S., Unrein, F., Mayora, G., Sarmento, H., and Devercelli, M. (2020). Environmental heterogeneity determines the ecological processes that govern bacterial Metacommunity assembly in a Floodplain River system. *ISME J.* 14, 2951–2966. doi: 10.1038/s41396-020-0723-2

Hughes, T. P., Huang, H., and Young, M. A. L. (2013). The wicked problem of china's disappearing coral reefs. *Conserv. Biol.* 27, 261–269. doi: 10.1111/j.1523-1739.2012.01957.x

Hughes, T. P., Kerry, J. T., Álvarez-Noriega, M., Álvarez-Romero, J. G., Anderson, K. D., Baird, A. H., et al. (2017). Global warming and recurrent mass bleaching of corals. *Nature* 543, 373–377. doi: 10.1038/nature2170

Ke, Z., Tan, Y., Huang, L., Liu, H., Liu, J., Jiang, X., et al. (2018). Spatial distribution patterns of phytoplankton biomass and primary productivity in six coral atolls in the central South China Sea. *Coral Reefs* 37, 919–927. doi: 10.1007/s00338-018-1717-7

Kemp, D. W., Rivers, A. R., Kemp, K. M., Lipp, E. K., Porter, J. W., and Wares, J. P. (2015). Spatial homogeneity of bacterial communities associated with the surface mucus layer of the reef-building coral Acropora palmata. *PLoS One* 10:e0143790. doi: 10.1371/journal.pone.0143790

Kleypas, J. A., McManus, J. W., and Menez, L. A. B. (1999). Environmental limits to coral reef development: where do we draw the line? *Am. Zool.* 39, 146–159. doi: 10.1093/icb/39.1.146

Laas, P., Ugarelli, K., Absten, M., Boyer, B., Briceño, H., and Stingl, U. (2021). Composition of prokaryotic and eukaryotic microbial communities in waters around the Florida reef tract. *Microorganisms* 9:1120. doi: 10.3390/microorganisms9061120

Liu, R., Wang, L., Liu, Q., Wang, Z., Li, Z., Fang, J., et al. (2018). Depth-resolved distribution of particle-attached and free-living bacterial communities in the water column of the New Britain trench. *Front. Microbiol.* 9:625. doi: 10.3389/fmicb.2018.00625

Magoč, T., and Salzberg, S. L. (2011). FLASH: fast length adjustment of short reads to improve genome assemblies. *Bioinformatics* 27, 2957–2963. doi: 10.1093/bioinformatics/btr507

Marie, D., Partensky, F., Vaulot, D., and Brussaard, C. (1999). Enumeration of phytoplankton, bacteria, and viruses in marine samples. *Curr. Protoc. Cytom.* Chapter 11:Unit 11.11. doi: 10.1002/0471142956.cy1111s10

Monismith, S. G., and Genin, A. (2004). Tides and sea level in the Gulf of Aqaba (Eilat). *J. Geophys. Res.* 109:C04015. doi: 10.1029/2003JC002069

Nelson, C. E., Alldredge, A. L., McCliment, E. A., Amaral-Zettler, L. A., and Carlson, C. A. (2011). Depleted dissolved organic carbon and distinct bacterial communities in the water column of a rapid-flushing coral reef ecosystem. *ISME J.* 5, 1374–1387. doi: 10.1038/ismej.2011.12

Ning, D., Yuan, M., Wu, L., Zhang, Y., Guo, X., Zhou, X., et al. (2020). A quantitative framework reveals ecological drivers of grassland microbial community assembly in response to warming. *Nat. Commun.* 11, 1–12. doi: 10.1038/s41467-020-18560-z

Oksanen, J., Blanchet, G. F., Friendly, M., Kindt, R., Legendre, P., McGlinn, D., et al. (2020). *Vegan: Community Ecology Package. R Package Version 2.5–7*. Available at: https://CRAN.R-project.org/package=vegan (Accessed November 22, 2021).

Padilla, C. C., Ganesh, S., Gantt, S., Huhman, A., Parris, D. J., Sarode, N., et al. (2015). Standard filtration practices may significantly distort planktonic microbial diversity estimates. *Front. Microbiol.* 6. doi: 10.3389/fmicb.2015.0054

Parada, A. E., Needham, D. M., and Fuhrman, J. A. (2016). Every base matters: assessing small subunit rRNA primers for marine microbiomes with mock communities, time series and global field samples. *Environ. Microbiol.* 18, 1403–1414. doi: 10.1111/1462-2920.13023

Payet, J. P., McMinds, R., Burkepile, D. E., and Vega Thurber, R. L. (2014). Unprecedented evidence for high viral abundance and lytic activity in coral reef waters of the South Pacific Ocean. *Front. Microbiol.* 5:493. doi: 10.3389/fmicb.2014.00493

Pendleton, L., Comte, A., Langdon, C., Ekstrom, J. A., Cooley, S. R., Suatoni, L., et al. (2016). Coral reefs and people in a high-CO_2 world: where can science make a difference to people? *PLoS One* 11:e0164699. doi: 10.1371/journal.pone.0164699

Quast, C., Pruesse, E., Yilmaz, P., Gerken, J., Schweer, T., Yarza, P., et al. (2013). The SILVA ribosomal RNA gene database project: improved data processing and web-based tools. *Nucleic Acids Res.* 41, D590–D596. doi: 10.1093/nar/gks1219

R Core Team (2014). *R: A Language and Environment for Statistical Computing*. R Foundation for Statistical Computing: Vienna, Austria.

Rädecker, N., Pogoreutz, C., Voolstra, C. R., Wiedenmann, J., and Wild, C. (2015). Nitrogen cycling in corals: the key to understanding holobiont functioning? *Trends Microbiol.* 23, 490–497. doi: 10.1016/j.tim.2015.03.008

Rahbek, C. (2005). The role of spatial scale and the perception of large-scale species-richness patterns. *Ecol. Lett.* 8, 224–239. doi: 10.1111/j.1461-0248.2004.00701.x

Rusch, D. B., Halpern, A. L., Sutton, G., Heidelberg, K. B., Williamson, S., Yooseph, S., et al. (2007). The sorcerer II global ocean sampling expedition: Northwest Atlantic through eastern tropical Pacific. *PLoS Biol.* 5:e77. doi: 10.1371/journal.pbio.0050077

Salazar, G., Cornejo-Castillo, F. M., Benitez-Barrios, V., Fraile-Nuez, E., Alvarez-Salgado, X. A., Duarte, C. M., et al. (2016). Global diversity and biogeography of deep-sea pelagic prokaryotes. *ISME J.* 10, 596–608. doi: 10.1038/ismej.2015.137

Shi, Y., Li, Y., Xiang, X., Sun, R., Yang, T., He, D., et al. (2018). Spatial scale affects the relative role of stochasticity versus determinism in soil bacterial communities in wheat fields across the North China plain. *Microbiome* 6, 27–12. doi: 10.1186/s40168-018-0409-4

Shi, Q., Liu, G. H., Yan, H. Q., and Zhang, H. L. (2012). Black disease (*Terpios hoshinota*): a probable cause for the rapid coral mortality at the northern reef of Yongxing Island in the South China Sea. *Ambio* 41, 446–455. doi: 10.1007/s13280-011-0245-2

Sloan, W. T., Lunn, M., Woodcock, S., Head, I. M., Nee, S., and Curtis, T. P. (2006). Quantifying the roles of immigration and chance in shaping prokaryote community structure. *Environ. Microbiol.* 8, 732–740. doi: 10.1111/j.1462-2920.2005.00956.x

Soininen, J., Mcdonald, R., and Hillebrand, H. (2007). The distance decay of similarity in ecological communities. *Ecography* 30, 3–12. doi: 10.1111/j.2006.0906-7590.04817.x

Somboonna, N., Wilantho, A., Assawamakin, A., Monanunsap, S., Sangsrakru, D., Tangphatsornruant, S., et al. (2014). Structural and functional diversity of free-living microorganisms in reef surface, Kra Island, Thailand. *BMC Genomics* 15:607. doi: 10.1186/1471-2164-15-607

Sorokin, Y. I., and Sorokin, P. Y. (2010). Plankton of the central great barrier reef: abundance, production and trophodynamic roles. *J. Mar. Biol. Assoc. U. K.* 90, 1173–1187. doi: 10.1017/S0025315410000597

Stachowicz, J. J. (2001). Mutualism, facilitation, and the structure of ecological communities: positive interactions play a critical, but underappreciated, role in ecological communities by reducing physical or biotic stresses in existing habitats and by creating new habitats on which many species depend. *Bioscience* 51, 235–246. doi: 10.1641/0006-3568(2001)051[0235:MFATSO]2.0.CO;2

Stegen, J. C., Lin, X., Fredrickson, J. K., Chen, X., Kennedy, D. W., Murray, C. J., et al. (2013). Quantifying community assembly processes and identifying features that impose them. *ISME J.* 7, 2069–2079. doi: 10.1038/ismej.2013.93

Sunagawa, S., Coelho, L. P., Chaffron, S., Kultima, J. R., Labadie, K., Salazar, G., et al. (2015). Structure and function of the global ocean microbiome. *Science* 348:1261359. doi: 10.1126/science.1261359

Suter, E. A., Pachiadaki, M., Taylor, G. T., Astor, Y., and Edgcomb, V. P. (2018). Free-living chemoautotrophic and particle-attached heterotrophic prokaryotes dominate microbial assemblages along a pelagic redox gradient. *Environ. Microbiol.* 20, 693–712. doi: 10.1111/1462-2920.13997

Tuomisto, H., Ruokolainen, K., and Yli-Halla, M. (2003). Dispersal, environment, and floristic variation of western Amazonian forests. *Science* 299, 241–244. doi: 10.1126/science.1078037

van Oppen, M. J. H., Bongaerts, P., Frade, P., Peplow, L. M., Boyd, S. E., Nim, H. T., et al. (2018). Adaptation to reef habitats through selection on the coral animal and its associated microbiome. *Mol. Ecol.* 27, 2956–2971. doi: 10.1111/mec.14763

Visser, P. M., Verspagen, J. M. H., Sandrini, G., Stal, L. J., Matthijs, H. C. P., Davis, T. W., et al. (2016). How rising CO2 and global warming may stimulate harmful cyanobacterial blooms. *Harmful Algae* 54, 145–159. doi: 10.1016/j.hal.2015.12.006

Wang, X. B., Lu, X. T., Yao, J., Wang, Z. W., Deng, Y., Cheng, W. X., et al. (2017). Habitat-specific patterns and drivers of bacterial beta-diversity in China's drylands. *ISME J.* 11, 1345–1358. doi: 10.1038/ismej.2017.11

Wang, D. R., Wu, Z. J., Li, Y. C., Chen, J. R., and Chen, M. (2011). Analysis on variation trend of coral reef in Xisha. *Acta. Ecol. Sin.* 31, 254–258. doi: 10.1016/j.chnaes.2011.06.005

Weber, L., González-Díaz, P., Armenteros, M., Ferrer, V. M., Bretos, F., Bartels, E., et al. (2020). Microbial signatures of protected and impacted northern Caribbean reefs: changes from Cuba to the Florida keys. *Environ. Microbiol.* 22, 499–519. doi: 10.1111/1462-2920.14870

Webster, N. S., Negri, A. P., Botté, E. S., Laffy, P. W., Flores, F., Noonan, S., et al. (2016). Host-associated coral reef microbes respond to the cumulative pressures of ocean warming and ocean acidification. *Sci. Rep.* 6:19324. doi: 10.1038/srep19324

Wu, P. F., Li, D. X., Kong, L. F., Li, Y. Y., Zhang, H., Xie, Z. X., et al. (2020). The diversity and biogeography of microeukaryotes in the euphotic zone of the northwestern Pacific Ocean. *Sci. Total Environ.* 698:134289. doi: 10.1016/j.scitotenv.2019.134289

Yang, Q., Dong, J., Zhang, Y., Ling, J., Wang, D., Wu, M., et al. (2015). Diversity analysis of diazotrophs associated with corals from Xisha and Sanya, South China Sea. *Aquat. Ecosyst. Health Manag.* 18, 433–442. doi: 10.1080/14634988.2015.1092850

Zhang, Y., Zhao, Z., Dai, M., Jiao, N., and Herndl, G. J. (2014). Drivers shaping the diversity and biogeography of total and active bacterial communities in the South China Sea. *Mol. Ecol.* 23, 2260–2274. doi: 10.1111/mec.12739

Zhou, J. Z., and Ning, D. L. (2017). Stochastic community assembly: does it matter in microbial ecology? *Microbiol. Mol. Biol. Rev.* 81:17. doi: 10.1128/MMBR.00002-17

Zuo, X., Su, F., Zhao, H., Zhang, J., Wang, Q., and Wu, D. (2017). Regional hard coral distribution within geomorphic and reef flat ecological zones determined by satellite imagery of the Xisha Islands, South China Sea. *Chin. J. Oceanol. Limn.* 35, 501–514. doi: 10.1007/s00343-017-5336-x

frontiers | Frontiers in Marine Science

TYPE Original Research
PUBLISHED 19 April 2023
DOI 10.3389/fmars.2023.1042527

OPEN ACCESS

EDITED BY
Ming Ma,
School of Pharmaceutical Sciences, Peking University, China

REVIEWED BY
Satya P. Singh,
Saurashtra University, India
Peng Jiang,
Institute of Oceanology (CAS), China

*CORRESPONDENCE
M. EL Bour
monia.elbour@instm.rnrt.tn

SPECIALTY SECTION
This article was submitted to Aquatic Microbiology, a section of the journal Frontiers in Marine Science

RECEIVED 12 September 2022
ACCEPTED 20 March 2023
PUBLISHED 19 April 2023

CITATION
Hmani I, Ktari L, Ismail A and EL Bour M (2023) Biotechnological potential of *Ulva ohnoi* epiphytic bacteria: enzyme production and antimicrobial activities. *Front. Mar. Sci.* 10:1042527. doi: 10.3389/fmars.2023.1042527

Biotechnological potential of *Ulva ohnoi* epiphytic bacteria: enzyme production and antimicrobial activities

I. Hmani, L. Ktari, A. Ismail and M. EL Bour*

Laboratory of Blue Biotechnology and Aquatic Bioproducts, National Institute of Marine Sciences and Technologies of Tunisia, Carthage University, Tunis, Tunisia

Seaweed surfaces harbor diverse epibiotic bacterial communities with functions related to morphogenesis, host health, and defense. Among seaweed holobionts, culturable strains can represent innovative sources of bioactive compounds and enzymes. The global industrial demand for microbial enzymes is continually growing in order to improve certain manufacturing processes with new perspectives of industrial exploitation. In this regard, the present study focuses on the enzymatic production and the antimicrobial activities of culturable epibiotic bacteria of *Ulva* from the Tunisian coast. Culturable associated bacteria were isolated and molecular identification was realized by 16S rRNA gene sequencing. For each strain, eight enzymatic activities were investigated: amylase, hemolysis, DNase, cellulase, lecithinase, lipase, gelatinase, and chitinase. The antimicrobial activity of *Ulva*-associated bacteria was evaluated against seven pathogenic bacteria, *Escherichia coli, Vibrio anguillarum, Vibrio alginoliticus, Pseudomonas aeruginosa, Aeromonas hydrophila, Salmonella typhymurium*, and *Staphylococcus aureus*, and one yeast, *Candida albicans*. The antibiotic resistance of isolated strains was determined for 15 commonly used antibiotics. The phylogenetic analysis revealed that the isolates belonged to Alphaproteobacteria (3), Gammaproteobacteria (5), Actinobacteria (3), and Firmicutes (4) phyllum. The majority of the isolates (66%) produced simultaneously more than one enzyme. Hemolysis was produced by 46.6% of isolates, while DNase was produced by 33% of strains. On the other hand, 13% of strains produced lecithinase, gelatinase, cellulase, and lipase. No chitinase was produced by the isolated bacteria. In addition, 60% of isolates displayed antimicrobial activity against at least one pathogenic strain. All *Ulva ohnoi*-associated bacteria were resistant to at least seven commonly used antibiotics. These results highlighted the occurrence of several enzymatic activities within *Ulva*-associated bacteria that can have potential uses in the industrial sector.

KEYWORDS

seaweed-epibiont, enzyme production, antimicrobial activity, bacterial phylogeny, antibiogram, *Ulva ohnoi*, antibioresistance

1 Introduction

Bacteria colonize almost all the planet's ecosystems; within the marine ecosystem, macro-organisms cannot live in total isolation and are exposed to bacteria. Each organism interacts directly and indirectly with its environment, and understanding the nature of interactions between organisms is a key step in the study of ecosystems and biological cycles. Marine bacteria draw the attention of marine specialists in the following aspects: biodiversity, recycling of waste and pollutants, remediation of polluted site, sustainable materials, and even renewable energy. Seaweed-associated bacteria interactions are an important component of the marine ecosystems. Understanding the mechanisms and pathways underlying these interactions is essential to explain the ecological distribution of bacteria, their physiology, and their responses to anthropogenic influences and environmental variations. It has been assumed for a long time that there is an association between algae and bacteria (Falkowski et al., 2004) and that they are the most abundant microorganisms on the algae's surface (Dobretsov and Qian, 2002). The host organism, also called basibiont, gives a suitable niche for the installation of associated bacteria (Califano et al., 2020) with optimal conditions for growth by providing oxygen, nutrients, and light. The associated bacteria provide hormones, vitamins, minerals, and carbon dioxide to its seaweed host (Martin et al., 2014; Kouzuma and Watanabe, 2015). Prior research confirmed that the composition and the nature of associated bacteria can be different from one seaweed to another and depends on the development stage of the alga (Ghaderiardakani et al., 2020; Qu et al., 2021).

Additionally, Ghaderiardakani et al. (2017) demonstrated that specific bacteria are essential to ensure proper algae growth and differentiation of stem and rhizoid cells. Recently, several studies highlighted the crucial and important role of *Ulva*-associated bacteria (Wichard et al., 2015; Weiss et al., 2017; Comba-González et al., 2021); in fact, special chemical mediators are used to ensure that the communication between alga and its associated bacteria and those mediators may be an important source of bioactive molecules and enzymes (Alsufyani et al., 2020).

The global industrial enzyme market is expected to grow from $5.5 billion in 2018 to $7.0 billion in 2023, according to Business Communication Company Research (BCC) (Guisan et al., 2020), which demonstrates how much this sector is important and also shows the increasing demand of the industry in enzymes that are recently used for eco-friendly textile processing (Kumar et al., 2021), drugs (Masci and Castagnolo, 2021), and bioremediation (Singh et al., 2021). Marine bacteria associated with algae are a potential source of new biomolecules having several biotechnological applications (Kandasamy et al., 2020; Kumar et al., 2022). They are an untapped source of enzymes; in fact, xylanases, amylases, and glycosidases are enzymes synthesized by bacteria associated with macroalgae (Chandrasekaran and Rajeev, 2010; Bakunina et al., 2012; Hehemann et al., 2014).

Marine bacteria have several uses (Samant et al., 2019); in fact, most enzymes used in different industries are of microbial origin and have specific characteristics, such as stability, high specific activity, and facilitated mass transfer. High-saline marine environments have proven to be a rich source of microorganisms harboring industrially important enzymes. Enzymes produced by marine microorganisms can provide numerous advantages compared to traditional enzymes due to their wide-ranging habitats. The quest for bacterial isolates producing enzymes with high efficacy and of commercial value is still ongoing to exploit enormous marine resources, one of which are marine macroalgae and bacteria associated with their surfaces, seaweeds – epiphytic bacteria are able to produce enzymes that are of biotechnological interest such as cellulases, lipases, amylases, agarases, laccases, and proteases (Comba-González et al., 2016).

Macroalgae, either green, red, or brown, can be the origin of a huge diversity of bacteria living on their surface. Ulva Linnaeus genus (Ulvales, Ulvophyceae) is commonly distributed in oceans and estuaries. It occupies the first 5 m of the marine areas' surfaces and can be found either in shallow water or in eutrophic zones. It is distinguished by a very thin thallus with a leaf-shaped, ribbon-like, or tubular form and green color that can be transparent under stress (Steinhagen et al., 2019). Currently, 102 species (accepted taxonomically) have been identified worldwide (Guiry and Guiry, 2022). Individuals of this genus are characterized by a broad range of environmental tolerance (Holzinger et al., 2015), high growth rate (Wichard et al., 2015), and photosynthetic activity leading to a relatively abundant natural biomass (Dominguez and Loret, 2019). The phylogenetic analysis of some *Ulva* sample on the Mediterranean Sea reports the presence of six non-indigenous species: *Ulva tepida, Ulva australis, Ulva californica, Ulva lactuca, Ulva chaugulii*. and *Ulva ohnoi*. The latter species *U. ohnoi* was found in the northern coast of Tunisia and it was previously described by Miladi et al. (2018) in Gabes (Southern cost of Tunisia).

In this study, the screening of *Ulva*-associated bacteria concerned different aspects from the molecular identification to biological activities. After bacterial sampling, a molecular identification for *Ulva*-associated bacteria was done, and then the antimicrobial activity was tested against pathogenic strains. In addition, the bioresistance of bacteria was tested and the enzymatic production was performed to test the production of amylase, hemolysis, DNase, cellulase, lecithinase, lipase, gelatinase, and chitinase. The main objectives of the present work are to isolate culturable *Ulva*-associated bacteria and evaluate their biological activities such as the capacity for enzyme production, antimicrobial activity, and their resistance to antibiotics.

2 Materials and methods

2.1 Isolation of bacterial strains and growth conditions

Ulva samples were collected from Ghar El Melh lagoon (37° 10'1.1568" N 10°10'54.9768" E) in May 2018 in shallow waters with an 18°C temperature and with 37‰ salinity. Sterile gloves and bags were used for sampling algae with the surrounding water to preserve the community of associated bacteria, which were then

transferred to the laboratory in a cooler. As the morphological identification of *Ulva* species can be tricky due to their phenotypic plasticity, the samples have been identified through DNA barcoding (Saunders and Kucera, 2010). A voucher specimen was kept in formaldehyde solution (2%).

Once in the laboratory, the samples were washed three times with autoclaved natural seawater to remove the non-attached bacteria (Burgess et al., 2003). Ten grams of seaweed was vortexed in a Stomacher for 6 min to detach surface-associated bacteria. Then, a 1-ml sample was taken for serial dilution up to 10^{-3} with sterile seawater. Under aseptic conditions, 100 µl of each dilution was spotted on marine agar (MA: Pronadisa Laboratories, CONDA) and then incubated in 20°C for 7 days at least for 1 month (Lemos et al., 1985).

Purification of bacteria was carried out and single colonies were selected based on morphological features and purified until pure cultures were obtained. Storage was done in stock solution made with glycerol 20% at −80°C. Thirty bacteria were isolated and 15 culturable bacteria were selected for the present study to carry out the different tests. Biochemical tests such as oxidase and catalase were performed according to Dalton et al. (1994).

2.2 Molecular identification of *Ulva*-associated bacteria

The molecular identification was carried out according to Ismail et al. (2018) using a single colony from each bacterium. 16S rRNA gene primers B8F (5′-AGAGTTTGATCMTGGCTCAG-3′) and U1492R (5′-GGTTACCTTGTTACGACTT-3′) were used. PCR reactions were performed using a Gene Biometra T1 DNA Thermal Cycler (Perkin-Elmer, USA) in 25-µl (final volume) reaction mixtures containing 0.1 µl of Hot Start DNA polymerase (Sigma), with each primer at a concentration of 10 pmol μl^{-1}, each deoxynucleoside triphosphate at a concentration of 10 mM, 2.5 µl of PCR buffer (with $MgCl_2$), and 1 µl of DNA template. The PCR protocol consisted of 40 cycles of denaturation at 94°C for 30 s, annealing at 55°C for 30 s, and extension at 72°C for 110 s. The cycles were preceded by 15 min of denaturation at 94°C and ended with a final extension for 7 min at 72°C. Negative controls contained all of the components of the PCR mixture except the DNA templates.

2.3 Phylogenetic analysis

The closest phylogenetic relatives of each isolate were identified by comparison of the 16S rRNA gene sequence to the National Center for Biotechnology Information (NCBI) GenBank database using the Basic Local Alignment Search Tool (BLAST) analysis tools (http://www.ncbi.nlm.nih.gov/BLAST). The phylogenetic analysis of isolates and close relative strains present in the NCBI nucleotide database was performed using the neighbor-joining method using MEGA software version 11 (Tamura et al., 2021). Numbers at nodes represent percentages of 1,000 bootstrap replications. The scale bar indicates mutations per nucleotide position.

2.4 Enzymatic production profile of *Ulva*-associated bacteria

2.4.1 Hemolysis

The hemolysis test was done in triplicate according to Satpute et al. (2008) with some modifications. Agar plates were prepared with horse blood; a streak of bacteria was added and incubated at 37°C. Results are observed after 48 to 72 h and distinguished with a colorless area.

2.4.2 DNase

This test was performed in triplicate on DNA agar medium with a single colony. After incubation for 48 h at 28°C, the surface of the agar was covered with the toluidine blue reagent, which makes it possible to demonstrate the presence or absence of DNA hydrolysis products. The pink halo around the culture means DNase positive; otherwise, it means DNase negative (Schreiber et al., 2016).

2.4.3 Lecithinase

The lecithinase test was carried out according to Garrity et al. (2010) by inoculating bacterial streaks on nutrient agar containing a sterile egg yolk emulsion followed by an incubation of 24 to 72 h at 30°C; this test was done in triplicate. Opaque areas in the transparent halo indicate degradation of the egg yolk lecithin by bacterial production of lecithinase enzyme.

2.4.4 Gelatinase

The gelatinase test was carried out on nutrient agar medium containing 1% gelatin (Smith and Goodner, 1958) in triplicate. Nutrient agar medium containing 1% gelatin was inoculated with the bacterial isolates and plates were incubated at 30 or 37°C for 2 to 5 days. For results, a solution of mercury chloride was used, which makes it possible to highlight the degradation of gelatin with a clear halo around the colonies.

2.4.5 Lipase

In triplicate, agar plates were prepared with tween 80 (Sierra, 1957) and then bacteria were streaked. The results of this test were readable after 24 h at 37°C through the formation of an opaque zone for lipase positive.

2.4.6 Amylase

This enzymatic test was carried out by preparing a specific starch agar according to Krishnan et al. (2011) in triplicate. Bacteria were inoculated in a single streak and then incubated for 24 to 72 h at 30°C. The hydrolysis of amylases was indicated by the presence of a clear zone around the colonies after the addition of lugol. The absence of staining around the culture shows the degradation of starch (amylase-positive bacteria) while areas containing starch stain brown (amylase-negative bacteria).

2.4.7 Cellulase

The cellulase test was carried out on agar prepared according to Sinha and Bedi (2018). The bacterial isolates were streaked on a plate and incubated for 72 h at 30°C. Afterwards, 1% Congo red

aqueous solution was added, which makes it possible to demonstrate the degradation of the cellulose after 15 min; this test was done in triplicate.

2.4.8 Chitinase

This test was carried out on nutrient agar supplemented with 1% chitin. After inoculation of bacteria in streaks, plates were incubated for 72 h at 30°C; this test was done in triplicate. The appearance of light areas around the colonies indicates the production of chitinase (Kaur et al., 2012). Diameters for all enzymatic activity were measured in centimeters. All tests were done in triplicate.

2.5 Antimicrobial activity of *Ulva*-associated bacteria

The drop test assay on Trypto-Casein-Soy agar (TSA) was used to test the antimicrobial activity of *Ulva*-associated bacteria against *Staphylococcus aureus* ATCC 25923, *Vibrio alginolyticus* ATCC 17749T and *Vibrio anguillarum* ATCC 12964T (clinical strain obtained from Pasteur Institute, Tunis), *Escherichia coli* ATCC 25922 and *Aeromonas hydrophila* B3 (fish pathogen obtained from RVAU-Denmark), *Salmonella typhimurium* C52 and *Pseudomonas aeruginosa* ATCC 27853 (clinical strain obtained from Laboratoire Hydrobiologie Marine et Continentale, Université de Montpellier II, France), *Vibrio alginolyticus* ATCC 17749T (clinical strain from Pasteur Institute, Tunis), and *Candida albicans* (yeast) ATCC 10231.

Fresh bacterial cultures of 24 h for both pathogenic and *Ulva*-associated strains were prepared for the antagonist test according to Rao et al. (2005) with modifications. The turbidity of the bacterial suspensions was adjusted to 0.5 McFarland. A drop of 0.5 cm of each bacterial suspension was placed in a petri dish containing the pathogenic bacteria grown on TSA. Agar plates were then incubated for 24 h at 20°C. Positive activity was obtained by the presence of a clear zone around the isolate and measured in millimeters. All tests were done in triplicate (n = 3).

2.6 Antibiotic resistance profile of *Ulva*-associated bacteria

Bacterial suspension in marine broth was prepared and several dilutions were applied to adjust the concentration to 0.5 McFarland. The culture is spread over the entire surface of Mueller-Hinton agar in order to obtain a homogeneous quantity of bacteria and left to dry. Using sterile forceps, antibiotic discs impregnated with standardized and fixed quantities of different antibiotics were placed in a petri dish. The following were the antibiotics used: azithromycin (AZM; 15 µg), spiramycin (SP; 100 µg), ceftazidime (CZD; 10 µg), ceftriaxone (CRO; 30 µg), vancomycin (VA; 30 µg), cefoxitin (FOX; 30 µg), ticarcillin (TIC; 75 µg), sulfonamides (SUL; 200 µg), amikacin (AN; 30 µg), gentamicin (GMN; 10 µg), kanamycin (KMN; 30 µg), chloramphenicol (C; 30 µg), tetracycline (TE; 30 µg), imipenem (IPM; 10 µg), and amoxicillin (AX; 25 µg). The antibiograms were incubated for 24 h at 20°C. Susceptibility measure for inhibitory zones in millimeters was evaluated in accordance with the standard measurement cited in Société Française de Microbiologie (2020) as sensitive (S), intermediary sensitive (I), and resistant (R). The multiple antibiotic resistance (MAR) index of the bacterial isolates was calculated based on the formula (Krumperman, 1983):

$$MAR\ index\ =\ NR/NT$$

where NR = number of antibiotics to which the isolate is resistant and NT = total number of antibiotics tested.

2.7 Statistical analysis

Data were analyzed by one-way analysis of variance (ANOVA), and significant differences at a level of 95% ($p< 0.05$) were determined by Tukey's test for the antimicrobial activity. Principal component analysis (PCA) for the enzymatic activity, antimicrobial activity, and antibiotic resistance of *Ulva*-associated bacteria was carried out to visualize the correlations and identify relationships between the different variables. For each strain, the capacity to give a positive result to a test has been taken into account. For antibiotic resistance, the index was calculated for each isolate by dividing the number of antibiotics to which the isolate is resistant by the total number of antibiotics tested (15), also defined as MAR (multiple antibiotic resistance) (Krumperman, 1983). The same principle has been applied for enzyme production and antibiotic activity. For each strain, "enzymatic capacity" was calculated by dividing the number of produced enzymes by the total number of enzymes tested (8), while "antimicrobial capacity" was calculated by dividing the number of inhibited bacteria by the total pathogenic bacteria used (8).

All statistical analyses were performed using XLSTAT 2021 by Addinsoft.

3 Results

3.1 Phylogenetic characterization of bacteria

Isolation of *Ulva*-associated bacteria led to the identification of 15 strains based on 16S rRNA gene sequencing. All nucleotide sequences of isolates were assigned to the GenBank database and were accession numbers (Table 1).

Acinetobacter was the predominant genus of the Gamma-Proteobacteria with three representative species followed by *Psychrobacter* with two representative species.

Most of *Ulva*'s isolates shared more than 98% identity with the identified closest matching strain except four strains (IH8, IH15, IH17, and IH3) that showed a lower identity percentage with the closest matching strain, leading to possible novel species or even a novel genus. The topology of the phylogenetic tree in Figure 1

10.3389/fmars.2023.1042527

TABLE 1 Epibiotic bacteria isolated from the *Ulva ohnoi* surface.

Isolates	Size (bp)	Closest species in NCBI	Standard strains accession number	Identity (%)	Accession number	Phylum	Oxydase	Catalase
IH25	850	*Dinoroseobacter shibae*	JQ660974	99	MZ150448	α-P	–	–
IH1	750	*Paracoccus marcusii*	MN931275	100	MZ150442		–	++
IH5	800	*Yoonia rosea*	MT406460	99	MZ150450		–	–
IH8	1,100	*Psychrobacter nivimaris*	KP717914	96	MZ150445	γ-P	–	–
IH24	850	*Psychrobacter celer*	MH256077	98	MZ150449		–	–
IH19	1,000	*Acinetobacter johnsonii*	MT226917	100	MZ150447		–	++
IH10	800	*Acinetobacter johnsonii*	MT226917	99	OL851810		–	–
IH15	1,145	*Acinetobacter johnsonii*	MN758792	95	MZ150452		–	++
IH17	600	*Exiguobacterium aestuarii*	MF426024	88	OL851812	F	–	++
IH7	800	*Enterococcus faecalis*	NR040789	100	MZ150446		–	–
IH21	900	*Alkalibacillus hwajinpoensis*	MT510155	99	MZ150451		–	–
IH3	161	*Enterococcus casseliflavus*	MT177112	92	OL851823		–	+
IH2	750	*Rathayibacter festucae*	MT431571	100	MZ150443	A	–	+
IH9	950	*Micrococcus aloeverae*	MZ496563	99	MZ150444		–	–
IH18	1,189	*Microbacterium phyllosphaerae*	MT533897	98	MZ150453		–	++

*α-P: α-proteobacteria, γ-P: γ-proteobacteria, F: firmicutes, A: actinobacteria, bp: base pair
Epibiotic bacteria isolated from the Ulva ohnoi sample were highly diverse. Most of the isolates (eight) belonged to Proteobacteria while four were Firmicutes and three of them belonged to Actinobacteria.

constructed with the neighbor-joining method shows the proximity of the isolated species in this study to the neighboring strains selected from the NCBI database in addition to the eight chosen strains previously isolated by Ismail et al. (2018) from *Ulva rigida* collected form Ghar El Melh or Cap Zebib. Interestingly, close matching occurred between IH1 and the isolate FN811323 from *Ulva* Cap Zebib (closely related to *Paracoccus* sp.). In addition, the position of *Acinetobacter* strains (IH10, IH15, and IH19) is close to *U. rigida* isolates from the same geographical area.

3.2 Enzymatic production

The majority of bacteria show enzymatic production. All the results obtained should be considered as preliminary screening. Thus, two-thirds of the isolated bacteria produced at least one enzyme as shown in Figure 2; some of them are able to produce several enzymes with a variety of functions (Supplementary Figure 1). Results of the enzymatic test show the following: 26% of isolates were able to produce amylase while only 33% can produce DNase; 13% of bacteria have lecithinase ability production; hemolysis is produced by 46% of bacteria; gelatinase, lipase, and cellulose were produced by 13% of tested bacteria; and no chitinase production was observed. Strains IH1 and IH2 demonstrated the ability to produce five enzymes among eight

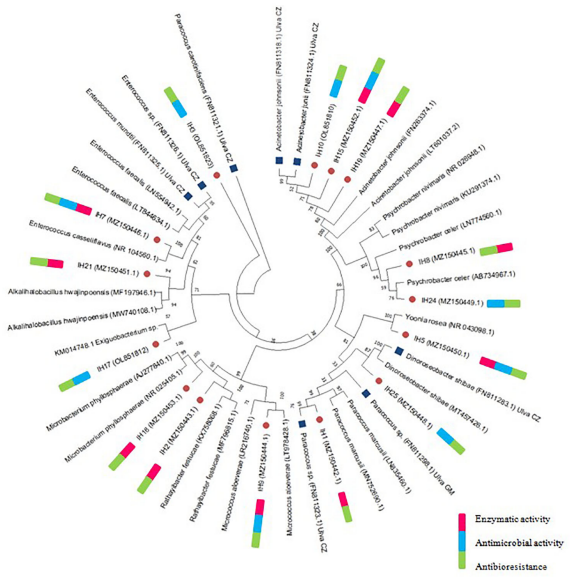

FIGURE 1
Neighbor-joining phylogenetic tree based on 16S rRNA gene sequences and different enzymatic and antimicrobial activities in comparison with isolates of *Ulva rigida* from Ismail et al. (2018): associated bacteria isolated from *Ulva ohnoi* (red spots) and *Ulva rigida*-associated bacteria (blue squares).

10.3389/fmars.2023.1042527

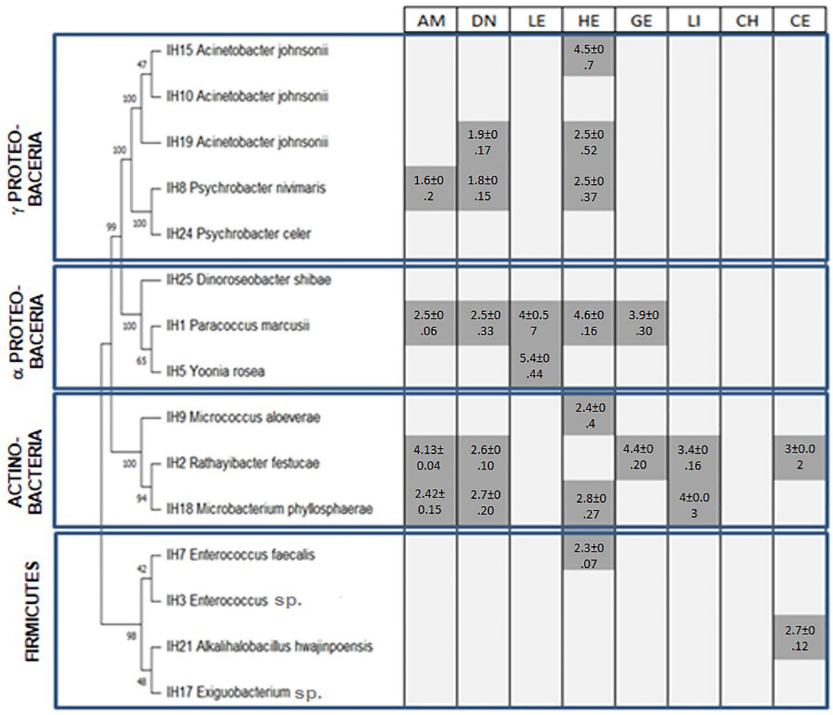

FIGURE 2
Enzymatic production of *Ulva ohnoi*-associated bacteria (dark gray is for production of enzyme, light gray is for no enzyme production, numbers are activity diameter expressed in cm) AM, amylase; HE, hemolysis; DN, DNase; CE, cellulase; LE, lecithinase; LI, lipase; GE, gelatinase; and CH, chitinase.

tested, followed by IH18, which showed the ability to produce four enzymes (amylase, DNase, hemolysis, and lipase). Seven strains were positive for hemolysis production: IH1, IH7, IH8, IH9, IH15, IH18, and IH19 with diameters of 4.6, 2.3, 2.5, 2.4, 4.5, 2.8, and 2.5 cm, respectively, while five strains were able to degrade DNA (IH1, IH2, IH8, IH18, and IH19) with diameters of 2.5, 2.6, 1.8, 2.7, and 1.9 cm, respectively. IH1 and IH2 are able to produce gelatinase with diameters of 3.9 and 4.4 cm. Cellulase was produced by both IH2 (3 cm) and IH21 (2.7 cm). Lecithinase is produced by IH1 and IH5 with diameters of 4 and 5.4 cm, respectively. IH2 and IH18 are able to produce lipase with diameters of 3.4 and 4 cm. All *Ulva* isolates were not able to produce chitinase.

3.3 Antimicrobial activities of *Ulva ohnoi*-associated bacteria

Antimicrobial activity obtained for isolated strains is presented in Table 2. Out of 15 strains, 9 displayed antimicrobial activity against pathogenic strains: 3 γ-Proteobacteria (IH24, IH10, and IH15), 3 Firmicutes (IH7, IH3, and IH17), 2 α-Proteobacteria (IH5 and IH25), and 1 Actinobacteria (IH9).

According to the results presented in Table 2, IH17 (closely related to *Exiguobacterium* sp.) was the most active stain inhibiting the growth of all the pathogenic tested strains except *S. aureus* and possesses the strongest antimicrobial activity as shown by the

TABLE 2 Antimicrobial activity of *Ulva ohnoi*-associated bacteria against pathogenic strains (mm).

ID	*C. a*	*V. an*	*S. t*	*P. a*	*V. al*	*E. c*	*A. h*	*S. a*
IH3	10.6 ± 0.8^{a}	10.3 ± 2.3^{a}	13 ± 2.8^{a}	12.7 ± 1.4^{a}	12.5 ± 1.7^{a}	9.9 ± 0.8^{a}	–	–
IH5	–	–	–	–	11 ± 1.6	–	–	–
IH7	–	–	–	–	9 ± 1.1	–	–	–
IH9	10 ± 1^{c}	10.8 ± 1.1^{bc}	13.2 ± 0.8^{a}	12.6 ± 0.8^{ab}	12 ± 0.5^{ab}	10.9 ± 0.6^{bc}	–	–
IH10	–	–	–	–	–	–	13.6 ± 1.3	–
IH15	9.5 ± 1.2^{b}	–	10 ± 1.1^{ab}	11.9 ± 1.3^{a}	10.3 ± 0.4^{ab}	–	–	–
IH17	10 ± 0.6^{b}	11.7 ± 0.7^{ab}	10.7 ± 2.9^{ab}	10 ± 1.3^{b}	11.4 ± 0.4^{ab}	10.5 ± 1.4^{ab}	13.8 ± 0.2^{a}	–
IH24	–	–	–	9.7 ± 0.3	–	–	–	–
IH25	–	–	–	9 ± 1	–	–	–	–

C. a: *Candida albicans*; V. an: *Vibrio anguillarum*; -: no activity; ± standard deviation; and n = 3; Values with the same letter are not significantly different at the level of 5% ($p < 0.05$).

10.3389/fmars.2023.1042527

inhibition diameter of 13.8 ± 0.02 against *A. hydrophila* with high significant variances at 95% confidence level. In addition, isolate IH3 (closely related to *Enterococcus casseliflavus*) displayed antimicrobial inhibition against five pathogenic bacteria and the yeast *C. albicans*. *Enterococcus faecalis* (IH7) inhibited the growth of *V. alginoliticus*. Fifty-five percent of the total active strains were isolated, and a significant variance exists for *Acinetobacter johnsonii* (IH10); however, *Yoonia rosea Acinetobacter* sp. (H15), *Psychrobacter celer* (IH24), and *Dinoroseobacter shibae* (IH25) were not significantly different.

Micrococcus aloeverae (IH9) showed a significant antimicrobial inhibition zone with a high significant variance at the level of 5%. *C. albicans* was inhibited by IH3, IH9, IH15, and IH17; on the other hand, *E. coli* was sensitive against IH3, IH9, and IH17; *S. typhymurium* was inhibited by four bacteria: IH3, IH9, IH15, and IH17. The pathogenic strain *V. anguillarum* was sensitive to three bacteria isolated from *Ulva*, IH3, IH9, and IH17, while *P. aeruginosa* and *V. alginoliticus* were the most sensitive pathogenic strains inhibited by six tested bacteria. *A. hydrophila* was less sensitive against the tested strains; it was inhibited only by two bacteria, *A. johnsonii* (IH10) and *Exiguobacterium* sp. (IH17).

3.4 Antibiotic resistance

Figure 3 presents the antibiotic resistance profile of the *U. ohnoi*-associated isolates.

All strains were resistant to spiramycin, cefoxitin, ticarcillin, and amoxicillin, while most of the strains were susceptible to vancomycin except IH25 (*D. shibae*), IH1 (*Paracoccus marcusii*), IH2 (*Rathayibacter festucae*), and IH18 (*Microbacterium phyllosphaerae*). The calculated MAR index for *Ulva*-associated bacteria ranged from 0.46 to 0.93, with 50% of the strains showing a very high resistance profile with an MAR index of 0.93 (Figure 3). Strains IH15, IH10, IH8, IH24 IH5, IH7, and IH17 presented the highest MAR index, while strain IH18 had the lowest one.

The PCA performed on enzymatic production (EA), antimicrobial activity (AA), and antibiotic resistance (AR) of bacterial strains led to the opposite loading of EA and AA, depicting an opposite correlation between them (Figure 4). Strains displaying antimicrobial activity presented a lower capacity to produce enzymes while enzyme-producing strains displayed few or no antimicrobial activity against the pathogenic strains tested. The PCA shows that there are three main clusters confirmed by the dissimilarity tree (Figure 4). The first cluster concerns the bacteria that are on the higher side of the second principal component, carried by AR and present high MAR indexes. It is composed of seven strains: IH10 (*A. johnsonii*), IH5 (*Yoonia rosea*), IH7 (*Enterococcus faecalis*), IH24 (*Psychrobacter celer*), IH21 (*Alkalihalobacillus hwajinpoensis*), IH19 (*A. johnsonii*), and IH8 (*Psychrobacter* nivimaris). The second cluster concerns strains with significant antimicrobial activity and characterized by three strains, IH17 (*Exiguobacterium* sp.), IH3 (*Enterococcus* sp.), and IH9 (*Micrococcus aloeverae*). These strains also have a high MAR index. The last group of isolates is represented by mainly two strains, IH1 (*P. marcusii*) and IH18 (*M. phyllosphaerae*), and these strains have a high enzyme production capacity while displaying no antimicrobial activity and the lowest MAR index.

4 Discussion

The *Ulva* surface represents a large and precious ecological niche for the installation of biofilm. Algae thallus can be colonized by Proteobacteria, Firmicutes, and Actinobacteria.

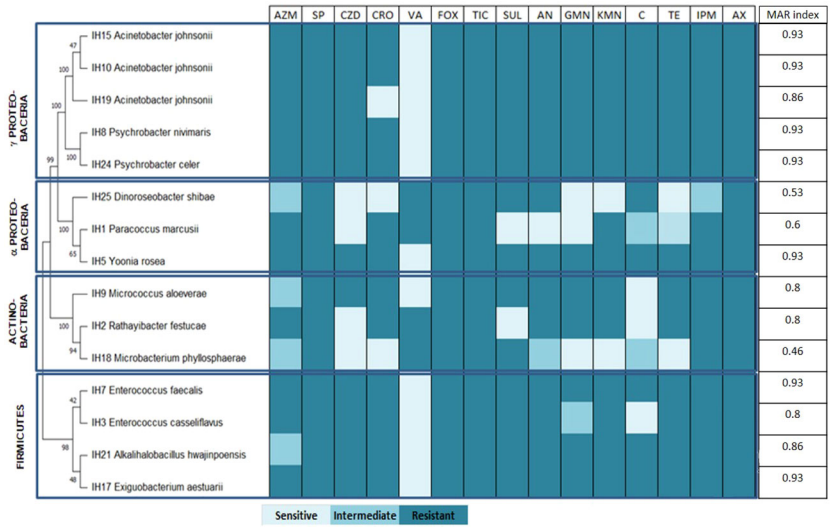

FIGURE 3
Antibiotic resistance profile of *Ulva ohnoi*-associated bacteria. AZM, azithromycin; SP, spiramycin; CZD, ceftazidime; CRO, ceftriaxone; VA, vancomycin; FOX, cefoxitin; TIC, ticarcillin; SUL, sulfonamides; AN, amikacin; GMN, gentamicin; KMN, kanamycin; C, chloramphenicol; TE, tetracycline; IPM, imipenem; AX, amoxicillin.

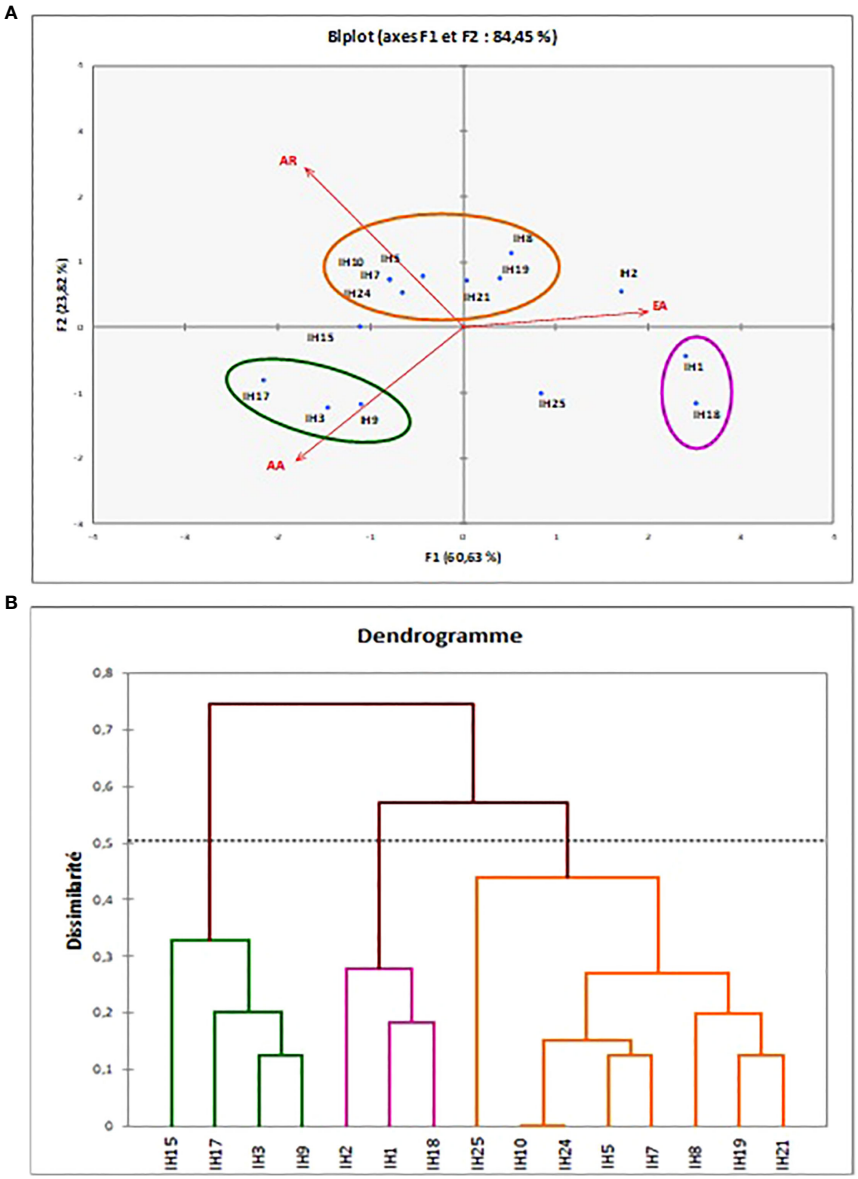

FIGURE 4
Different clusters obtained for the enzymatic, antimicrobial, and antibiotic resistance tests of *Ulva ohnoi*-associated bacteria strains obtained by PCA **(A)** and dissimilarity tree **(B)**.

In the present study, Proteobacteria was the most represented taxonomic group (53%) of the total identified strains. This result is in accordance with literature reporting Proteobacteria generally being the most abundant taxonomic group on seaweed surfaces (Ismail et al., 2018). More specifically, Burke et al. (2011) showed that the clade of Proteobacteria are more likely associated with green macroalgae.

Two subclasses were found to be associated with *U. ohnoi*, the α-Proteobacteria represented by strains closely related to *D. shibae*, *P. marcusii*, and *Yoonia rosea*, and the γ-Proteobacteria represented by isolates closely related to *A. johnsonii. Psychrobacter celer* and *Psychrobacter nivimaris* Actinobacteria representatives occupied a minor proportion of isolated bacteria with 3 strains out of 15. These findings are in agreement with those of Choi et al. (2016) who found a few representatives of Actinobacteria (4%) among *Ulva pertusa*-associated strains.

In a previous study conducted by Ismail et al. (2018), epiphytic bacteria isolated from *U. rigida* collected from the same sampling site, Ghar El Melh, were identified. Among the isolated strains, these authors identified one strain closely related to *Paracoccus* sp. Interestingly, *Paracoccus* sp. have been described to have growth-promoting and morphogenesis-inducing function in *Ulva* (Ghaderiardakani et al., 2017). In this study, isolate IH1 has been found to belong to *Paracoccus* genus, supporting that species of this genus belong to the resident flora of epiphytic community of *Ulva* sp. in Ghar El Melh Lagoon.

Similarly, strains closely related to *D. shibae* were isolated from both Ghar El Melh Lagoon samples *U. rigida* (Ismail et al., 2018)

and *U. ohnoi* (present study). This species belongs to the Roseobacter group, which have been described as playing an important role in host health by producing bioactive secondary metabolites (Tujula et al., 2010; Wienhausen et al., 2017).

Except for these two species described above (*Paracoccus* sp. and *D. shibae*), all other isolates were different from Ismail et al. (2018) *U. rigida* isolates. This finding is in accordance with Lachnit et al. (2011) who demonstrated that at different sampling intervals, epibacterial community profiles differ significantly at a bacterial phylum level among algal species.

As most enzymes used in different industries are of microbial origin, associated bacteria with sedentary marine organisms including seaweeds represent an important reservoir as a novel source of industrial enzymes with possible commercial applications (Mohapatra et al., 2003). In this study, majority of *U. ohnoi* culturable associated isolates had the capacity to produce at least one extracellular enzyme. Enzymes isolated from marine bacteria attract the attention of several researchers, which is due to their availability and cheap production from marine bacteria.

Comba-González et al. (2016) highlighted several enzymes of biotechnological interest potentially produced by epiphytic bacteria associated with *Ulva* including lipase and amylase. In the present study, *R. festucae* and *M. phyllosphaerae* displayed lipolytic ability and can be a potential source for lipase production in several fields. For instance, lipases are used in nanomedicine (Khan et al., 2017), the cheese industry (Kumar and Ray, 2014), animal feed (Ferreira-Dias et al., 2013), and the biodiesel industry (Najjar et al., 2021). Joseph and Ramteke (2013) reported the production of lipase by *M. phyllosphaerae* and its possible use as a detergent additive. To the best of our knowledge, *R. festucae* is described for the first time as capable of synthesizing lipase.

Four isolates were found to be capable of producing amylase. Microbial amylases have a wide range of applications in several industries such as food, textile, or biofuel (Raveendran et al., 2018). Amylases are enzymes used in starch conversion (Van der Maarel et al., 2002), the detergent industry (Gupta et al., 2003), and the textile industry (Feitkenhauer, 2003). Matsumoto et al. (2003) highlighted the potential use amylase produced by the marine bacteria *Pseudoalterimonas undina* isolated from green microalgae for ethanol production. On the other hand, Kalpana et al. (2012) confirm that α-amylase from *Bacillus subtilis* is used against biofilm-forming human bacterial pathogens.

Another enzyme of interest is extracellular cellulase, which has several biotechnological applications in the food industry and textile (Raveendran et al., 2018). Two isolates, IH2 and IH21, closely related to *R. festucae* and *Alkalibacillus hwajinpoensis* presented cellulase production ability. All these findings confirm the potential use of *U. ohnoi* epiphytic bacteria for several industrial applications.

Isolates IH1 and IH5 identified as *P. marcusii* and *Yoonia rosea*, respectively, produce lecithinase and the two isolates IH1 and IH2 were found to be positive for gelatinase. Lecithinase is a type of phospholipase that acts upon lecithin; in the present study, two strains produce this enzyme, which are *P. marcusii* and *Yoonia rosea*. This enzyme is used as antibodies in serum according to the study of Kyle et al. (1971). For gelatinase, it has several applications in the culinary industry and pharmaceutical products, and it is also an essential ingredient in the food industry. To the best of our knowledge, this is the first mention of gelatinase production from *Ulva*-associated bacteria.

DNase is also recommended for the degradation of biofilm associated with the most common upper respiratory tract diseases, which is chronic rhinosinusitis (Shields et al., 2013), and interestingly, in the present study, five bacteria produce DNase and can be valuable source for the extraction of this enzyme.

Seaweed-associated bacteria have the ability to produce active enzyme carbohydrates; in fact, seaweeds present approximately half of the global primary production and contribute to the production of large amounts of polysaccharides that will be consumed by microbes that utilize carbohydrate-active enzymes (CAZymes) able to degrade agars, carrageenan, alginate, and ulvan-polysaccharides from red, brown, and green algae as described by Hehemann et al. (2014).

Hemolytic ability screening allowed the identification of seven isolates with the ability to destroy red blood cells. Among these strains, *P. marcusii* (IH1) is in agreement with the hemolysis ability being commonly observed within *Paracoccus* spp. (Leinberger et al., 2021). The screening of the hemolysis ability degradation of 15 bacterial isolates collected from seawater, sediment, and shell samples from the Indian coasts shows that 12 isolates have α-hemolytic activity according to Satpute et al. (2008), which in accordance with our finding where majority of the strains (8 out of 15) demonstrated hemolysis capacity.

U. ohnoi-associated strains in the present study were not able to produce chitinase. Naik et al. (2019) obtained chitinase production from *Ulva*-associated bacteria and suggested the possible use of bacterial genes to enhance the degradation of crab shell.

Concerning the antimicrobial activity of *U. ohnoi*-associated bacteria, nine strains displayed positive activity in the present study. This result is in agreement with that found by Ismail et al. (2018) and Wu et al. (2014) who showed that several bacterial strains isolated from *Ulva* surface have an important antimicrobial activity. Accordingly, these authors described significant antibacterial activity for the isolate *D.* shibae, which has been found to be closely related to IH25. Contrary to our findings, *P. marcusii* isolated from a crustacean displayed antibacterial activity (Leinberger et al., 2021). This difference may be due to the biotic or abiotic conditions as bacterial metabolism is dynamic and flexible, depending on the host and environmental conditions, and will lead to different metabolic capacities (Passalacqua et al., 2016).

Dhanya et al. (2016) and Trivedi et al. (2011) demonstrated not only that *Ulva*-associated bacteria have antimicrobial activity but also that its endophytes can display significant antibacterial properties against human pathogens like *Staphylococcus aureus*, *Escherichia coli*, *Pseudomonas aeruginosa*, *Salmonella typhymurium*, or *Bacillus subtilis* and maybe a new source for drug research against multidrug-resistant pathogens.

The intense use of antibiotics allows the bacteria to acquire a certain resistance due to gene modifications (Munita and Arias, 2016). Antibiotic resistance is a global phenomenon; resistance to

anti-infectives could be responsible for more than 10 million deaths per year and thus might become the major cause of death by 2050 according to O'Neill (2016). Currently, humans are consuming 37 antibiotics used in aquaculture farms *via* seafood composed of shrimp, crab, mollusks, and fish (Hui et al., 2015), which increase bioresistance to these antibiotics.

On the other hand, not only did bioresistance increase but also some pathogenic bacteria became resistant due to the wide use of antibiotics (Miranda et al., 2018). Until now, the antibiotic resistance of bacteria from marine environment is very little studied. In particular, this is the first report of antibiotic resistance of bacterial strains associated with the green alga *U. ohnoi*. A better knowledge of environmental resistance could be of great importance to predict the emergence of new resistance of clinical concern (Lupo et al., 2012). Results obtained demonstrated the multiple drug resistance profile of *Ulva*-associated bacteria, suggesting their adaptation and ability to encode antibiotic resistance genes. In the present study, three *Acinetobacter* of marine origin were mentioned, and they are all resistant to all the antibiotics except vancomycin. The same genus is clinically important in terms of causing several infections; in fact, Gupta et al. (2015) studied this genus isolated from human origin, and they show that this group is highly resistant to several antibiotics especially ceftriaxone and ceftazidime.

The *Acinetobacter* genus either of marine origin or of clinical origin is always resistant to antibiotics. Tetracyclines are antibiotics used in aquaculture especially for fish farming of salmon (Higuera-Llanten et al., 2018); in the present study, all γ-Proteobacteria and Firmicutes were resistant to this antibiotic.

Compared with Ktari et al. (2022), the MAR index of *A. taxiformis*-associated bacteria ranged from 0.11 to 0.78, with more than 60% of strains showing resistance to antibiotics. However, in the present study, the MAR index was between 0.46 and 0.93, which shows that bacteria isolated from *Ulva* thallus were more resistant to antibiotics; this resistance may be due to a high level of expose to antibiotics through anthropic pollution characterizing the sampling site Ghar El Melh lagoon. In fact, wastewater from the urban area of the Ghar El Melh region is poured directly into the lagoon without treatment, and the water quality and the vegetation of the lagoon have changed considerably over the years according to Moussa et al. (2005).

The functional role of associated bacteria in maintaining their host health has been described in several studies leading to the holobiont concept (Egan et al., 2013; Ghaderiardakani et al., 2020). Ghaderiardakani et al. (2017) demonstrated in *Ulva* holobiont that there are always specific strains with functions related to growth and morphological development. These authors identified *Microbacterium* sp. and *Paracoccus* sp. among the strains that have an algal morphogenesis-inducing function. Interestingly, our finding showed that IH1 and IH18 closely related to *P. marcusii* and *M.* phyllosphaerae, respectively, were grouped in the same cluster. These two strains displayed high enzymatic production capacity and no antimicrobial activity and had a lower multidrug-resistant index. In fact, enzymes produced by bacteria do not necessarily have antibiotic activity, and each strain has a particular interest that benefits the host.

5 Conclusion

U. ohnoi-associated bacteria were screened for their enzymatic production, antimicrobial potential, and antibiotic resistance. Fifteen strains were phylogenetically identified and analyzed. Isolates belonged to three major phyla: Proteobacteria, Firmicutes, and Actinobacteria. The enzymatic production of *Ulva* epiphytes was studied and showed that 67% of the tested bacteria produce enzymes that can be useful in several industrial fields like food, pharmacology, textile, and biofuel. Nevertheless, the development and application of the enzymes need further quantitative evaluation. On the other hand, nine bacteria strains displayed antibacterial activity. This study highlighted that *Ulva*-associated bacteria can potentially contribute to the development of different industrial sectors.

Data availability statement

The datasets presented in this study can be found in online repositories. The names of the repository/repositories and accession number(s) can be found in the article/Supplementary Material.

Author contributions

IH – carried out the experiment and drafted the first version of the manuscript. AI – supervised molecular analysis and provided critical feedback. LK and MEB supervised, reviewed and edited the manuscript. All authors contributed to the article and approved the submitted version.

Conflict of interest

The authors declare that the research was conducted in the absence of any commercial or financial relationships that could be construed as a potential conflict of interest.

Publisher's note

Supplementary material

The Supplementary Material for this article can be found online at: https://www.frontiersin.org/articles/10.3389/fmars.2023.1042527/full#supplementary-material

References

Alsufyani, T., Califano, G., Deicke, M., Grueneberg, J., Weiss, A., Engelen, A. H., et al. (2020). Macroalgal–bacterial interactions: identification and role of thallusin in morphogenesis of the seaweed ulva (Chlorophyta). *J. Exp. Bot.* 71, 3340–3349. doi: 10.1093/jxb/eraa066

Bakunina, I., Nedashkovskaya, O., Kim, S., Zvyagintseva, T., and Mikhailov, V. (2012). Distribution of α-n-acetylgalactosaminidases among marine bacteria of the phylum bacterioidetes, epiphytes of marine algae of the seas of Okhotsk and Japan. *Microbiology* 81, 373–378. doi: 10.1134/S0026261712030022

Burgess, J. G., Boyd, K. G., Armstrong, E., Jiang, Z., Yan, L., Berggren, M., et al. (2003). The development of a marine natural product-based antifouling paint. *Biofouling* 19, 197–205. doi: 10.1080/0892701031000061778

Burke, C., Steinber, P., Rusch, D., Kjelleberg, S., and Thomas, T. (2011). Bacterial community assembly based on functional genes rather than species. *Proc. Natl. Acad. Sci. U.S.A.* 108, 14288–14293. doi: 10.1073/pnas.1101591108

Califano, G., Kwantes, M., Abreu, M. H., Costa, R., and Wichard, T. (2020). Cultivating the macroalgal holobiont: effects of integrated multi-trophic aquaculture on the microbiome of *Ulva rigida* (chlorophyta). *Front. Mar. Sci.* 7. doi: 10.3389/fmars.2020.00052

Chandrasekaran, M., and Rajeev, K. (2010). Marine microbial enzymes. *Biotechnology.* 9, 1–15.

Choi, H. R., Park, S. H., Kim, D. H., Kim, J. Y., and Heo, M. S. (2016). Analysis of the phylogenetic diversity and community structure of marine bacteria inhabiting *Ulva pertusa.* J. *Life. Sci.* 26, 819–825. doi: 10.5352/JLS.2016.26.7.819

Comba-González, N. B., Niño Corredor, A. N., López Kleine, L., and Castaño, D. M. (2021). Temporal changes of the epiphytic bacteria community from the marine macroalga *Ulva lactuca* (Santa Marta, Colombian-Caribbean). *Curr. Microbiol.* 78, 534–543. doi: 10.1007/s00284-020-02302-x

Comba-González, N. B., Ruiz-Toquica, J. S., López-Kleine, L., and Montoya-Castaño, D. (2016). Epiphytic bacteria of macroalgae of the genus ulva and their potential in producing enzymes having biotechnological interest. *J. Mar. Biol. Oceanogr.* 5, 2. doi: 10.4172/2324-8661.1000153

Dalton, H. M., Poulsen, L. K., Halasz, P., Angles, M. L., Goodman, A. E., and Marshall, K. C. (1994). Substratum induced morphological changes in a marine bacterium and their relevance to bioflm structure. *J. Bacteriol* 176, 6900–6906. doi: 10.1128/jb.176.22.6900-6906.1994

Dhanya, K. I., Swati, V. I., Vanka, K., and Osborne, J. (2016). Antimicrobial activity of *Ulva reticulata* and its endophytes. *J. Ocean. Univ. China.* 15, 363–369. doi: 10.1007/s11802-016-2803-7

Dobretsov, S. V., and Qian, P. Y. (2002). Effect of bacteria associated with the green alga *Ulva reticulata* on marine micro-and macrofouling. *Biofouling.* 18, 217–228. doi: 10.1080/08927010290013026

Dominguez, H., and Loret, E. P. (2019). *Ulva lactuca*, a source of troubles and potential riches. *Mar. Drugs* 17, 357. doi: 10.3390/md17060357

Egan, S., Harder, T., Burke, C., Steinberg, P., Kjelleberg, S., and Thomas, T. (2013). The seaweed holobiont: understanding seaweed–bacteria interactions. *FEMS. Microbiol. Rev.* 37, 462–476. doi: 10.1111/1574-6976.12011

Falkowski, P. G., Katz, M. E., Knoll, A. H., Quigg, A., Raven, J. A., Schofield, O., et al. (2004). The evolution of modern eukaryotic phytoplankton. *Science* 305, 354–360. doi: 10.1126/science.1095964

Feitkenhauer, H. (2003). Anaerobic digestion of desizing wastewater: influence of pretreatment and anionic surfactant on degradation and intermediate accumulation. *Enzyme. Microb. Technol.* 33, 250–258. doi: 10.1016/S0141-0229(03)00125-X

Ferreira-Dias, S., Sandoval, G., Plou, F., and Valero, F. (2013). The potential use of lipases in the production of fatty acid derivatives for the food and nutraceutical industries. *Electron J. Biotechnol.* 16 (3), 12. doi: 10.2225/vol16-issue3-fulltext-5

Garrity, G., De Vos, P., Jones, D., Kreig, N., Ludwig, W., Rainey, F., et al. (2010). *Bergey's manual of systematic bacteriology: The firmicutes* (USA: University of Georgia).

Ghaderiardakani, F., Coates, J., and Wichard, T. (2017). Bacteria-induced morphogenesis of *Ulva intestinalis* and *Ulva mutabilis* (Chlorophyta): a contribution to the lottery theory. *FEMS Microbiol. Ecol.* 93, 8. doi: 10.1093/femsec/fix094

Ghaderiardakani, F., Quartino, M., and Wichard, T. (2020). Microbiome-dependent adaptation of seaweeds under environmental stresses: A perspective. *Front. Mar. Sci.* 7. doi: 10.3389/fmars.2020.575228

Guiry, M. D., and Guiry, G. M. (2022) *AlgaeBase*. Available at: https://www.algaebase.org (Accessed December 22, 2021).

Guisan, J. M., Bolivar, J. M., López-Gallego, F., and Rocha-Martín, J. (2020). *Methods in molecular biology immobilization of enzymes and cells* (New Yorks: Humana New York).

Gupta, N., Gandham, N., Jadhav, S., and Mishra, R. N. (2015). Isolation and identification of acinetobacter species with special reference to antibiotic resistance. *J. Nat. Sc. Biol. Med.* 6, 159–162. doi: 10.4103/0976-9668.149116

Gupta, R., Gigras, P., Mohapatra, H., Goswami, V. K., and Chauhan, B. (2003). Microbial -amylases: a biotechnological perspective. *Process. Biochem.* 38, 1599–1616. doi: 10.1016/S0032-9592(03)00053-0

Hehemann, J., Boraston, A., and Czjzek, M. (2014). A sweet new wave: structures and mechanism of enzymes that digest polysaccharides from marine algae. *Curr. Opin. Struc. Biol.* 28, 77–86. doi: 10.1016/j.sbi.2014.07.009

Higuera-Llanten, S., Vasquez-Ponce, F., Barrientos-Espinoza, B., Mardones, F. O., Marshall, S. H., and Olivares-Pacheco, J. (2018). Extended antibiotic treatment in salmon farms select multiresistant gut bacteria with a high prevalence of antibiotic resistance genes. *PloS One* 13, e0203641. doi: 10.1371/journal.pone.0203641

Holzinger, A., Herburger, K., Kaplan, F., and Louise, A. L. (2015). Desiccation tolerance in the chlorophyte green alga *Ulva* compressa: does cell wall architecture contribute to ecological success? *Planta.* 242, 477–492. doi: 10.1007/s00425-015-2292-6

Hui, C., Shan, L., Xiang-Rong, X., Shuang-Shuang, L., Guang-Jie, Z., Kai-Feng, S., et al. (2015). Antibiotics in typical marine aquaculture farms surrounding hailing island, south China: Occurrence, bioaccumulation and human dietary exposure. *Mar. pollut. Bull.* 90, 181–187. doi: 10.1016/j.marpolbul.2014.10.053

Ismail, A., Ktari, L., Ahmed, M., Bolhuis, H., Bouhaouala-Zahar, B., Stal, L., et al. (2018). Heterotrophic bacteria associated with the green alga *Ulva rigida*: identification and antimicrobial potential. *J. Appl. Phycol.* 30, 2883–2899. doi: 10.1007/s10811-018-1454-x

Joseph, B., and Ramteke, P. W. (2013). Extracellular solvent stable cold active lipase from psychrotrophic bacillus sphaericus MTCC 7526: partial purification and characterization. *Ann. Microbiol.* 63, 363–370. doi: 10.1007/s13213-012-0483-y

Kalpana, B. J., Aarthy, S., and Pandian, S. K. (2012). Antibiofilm activity of α-amylase from bacillus subtilis S8-18 against biofilm forming human bacterial pathogens. *Appl. Biochem. Biotechnol.* 167, 1778–1794. doi: 10.1007/s12010-011-9526-2

Kandasamy, P., Radhesh, K. S., Radhakrishnan, S., Sengali, R., Balaji, G., Gracy, M., et al. (2020). Shewanella algae and microbulbifer elongatus from marine macro-algae – isolation and characterization of agarhydrolysing bacteria. *Access Microbiol.* 10, 2. doi: 10.1099/acmi.0.000170

Kaur, K., Dattajirao, V., Shrivastava, V., and Bhardwaj, U. (2012). Isolation and characterization of chitosan-producing bacteria from beaches of chennai, India. *Enzyme. Res.* 2012, 421683. doi: 10.1155/2012/421683

Khan, I., Dutta, J. R., and Ganesan, R. (2017). *Lactobacillus* sps. lipase mediated poly (ϵ-caprolactone) degradation. *Int. J. Biol. Macromol.* 95, 126–131. doi: 10.1016/j.ijbiomac.2016.11.040

Kouzuma, A., and Watanabe, K. (2015). Exploring the potential of algae/bacteria interactions. *Curr. Opin. Biotechnol.* 33, 125–129. doi: 10.1016/j.copbio.2015.02.007

Krishnan, A., Kumar, G., Loganathan, K., and Rao, B. (2011). Optimization, production and partial purification of extracellular αamylase from *Bacillus* sp. *Marini. Arch. Appl. Sci. Res.* 3, 33–42.

Krumperman, P. H. (1983). Multiple antibiotic resistance indexing of escherichia coli to identify high-risk sources of fecal contamination of foods. *Appl. Environ. Microbiol.* 46, 165–170. doi: 10.1128/aem.46.1.165-170.1983

Ktari, L., Ismail, A., Selmi, H., Hmani, I., and Elbour, M. (2022). Biological potential of the alien red alga asparagopsis taxiformis and characterization of its culturable associated bacteria. *J. Appl. Phycol* 34, 2769–2782. doi: 10.1007/s10811-022-02818-8

Kumar, D., Bhardwaj, R., Jassal, S., Goyal, A., Khullar, A., and Gupta, N. (2021). Application of enzymes for an eco-friendly approach to textile processing. *Environ. Sci. pollut. Res*. doi: 10.1007/s11356-021-16764-4

Kumar, D. S., and Ray, S. (2014). Fungal lipase production by solid state fermentation–an overview. *J. Anal. Bioanal. Tech* 6, 1–10. doi: 10.4172/2155-9872.1000230

Kumar, P., Verma, A., Sundharam, S. S., Ojha, A. K., and Krishnamurthi, S. (2022). Exploring diversity and polymer degrading potential of epiphytic bacteria isolated from marine macroalgae. *Microorganisms* 10 (12), 2513. doi: 10.3390/microorganisms10122513

Kyle, H. S., Freddie, A. B., Karen, D. P., and Robert, L. V. (1971). Lecithin-agar assay for lecithinase antibodies serum. *Appl. Microbiol.* 21, 98–103. doi: 10.1128/am.21.1.98-103.1971

Lachnit, T., Meske, D., Wahl, M., Harder, T., and Schmitz, R. (2011). Epibacterial community patterns on marine macroalgae are host-specific but temporally variable. *Environ. Microbiol.* 13 (3), 655–665. doi: 10.1111/j.1462-2920.2010.02371.x

Leinberger, J., Holste, J., Bunk, B., Freese, H. M., Spröer, C., Dlugosch, L., et al. (2021). High potential for secondary metabolite production of paracoccus marcusii CP157, isolated from the crustacean cancer pagurus. *Front. Microbiol.* 12. doi: 10.3389/fmicb.2021.688754

Lemos, M. L., Toranzo, A. E., and Barja, J. L. (1985). Antibiotic activity of epiphytic bacteria isolated from intertidal seaweeds. *Microb. Ecol.* 11, 149–163. doi: 10.1007/BF02010487

Lupo, A., Coyne, S., and Berendonk, T. U. (2012). Origin and evolution of antibiotic resistance: The common mechanisms of emergence and spread in water bodies. *Front. Microbiol.* 3. doi: 10.3389/fmicb.2012.00018

Martin, M., Portetelle, D., Michel, G., and Vandenbol, M. (2014). Microorganisms living on macroalgae: diversity, interactions, and biotechnological applications. *Appl. Microbiol. Biotech.* 98, 2917–2935. doi: 10.1007/s00253-014-5557-2

Masci, D., and Castagnolo, D. (2021). "An introduction. exploiting enzymes as green catalysts in the synthesis of chemicals and drugs," in *Book the royal society of chemistry*, vol. 68. , 118.

Matsumoto, M., Yokouchi, H., Suzuki, N., Ohata, H., and Matsunaga, T. (2003). Saccharification of marine microalgae using marine bacteria for ethanol production. *Appl. Biochem. Biotechnol.* 5, 247–254. doi: 10.1385/ABAB:105:1-3:247

Miladi, R., Manghisi, A. A., Minicante, S., Genovese, G., Abdelkafi, S., and Morabito, M. (2018). A DNA barcoding survey of *Ulva* (Chlorophyta) in Tunisia and Italy reveals the presence of the overlooked alien u. ohnoi. *Cryptogamie Algologie.* 39, 85–107. doi: 10.7872/crya/v39.iss1.2018.85

Miranda, C. D., Godoy, F. A., and Lee, M. R. (2018). Current status of the use of antibiotics and the antimicrobial resistance in the Chilean salmon farms. *Front. Microbiol.* 9. doi: 10.3389/fmicb.2018.01284

Mohapatra, B. R., Bapuji, M., and Sree, A. N. (2003). Production of industrial enzymes (Amylase, carboxymethylcellulase and protease) by bacteria isolated from marine sedentary organisms. *Acta Biotechnol.* 23, p75–pp84. doi: 10.1002/abio.200390011

Moussa, M., Baccar, L., and Ben Khemis, R. (2005). La lagune de ghar El melh : Diagnostic écologique et perspectives d'aménagement hydraulique. *Rev. Des. Sci. l'Eau / J. Water Sci.* 18, 13–26.

Munita, J. M., and Arias, C. A. (2016). Mechanisms of antibiotic resistance. *Microbiol. Spectr.* 4, 10. doi: 10.1128/microbiolspec.VMBF-0016-2015

Naik, S., Sanika Naik, M., Vaingankar, D., Mujawar, S., Parab, P., and Meena, S. (2019). Biodegradation of seafood waste by seaweed-associated bacteria and application of seafood waste for ethanol production. *Adv. Biol. Sci. Res.*, 149–159.

Najjar, A., Hassan, E. A., Zabermawi, N., Saber, S. H., Bajrai, L. H., Almuhayawi, M. S., et al. (2021). Optimizing the catalytic activities of methanol and thermotolerant *Kocuria flava* lipases for biodiesel production from cooking oil wastes. *Sci. Rep.* 11, 13659. doi: 10.1038/s41598-021-93023-z

O'Neill, J. (2016). Tackling drug-resistant infections globally: Final report and recommendations. *Microbiol. Spectr.* 4, 10. doi: 10.1128/microbiolspec.VMBF-0016-2015

Passalacqua, K. D., Charbonneau, M. E., and O'Riordan, M. X. D. (2016). Bacterial metabolism shapes the host-pathogen interface. *Microbiol. Spectr.* 4, 10. doi: 10.1128/microbiolspec.VMBF-0027-2015

Qu, T., Chengzong, H., Xinyu, Z., Yi, Z., Chen, G., Zhihao, L., et al. (2021). "Bacteria associated with *Ulva* prolifera: A vital role in green tide formation and migration.". *Harmful Algae* 108 (2021), 102104. doi: 10.1016/j.hal.2021.102104

Rao, D., Webb, J. S., and Kjelleberg, S. (2005). Competitive interactions in mixedspecies biofilms containing the marine bacterium *Pseudoalteromonas tunicata*. *Appl. Environ. Microbiol.* 71, 1729–1736. doi: 10.1128/AEM.71.4.1729-1736.2005

Raveendran, S., Parameswaran, B., and Ummalyma, S. B. (2018). Applications of microbial enzymes in food industry. *Food Technol. Biotechnol.* 56 (1), 16–30. doi: 10.17113/ftb.56.01.18.5491

Samant, S., Naik, M. M., Vaingankar, D. C., Mujawar, S. Y., Parab, P., and Meena, S. N. (2019). "Biodegradation of seafood waste by seaweed-associated bacteria and application of seafood waste for ethanol production," in *Advances in biological science research* (Academic Press), 149–159.

Satpute, S., Bhawsar, B. D., Dhakephalkar, P., and Chopade, B. (2008). Assessment of different screening methods for selecting biosurfactant producing marine bacteria. *Indian. J. Mar. Sci.* 37, 243–250.

Saunders, G. W., and Kucera, H. (2010). An evaluation of rbcL, tufA, UPA, LSU and ITS as DNA barcode markers for the marine green macroalgae. *Cryptogamie Algologie* 31 (4), 487.

Schreiber, L., Kjeldsen, K. U., Funch, P., Jensen, J., Obst, M., López-Legentil, S., et al. (2016). Endozoicomonas are specific, facultative symbionts of Sea squirts. *Front. Microbiol.* 7. doi: 10.3389/fmicb.2016.01042

Shields, R. C., Mokhtar, N., Ford, M., Hall, M. J., Burgess, J. G., ElBadawey, M. R., et al. (2013). Efficacy of a marine bacterial nuclease against biofilm forming microorganisms isolated from chronic rhinosinusitis. *PLoS. One* 8, 55339. doi: 10.1371/journal.pone.0055339

Sierra, G. (1957). A simple method for the detection of lipolytic activity of microorganisms and some observations on the influence of the contact between cells and fatty substrates. *Antonie. Van. Leeuwenhoek.* 23, 15–22. doi: 10.1007/BF02545855

Singh, A. K., Bilal, M., Hafiz, M. N. I., Anne, S., and Meyer Abhay, R. (2021). Bioremediation of lignin derivatives and phenolics in wastewater with lignin modifying enzymes: Status, opportunities and challenges. *Sci. Total. Environ.* 777, 1459883. doi: 10.1016/j.scitotenv.2021.145988

Sinha, P., and Bedi, S. (2018). Production of sugars from cellulosic wastes by enzymatic hydrolysis. *Int. J. Curr. Res.* 10, 72141–72144. doi: 10.24941/ijcr.31694.08.2018

Smith, H. L., and Goodner, K. (1958). Detection of bacterial gelatinases by gelatin-agar plate methods. *J. Bacteriol.* 76, 662–665. doi: 10.1128/jb.76.6.662-665.1958

Société Française de Microbiologie (2020). "Comité de l'antibiogramme de la société française de microbiologie," in *CASFM / EUCAST : Société française de microbiologie*, 6–181.

Steinhagen, S., Weinberger, F., and Karez, R. (2019). Molecular analysis of *Ulva compressa* (Chlorophyta, *Ulva*les) reveals its morphological plasticity, distribution and potential invasiveness on German north Sea and Baltic Sea coasts. *Eur. J. Phycol.* 54, 102–114. doi: 10.1080/09670262.2018.1513167

Tamura, K., Stecher, G., and Kumar, S. (2021). MEGA11: Molecular evolutionary genetics analysis version 11. *Mol. Biol. Evol.* 38, 3022–3027. doi: 10.1093/molbev/msab120

Trivedi, N., Gupta, V., Kumar, M., Kumari, P., and Reddy, B. (2011). An alkali-halotolerant cellulase from bacillus flexus isolated from green seaweed *Ulva lactuca*. carbohyd. *Polym.* 83, 891–897. doi: 10.1016/j.carbpol.2010.08.069

Tujula, N. A., Crocetti, G. R., Burke, C., Thomas, T., Holmström, C., and Kjelleberg, S. (2010). Variability and abundance of the epiphytic bacterial community associated with a green marine ulvacean alga. *ISME J.* 4 (2), 301–311. doi: 10.1038/ismej.2009.107

Van der Maarel, M. J., van der Veen, B., Uitdehaag, J. C., Leemhuis, H., and Dijkhuizen, L. (2002). Properties and applications of starch-converting enzymes of the alpha-amylase family. *J. Biotechnol.* 94, 137–155. doi: 10.1016/s0168-1656(01)00407-2

Weiss, A., Costa, R., and Wichard, T. (2017). Morphogenesis of *Ulva mutabilis* (Chlorophyta) induced by maribacter species (Bacteroidetes, flavobacteriaceae). *Botanica. Marina.* 60, 197–206. doi: 10.1515/bot-2016-0083

Wichard, T., Charrier, B., Mineur, F., Bothwell, J. H., De Clerck, O., and Coates, J. C. (2015). The green seaweed *Ulva*: a model system to study morphogenesis. *Front. Plant Sci.* 6. doi: 10.3389/fpls.2015.00072

Wienhausen, G., Noriega-Ortega, B. E., Niggemann, J., Dittmar, T., and Simon, M. (2017). The exometabolome of two model strains of the roseobacter group: a marketplace of microbial metabolites. *Front. Microbiol.* 8, 1985. doi: 10.3389/fmicb.2017.01985

Wu, G., Qin, Y., Cheng, Q., and Liu, Z. (2014). Characterization of a novel alkali-stable and salt-tolerant α-amylase from marine bacterium *Zunongwangia profunda*. *J. Mol. Catal. B-Enzym* 110, 8–15. doi: 10.1016/j.molcatb.2014.08.023

Frontiers in Microbiology

Explores the habitable world and the potential of microbial life

The largest and most cited microbiology journal which advances our understanding of the role microbes play in addressing global challenges such as healthcare, food security, and climate change.

Discover the latest Research Topics

See more →

Frontiers

Avenue du Tribunal-Fédéral 34
1005 Lausanne, Switzerland
frontiersin.org

Contact us

+41 (0)21 510 17 00
frontiersin.org/about/contact